AD-A179 718 VORTEX INTERACTION ON A CANARD-WING CONFIGURATION(U) 1/3
AIR FORCE WRIGHT AERONAUTICAL LABS WRIGHT-PATTERSON AFB
OH W CALARESE OCT 86 AFWAL-TR-86-3100

UNCLASSIFIED F/G 1/1 NL

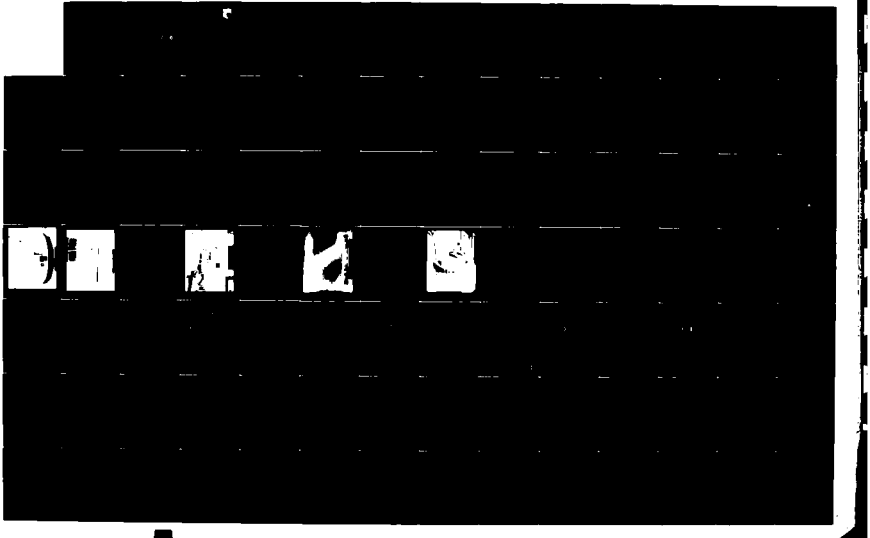

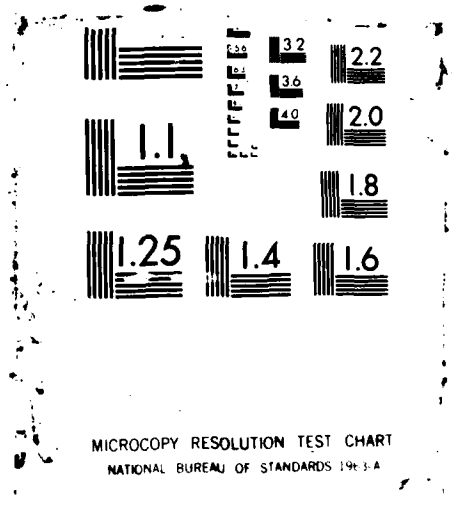
3.2
3.6
4.0
2.2
2.0
1.8
1.1
1.25
1.4
1.6
MICROCOPY RESOLUTION TEST CHART
NATIONAL BUREAU OF STANDARDS 1963-A

DTIC FILE COPY

PHOTOGRAPH THIS SHEET

AD-A179 718

DTIC ACCESSION NUMBER

LEVEL

AFWAL-TR-86-3100
VORTEX INTERACTION ON A CANARD WING CONFIGURATION

(1)

INVENTORY

OCT. 1986

DOCUMENT IDENTIFICATION

DISTRIBUTION STATEMENT A
Approved for public release;
Distribution Unlimited

DISTRIBUTION STATEMENT

ACCESSION FOR		
NTIS	GRA&I	☑
DTIC	TAB	☐
UNANNOUNCED		☐
JUSTIFICATION		
BY		
DISTRIBUTION /		
AVAILABILITY CODES		
DIST	AVAIL AND/OR SPECIAL	
A-1		

DISTRIBUTION STAMP

QUALITY INSPECTED 2

*Original contains color plates; All DTIC reproductions will be in black and white.

DTIC
SELECTED
APR 30 1987
D

DATE ACCESSIONED

DATE RETURNED

87 4 29 042

DATE RECEIVED IN DTIC

REGISTERED OR CERTIFIED NO.

PHOTOGRAPH THIS SHEET AND RETURN TO DTIC-FDAC

DTIC FORM 70A
MAR 86

DOCUMENT PROCESSING SHEET

PREVIOUS EDITION MAY BE USED UNTIL STOCK IS EXHAUSTED.

AFWAL-TR-86-3100

VORTEX INTERACTION ON A CANARD-WING CONFIGURATION

W. CALARESE
High Speed Aero Performance Branch
Aeromechanics Division

October 1986

Final Report for Period October 1982 - March 1985

FLIGHT DYNAMICS LABORATORY
AIR FORCE WRIGHT AERONAUTICAL LABORATORIES
AIR FORCE SYSTEMS COMMAND
WRIGHT-PATTERSON AIR FORCE BASE, OHIO 45433-6553

REPORT DOCUMENTATION PAGE

Form Approved OMB No. 0704-0188

1a. REPORT SECURITY CLASSIFICATION: UNCLASSIFIED	1b. RESTRICTIVE MARKINGS
2a. SECURITY CLASSIFICATION AUTHORITY	3. DISTRIBUTION/AVAILABILITY OF REPORT: Approved for Public Release; Distribution Unlimited
2b. DECLASSIFICATION/DOWNGRADING SCHEDULE	
4. PERFORMING ORGANIZATION REPORT NUMBER(S): AFWAL-TR-86-3100	5. MONITORING ORGANIZATION REPORT NUMBER(S)
6a. NAME OF PERFORMING ORGANIZATION: Air Force Wright Aeronautical Laboratories; 6b. OFFICE SYMBOL (If applicable): AFWAL/FIMG	7a. NAME OF MONITORING ORGANIZATION
6c. ADDRESS (City, State, and ZIP Code): Wright-Patterson AFB, OH 45433-6553	7b. ADDRESS (City, State, and ZIP Code)
8a. NAME OF FUNDING/SPONSORING ORGANIZATION; 8b. OFFICE SYMBOL (If applicable)	9. PROCUREMENT INSTRUMENT IDENTIFICATION NUMBER
8c. ADDRESS (City, State, and ZIP Code)	10. SOURCE OF FUNDING NUMBERS

PROGRAM ELEMENT NO.	PROJECT NO.	TASK NO.	WORK UNIT ACCESSION NO.
61102F	2307	N4	54

11. TITLE (Include Security Classification)

Vortex Interaction on a Canard-Wing Configuration.

12. PERSONAL AUTHOR(S)

Wladimiro Calarese

13a. TYPE OF REPORT	13b. TIME COVERED	14. DATE OF REPORT (Year, Month, Day)	15. PAGE COUNT
Final Report	FROM 10/1/82 TO 3/3/85	October 1986	254

16. SUPPLEMENTARY NOTATION

17. COSATI CODES			18. SUBJECT TERMS (Continue on reverse if necessary and identify by block number)
FIELD	GROUP	SUB-GROUP	Vortex Flow, Subsonic Flow, Close-Coupled Canards.
0102	2004	0101	

19. ABSTRACT (Continue on reverse if necessary and identify by block number)

The present experiment studies the interaction of vorticles shed by the canard and wing's leading edges, and their effect on the aircraft aerodynamic characteristics. A close-coupled canard-wing configuration was selected and tested in different wind tunnels and at different conditions. Tunnel and model size effects, Mach number, angle of attack, and spanwise blowing effects on the vortex interaction were analyzed. Intrusive (hot wires) and non-intrusive (laser doppler velocimeters) data acquisition techniques were used and compared to enhance the reliability of the results. Flow visualization by tufts, oil, and laser light sheets were employed. Mean velocities, vortex turbulence intensities, and Reynolds stresses obtained for different conditions were compared and found to be generally consistent. Mach number, wind tunnel, and model size effects were in general small. Turbulence intensities and stresses increased with angles of attack. Spanwise blowing produced a small favorable effect. The use of a coplanar canard produced a small favorable interaction between the leading edge vorticles. while the off-set (Con't)

20. DISTRIBUTION/AVAILABILITY OF ABSTRACT	21. ABSTRACT SECURITY CLASSIFICATION
☒ UNCLASSIFIED/UNLIMITED ☐ SAME AS RPT. ☐ DTIC USERS	UNCLASSIFIED

22a. NAME OF RESPONSIBLE INDIVIDUAL	22b. TELEPHONE (Include Area Code)	22c. OFFICE SYMBOL
Wladimiro Calarese	513-255-2052	AFWAL/FIMG

(Con't)

canard produced a considerable increase in the lift/drag ratio.

NOTICE

When Government drawings, specifications, or other data are used for any purpose other than in connection with a definitely related Government procurement operation, the United States Government thereby incurs no responsibility nor any obligation whatsoever; and the fact that the government may have formulated, furnished, or in any way supplied the said drawings, specifications, or other data, is not to be regarded by implication or otherwise as in any manner licensing the holder or any other person or corporation, or conveying any rights or permission to manufacture, use, or sell any patented invention that may in any way be related thereto.

This technical report has been reviewed and is approved for publication.

WLADIMIRO CALARESE, Aerospace Engineer
High Speed Aero Performance Branch
Aeromechanics Division

VALENTINE DAHLEM, Chief
High Speed Aero Performance Branch
Aeromechanics Division

FOR THE COMMANDER:

Donald A. Dreesbach
Colonel, USAF
Chief
Aeromechanics Division

"If your address has changed, if you wish to be removed from our mailing list, or if the addressee is no longer employed by your organization please notify AFWAL/FIMG **, W-P AFB, OH 45433 to help maintain a current mailing list".**

Copies of this report should not be returned unless return is required by security considerations, contractual obligations, or notice on a specific document.

FOREWORD

This report was prepared by Dr Wladimiro Calarese of the High Speed Aerodynamics Group, High Speed Aero Performance Branch, Aeromechanics Division, Flight Dynamics Laboratory, Wright Aeronautical Laboratories, Wright-Patterson Air Force Base, Ohio. The research was performed in-house under work unit No. 2307N454 and covers work performed between January 1984 and January 1985.

The author wishes to thank Mr Glenn Gustafson, Capt Wendell Baker, Mr Noel Allen, and the other members of the Experimental Aerodynamics Group of AFWAL/FIMM, Dr George Seibert and the members of the Aero Optics Group of AFWAL/FIMN, Mr Glenn Williams, Mr Gary Dale, and the Trisonic Gasdynamics Facility support group for their invaluable assistance and support in the data collection of the present experiments.

TABLE OF CONTENTS

LIST OF SYMBOLS

C_D	drag coefficient based on wing area
C_L	lift coefficient based on wing area
C_M	pitching moment coefficient based on wing area and mean wing chord; reference point located at 66% of fuselage centerline
C_μ	blowing coefficient based on wing area; C=MDOT $V_j/qS_w g$
d	laser fringe spacing
D	drag
e_1, e_2	A.C. voltage output for wire 1, and 2 of the hot wire anemometer
$\overline{e_1^2}$, $\overline{e_2^2}$	mean value of the square of the A.C. voltage output for wire 1 and 2
E_1, E_2	D.C. voltage output for wire 1 and 2 of the hot wire anemometer
$\overline{f}$	Doppler frequency function
f	function
g	acceleration of gravity
H.W.	hot wire anemometer
L	lift
LDV	laser Doppler velocimeter
M	Mach number
MDOT	mass flux, pounds/sec.
q	dynamic pressure
R	autocorrelation function, i.e. $R = u^*(t)\, u^*(t + \tau_1)$
R^*	crosscorrelation function, i.e. $R^* = u^*(t)\, w^*(t + \tau_1)$
RMS	root mean square
Sw	wing planform area
t	time
TGF	Trisonic Gasdynamics Facility
TPN	test point number

LIST OF SYMBOLS (continued)

$\bar{u}$	mean axial velocity
u^*	axial velocity fluctuation
u', $\bar{u}'$	axial (longitudinal) turbulence intensity $\sqrt{\overline{u^{*2}}}$
$\frac{\overline{u'w'}}{V^2}$	Reynolds stresses in the axial plane
$\frac{u\,w}{V}$	abbreviation for $\frac{\overline{u'w'}}{V^2} \times 10^2$
V_j	blowing velocity
V	free stream velocity
VWT, V.T., V.W.T.	vertical wind tunnel
$\bar{w}$	mean vertical velocity
w^*	vertical velocity fluctuation
w', $\bar{w}'$	vertical turbulence intensity, $\sqrt{\overline{w^{*2}}}$
X,Y,Z	cartesian coordinate system aligned with the wind tunnel coordinates with origin at the body nose vertex, X in the direction of the wind tunnel axis (free stream direction), Y in the lateral direction, Z in the direction perpendicular to the wind tunnel axis in the pitch plane.
$\bar{x}$	hot wire longitudinal distance from the wing's trailing edge tip, parallel to the tunnel axis, with the negative direction downstream
$\bar{y}$	hot wire lateral distance from the wing or canard's trailing edge tip, positive toward the fuselage
Y_s	lateral distance from the model's fuselage

LIST OF SYMBOLS (continued)

Z_{MAX}, Z_m, Z_M	wing's maximum semi-thickness at the root
α	angle of attack
β_1	angle between the canards trailing edge and the perpendicular to the fuselage centerline
β_2	angle between the wing's trailing edge and the perpendicular to the fuselage centerline
θ	semi-angle of laser interfering beams
λ	laser wavelength
Λ	wing or canard sweep angle
ρ	density
τ	local airfoil thickness
τ_1	characteristic time

Subscript

cls, CLS	height over the canard's local surface where data are taken
cte, CTE	height over the canard's trailing edge where data are taken
wls, WLS	height over the wing's local surface where data are taken
wte, WTE	height over the wing's trailing edge where data are taken

In the computer plotted figures, 1) the appropriate subscripts above should be used with the Z letter in the abscissa. For example, if the data refers to the wing, then Z/Z_{MAX} should be interpreted as Z_{WLS}/Z_{MAX}, etc., 2) the capital X's refer to off-scale data

LIST OF ILLUSTRATIONS

LIST OF ILLUSTRATIONS (Cont'd)

LIST OF ILLUSTRATIONS (Cont'd)

LIST OF ILLUSTRATIONS (Cont'd)

LIST OF ILLUSTRATIONS (Cont'd)

LIST OF ILLUSTRATIONS (Cont'd)

LIST OF ILLUSTRATIONS (Cont'd)

SECTION I

INTRODUCTION

The advent of high maneuverability aircraft, which use coupled and closely coupled canards, has stimulated research directed to ascertaining the effect of canards on the overall aerodynamic characteristics of the aircraft and to determining whether a favorable interference between the canard and the wing leading edge vortices can be found to enhance the value of the lift/drag ratio (Reference 1-4).

The flow at the leading edges of sweptback wings at an angle of attack separates and produces vortex sheets which roll up into vortices on the wing's upper surface. The presence of canards closely coupled with the wings produces an interference between the leading edge vortices (Figure 1). The interference changes the turbulence characteristics and the trajectories of the vortices, which in turn can change the wing's aerodynamic characteristics. The present research was directed at acquiring experimental data on the leading edge vortices and their interaction.

In order to be certain of the reliability of the collected data, two different data acquisition systems were used. An intrusive hot wire anemometer system was compared to a non intrusive laser doppler velocimeter system. In addition, tests were performed with different size models in different wind tunnels at different Mach numbers to ascertain whether differences in these parameters would alter the vortex interaction process.

Detailed turbulence intensities and Reynolds stress measurements were performed in the rolled-up vortices by means of hot film anemometers and laser doppler velocimeters for various canard-wing configurations tested in different wind tunnels. These measurements gave an extensive picture of boundary layer separation and vortex formation on the canard-wing upper surface. Spanwise wing blowing was used in some tests to ascertain whether changing the vortex trajectory would enhance the wing lift. Laser light sheets, photography, oil flow, and tufts were used for flow visualization.

The Reynolds stress data obtained in the present experiment can be used to improve eddy viscosity models used in the solution of the unsteady Navier-Stokes equations, applied to the present aerodynamic configuration, and to compare with theoretical results.

SECTION II

EQUIPMENT AND TEST DESCRIPTION

The tests were performed in the 12 foot vertical wind tunnel (VWT) and in the Trisonic Gasdynamics Facility (TGF) 2 foot wind tunnel of the Flight Dynamics Laboratory. Similar tests were previously performed in the 5 foot wind tunnel of the Air Force Institute of Technology (Reference 1).

a. Vertical Wind Tunnel

The vertical wind tunnel is an open return tunnel. Its test section is 12 feet wide and 15 feet high with a contraction ratio of 9.9 to 1. The maximum velocity attained in the tunnel is 102 mph, the maximum Mach number is 0.14 and the Reynolds number per foot equals 0.95×10^6. It runs at atmospheric conditions. A sketch of the tunnel is shown in Figure 2. Electronic data recording equipment is available and consists of an analog to digital converter and a Hewlett-Packard HP85 digital data acquisition system with 20 signal conditioning amplifiers.

The tests were performed at a freestream velocity of 100 mph (Mach number approximately equal to 0.14) and at a Reynolds number per foot of 8.80×10^5. Three angles of attack were used, α = 10°, 16°, 20° (nominal values). The sting mounted model is shown in Figures 3-4. It was mounted off center of the test section in order to allow the LDV system to be within range for good beam focusing, since its focal length did not reach the tunnel centerline, and also to place the model where pre-test surveys showed the free stream turbulence levels to be at a minimum.

The canards could be coplanar with the wings or could be raised vertically and inserted in slots in an off-set position with respect to the wings (Figure 5). No canard deflections were used. The 60° sweptback wing was untwisted and had uncambered circular arc airfoil sections. Its aspect ratio was 2.5. The maximum thickness distribution varied linearly from 6 percent of the chord at the root to 4 percent at the tip. The maximum semi-thickness at the root was equal to 0.3 in. The angle between the trailing edge and the

perpendicular to the fuselage centerline was δ_2=34.77°. The 51.7° sweptback canard was also untwisted and had an uncambered circular-arc airfoil section with the same thickness distribution as the wing. The canard area was 28 percent of the wing area, and its aspect ratio was 4.12. The angle between the trailing edge and the perpendicular to the fuselage centerline was δ_1=13.8°. A six component strain gauge balance was incorporated in the models capable of measuring normal, axial, and side forces up to 50, 15, and 25 lbs. respectively. The balance was properly calibrated and performed satisfactorily. The configuration tested comprised two canard positions, coplanar (mid) and off set (high) by 1.69 in.

b. Trisonic Gasdynamics Facility

The TGF wind tunnel is a close-circuit, variable density, continuous flow wind tunnel, which can operate at subsonic, transonic, and supersonic speeds (Figure 6A). The two foot subsonic test section can provide Mach numbers from 0.23 to 0.85. The maximum Reynolds number per foot that can be obtained is 7.5 million. For more details, consult Reference 5. The Mach numbers used were M=0.3 and M=0.5 and the Reynolds numbers per foot were 1.8×10^6 and 2.2×10^6, respectively. Three angles of attack were also used, namely α = 10°, 16°, 19° (nominal values). The model used was sting mounted and it was a 55% replica of the VWT model. The balance malfunctioned when spanwise blowing was used at high dynamic pressures and could not be calibrated properly. Therefore, the force data with blowing were disregarded since lift changes due to blowing could not be ascertained. The configurations tested were with the mid canard and without canard.

c. Data Acquisition

The data acquisition system in both tunnels consisted of an argon ion laser doppler velocimeter. Two orthogonal velocity components (axial and vertical) were measured simultaneously. Each component was bragg shifted to eliminate directional ambiguity, and facilitate band pass filtering. An off-axis backscatter configuration was used. A traverse mechanism was employed with an overall precision accuracy of approximately ± 0.25% of the distance traveled. The digital data were channeled to a microcomputer for

on-line analysis and then transferred to a minicomputer for final processing and analysis. The power output for the VWT system was 4 watts for full wave output, while in the TGF was 15 watts. The seeding in the VWT was accomplished by atomizing water using pressurized air from 80 to 200 psi, while in the TGF, silicon oil was used and atomized with 300 psi pressurized air. The TGF LDV system is shown in Figure 6A and a schematic of the laser configuration is shown in Figure 6B.

The mean velocities were obtained by calculating the fringe spacing obtained by crossing the interfering blue and green laser beams at the point under investigation in the flow field,

$$d = \frac{\lambda}{2\sin\theta} \tag{1}$$

where λ is the beam wavelength and θ is the semi-angle of the interfering beams. Then the value of the fringe spacing is multiplied by the doppler frequency of the particles traversing the fringe spacing,

$$\bar{u} = d\bar{f} \tag{2}$$

The turbulence intensities were obtained directly from the autocorrelation function while the Reynolds stresses were derived from the crosscorrelation function,

$$\bar{u}' = \sqrt{\overline{u'^2}} = f(R) \tag{3}$$

$$\overline{u'w'} = f(R^*) \tag{4}$$

Similar equations were used for the vertical mean velocity and turbulence intensity.

Flow visualization was obtained by using tufts, oil flow, and laser light sheets generated by removing the front transmission lense of the laser and replacing it with a cylindrical lense. For more details about the laser velocimeter apparatus, refer to Reference 6.

A cross-shaped hot film anemometer was used in the TGF in conjunction with the LDV and mounted on an off-set probe support, (Figure 7A) The film length was 0.05 in, its sensing length 0.02 in, its diameter 0.001 in, and its dynamic response greater than 80 KHZ, (Figure 7B). It was mounted on a traverse mechanism shown in Figure 8, which allowed motion in all three axes. All the data presented were obtained with the probe aligned with the free-stream direction and at different positions in the Z direction, which is perpendicular to the wind tunnel axis. The hot film output was monitored with a RMS meter and recorded on tape. Auto correlations and power spectral densities were obtained using a Fourier analyzer. Mean velocities, turbulence intensities, and Reynolds stresses were calculated using the D.C. and A.C. voltage outputs. For example:

$$\bar{u} = \frac{0.707}{\rho}\left[E_1 + E_2\right] \tag{5}$$

$$\bar{w} = \frac{0.707}{\rho}\left[E_1 - E_2\right] \tag{6}$$

$$\bar{u}' = \frac{0.707}{\rho}\,\mathrm{RMS}\left[e_1 + e_2\right] \tag{7}$$

$$\bar{w}' = \frac{0.707}{\rho}\,\mathrm{RMS}\left[e_1 - e_2\right] \tag{8}$$

$$\overline{u'w'} = \frac{0.5}{\rho^2}\left[\overline{e_1^2} - \overline{e_2^2}\right] \tag{9}$$

The procedure used is similar to those outlined in References 7 & 8. In both tunnels, spanwise mass blowing was used in some tests to alter the vortex trajectory of the wing leading edge vortex for lift enhancement. High pressure air of up to 150 psi was injected at 50% of the wing root chord, which resulted in a mass flux of 1/4 pound/sec and a corresponding blowing coefficient of $C_\mu \approx 0.05$.

Figure 4 shows the external injection lines on the VWT model, and the injection ports located just aft the wing's root maximum thickness, at 26.18 in from the model tip. Figure 8 shows the internal injection lines beside the sting and the injection port below the wing in the TGF configuration located at 14.41 in from the model tip. Data were recorded at 18 locations, A through R, for 18 different conditions (Figure 9), namely three angles of attack, two canard positions, two Mach numbers, with and without mass blowing, using the LDV system in the VWT and the LDV and the hot wire probe in the TGF. At each canard, wing, or flow field location, 10 measurements were taken in the vertical direction. In Figure 9, the first dimensions refer to the model used in the VWT, while the dimensions in parenthesis refer to the 55% replica used in the TGF tunnel.

For the different angles of attack used, corrections to the angle of attack were made to compensate for the sting and model deflections due to the dynamic loads. The probe position would vary within ± 0.04 in accuracy for different tests due to some slack in the traverse mechanism. In order to evaluate probe interference effects, some LDV measurements were obtained with the probe in the flow filed. A 1% difference was recorded between the data collected with the probe in the flow field and without the probe. Some uncertainty was introduced in the model deflection when spanwise injection was used because of the balance sensitivity to the thrust introduced by the blowing. Free stream turbulence intensity in the vertical tunnel was approximately 1%, while in the TGF was 0.5% of the freestream velocity, and it was measured with both the hot wire and the LDV.

The zero probe position was coincident with a cartesian coordinate system centered on the wing tip trailing edge. The vertical distance of the probe from the surface of the canard or wing was calculated as follows:

$$\tilde{Z}_{cls/wls} = Z_p - \tilde{Z}_{os} \qquad (10)$$

where Z_p is the probe vertical reading and

$$\tilde{Z}_{os} = \bar{x} \tan\alpha + \tau/2\cos\alpha \qquad (11)$$

is the location of the canard or wing surface at any given measuring station.

The vertical distance of the probe from the canard or wing trailing edge was

$$\tilde{Z}_{cte/wte} = Z_p - \tilde{Z}_{off} \tag{12}$$

where

$$\tilde{Z}_{off} = \bar{y} \tan \beta_{1,2} \sin\alpha \tag{13}$$

is the location of the canard or wing trailing edge in the flow field. In all the plots presented, the UW/V symbol on the ordinate stands for $\frac{\overline{u'w'}}{V^2} \times 10^2$.

Two or more numbers shown under the test point number (TPN) in the figures signify that the data were repeated one or more times. No attempt was made to investigate Reynolds number effects since the Reynolds numbers in the two tunnels were very close to each other.

SECTION III

VORTEX FLOW FIELD

The vortical flow field over a close-coupled canard-wing configuration at angle of attack is examined. At angles of attack, the flow over a sweptback wing separates forming a free vortex sheet which rolls up over the wing's upper surface. This leading edge vortex produces an additional lift which is nonlinearly dependent on the angle of attack and might interact with the trailing edge vortex sheet which results from the circulation on the wing and is generated by the vorticity from the wing's potential lift. The same vortex system occurs on the canard and may interact with the wing vortex flow. Also present in the flow field are secondary vortices, spanwise trailing edge vortices caused by the trailing edge sweep, and wing tip vortices, generating at times very complex interactions. Spanwise air blowing is used to alter the leading edge vortex trajectory in an effort to keep it locked to the wing's leading edge for lift enhancement.

An effort is made to analyze the vortical flow field over the configuration and to interpret the behavior of the turbulence intensities, the stresses, and the vortices at different stations.

The local effect of these parameters is considered in relation to the overall L/D ratio behavior.

SECTION IV

RESULTS

It must be stated that data taken with the hot wire and LDV systems agree only in the general trends and distribution. At times only, there is agreement in the magnitudes too. In general, there is a lot of scatter in the Reynolds stress measurements. Bigger symbols in the figures signify that the values are off scale.

Figures 10-13 show the results obtained in the TGF at various points (stations) over the canard and the wing with measurements repeated at least twice. The repeated runs were performed after an interval of several days, changing the model configuration and then going back to the original one. The data in Figures 10-11, obtained with the hot wire, are repeatable except for a small variation in the mean vertical velocities. In general, the data are repeatable within a small degree of difference, which is acceptable due to the unstable vortical flow characteristics. In Figures 12-13, data obtained with the LDV are shown. They repeat themselves with a greater degree of accuracy than observed with the hot wire, which indicates a better reliability on non intrusive diagnostic techniques. It is evident that the hot wire probe produces a greater disturbance in the flow field than the micron size seeding used for the LDV measurements. For some configurations (see Appendix A), the hot wire data repeatability is not as accurate.

a. Comparison of H.W. and LDV Data With mid (coplanar) Canard, $\alpha = 10°$

The Mach number is 0.14 for the VWT and 0.3 for the TGF data. Spanwise air blowing was used in the TGF and the data were collected with the hot wire and the LDV systems in the TGF, and with the LDV in the VWT. Figures 14-16 show the results obtained for various flow field quantities at the point Q (Figure 9) in the wake of the wing. There is in general a good agreement between the hot wire and the LDV data of the TGF tunnel and the LDV data of the VWT. It is evident that a vortex is present in the flow field because of the change of sign in the vertical mean velocity w/V and the maximum values reached by the turbulence intensity w'/V at the point where the magnitude of

the vertical mean velocity is close to zero, which both occur when a vortex is traversed. The spanwise blowing produces a very small change; i.e., it moves the vortex closer to the surface (compare the values of w/V with and without blowing). The discrepancy between H.W. and LDV data is more pronounced with blowing. In the VWT, the values of the vertical turbulence intensity and of the axial Reynolds stresses are somewhat off the TGF values, even considering the unsteady characteristics of the flow field, up to $Z/Z_m = 0.4$, then they agree quite well up to the end of the vertical excursion.

Figures 17-19 refer to quantities measured at point M, which is located near the wing tip (Figure 9). The comparison of velocities and stresses between hot wire and LDV data is good, but the LDV data for the vertical mean velocity and turbulence intensity are somewhat higher, away from the wing. Blowing does not substantially change the flow field. Only the Reynolds stresses change sign near the wing surface because of it. The VWT LDV data show the same distribution of vertical mean velocity and turbulence intensity except that the peak values for the velocity between $Z_{wls}/Z_m = 2$ and 4 are considerably lower. In all the figures, there is a decrease of axial velocity near the wing surface which indicates the incipient formation of the wing tip vortex.

Figures 20-22 show the data measured at point H, which is located near the wing leading edge at about half span (Figure 9). Again, the data agree qualitatively, and the effect of blowing seems to be confined to increasing the values of the vertical mean velocity and turbulence intensity. The plots show the location of the leading edge vortex to be at about $Z_{wls}/Z_m = 4$. In the VWT, the leading edge vortex is closer to the wing surface at $Z_{wls}/Z_m = 2$ (Figure 21). The Reynolds stresses at times have discrepancies in their distribution and some isolated high values which do not repeat. This behavior shows the difficulties inherent in the acquisition of the Reynolds stresses in unsteady turbulent flows.

Figures 23-25 depict the flow field behind the canard trailing edge at the point E (Figure 9). The data from the TGF agree quite well. Analyzing the axial and vertical mean velocities, the wake and associated vortex flow can be detected at $Z_{cte}/Z_m = 0.2$. At that point, the distributions have an

inflection and the turbulence intensities reach a maximum. Unfortunately, the data from the VWT do not show this behavior and actually they do not agree with the TGF data. It is possible that the seeding for the LDV in the VWT was done incorrectly.

In Figures 26-28, the data from the tip of the canard at point D are plotted (Figure 9). There is agreement in the overall results. The blowing increases the intensities of the stresses and the mean and fluctuating velocites, except for the hot wire measurements of the w/V which shows a lower velocity with blowing. This occurrence might be due to probe interference. Also, the value of w/V in the VWT is much lower than the one in the TGF. The canard tip vortex is picked up at $Z_{cls}/Z_m \approx 0.1$ (check w/V distribution), which is very close to the surface. In fact, the vortex just starts to roll up at that height.

The flow over the point B, located at mid span on the canard (Figure 9), is analyzed in Figures 29-31. The distribution of the vertical mean velocity shows that the canard leading edge vortex core is located at $Z_{cls}/Z_m \approx 0.1$ and it just passes over point B, but a discrepancy on the vortex rotation is noticed by comparing the VWT and the TGF results. Again, this is attributed to probe interference.

The same degree of agreement is found for the H.W. and LDV measurements at higher angles of attack (see Appendix B).

b. Comparison of data with high (off-set) canard and with mid canard, VWT, $\alpha = 10°$

Data with the canard placed 1.69 in above the wing plane were obtained in the VWT. It is useful to compare these data with the mid canard data in order to establish the extent of influence of the canards position on the wing's flow field.

At the wing's leading edge, point F, it is clear that the mid canard presence influences appreciably the flow field, while the high canard causes much less interference (Figures 32-33). The vertical mean velocity, the

turbulence intensity, and the Reynolds stresses have much higher values for the mid canard position. The excessive turbulence reaching the wing is detrimental to the lift. The balance data confirm that the interference caused by the mid canard is unfavorable compared with the conditions with the high canard configuration at $\alpha = 10°$. The lift coefficient for the high canard is $C_L = 0.59$, while for the mid canard $C_L = 0.525$. The L/D ratio with the high canard is 12% higher than with the mid canard.

Plots for other locations are shown in Appendix C.

c. Comparison of data with high (off-set) canard and with mid canard, VWT, $\alpha = 16°$

At the point R, the wing tip vortex for the high canard is centered at $Z_{wte}/Z_m \cong 3.2$ while the mid canard produces a shift of the vortex in the vertical direction, since its center is approximately located at $Z_{wte}/Z_m = 6$. The high canard produces also an inversion in the vertical mean velocity direction close to the wing plane and a higher vertical turbulence intensity (Figure 34). The other quantities are comparable (Figure 35).

On the wing tip, point M, the vertical mean velocity is higher for the high canard (Figure 36). In addition, with the high canard, the vortex core is smaller than with the mid canard, indicating that a slower vortex growth, and therefore a less dissipating action is taking place, while the momentum is conserved. The velocity, turbulence, and stresses in the axial direction and axial plane are much higher in presence of the mid canard which indicates a stronger interference (Figure 37). The same conditions are found at point H on the wing, where a bigger vortex and higher turbulence with the mid canard indicate a stronger interaction (Figures 38-39).

The balance data indicate that an overall favorable interference is obtained with the high canard since the L/D ratio is about 12% higher than with the mid canard.

d. Comparison of data with high (off-set) canard and with mid canard, VWT, $\alpha = 20°$

As was the case for $\alpha = 16°$, at $\alpha = 20°$ the mid canard shifts the wing tip vortex up in the vertical direction at point Q (Figure 40). The plot of the vertical mean velocity for the high canard shows two distinct vortices, the wing tip vortex, the center of which is located at $Z_{wte}/Z_m \cong 0$ and the canard tip vortex located at $Z_{wte}/Z_m \cong 9$. The turbulence intensity increases considerably at the second vortex location as do the Reynolds stresses for the high canard (Figure 41). At the wing tip, point M, the high canard causes higher turbulence and stresses, but the mid canard produces a higher vortex vertical velocity (Figures 42-43), which is beneficial to the lift.

At the wing's leading edge, point H, the mid canard causes a lift of the leading edge vortex from $Z_{wls}/Z_m = 1.75$ to $Z_{wls}/Z_m = 4$. In addition, the vortex is completely rolled up (Figures 44-45). The turbulence intensities and the stresses are comparable. Results at other locations are shown in Appendix C.

The balance data show that at $\alpha = 20°$, the high canard location produces an overall favorable interference, since the L/D ratio is 7% higher.

e. Comparison of data with mid canard and without canard, TGF, $\alpha = 10°$

The comparison of Figures 46 and 47 shows that, without canard, the turbulence and wake effects recorded with the hot wire at point Q are higher while the negative vertical mean velocity is smaller than with the presence of the canard. This effect is considered to be a favorable interference of the mid canard with the wing, due to the development of a less dissipative flow with a greater downwash behind the wing, which generates a bigger lift. This effect was already noticed in Reference 1. The balance data confirm this conclusion showing a lift increase of about 7% by using the coplanar canard. However, the L/D ratio with the coplanar canard increases by only about 2%. Measurements taken with the H.W. with blowing without canard show a change in the stress behavior and an increase in the wake longitudinal velocity, but blowing leaves the other parameters almost unchanged (Figures 47-48).

f. Comparison of Data with mid canard and without canard TGF, $\alpha = 16°$

In the wake of the wing's tip, point R, the wake axial and vertical mean velocity are much higher with the canard, while the turbulence intensity is lower, which indicates a favorable canard interference (Figures 49-50). At point Q, in the wake of the wing leading edge vortex, which is located at $Z_{wte}/Z_m \cong 6$, the blowing increases the turbulence and stresses, especially when the measurements are made with the LDV (Figures 51-52). On the wing tip, point M, the same favorable canard interference experienced at point R is recorded. The blowing increases the axial mean velocity and the stresses over the wing tip (Figures 53-54).

On the wing leading edge, point H, the wake of the canard and its vortex produce a higher axial mean velocity and lower axial turbulence intensity than the configuration without canard, but a lower vertical mean velocity and a higher vertical turbulence intensity. Furthermore, the flow from the canard helps the wing's leading edge vortex roll up and position its center at $Z_{wls}/Z \cong 4.0$, which is the point of sign change of the vertical mean velocity and of maximum turbulence intensity. Without canard, the vortex flow is still moving vertically, it is retarded in the longitudinal direction, and it is not rolled up (Figures 55-56). Again, the mid canard leading edge vortex seems to interact favorably with the wing vortex. The balance data at $\alpha = 16°$ show that the canard increases substantially the lift coefficient about 15%, but the L/D ratio increases only slightly, just about 4%.

Results at other locations and angles of attack are similar to those presented and are shown in Appendix D.

a. Mach number effects on the wing's outboard span with mid canard, TGF, $\alpha = 16°$

In Figures 57-59, hot wire results at points R, M, and E for M = 0.3 and 0.5 show comparable values for the flow parameters measured. Only the vertical mean velocity for M = 0.3 in Figure 57 could be higher or lower according to two different runs.

At midspan in the wake of the wing, point I, an increase in Mach number has the effect to reduce the mean velocities, the axial turbulence intensity,

and the Reynolds stresses near the wake's center (Figure 60). The same effects are seen at the wing's trailing edge, point J (Figure 61) and on the wing itself, at points K and L (Figures 62-63). The leading edge vortex location can clearly be seen to be at point K (Figure 62). Its center is located at $Z_{wls}/Z_m \approx 4$ where the axial mean velocity is minimal and the intensity and stresses are maximum and where the vertical mean velocity changes sign and corresponds to a maximum turbulence intensity.

h. Force and Moment Measurements

Balance measurements obtained in both wind tunnels show a good agreement for the values of the lift, drag, and pitching moment coefficients (Figures 64-65).

Figure 64 refers to data obtained in the vertical wind tunnel. It is evident that the high canard produces a favorable interference and a better lift/drag ratio than the mid canard, up to about 10% higher.

Figure 65 refers to data obtained in the TGF, with the coplanar canard and without canard. The use of the canard gives a higher lift/drag ratio, but the improvement is fairly small (about 4%).

It is believed that the reason for the high canards favorable results is partly due to its vortex and wake flow missing the wing and, therefore, causing less adverse interference.

For the range tested, as expected, the Mach number has in general a small influence on the lift/drag ratios, which are basically functions of Reynolds number (Figure 66). The Reynolds number difference between the tunnels is small enough not to affect the coefficients' values.

Normal force measurements taken with and without blowing with the VWT balance showed a very slight increase in normal force with blowing, but this increase is inconclusive since it lies within the experimental error range, which lies in the 2% to 3% range. As stated before, the TGF balance data with blowing were unreliable and could not be presented.

SECTION V

FLOW VISUALIZATION

Flow visualization was obtained in both the VWT and the TGF tunnels. In the VWT, tufts, oil flow, and laser light sheets were used, while in the TGF tunnel, only light sheets were used. Figures 67-72 show the flow field in the VWT for both the mid and high canard at angles of attack of 10°, 16°, and 20° using tufts. The size of the leading edge vortices increases with increasing angle of attack. The mid canard shields the wing's leading edge and, consequently, the wing's leading edge vortex starts forming a short distance outboard and ends well ahead of the wing tip, while, for the high canard, the wing's leading edge vortex extends from the wing's root almost to the wing's tip. This can clearly be seen in the oil flow photographs (Figures 73-78). This better vortex formation is beneficial to the overall lift.

At all angles of attack, the leading edge vortex for the mid canard sheds at 3/4 span on the canard and at mid chord near the wing tip on the wing (notice the vortex separation line). When the high canard is used, the canards leading edge vortex sheds at a span location closer to the canard tip when the wing's leading edge vortex remains close to the wing's surface up to the tip's trailing edge. The earlier vortex shedding for the mid canard produces an unfavorable interference and a lower L/D ratio. At α = 16°, and 20°, two secondary separation lines are visible on the wing. Figure 79 shows the vortex system obtained with the laser light sheets in the VWT. The model configuration refers to the mid canard at α = 16°. On the model's left side is clearly seen the interaction between the canard and wing vortices.

Figure 80 shows the application of laser light sheets in the TGF tunnel. The air injection port at the wing's root mid span is visible. Figures 81-85 show the vortex interaction at different angles of attack at M= 0.3 and 0.5. In Figures 81-82, the tip (or secondary) vortex, the wing's and the canards leading edge vortices are clearly seen closely interacting with each other at α = 18° and M = 0.30. The vortex system is slightly bigger at M = 0.5. Figures 83-84 show the vortex system at α = 16° and at M = 0.3 and 0.5

respectively. Again, the higher Mach number produces bigger vortices. Comparing Figures 81-83 and 82-84, it is easy to see, as expected, that the vortex system is bigger at higher angles of attack; therefore, the effect of increasing the Mach numbers is similar to increasing slightly the angle of attack.

In Figure 85, the wing vortex for $\alpha = 10^{\circ}$ can be seen on the opposite side of the model; i.e., on the right wing.

Complete movies have been taken for different configurations at all angles of attack up to $\alpha = 18^{\circ}$ and are available for reviewing at the Flight Dynamics Laboratory.

SECTION VI

CONCLUSION

An experimental investigation was performed on a close-coupled canard-wing model using two different wind tunnels and two diagnostic systems. The conclusions are:

a. In general, the data repeatability shows some small degree of inaccuracy, due to the unstable (time dependent) nature of vortical flows. Usually the LDV repeatability is better than the hot wire anemometry is, because of the non intrusive technique, but for some configurations, the hot wire repeatability is quite good. The comparison of data taken with the hot wire and the LDV system shows an agreement in the general trends and distributions. The magnitudes usually differ and only at times are they in agreement. Also, a lot of scatter and discrepancies are noticed in the Reynolds stress measurements taken with the two systems, which make them unreliable.

b. There is in general agreement between the hot wire and LDV data of the TGF tunnel and the LDV data of the VWT. This signifies that the size of the tunnel and of the model have a negligible effect on the data.

c. For the Mach number range tested, the Mach number effect is in general small except at some discrete stations on the wing and when no canard is used. In this case, the increase in Mach number reduces somewhat the values of the mean velocities, intensities, and stresses. Another Mach number effect is to increase the vortex size with increasing Mach numbers.

d. Spanwise blowing usually produces a small favorable effect.

e. The vortex interaction remains unchanged with angle of attack. The only influence of increasing the angle of attack consists of increasing the mean and fluctuating properties of the vortical flow field.

f. At all angles of attack, the presence of the high (off-set) canard creates a favorable interaction between the leading edge vortices by

increasing the vortex core and its strength over the wing plane and is more effective than the mid (coplanar) canard in improving the wing's vortex flow.

a. The use of the mid (coplanar) canard increases the lift coefficient of all the configurations tested, but the lift/drag ratio increase is small when compared with configurations without canard. The high (off-set) canard instead produces a marked improvement on the lift/drag ratio at all the angles of attack tested.

REFERENCES

1. Calarese, W., "Close-Coupled Canard-Wing Vortex Interaction and Reynolds Stress Acquisition," AIAA-82-1368, August 1982.

2. Washburn, K. E., and Gloss, B. B., "Aerodynamics Load Distributions at Transonic Speeds for a Close-Coupled Wing-Canard Configuration: Tabulated Pressure Data," NASA TM-78780, October 1978.

3. Gloss, B. B., and Washburn, K. E., "A Study of Canard-Wing Interference Using Experimental Pressure Data at Transonic Speeds," NASA Technical Paper 1355, 1979.

4. Gloss, B. B., and McKinney, L. W., "Canard-Wing Lift Interference Related to Maneuvering Aircraft at Subsonic Speeds," NASA TMX-2897, Dec 1973.

5. Clark, G. F., "Trisonic Gasdynamics Facility User Manual," AFWAL-TM-82-176-FIMM, April 1982.

6. O'Heren, C. H. Parobek, D. M., and Weissman, C. B., "Laser Velocimeter Developments for Surveying Thin Boundary Layers in a Mach 6 High Reynolds Number Flow," AFWAL-TR-82-3111.

7. Swanson, R. C., and Schetz, J. A., "Turbulent Wake Behind Slender Bodies Including Self-Propelled Configurations," VPI-AERO-024, September 1974

8. Chieng, C. C., Jakubowski, A. K., and Schetz, J. A., "Investigation of the Turbulent Properties of the Wake Behind Self-Propelled, Axisymmetric Bodies," VPI-AERO-025, September 1974

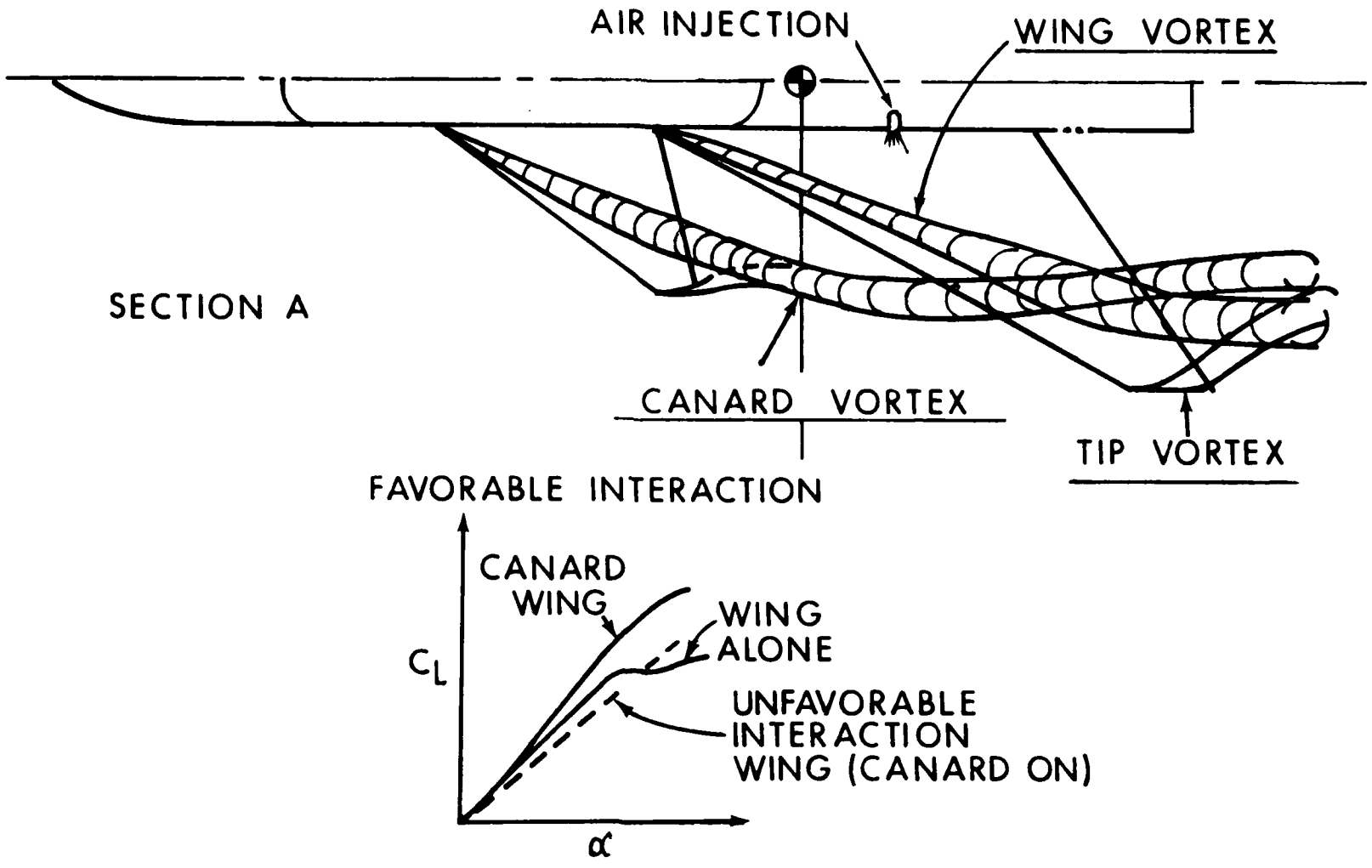

FIG. 1 COPLANAR CANARD CONFIGURATION AT ANGLE OF ATTACK, VORTEX INTERACTION

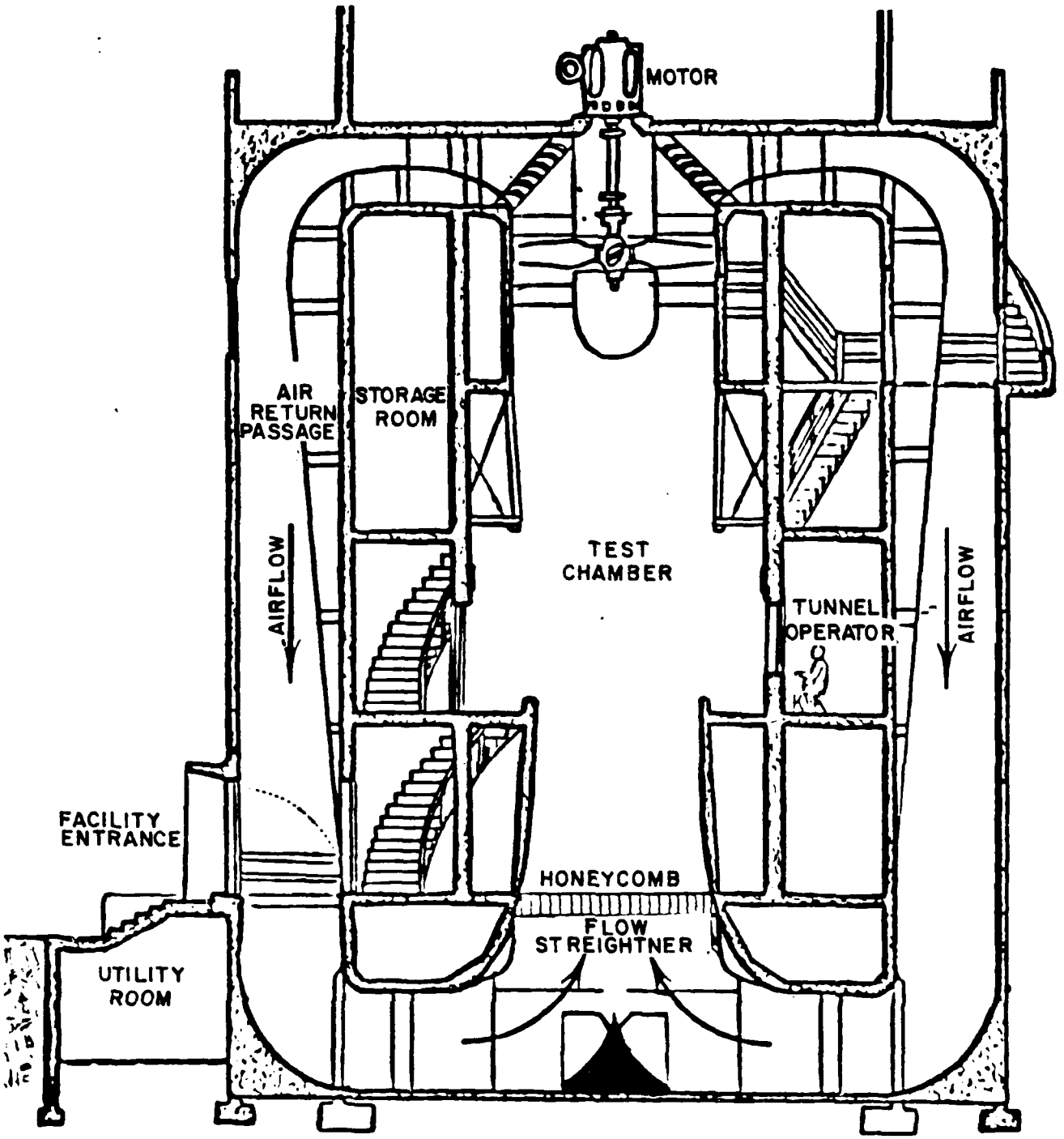

FIG. 2 VERTICAL WIND TUNNEL (VWT)
WRIGHT FIELD
SCALE 1"-126"

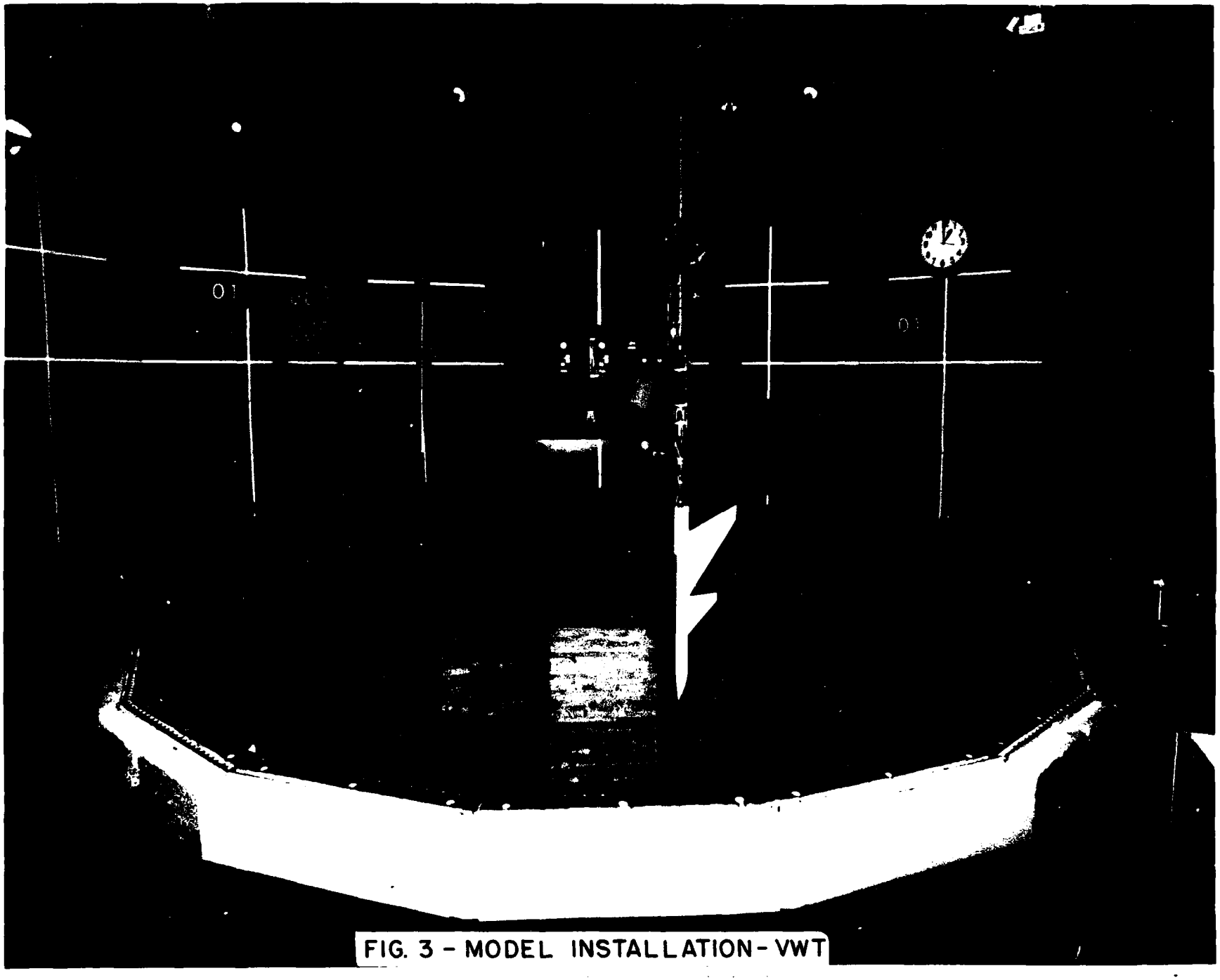

FIG. 3 - MODEL INSTALLATION - VWT

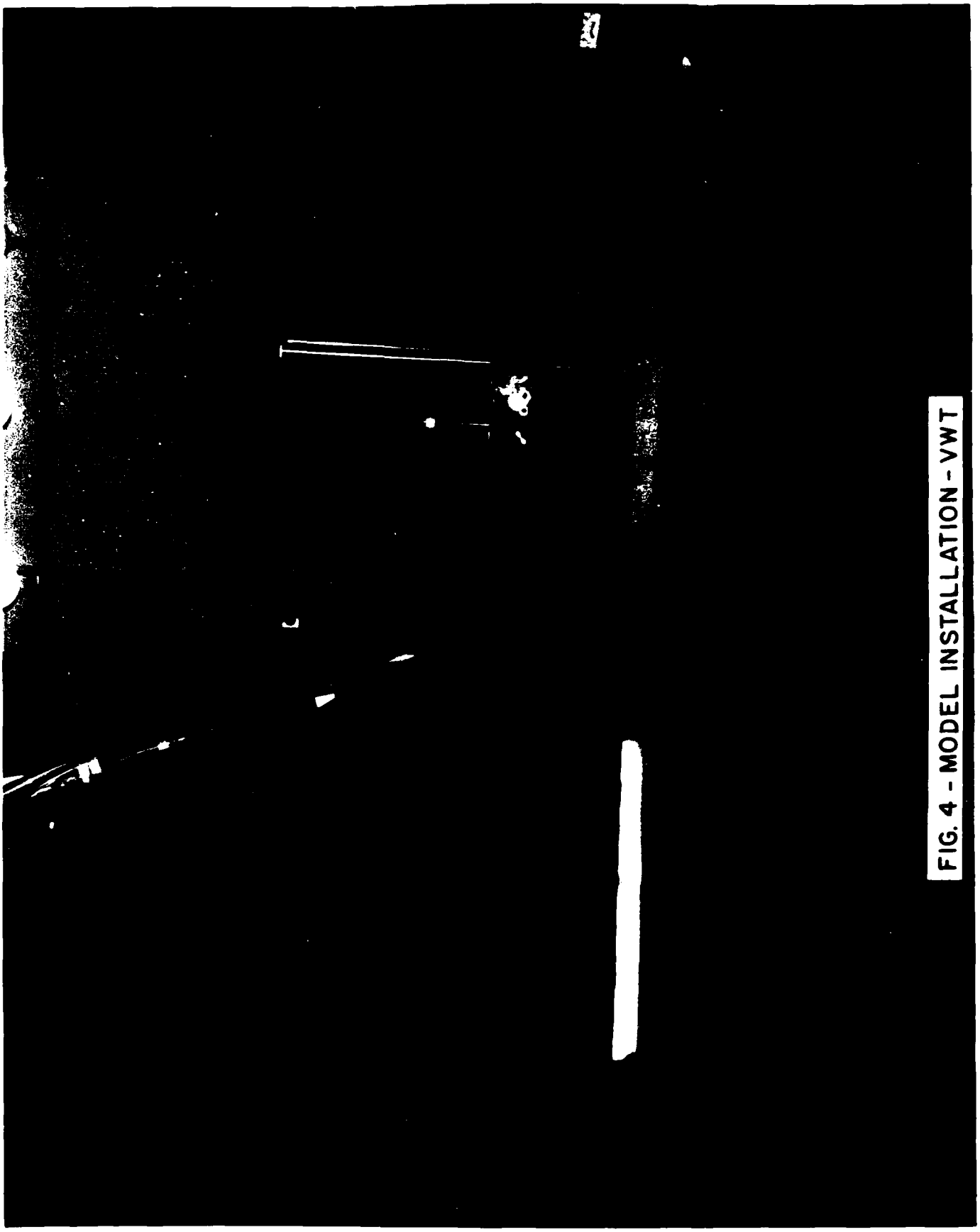

FIG. 4 - MODEL INSTALLATION - VWT

CANARD CONFIGURATION

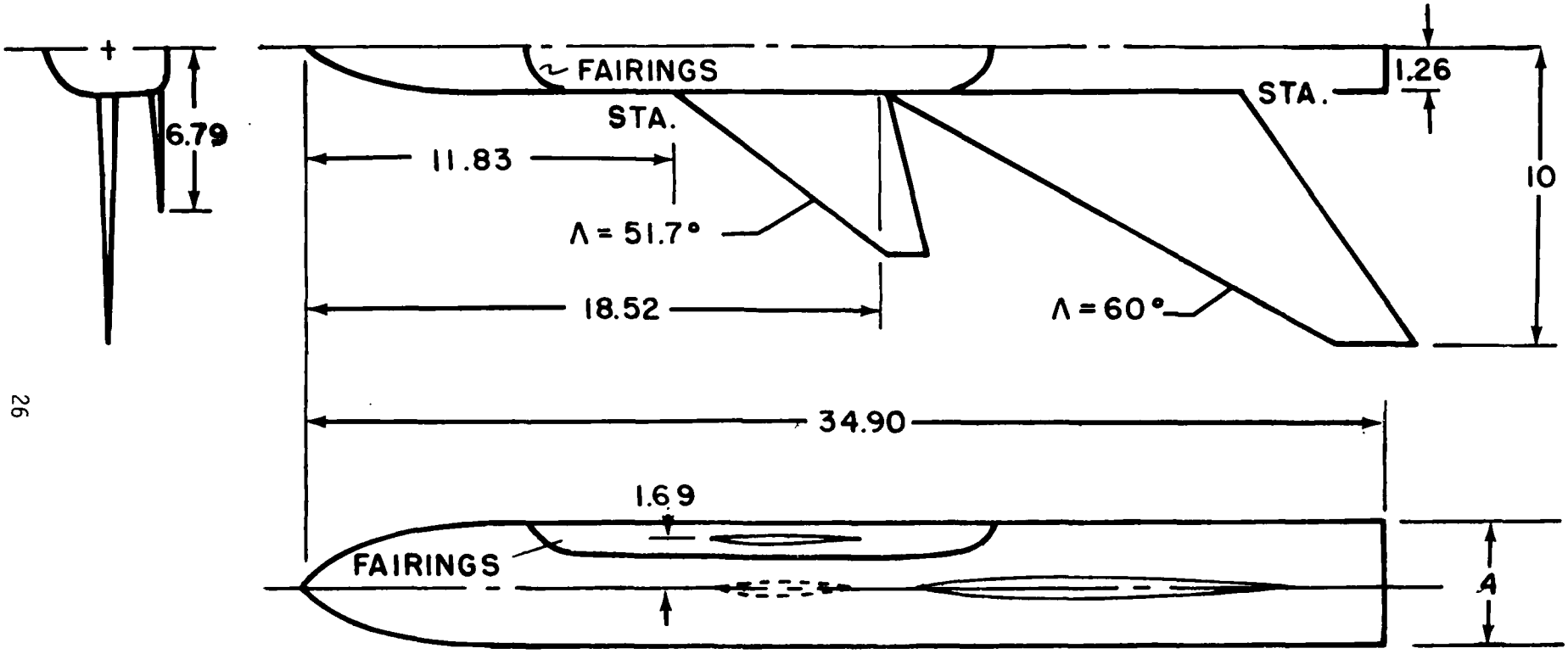

ALL DIMENSIONS IN INCHES

FIG. 5 SKETCH OF MODEL - VWT

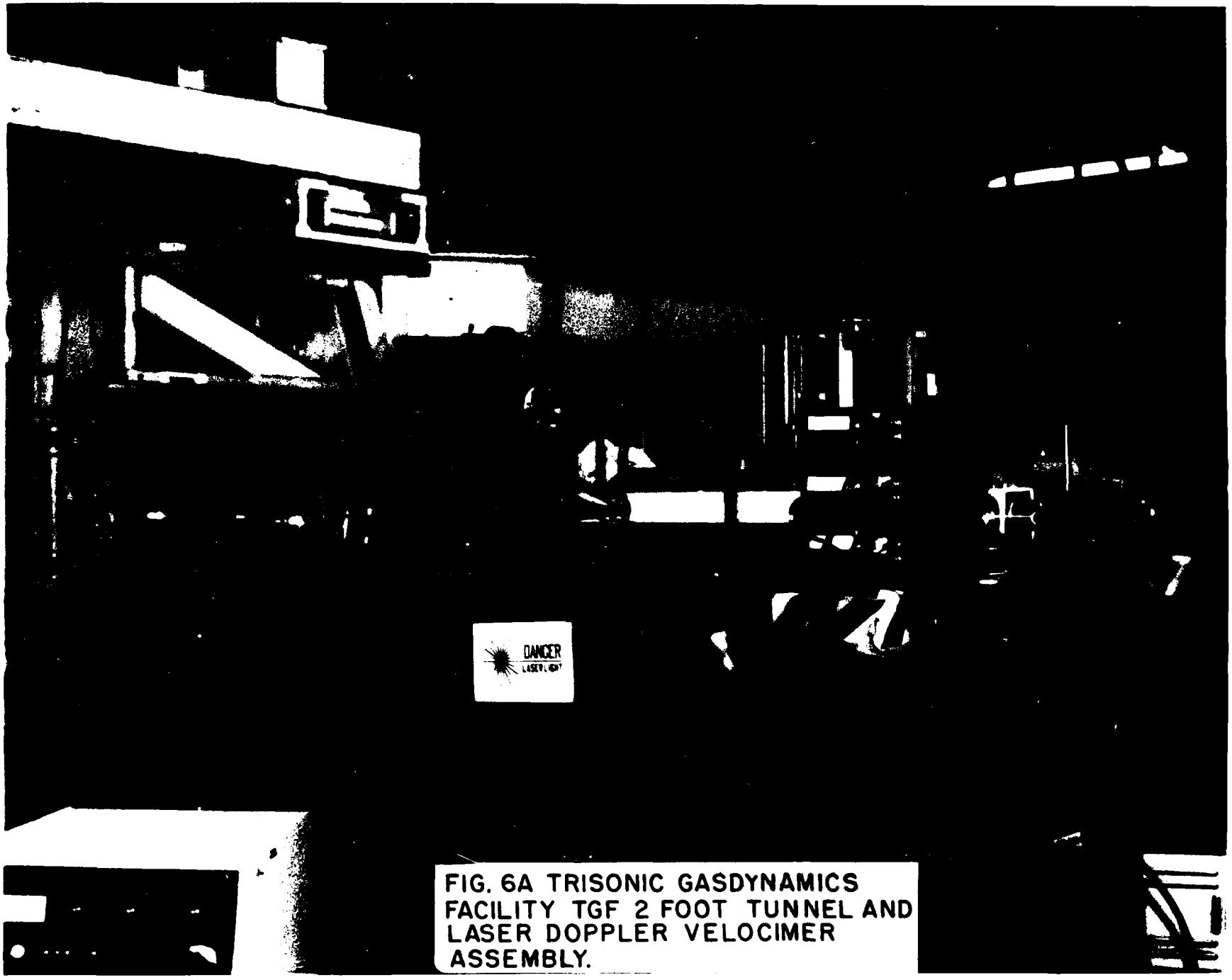

FIG. 6A TRISONIC GASDYNAMICS FACILITY TGF 2 FOOT TUNNEL AND LASER DOPPLER VELOCIMER ASSEMBLY.

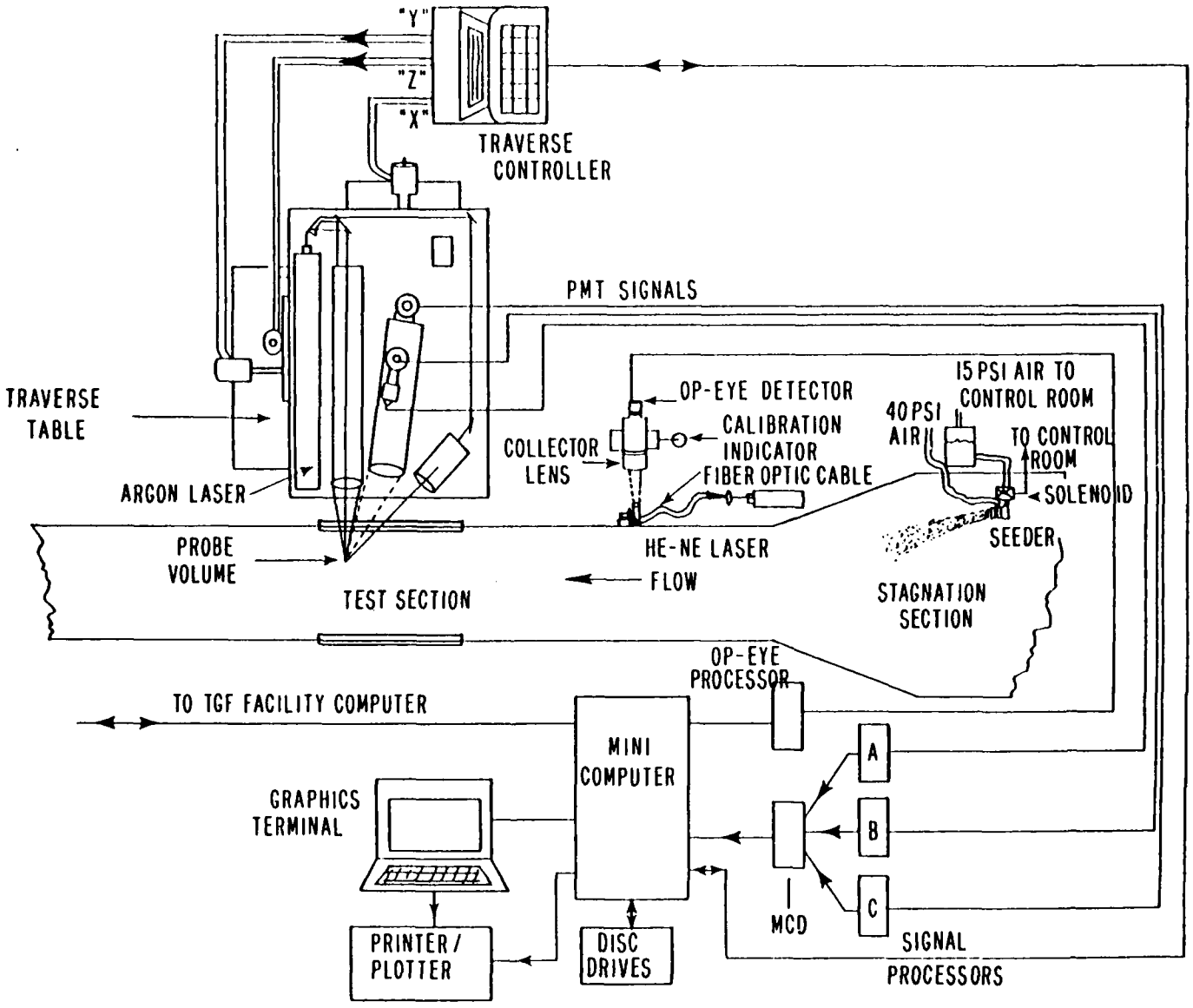

FIGURE 6B-SYSTEM CONFIGURATION IN THE TGF.

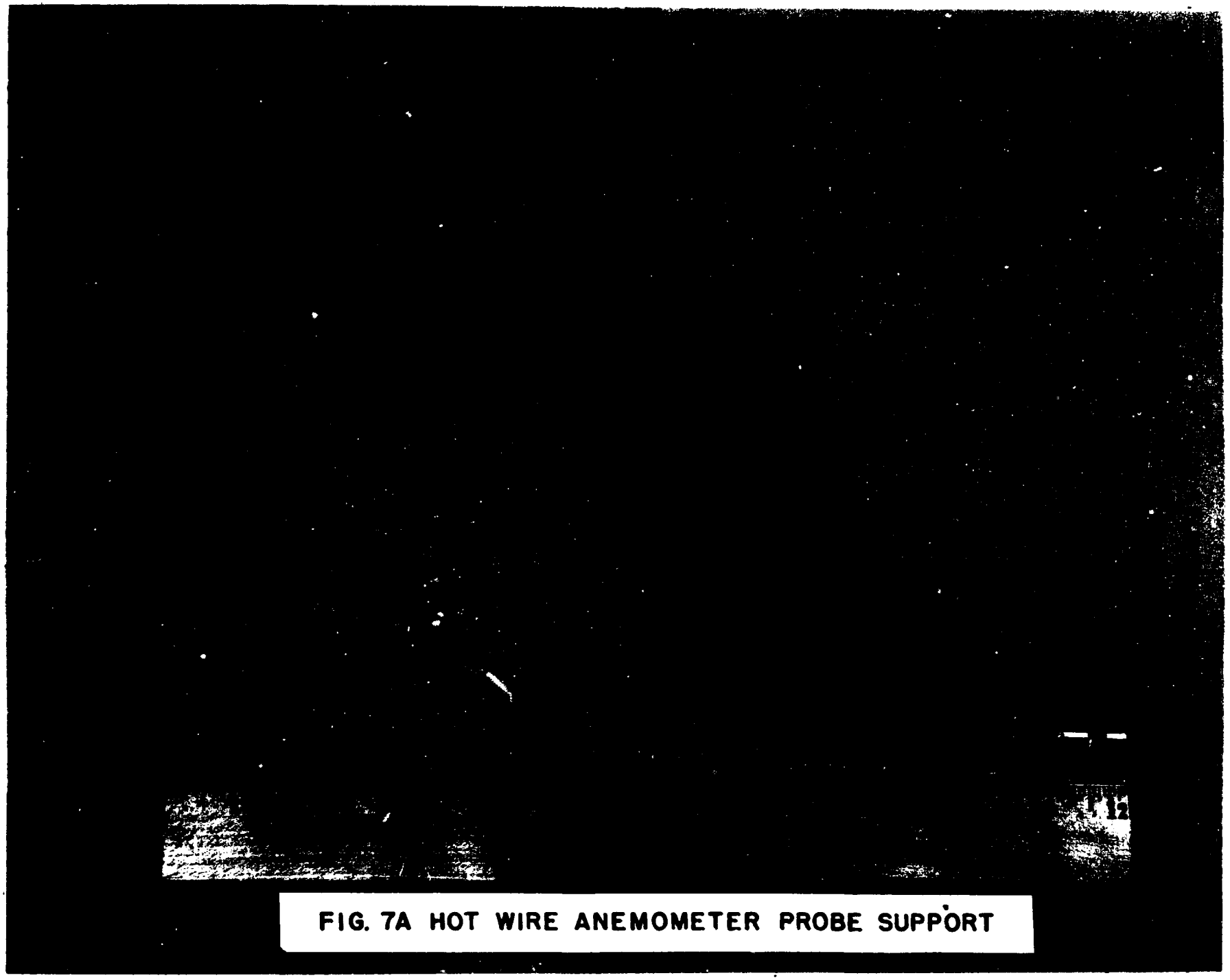

FIG. 7A HOT WIRE ANEMOMETER PROBE SUPPORT

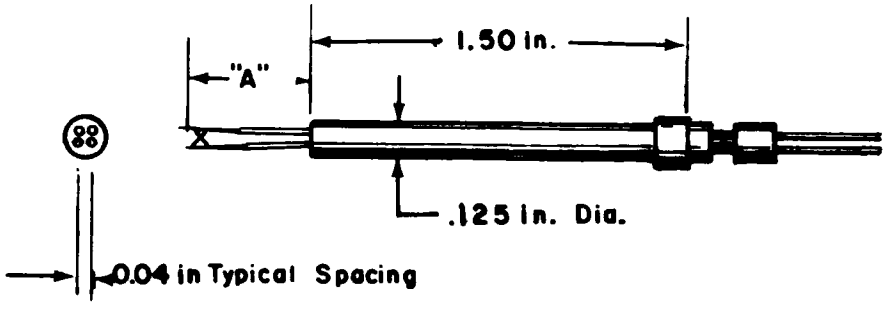

FIGURE 7B SKETCH OF CROSS WIRE SENSORS

FIG. 8 MODEL AND HOT WIRE PROBE INSTALLATION - TGF

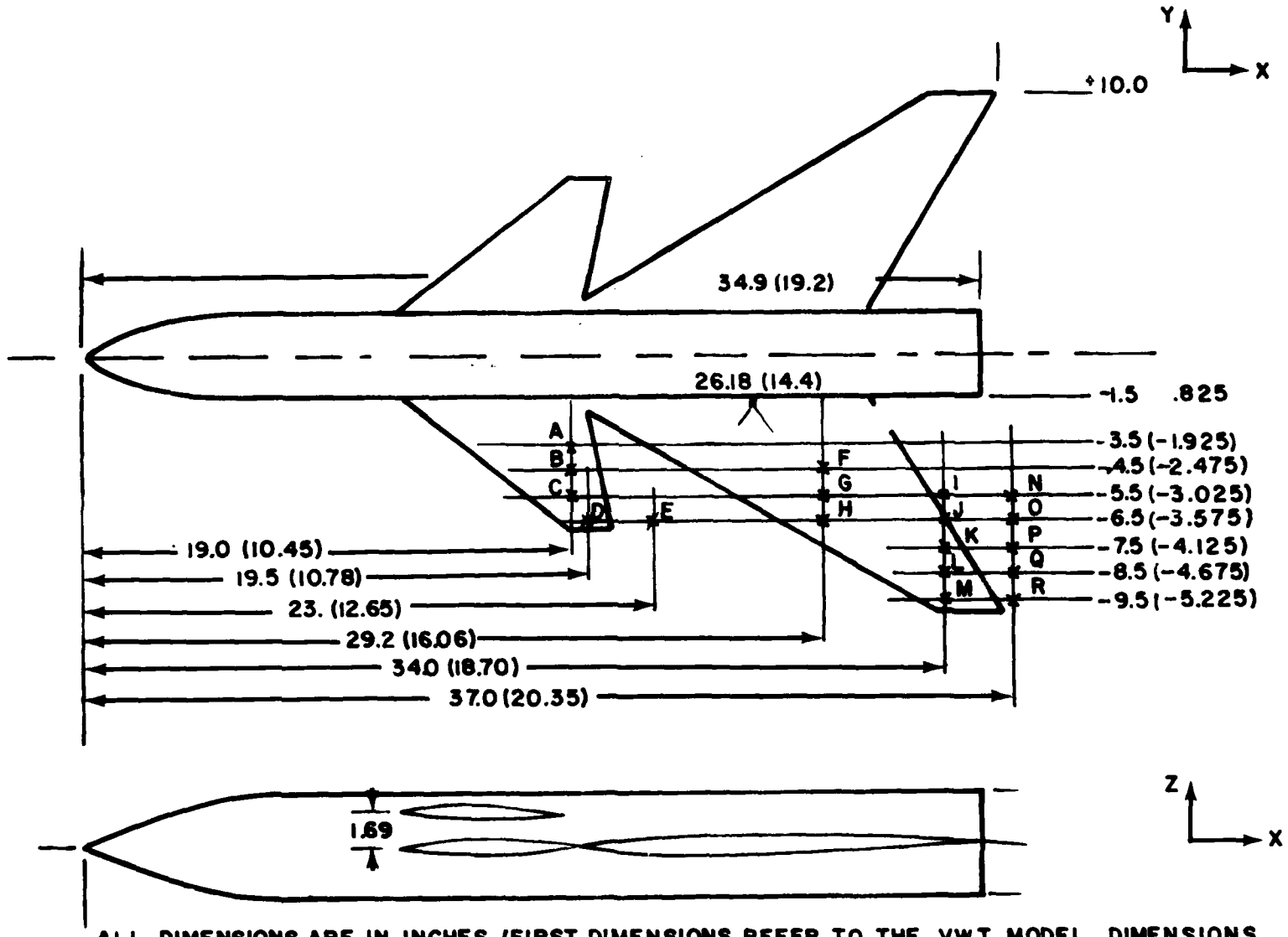

ALL DIMENSIONS ARE IN INCHES (FIRST DIMENSIONS REFER TO THE VWT MODEL, DIMENSIONS IN PARENTHESIS REFER TO THE 55% REPLICA USED IN THE TGF TUNNEL)

FIG. 9 MODEL LOCATIONS FOR HOT WIRE AND LDV TESTING

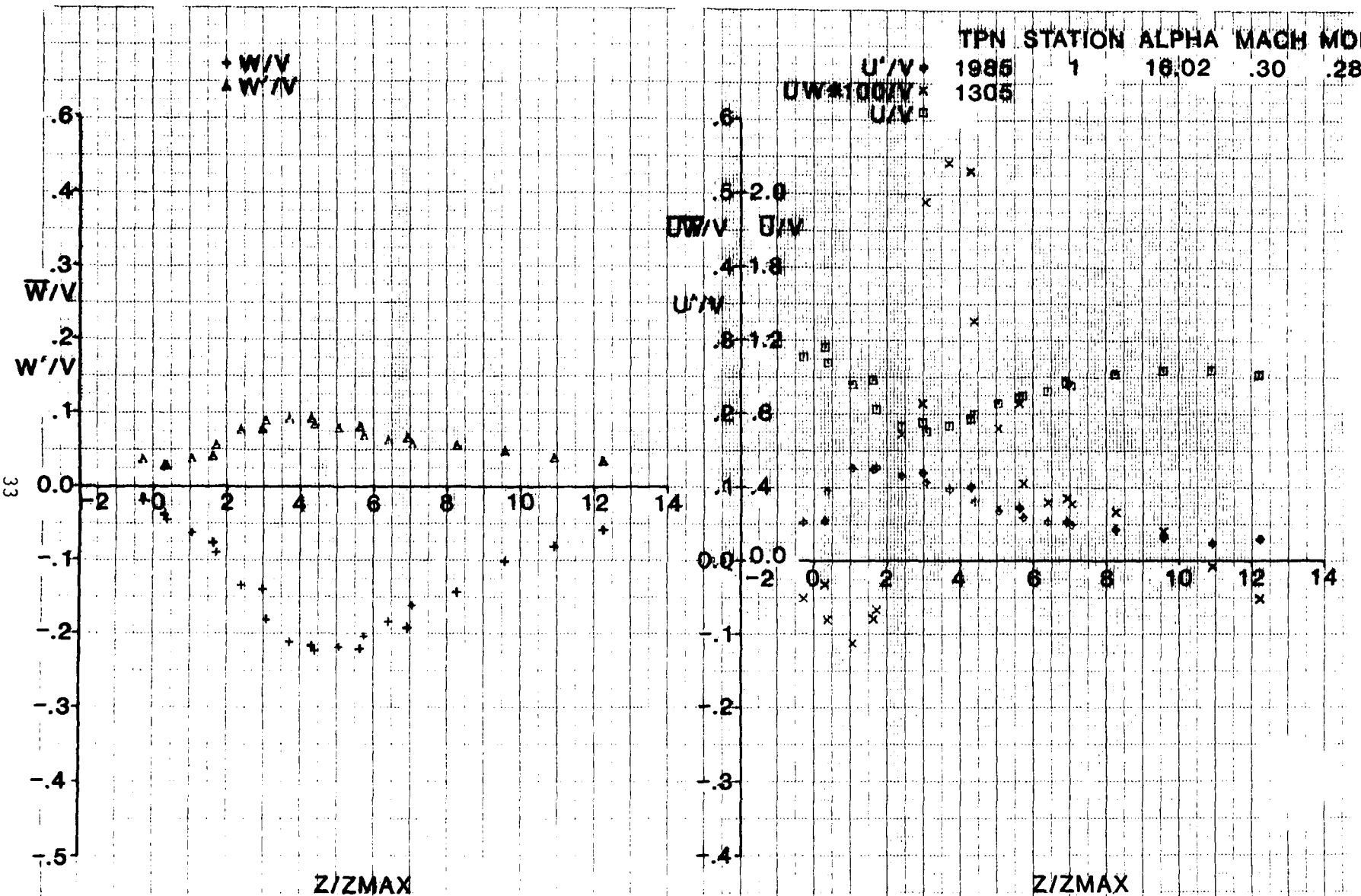

FIG.10. REPEATED HOT WIRE MEASUREMENTS OF MEAN VELOCITIES, TURBULENCE INTENSITIES, AND REYNOLDS STRESSES WITH THE COPLANAR CANARD - TGF - STATION I - $\alpha = 16°$

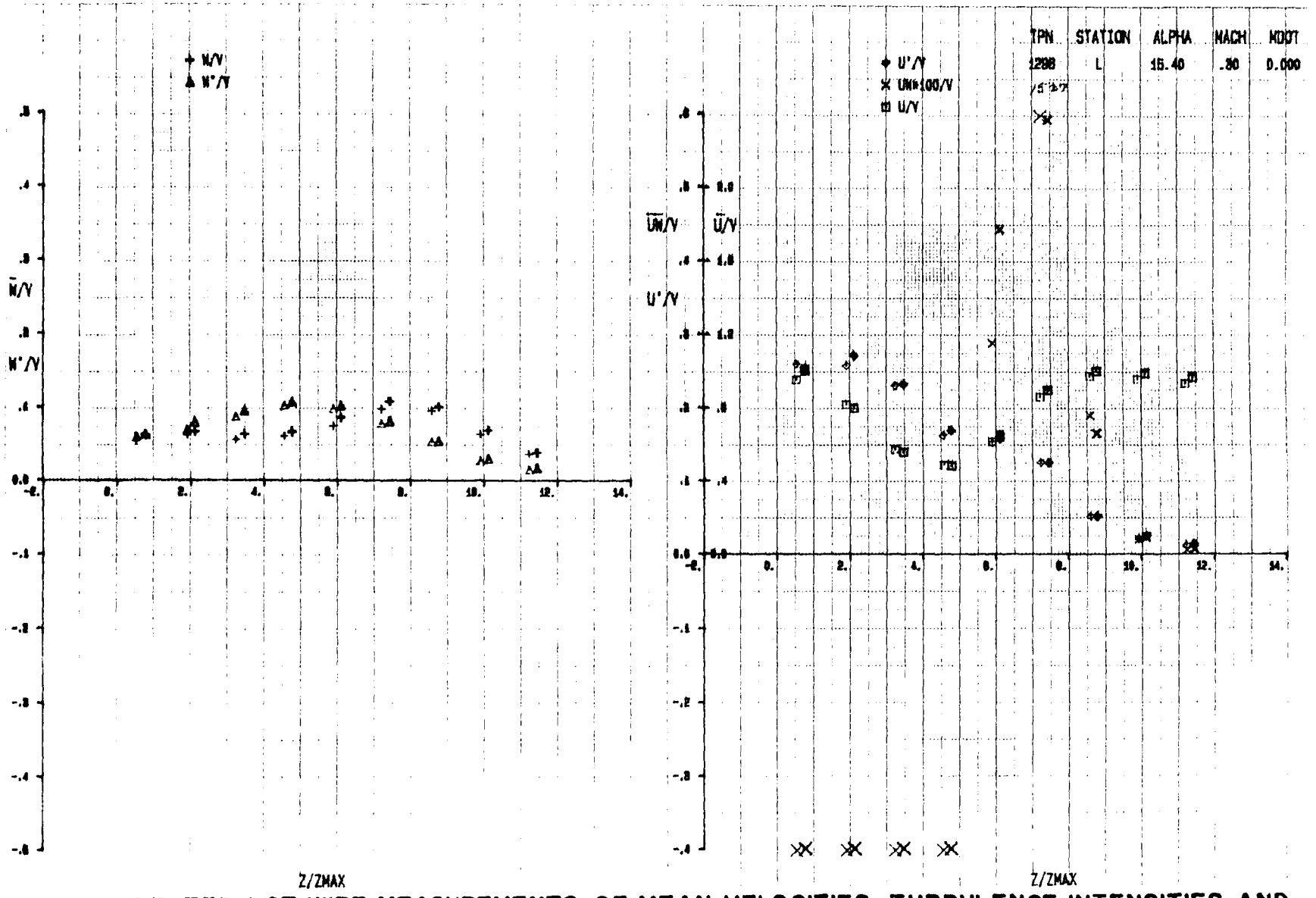

FIG 11 REPEATED HOT WIRE MEASUREMENTS OF MEAN VELOCITIES, TURBULENCE INTENSITIES AND REYNOLDS STRESSES WITHOUT CANARD - TGF - α = 16° STATION L

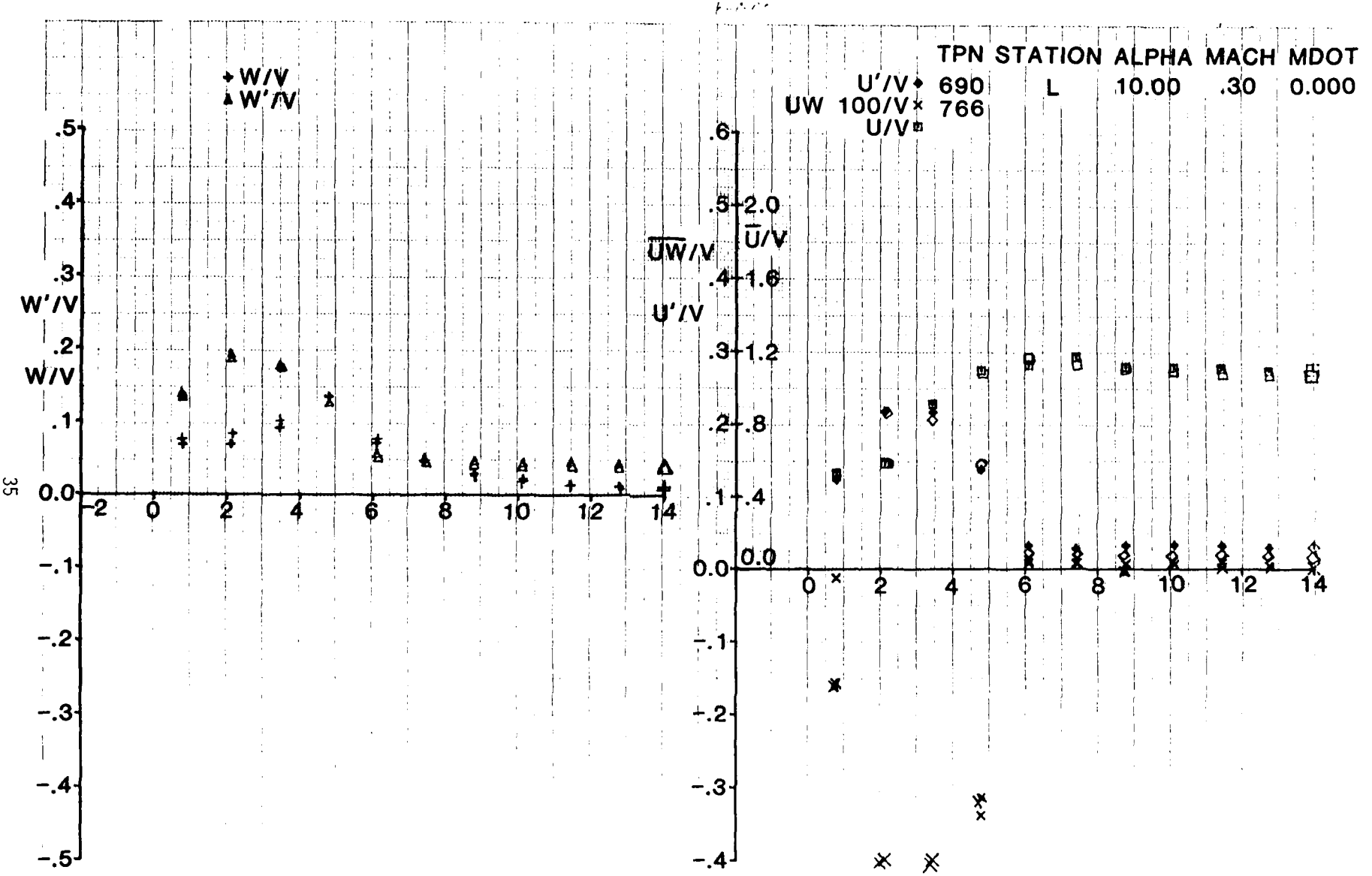

FIG. 12. REPEATED LDV MEASUREMENTS OF MEAN VELOCITIES, TURBULENCE INTENSITIES, AND REYNOLDS STRESSES WITHOUT CANARD - TGF - $\alpha = 10°$ - STATION L

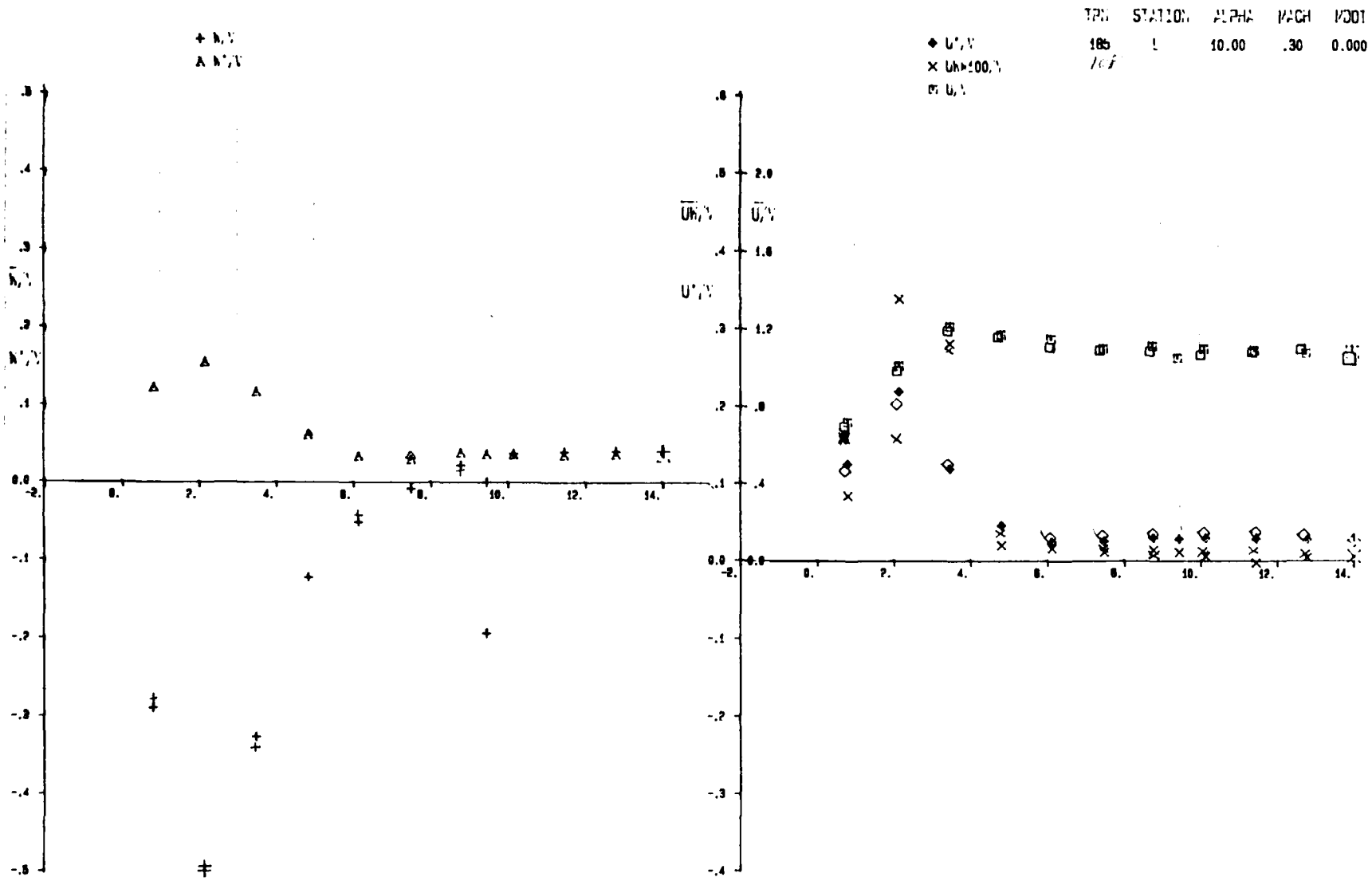

FIG. 13 REPEATED LDV MEASUREMENTS OF MEAN VELOCITIES, TURBULENCE INTENSITIES, AND REYNOLDS STRESSES WITH THE COPLANAR CANARD-TGF - $\alpha = 10°$ - STATION L

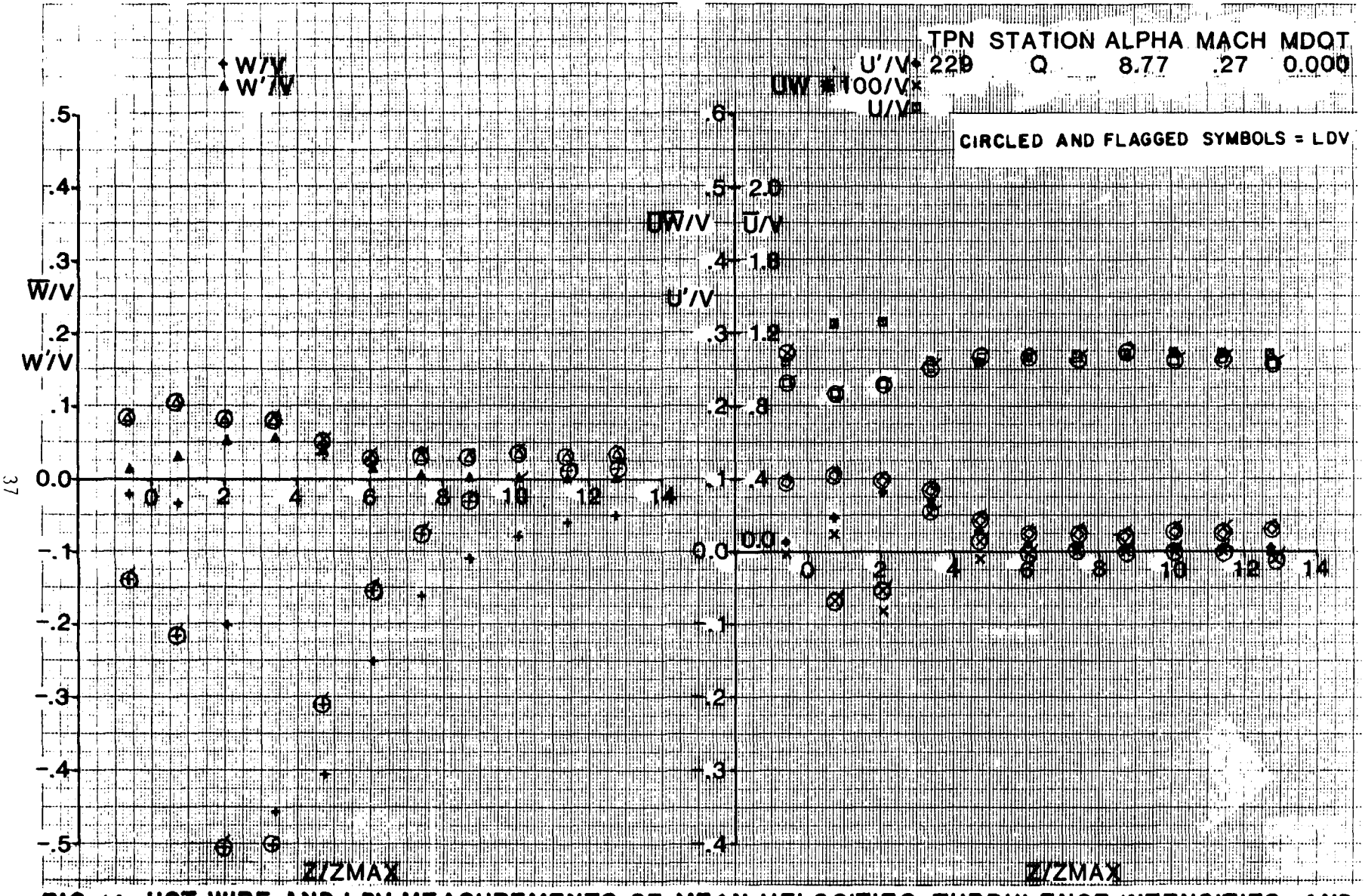

FIG. 14. HOT WIRE AND LDV MEASUREMENTS OF MEAN VELOCITIES, TURBULENCE INTENSITIES, AND REYNOLDS STRESSES WITHOUT BLOWING - COPLANAR CANARD - TGF - $\alpha = 10°$ STATION Q

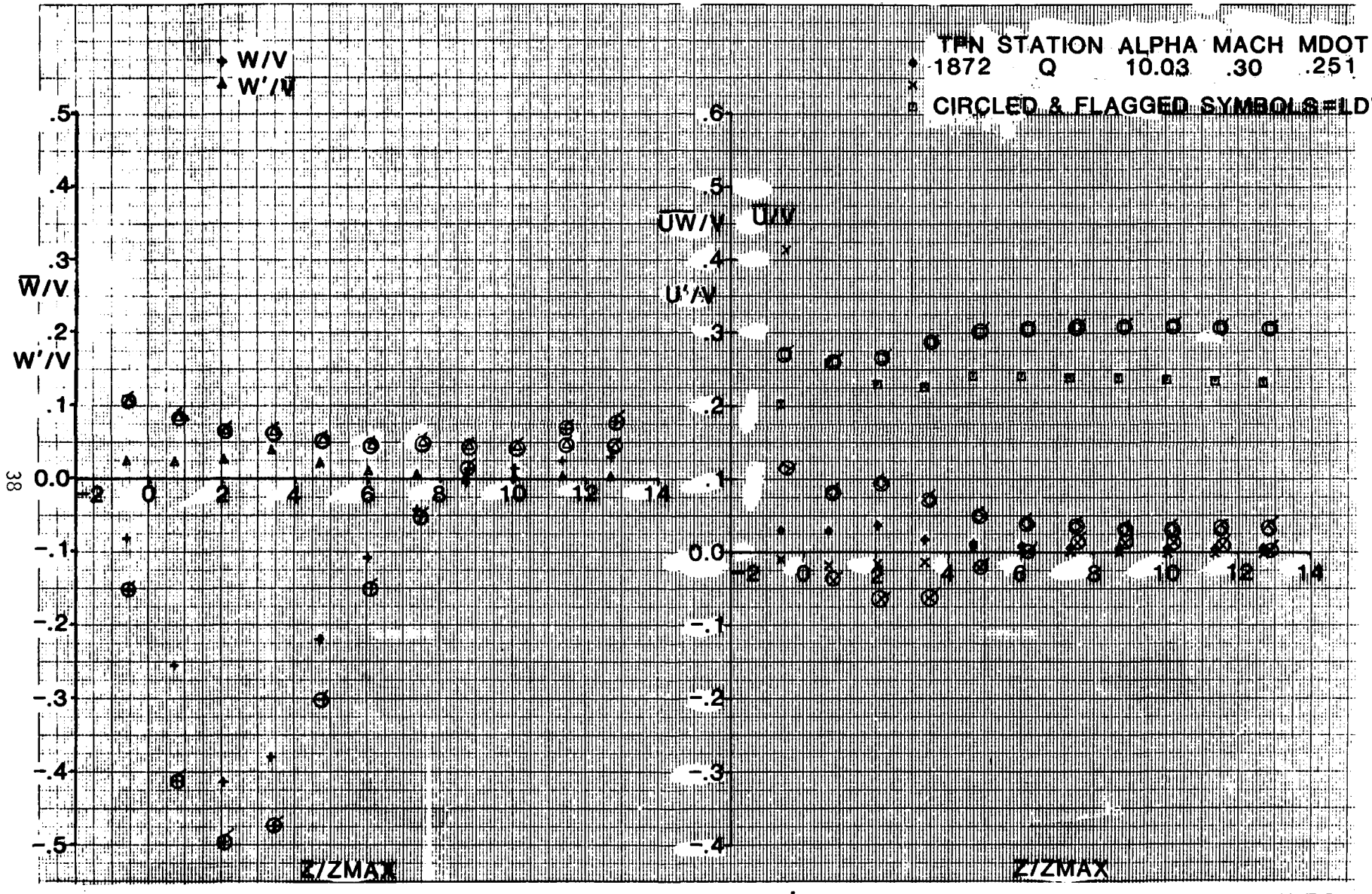

FIG. 15. HOT WIRE AND LDV MEASUREMENTS OF MEAN VELOCITIES, TURBULENCE INTENSITIES, AND REYNOLDS STRESSES WITH BLOWING - COPLANAR CANARD - TGF - $\alpha = 10°$ - STATION Q

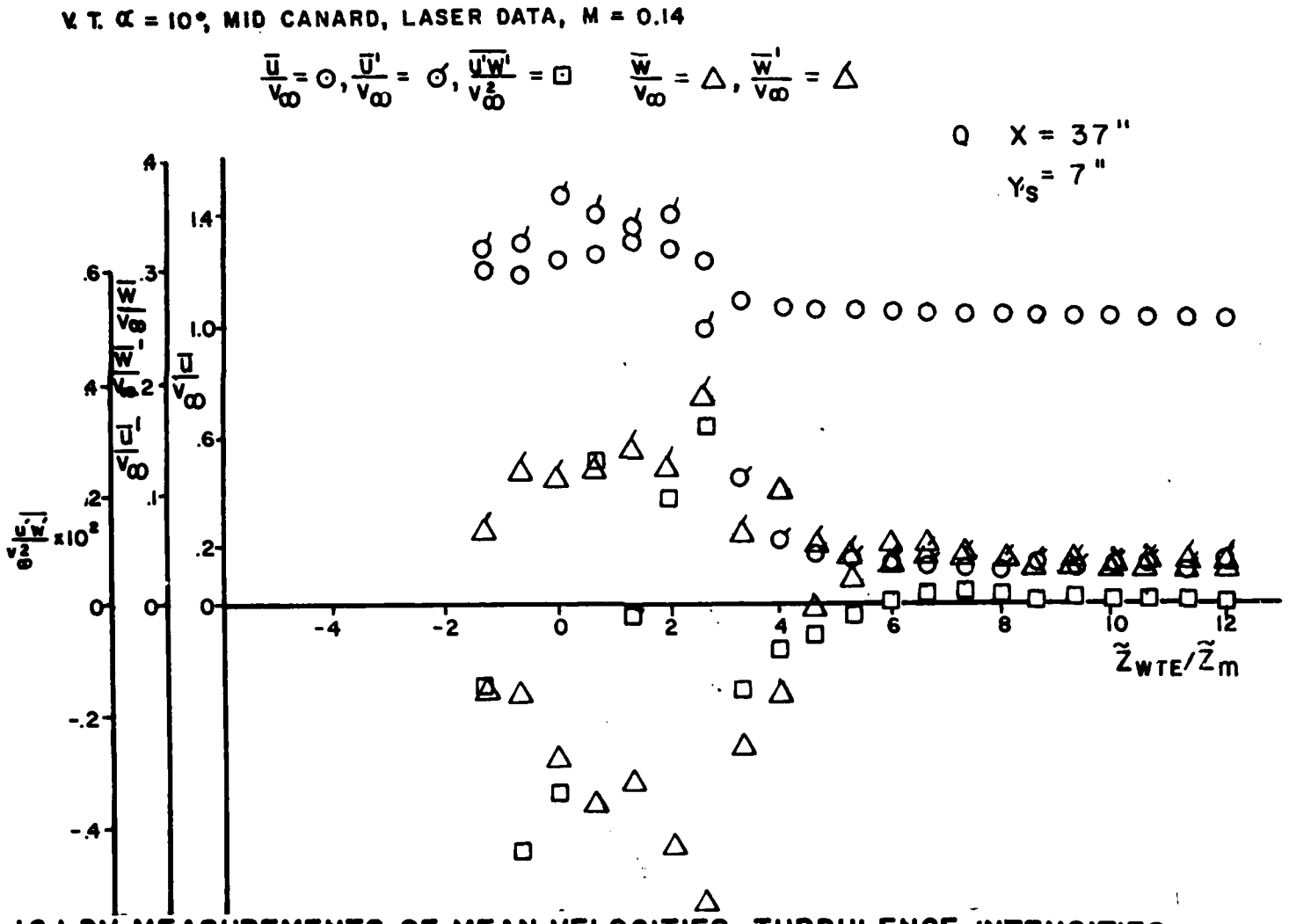

FIG. 16 LDV MEASUREMENTS OF MEAN VELOCITIES, TURBULENCE INTENSITIES, AND REYNOLDS STRESSES WITH THE COPLANAR CANARD WITHOUT BLOWING V. W. T. - α = 10° STATION Q

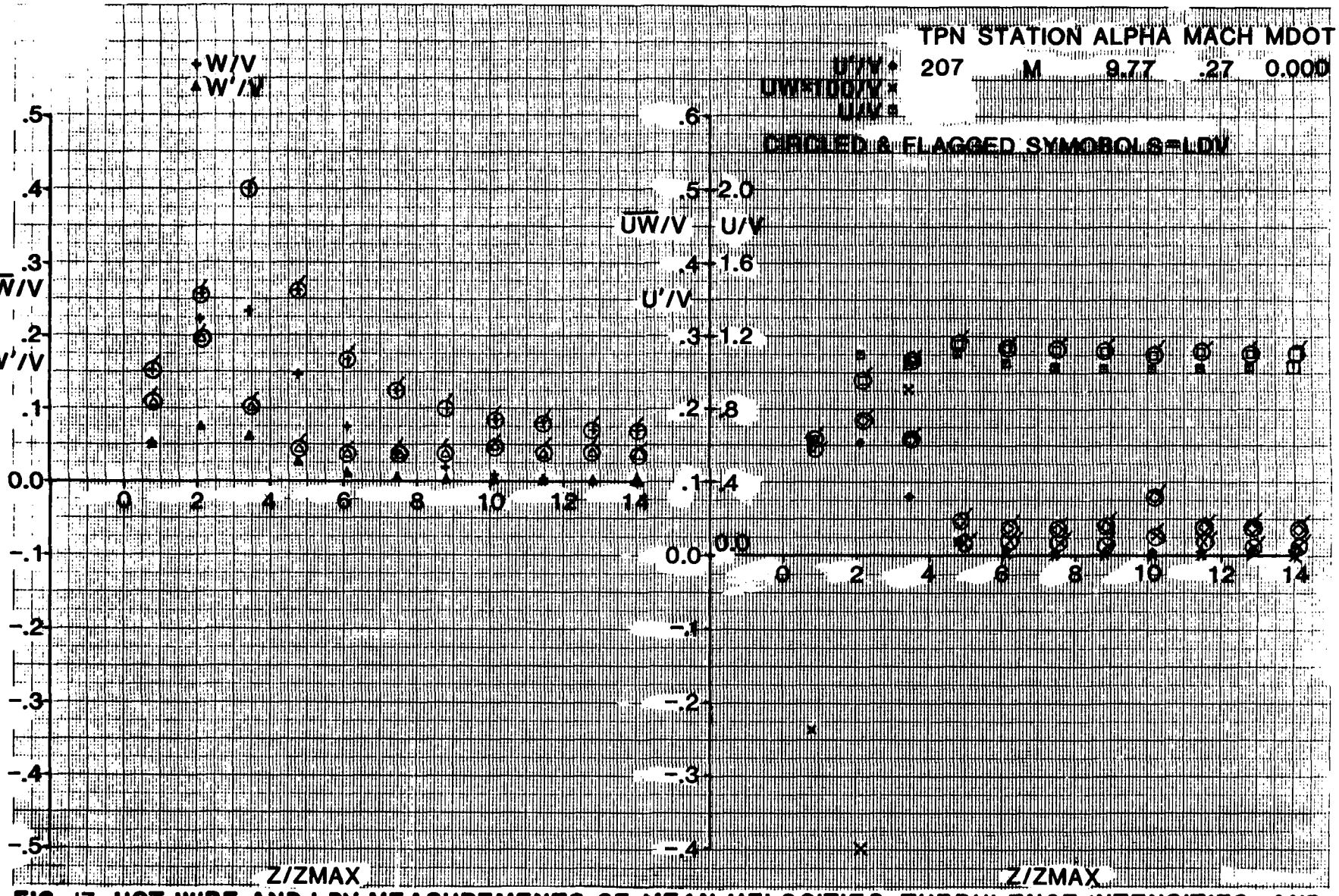

FIG. 17. HOT WIRE AND LDV MEASUREMENTS OF MEAN VELOCITIES, TURBULENCE INTENSITIES, AND REYNOLDS STRESSES WITHOUT BLOWING - COPLANAR CANARD - TGF - α = 10° STATION M

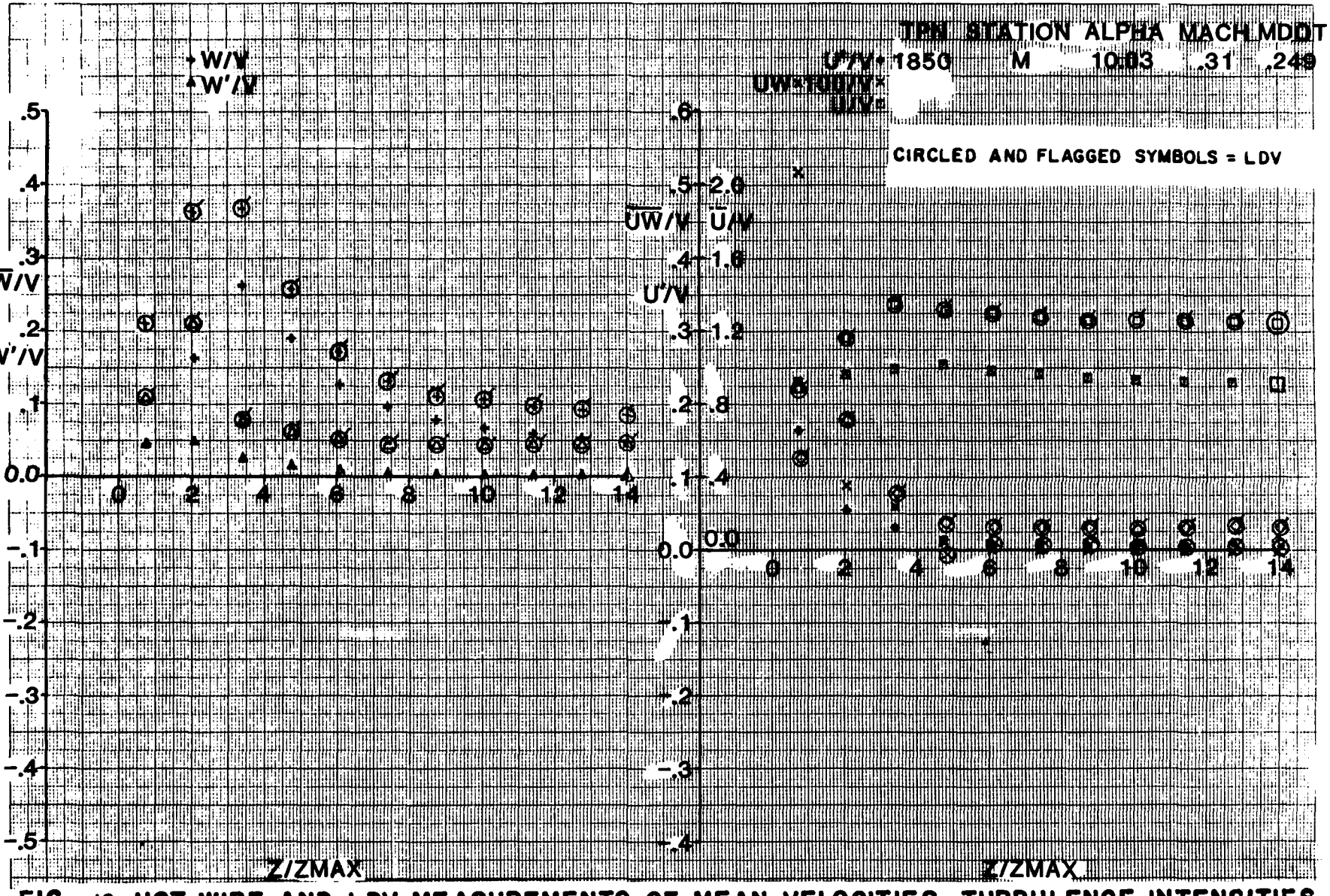

FIG. 18. HOT WIRE AND LDV MEASUREMENTS OF MEAN VELOCITIES, TURBULENCE INTENSITIES, AND REYNOLDS STRESSES WITH BLOWING - COPLANAR CANARD - TGF - $\alpha = 10^{\circ}$ - STATION M

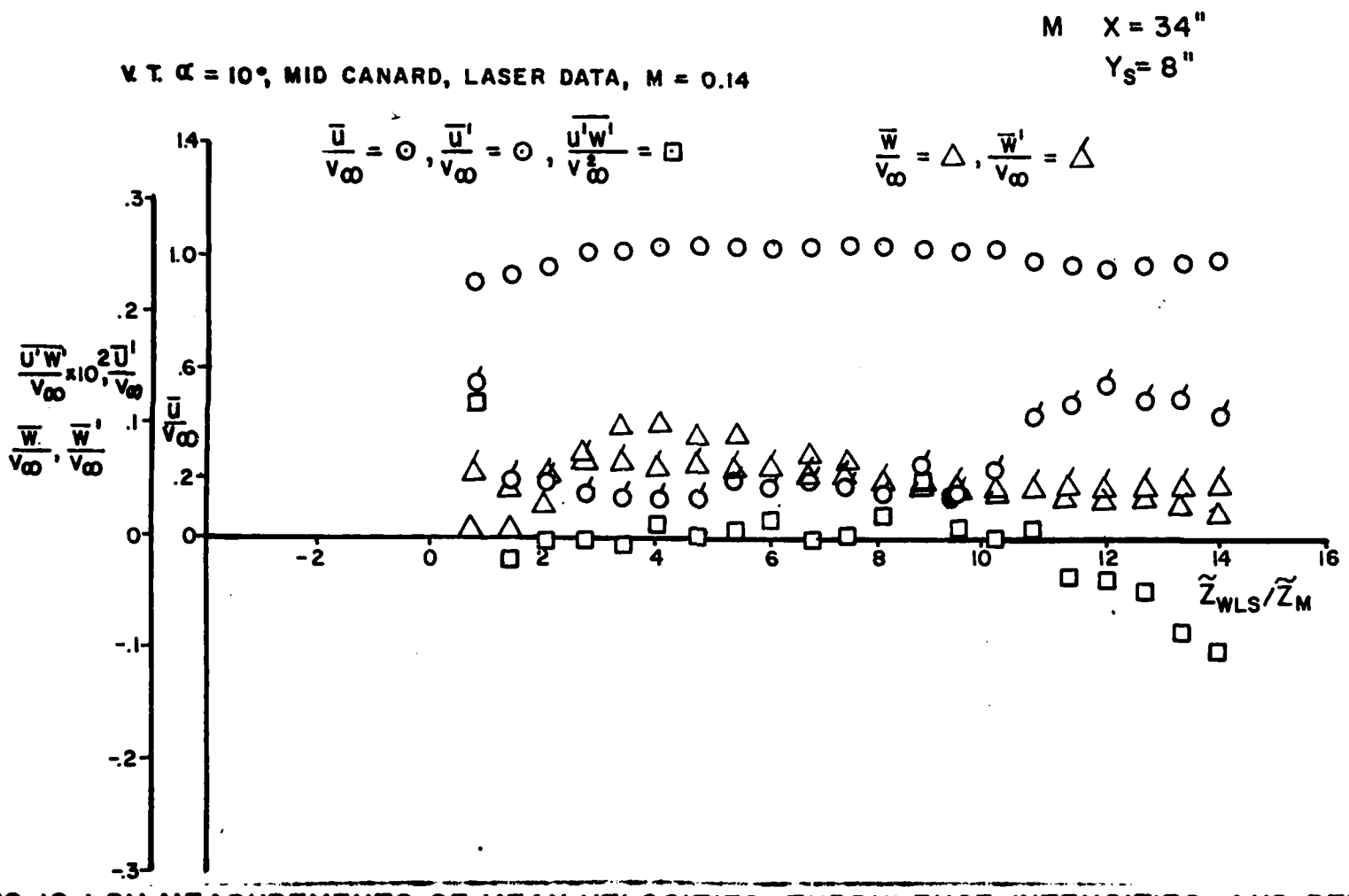

FIG. 19 LDV MEASUREMENTS OF MEAN VELOCITIES, TURBULENCE INTENSITIES, AND REYNOLDS STRESSES WITHOUT BLOWING - COPLANAR CANARD - V.W.T. - α = 10° - STATION M

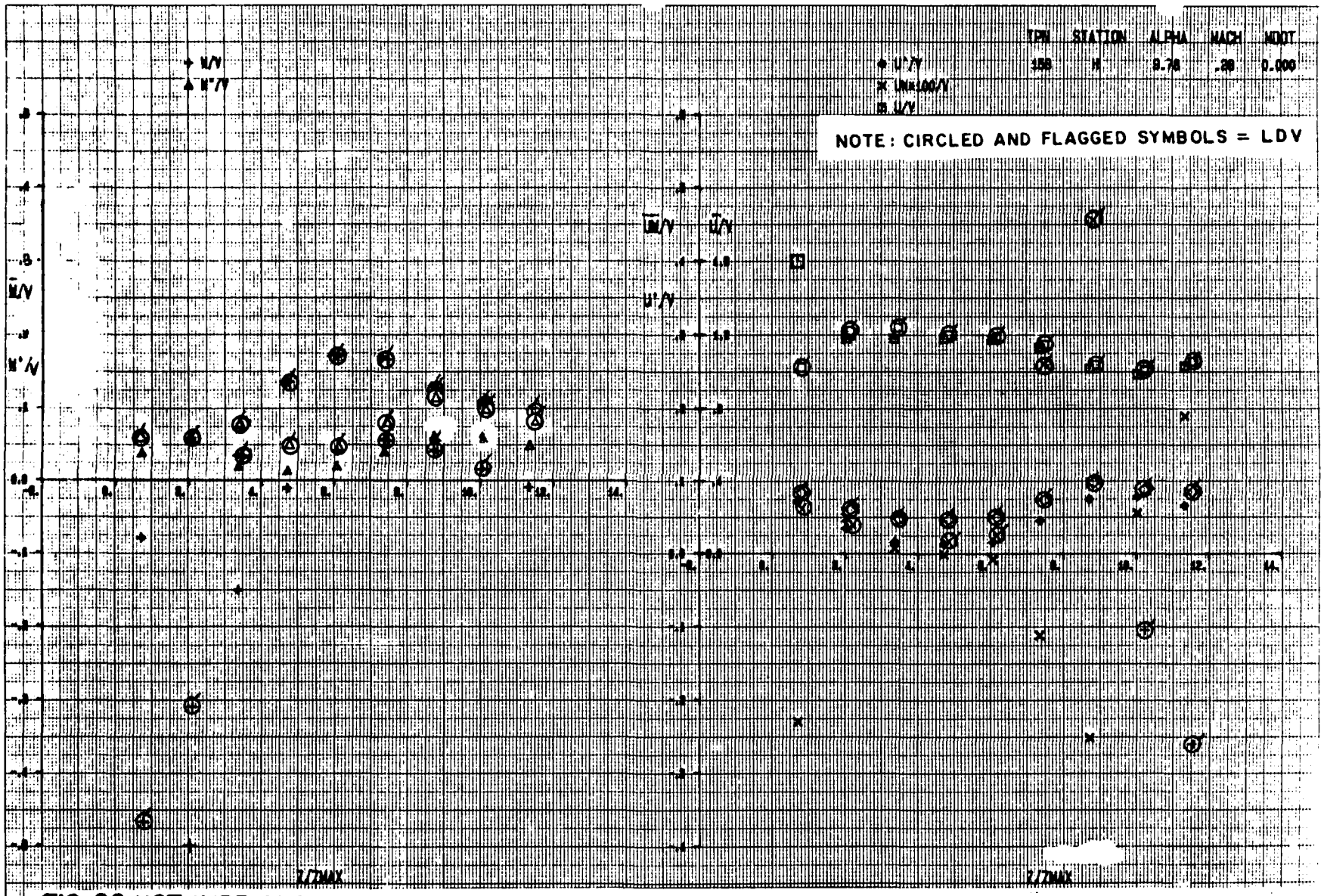

FIG. 20 HOT WIRE AND LDV MEASUREMENTS OF MEAN VELOCITIES, TURBULENCE INTENSITIES, AND REYNOLDS STRESSES WITHOUT BLOWING - COPLANAR CANARD - TGF - α = 10°- STATION H

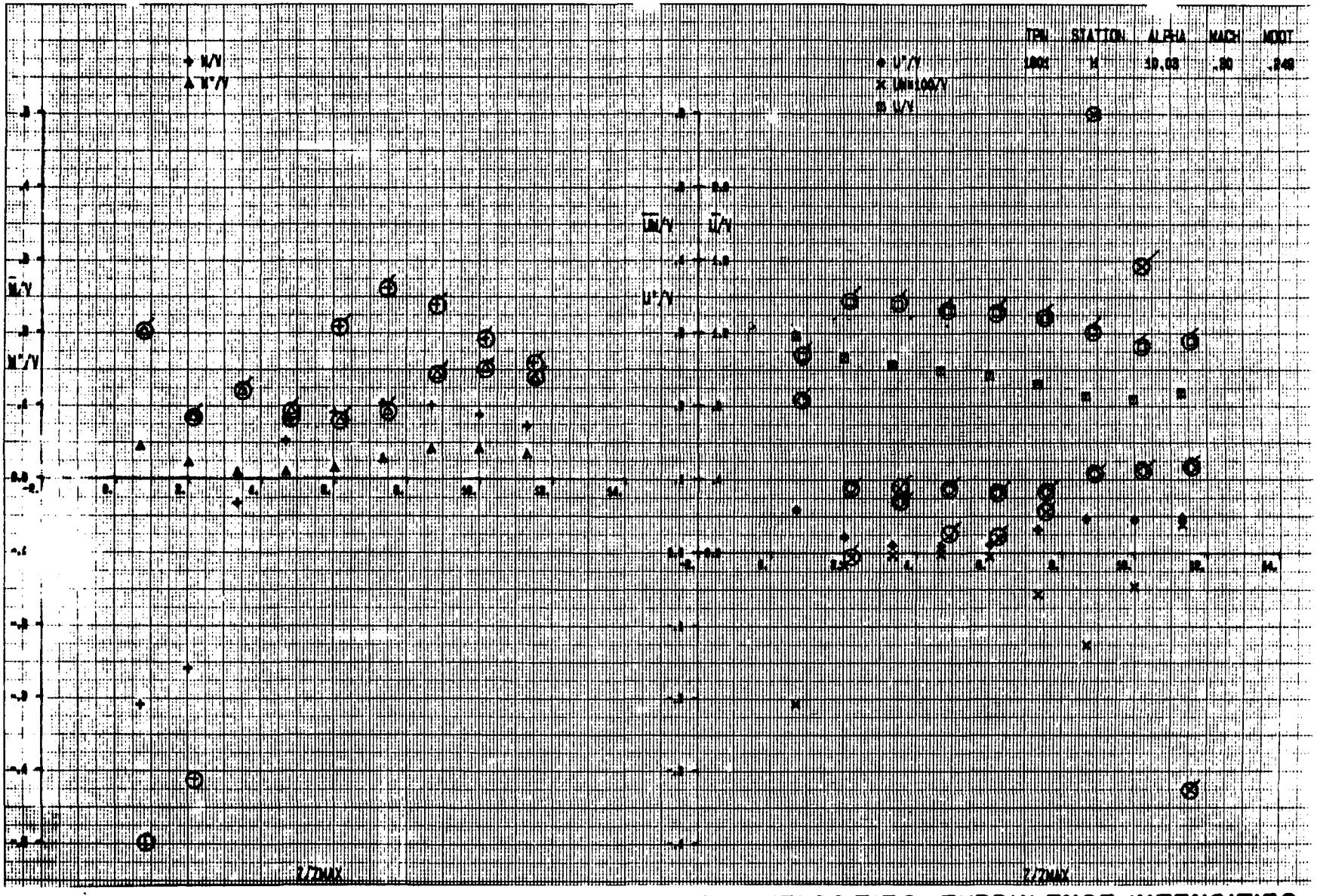

FIG. 21 HOT WIRE AND LDV MEASUREMENTS OF MEAN VELOCITIES, TURBULENCE INTENSITIES, AND REYNOLDS STRESSES WITH BLOWING - COPLANAR CANARD - TGF - $\alpha = 10°$ - STATION H

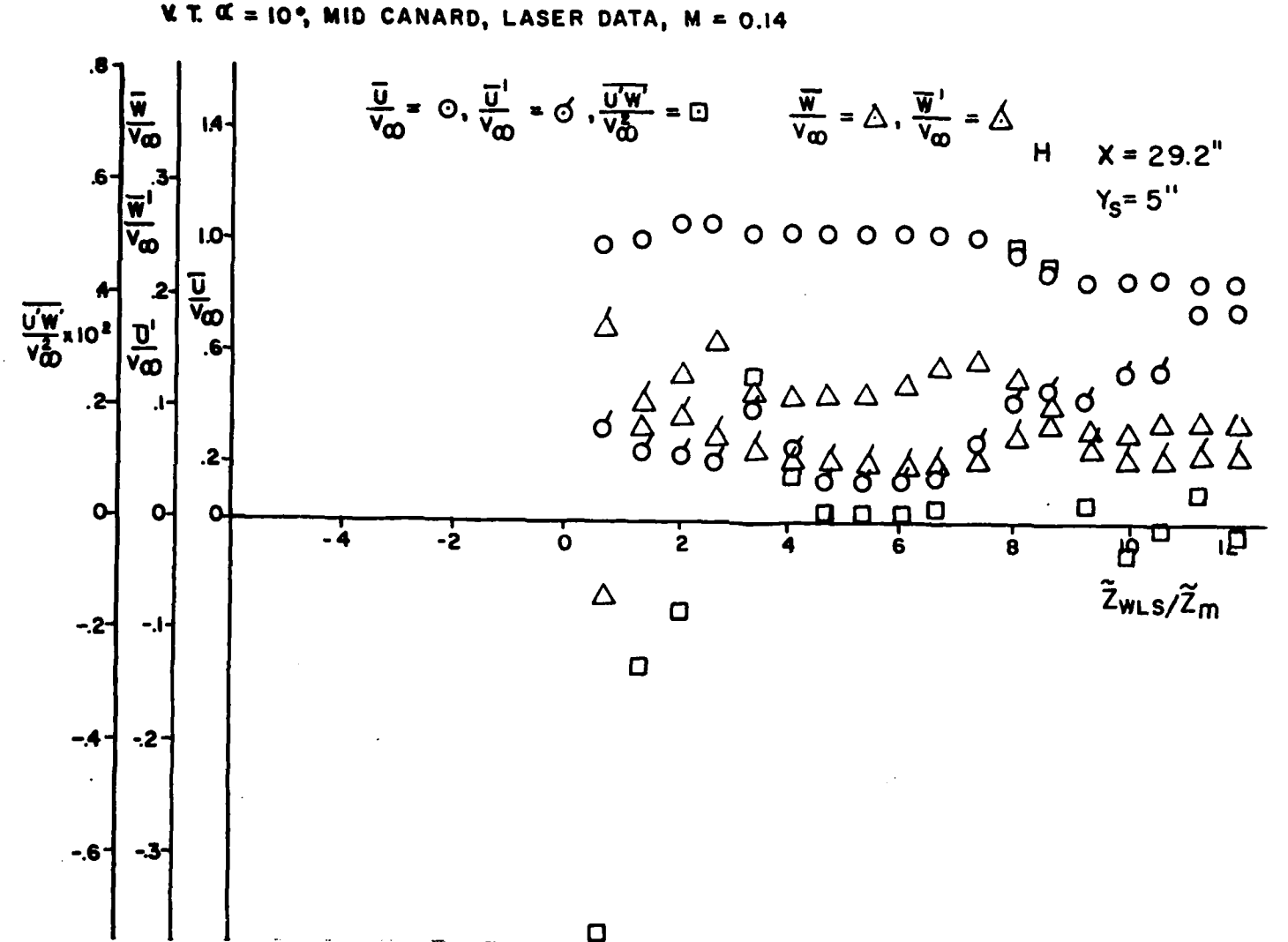

FIG. 22 LDV MEASUREMENTS OF MEAN VELOCITIES, TURBULENCE INTENSITIES, AND REYNOLDS STRESSES WITHOUT BLOWING - COPLANAR CANARD -V.W.T.- α = 10°-STATION H

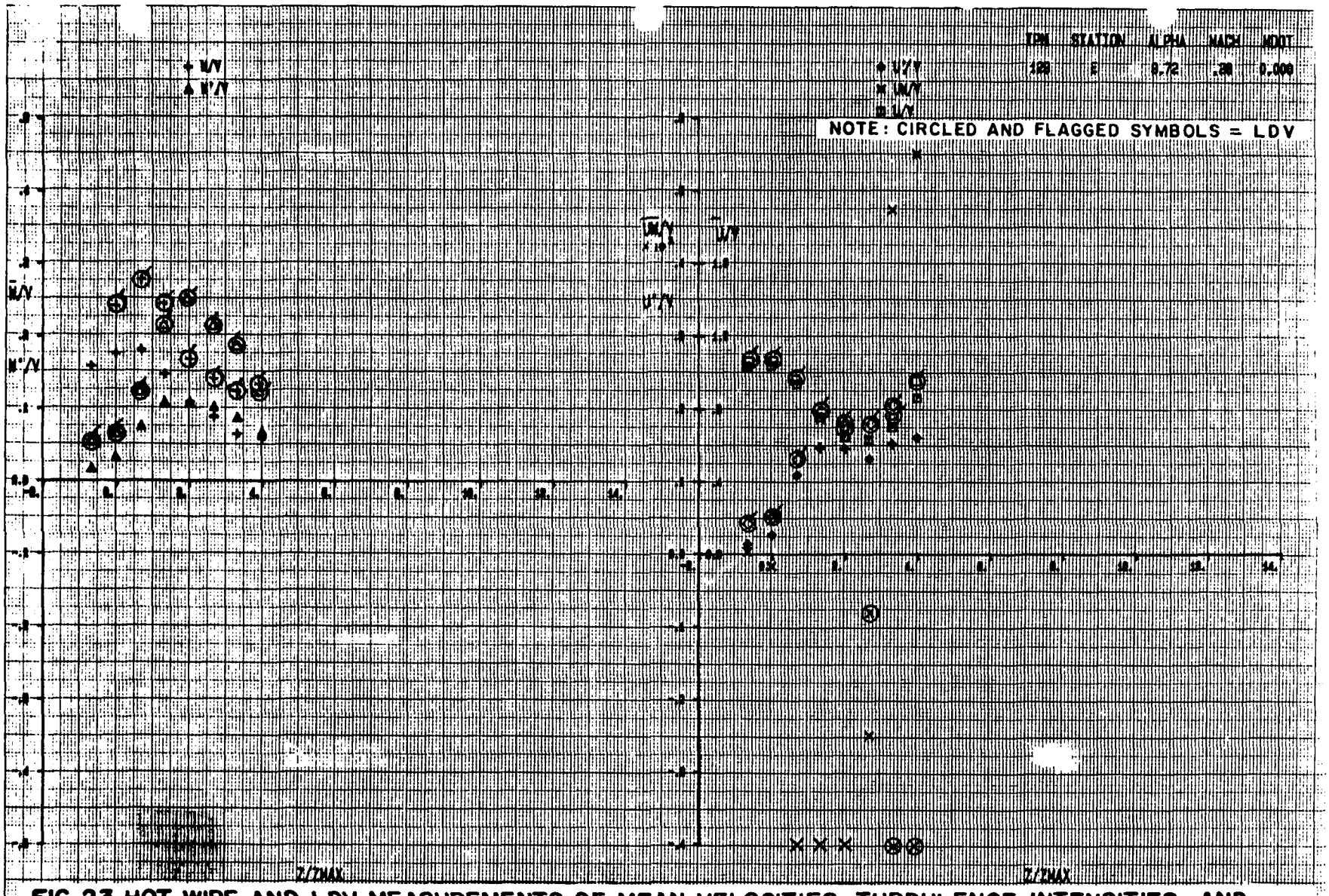

FIG. 23 HOT WIRE AND LDV MEASUREMENTS OF MEAN VELOCITIES, TURBULENCE INTENSITIES, AND REYNOLDS STRESSES WITHOUT BLOWING - COPLANAR CANARD - TGF - α = 10°- STATION E

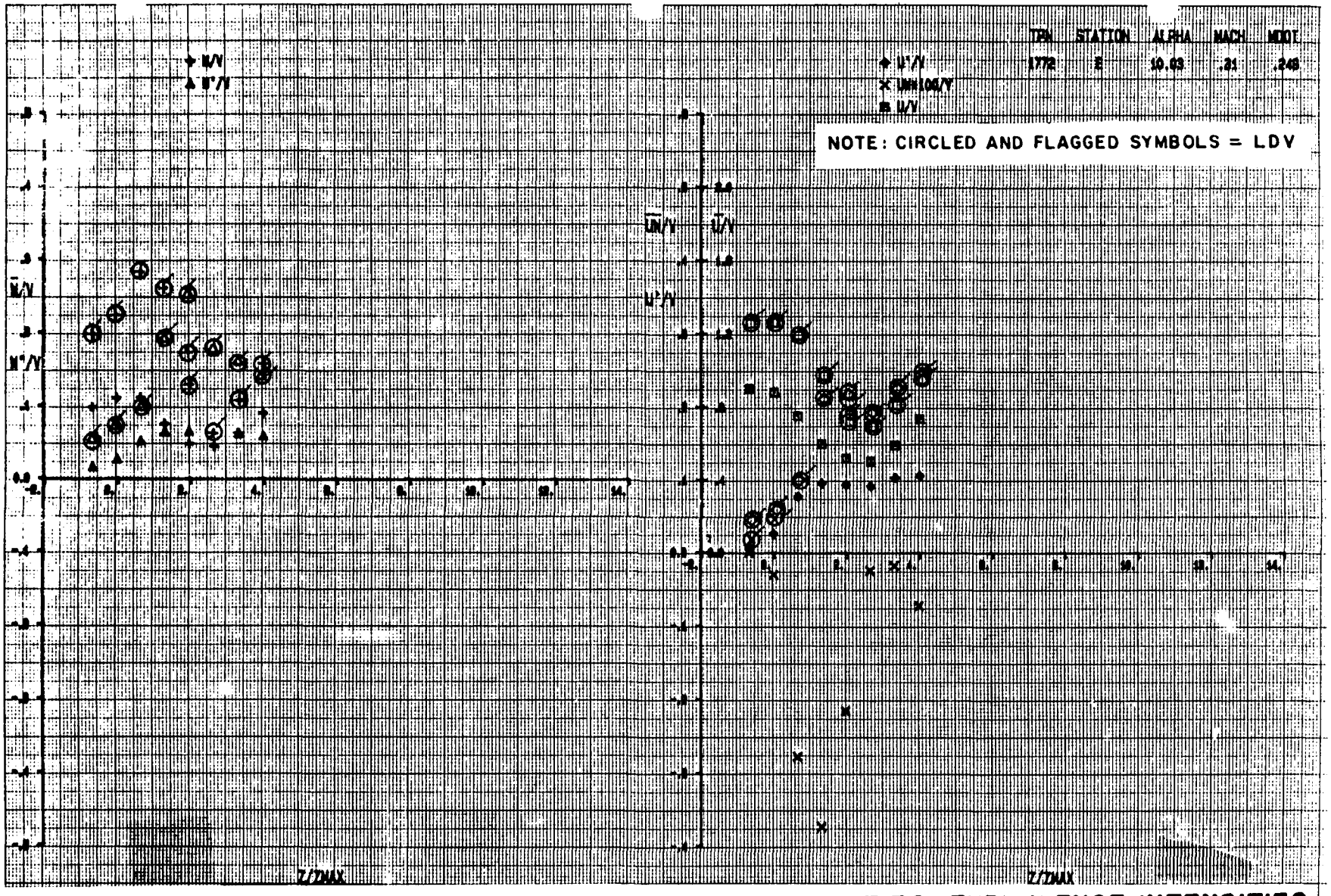

FIG. 24 HOT WIRE AND LDV MEASUREMENTS OF MEAN VELOCITIES, TURBULENCE INTENSITIES, AND REYNOLDS STRESSES WITH BLOWING - COPLANAR CANARD - TGF - $\alpha = 10°$ - STATION E

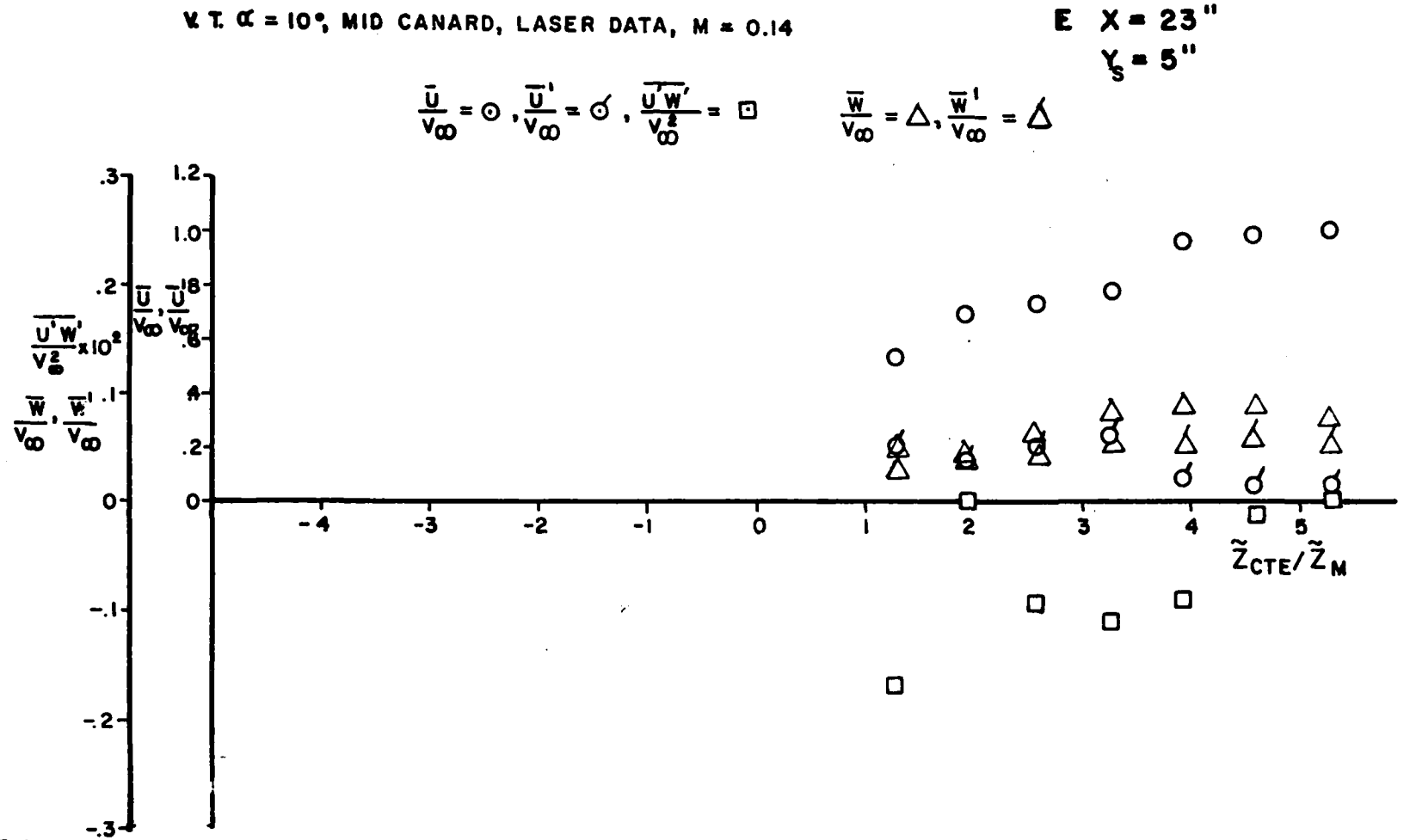

FIG.25 LDV MEASUREMENTS OF MEAN VELOCITIES, TURBULENCE INTENSITIES, AND REYNOLDS STRESSES WITHOUT BLOWING - COPLANAR CANARD - V.W.T. - α = 10° - STATION E

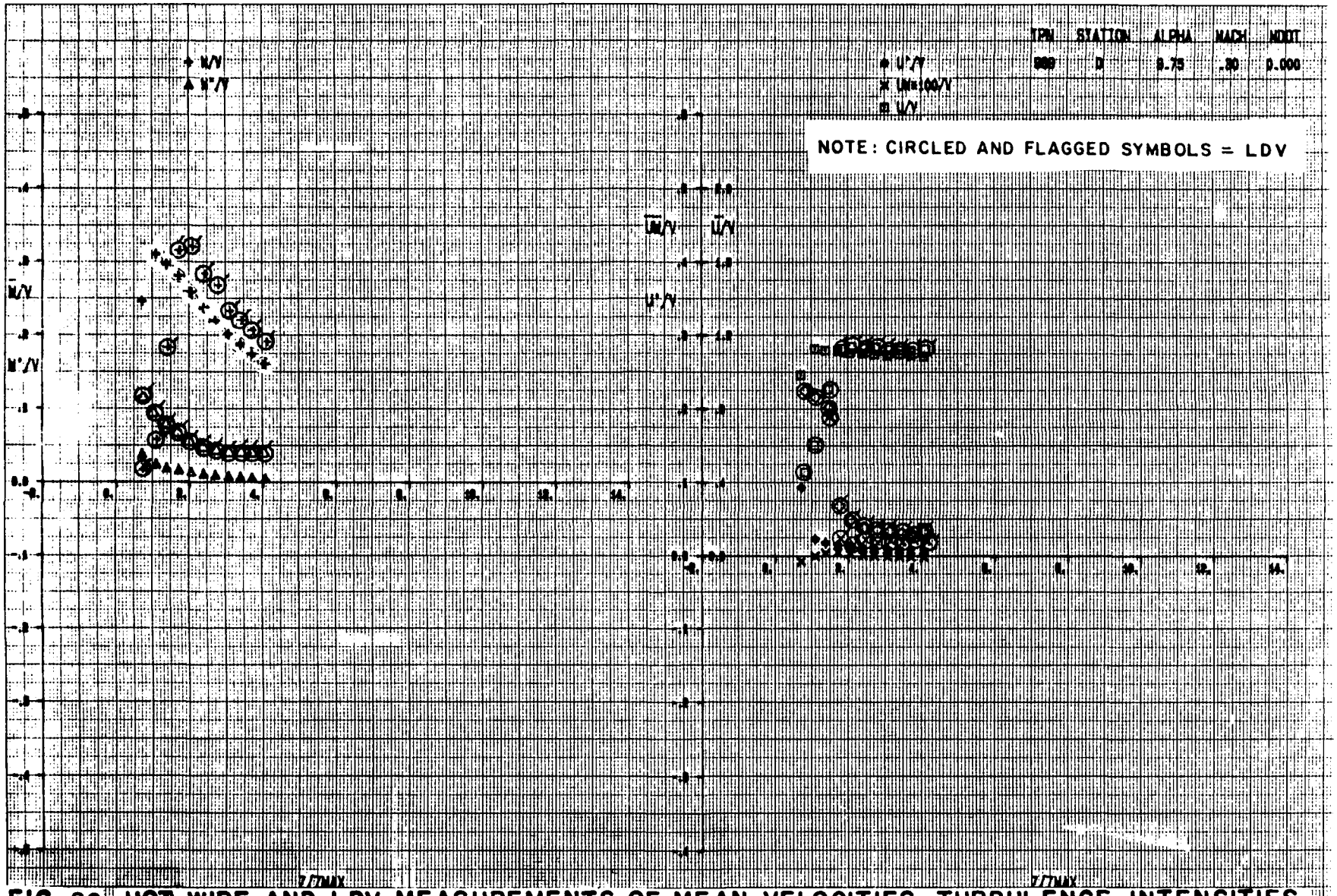

FIG. 26 HOT WIRE AND LDV MEASUREMENTS OF MEAN VELOCITIES, TURBULENCE INTENSITIES, AND REYNOLDS STRESSES WITHOUT BLOWING - COPLANAR CANARD - TGF - $\alpha = 10°$ - STATION D

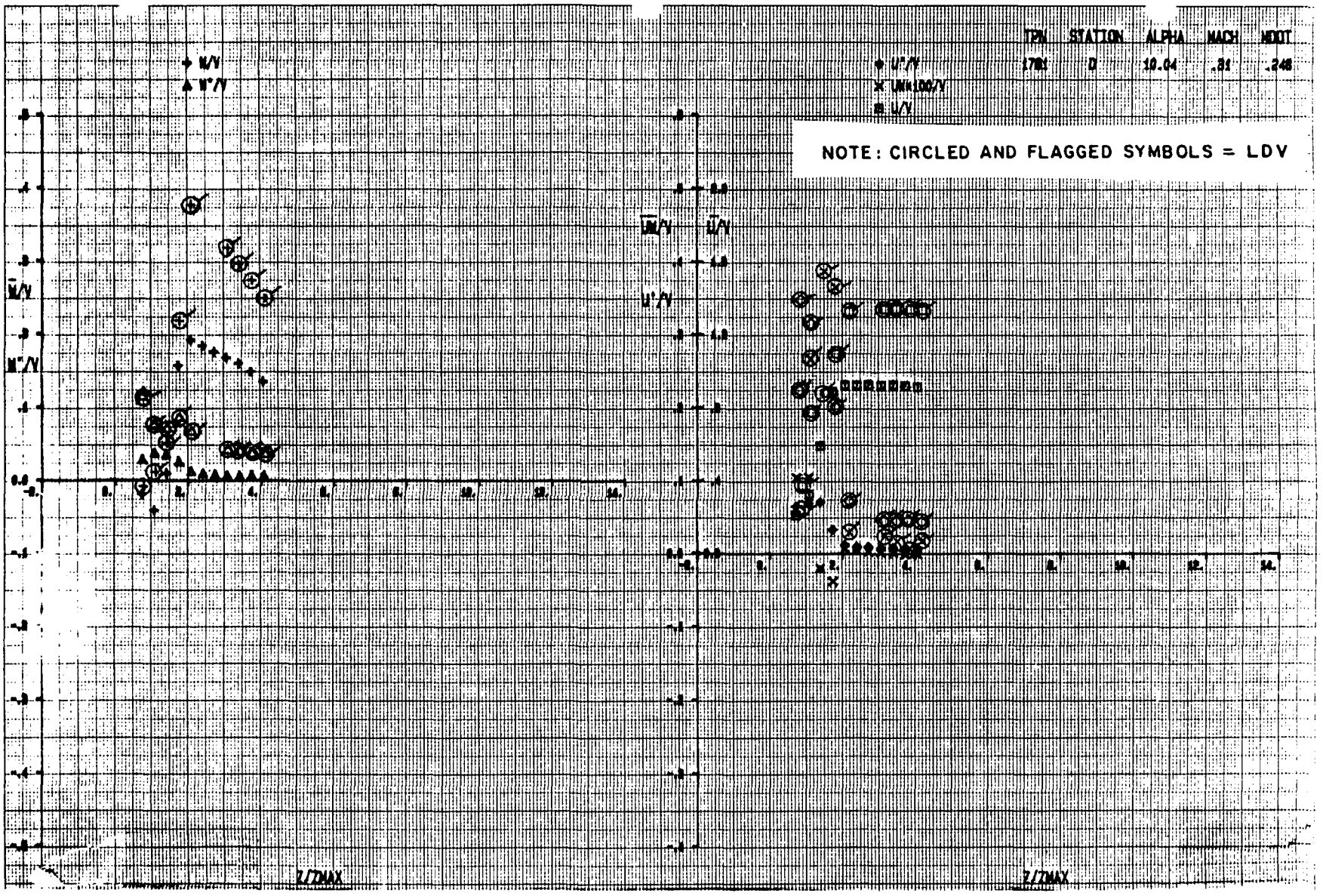

FIG. 27 HOT WIRE AND LDV MEASUREMENTS OF MEAN VELOCITIES, TURBULENCE INTENSITIES, AND REYNOLDS STRESSES WITH BLOWING - COPLANAR CANARD - TGF - $\alpha = 10°$ - STATION D

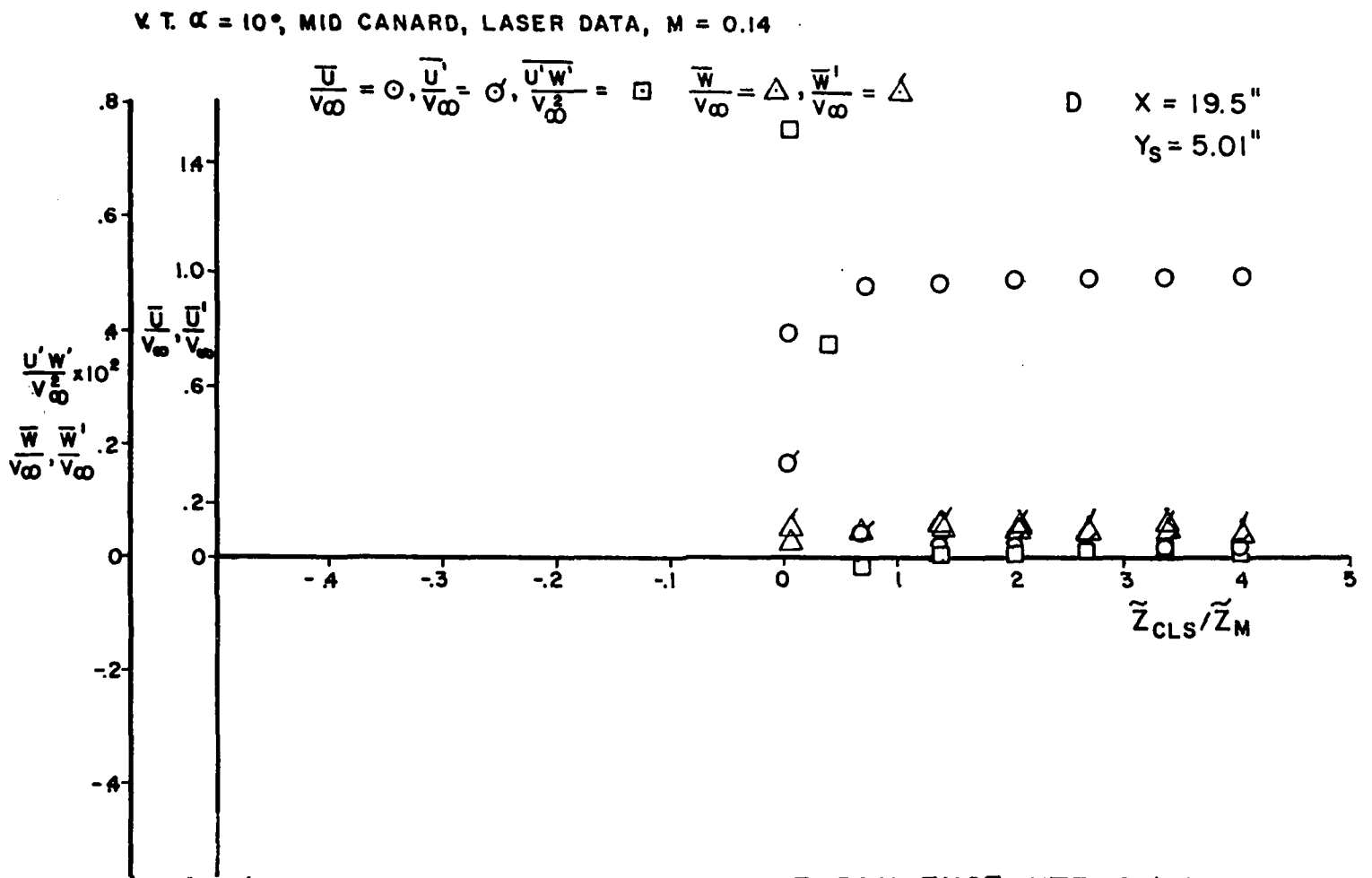

FIG. 28 LDV MEASUREMENTS OF MEAN VELOCITIES, TURBULENCE INTENSITIES, AND REYNOLDS STRESSES WITH THE COPLANAR CANARD WITHOUT BLOWING V. W. T. - α = 10° STATION D

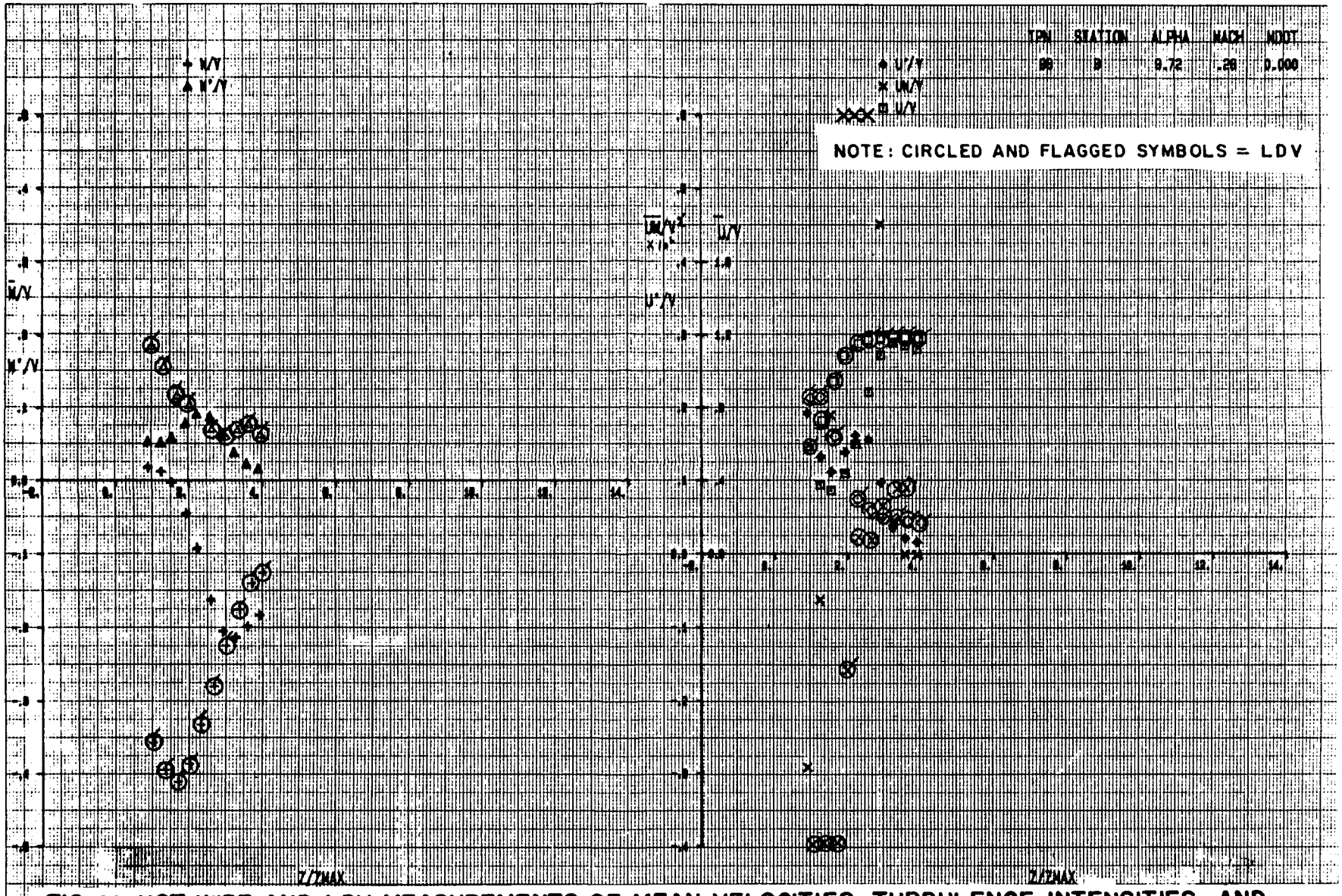

FIG. 29 HOT WIRE AND LDV MEASUREMENTS OF MEAN VELOCITIES, TURBULENCE INTENSITIES, AND REYNOLDS STRESSES WITHOUT BLOWING – COPLANAR CANARD – TGF – α = 10°– STATION B

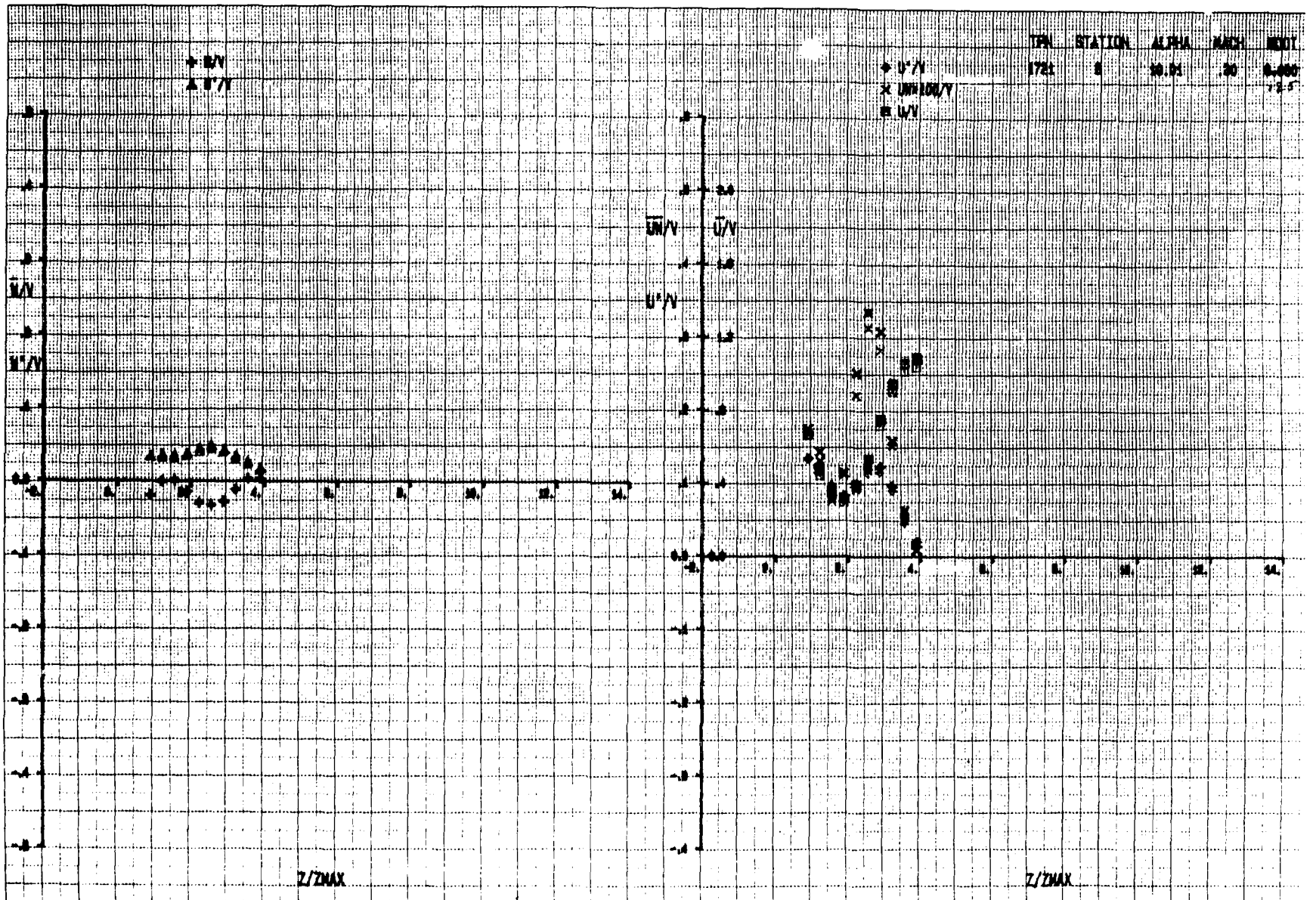

FIG.30 HOT WIRE MEASUREMENTS OF MEAN VELOCITIES, TURBULENCE INTENSITIES, AND REYNOLDS STRESSES WITH BLOWING - COPLANAR CANARD - TGF - $\alpha = 10°$ - STATION B

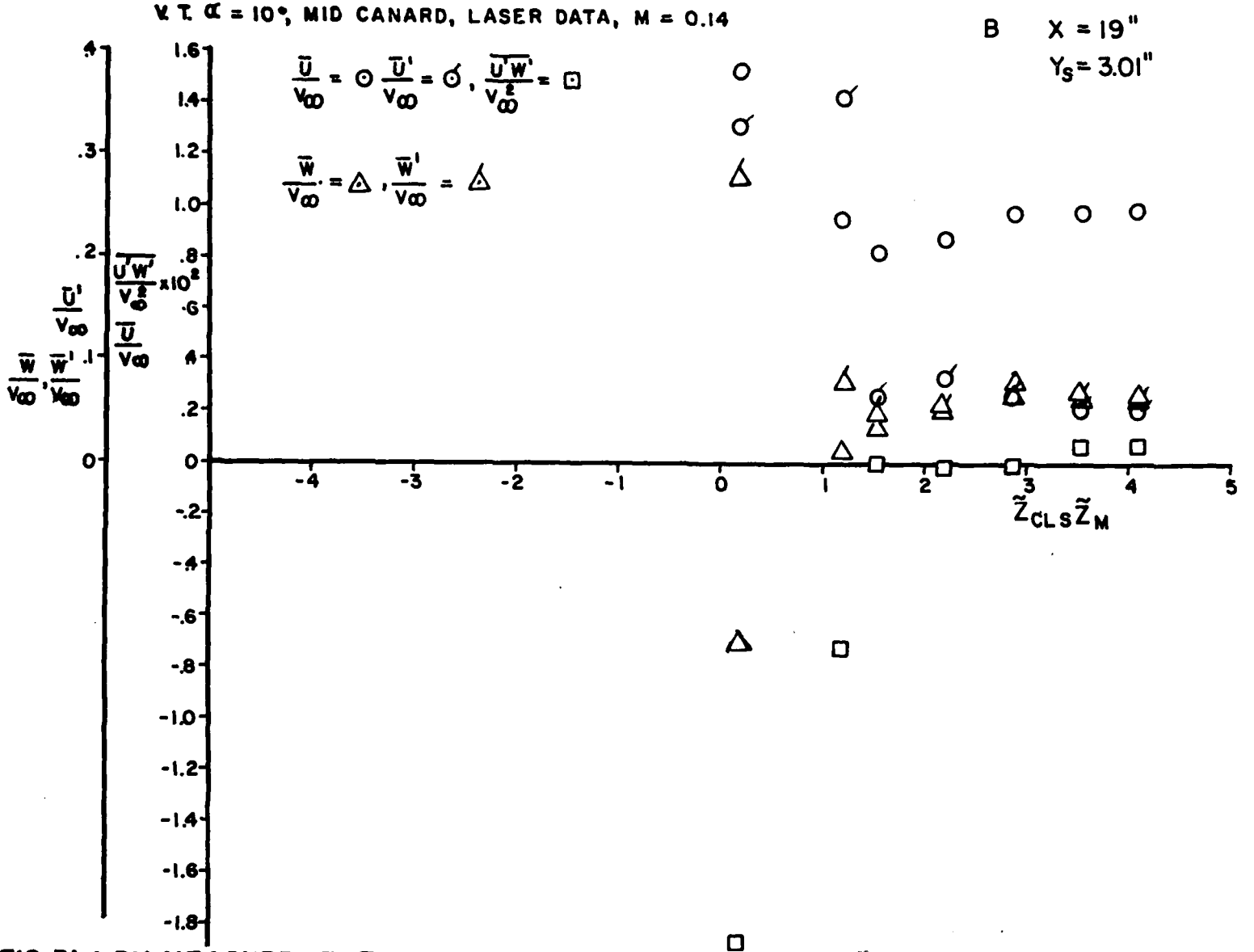

FIG. 31 LDV MEASUREMENTS OF VERTICAL MEAN VELOCITY AND TURBULENCE INTENSITY WITH THE COPLANAR CANARD WITHOUT BLOWING - V.W.T. - α = 10 - STATION B

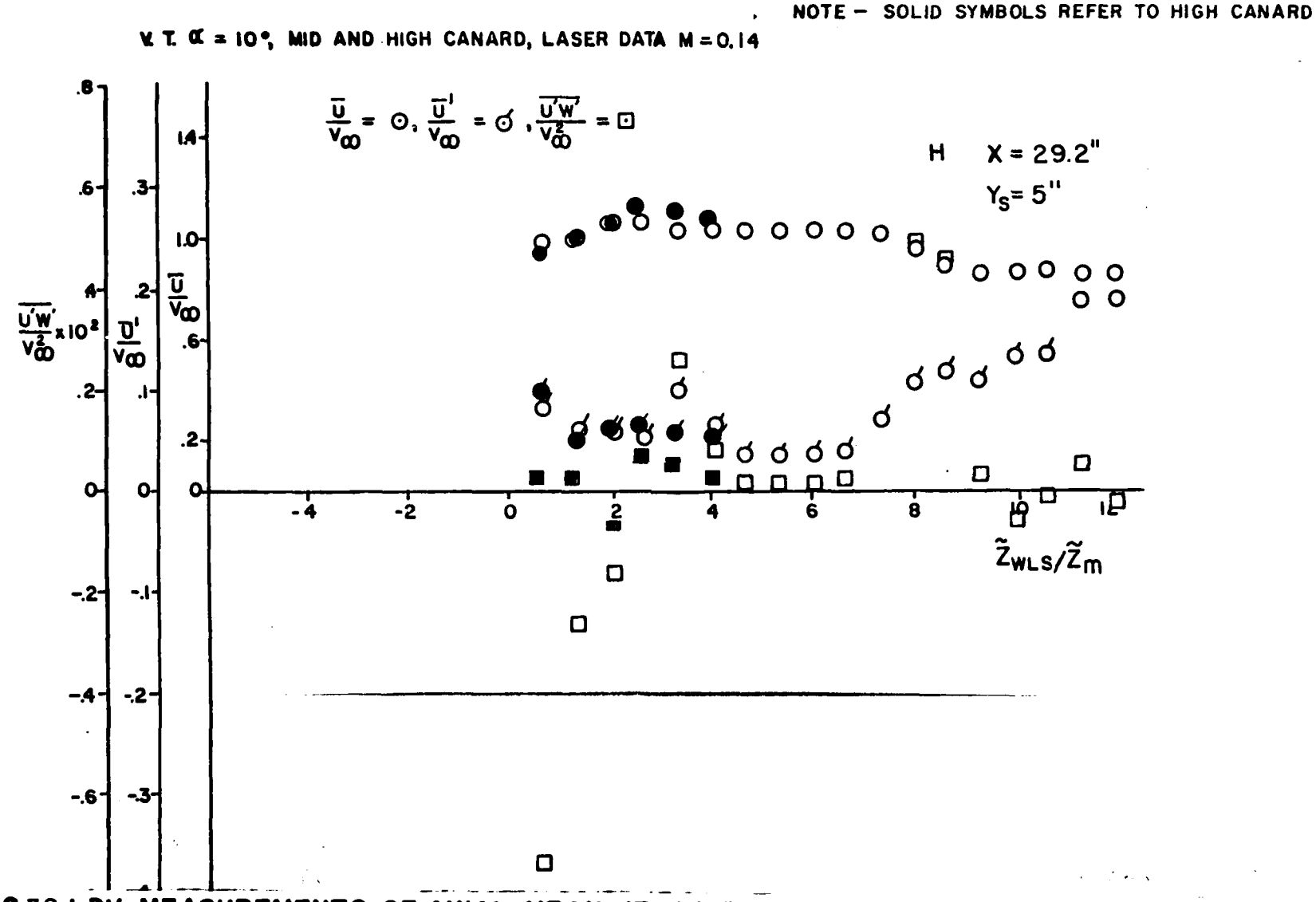

FIG.32 LDV MEASUREMENTS OF AXIAL MEAN VELOCITY, TURBULENCE INTENSITY, AND REYNOLDS STRESSES WITH THE COPLANAR CANARD AND THE HIGH CANARD WITHOUT BLOWING – V. W. T. – α = 10° – STATION H

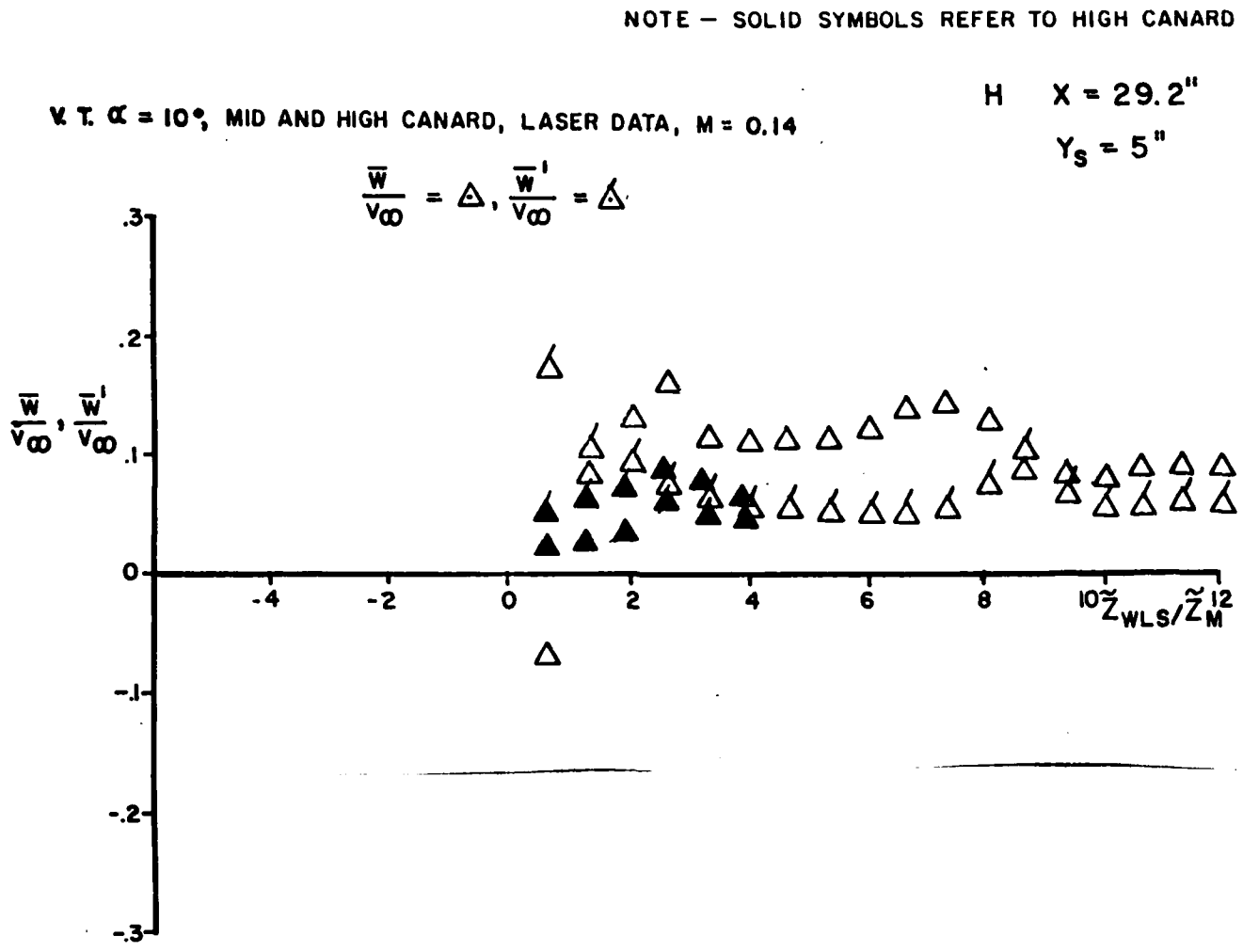

FIG.33 LDV MEASUREMENTS OF VERTICAL MEAN VELOCITY AND TURBULENCE INTENSITY WITH THE COPLANAR CANARD AND THE HIGH CANARD WITHOUT BLOWING - V.W.T. - α = 10° - STATION H

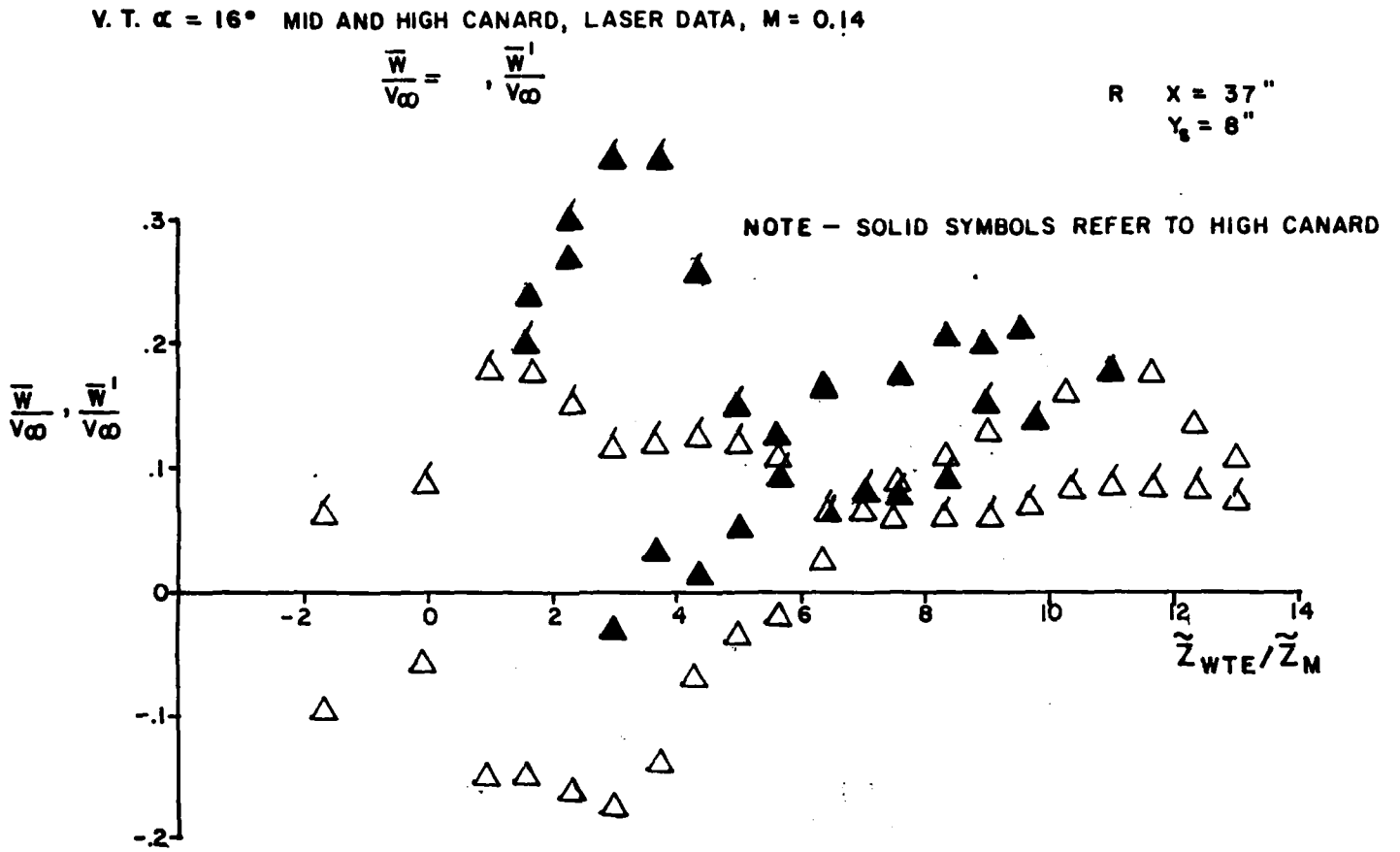

FIG.34 LDV MEASUREMENTS OF VERTICAL MEAN VELOCITY AND TURBULENCE INTENSITY WITH THE COPLANAR CANARD AND THE HIGH CANARD WITHOUT BLOWING - V.W.T. - α = 16° - STATION R

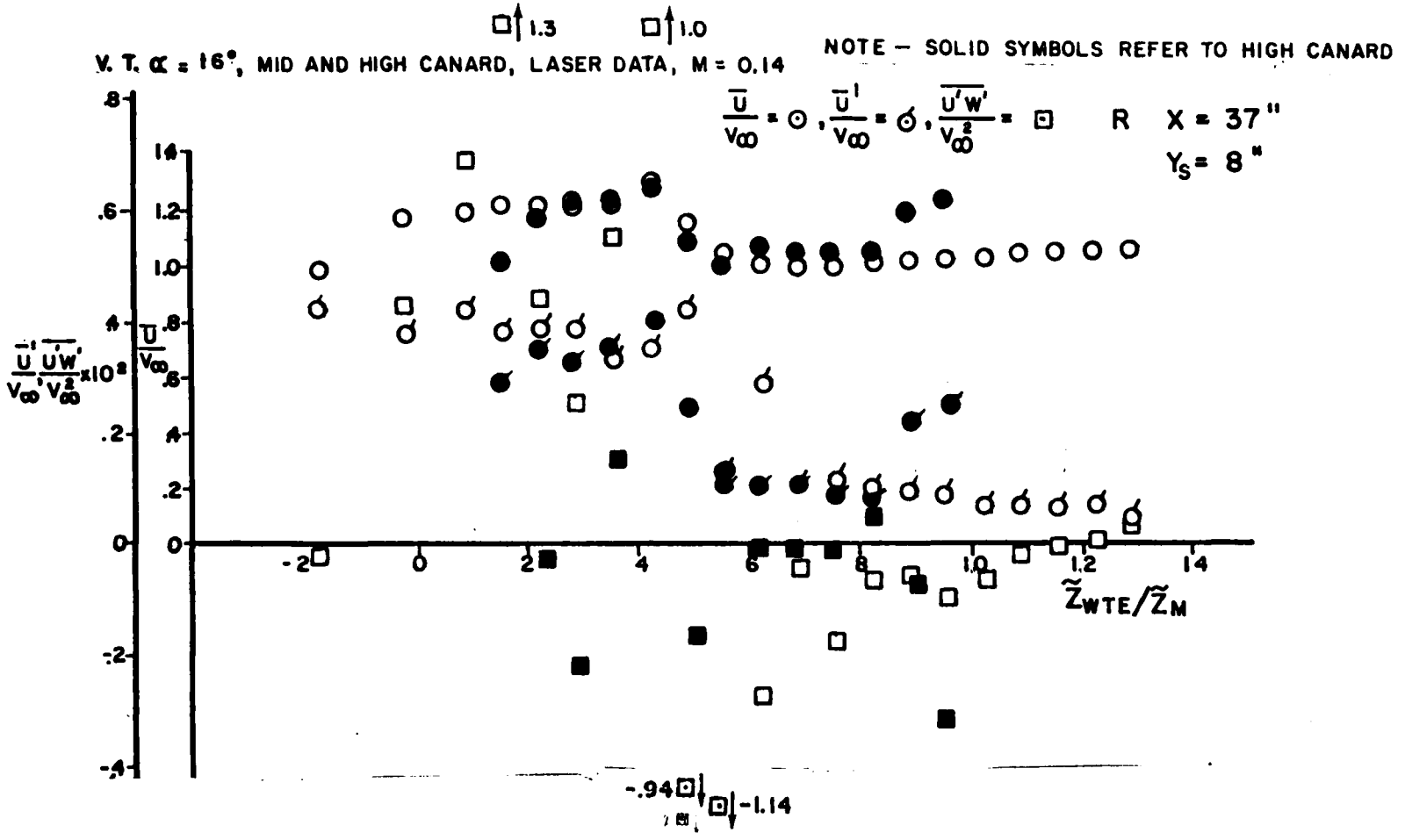

FIG.35 LDV MEASUREMENTS OF AXIAL MEAN VELOCITY, TURBULENCE INTENSITY, AND REYNOLDS STRESSES WITH THE COPLANAR CANARD AND THE HIGH CANARD WITHOUT BLOWING – V. W. T. – α =16° – STATION R

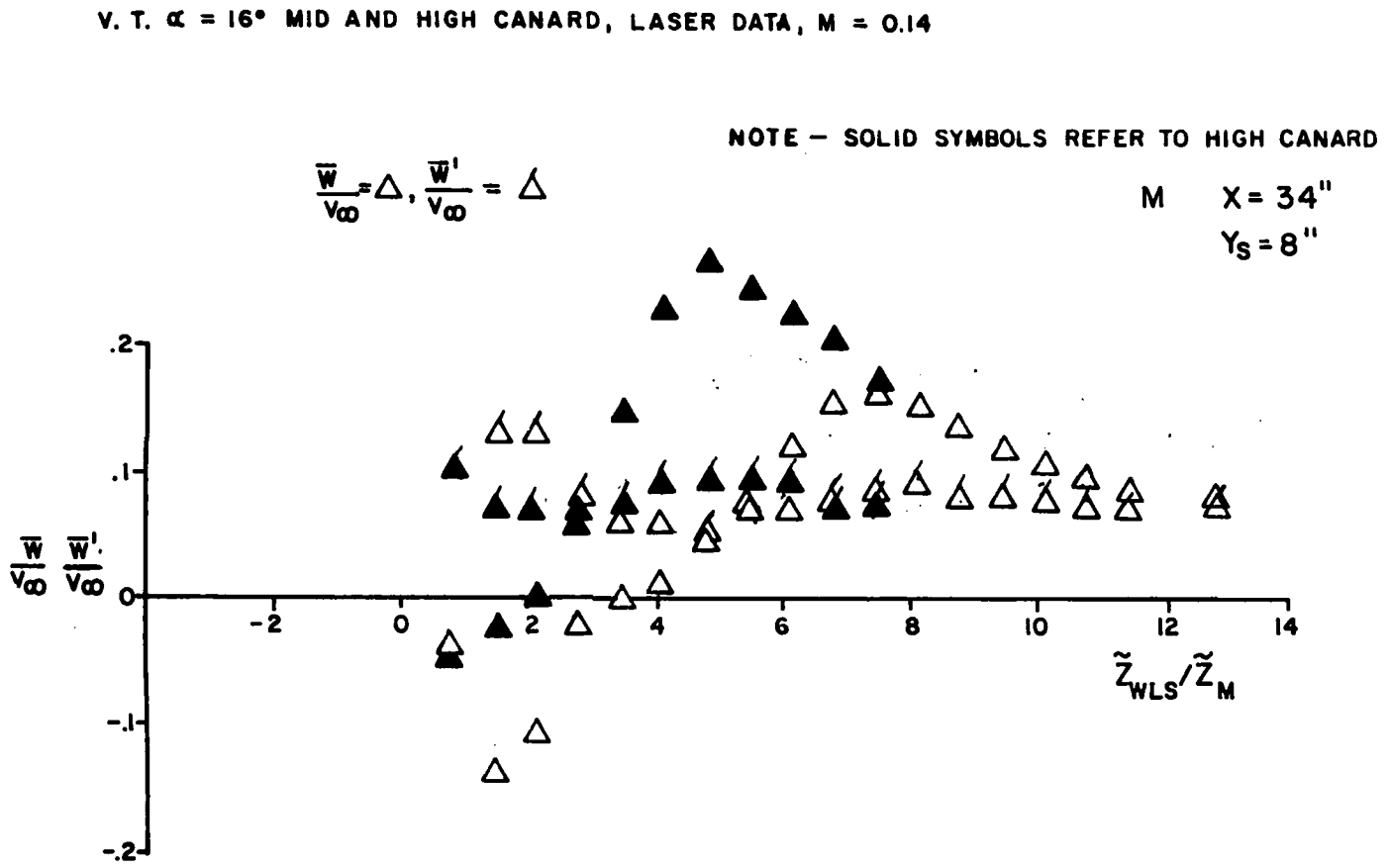

FIG. 36 LDV MEASUREMENTS OF VERTICAL MEAN VELOCITY AND TURBULENCE INTENSITY WITH THE COPLANAR CANARD AND THE HIGH CANARD WITHOUT BLOWING - V.W.T. - α = 16° STATION M

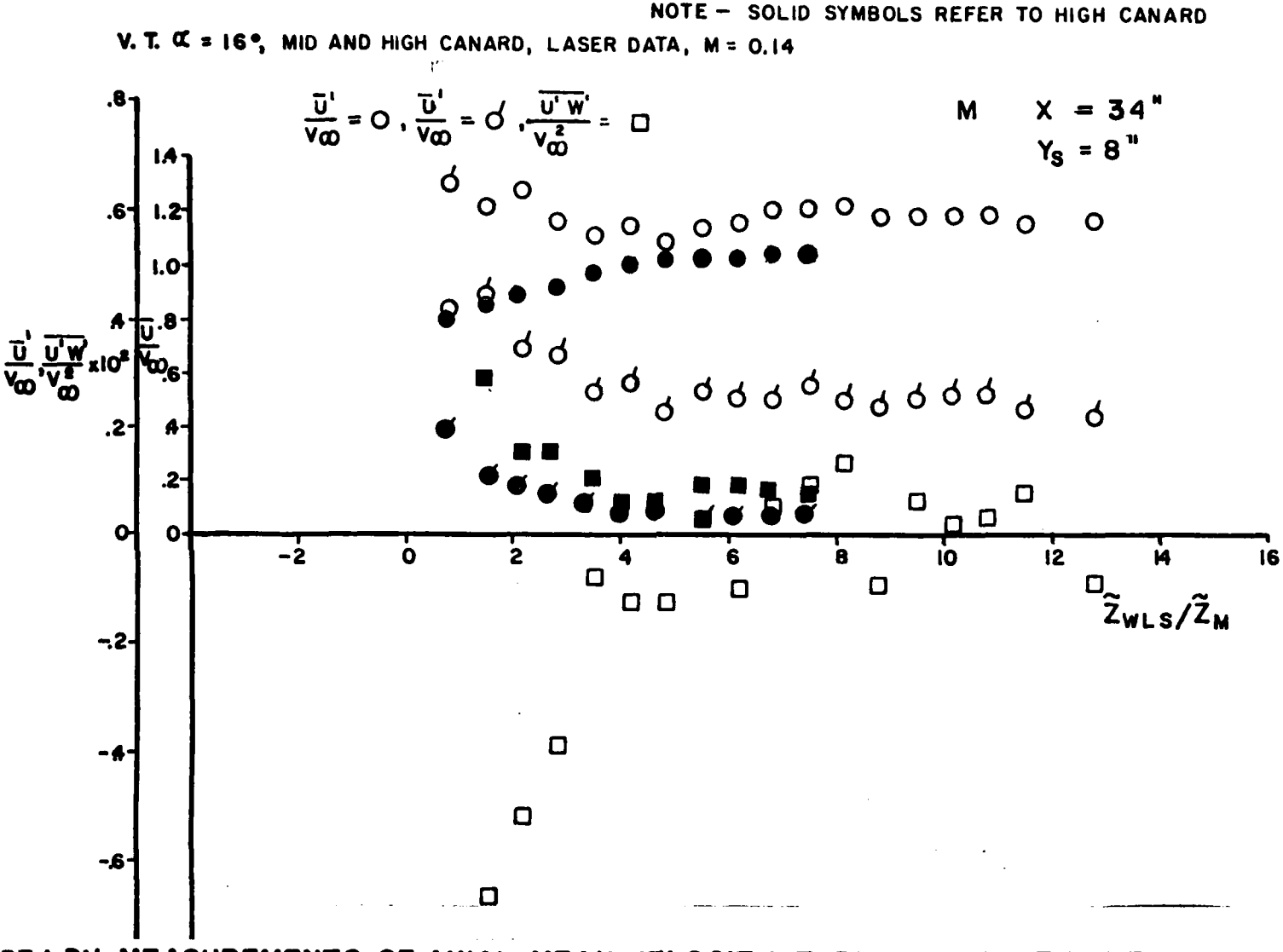

FIG.37 LDV MEASUREMENTS OF AXIAL MEAN VELOCITY, TURBULENCE INTENSITY, AND REYNOLDS STRESSES WITH THE COPLANAR CANARD AND THE HIGH CANARD WITHOUT BLOWING – V. W. T. – α = 16° – STATION M

NOTE – SOLID SYMBOLS REFER TO HIGH CANARD

V. T. α = 16°, MID AND HIGH CANARD, LASER DATA M = 0.14

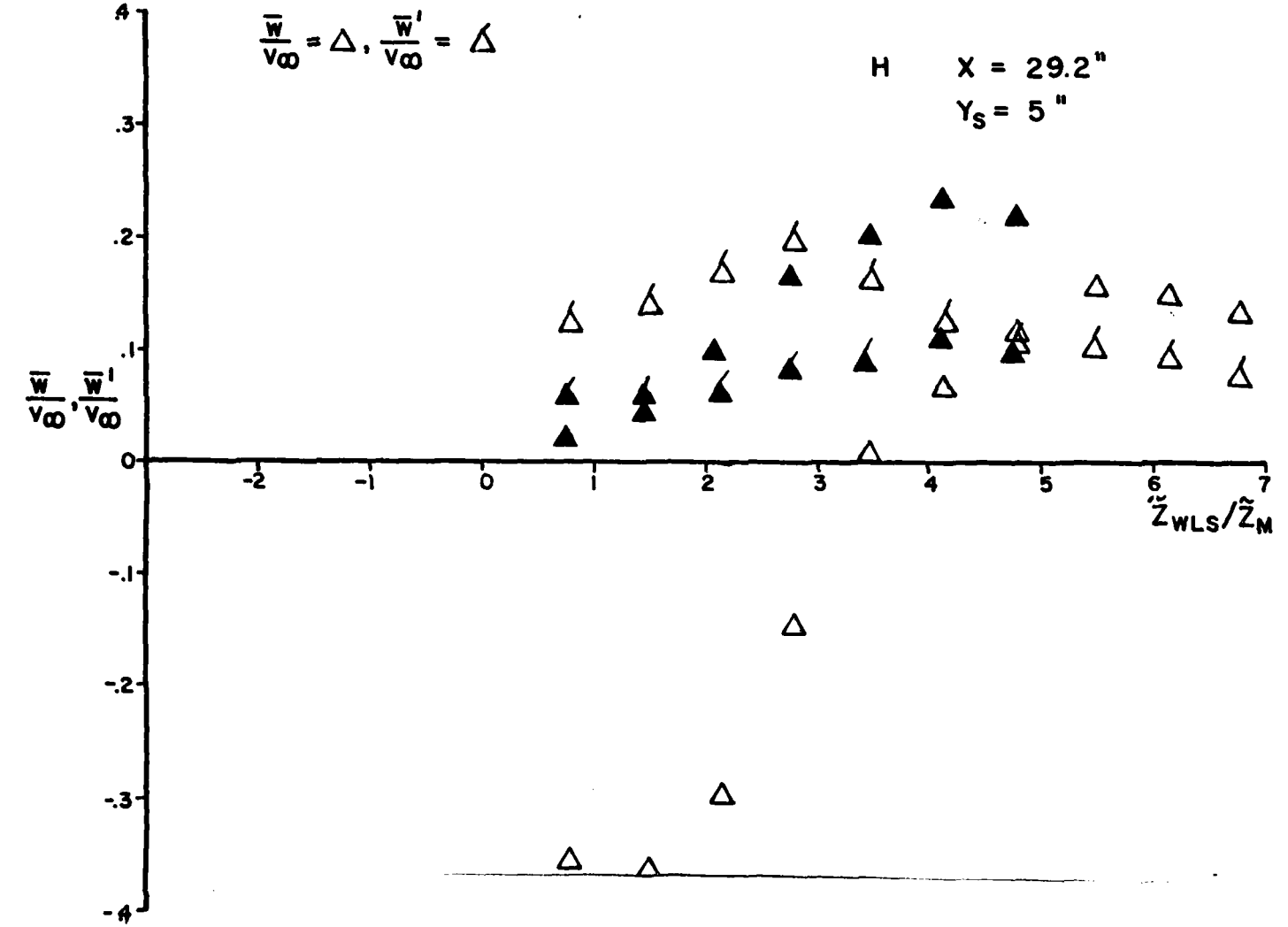

FIG.38 LDV MEASUREMENTS OF VERTICAL MEAN VELOCITY AND TURBULENCE INTENSITY WITH THE COPLANAR CANARD AND THE HIGH CANARD WITHOUT BLOWING - V.W.T. - α = 16° - STATION H

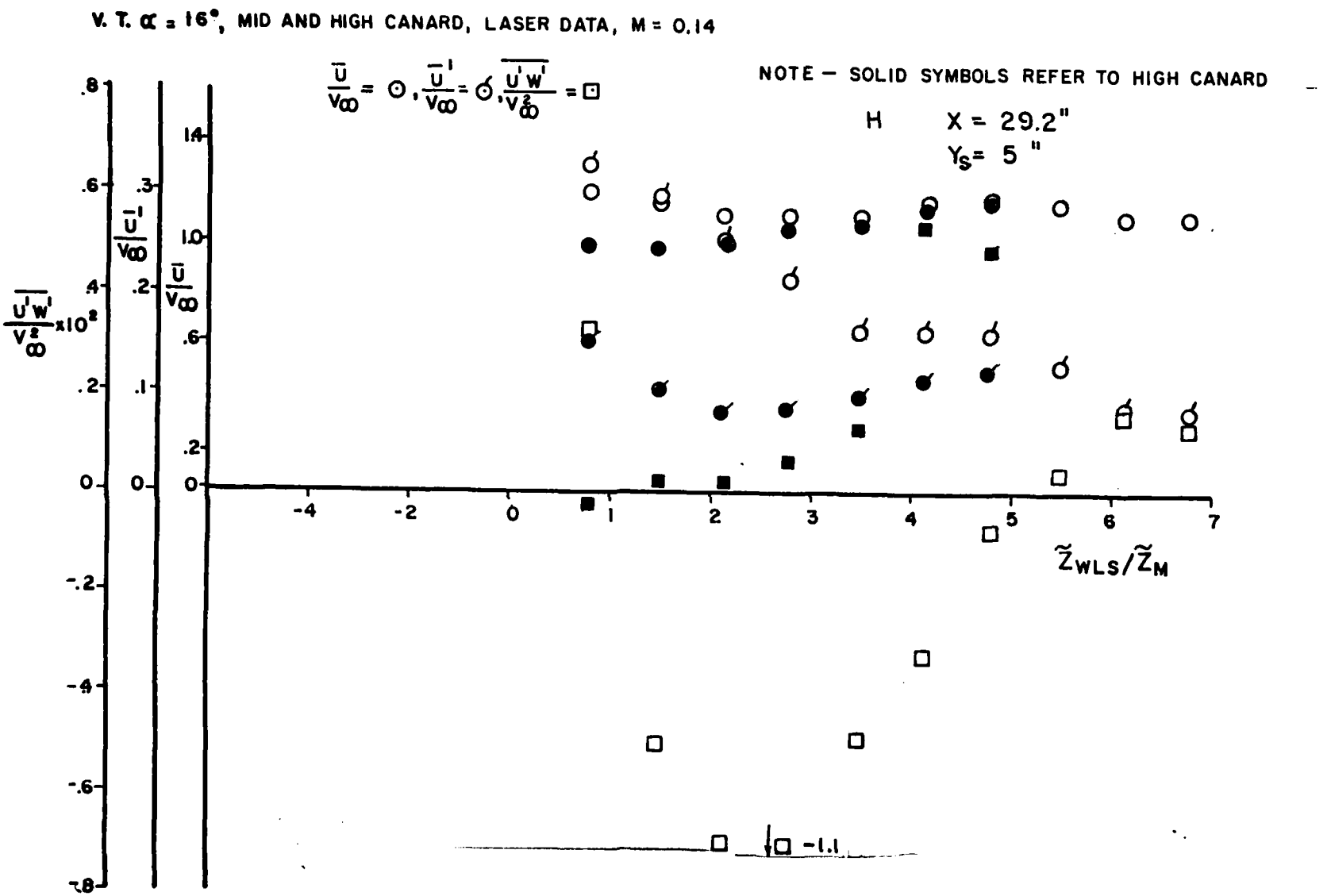

FIG. 39 LDV MEASUREMENTS OF AXIAL MEAN VELOCITY, TURBULENCE INTENSITY, AND REYNOLDS STRESSES WITH THE COPLANAR CANARD AND THE HIGH CANARD WITHOUT BLOWING – V. W. T. – α = 16° – STATION H

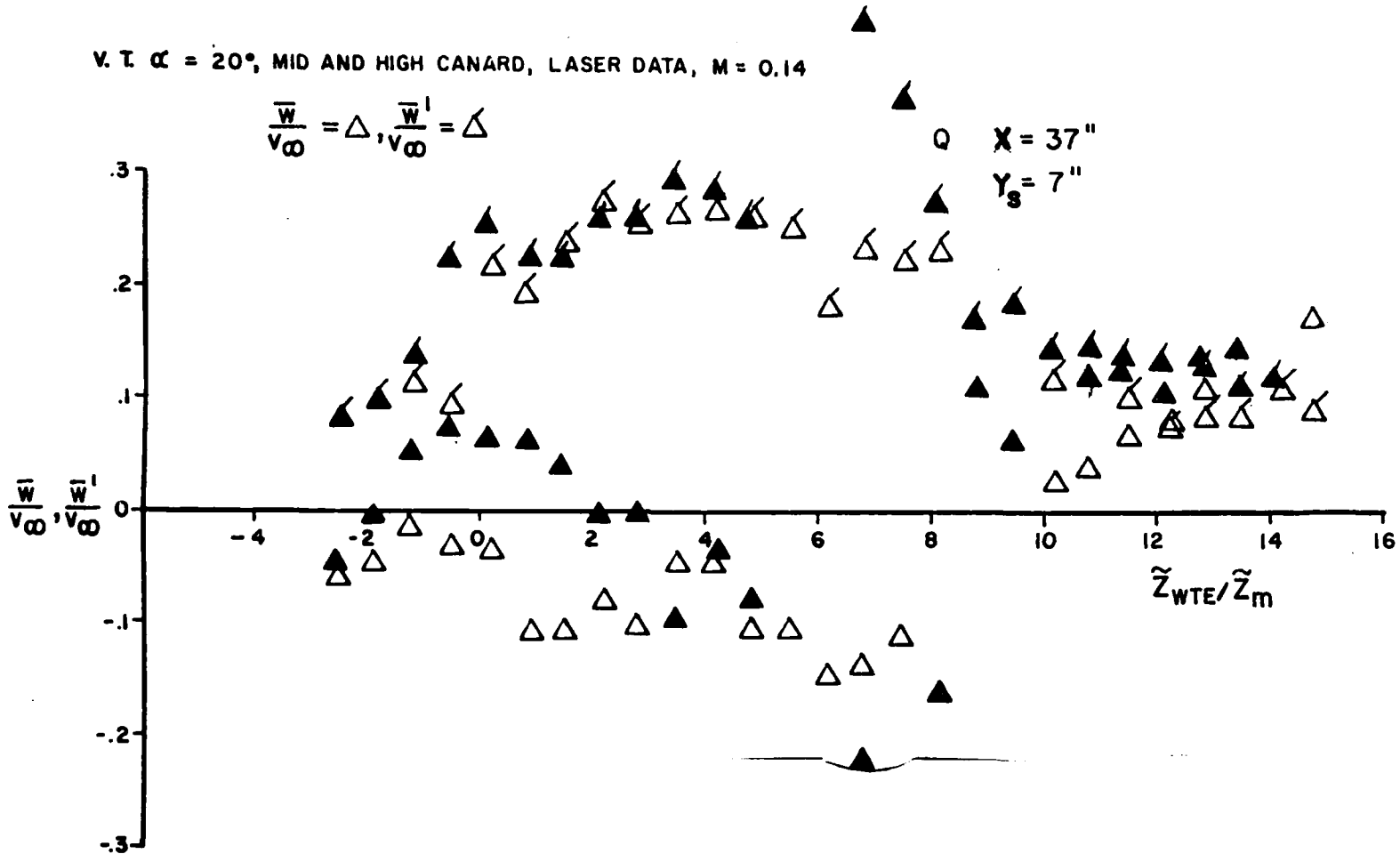

FIG. 40 LDV MEASUREMENTS OF VERTICAL MEAN VELOCITY AND TURBULENCE INTENSITY WITH THE COPLANAR CANARD AND THE HIGH CANARD WITHOUT BLOWING - V.W.T. - α = 20° - STATION Q

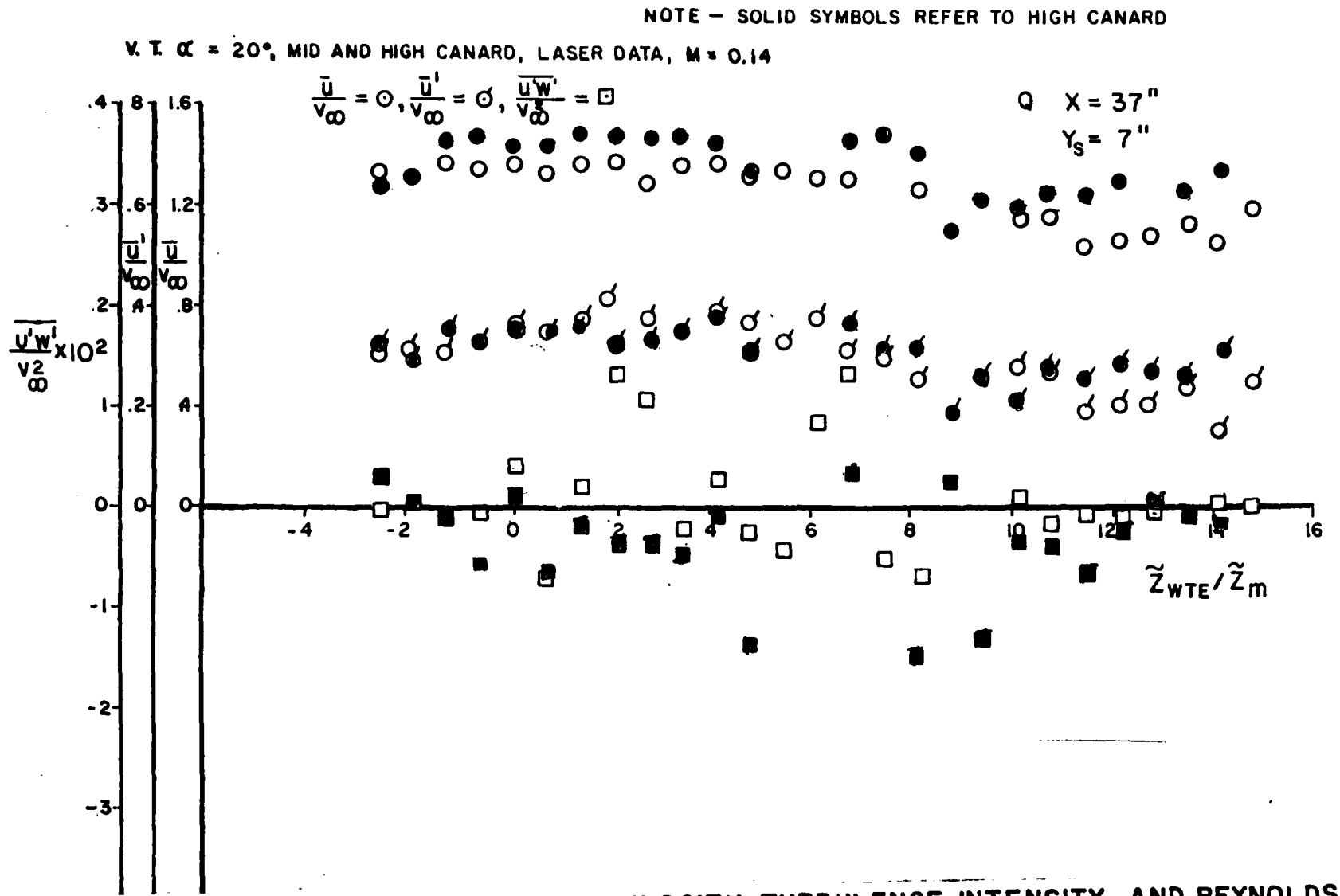

FIG. 41 LDV MEASUREMENTS OF AXIAL MEAN VELOCITY, TURBULENCE INTENSITY, AND REYNOLDS STRESSES WITH THE COPLANAR CANARD AND THE HIGH CANARD WITHOUT BLOWING – V. W. T. – α = 20° – STATION Q

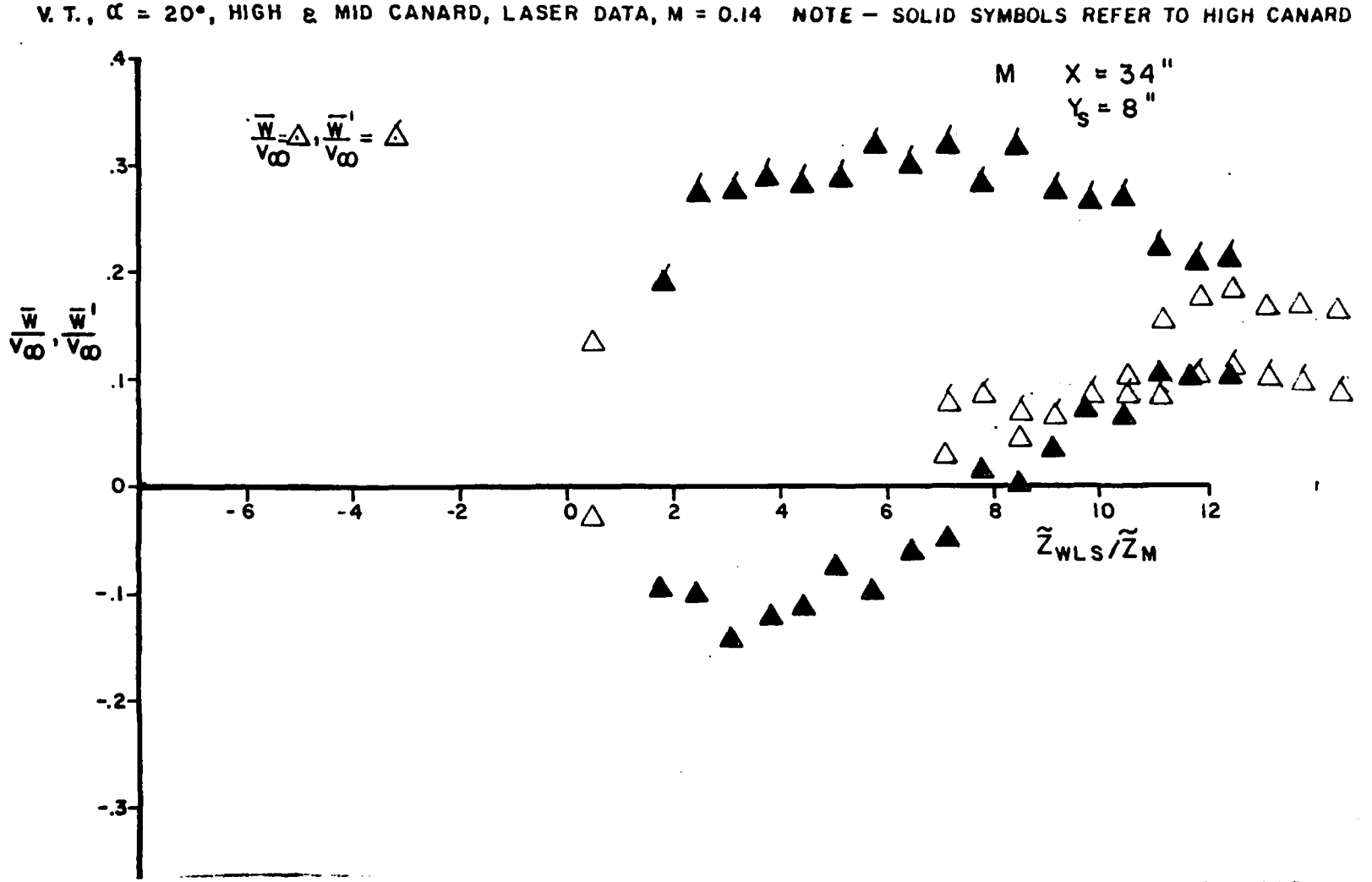

FIG.42 LDV MEASUREMENTS OF VERTICAL MEAN VELOCITY AND TURBULENCE INTENSITY WITH THE COPLANAR CANARD AND THE HIGH CANARD WITHOUT BLOWING - V.W.T. - α = 20° STATIONM

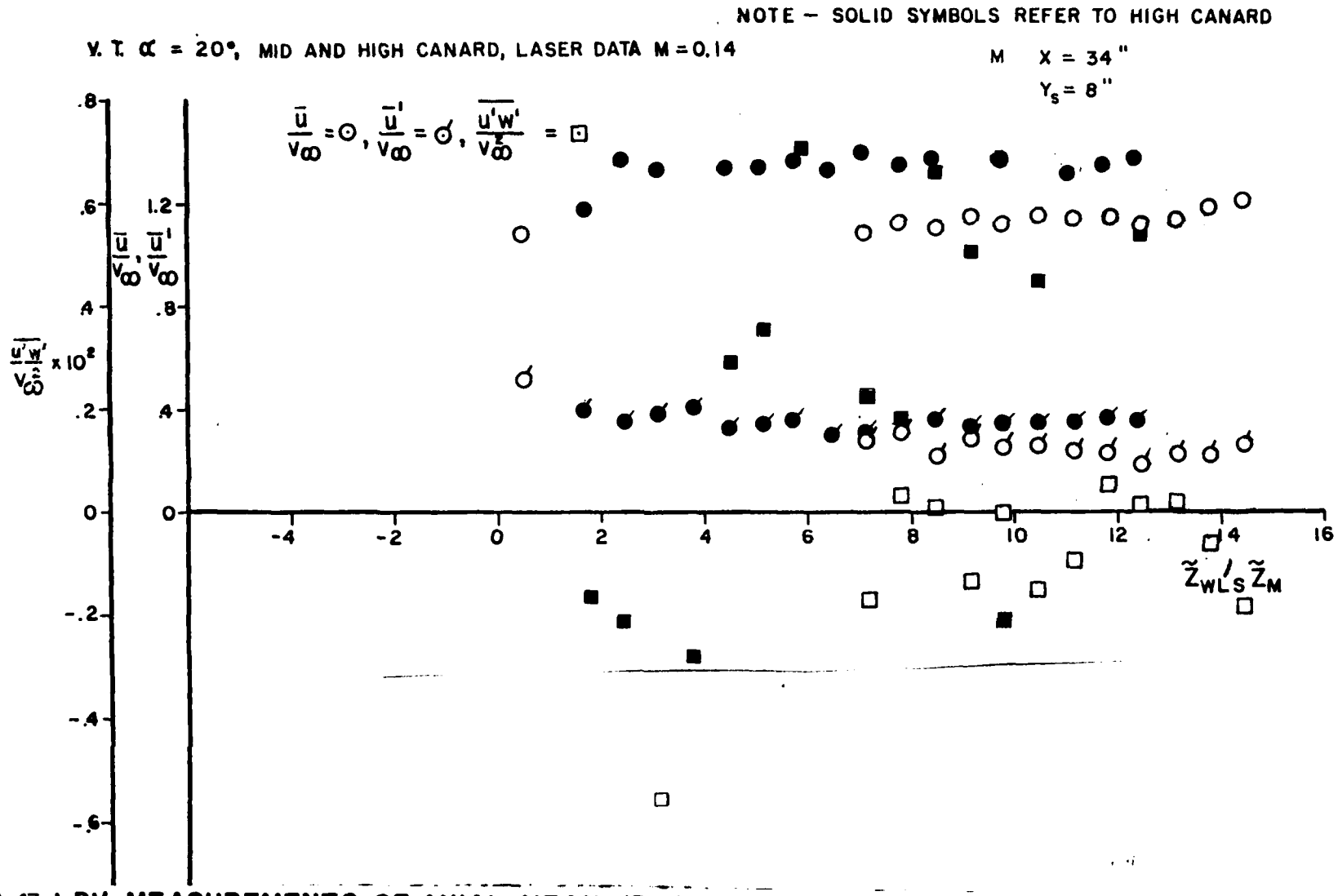

FIG. 43 LDV MEASUREMENTS OF AXIAL MEAN VELOCITY, TURBULENCE INTENSITY, AND REYNOLDS STRESSES WITH THE COPLANAR CANARD AND THE HIGH CANARD WITHOUT BLOWING – V. W. T. – α = 20° – STATION M

NOTE – SOLID SYMBOLS REFER TO HIGH CANARD

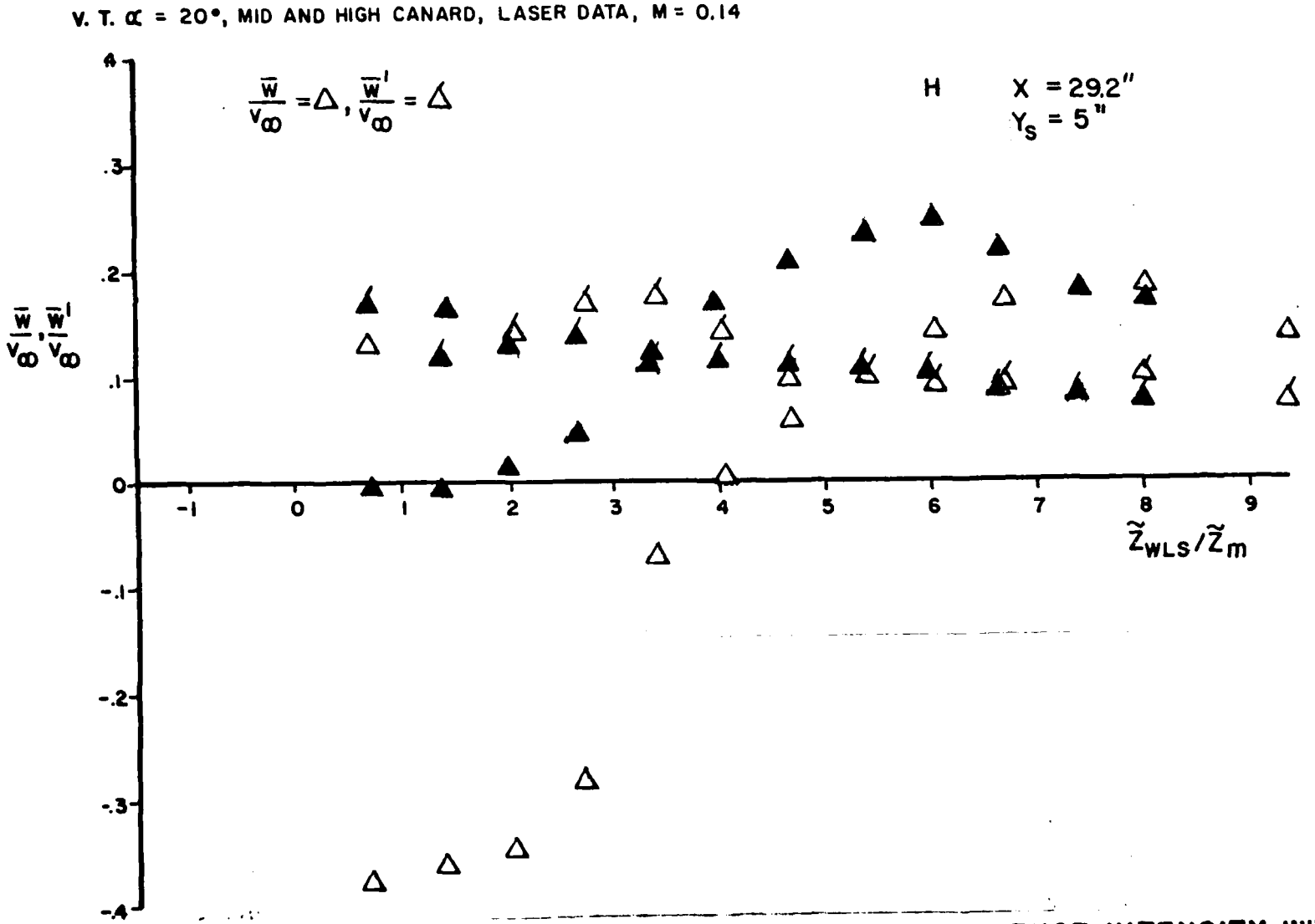

FIG.44 LDV MEASUREMENTS OF VERTICAL MEAN VELOCITY AND TURBULENCE INTENSITY WITH THE COPLANAR CANARD AND THE HIGH CANARD WITHOUT BLOWING - V.W.T. - $\alpha = 20^\circ$ - STATION H

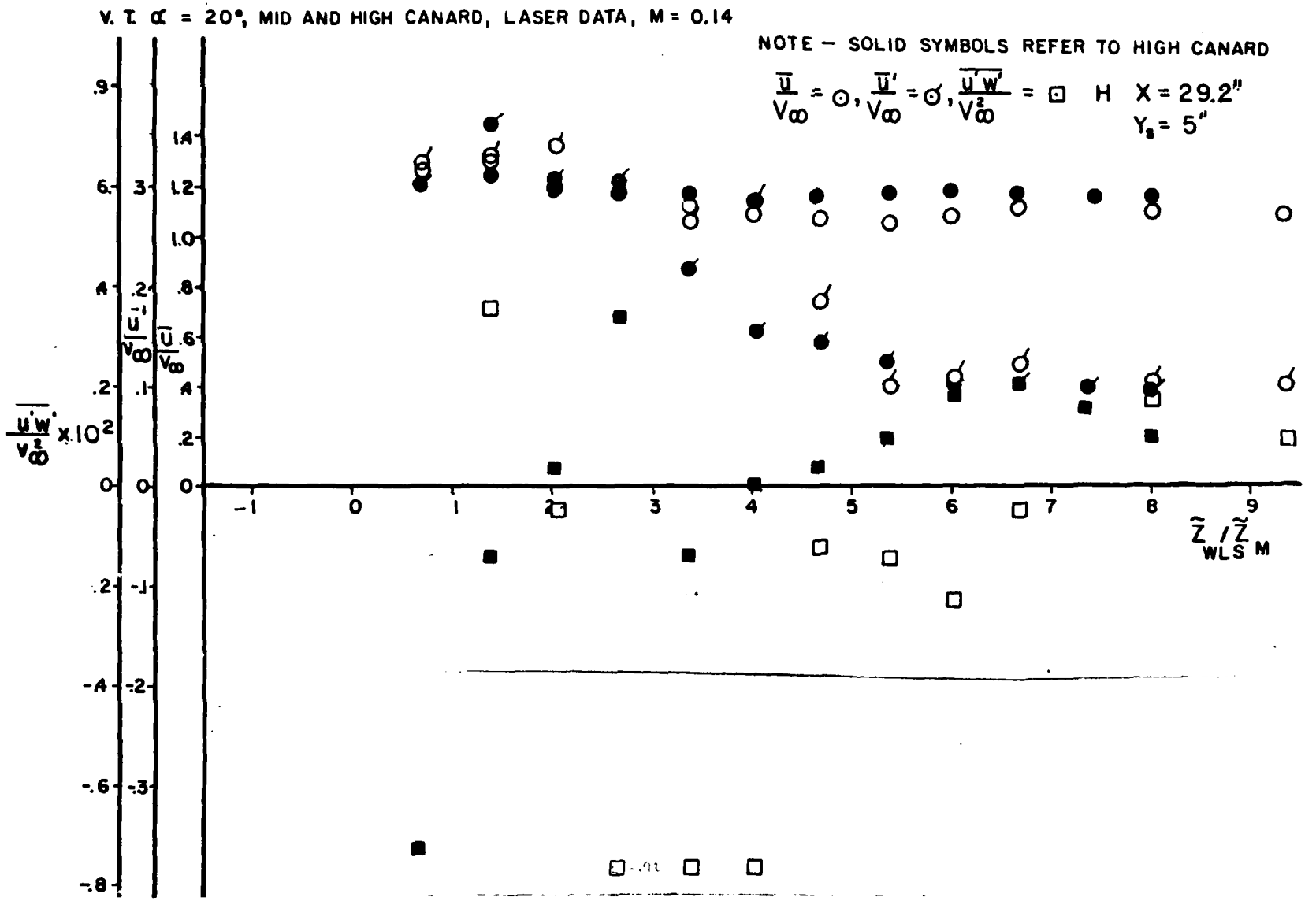

FIG.45 LDV MEASUREMENTS OF AXIAL MEAN VELOCITY, TURBULENCE INTENSITY, AND REYNOLDS STRESSES WITH THE COPLANAR CANARD AND THE HIGH CANARD WITHOUT BLOWING – V. W. T. – α = 20° – STATION H

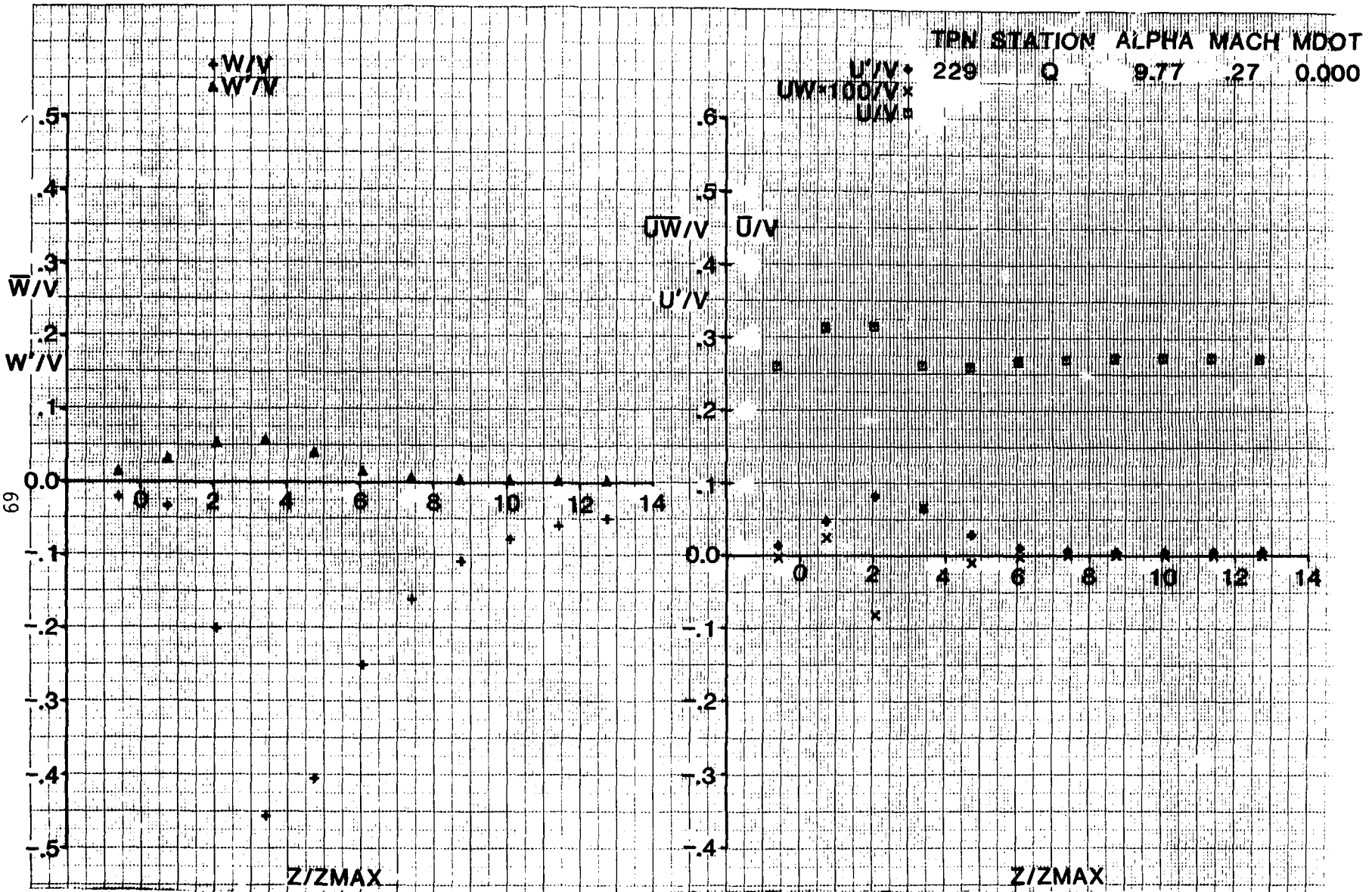

FIG. 46. HOT WIRE MEASUREMENTS OF MEAN VELOCITIES, TURBULENCE INTENSITIES, AND REYNOLDS STRESSES WITHOUT BLOWING - COPLANAR CANARD - TGF - α = 10°-STATION Q

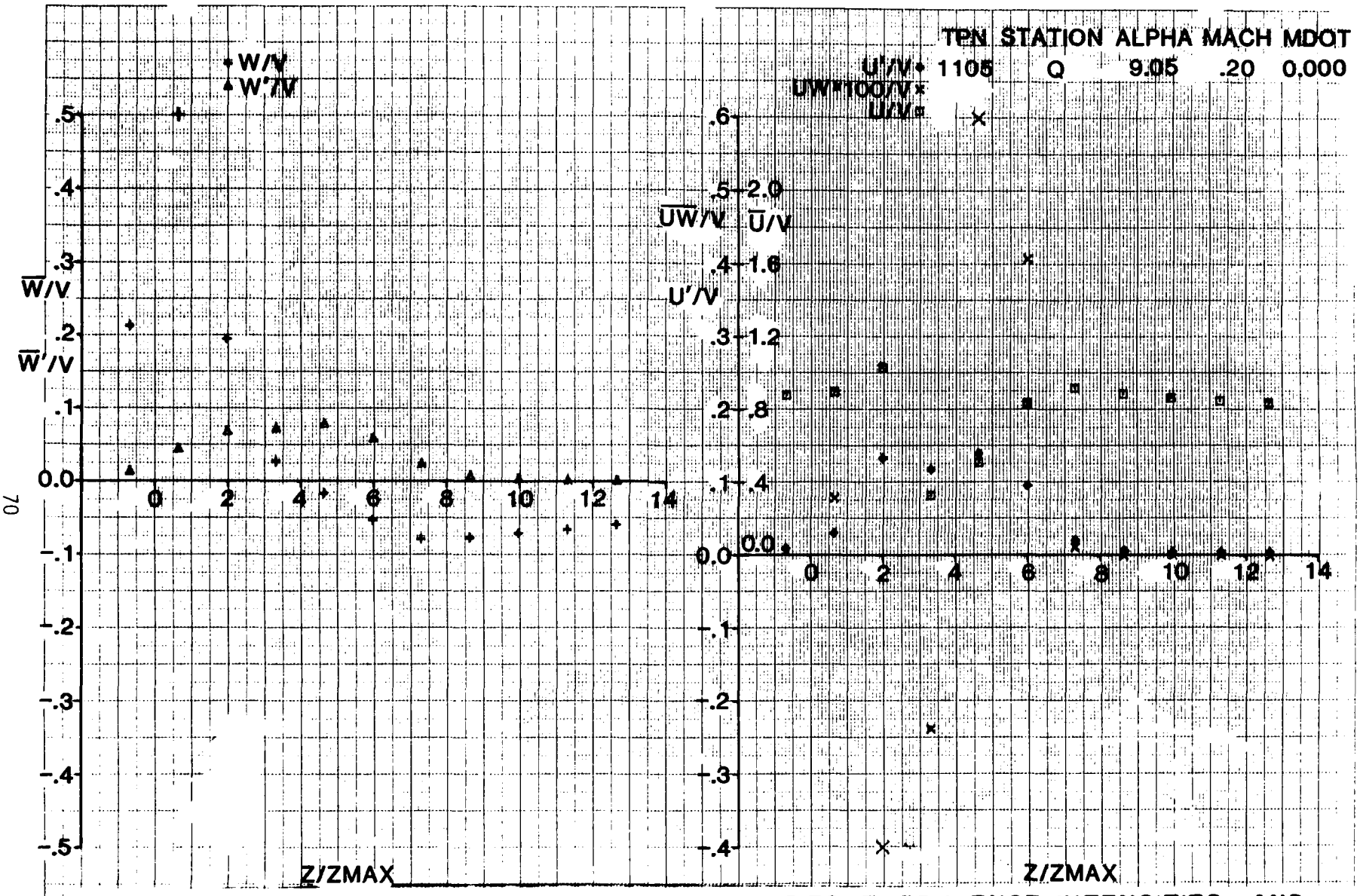

FIG. 47. HOT WIRE MEASUREMENT OF MEAN VELOCITIES, TURBULENCE INTENSITIES, AND REYNOLDS STRESSES WITHOUT BLOWING - NO CANARD - TGF - α = 10° STATION Q

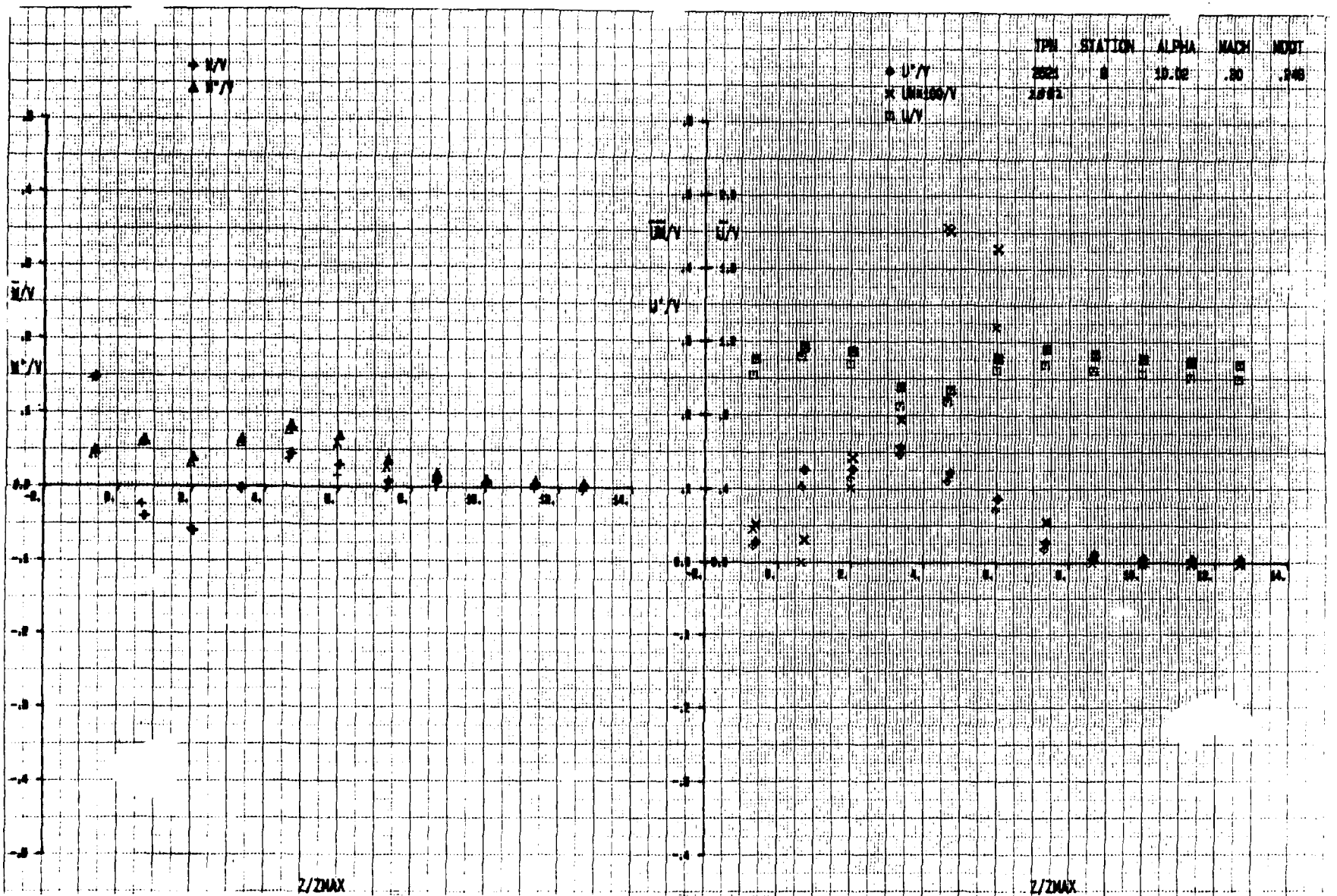

FIG 48 REPEATED HOT WIRE MEASUREMENTS OF MEAN VELOCITIES, TURBULENCE INTENSITIES AND REYNOLDS STRESSES WITH BLOWING- NO CANARD -TGF - α = 10° STATION Q

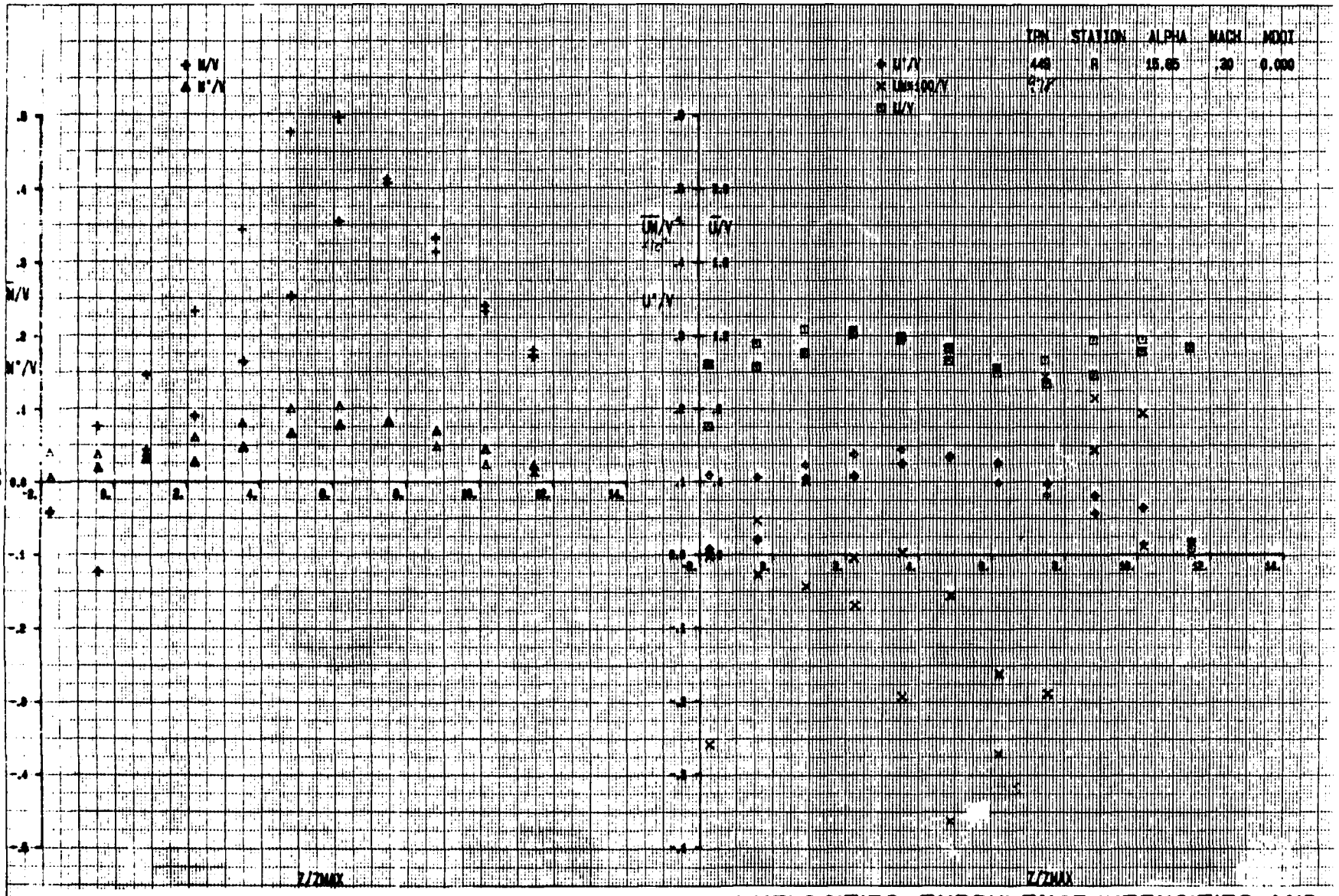

FIG 49 REPEATED HOT WIRE MEASUREMENTS OF MEAN VELOCITIES, TURBULENCE INTENSITIES AND REYNOLDS STRESSES WITHOUT BLOWING - COPLANAR CANARD - TGF - α = 16° STATION R

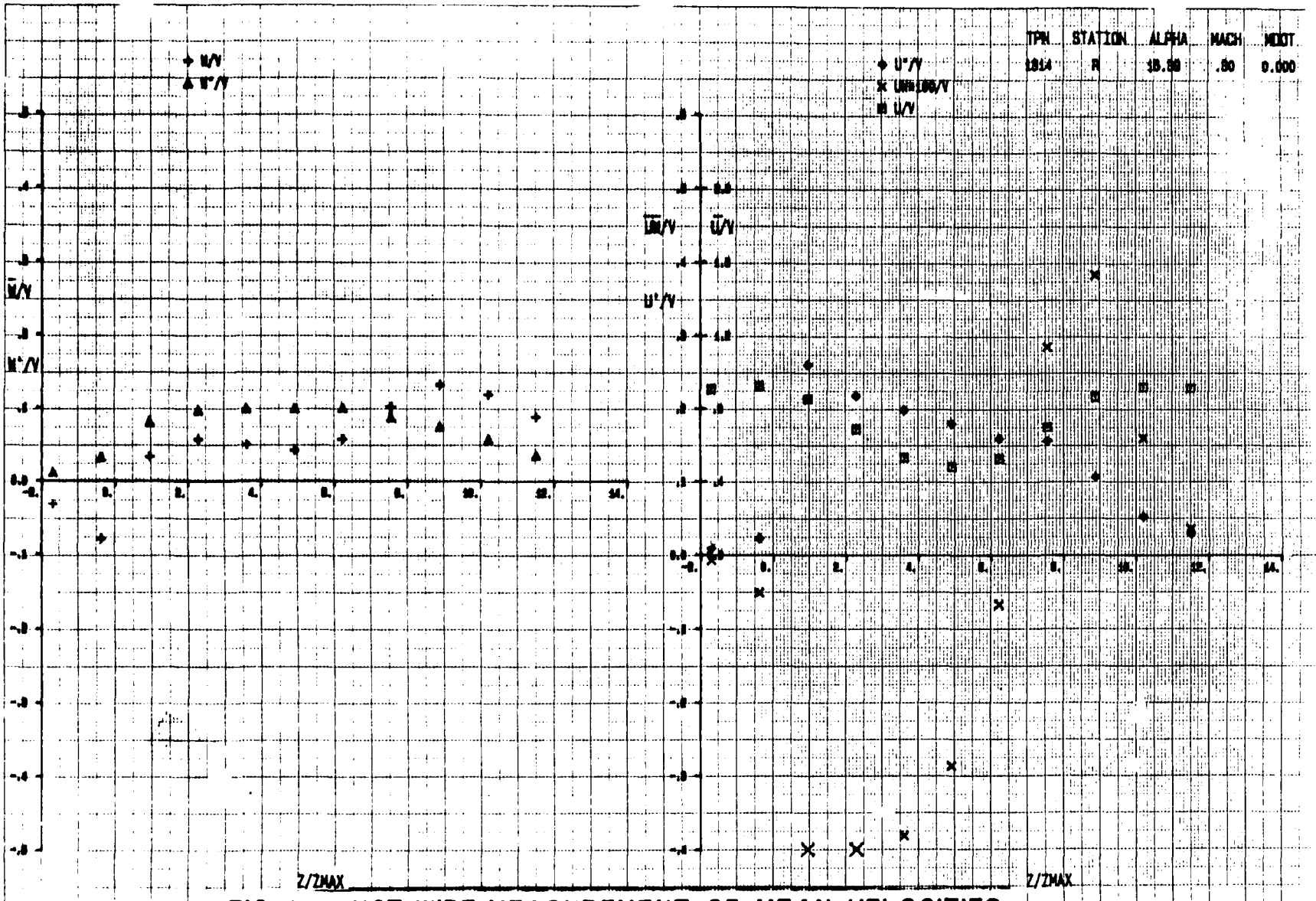

FIG. 50 HOT WIRE MEASUREMENT OF MEAN VELOCITIES, TURBULENCE INTENSITIES, AND REYNOLDS STRESSES WITHOUT BLOWING - NO CANARD - TGF - $\alpha = 16°$ STATION R

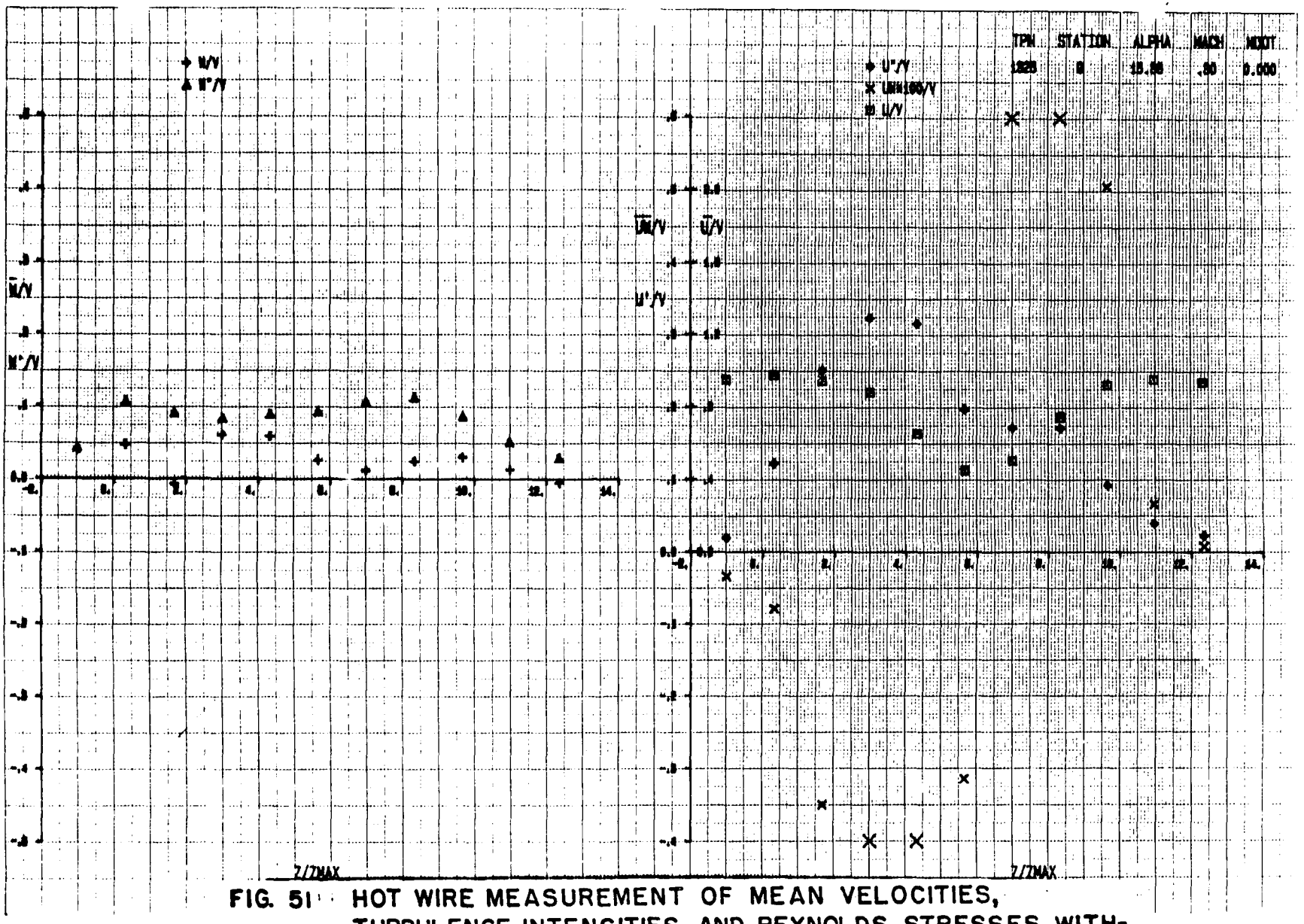

FIG. 51 HOT WIRE MEASUREMENT OF MEAN VELOCITIES, TURBULENCE INTENSITIES, AND REYNOLDS STRESSES WITHOUT BLOWING - NO CANARD - TGF - $\alpha = 16°$ STATION Q

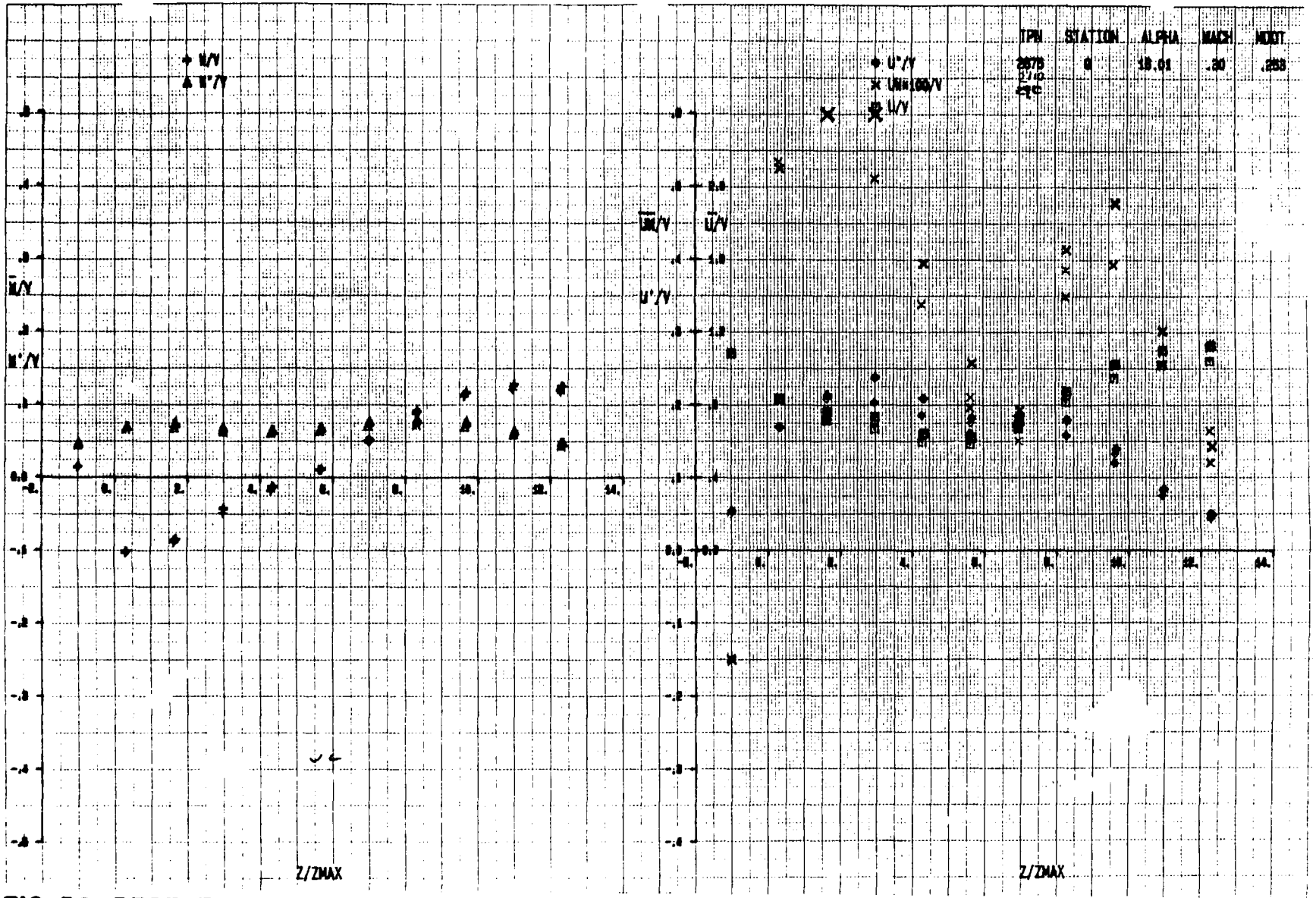

FIG 52 REPEATED HOT WIRE MEASUREMENTS OF MEAN VELOCITIES, TURBULENCE INTENSITIES AND REYNOLDS STRESSES WITH BLOWING - NO CANARD - TGF - α = 16° STATION Q

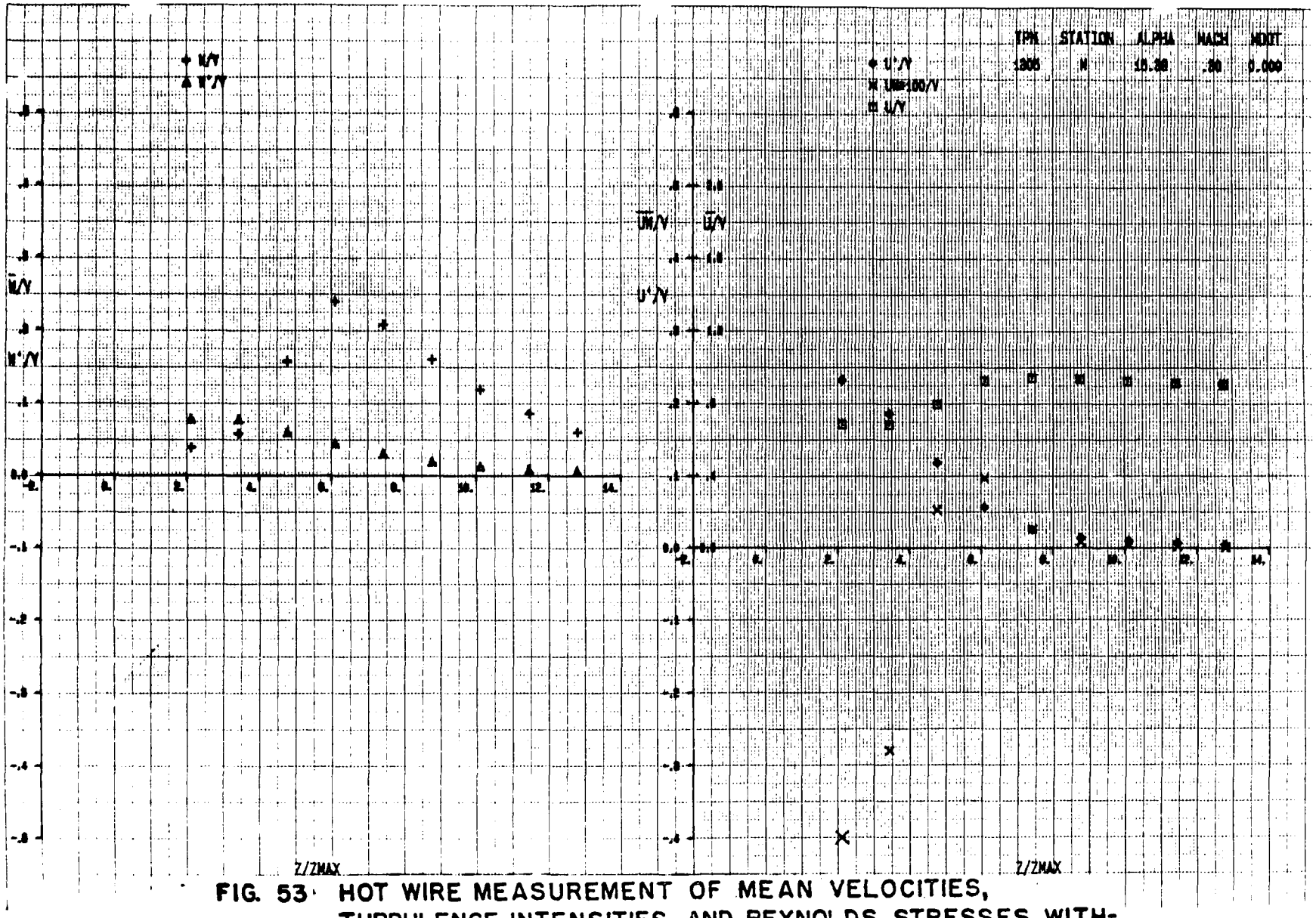

FIG. 53 HOT WIRE MEASUREMENT OF MEAN VELOCITIES, TURBULENCE INTENSITIES, AND REYNOLDS STRESSES WITHOUT BLOWING - NO CANARD - TGF - $\alpha = 16°$ STATION M

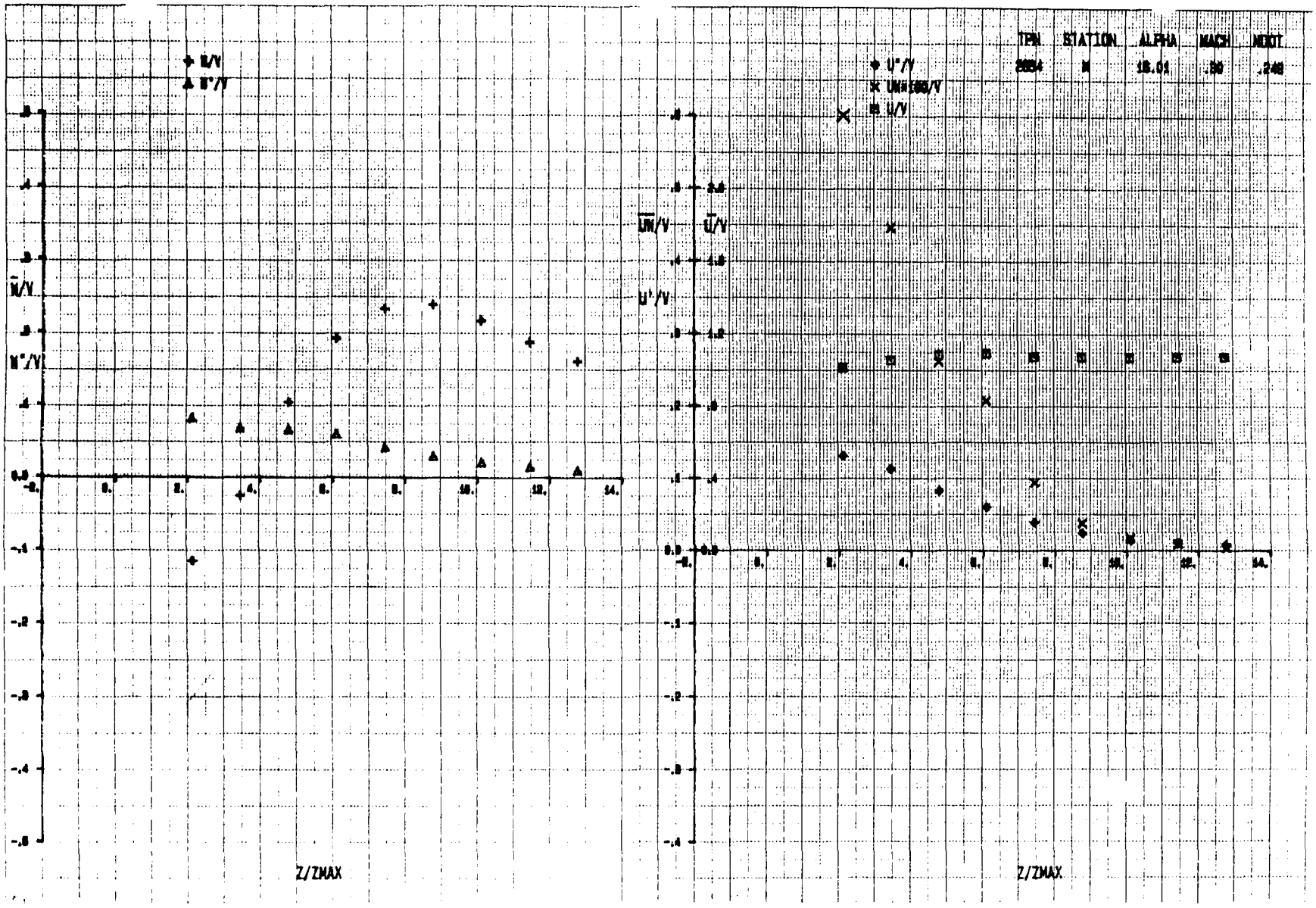

FIG. 54 HOT WIRE MEASUREMENT OF MEAN VELOCITIES, TURBULENCE INTENSITIES, AND REYNOLDS STRESSES WITH BLOWING - NO CANARD - TGF - $\alpha = 16°$ STATION M

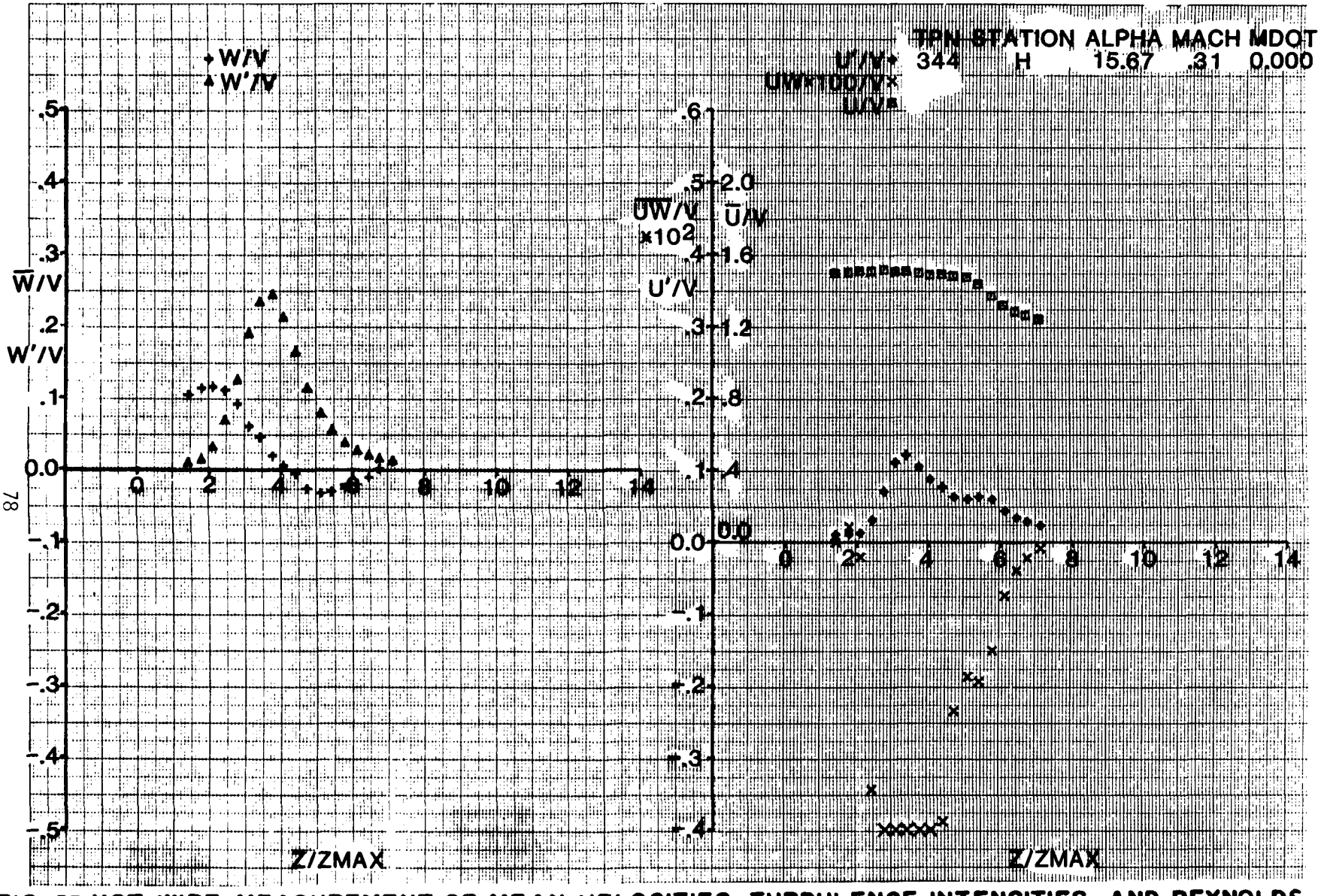

FIG. 55.HOT WIRE MEASUREMENT OF MEAN VELOCITIES, TURBULENCE INTENSITIES, AND REYNOLDS STRESSES WITHOUT BLOWING - COPLANAR CANARD - TGF - α = 16° STATION H

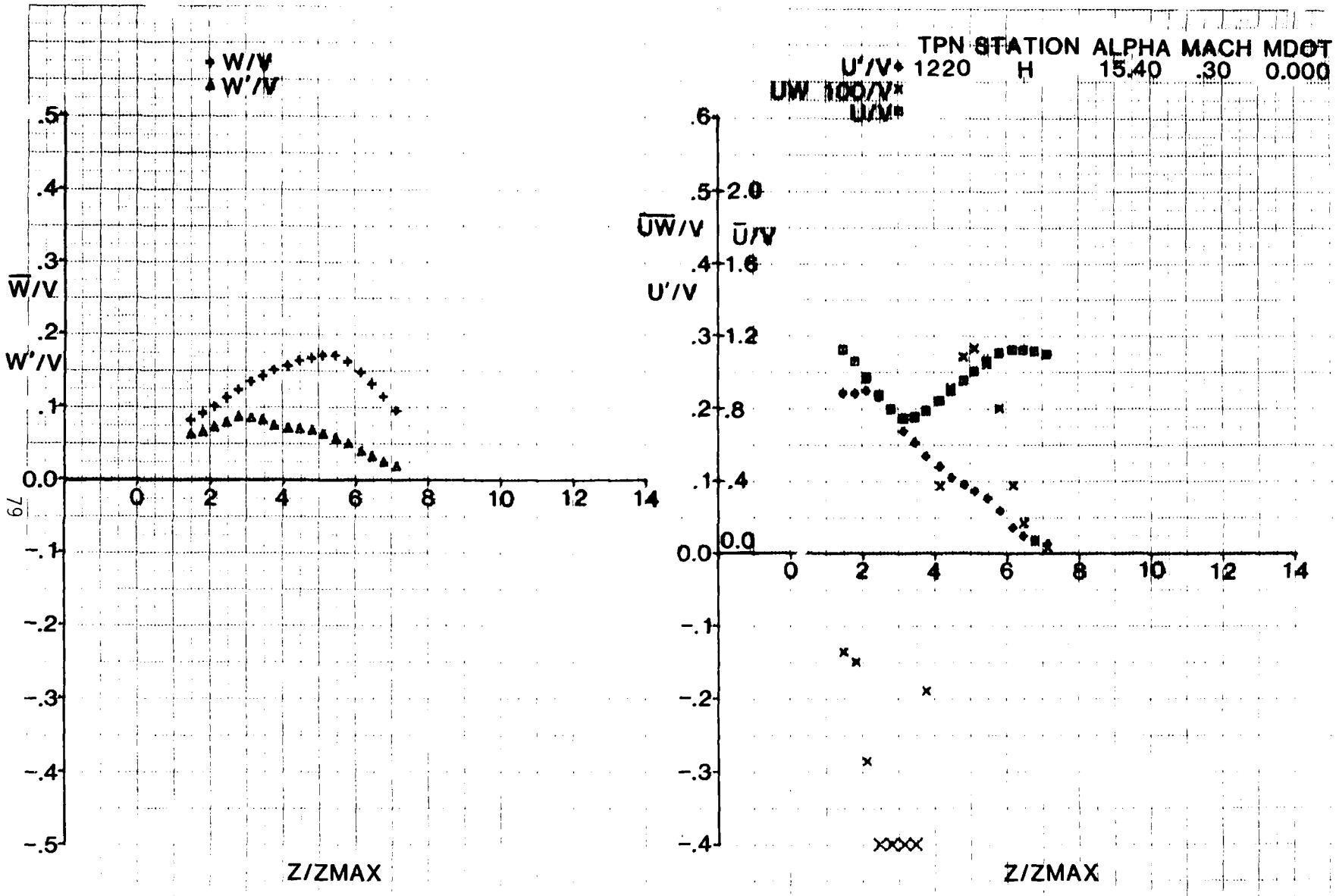

FIG.56.HOT WIRE MEASUREMENT OF MEAN VELOCITIES, TURBULENCE INTENSITIES, AND REYNOLDS STRESSES WITHOUT BLOWING - NO CANARD - TGF - $\alpha = 16°$ STATION H

AD-A179 718 VORTEX INTERACTION ON A CANARD-WING CONFIGURATION(U) 2/3
AIR FORCE WRIGHT AERONAUTICAL LABS WRIGHT-PATTERSON AFB
OH W CALARESE OCT 86 AFWAL-TR-86-3100

UNCLASSIFIED F/G 1/1 NL

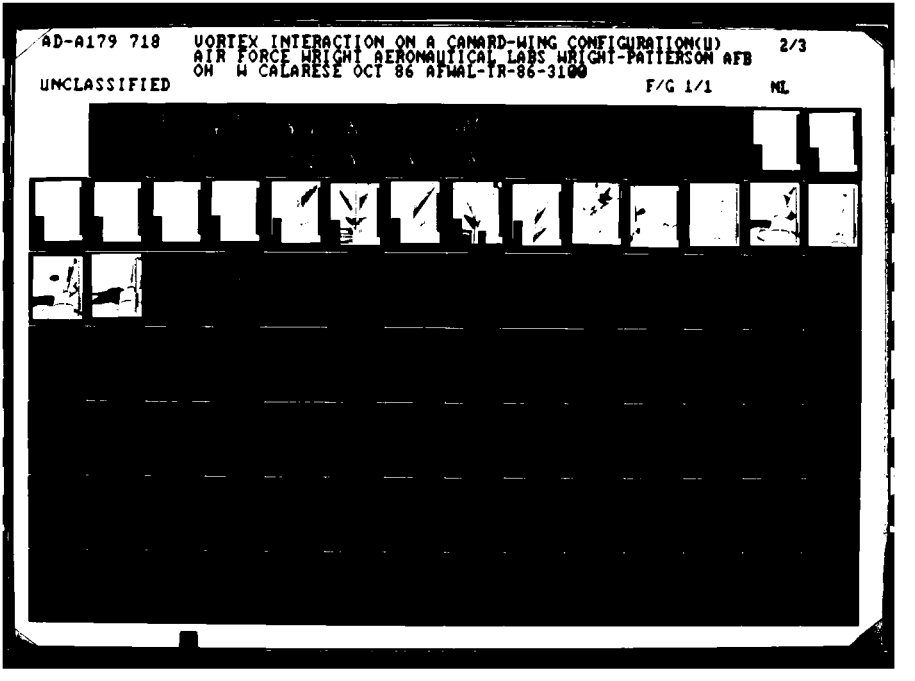

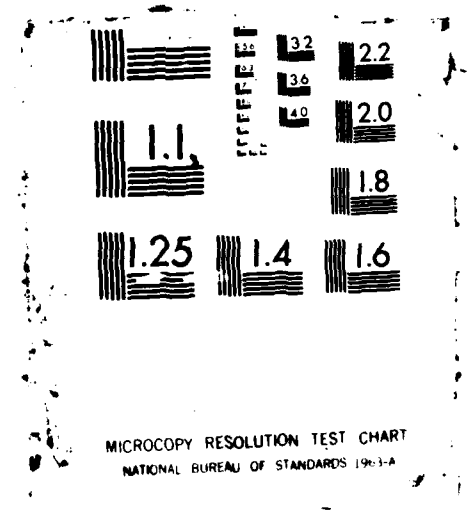
3.2
3.6
4.0
2.2
2.0
1.8
1.1
1.25
1.4
1.6
MICROCOPY RESOLUTION TEST CHART
NATIONAL BUREAU OF STANDARDS 1963-A

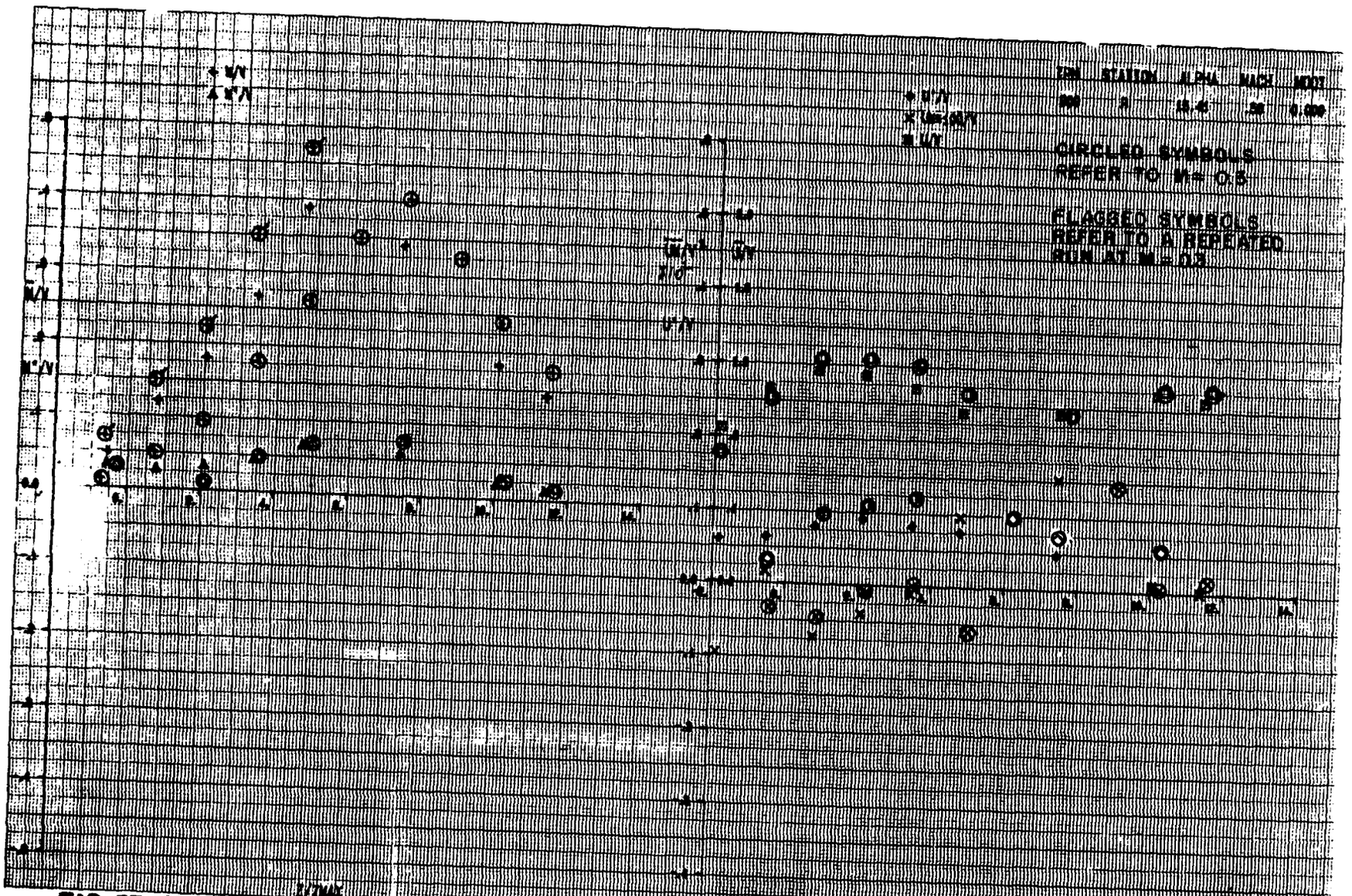

FIG. 57 MACH NUMBER EFFECT ON HOT WIRE MEASUREMENTS OF MEAN VELOCITIES, TURBULENCE INTENSITIES, AND REYNOLDS STRESSES WITHOUT BLOWING - COPLANAR CANARD - TGF - $\alpha = 16°$ - STATION R

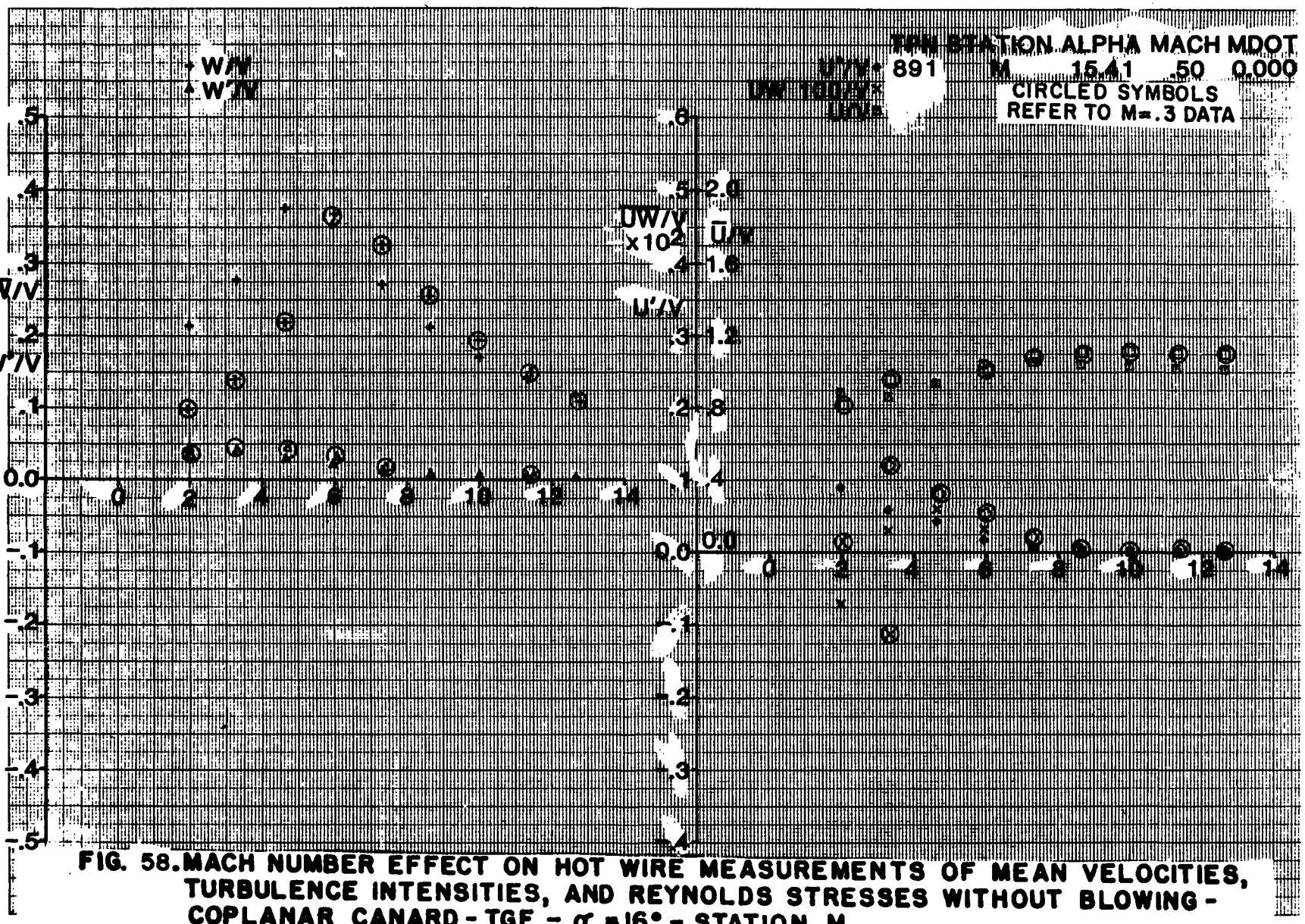

FIG. 58. MACH NUMBER EFFECT ON HOT WIRE MEASUREMENTS OF MEAN VELOCITIES, TURBULENCE INTENSITIES, AND REYNOLDS STRESSES WITHOUT BLOWING - COPLANAR CANARD - TGF - α = 16° - STATION M

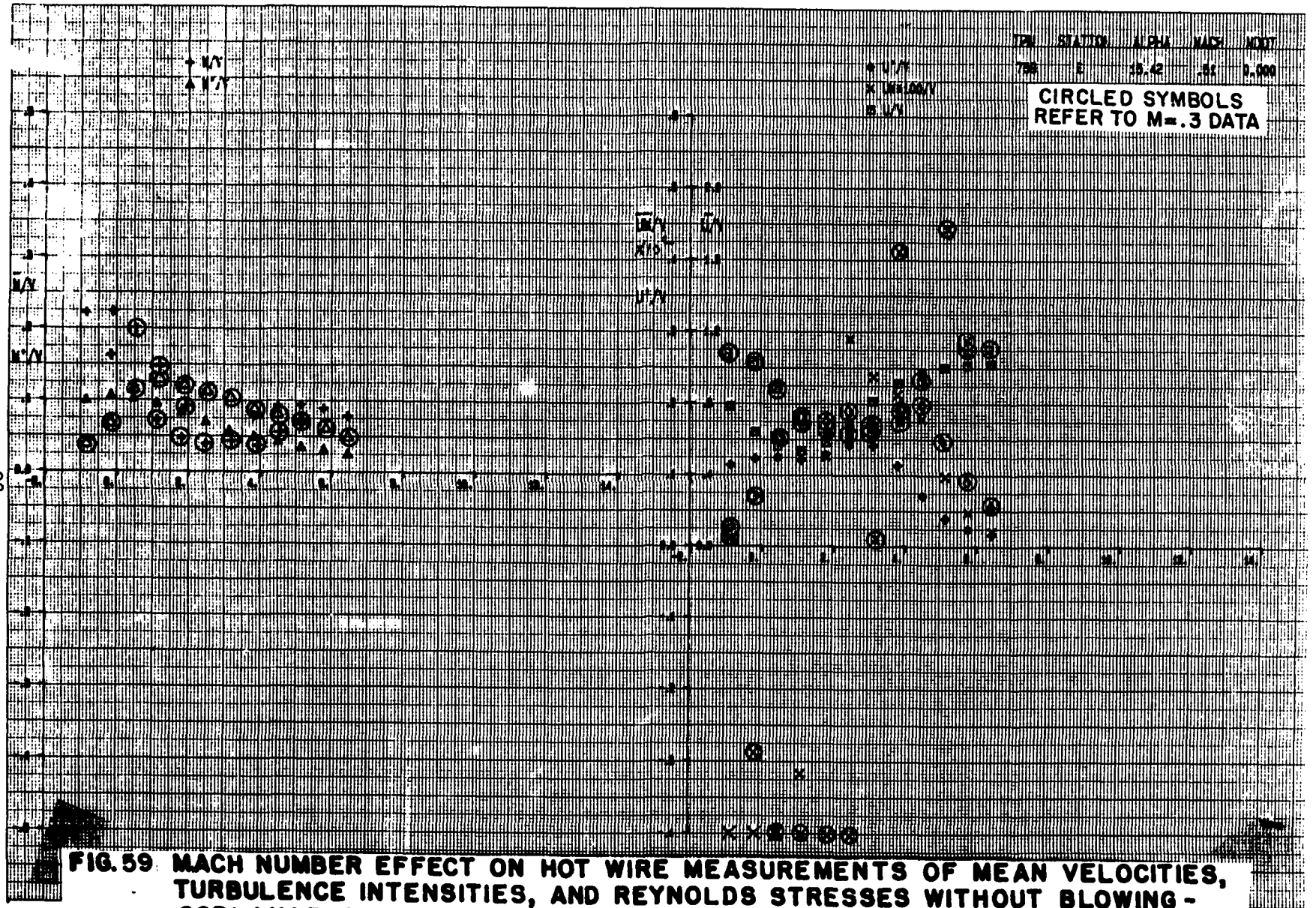

FIG. 59 MACH NUMBER EFFECT ON HOT WIRE MEASUREMENTS OF MEAN VELOCITIES, TURBULENCE INTENSITIES, AND REYNOLDS STRESSES WITHOUT BLOWING - COPLANAR CANARD - TGF - $\alpha = 16°$ - STATION E

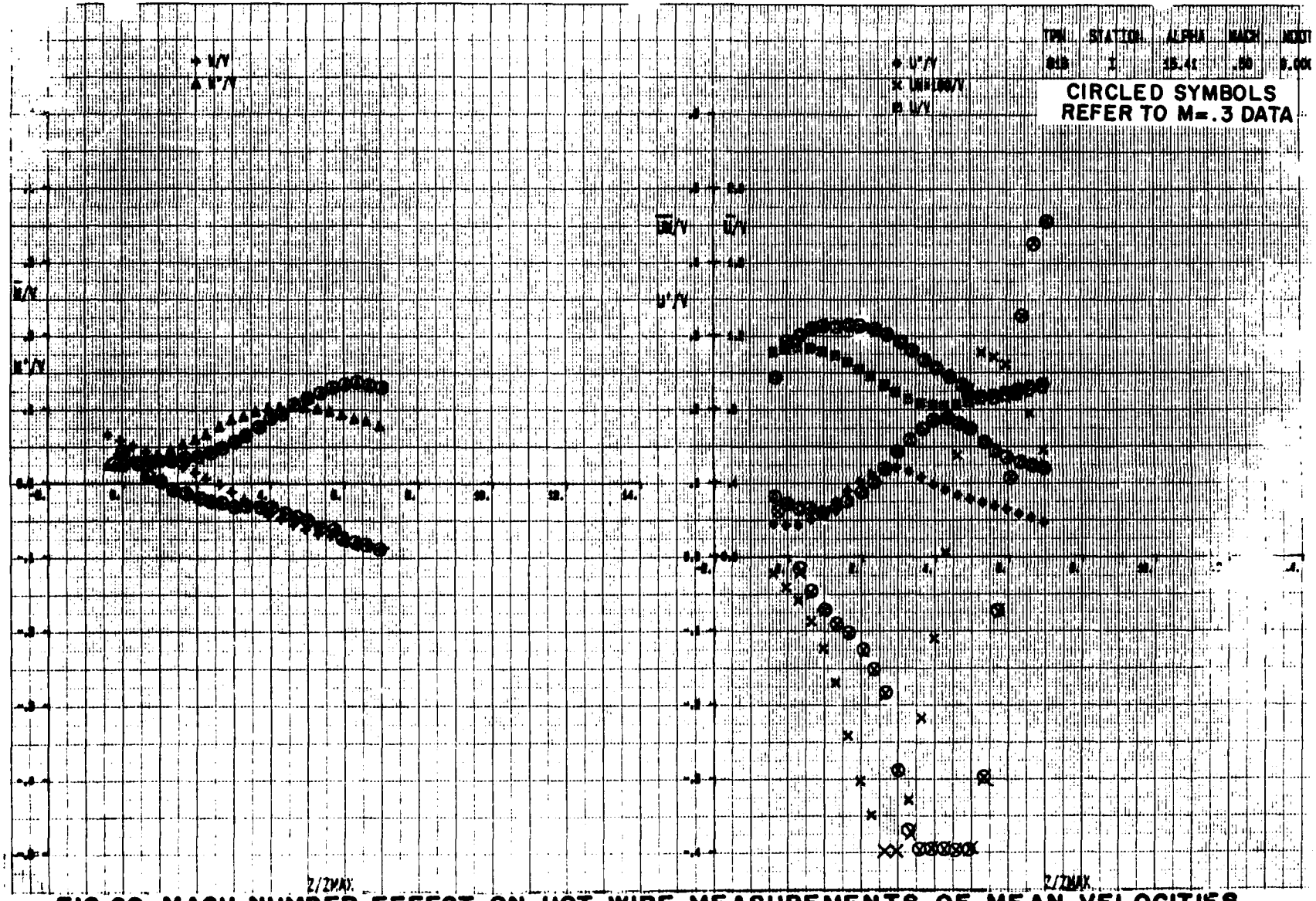

FIG. 60 MACH NUMBER EFFECT ON HOT WIRE MEASUREMENTS OF MEAN VELOCITIES, TURBULENCE INTENSITIES, AND REYNOLDS STRESSES WITHOUT BLOWING - COPLANAR CANARD - TGF - $\alpha = 16°$ - STATION I

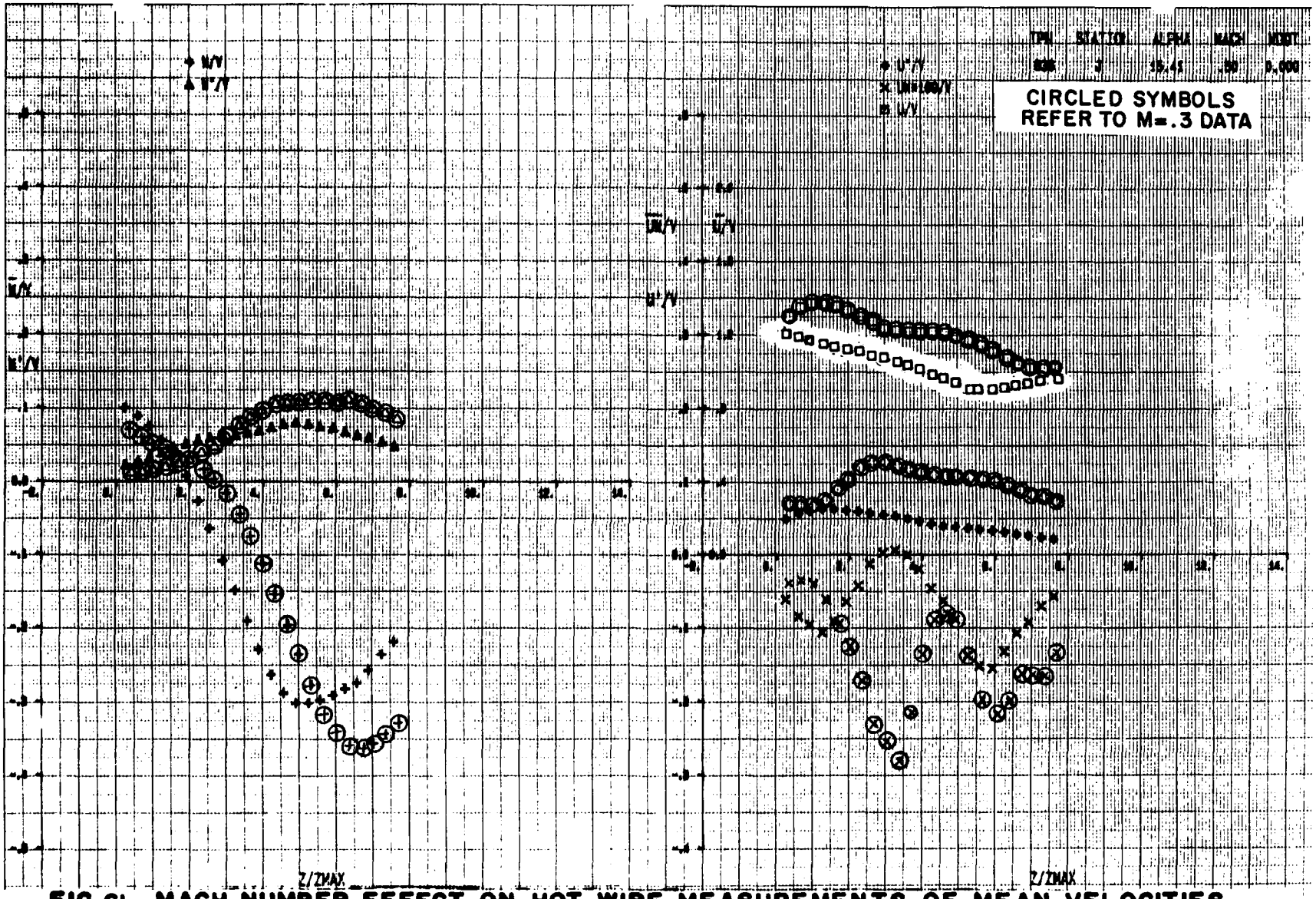

FIG. 61 MACH NUMBER EFFECT ON HOT WIRE MEASUREMENTS OF MEAN VELOCITIES, TURBULENCE INTENSITIES, AND REYNOLDS STRESSES WITHOUT BLOWING - COPLANAR CANARD - TGF - $\alpha = 16°$ - STATION J

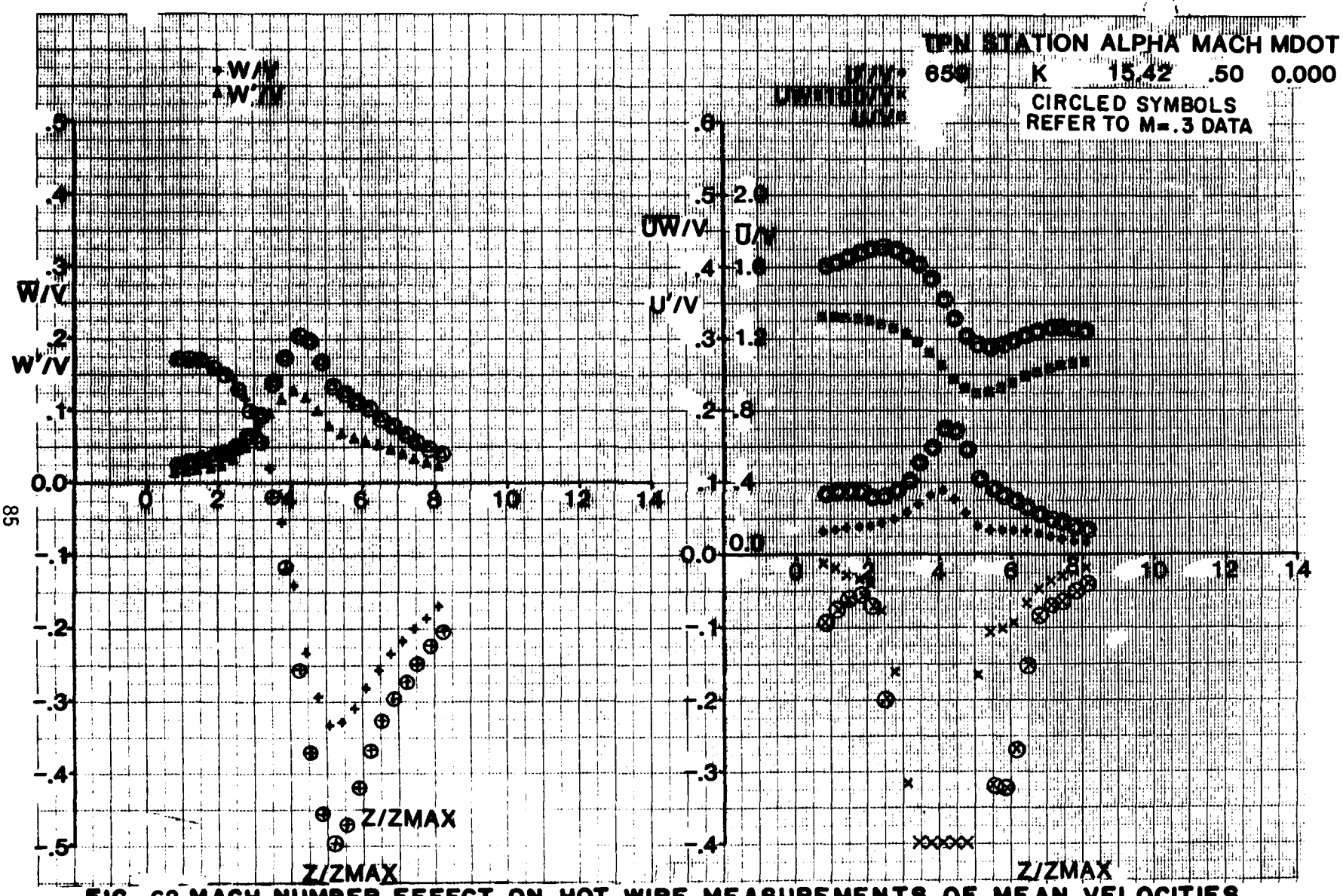

FIG. 62. MACH NUMBER EFFECT ON HOT WIRE MEASUREMENTS OF MEAN VELOCITIES, TURBULENCE INTENSITIES, AND REYNOLDS STRESSES WITHOUT BLOWING - COPLANAR CANARD - TGF - α = 16° - STATION K

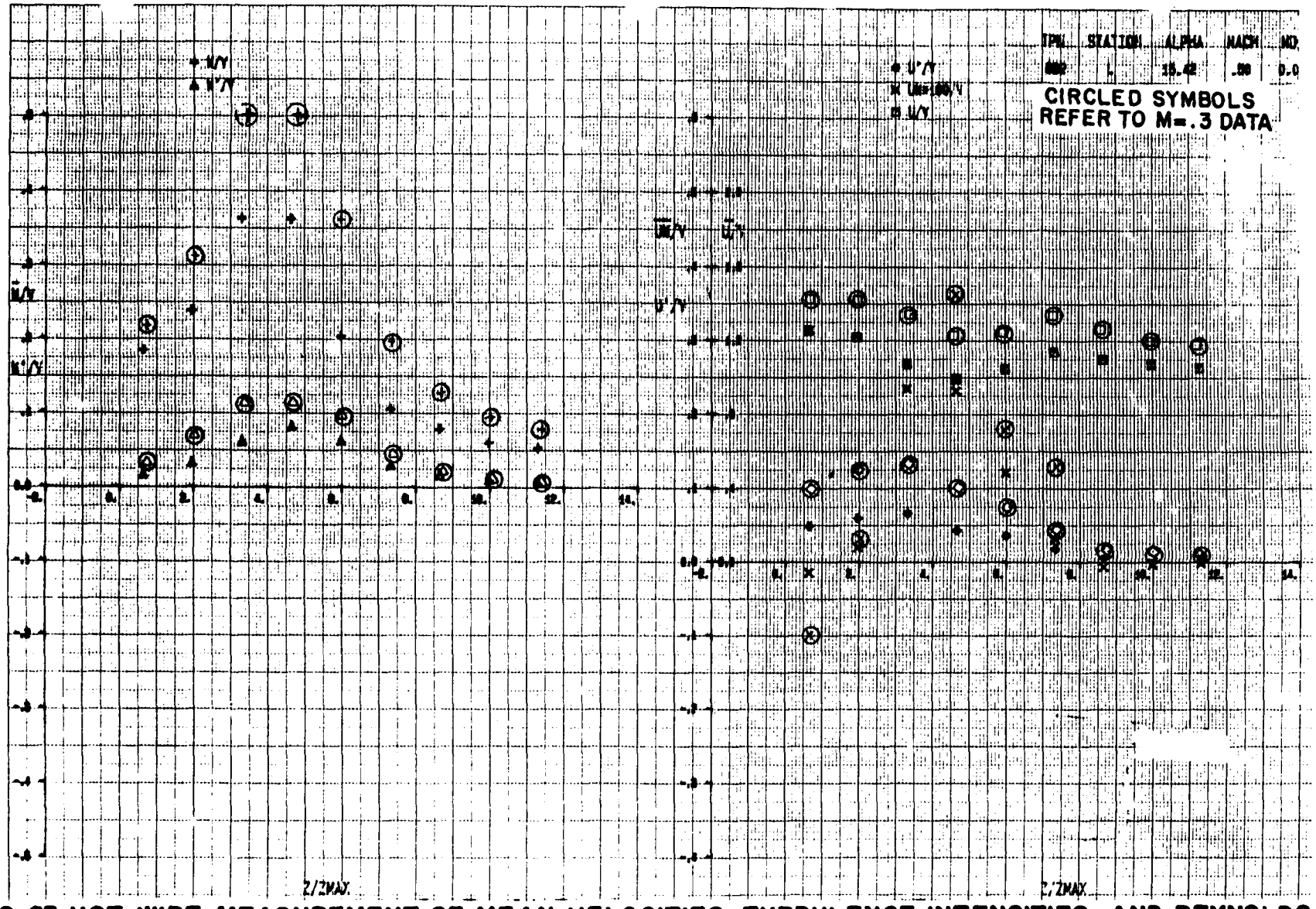

FIG. 63 HOT WIRE MEASUREMENT OF MEAN VELOCITIES, TURBULENCE INTENSITIES, AND REYNOLDS STRESSES WITHOUT BLOWING - COPLANAR CANARD - TGF - $\alpha = 16°$ STATION L

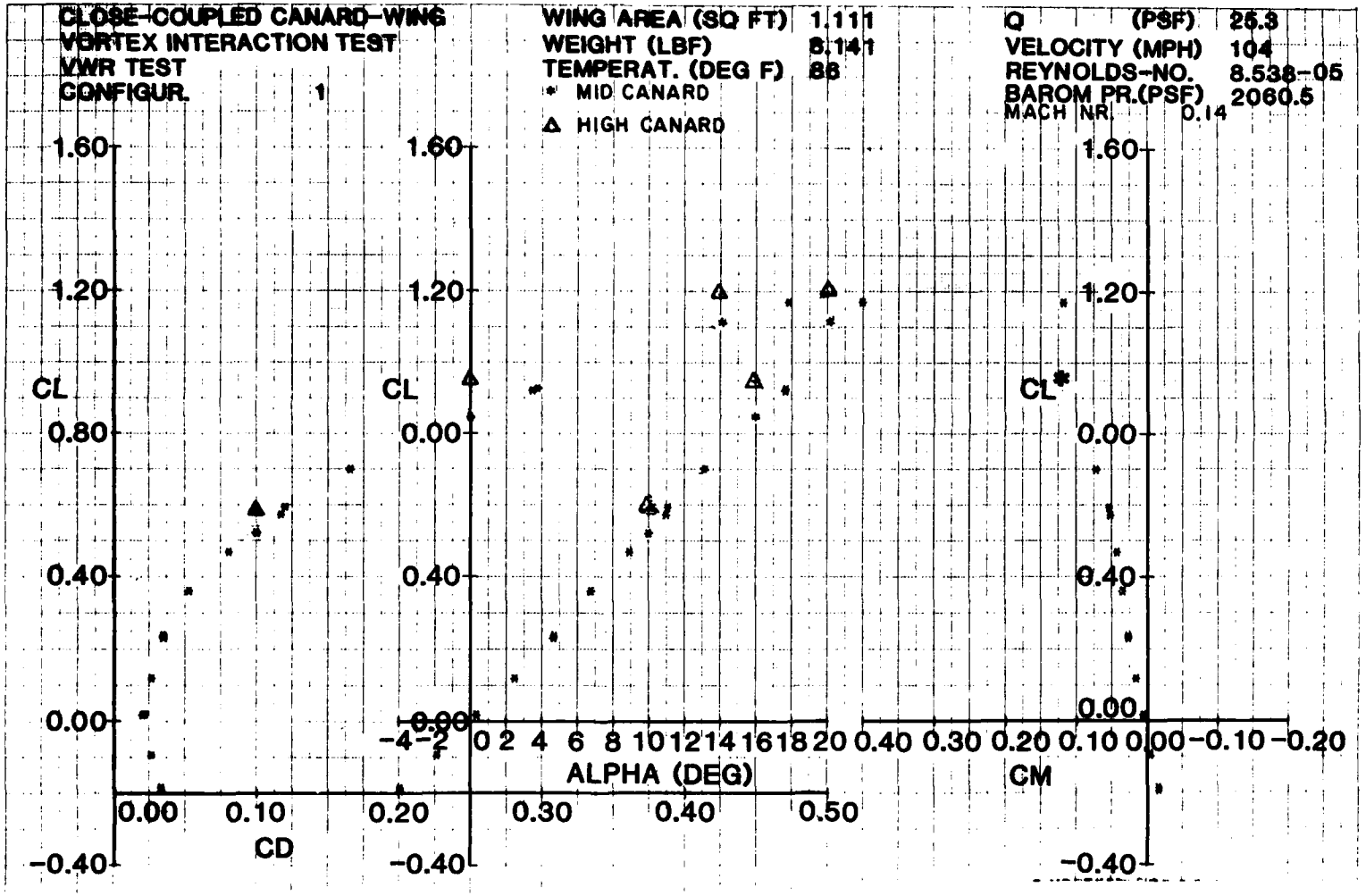

FIG. 64. COMPARISON OF LIFT COEFFICIENTS AND DRAG POLARS FOR MID AND HIGH CANARD WITHOUT BLOWING - V.W.T.

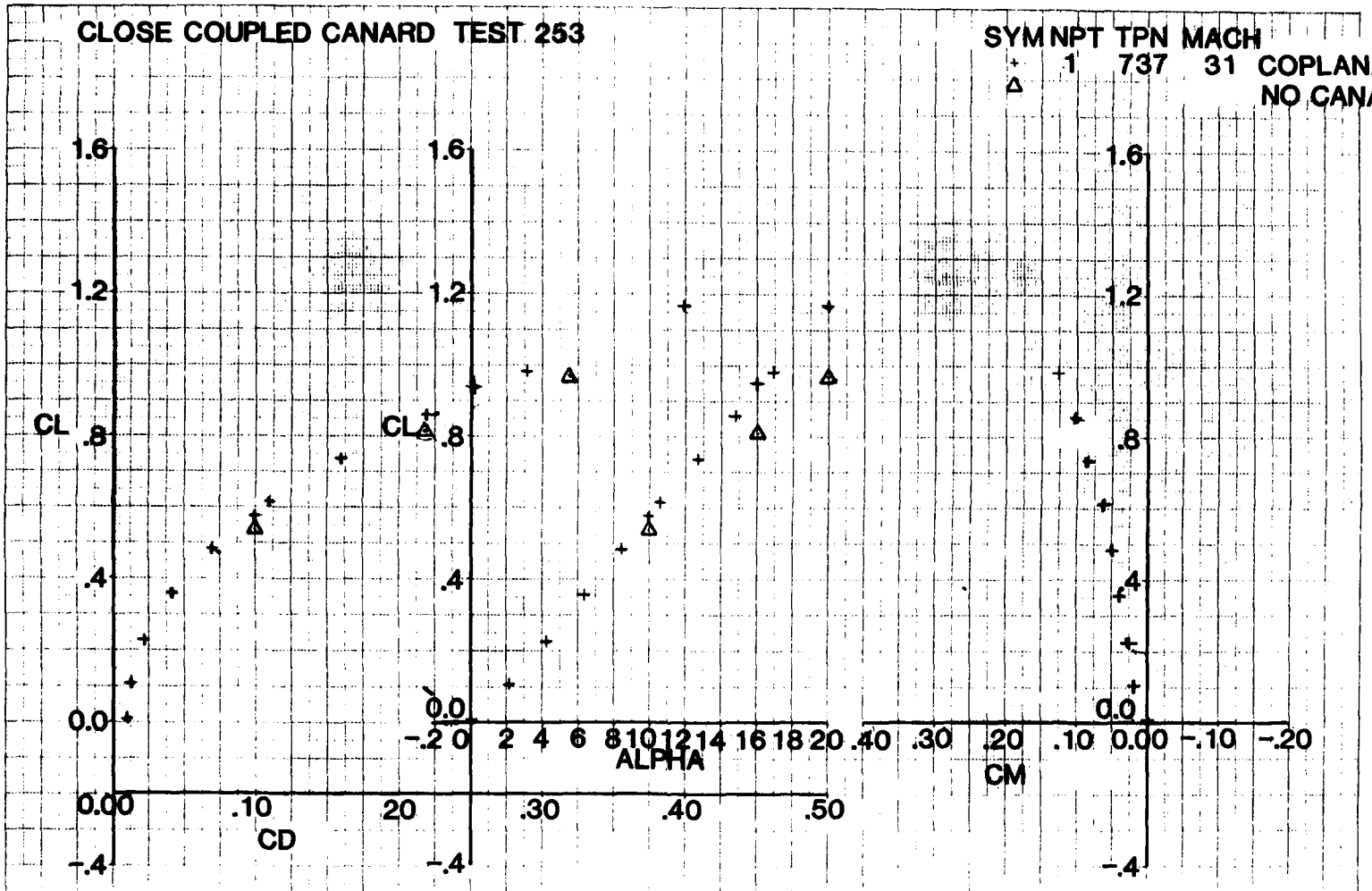

FIG. 65. COMPARISON OF LIFT COEFFICIENTS AND DRAG POLARS OBTAINED WITH THE COPLANAR CANARD AND WITHOUT CANARD - TGF

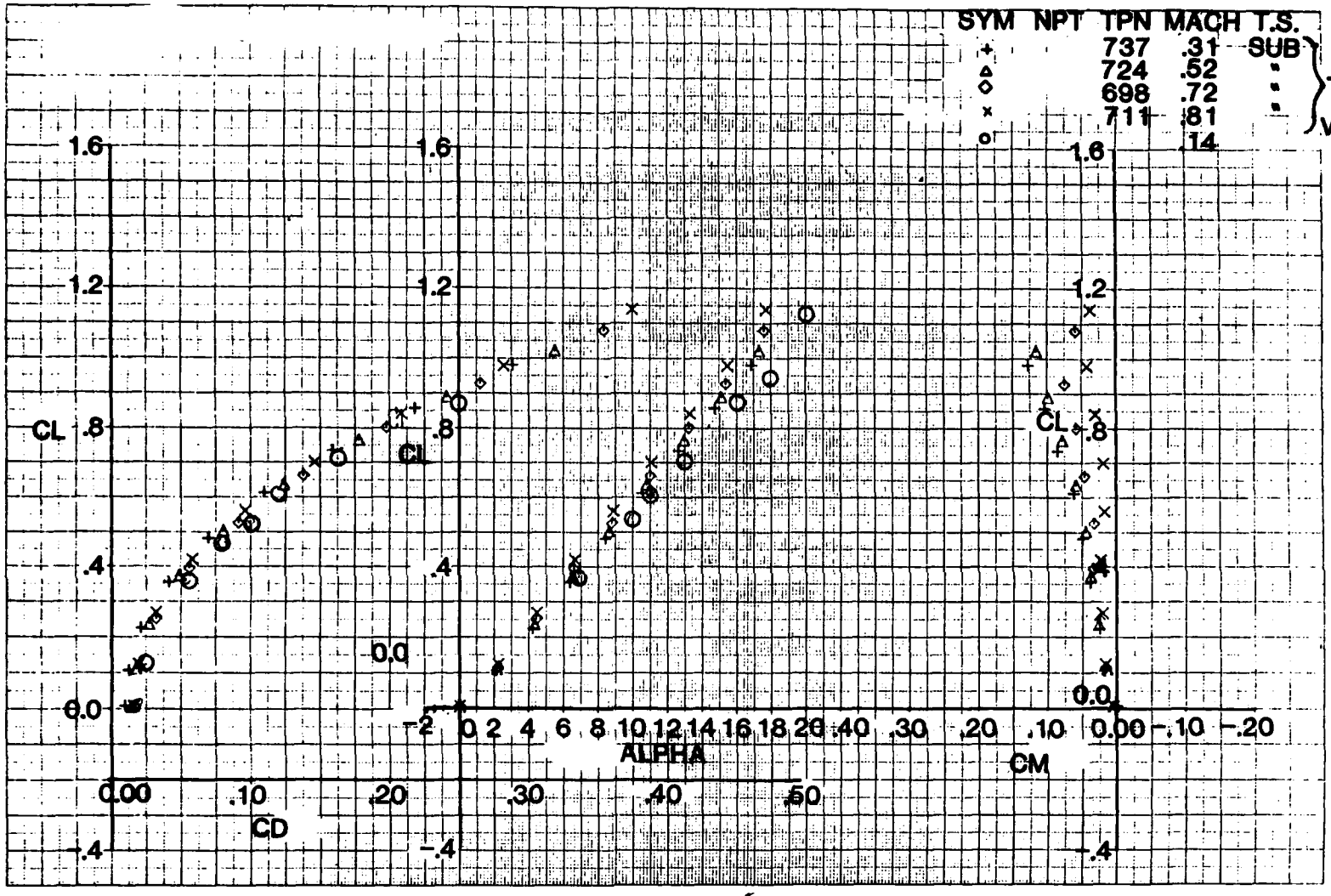

FIG. 66.MACH NUMBER EFFECT ON LIFT COEFFICENTS AND DRAG POLARS WITH THE COPLANAR CANARD - VWT AND TGF

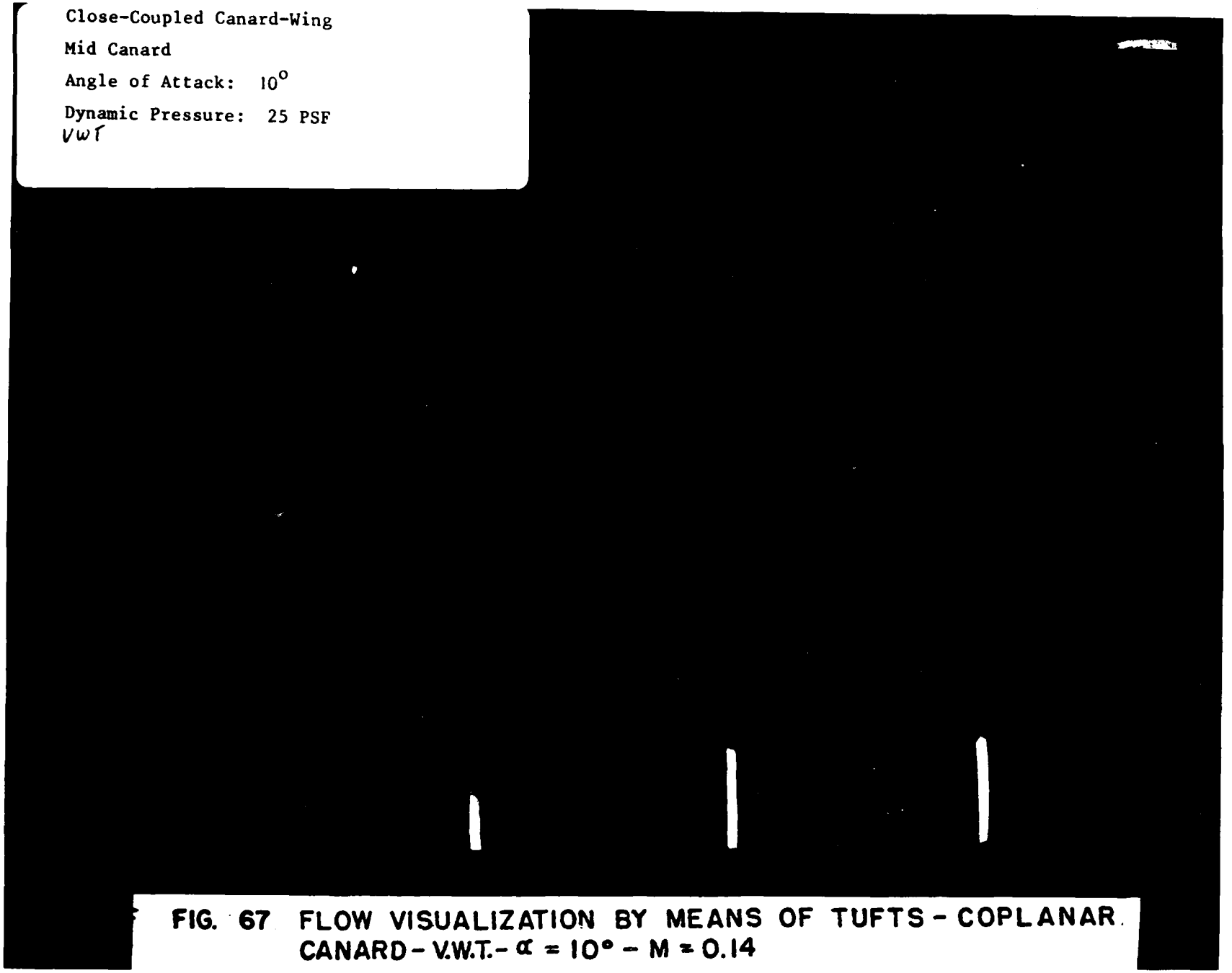

FIG. 67 FLOW VISUALIZATION BY MEANS OF TUFTS - COPLANAR CANARD - V.W.T. - $\alpha = 10° - M = 0.14$

Close-Coupled Canard-Wing
High Canard
Angle of Attack: 10^{o}
Dynamic Pressure: 25 PSF

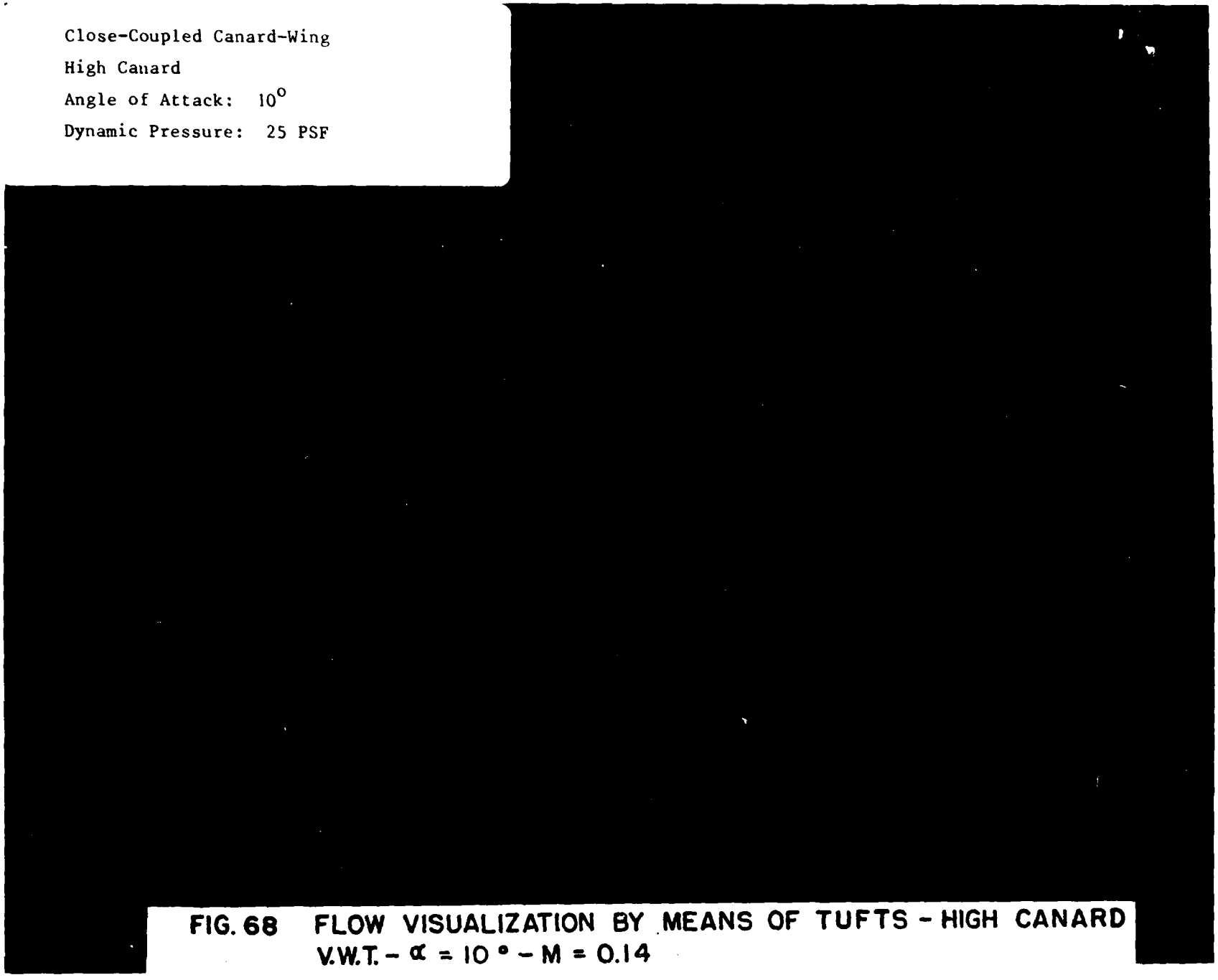

FIG. 68 FLOW VISUALIZATION BY MEANS OF TUFTS - HIGH CANARD
V.W.T. - α = 10° - M = 0.14

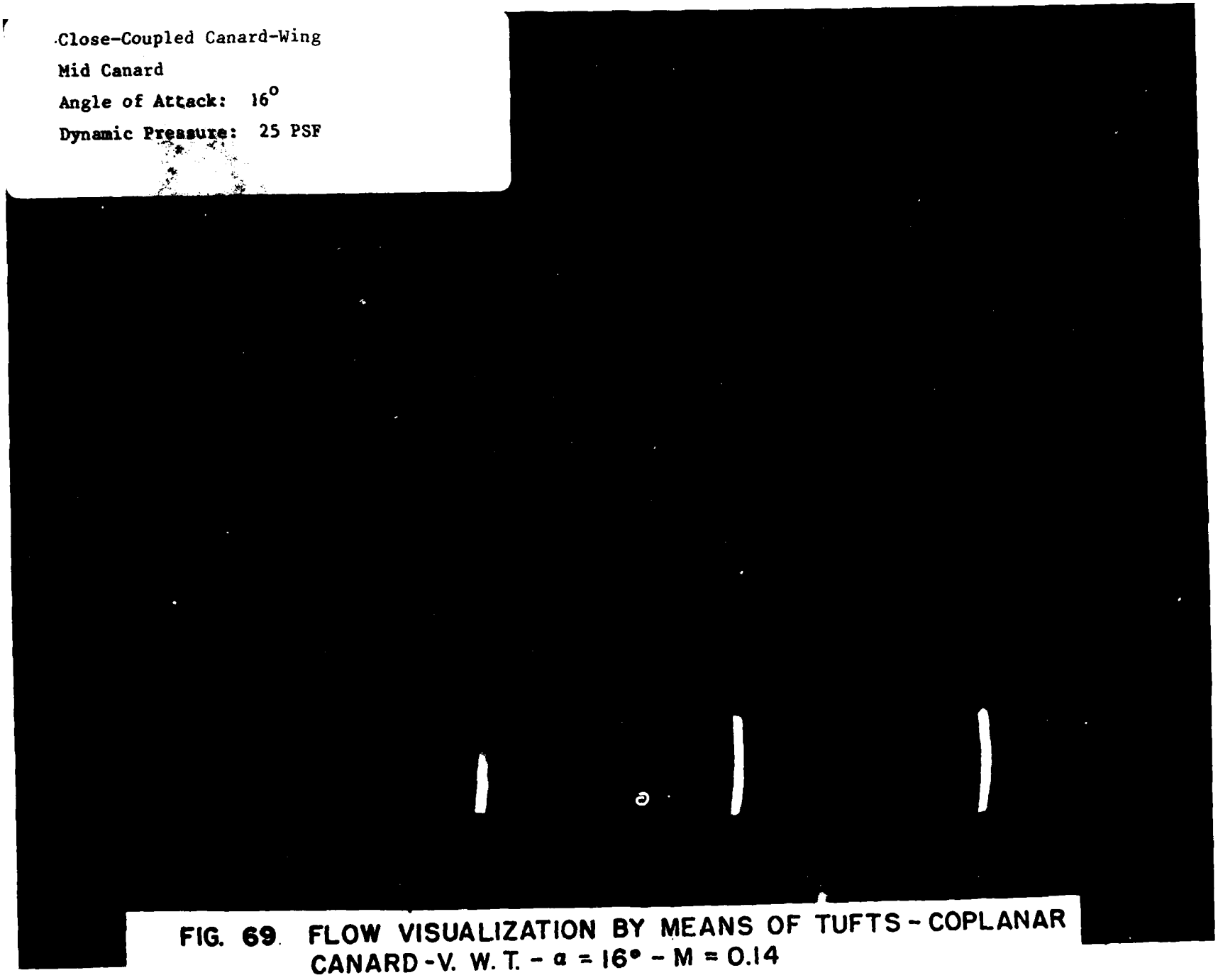

FIG. 69 FLOW VISUALIZATION BY MEANS OF TUFTS - COPLANAR CANARD - V. W. T. - $\alpha = 16°$ - M = 0.14

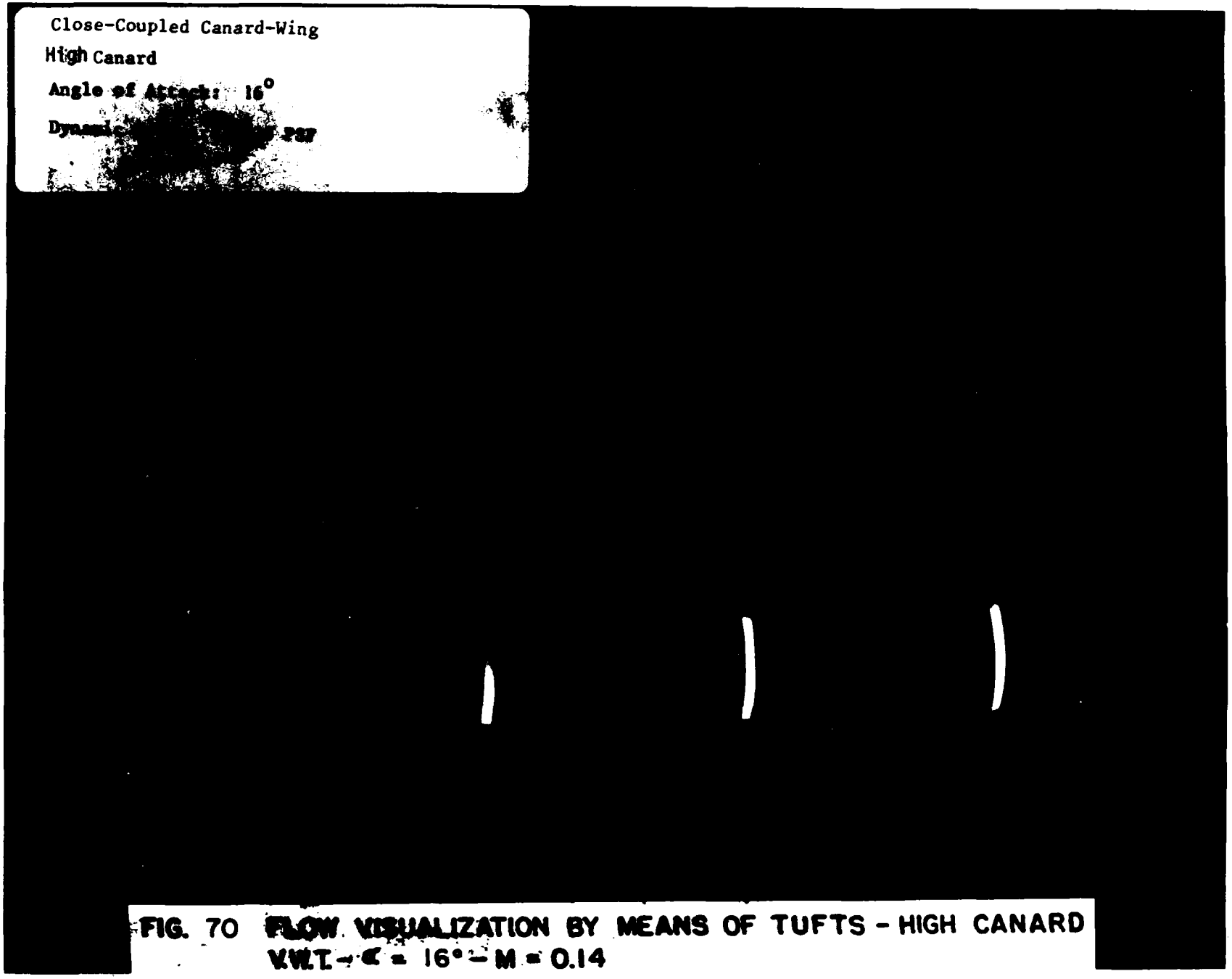

FIG. 70 FLOW VISUALIZATION BY MEANS OF TUFTS - HIGH CANARD
V.W.T. - α = 16° - M = 0.14

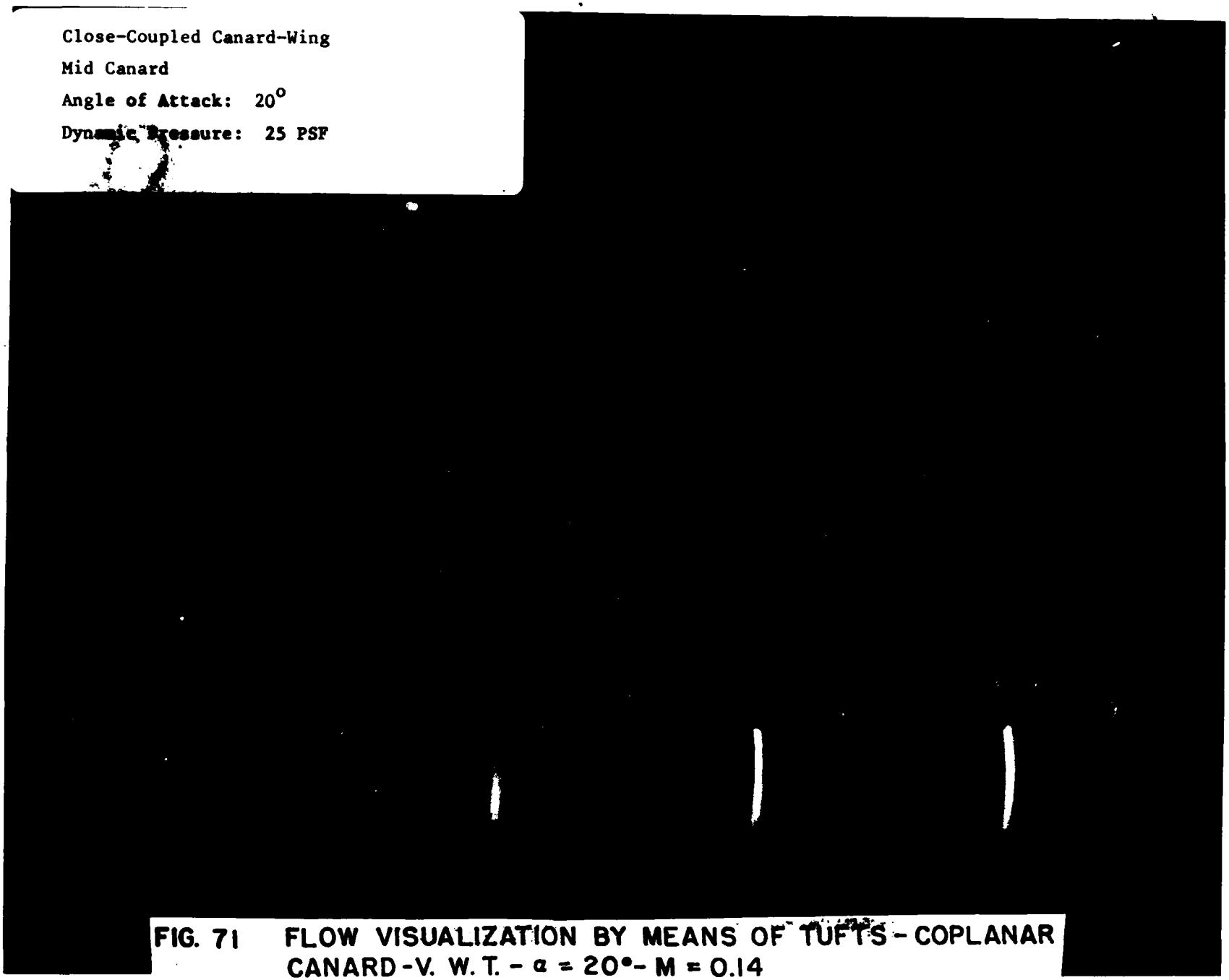

FIG. 71 FLOW VISUALIZATION BY MEANS OF TUFTS - COPLANAR CANARD - V. W. T. - $\alpha = 20°$ - M = 0.14

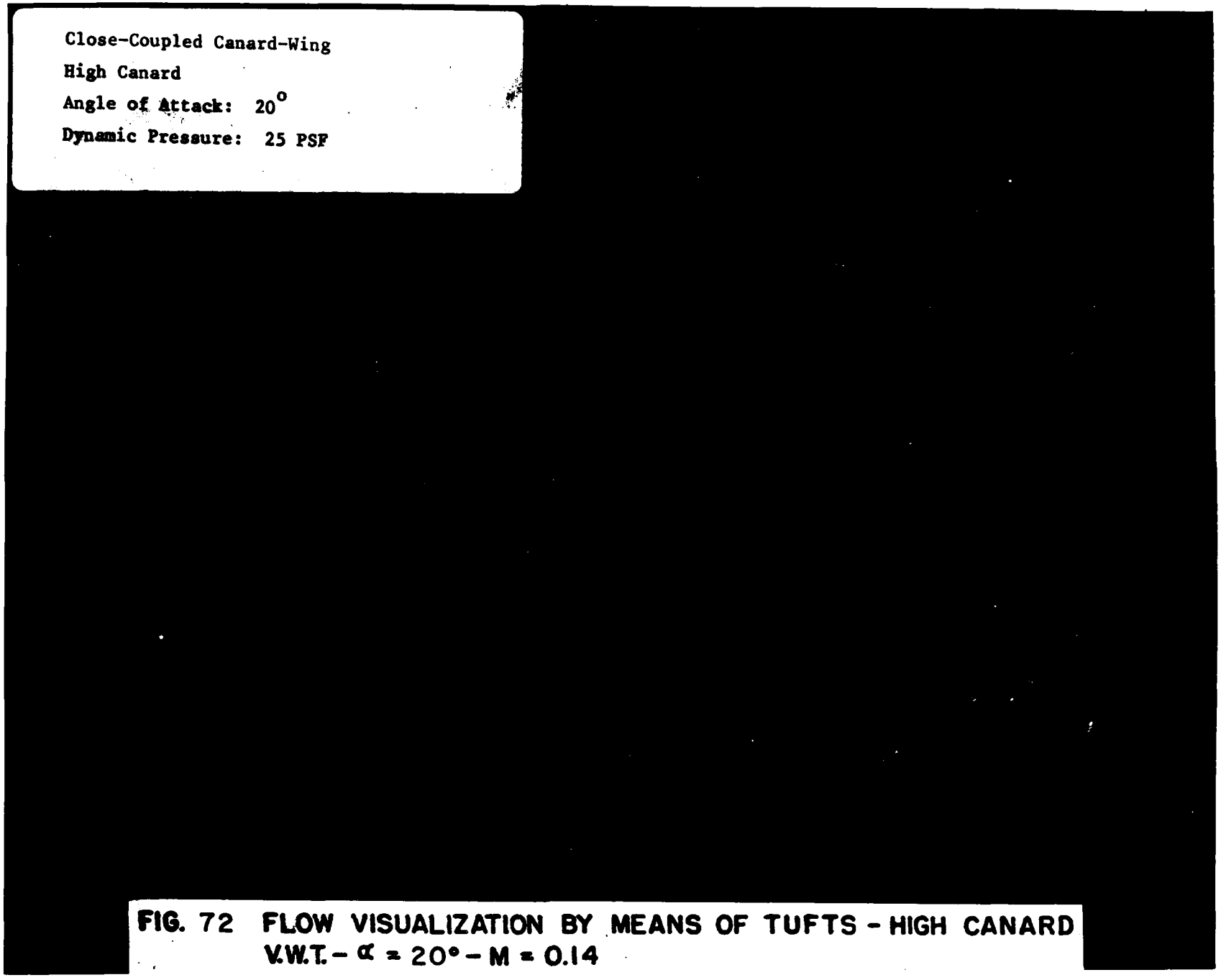

FIG. 72 FLOW VISUALIZATION BY MEANS OF TUFTS - HIGH CANARD
V.W.T. - α = 20° - M = 0.14

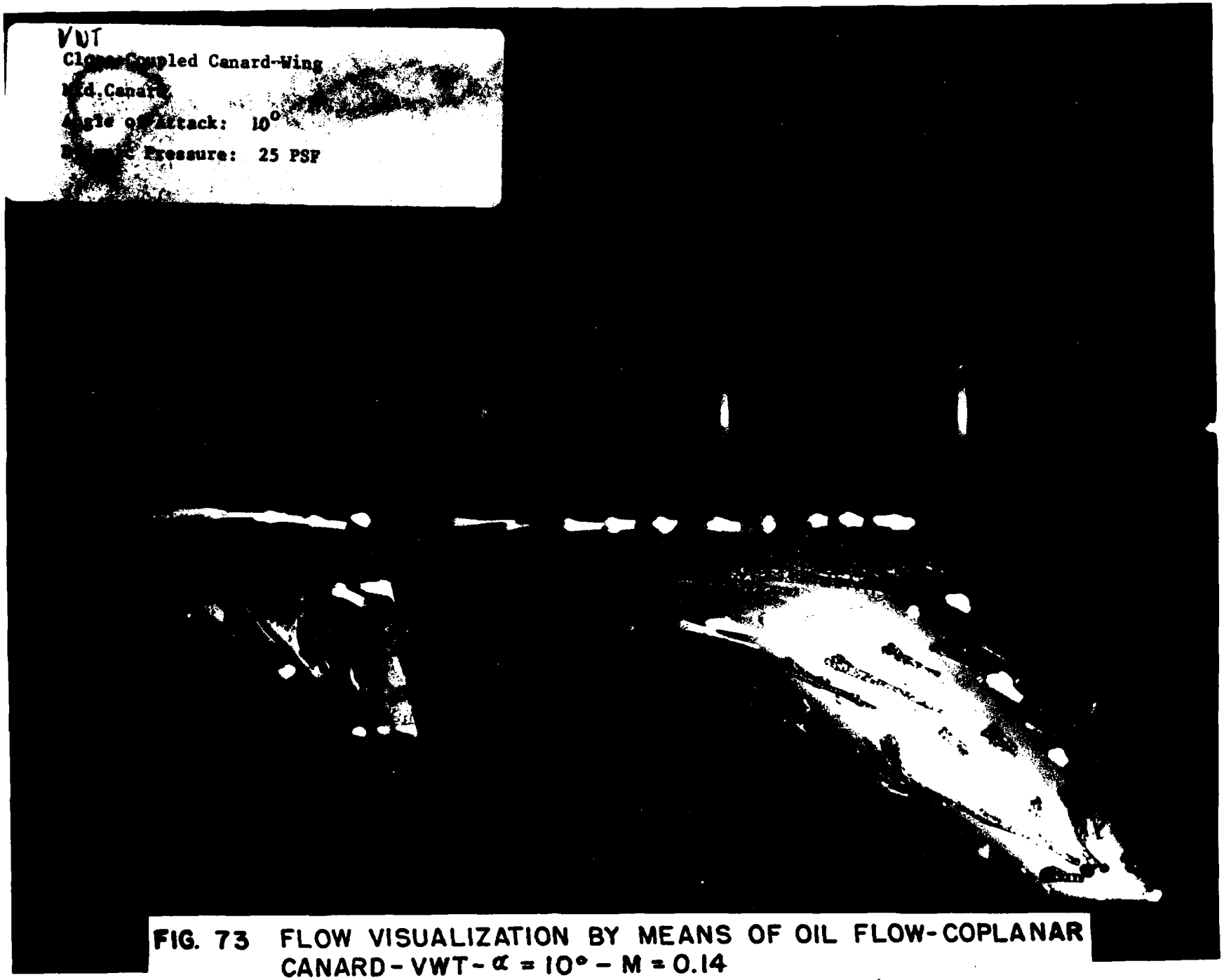

FIG. 73 FLOW VISUALIZATION BY MEANS OF OIL FLOW-COPLANAR CANARD-VWT-$\alpha = 10° - M = 0.14$

Close-Coupled Canard-Wing
High Canard
Angle of Attack: 10^{o}
Dynamic Pressure: 25 PSF

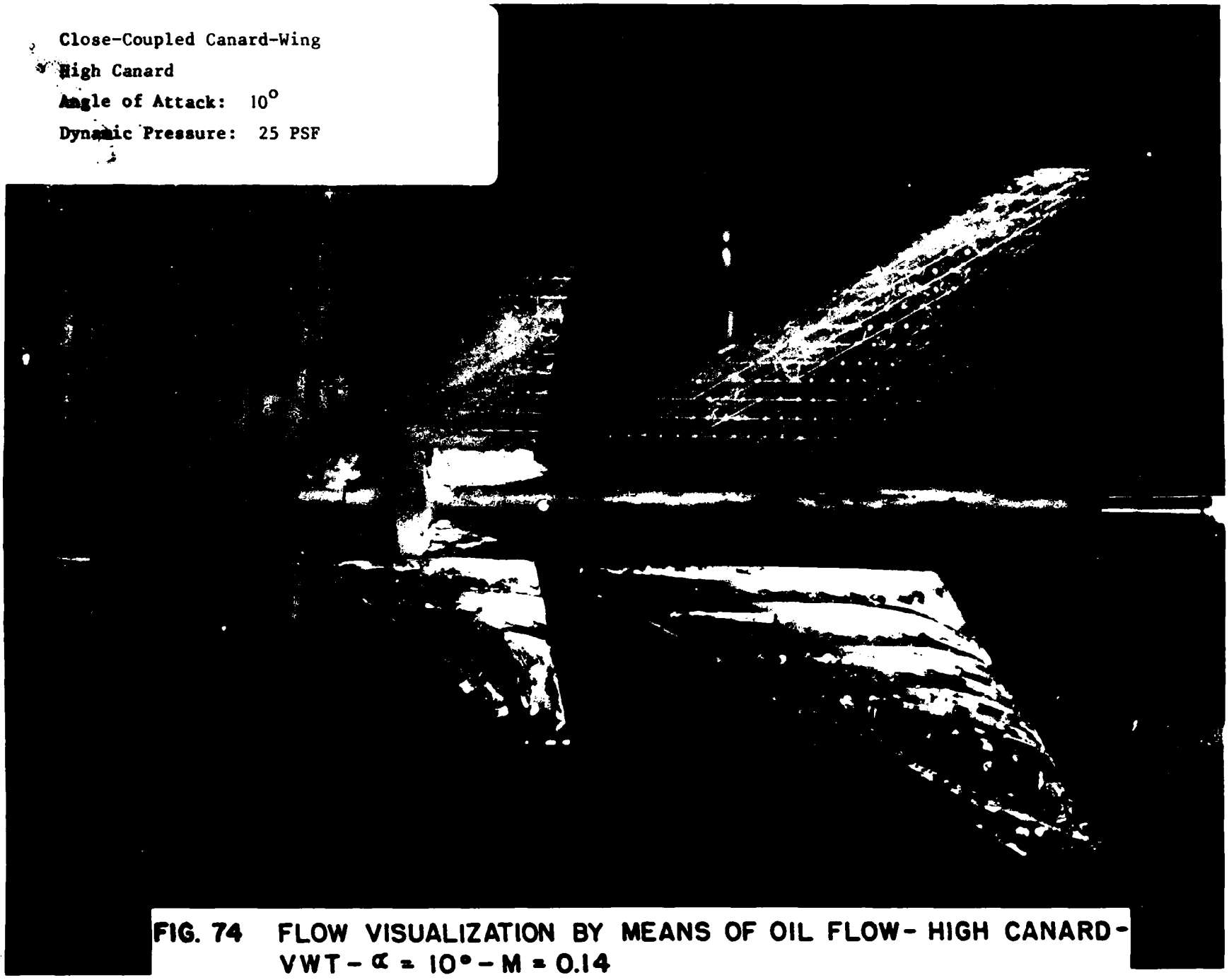

FIG. 74 FLOW VISUALIZATION BY MEANS OF OIL FLOW- HIGH CANARD- VWT - α = 10° - M = 0.14

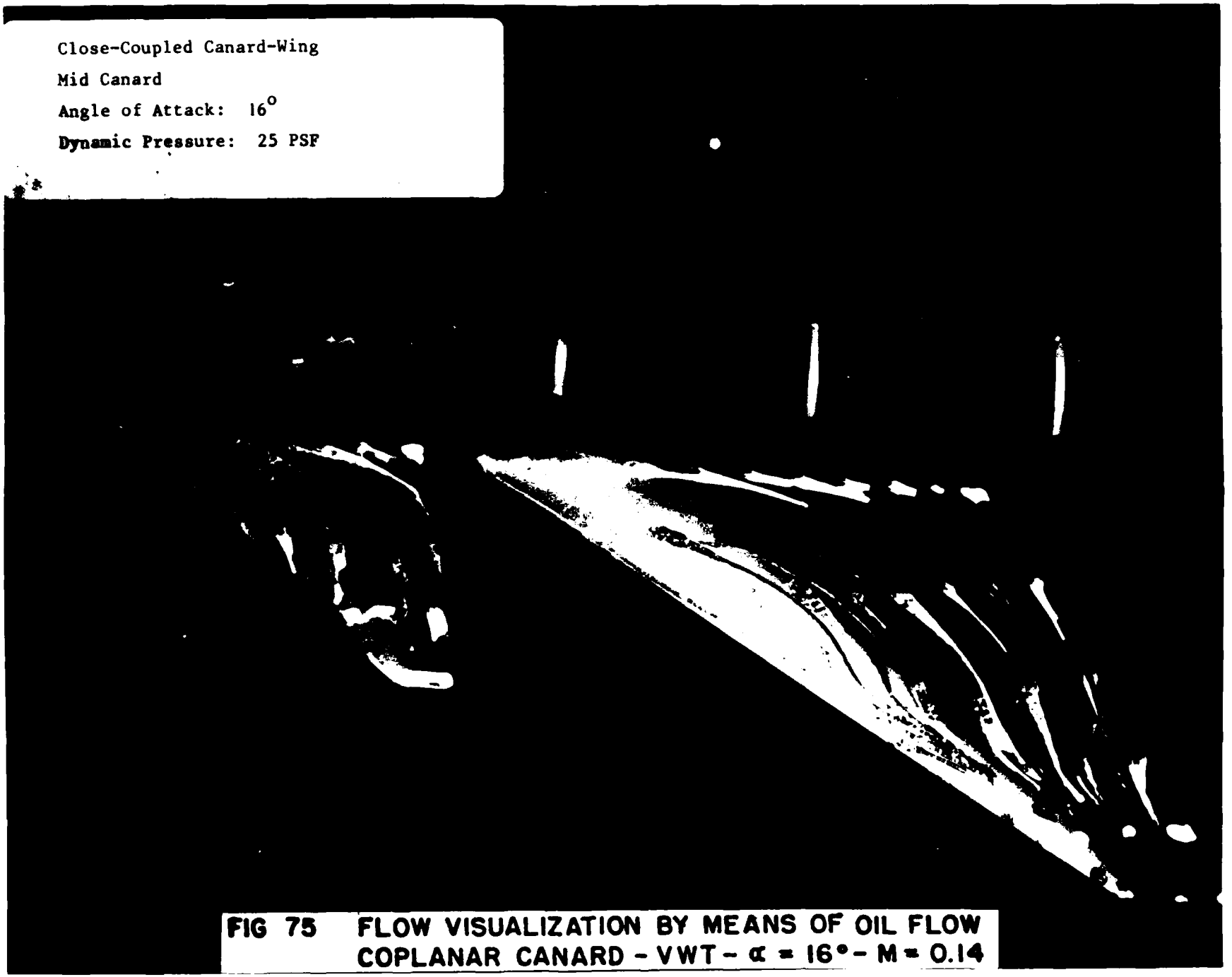

FIG 75 FLOW VISUALIZATION BY MEANS OF OIL FLOW
COPLANAR CANARD - VWT - α = 16° - M = 0.14

Close-Coupled Canard-Wing
High Canard
Angle of Attack: 16^{o}
Dynamic Pressure: 25 PSF

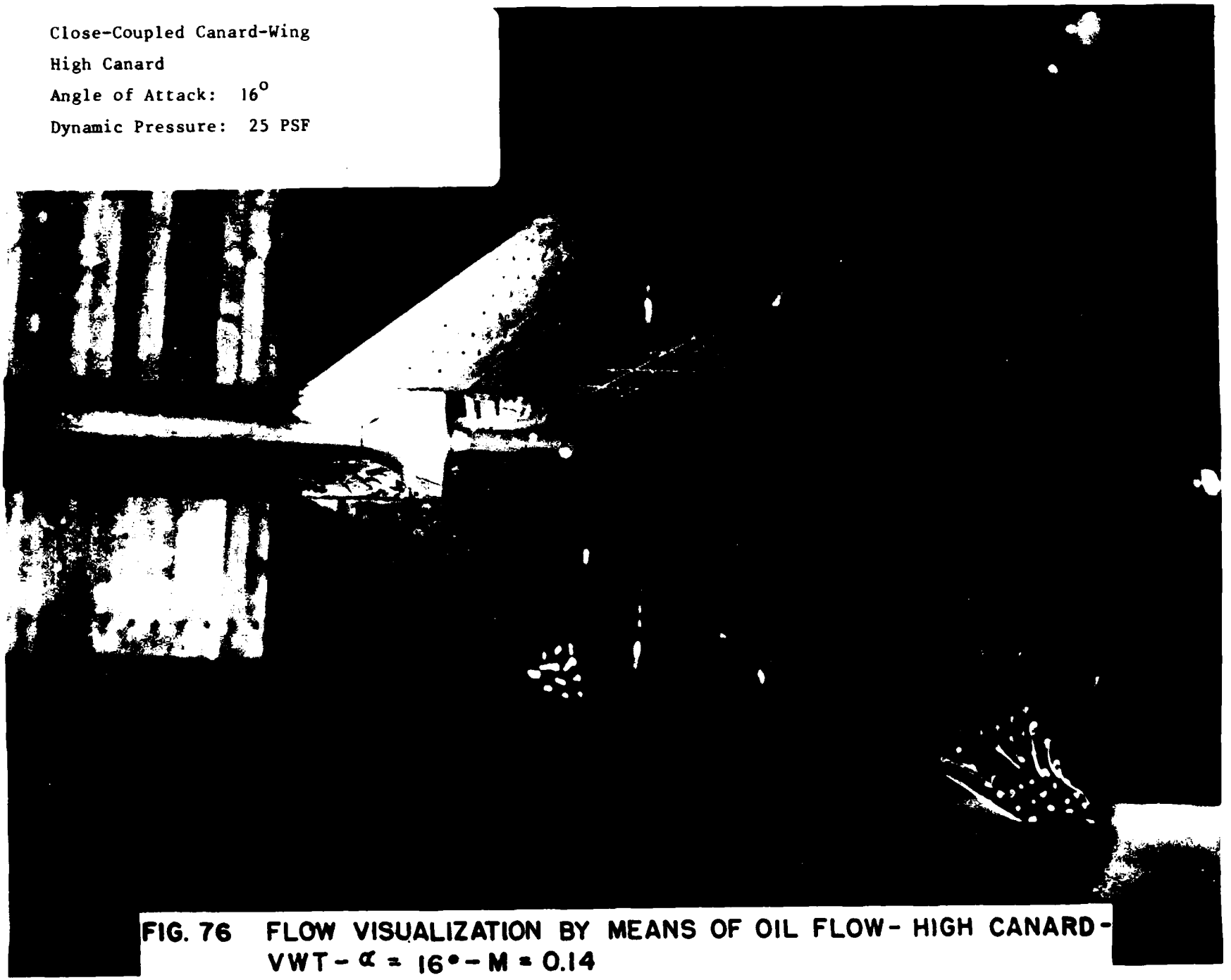

FIG. 76 FLOW VISUALIZATION BY MEANS OF OIL FLOW- HIGH CANARD- VWT- α = 16°- M = 0.14

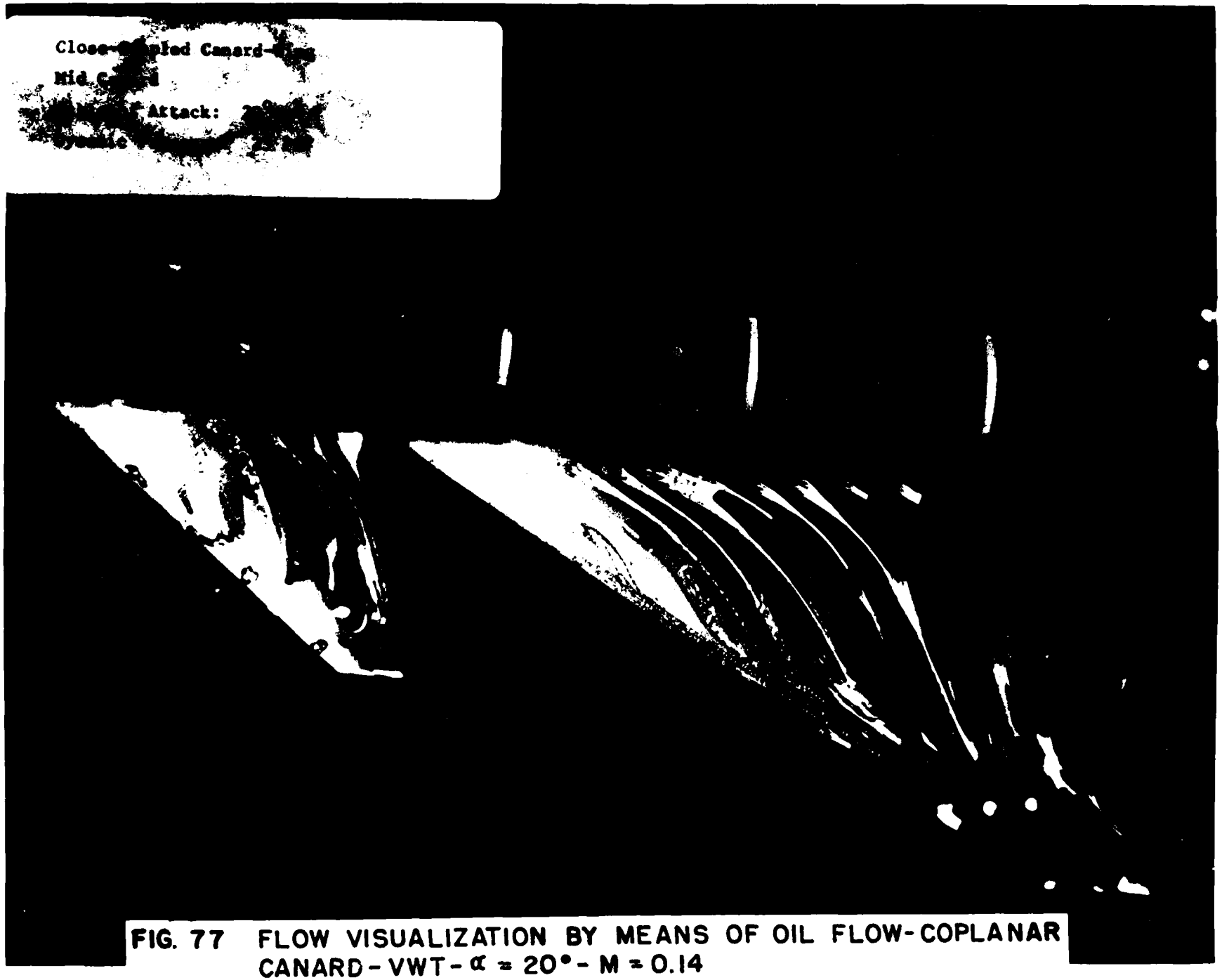

FIG. 77 FLOW VISUALIZATION BY MEANS OF OIL FLOW-COPLANAR CANARD-VWT-$\alpha \approx 20°$-$M \approx 0.14$

FIG. 79 FLOW VISUALIZATION BY MEANS OF LASER LIGHT SHEETS - COPLANAR CANARD - VWT - α = 16° - M = 0.14

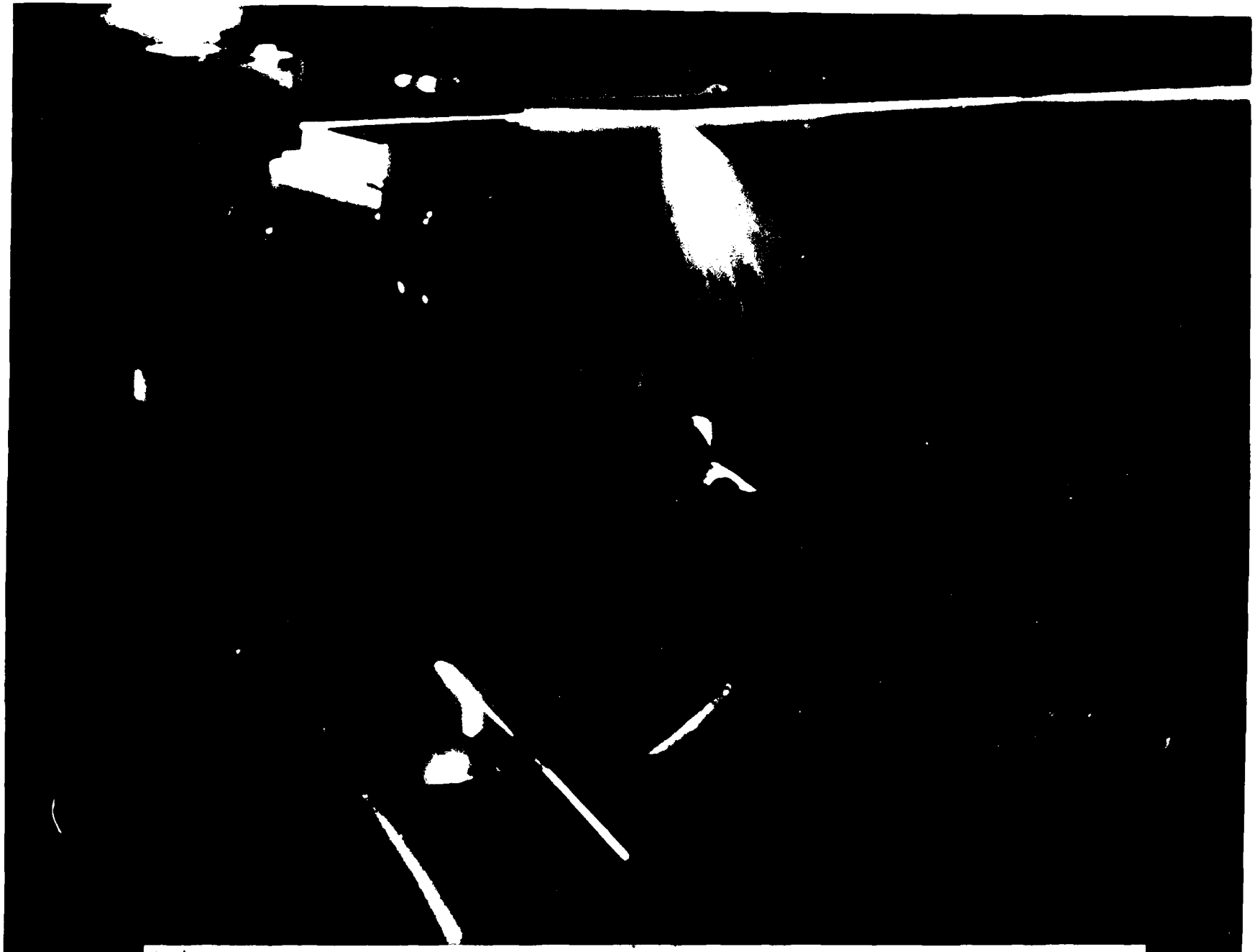

FIG. 80 FLOW VISUALIZATION BY MEANS OF LASER LIGHT SHEETS- NO CANARD - $\alpha = 0° - M \approx 0$

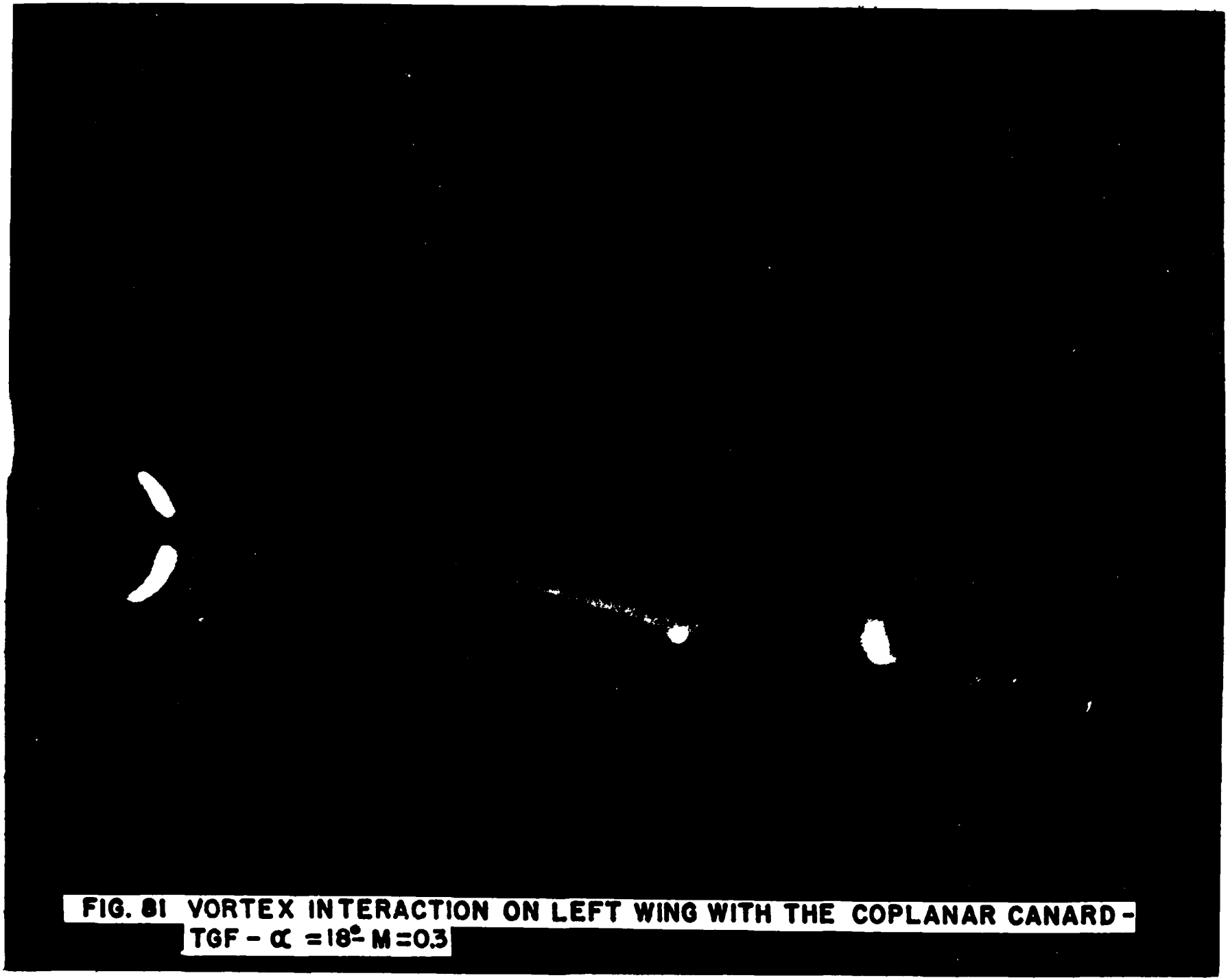

FIG. 81 VORTEX INTERACTION ON LEFT WING WITH THE COPLANAR CANARD - TGF - $\alpha = 18^{\circ}$ - M = 0.3

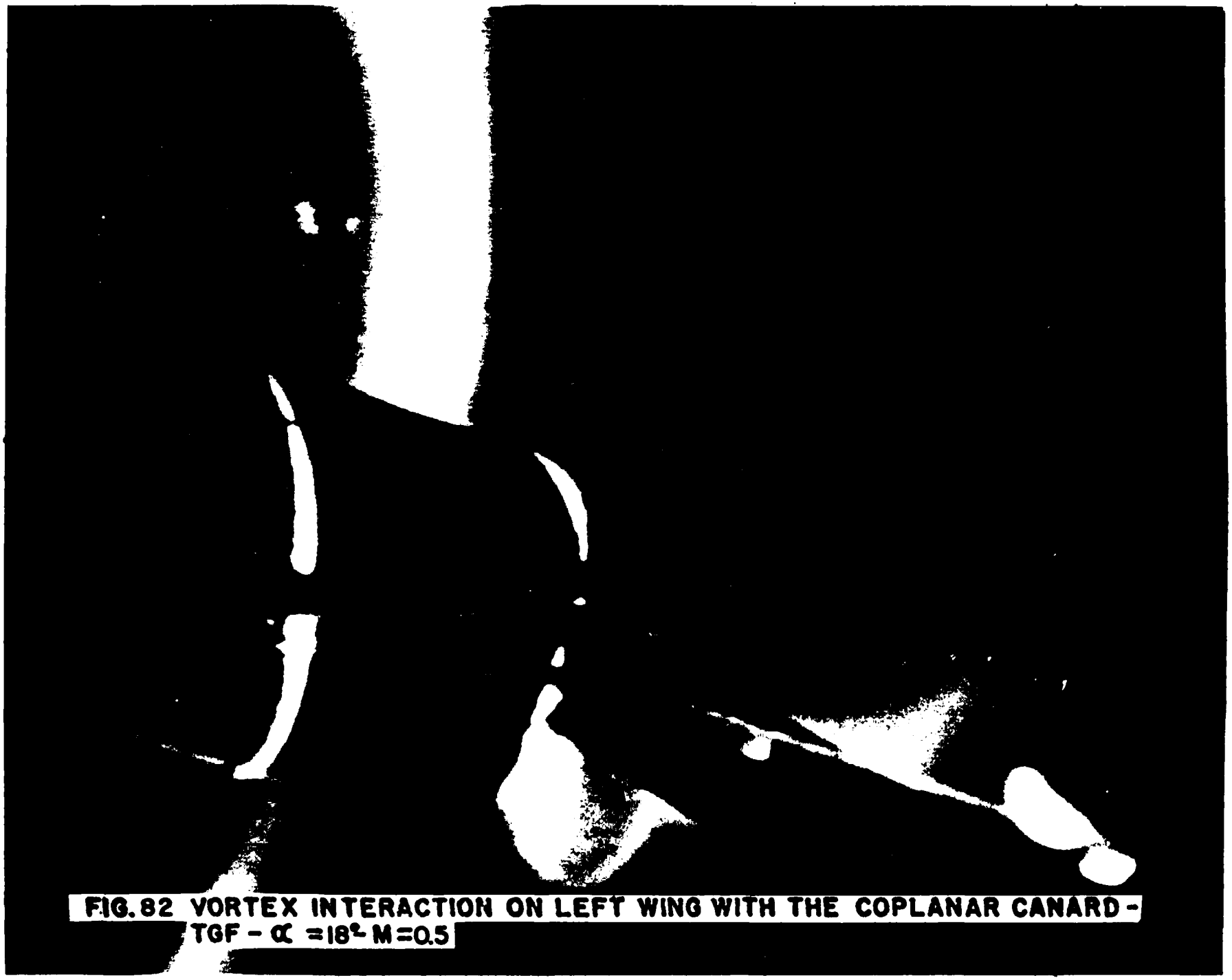

FIG. 82 VORTEX INTERACTION ON LEFT WING WITH THE COPLANAR CANARD - TGF - α = 18° M = 0.5

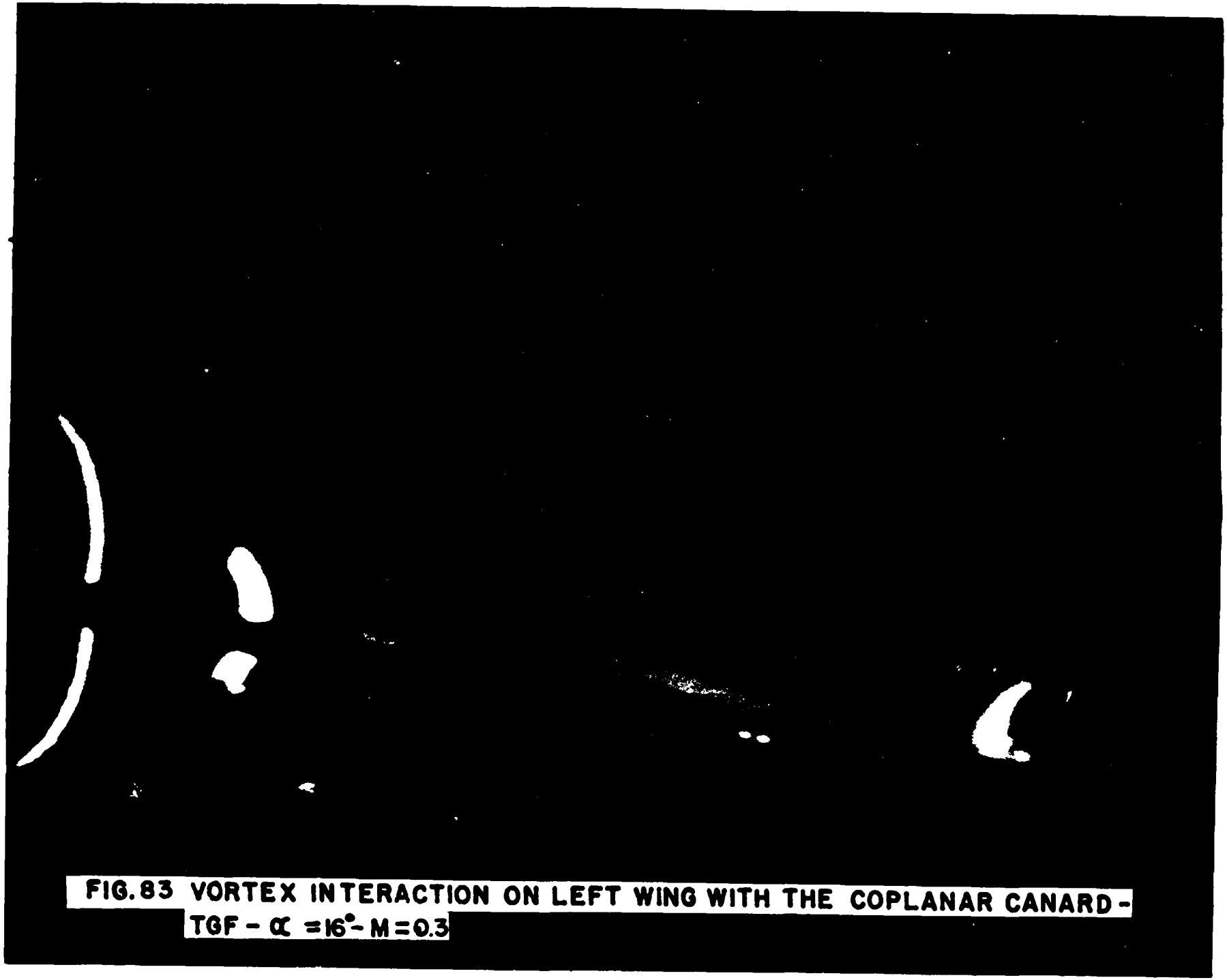

FIG. 83 VORTEX INTERACTION ON LEFT WING WITH THE COPLANAR CANARD - TGF - $\alpha = 16^{\circ}$ - M = 0.3

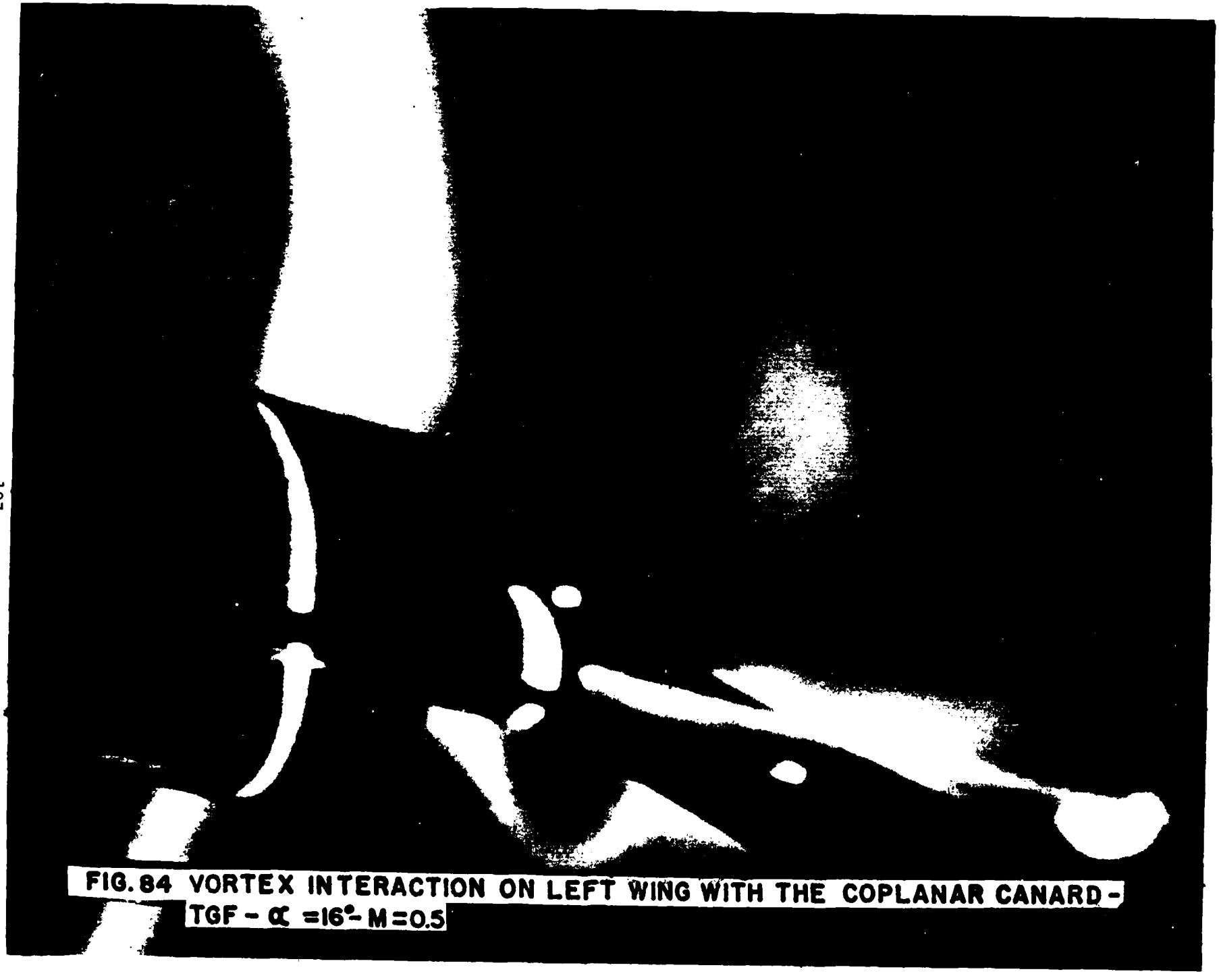

FIG. 84 VORTEX INTERACTION ON LEFT WING WITH THE COPLANAR CANARD - TGF - α =16°- M=0.5

FIG.85 VORTEX INTERACTION ON LEFT WING WITH THE COPLANAR CANARD-
TOF - α 10.° - M = 0.5

APPENDIX A

The figures A1 to A19 show repeated runs for different configurations at different stations, measured with the H.W. and the LDV.

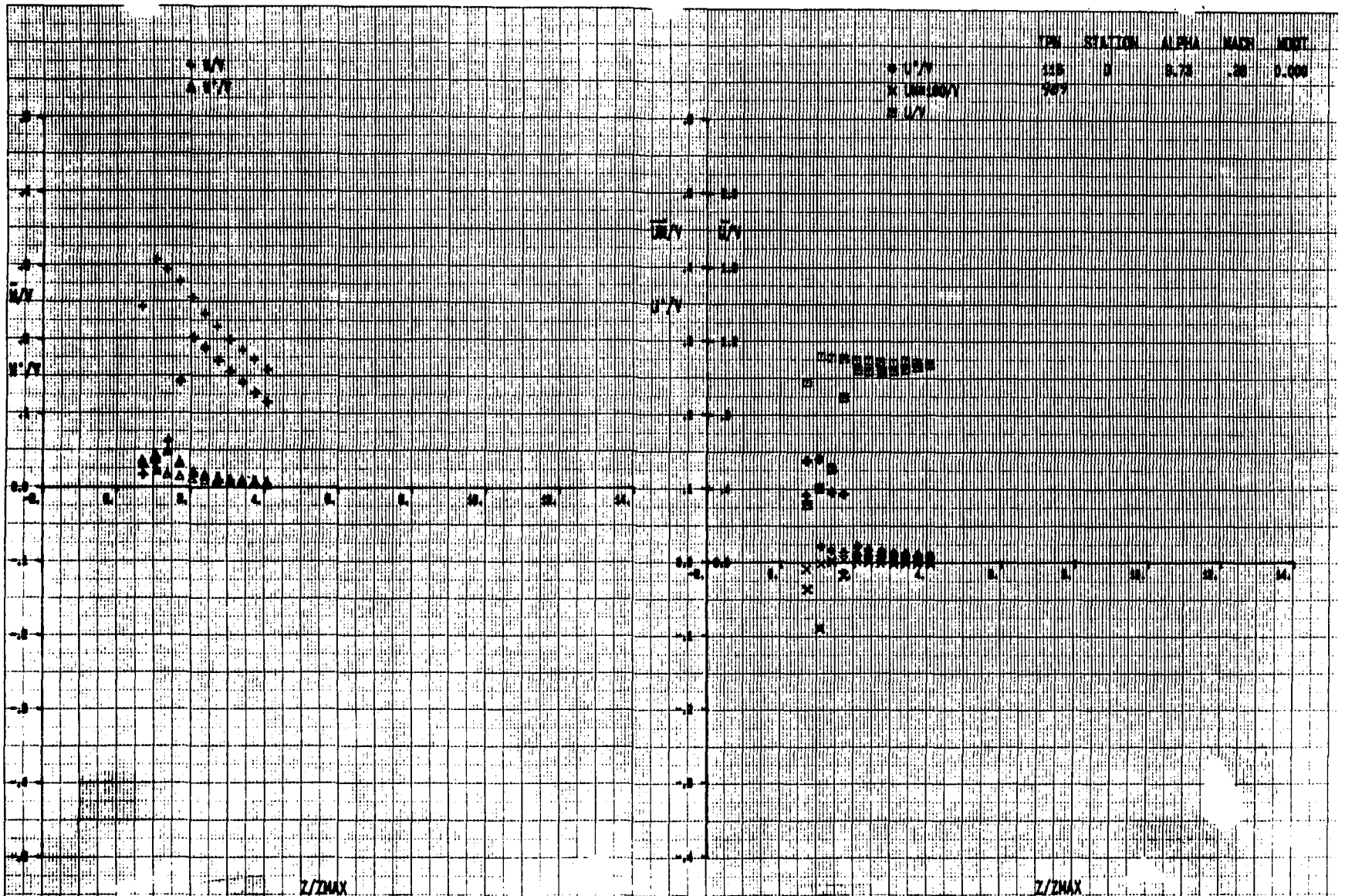

FIG A1 REPEATED HOT WIRE MEASUREMENTS OF MEAN VELOCITIES, TURBULENCE INTENSITIES AND REYNOLDS STRESSES WITH THE COPLANAR CANARD-TGF- $\alpha = 10°$ STATION D

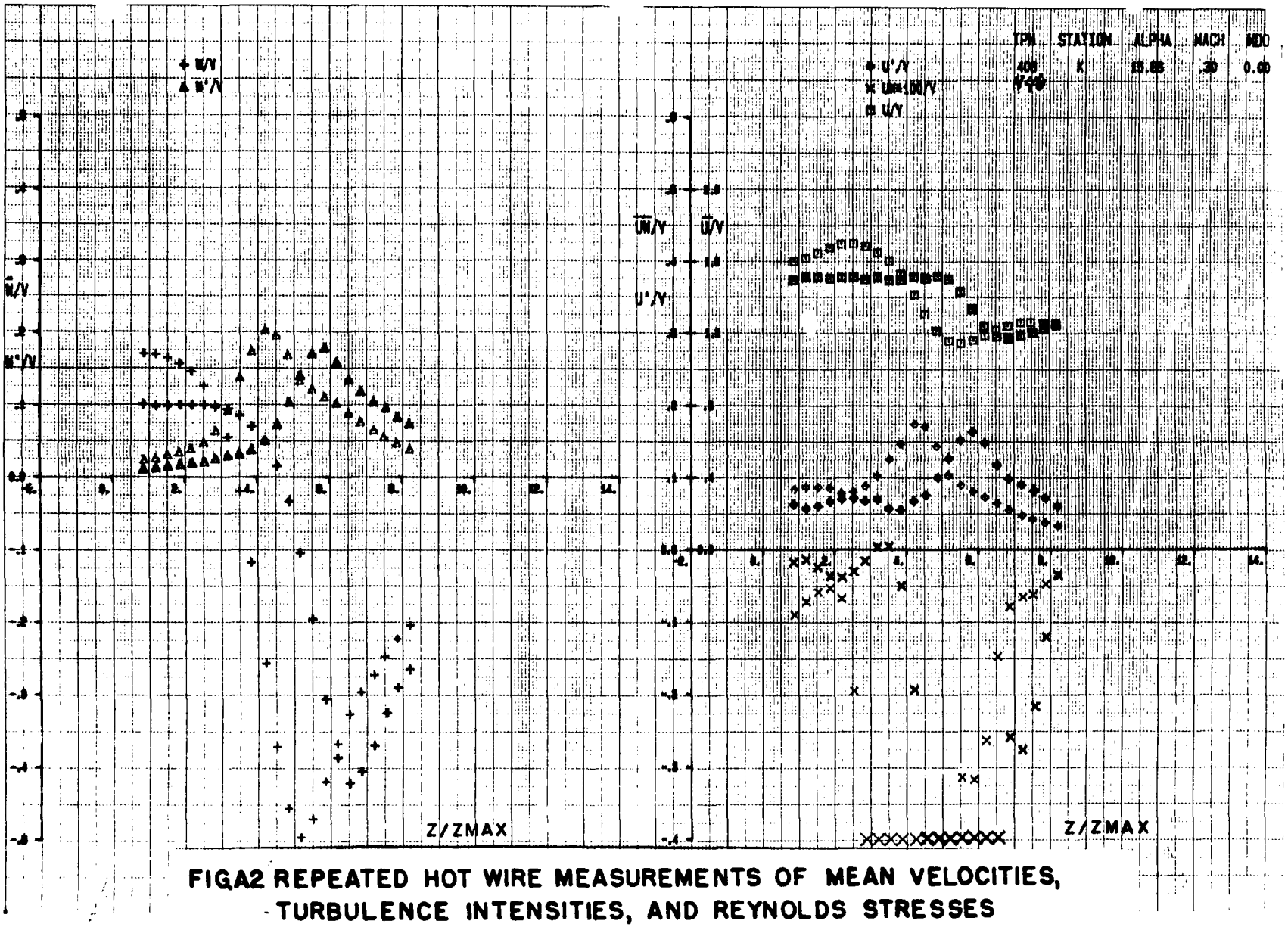

FIG.A2 REPEATED HOT WIRE MEASUREMENTS OF MEAN VELOCITIES, TURBULENCE INTENSITIES, AND REYNOLDS STRESSES WITH THE COPLANAR CANARD - TGF-, $\alpha = 16°$ STATION K

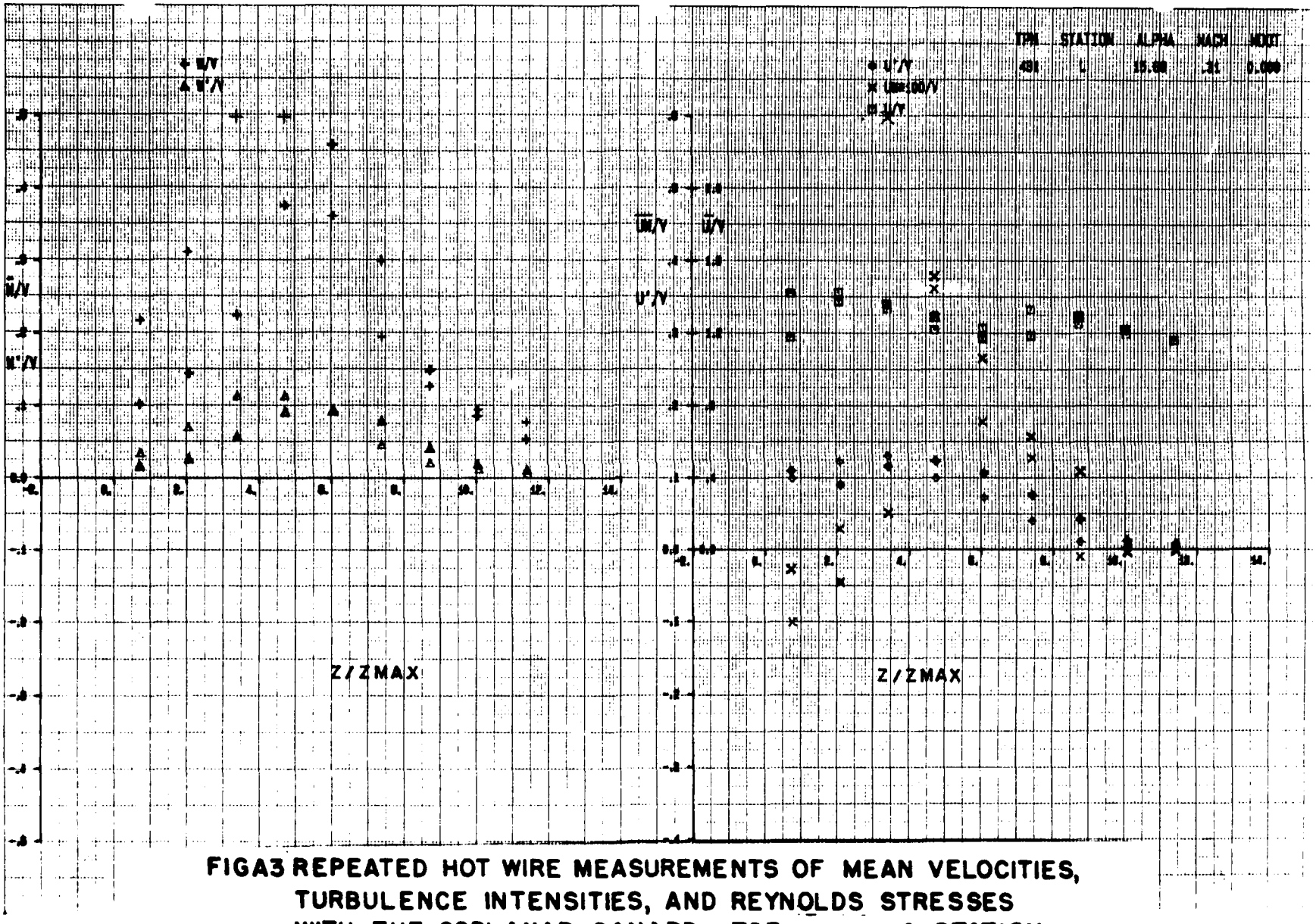

FIG A3 REPEATED HOT WIRE MEASUREMENTS OF MEAN VELOCITIES, TURBULENCE INTENSITIES, AND REYNOLDS STRESSES WITH THE COPLANAR CANARD - TGF - α = 16° STATION L

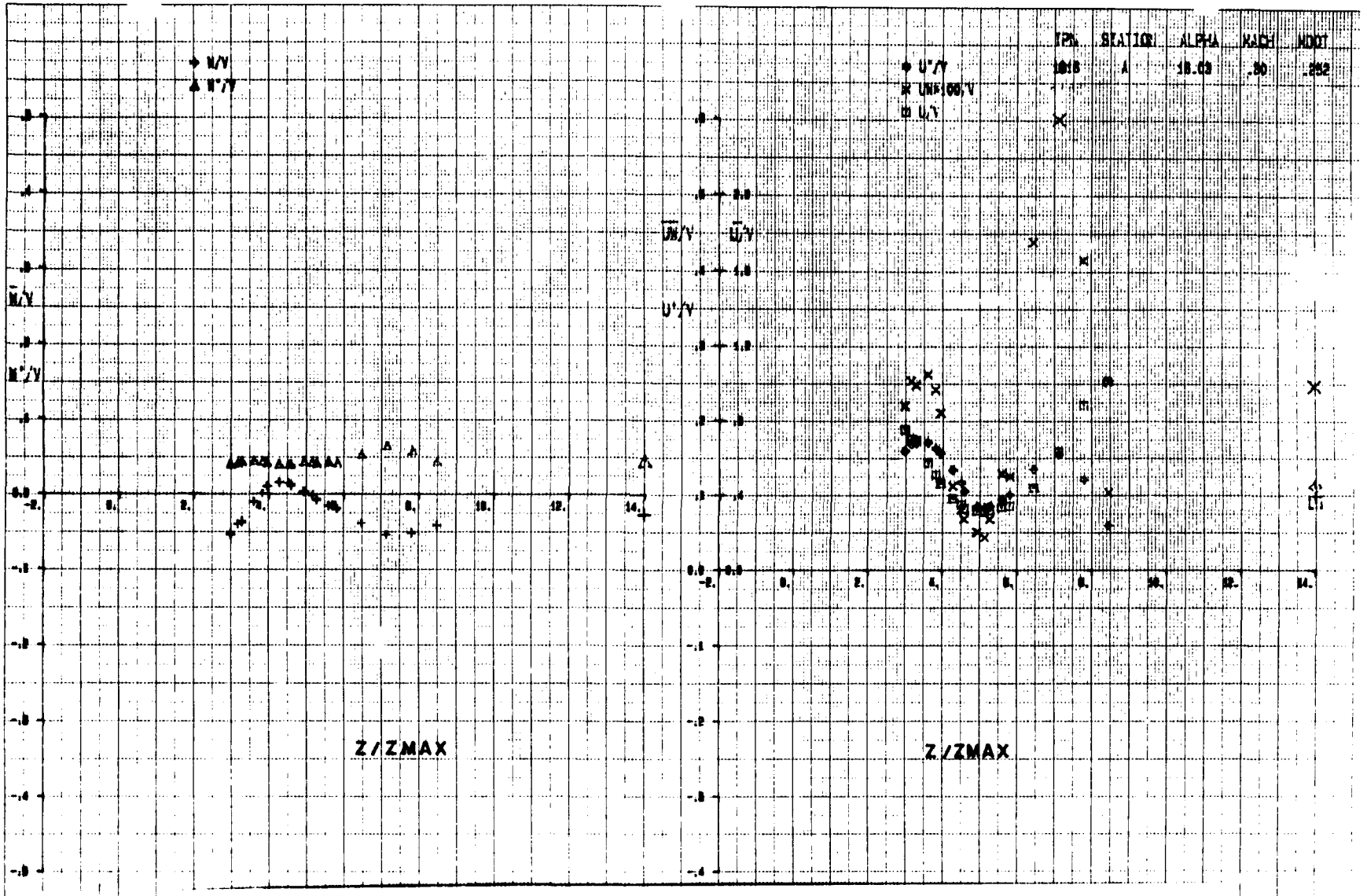

FIGA4 REPEATED HOT WIRE MEASUREMENTS OF MEAN VELOCITIES, TURBULENCE INTENSITIES, AND REYNOLDS STRESSES WITH THE COPLANAR CANARD - TGF - $\alpha = 16°$ STATION A

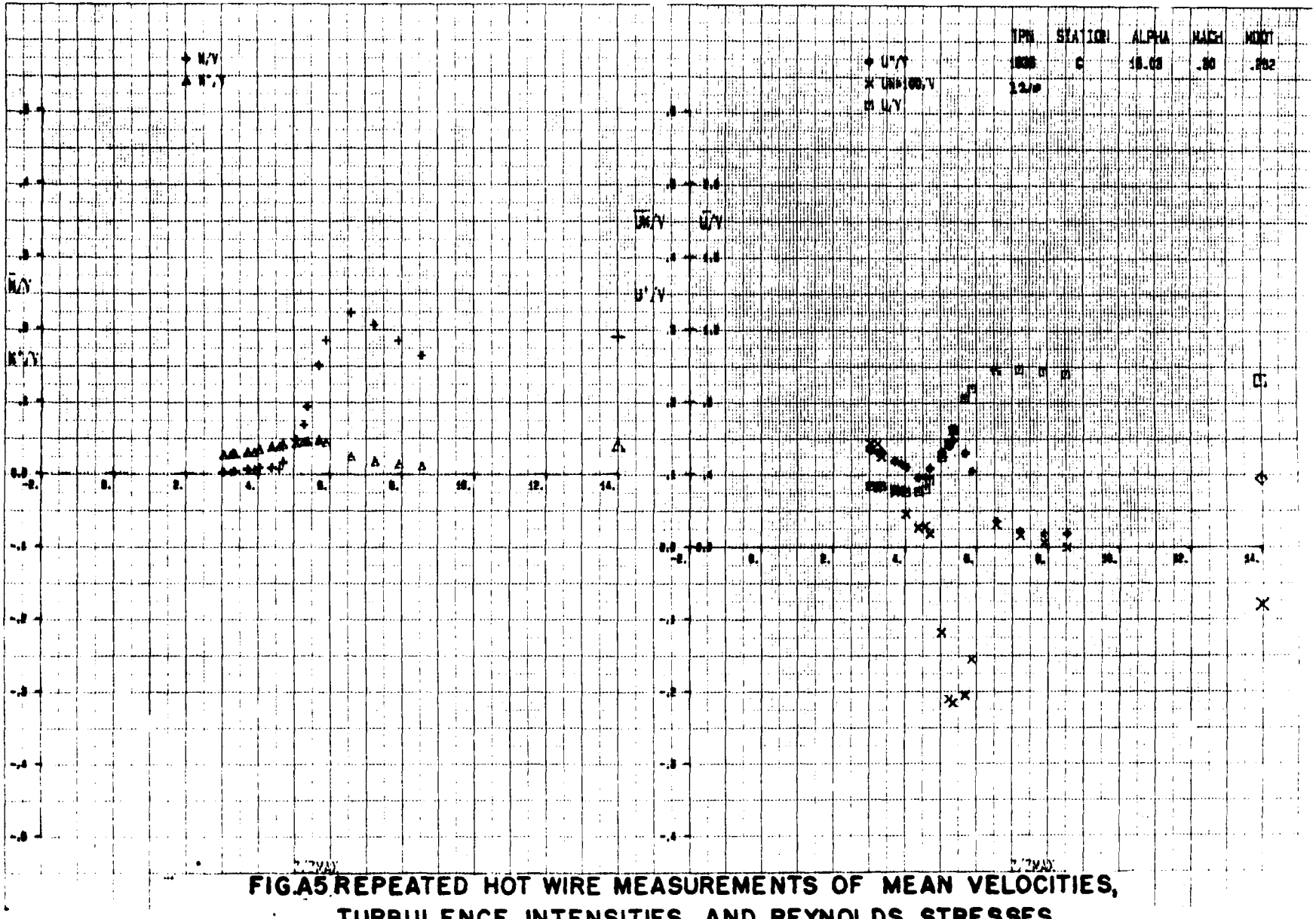

FIG.A5 REPEATED HOT WIRE MEASUREMENTS OF MEAN VELOCITIES, TURBULENCE INTENSITIES, AND REYNOLDS STRESSES WITH THE COPLANAR CANARD - TGF. - α =16 ° STATION C

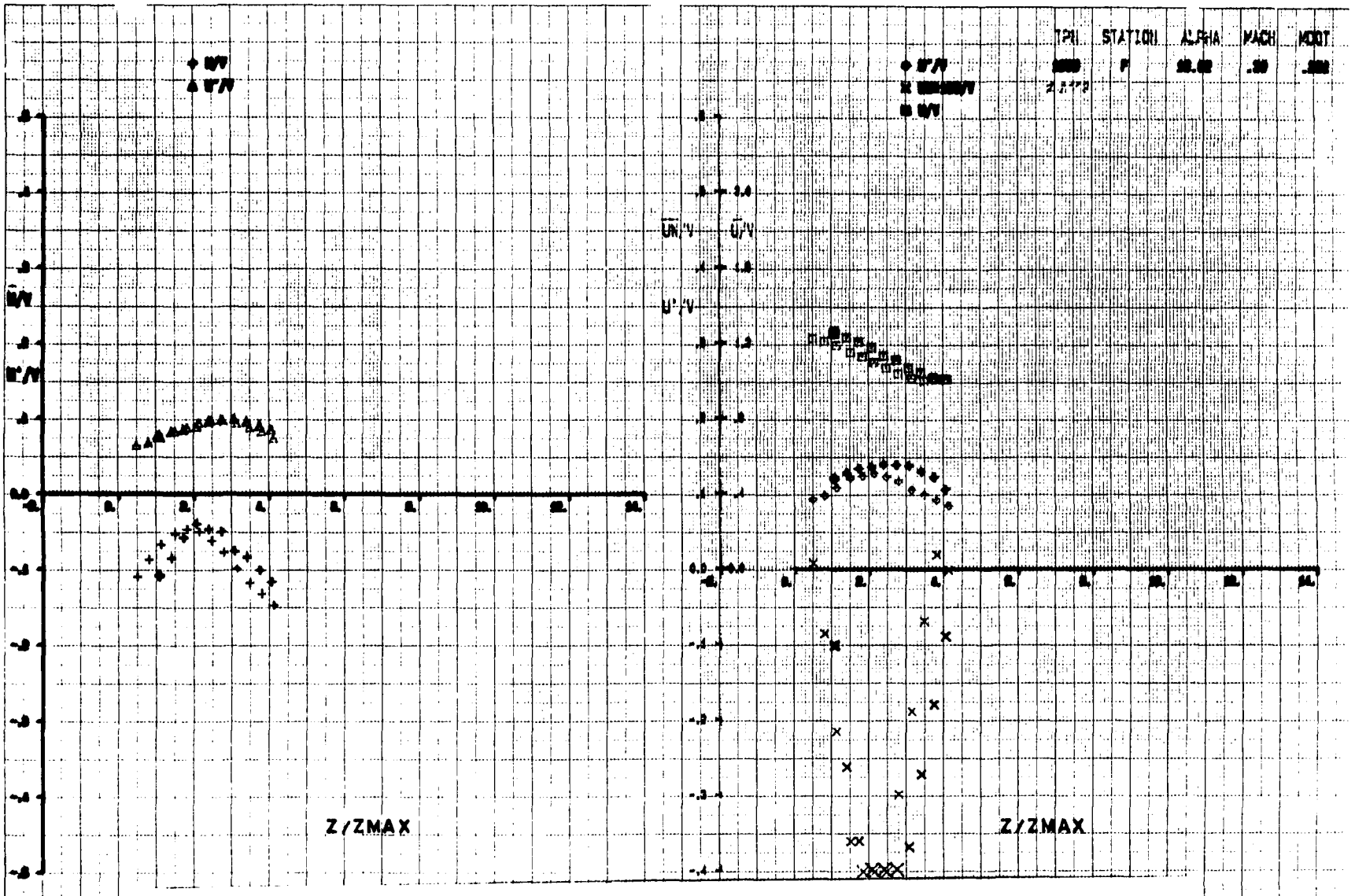

FIGA6 REPEATED HOT WIRE MEASUREMENTS OF MEAN VELOCITIES, TURBULENCE INTENSITIES, AND REYNOLDS STRESSES WITH THE COPLANAR CANARD - TGF - $\alpha = 16°$ STATION F

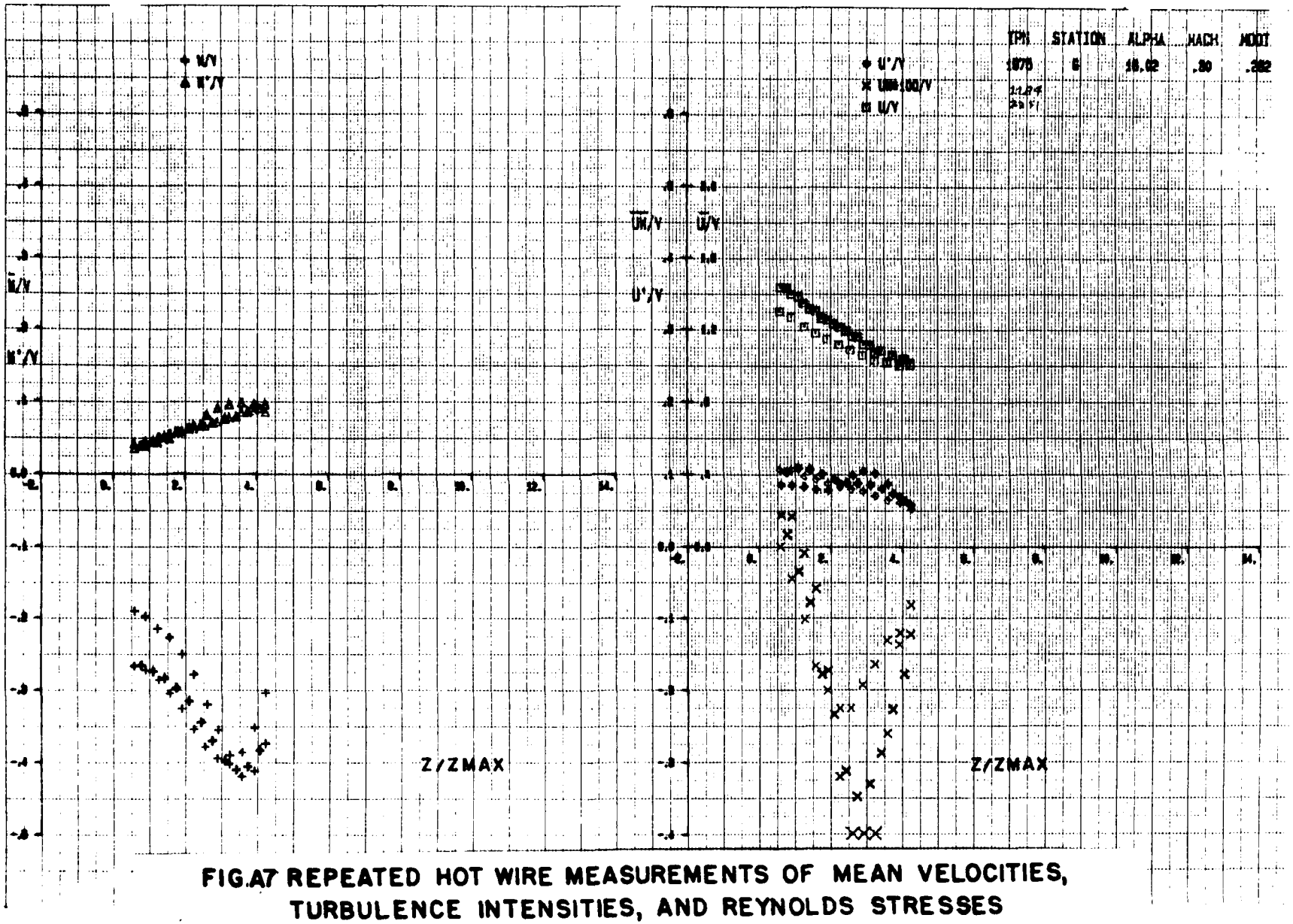

FIG.A7 REPEATED HOT WIRE MEASUREMENTS OF MEAN VELOCITIES, TURBULENCE INTENSITIES, AND REYNOLDS STRESSES WITH THE COPLANAR CANARD - TGF - α=16°-STATION G

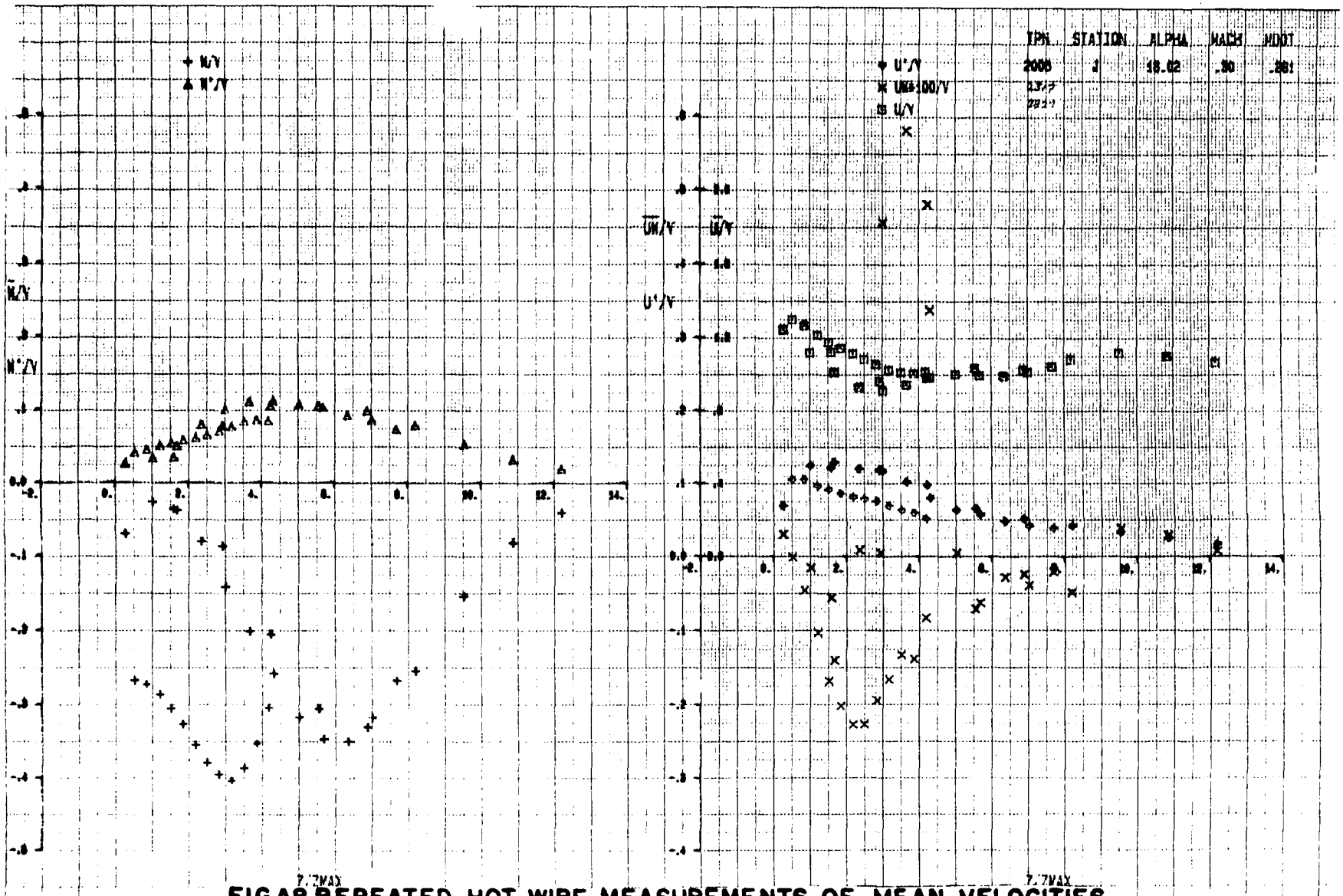

FIG.A8 REPEATED HOT WIRE MEASUREMENTS OF MEAN VELOCITIES, TURBULENCE INTENSITIES, AND REYNOLDS STRESSES WITH THE COPLANAR CANARD - TGF - $\alpha = 16°$ STATION J

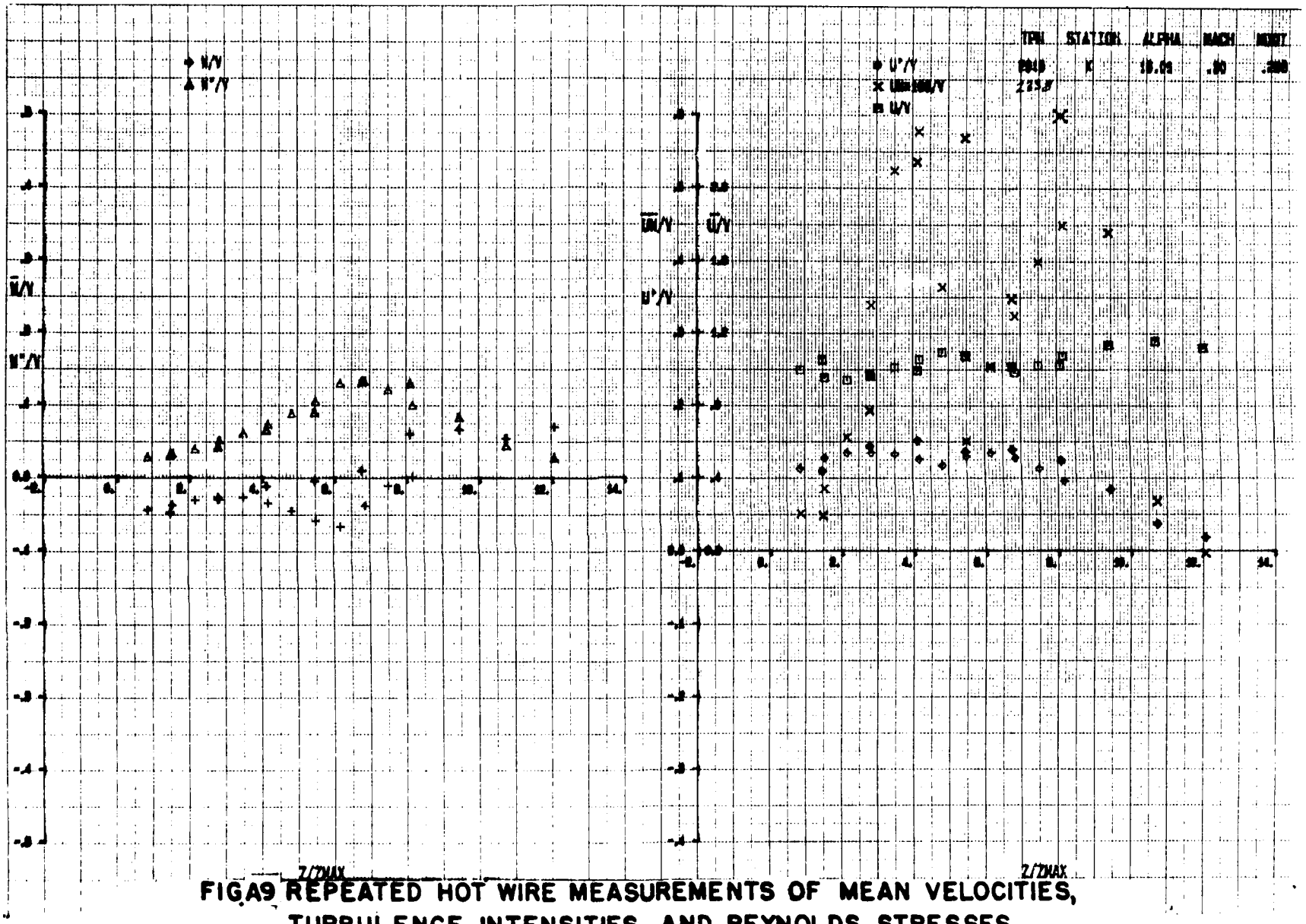

FIG.A9 REPEATED HOT WIRE MEASUREMENTS OF MEAN VELOCITIES, TURBULENCE INTENSITIES, AND REYNOLDS STRESSES WITH THE COPLANAR CANARD - TGF $\alpha = 16°$ STATION K

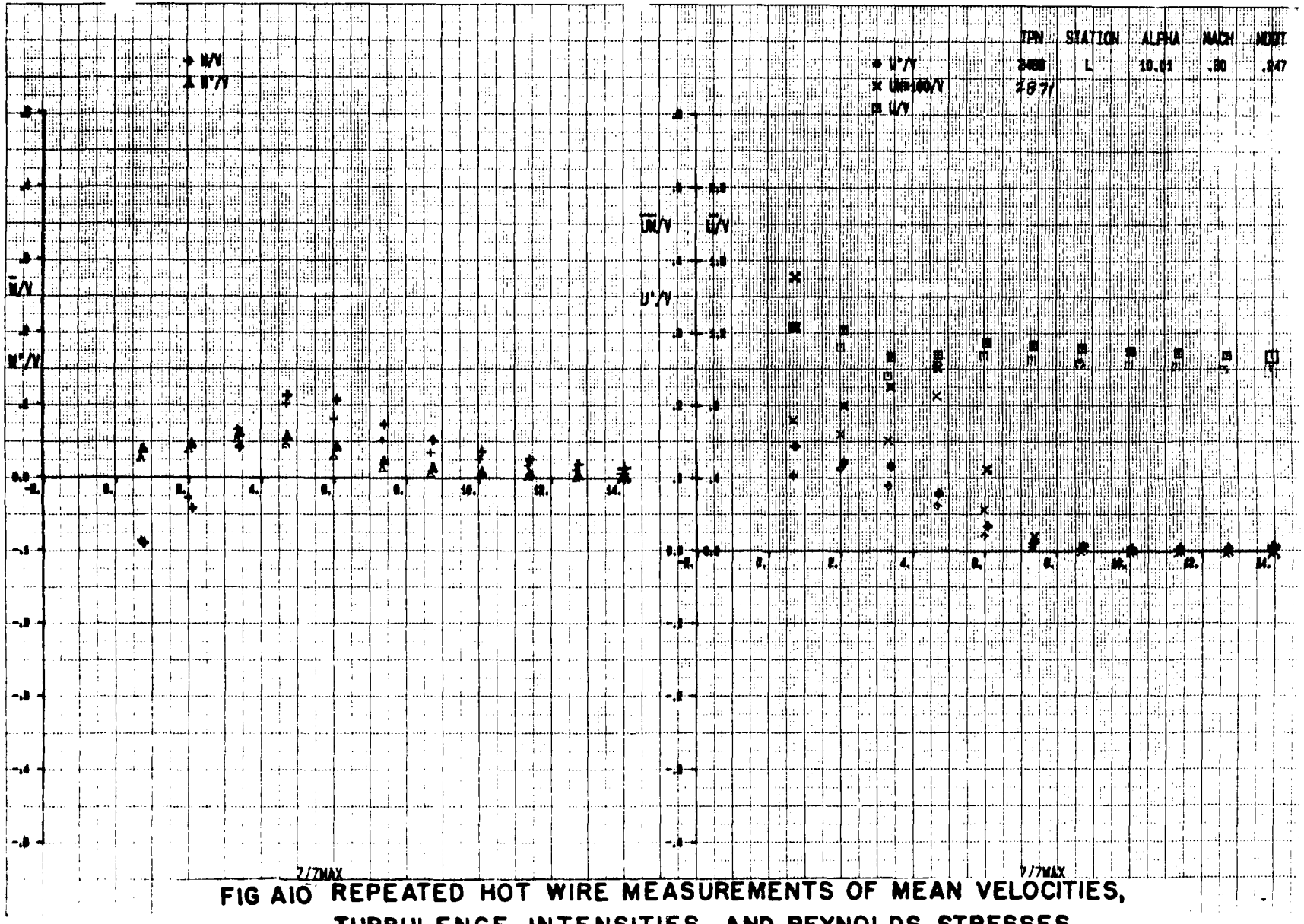

FIG A10 REPEATED HOT WIRE MEASUREMENTS OF MEAN VELOCITIES, TURBULENCE INTENSITIES, AND REYNOLDS STRESSES WITHOUT CANARD - TGF STATION L - α = 10°

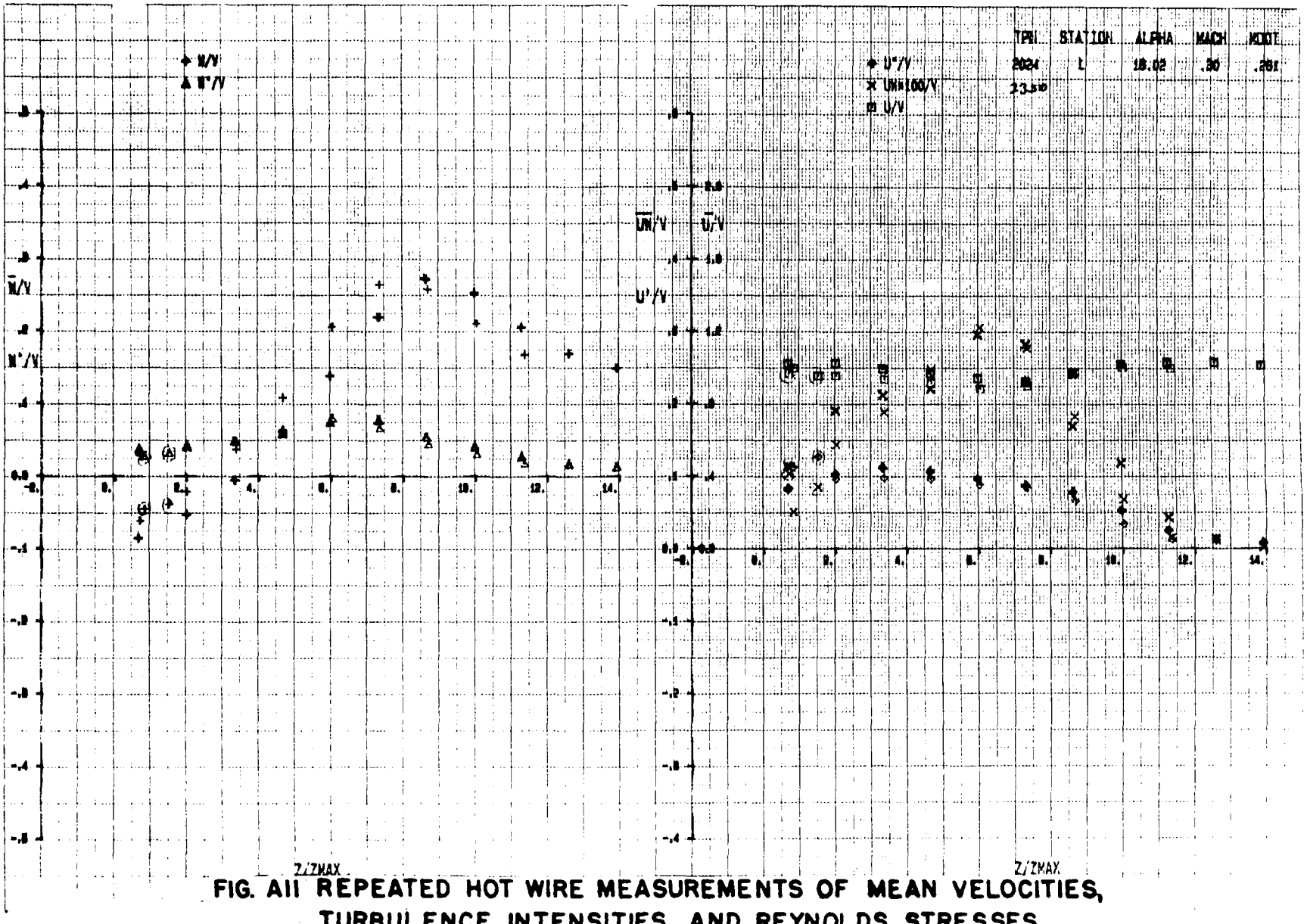

FIG. AII REPEATED HOT WIRE MEASUREMENTS OF MEAN VELOCITIES, TURBULENCE INTENSITIES, AND REYNOLDS STRESSES WITH THE COPLANAR CANARD - TGF - STATION L - α = 16°

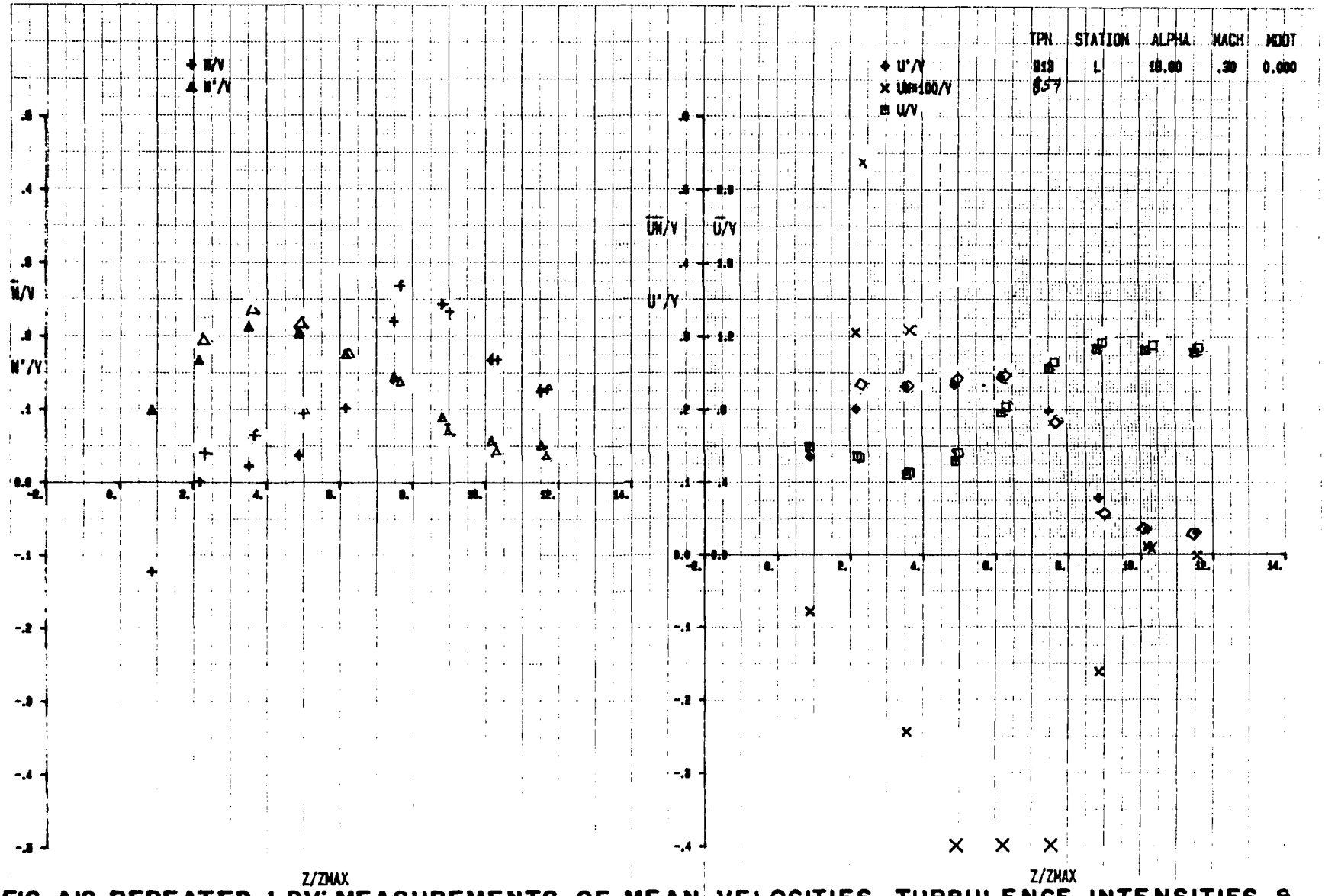

FIG. A12 REPEATED LDV MEASUREMENTS OF MEAN VELOCITIES, TURBULENCE INTENSITIES & REYNOLDS STRESSES WITHOUT CANARD - TGF - α = 16° STATION L

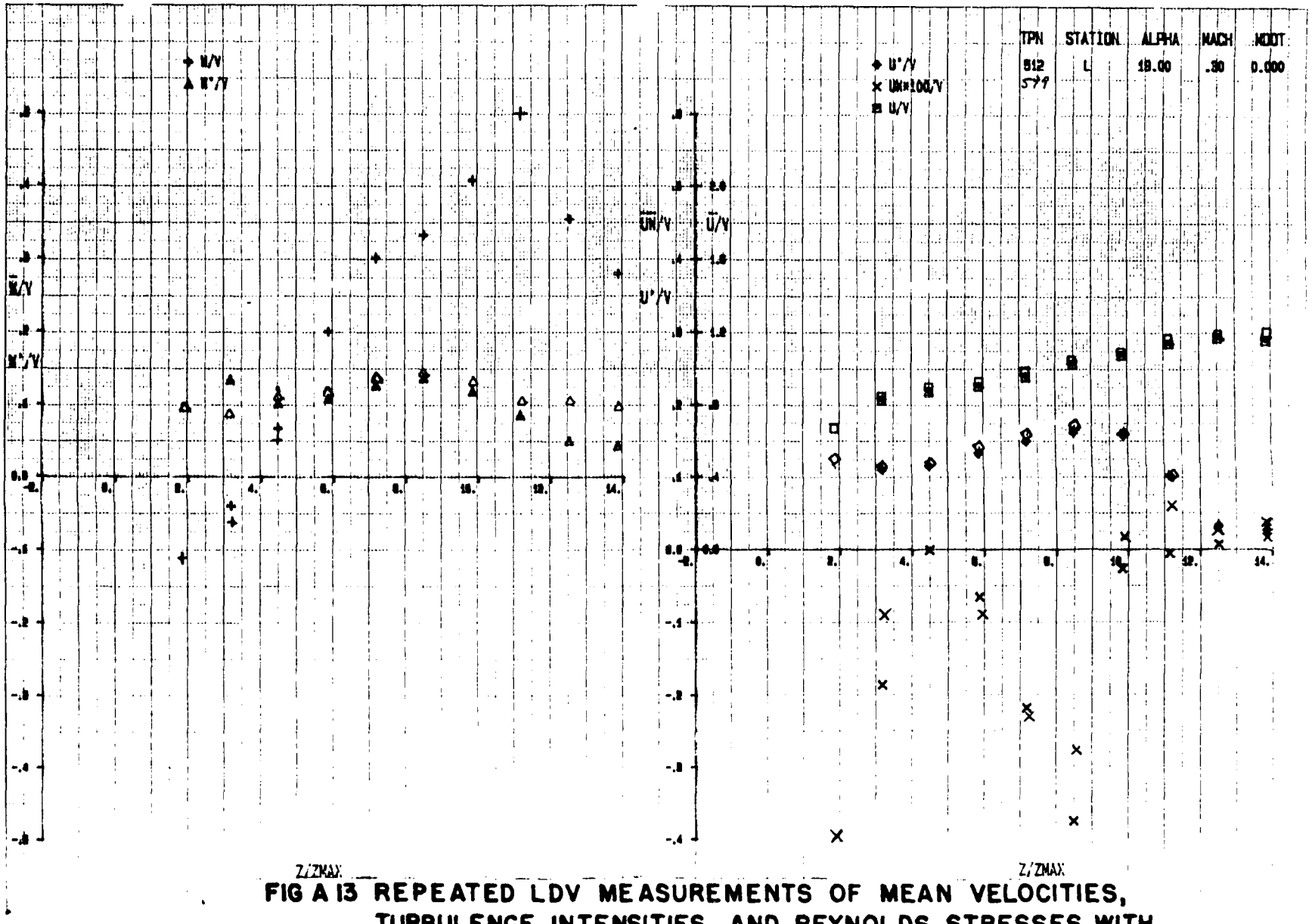

FIG A 13 REPEATED LDV MEASUREMENTS OF MEAN VELOCITIES, TURBULENCE INTENSITIES, AND REYNOLDS STRESSES WITH THE COPLANAR CANARD-TGF - $\alpha = 20°$ - STATION L

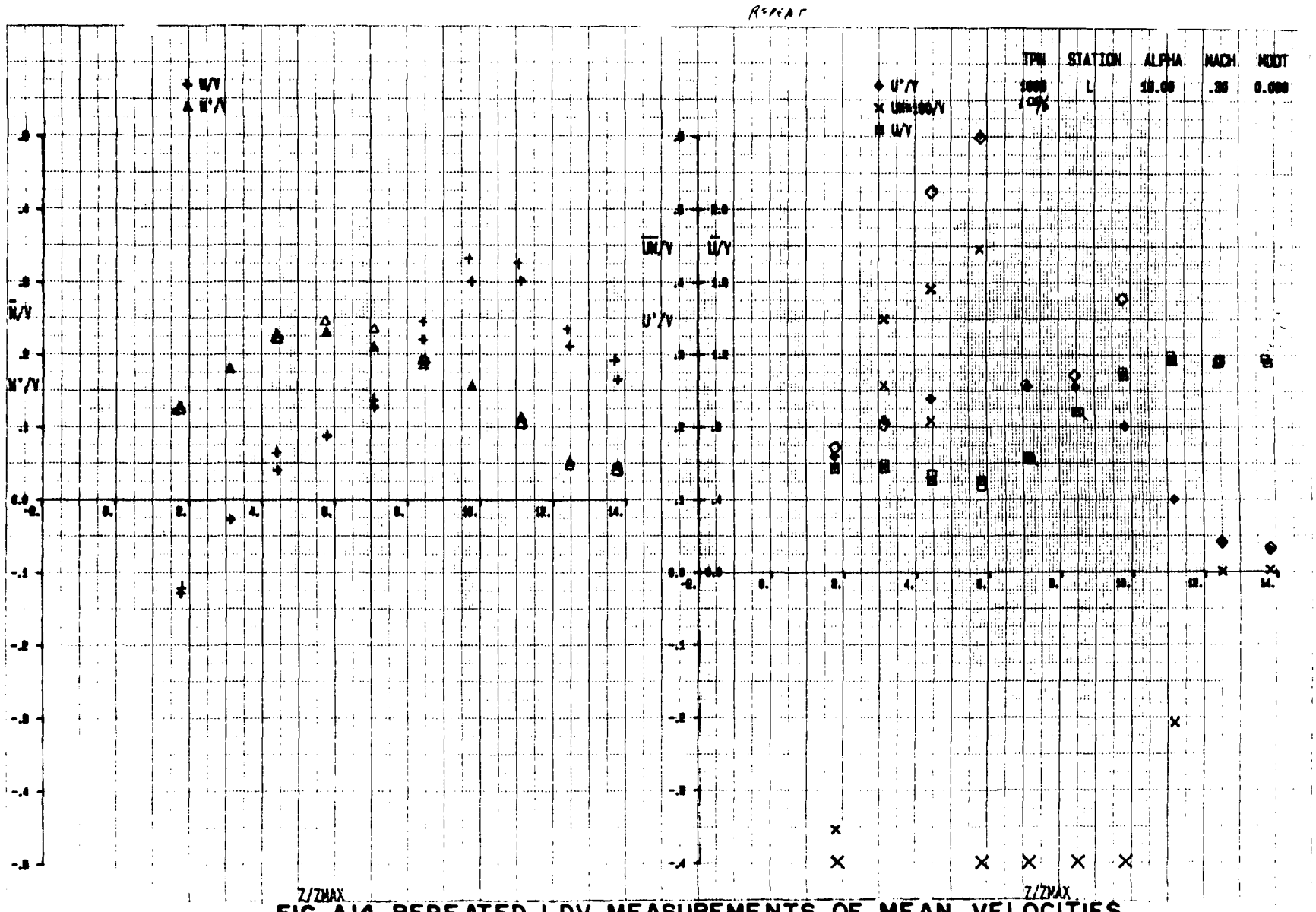

FIG. A14 REPEATED LDV MEASUREMENTS OF MEAN VELOCITIES, TURBULENCE INTENSITIES, AND REYNOLDS STRESSES WITHOUT CANARD - TGF-α =20°-STATION L

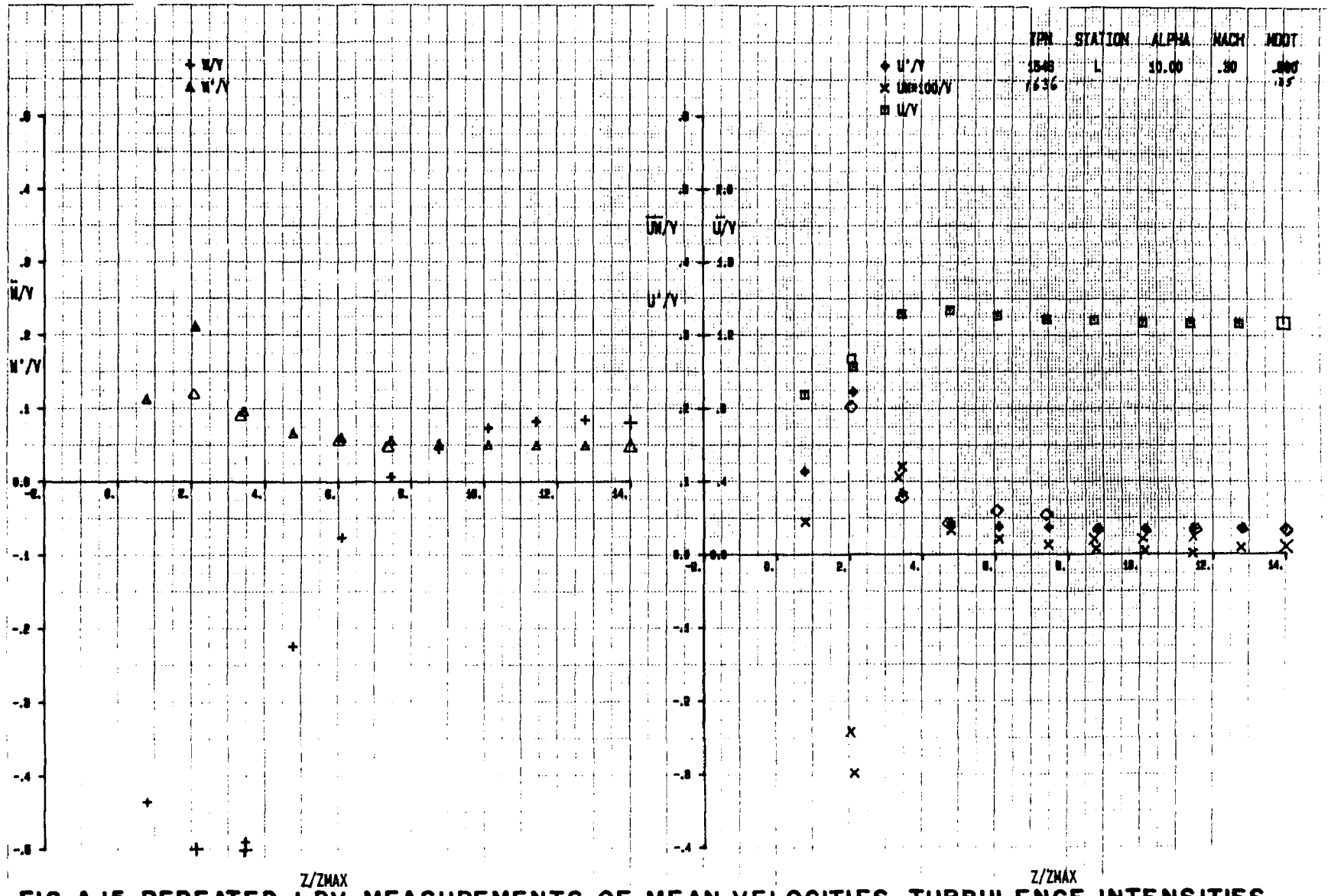

FIG A 15 REPEATED LDV MEASUREMENTS OF MEAN VELOCITIES, TURBULENCE INTENSITIES, AND REYNOLDS STRESSES WITH THE COPLANAR CANARD-TGF - α = 10° STATION L

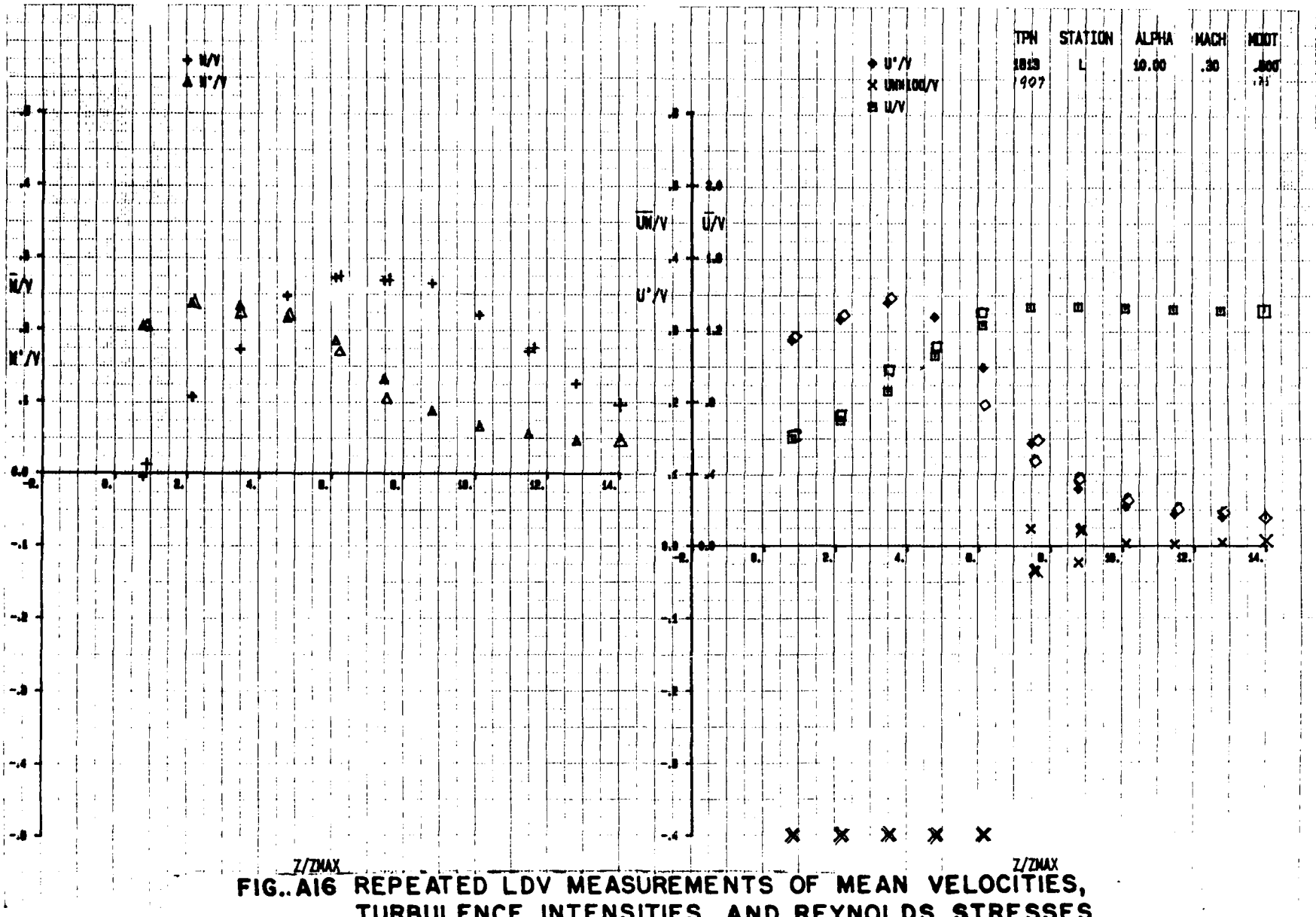

FIG. A16 REPEATED LDV MEASUREMENTS OF MEAN VELOCITIES, TURBULENCE INTENSITIES, AND REYNOLDS STRESSES WITHOUT CANARD - TGF - $\alpha = 10°$ STATION L -

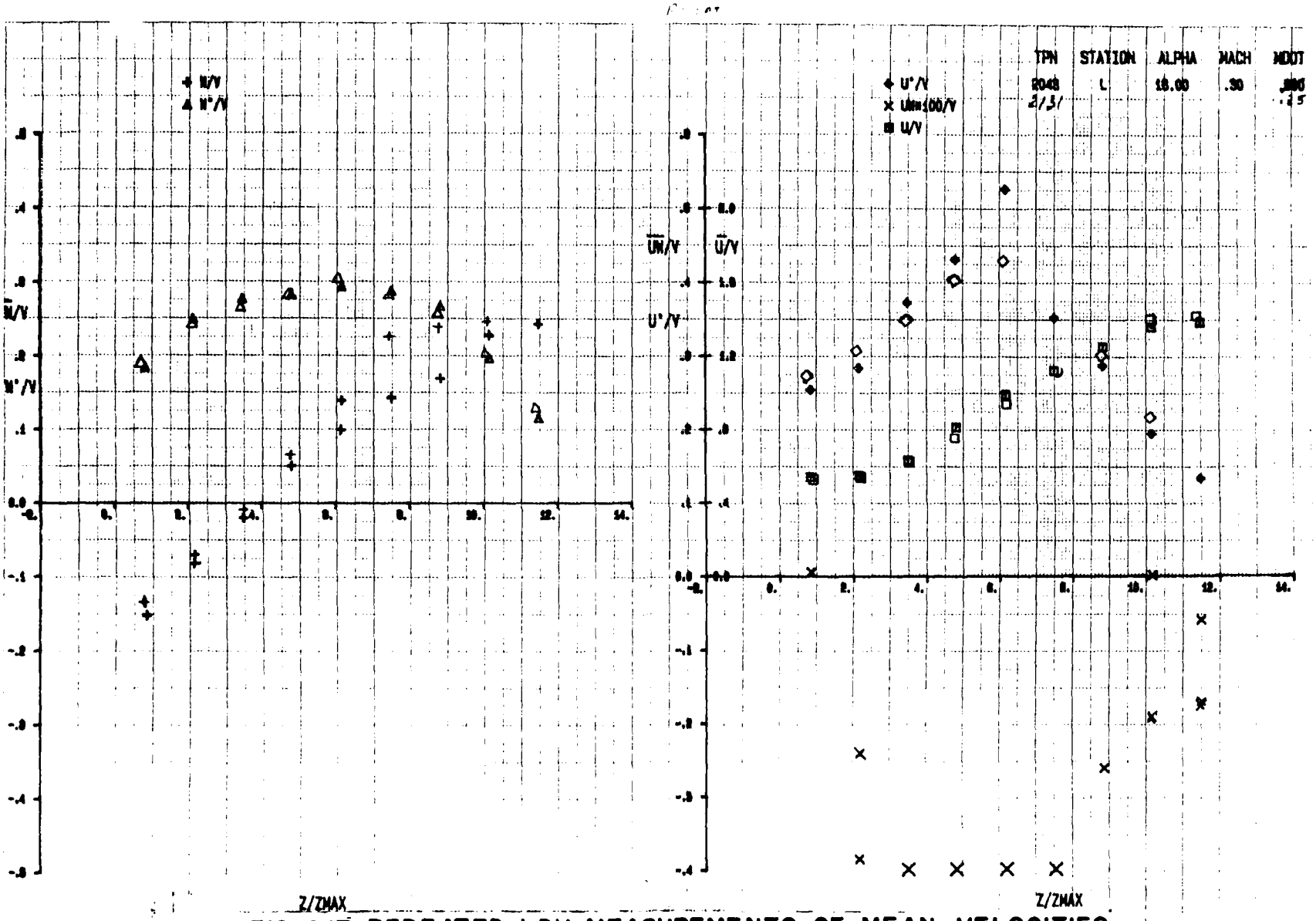

FIG. A17 REPEATED LDV MEASUREMENTS OF MEAN VELOCITIES, TURBULENCE INTENSITIES, AND REYNOLDS STRESSES WITHOUT CANARD - TGF - $\alpha = 16°$ STATION L

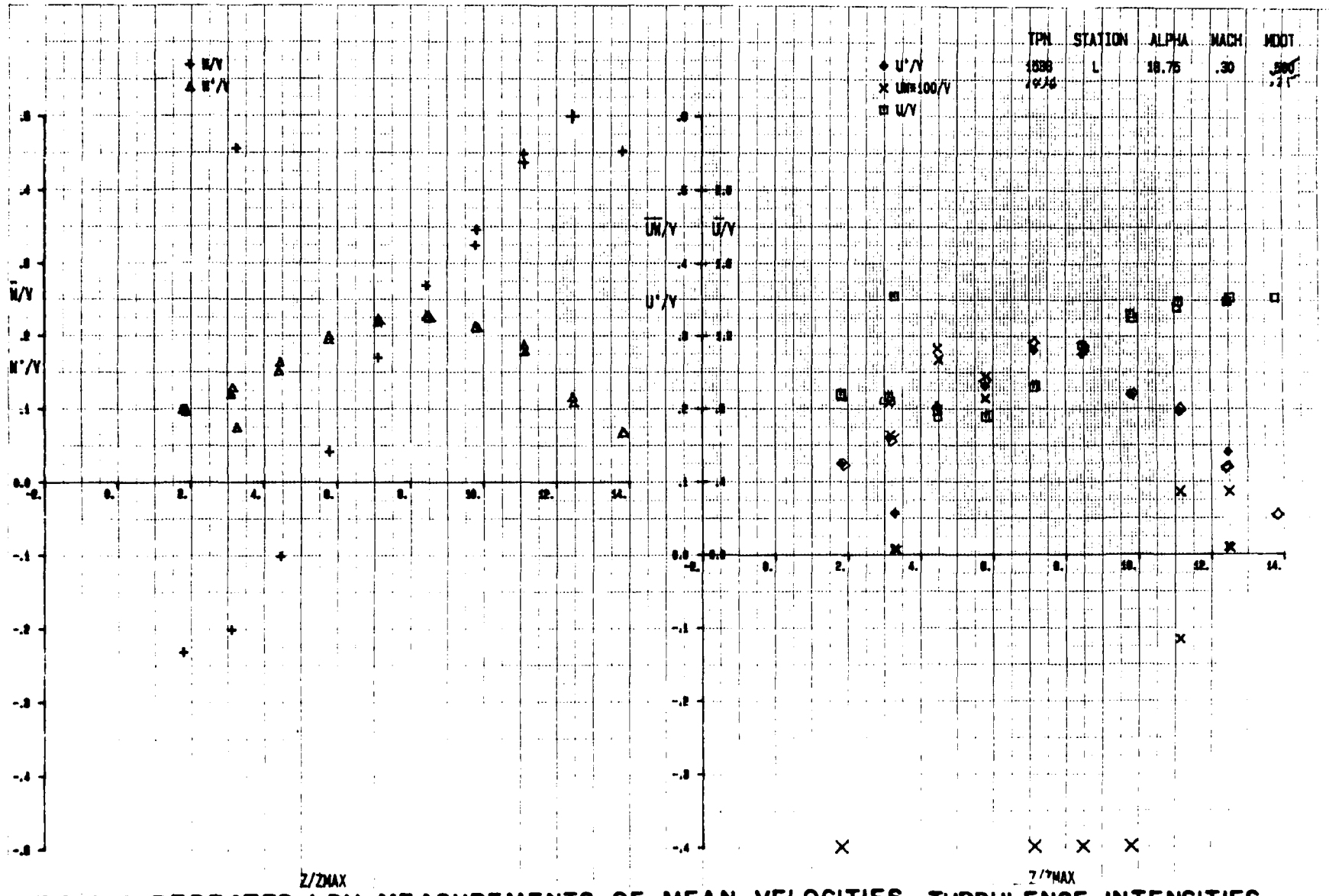

FIG. A 18 REPEATED LDV MEASUREMENTS OF MEAN VELOCITIES, TURBULENCE INTENSITIES, AND REYNOLDS STRESSES WITH THE COPLANAR CANARD-TGF $\alpha = 20°$ STATION L

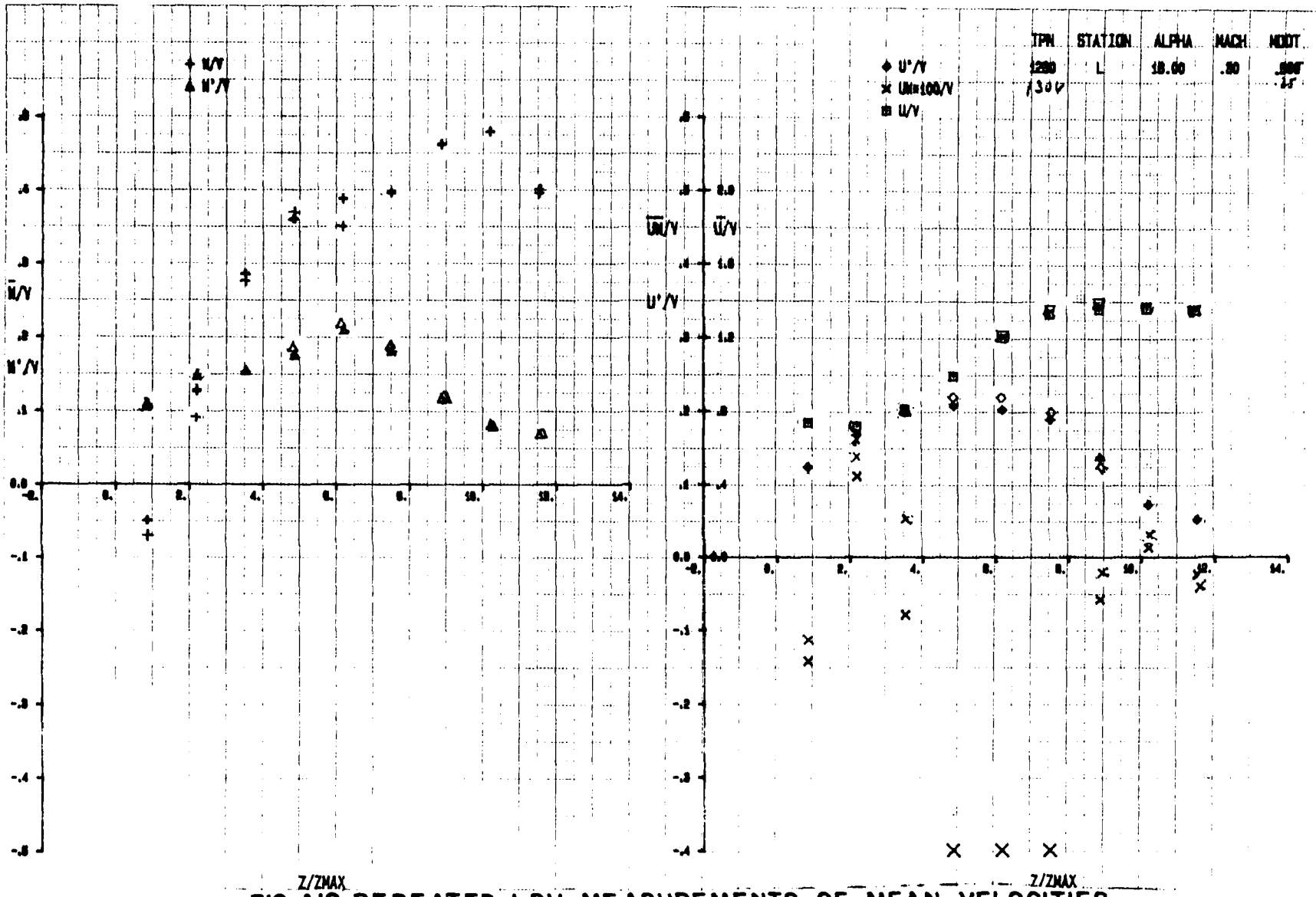

FIG. A19 REPEATED LDV MEASUREMENTS OF MEAN VELOCITIES, TURBULENCE INTENSITIES, AND REYNOLDS STRESSES WITH THE COPLANAR CANARD-TGF STATION L - α 16°

APPENDIX B

The figures B1 to B70 compare data obtained with the H.W. and the LDV for different configurations at different stations, for $\alpha = 16°$ and $\alpha = 20°$.

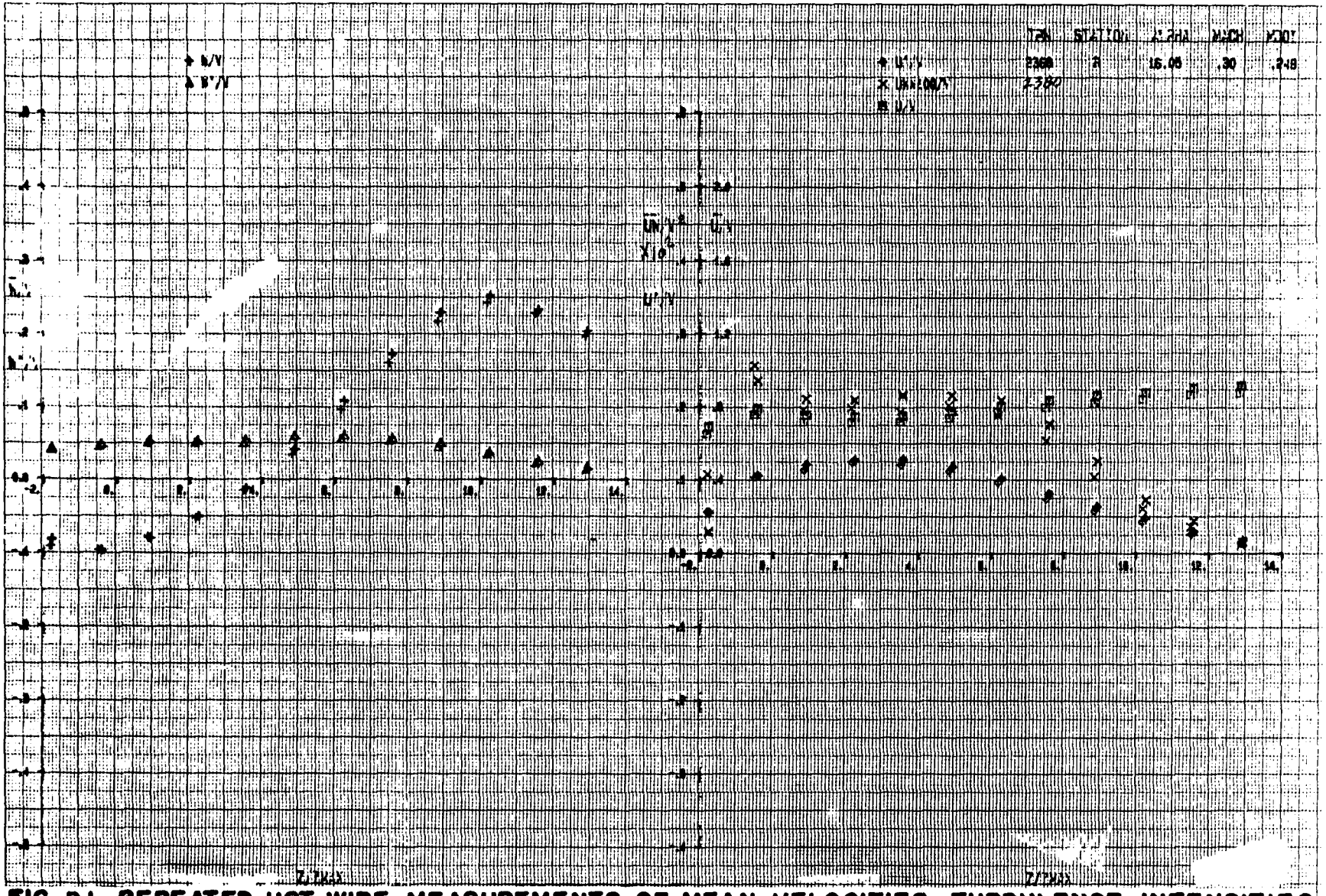

FIG B1 REPEATED HOT WIRE MEASUREMENTS OF MEAN VELOCITIES, TURBULENCE INTENSITIES AND REYNOLDS STRESSES WITH BLOWING -COPLANAR CANARD - TGF - α =16° STATION R

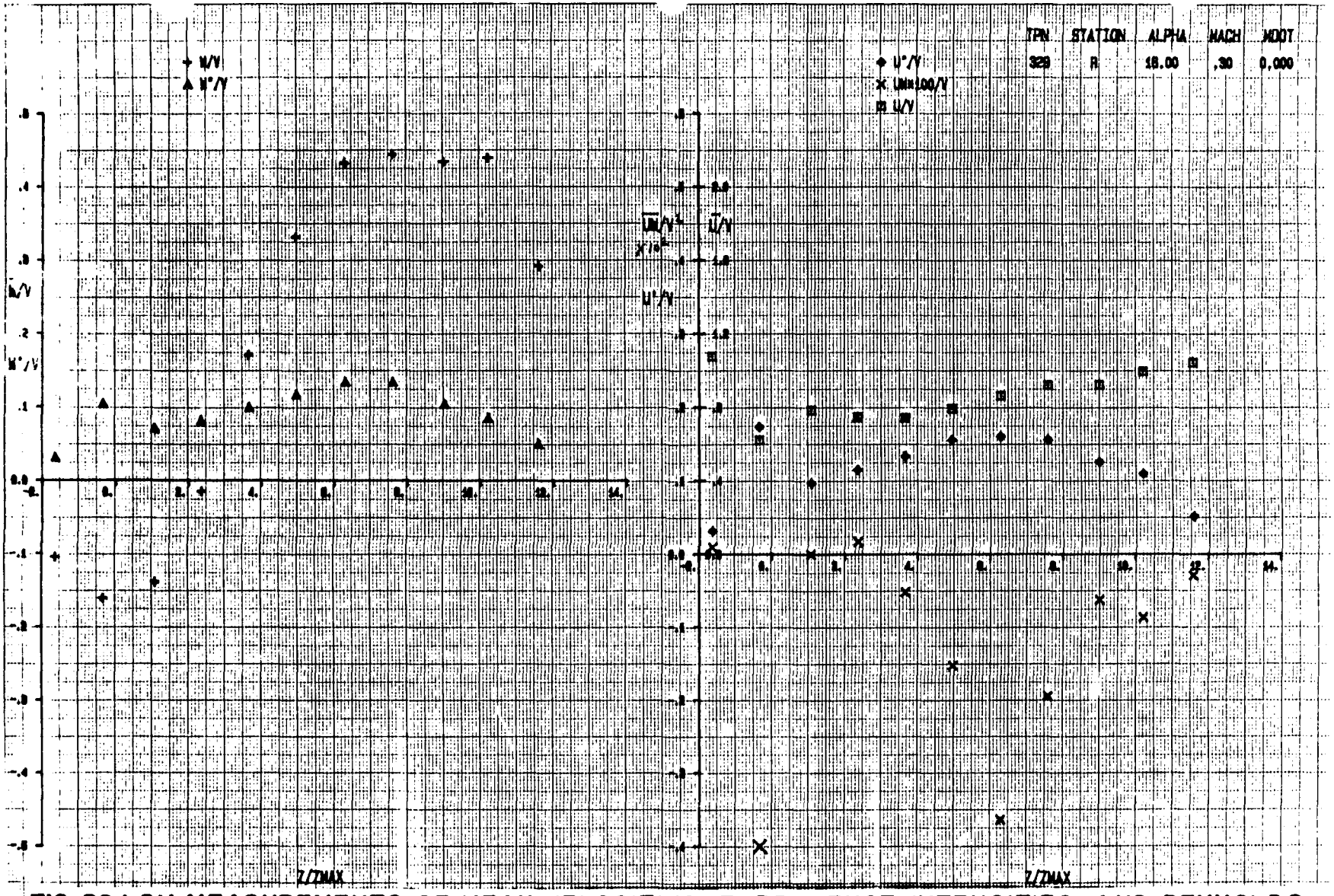

FIG. B2 LDV MEASUREMENTS OF MEAN VELOCITIES, TURBULENCE INTENSITIES, AND REYNOLDS STRESSES WITHOUT BLOWING - COPLANAR CANARD - TGF - α = 16°-STATION R

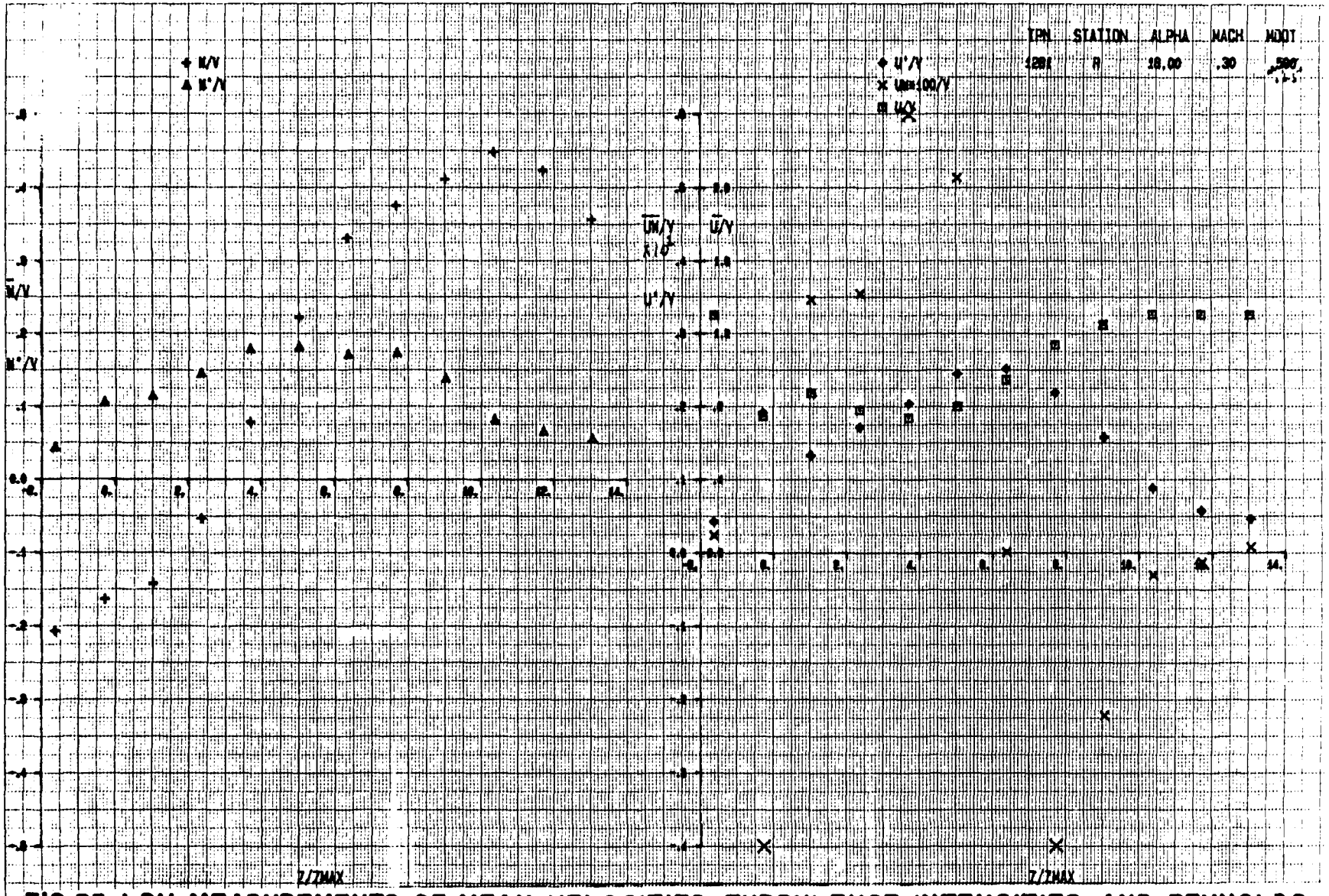

FIG. B3 LDV MEASUREMENTS OF MEAN VELOCITIES, TURBULENCE INTENSITIES, AND REYNOLDS STRESSES WITH BLOWING - COPLANAR CANARD - TGF - α = 16° -STATION R

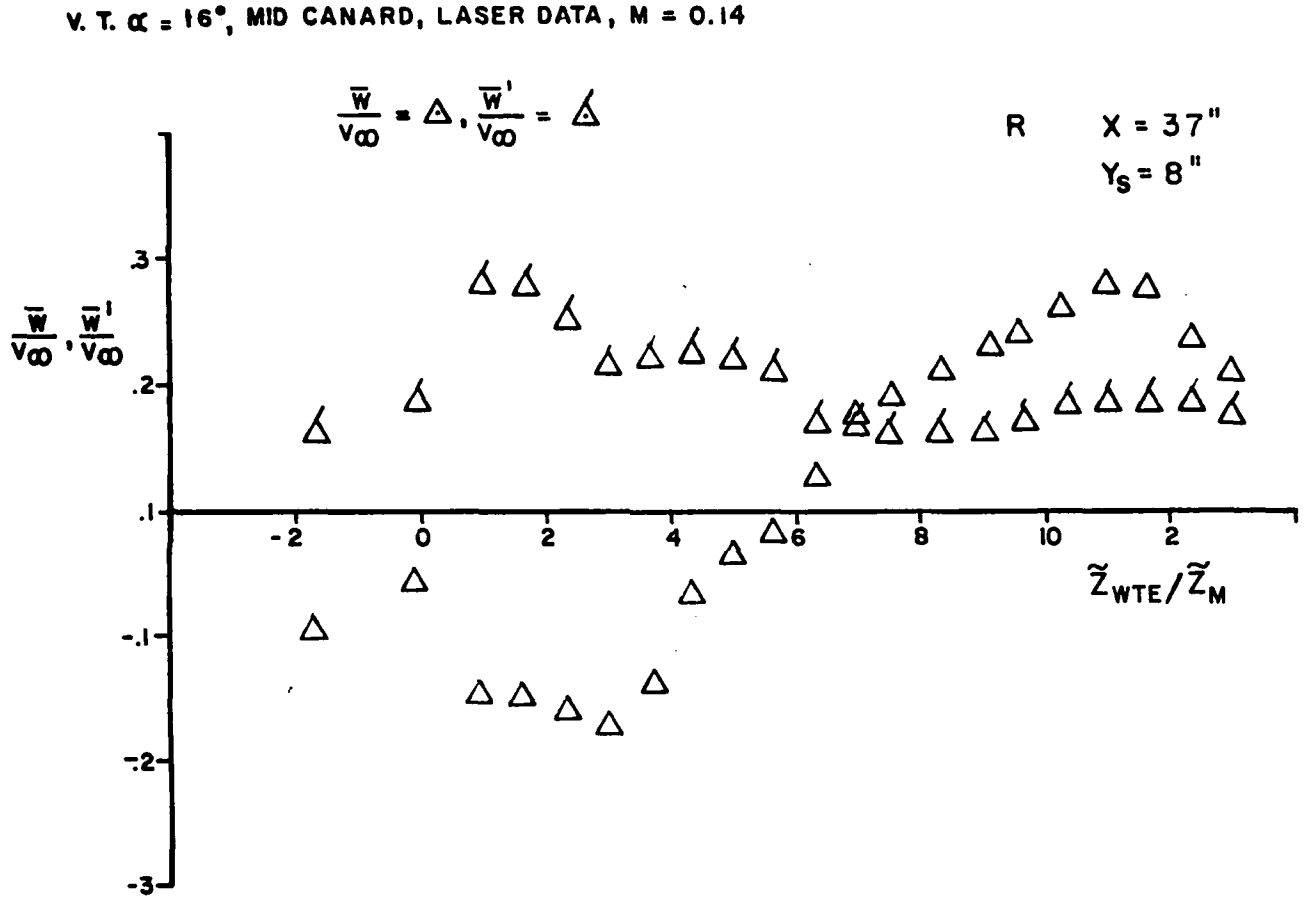

FIG. B4 LDV MEASUREMENTS OF VERTICAL MEAN VELOCITY AND TURBULENCE INTENSITY WITH THE COPLANAR CANARD WITHOUT BLOWING - V.W.T. - α = 16° - STATION R

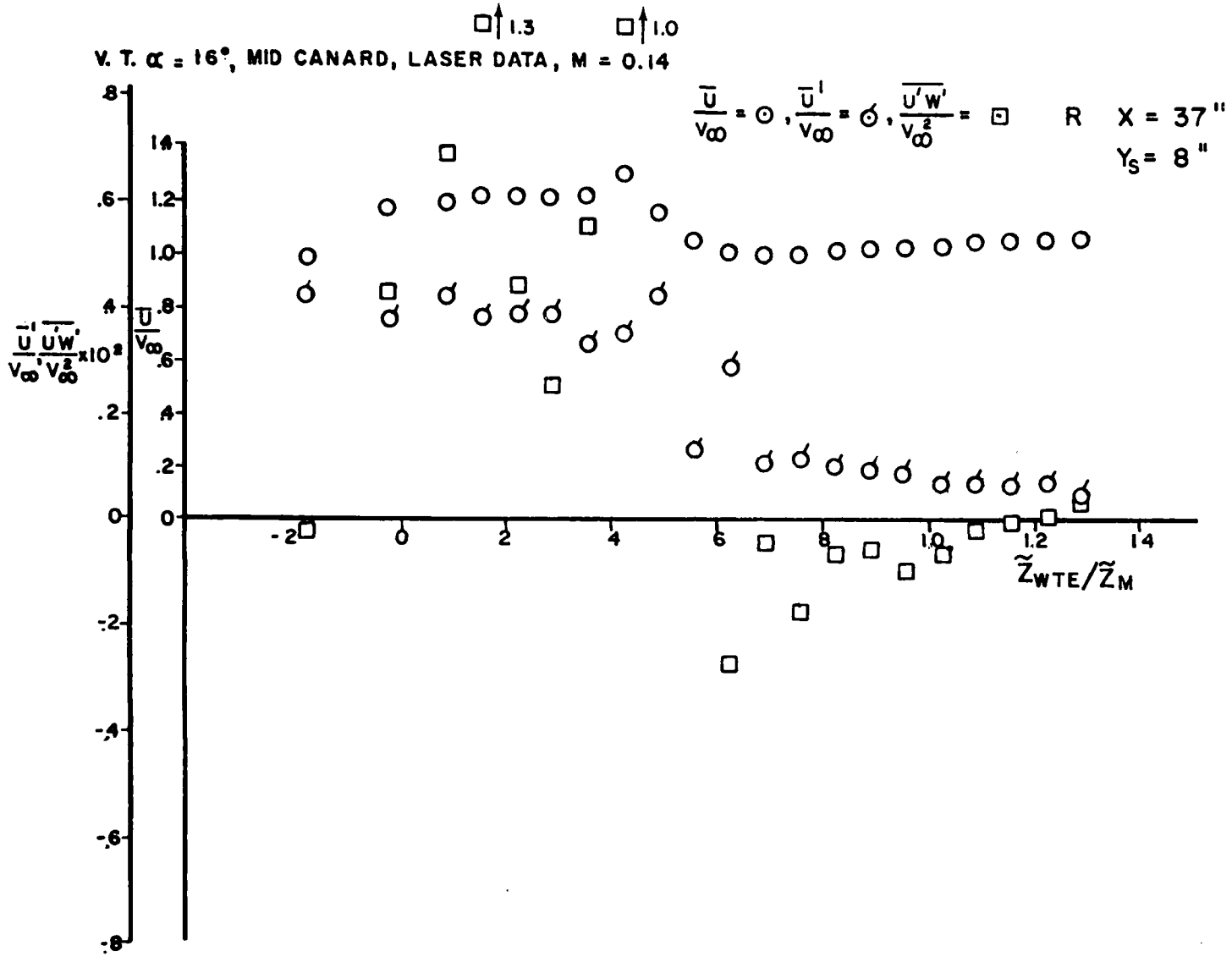

FIG. B5 LDV MEASUREMENTS OF AXIAL MEAN VELOCITY, TURBULENCE INTENSITY, AND REYNOLDS STRESSES WITH THE COPLANAR CANARD WITHOUT BLOWING - V. W. T. - α = 16° STATION R

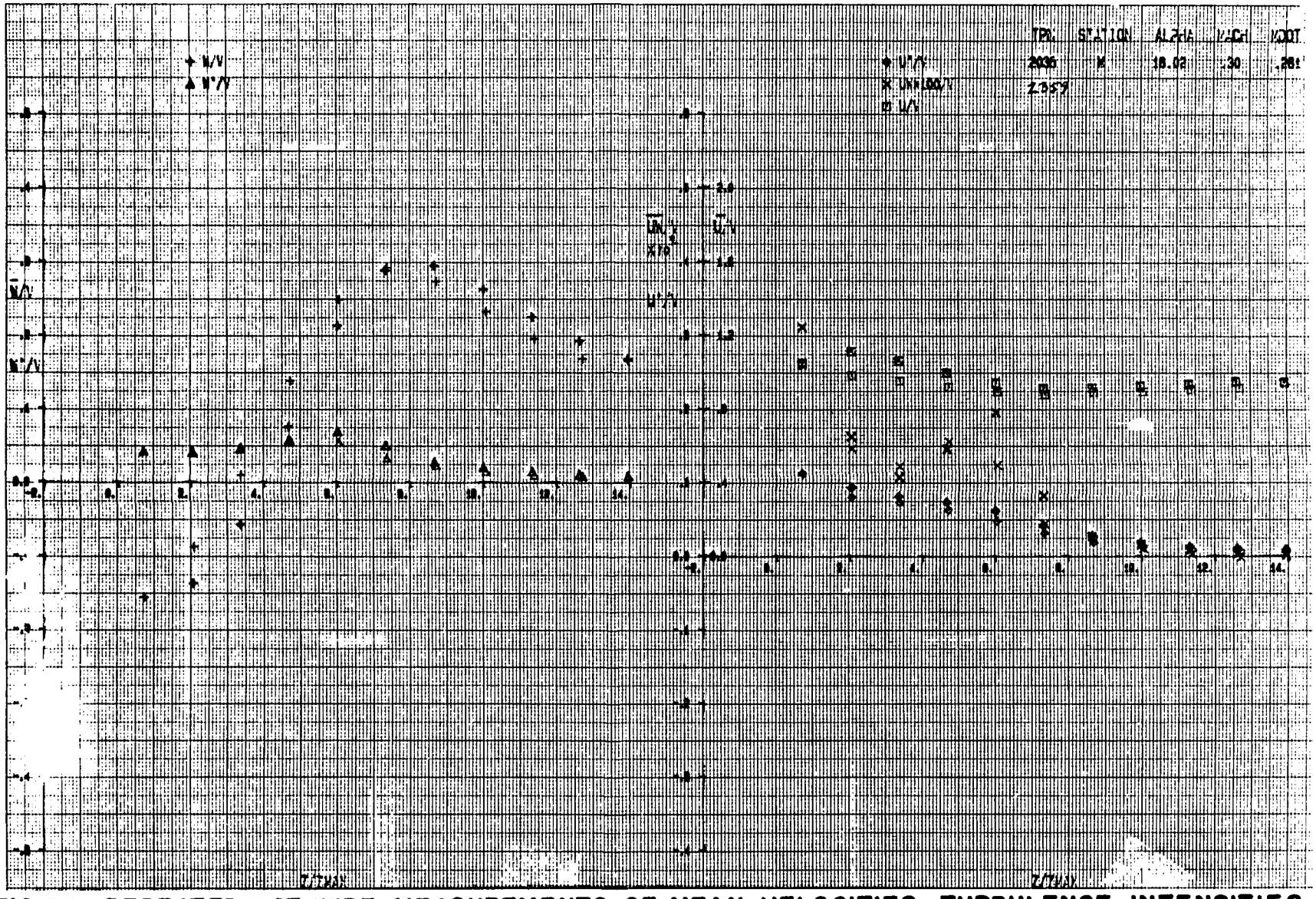

FIG B6 REPEATED HOT WIRE MEASUREMENTS OF MEAN VELOCITIES, TURBULENCE INTENSITIES AND REYNOLDS STRESSES WITH BLOWING - COPLANAR CANARD - TGF - α = 16° STATION M

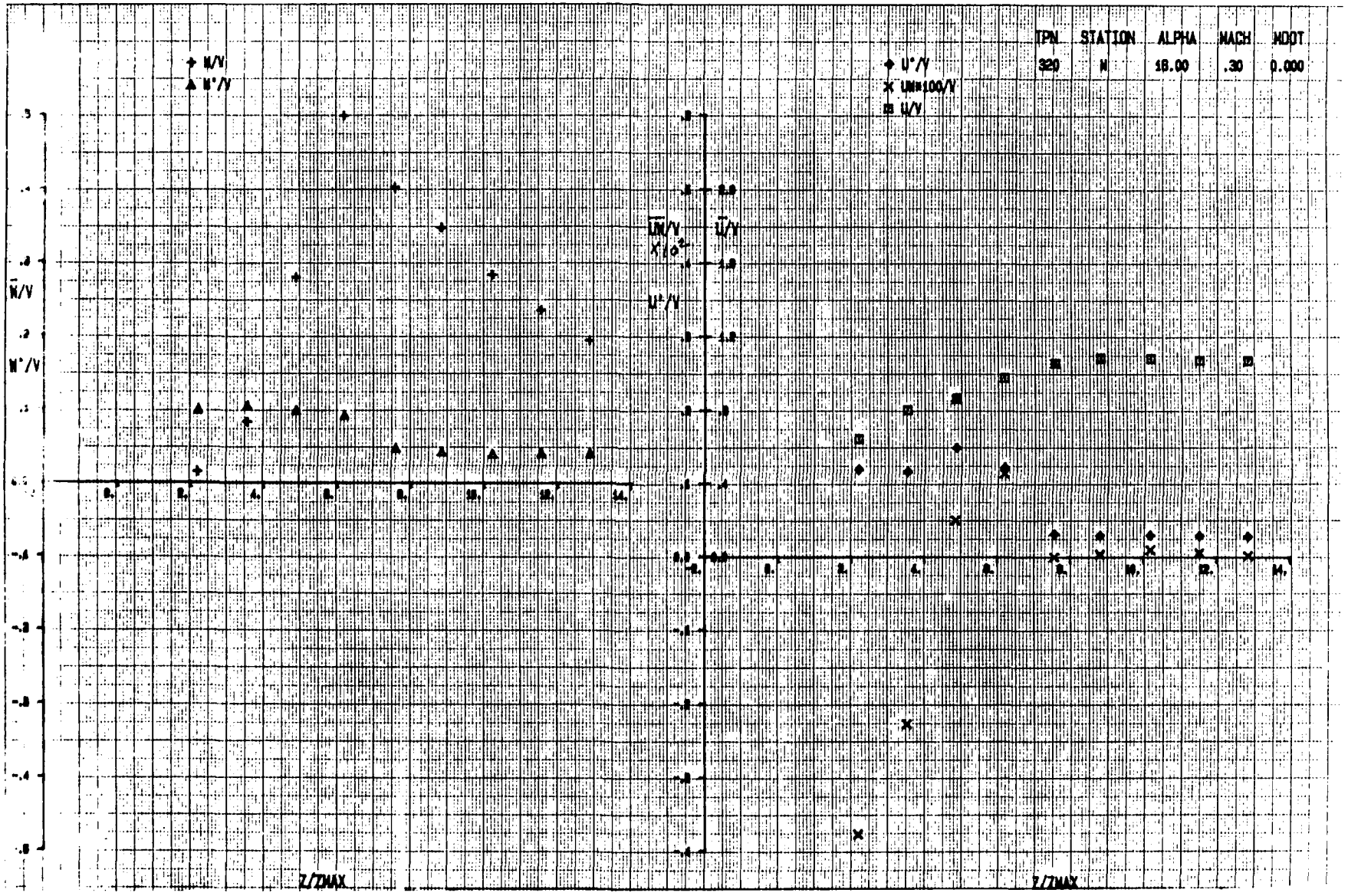

FIG. B7 LDV MEASUREMENTS OF MEAN VELOCITIES, TURBULENCE INTENSITIES, AND REYNOLDS STRESSES WITHOUT BLOWING - COPLANAR CANARD - TGF - α = 16°-STATION M

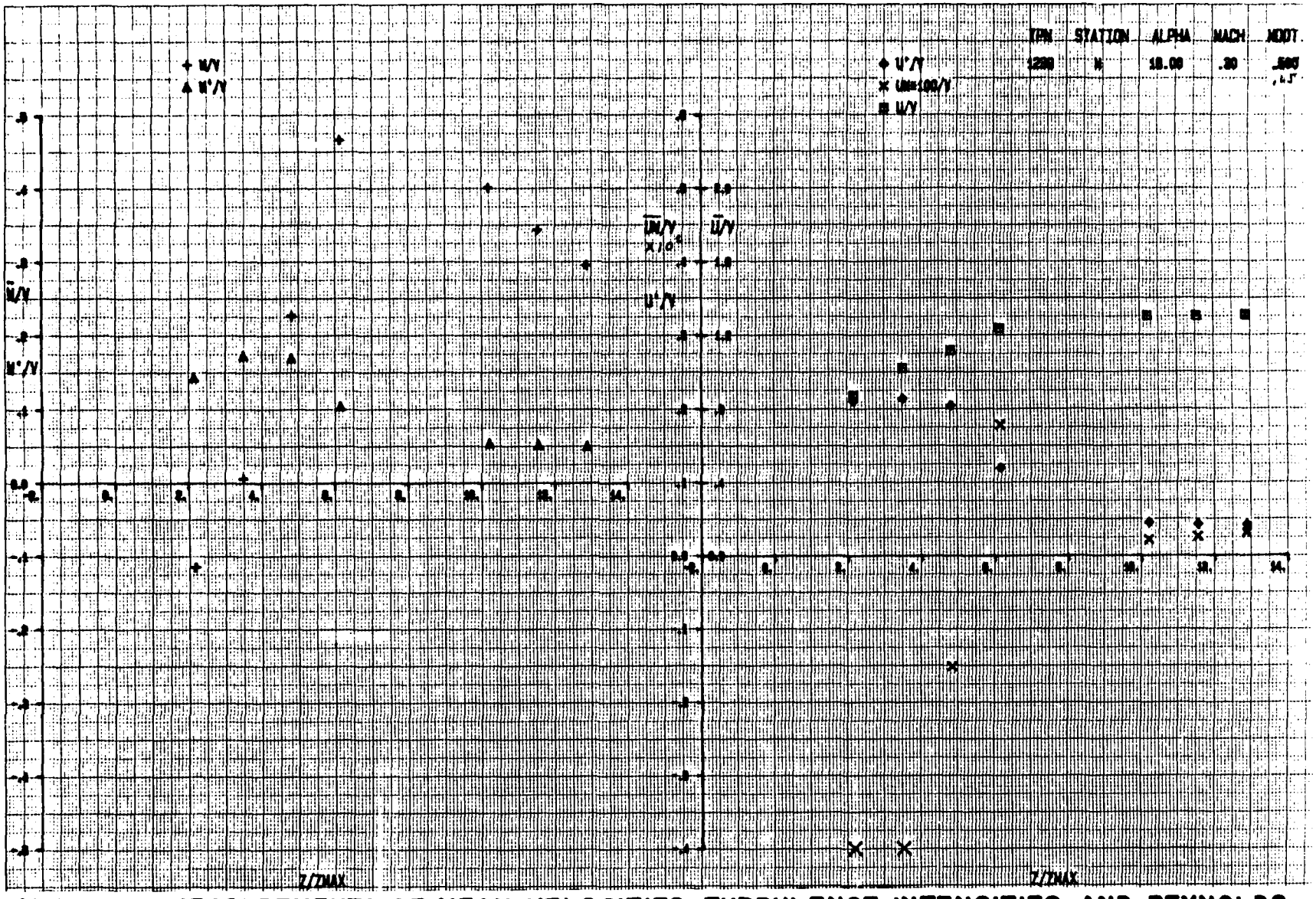

FIG. B8 LDV MEASUREMENTS OF MEAN VELOCITIES, TURBULENCE INTENSITIES, AND REYNOLDS STRESSES WITH BLOWING - COPLANAR CANARD - TGF - α = 16°-STATION M

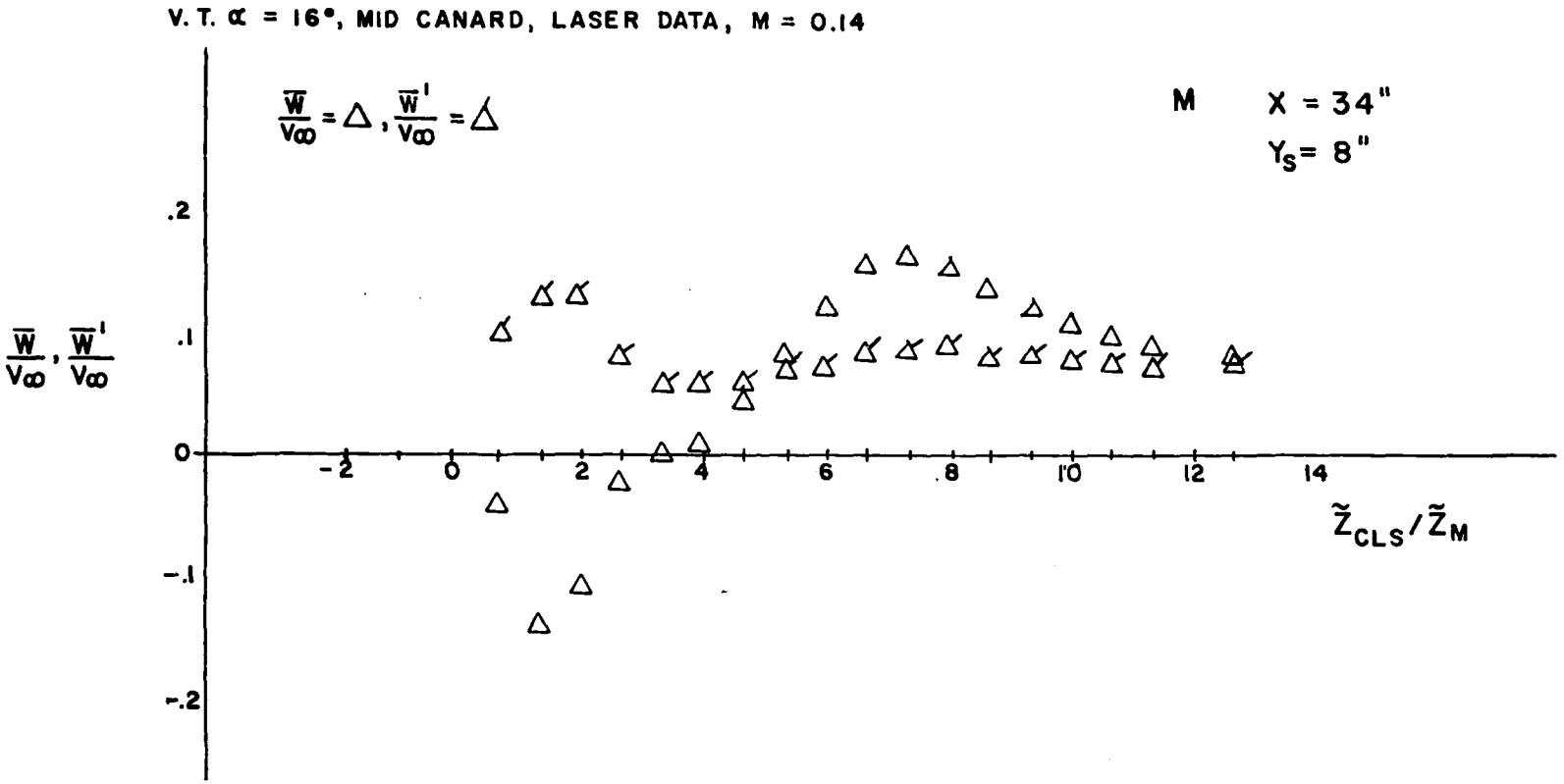

FIG. B9 LDV MEASUREMENTS OF VERTICAL MEAN VELOCITY AND TURBULENCE INTENSITY WITH THE COPLANAR CANARD - WITHOUT BLOWING - V.W.T. - α = 16° - STATION M

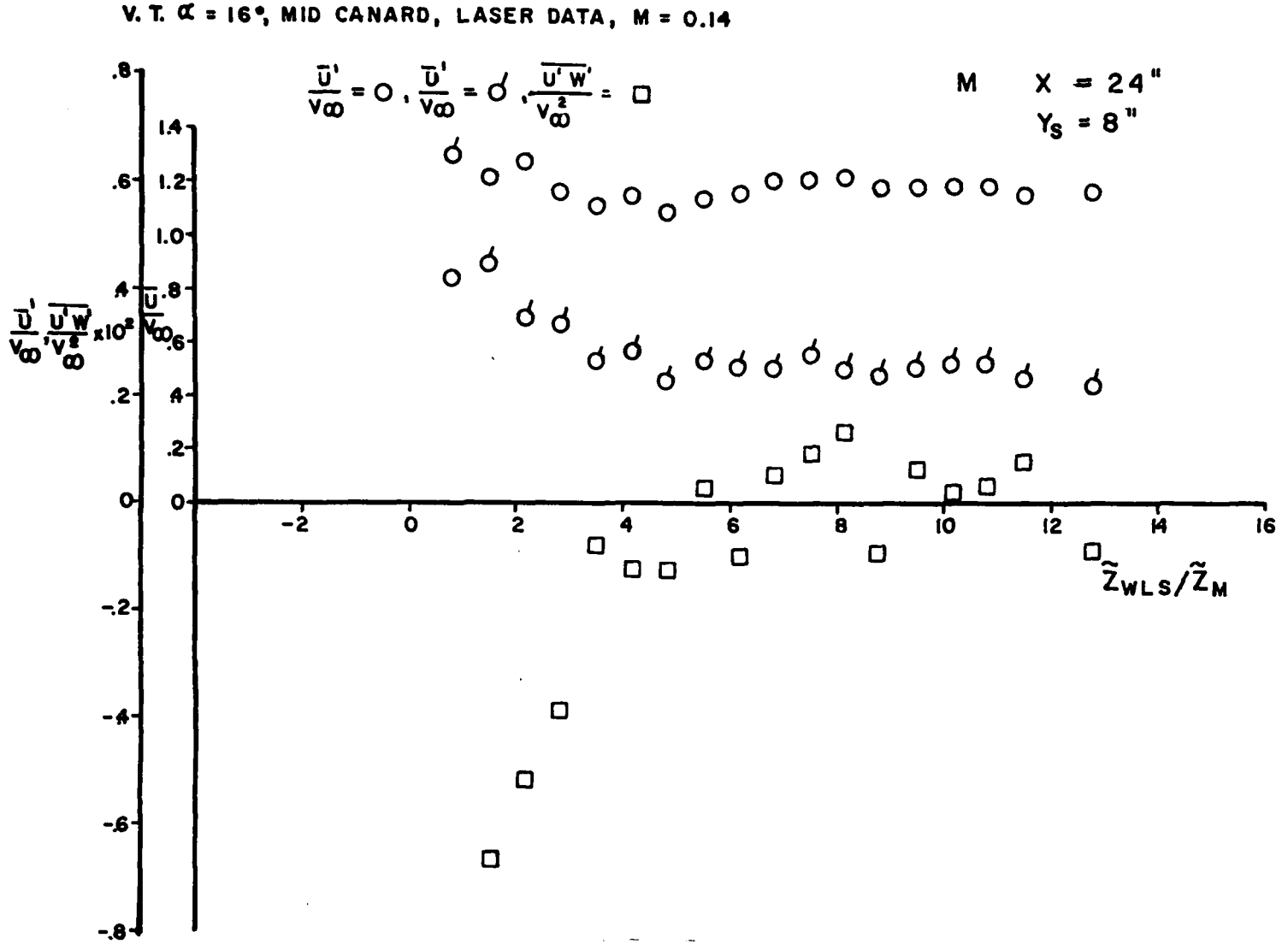

FIG. BIOLDV MEASUREMENTS OF AXIAL MEAN VELOCITY, TURBULENCE INTENSITY, AND REYNOLDS STRESSES WITH THE COPLANAR CANARD WITHOUT BLOWING - V. W. T. - α = 16° - STATION M

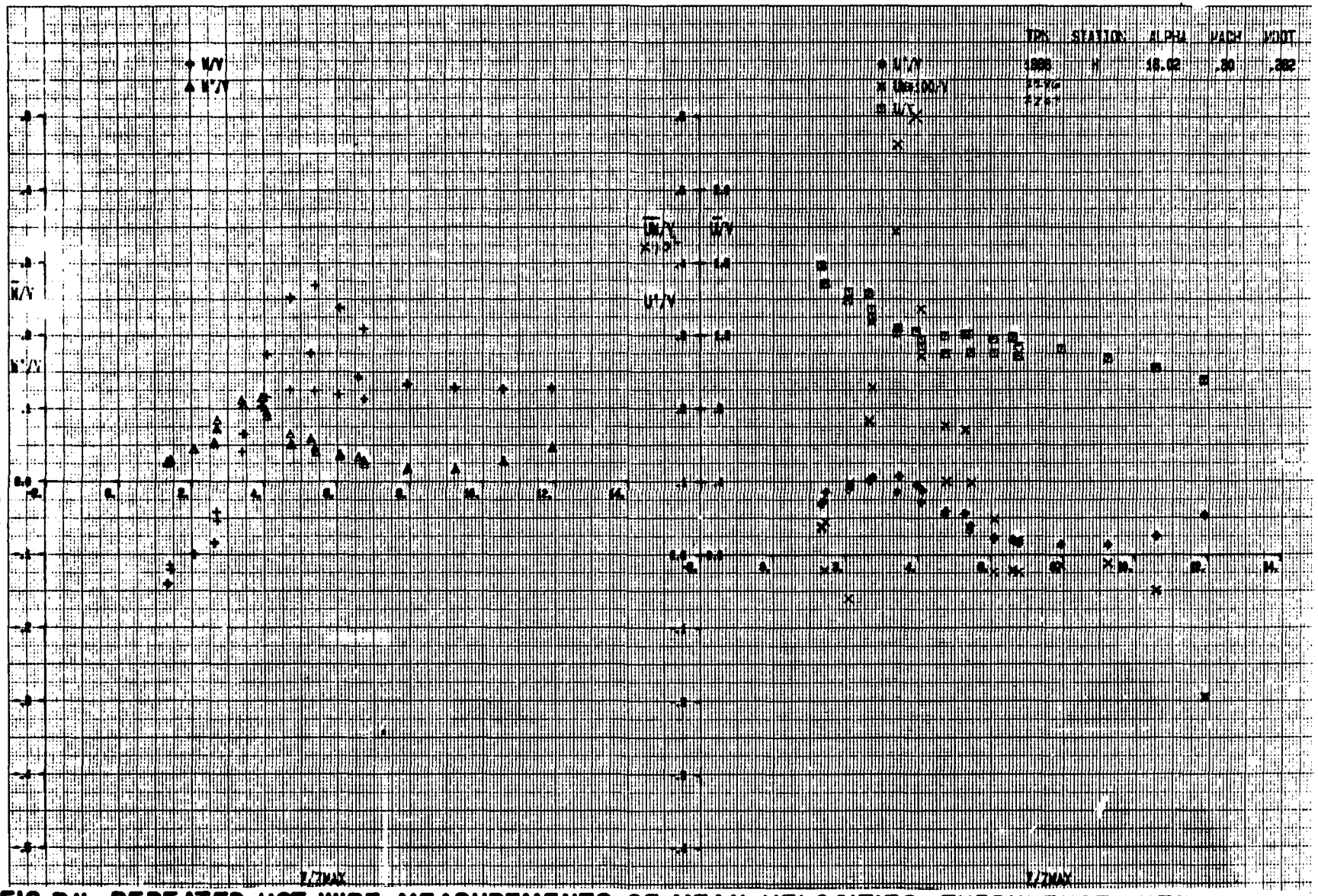

FIG B11 REPEATED HOT WIRE MEASUREMENTS OF MEAN VELOCITIES, TURBULENCE INTENSITIES AND REYNOLDS STRESSES WITH BLOWING - COPLANAR CANARD - TGF - α = 16° STATION H

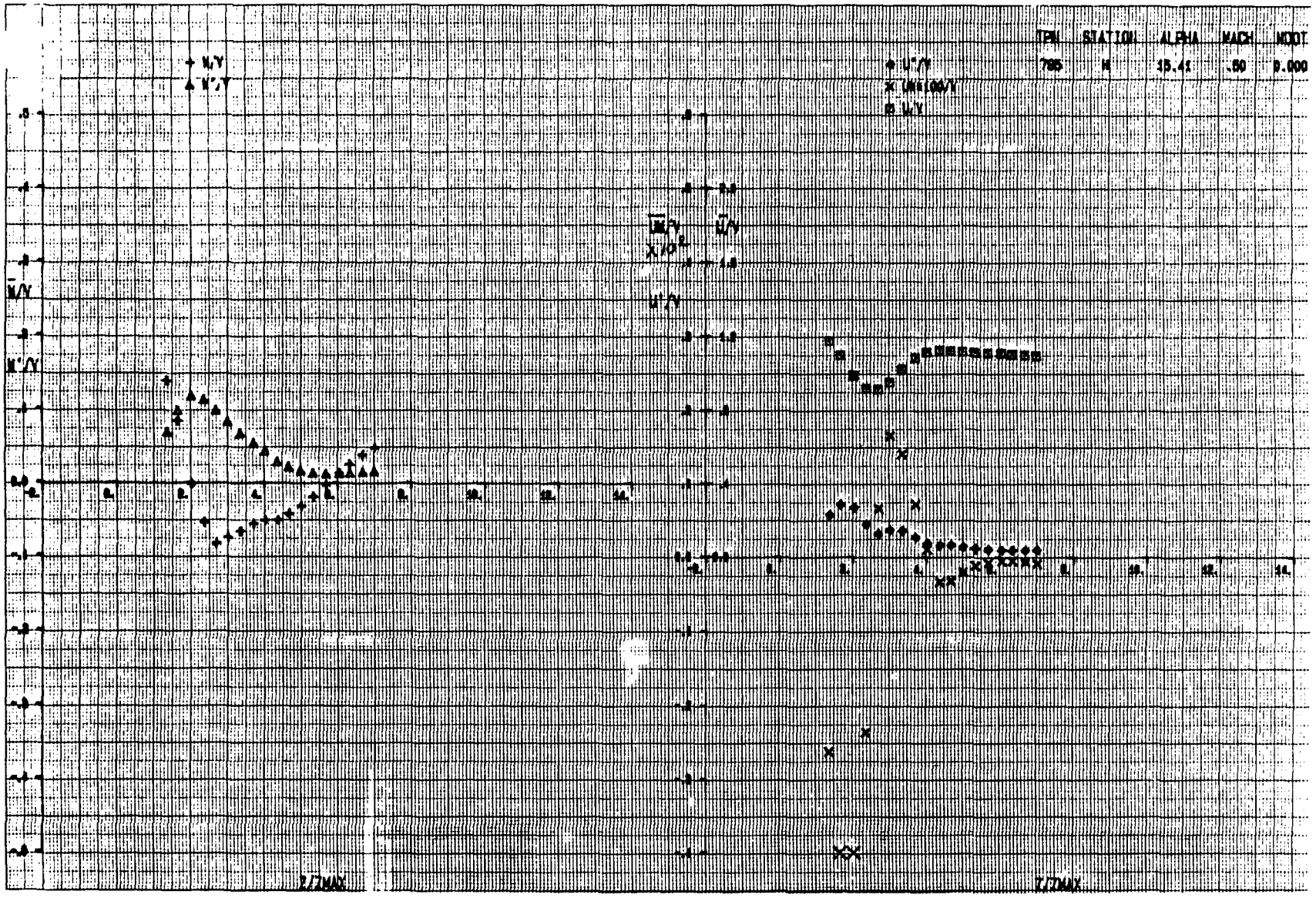

FIG. B12 HOT WIRE MEASUREMENT OF MEAN VELOCITIES, TURBULENCE INTENSITIES, AND REYNOLDS STRESSES WITHOUT BLOWING - COPLANAR CANARD - TGF - $\alpha = 16°$ STATION H

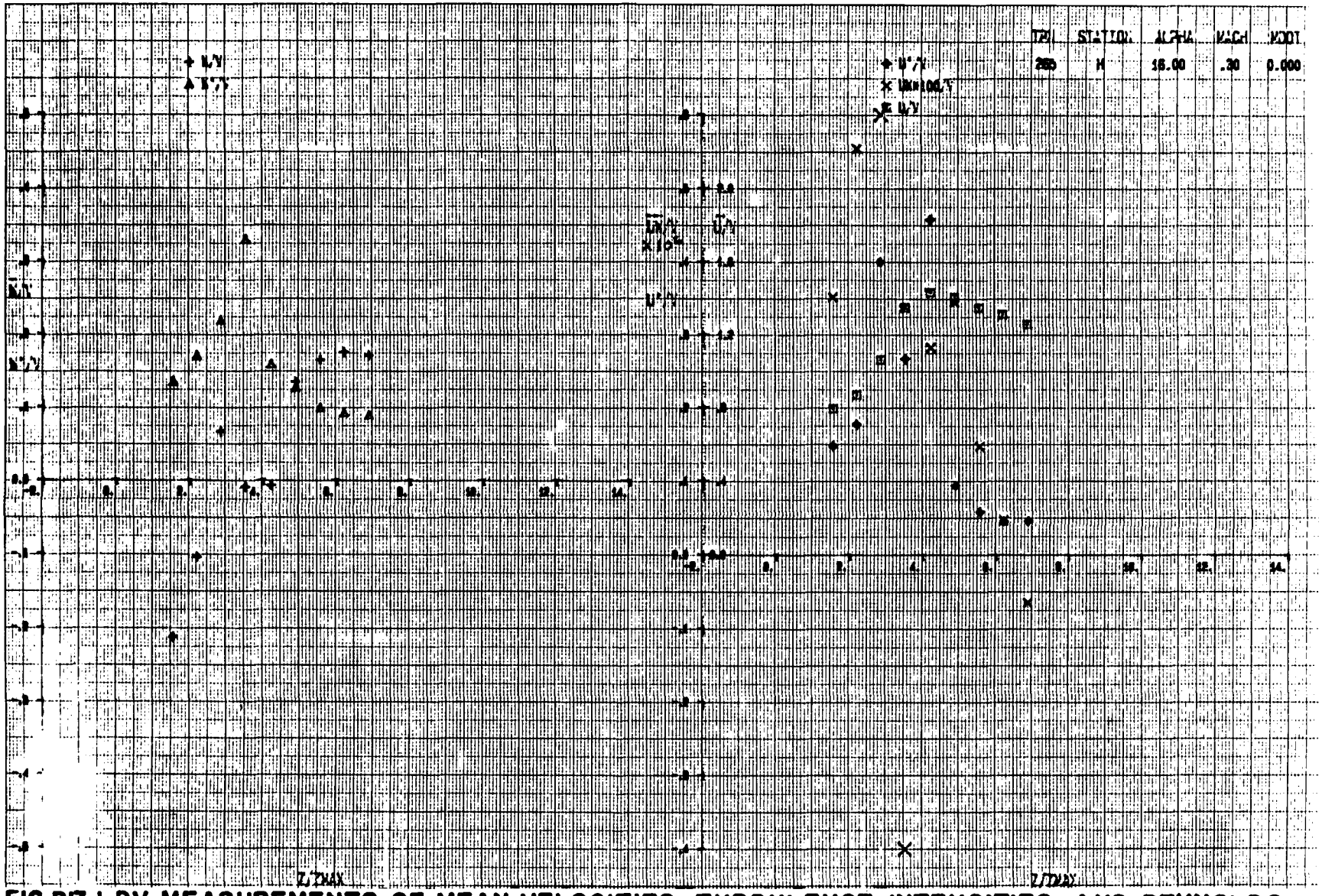

FIG.B13 LDV MEASUREMENTS OF MEAN VELOCITIES, TURBULENCE INTENSITIES, AND REYNOLDS STRESSES WITHOUT BLOWING - COPLANAR CANARD - TGF - α = 16°-STATION H

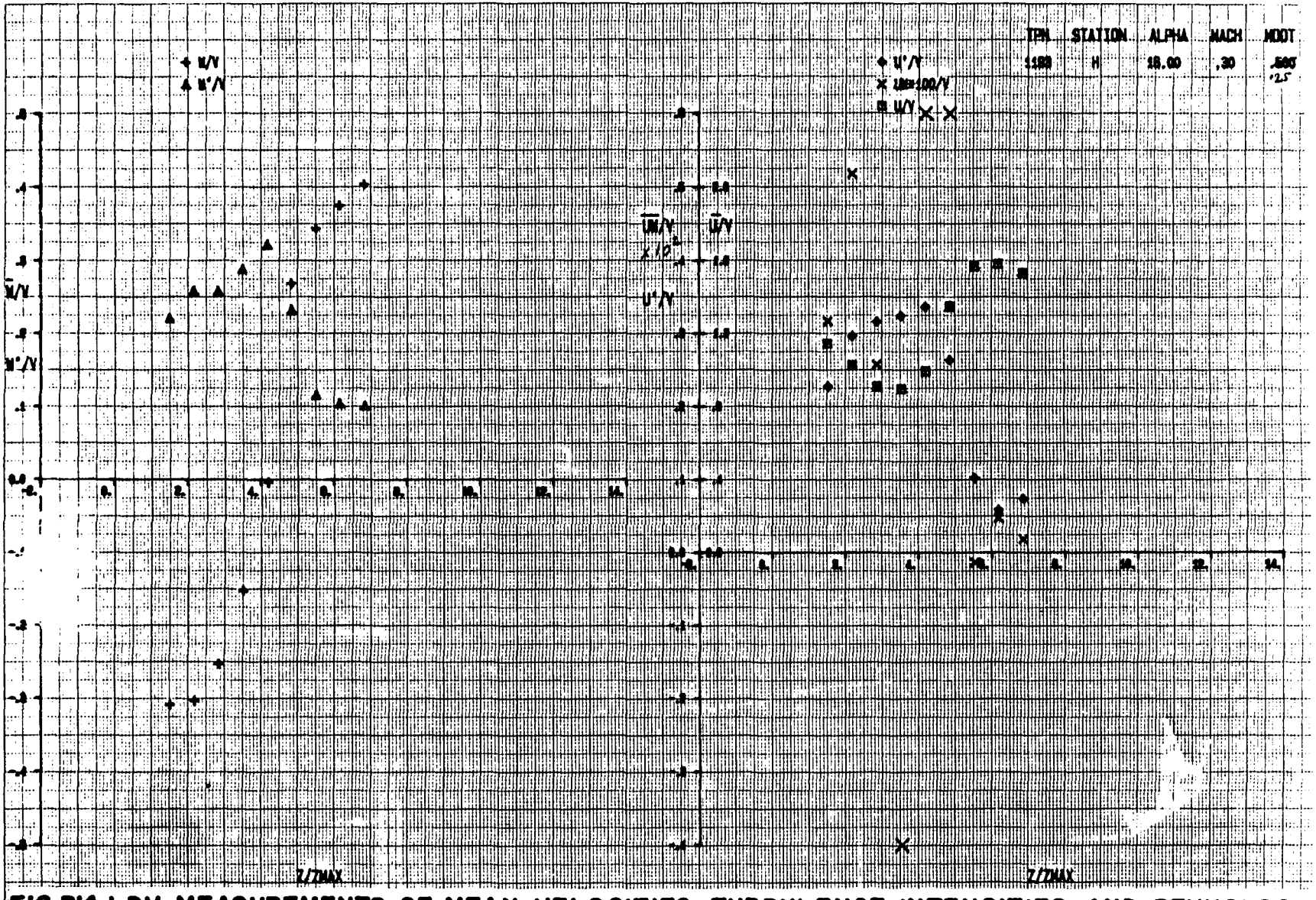

FIG.B14 LDV MEASUREMENTS OF MEAN VELOCITIES, TURBULENCE INTENSITIES, AND REYNOLDS STRESSES WITH BLOWING - COPLANAR CANARD - TGF - α = 16° -STATION H

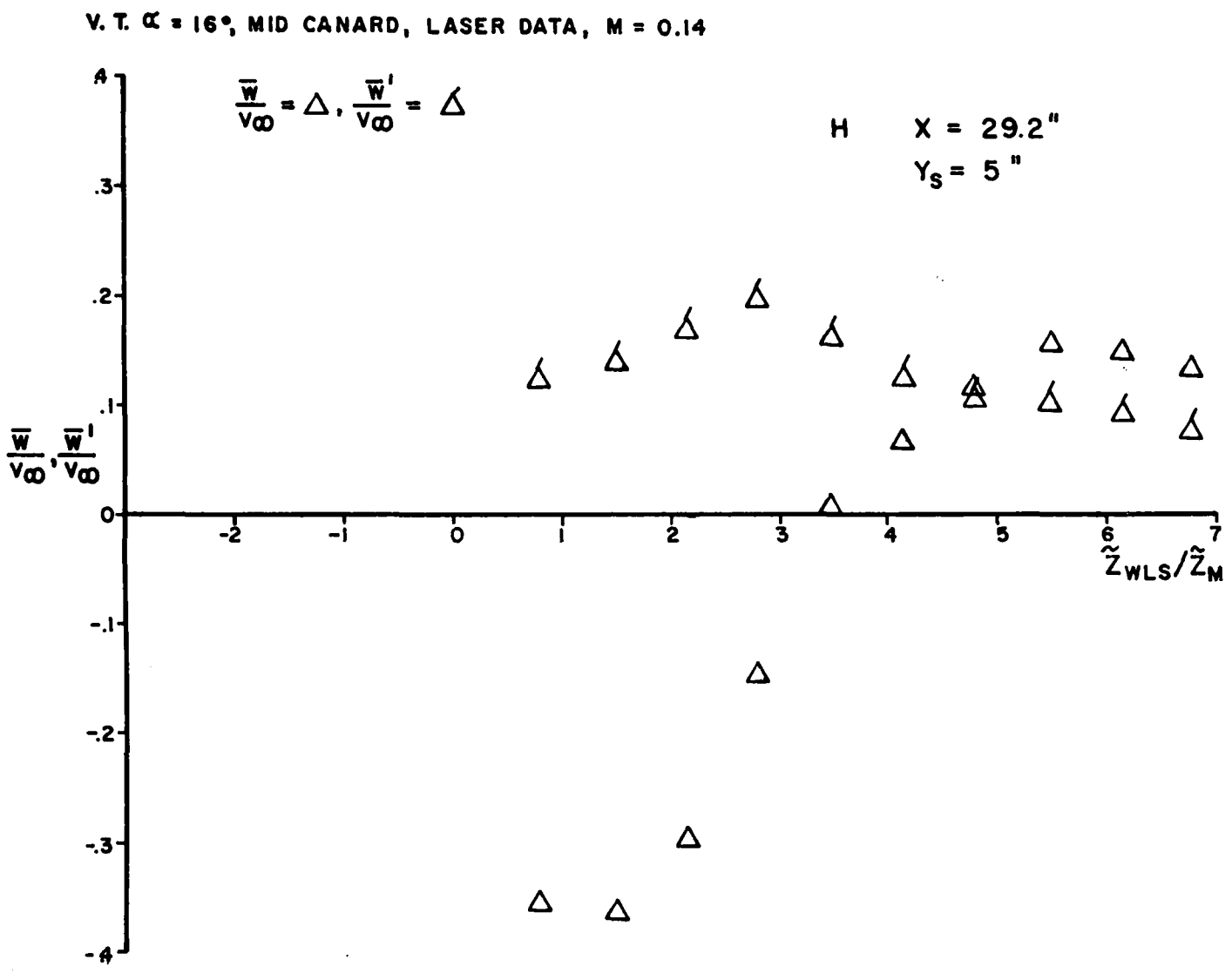

FIG. B15 LDV MEASUREMENTS OF VERTICAL MEAN VELOCITY AND TURBULENCE INTENSITY WITH THE COPLANAR CANARD WITHOUT BLOWING - V.W.T. - α = 16° - STATION H

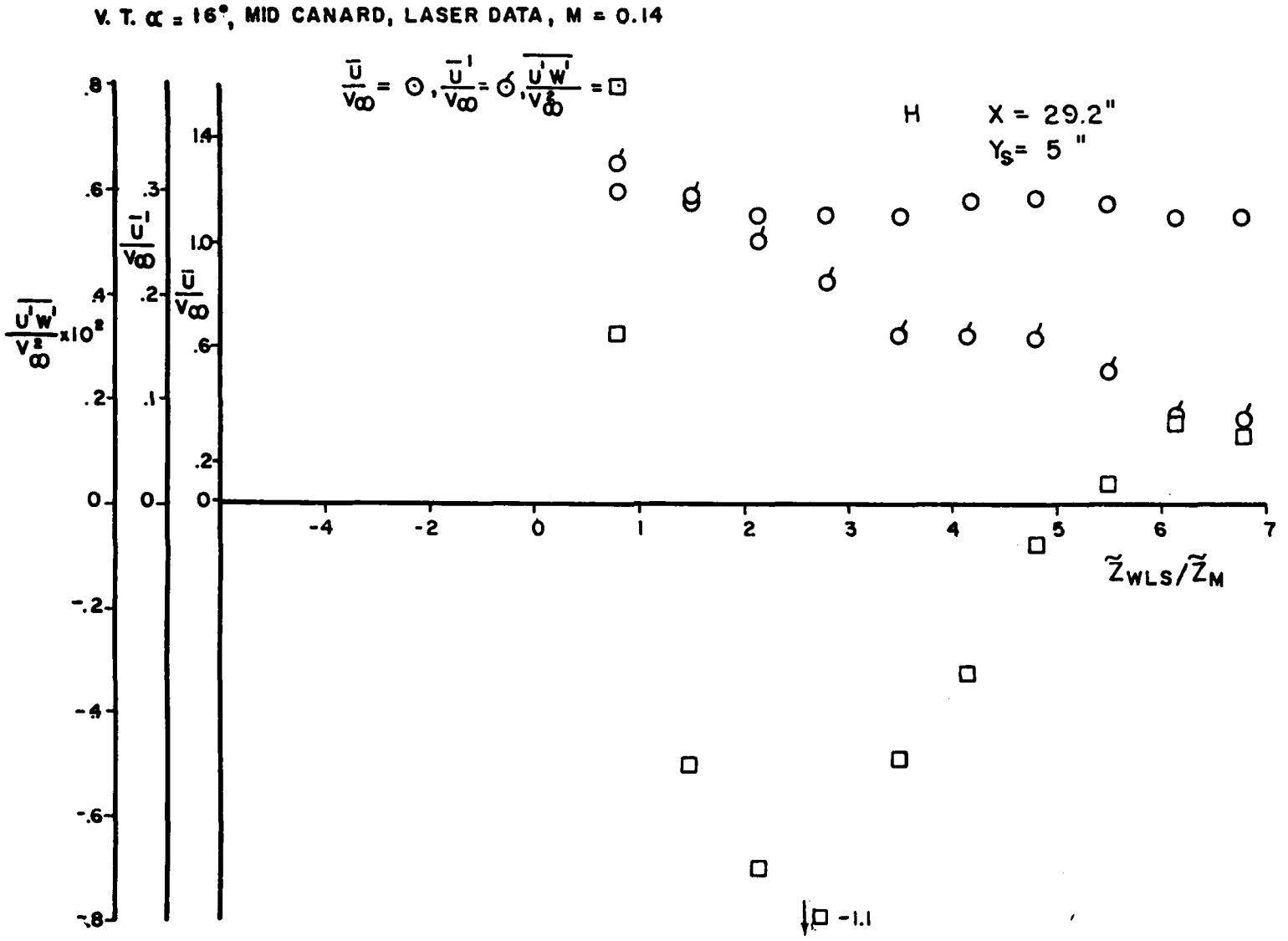

FIG. B16LDV MEASUREMENTS OF AXIAL MEAN VELOCITY, TURBULENCE INTENSITY, AND REYNOLDS STRESSES WITH THE COPLANAR CANARD WITHOUT BLOWING – V. W. T. – α = 16° STATION H

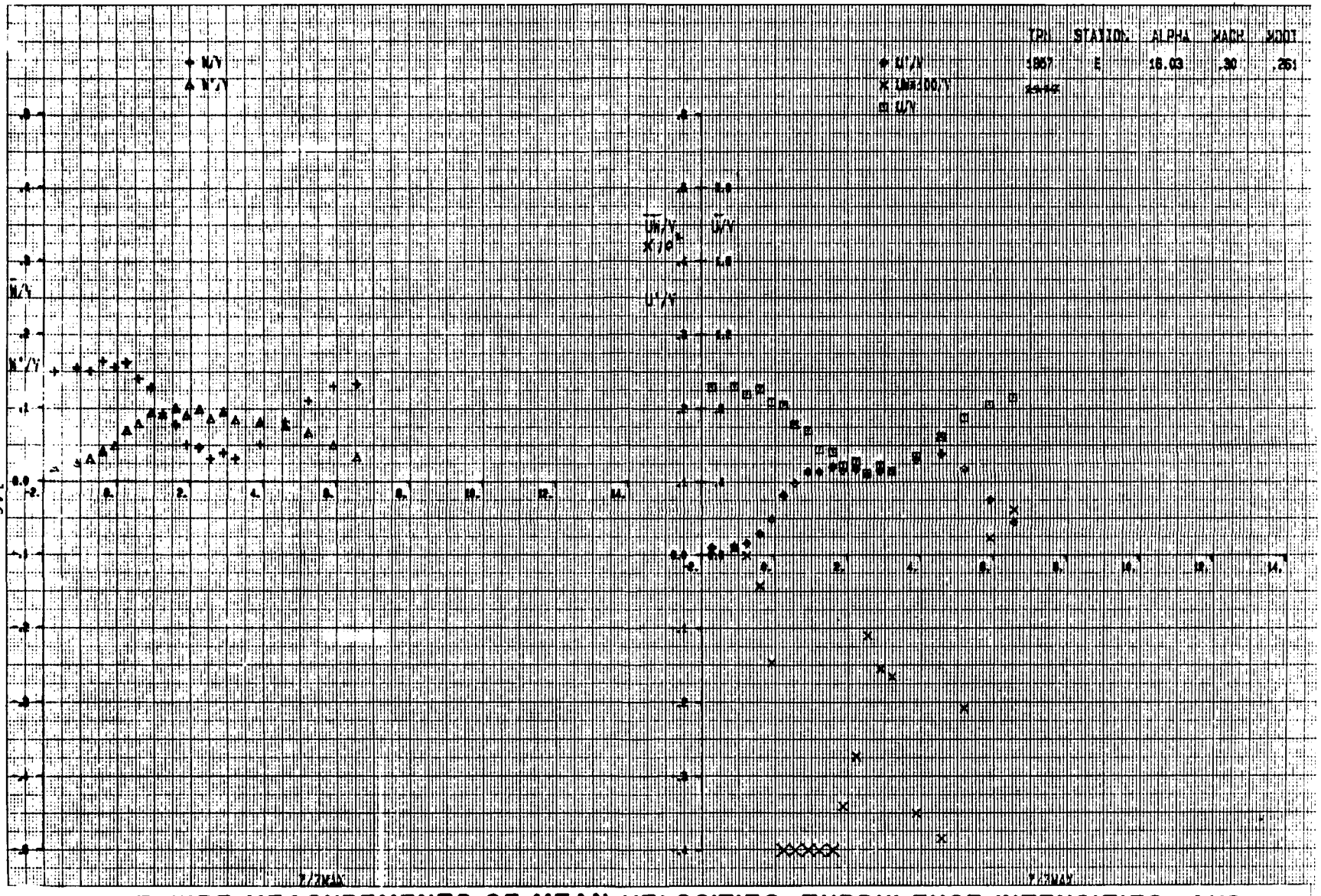

FIG.B17 HOT WIRE MEASUREMENTS OF MEAN VELOCITIES, TURBULENCE INTENSITIES, AND REYNOLDS STRESSES WITH BLOWING - COPLANAR CANARD - TGF - α=16°-STATION E

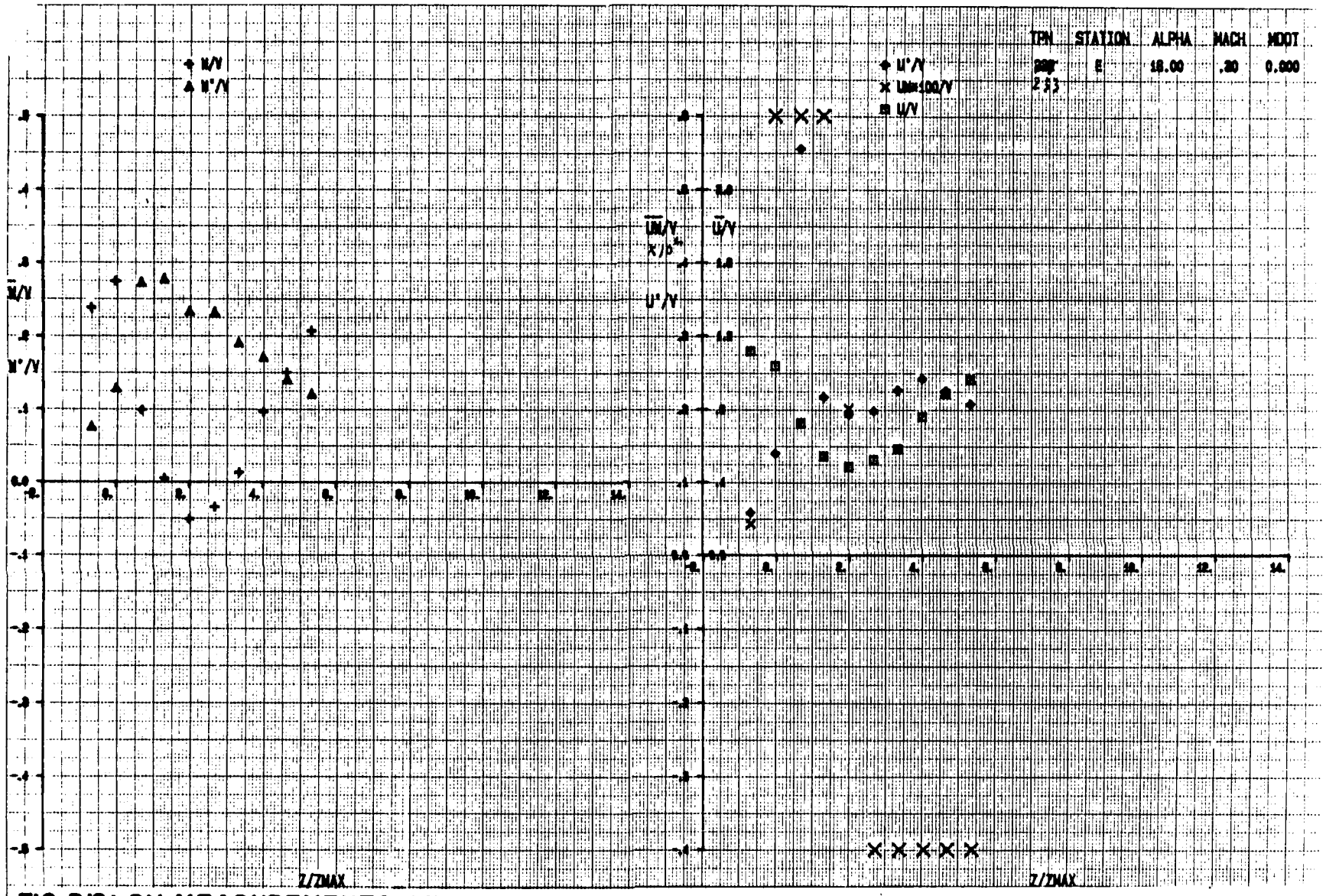

FIG. B18 LDV MEASUREMENTS OF MEAN VELOCITIES, TURBULENCE INTENSITIES, AND REYNOLDS STRESSES WITHOUT BLOWING - COPLANAR CANARD - TGF - α = 16° - STATION E

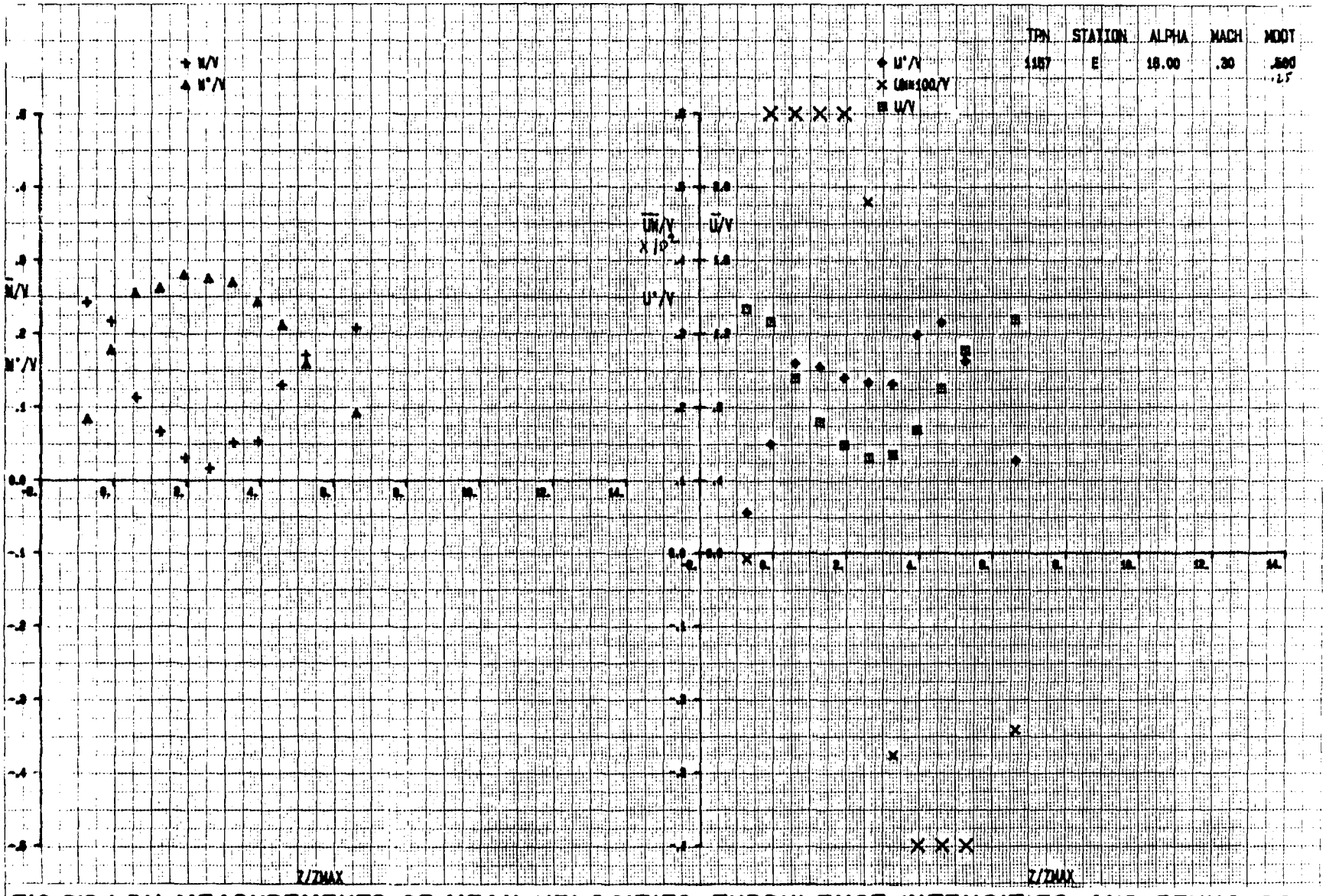

FIG. 819 LDV MEASUREMENTS OF MEAN VELOCITIES, TURBULENCE INTENSITIES, AND REYNOLDS STRESSES WITH BLOWING - COPLANAR CANARD - TGF - α = 16° -STATION E

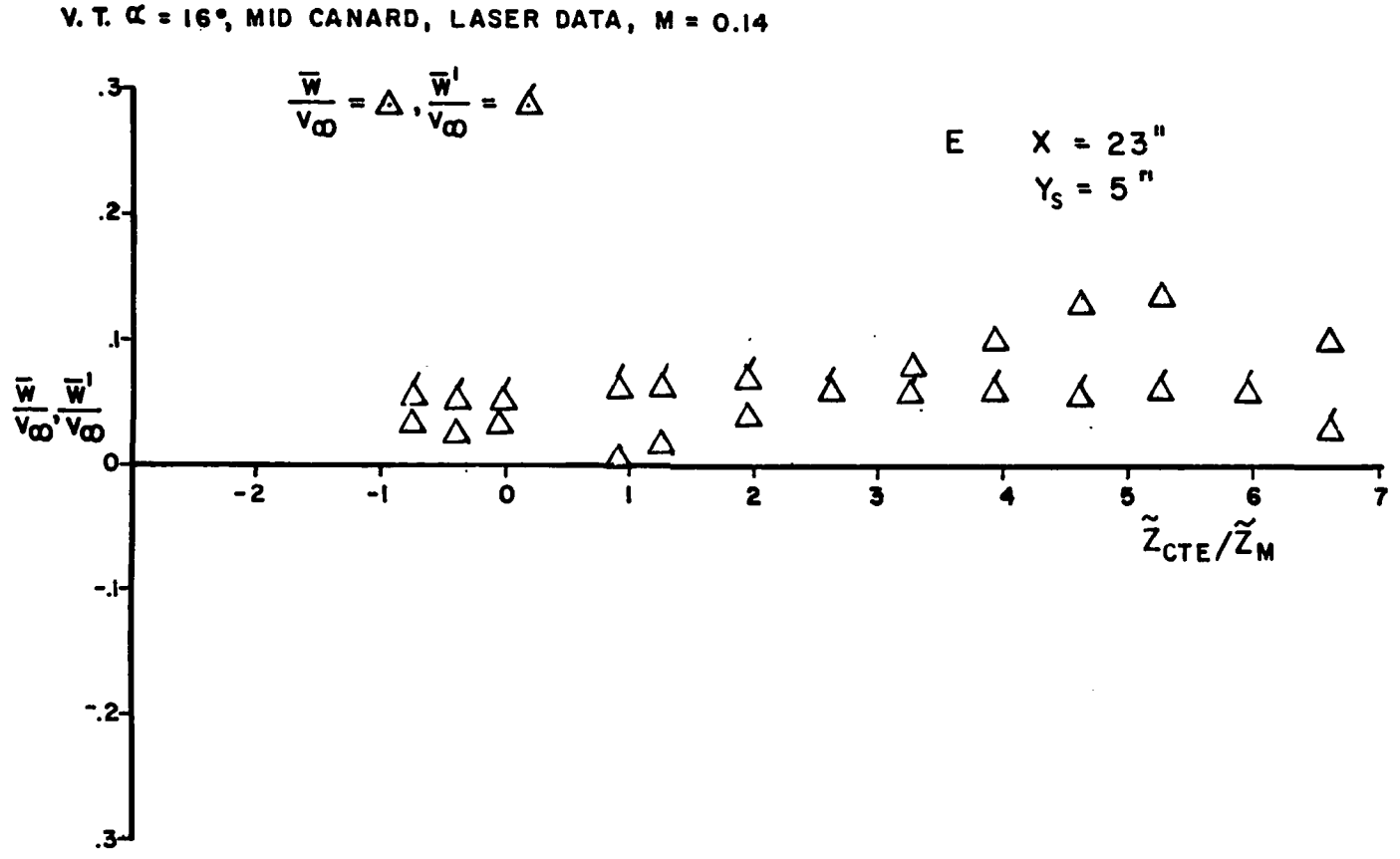

FIG. 82 LDV MEASUREMENTS OF VERTICAL MEAN VELOCITY AND TURBULENCE INTENSITY WITH THE COPLANAR CANARD WITHOUT BLOWING - V.W.T. - α = 16° - STATION E

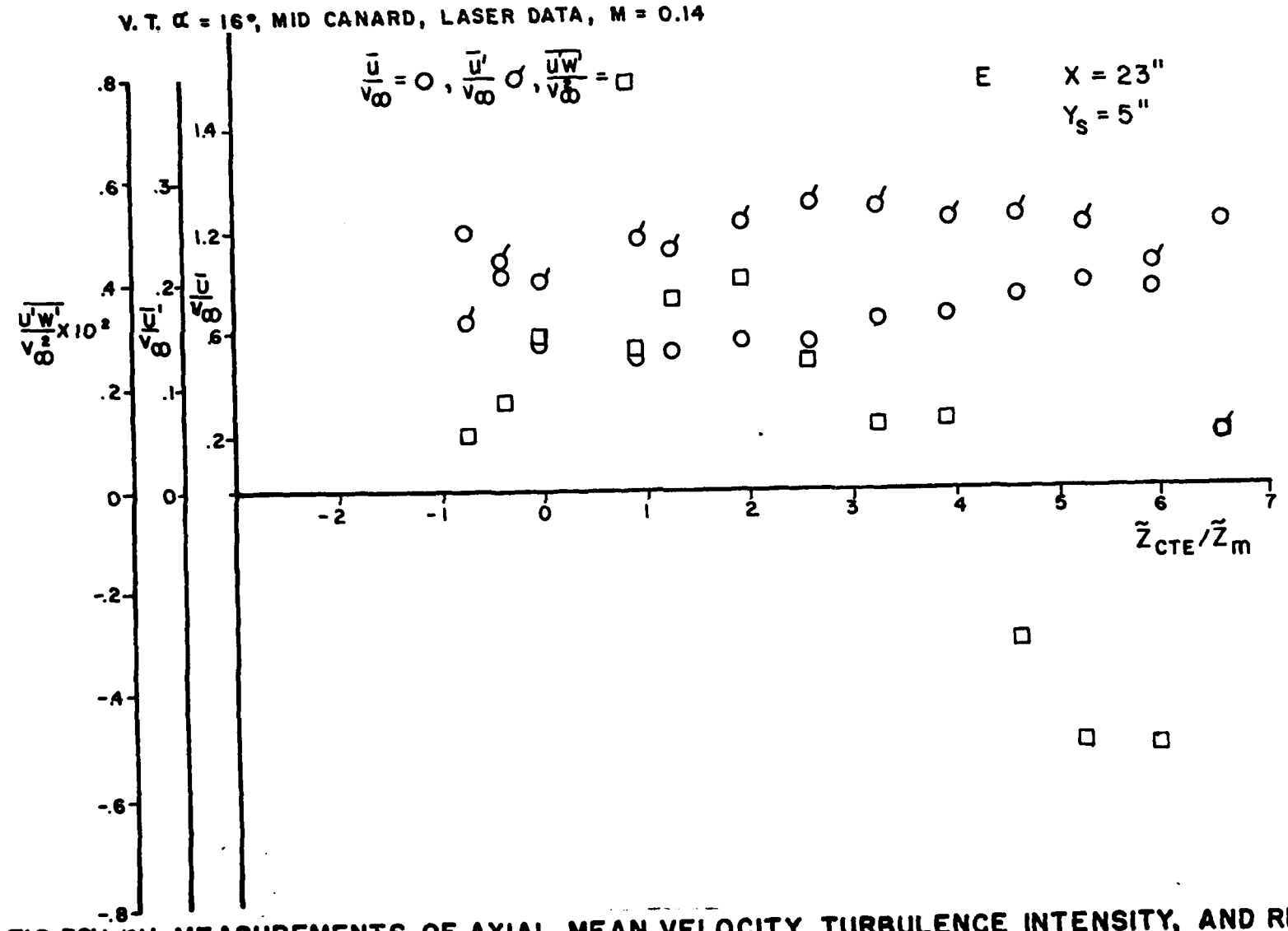

FIG. B21 LDV MEASUREMENTS OF AXIAL MEAN VELOCITY, TURBULENCE INTENSITY, AND REYNOLDS STRESSES WITH THE COPLANAR CANARD WITHOUT BLOWING - W.T. - α = 16° STATION E

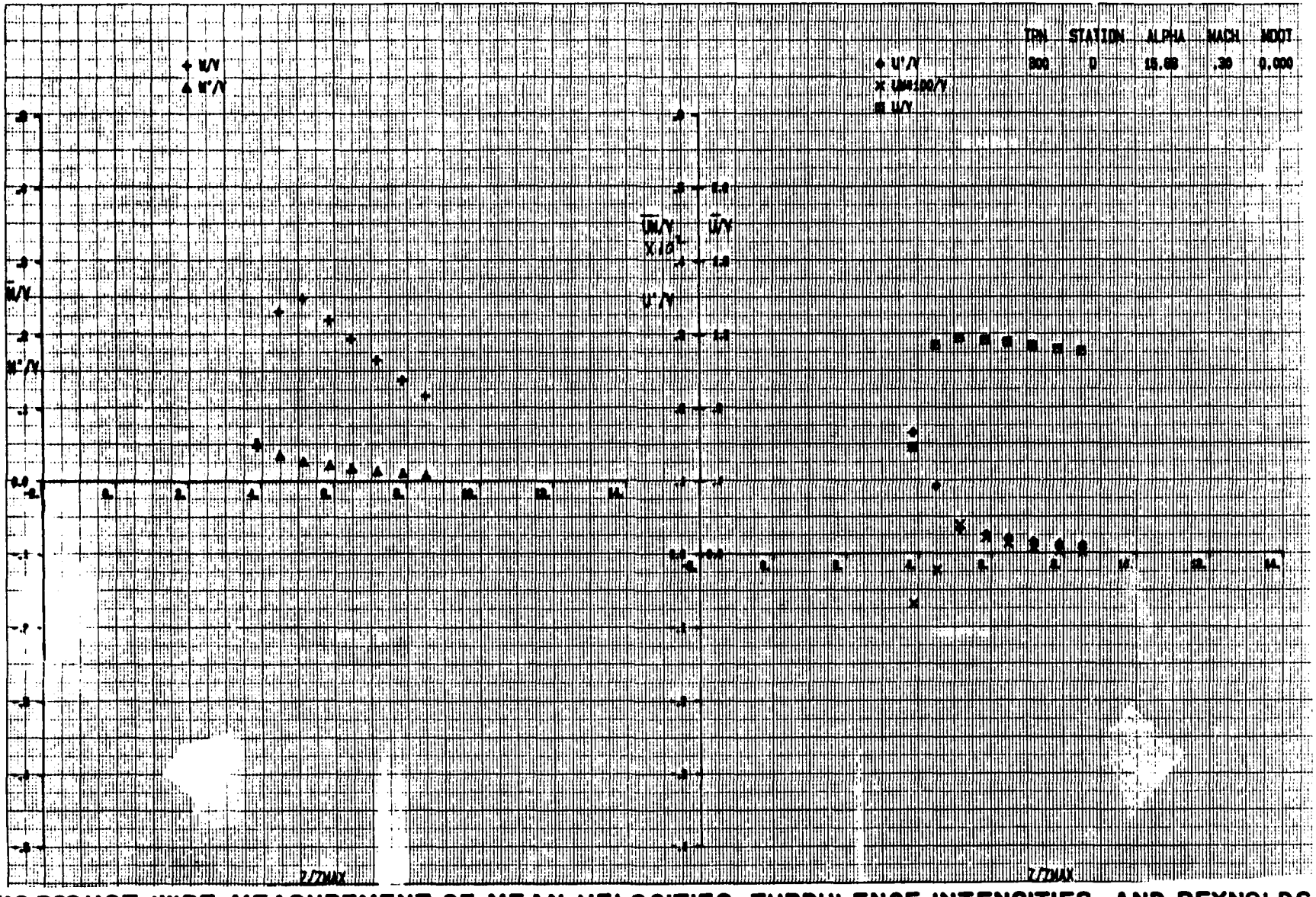

FIG.B22 HOT WIRE MEASUREMENT OF MEAN VELOCITIES, TURBULENCE INTENSITIES, AND REYNOLDS STRESSES WITHOUT BLOWING - COPLANAR CANARD - TGF - $\alpha = 16°$ STATION D

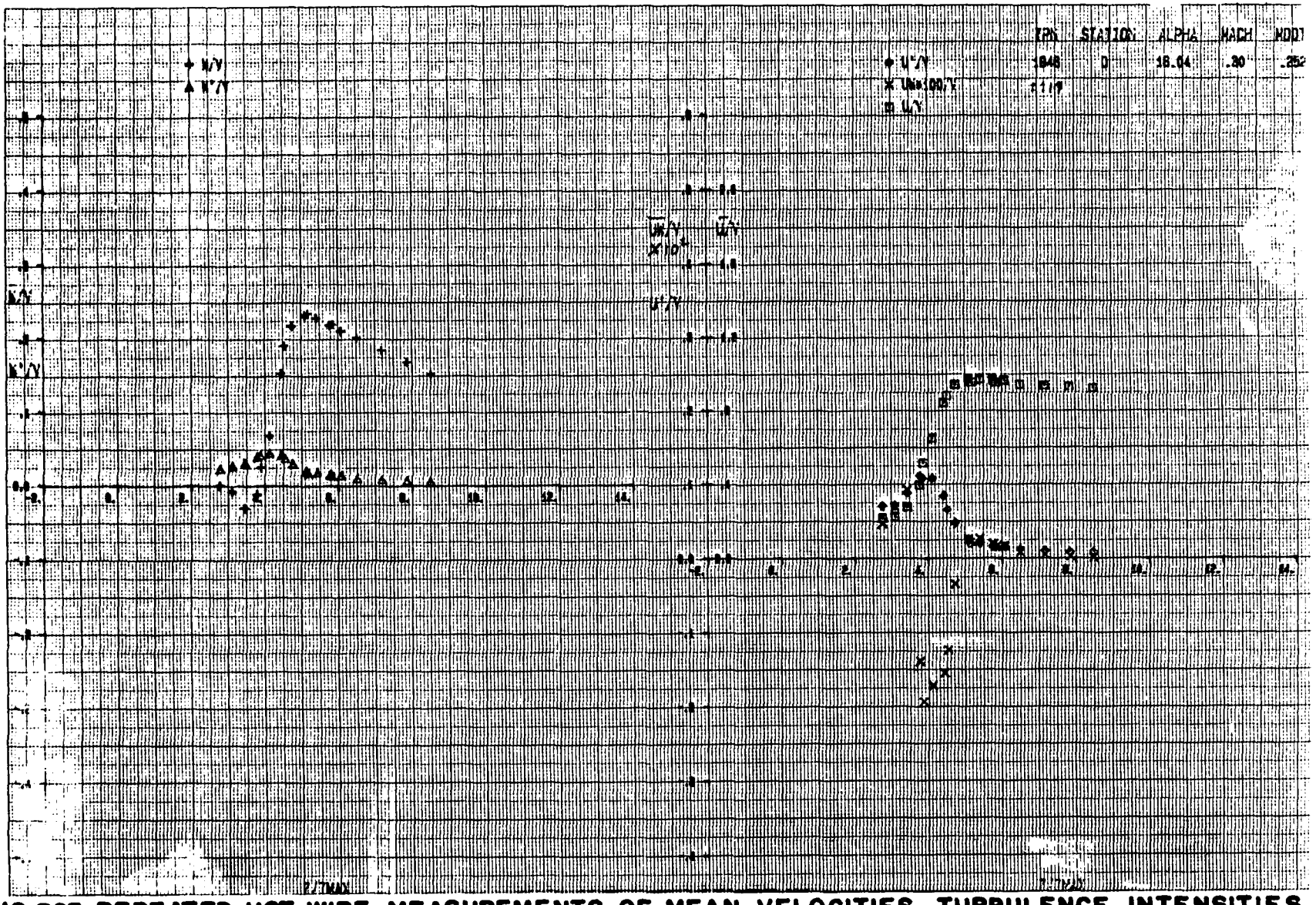

FIG B23 REPEATED HOT WIRE MEASUREMENTS OF MEAN VELOCITIES, TURBULENCE INTENSITIES AND REYNOLDS STRESSES WITH BLOWING - COPLANAR CANARD - TGF - $\alpha = 16°$ STATION D

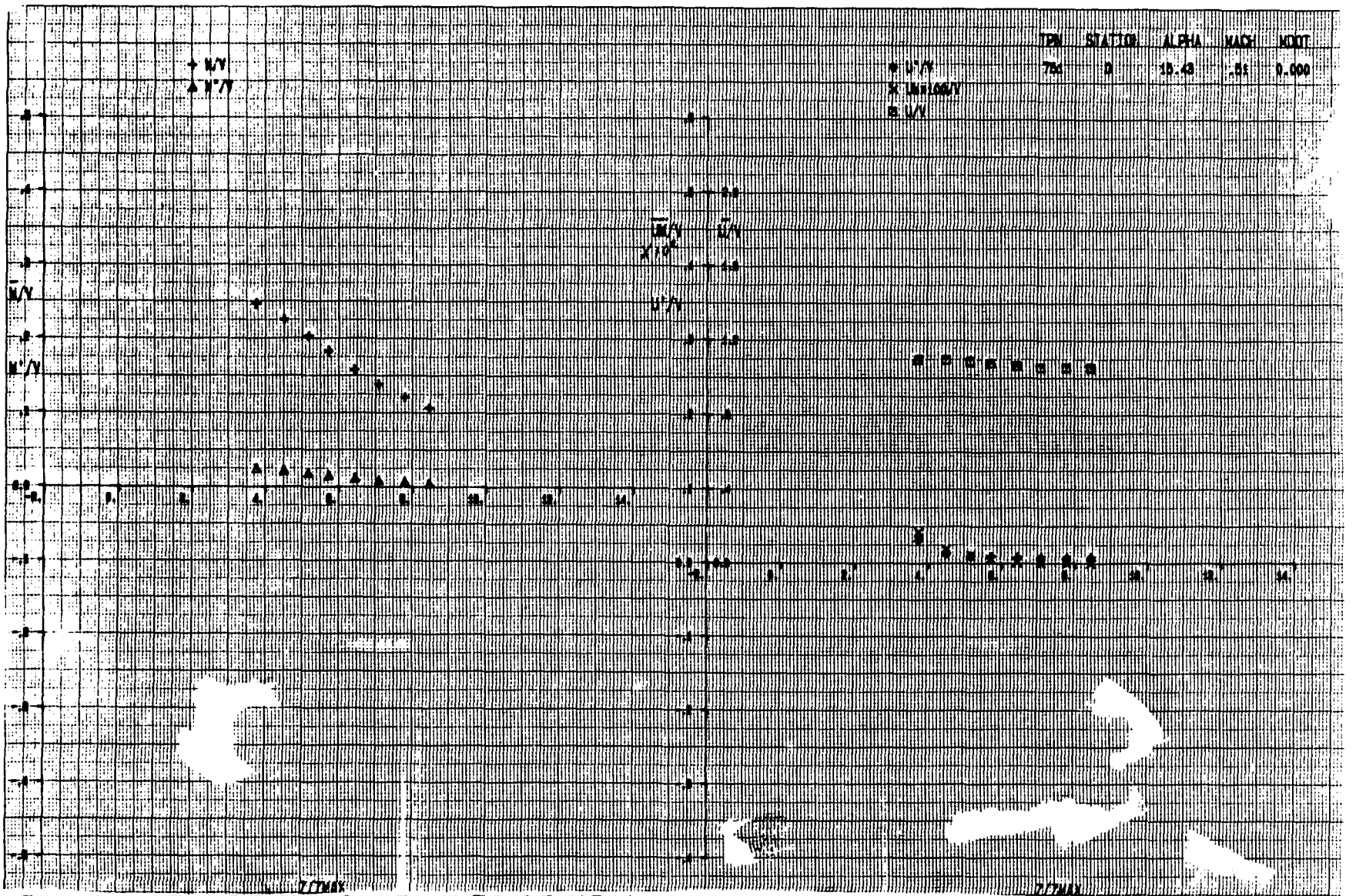

FIG. B24 HOT WIRE MEASUREMENTS OF MEAN VELOCITIES, TURBULENCE INTENSITIES, AND REYNOLDS STRESSES WITHOUT BLOWING - COPLANAR CANARD - TGF - α 16°- STATION D

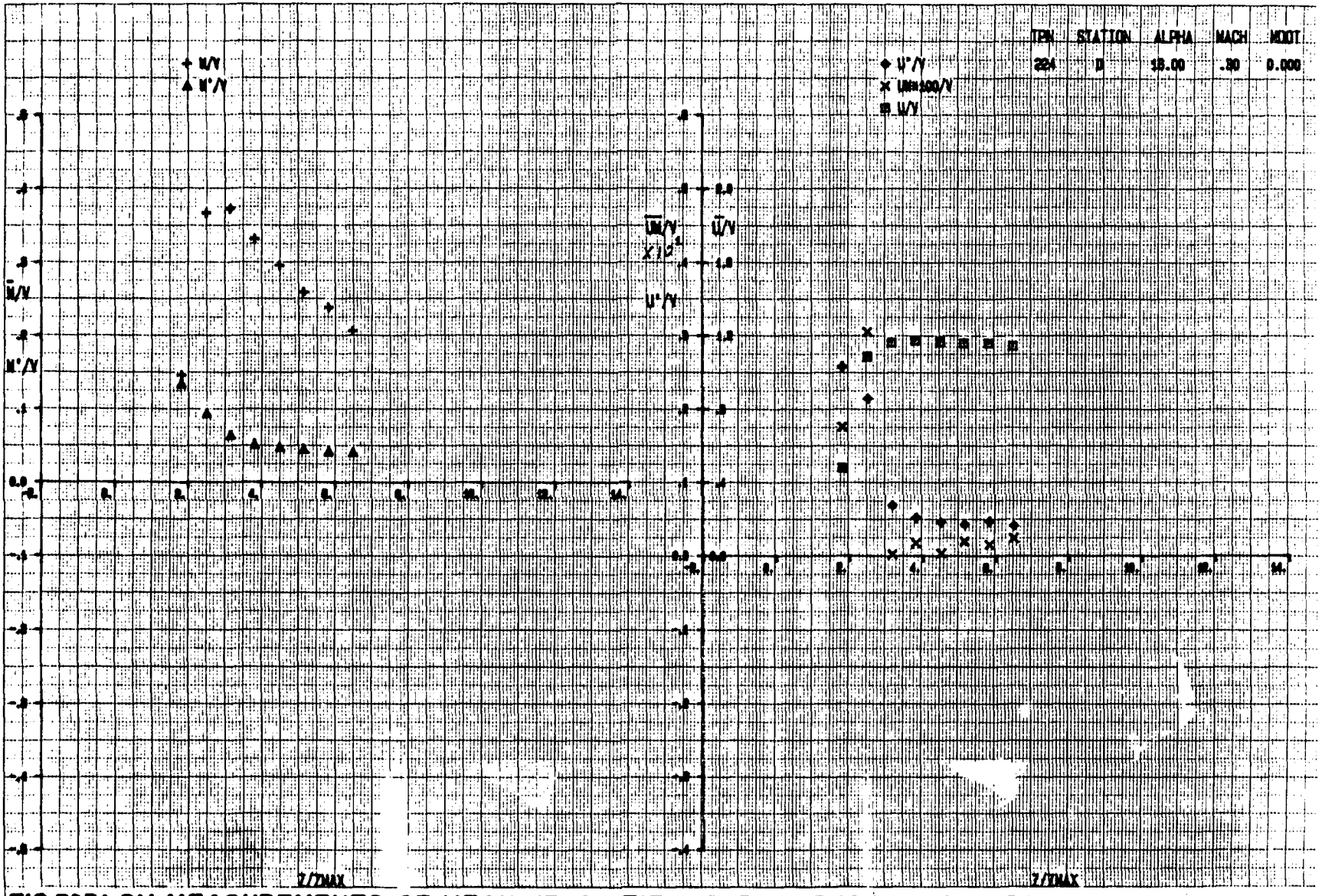

FIG.B25 LDV MEASUREMENTS OF MEAN VELOCITIES, TURBULENCE INTENSITIES, AND REYNOLDS STRESSES WITHOUT BLOWING - COPLANAR CANARD - TGF - α = 16°-STATION D

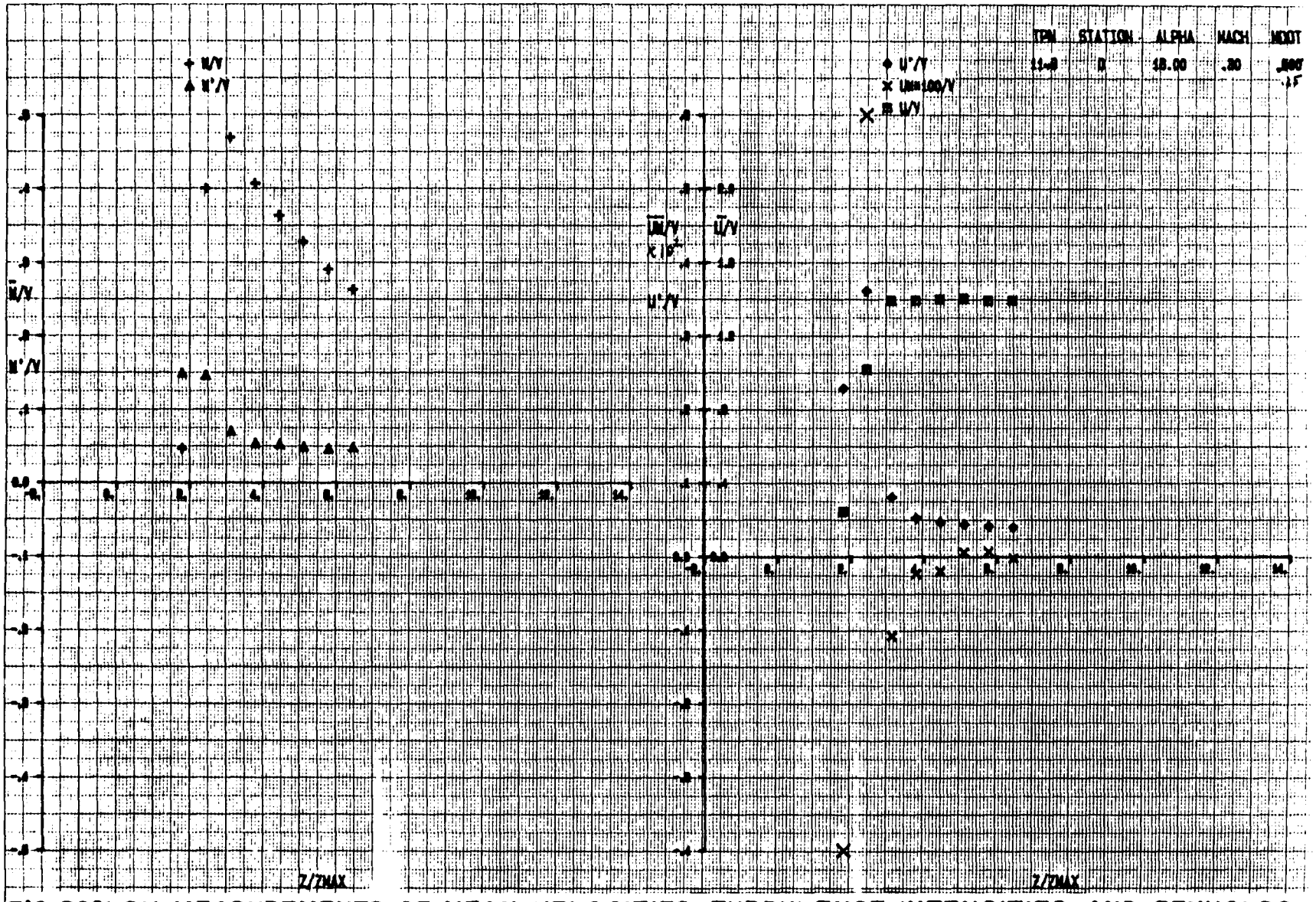

FIG. B26 LDV MEASUREMENTS OF MEAN VELOCITIES, TURBULENCE INTENSITIES, AND REYNOLDS STRESSES WITH BLOWING - COPLANAR CANARD - TGF - α = 16° -STATION D

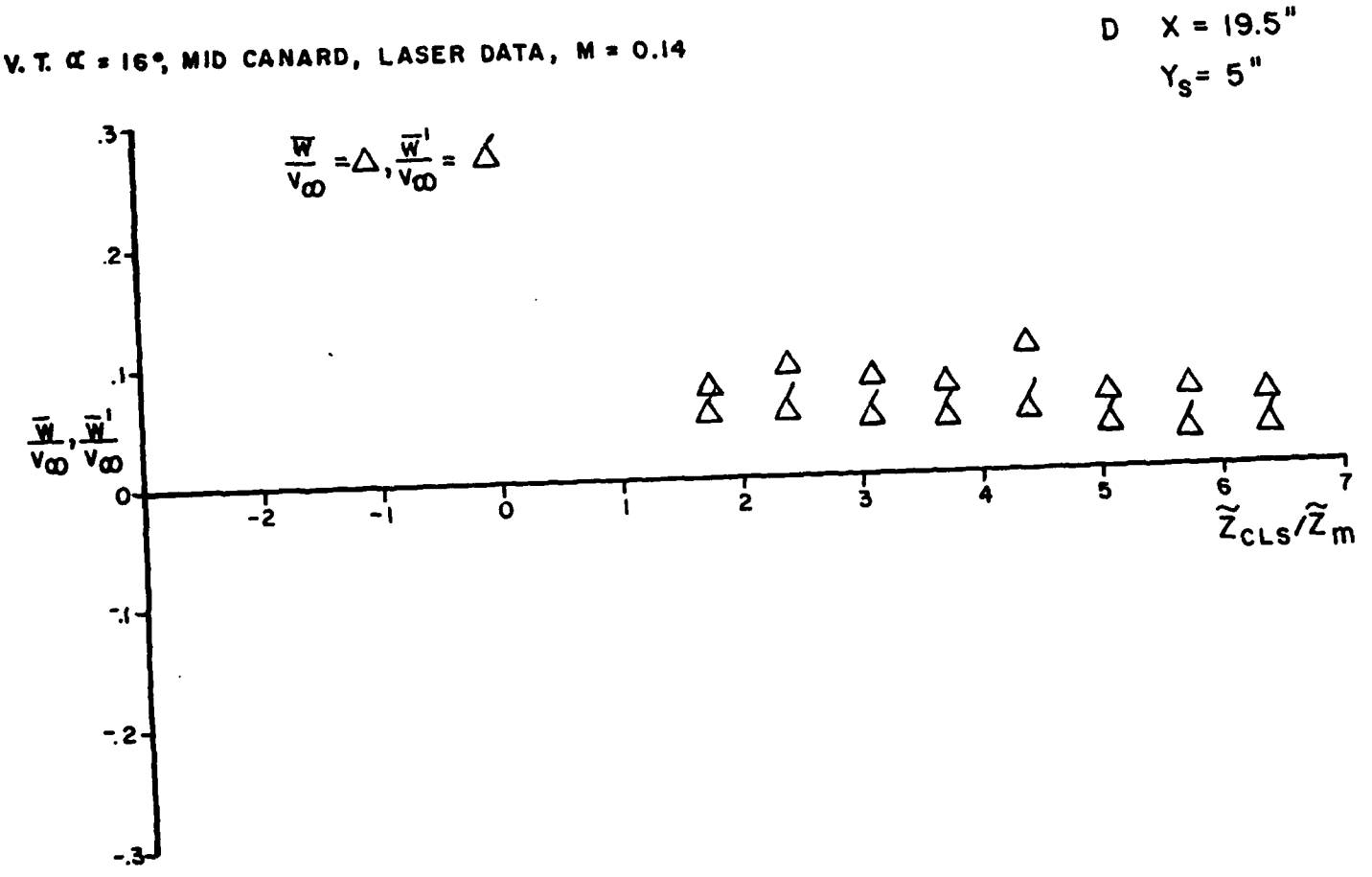

FIG.B27LDV MEASUREMENTS OF VERTICAL MEAN VELOCITY AND TURBULENCE INTENSITY WITH THE COPLANAR CANARD WITHOUT BLOWING -V.W.T.- α = 16° STATION D

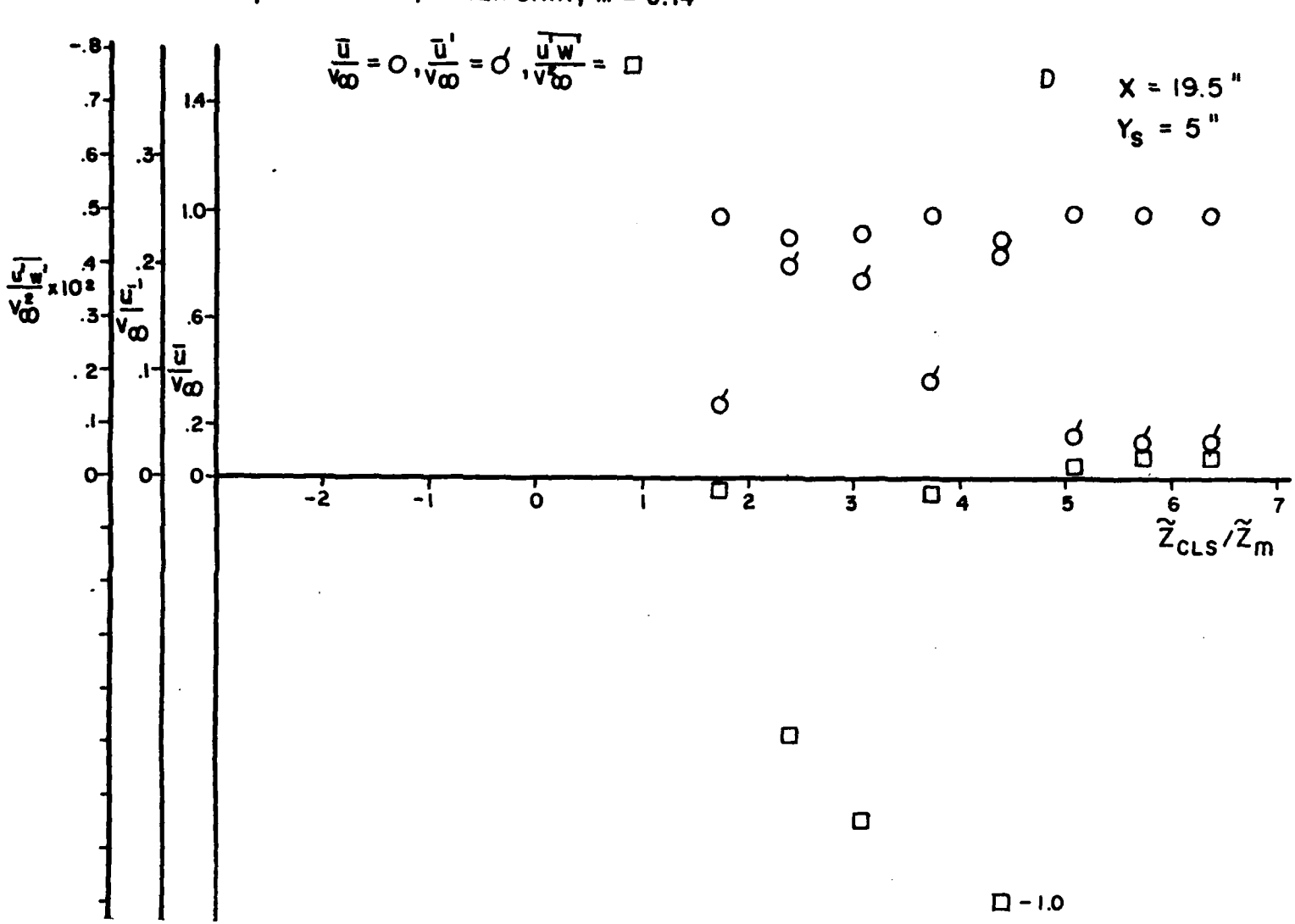

FIG.B28LDV MEASUREMENTS OF AXIAL MEAN VELOCITY, TURBULENCE INTENSITY, AND REYNOLDS STRESSES WITH THE COPLANAR CANARD WITHOUT BLOWING - V. W. T. - α = 16° STATION D

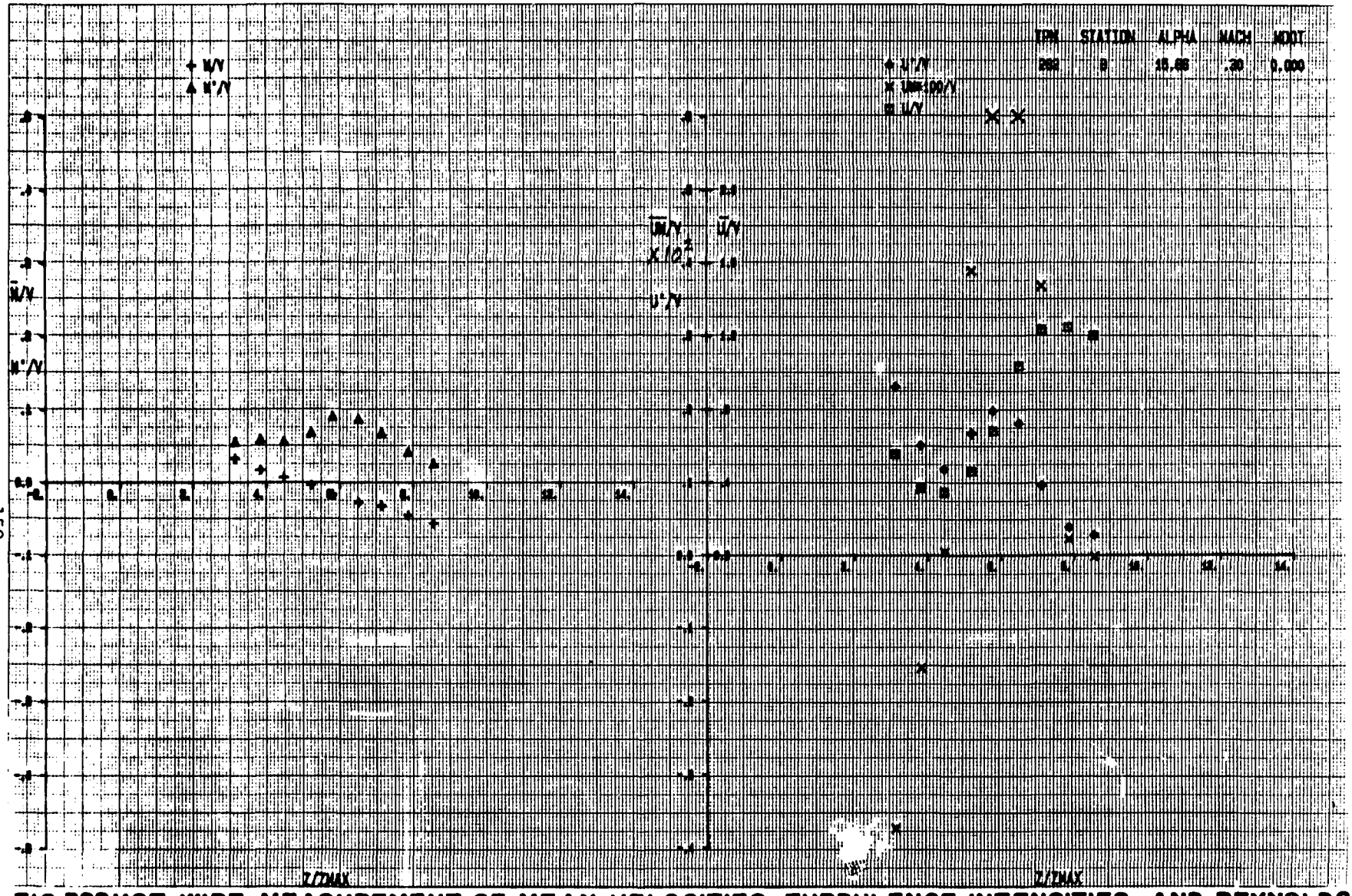

FIG. B29 HOT WIRE MEASUREMENT OF MEAN VELOCITIES, TURBULENCE INTENSITIES, AND REYNOLDS STRESSES WITHOUT BLOWING - COPLANAR CANARD - TGF - α = 16° STATION B

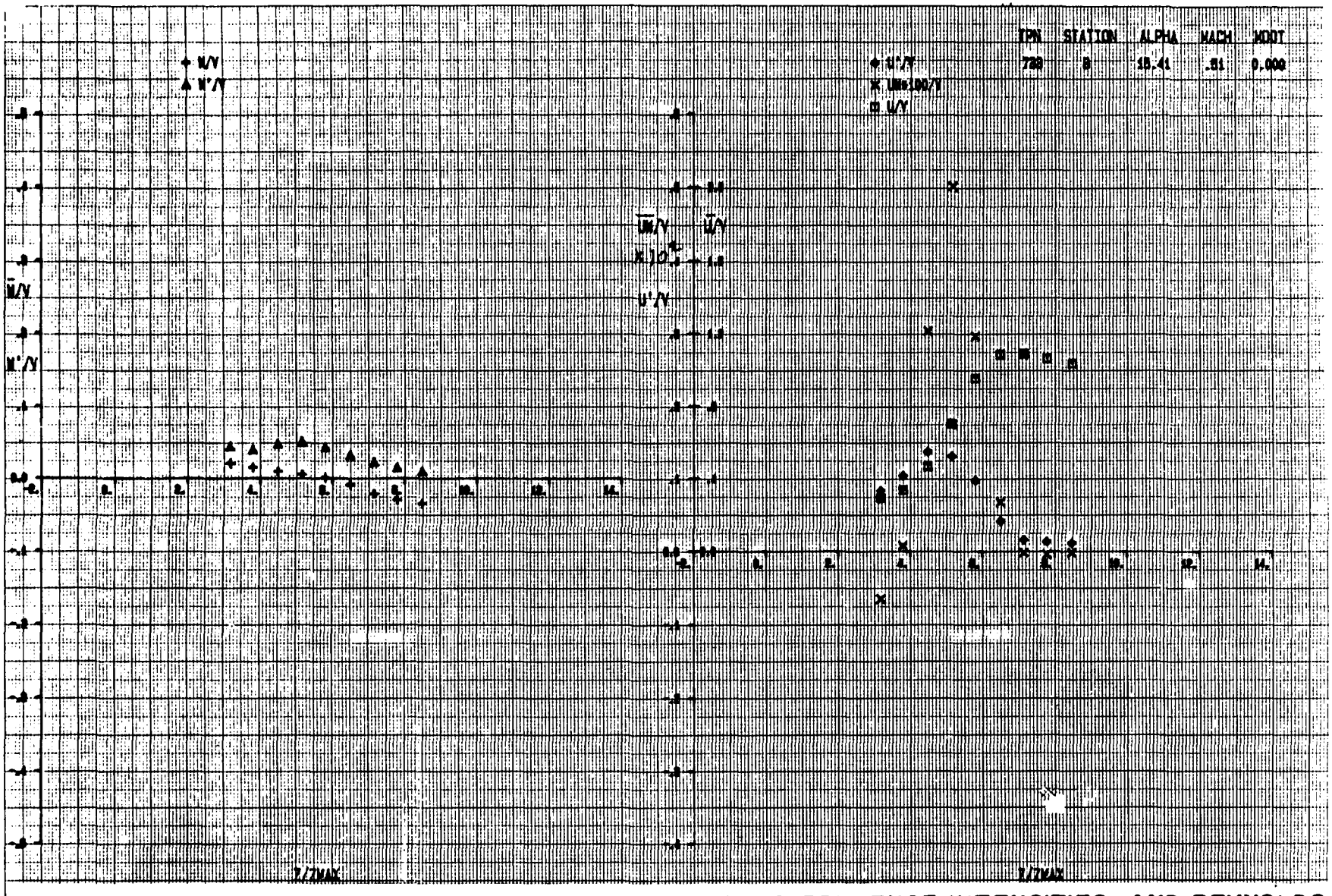

FIG.B30HOT WIRE MEASUREMENT OF MEAN VELOCITIES, TURBULENCE INTENSITIES, AND REYNOLDS STRESSES WITHOUT BLOWING - COPLANAR CANARD - TGF - α = 16 STATION B

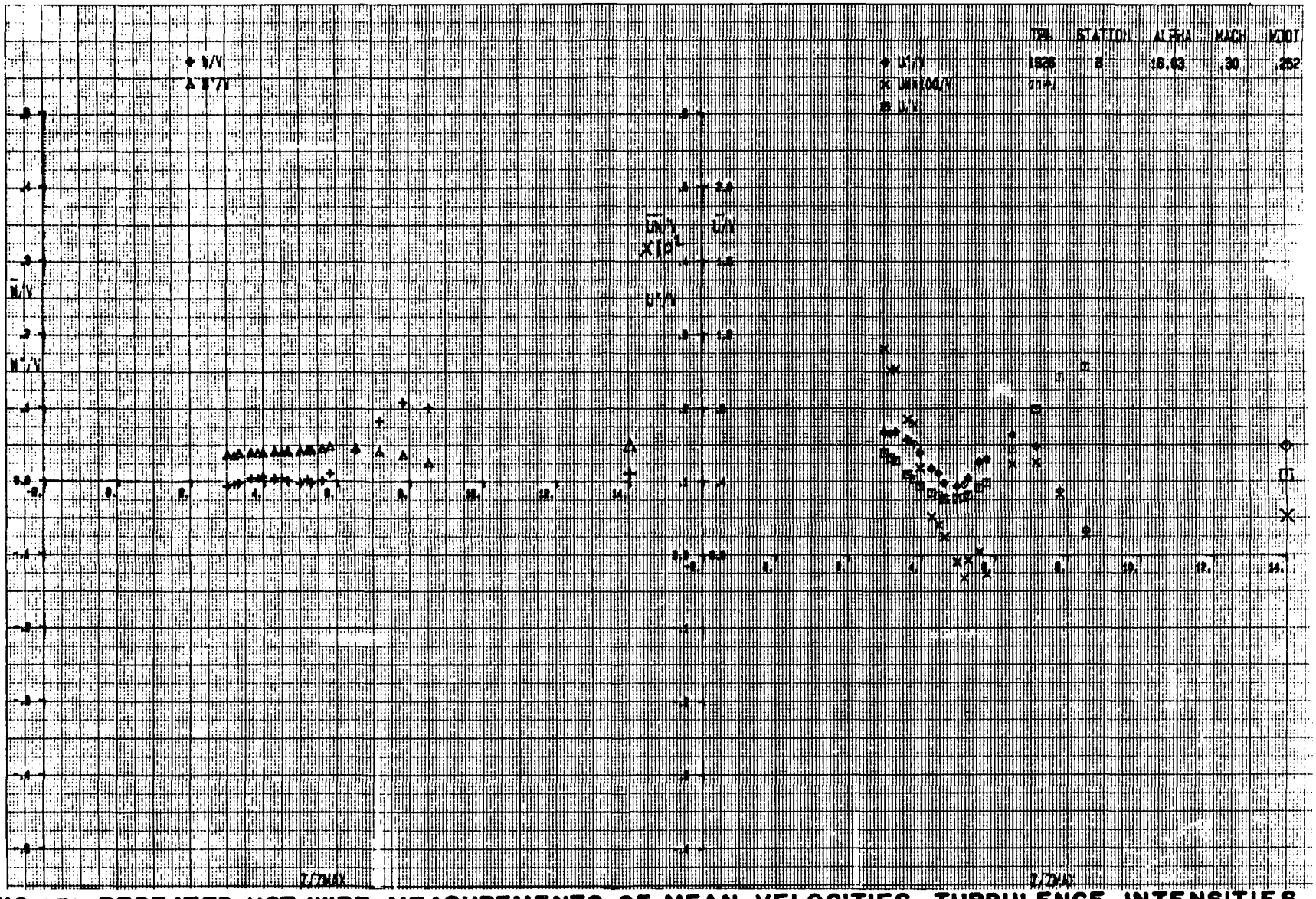

FIG B31 REPEATED HOT WIRE MEASUREMENTS OF MEAN VELOCITIES, TURBULENCE INTENSITIES AND REYNOLDS STRESSES WITH BLOWING - COPLANAR CANARD - TGF - α = 16° STATION B

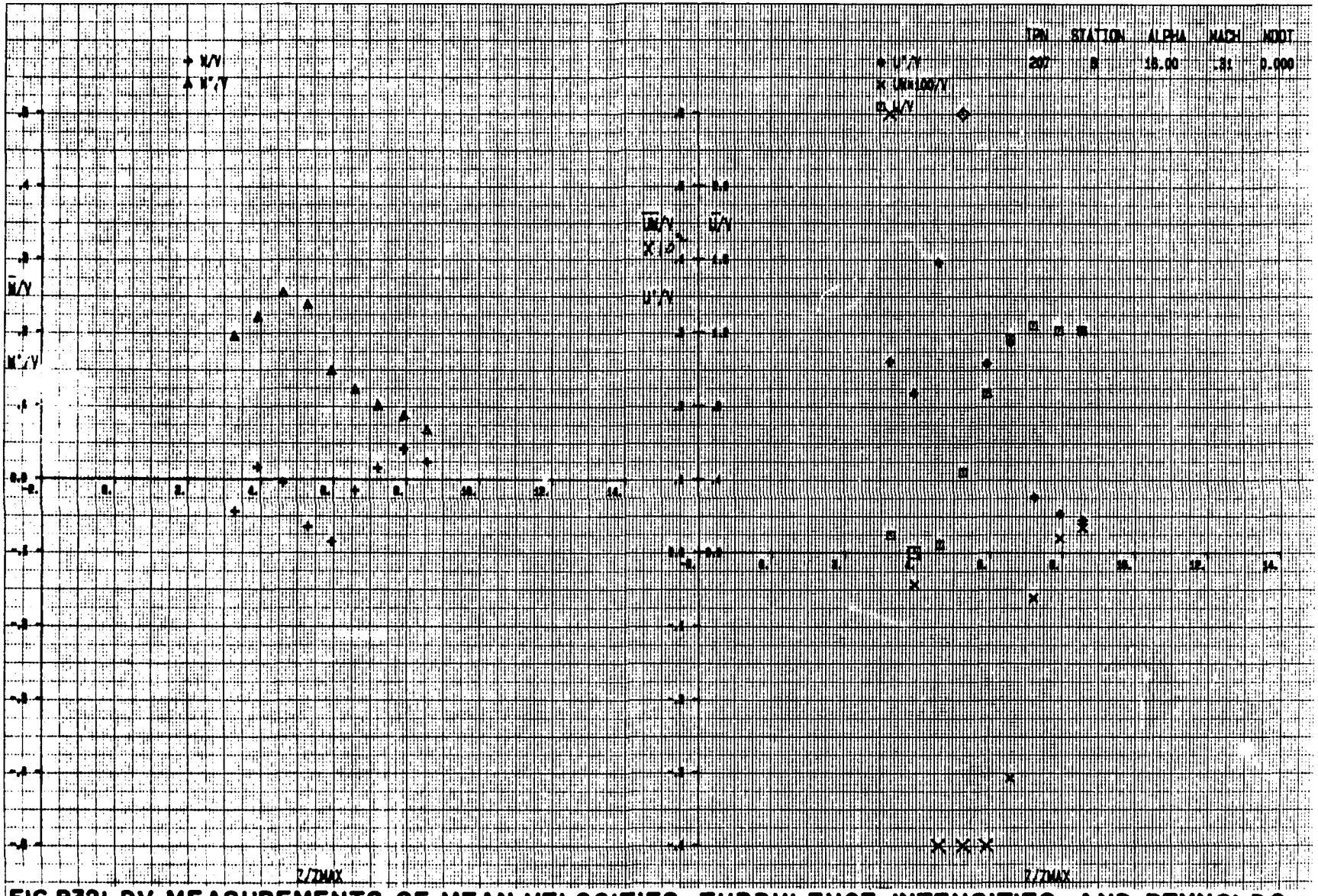

FIG. B32 LDV MEASUREMENTS OF MEAN VELOCITIES, TURBULENCE INTENSITIES, AND REYNOLDS STRESSES WITHOUT BLOWING - COPLANAR CANARD - TGF - α = 16°-STATION B

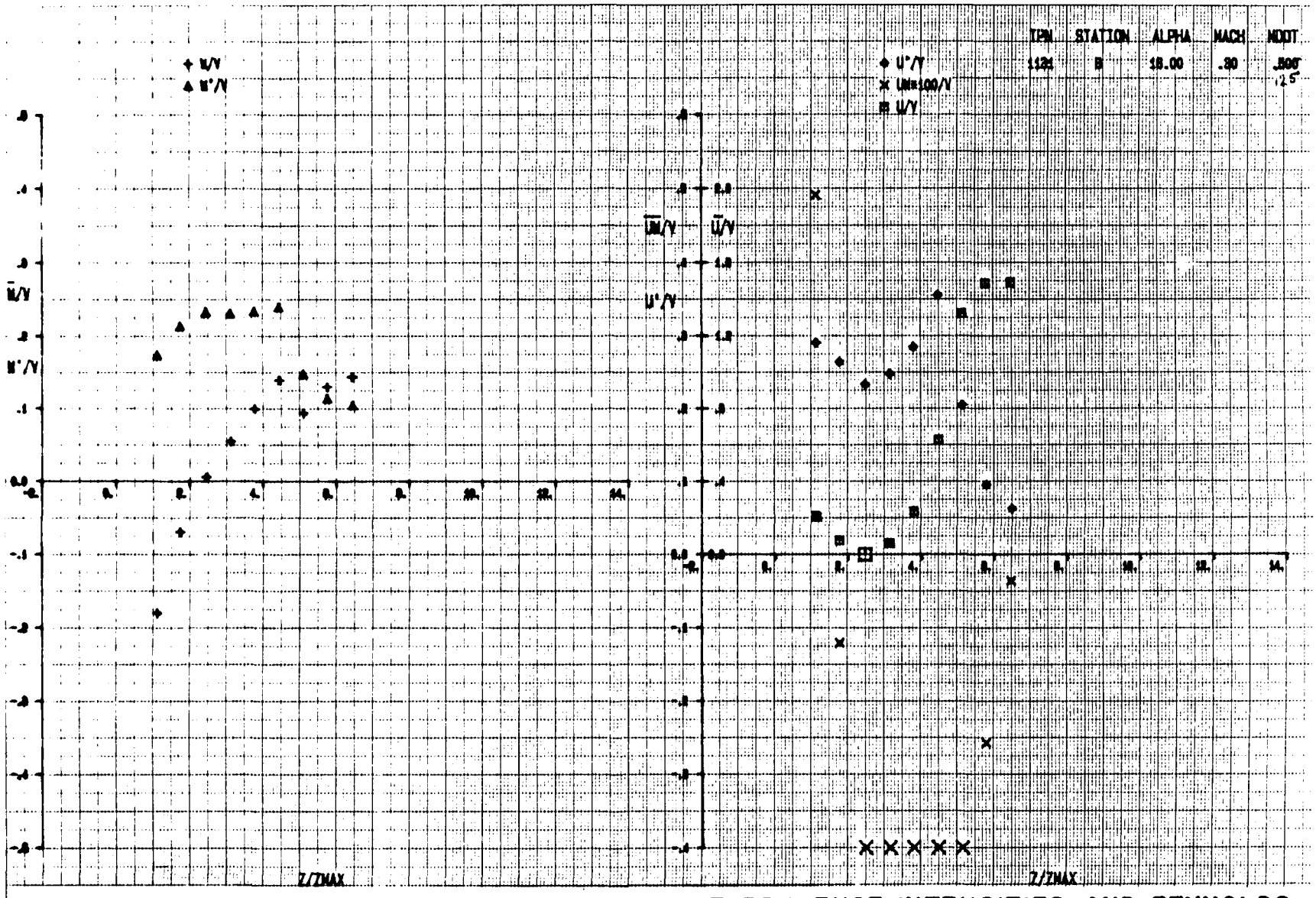

FIG.B33 LDV MEASUREMENTS OF MEAN VELOCITIES, TURBULENCE INTENSITIES, AND REYNOLDS STRESSES WITH BLOWING - COPLANAR CANARD - TGF - α = 16° -STATION B

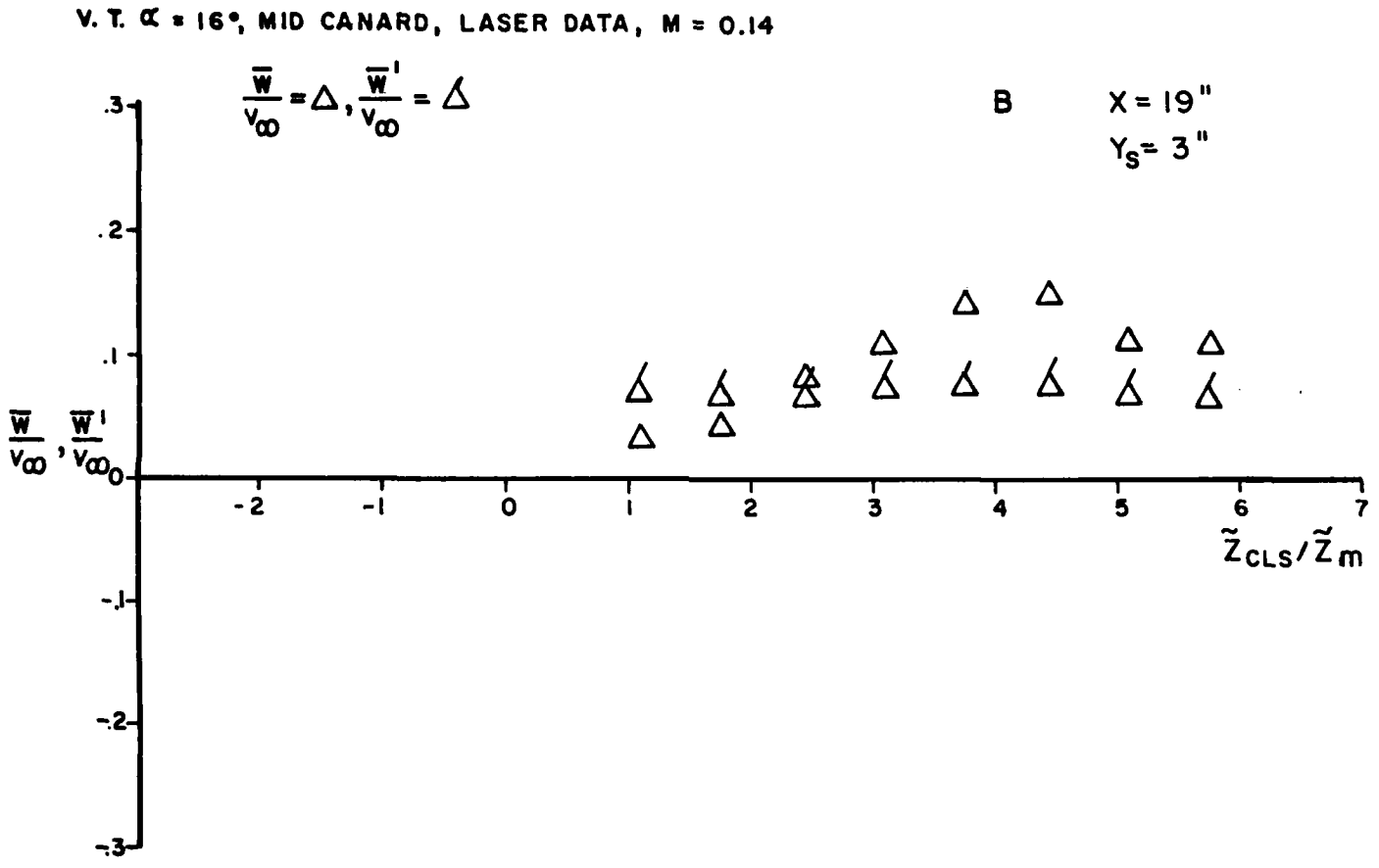

FIG.B34 LDV MEASUREMENTS OF VERTICAL MEAN VELOCITY AND TURBULENCE INTENSITY WITH THE COPLANAR CANARD WITHOUT BLOWING - V.W.T. - α = 16° - STATION B

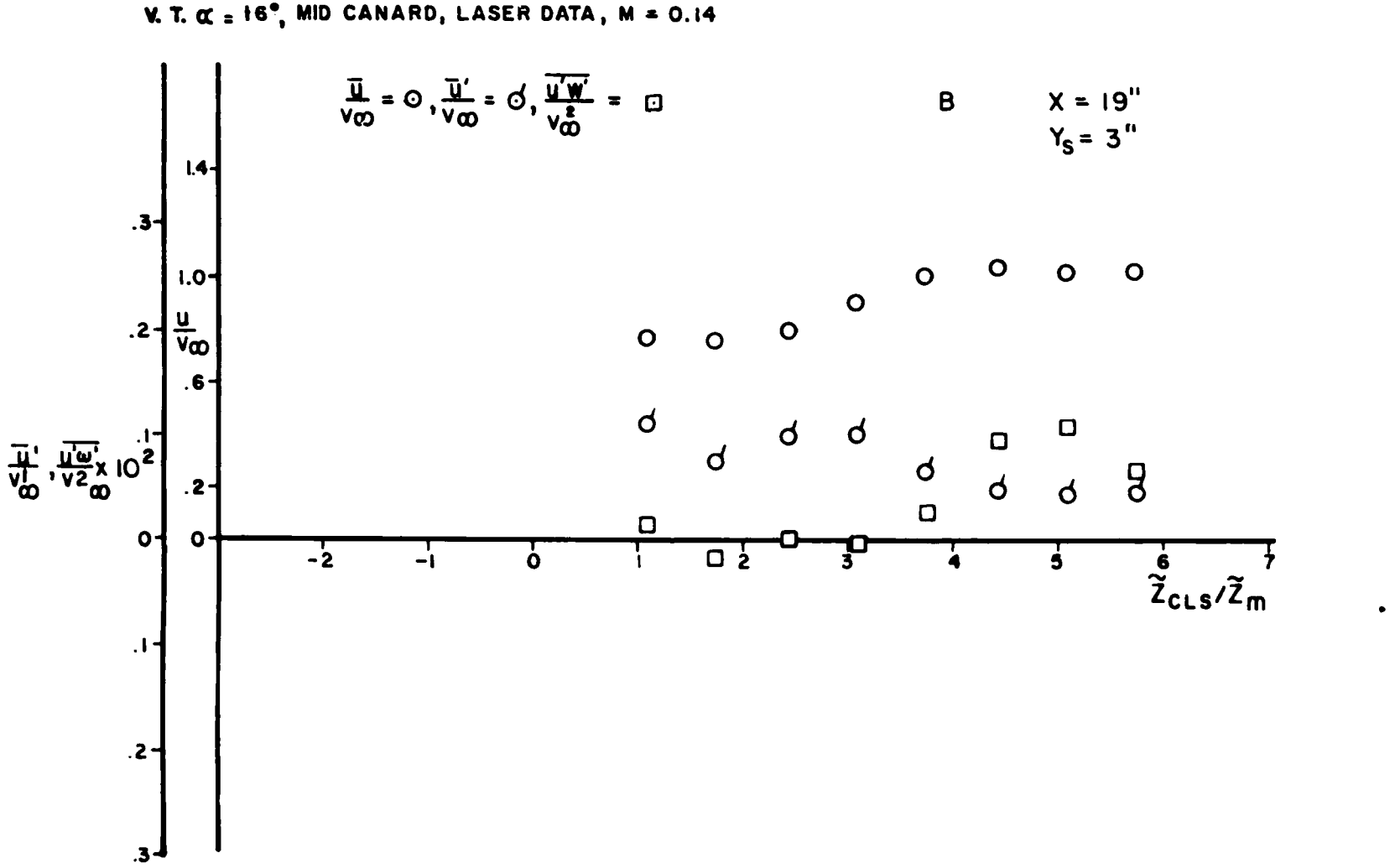

FIG. B35LDV MEASUREMENTS OF AXIAL MEAN VELOCITY, TURBULENCE INTENSITY, AND REYNOLDS STRESSES WITH THE COPLANAR CANARD WITHOUT BLOWING – V. W. T. – α = 16° – STATION B

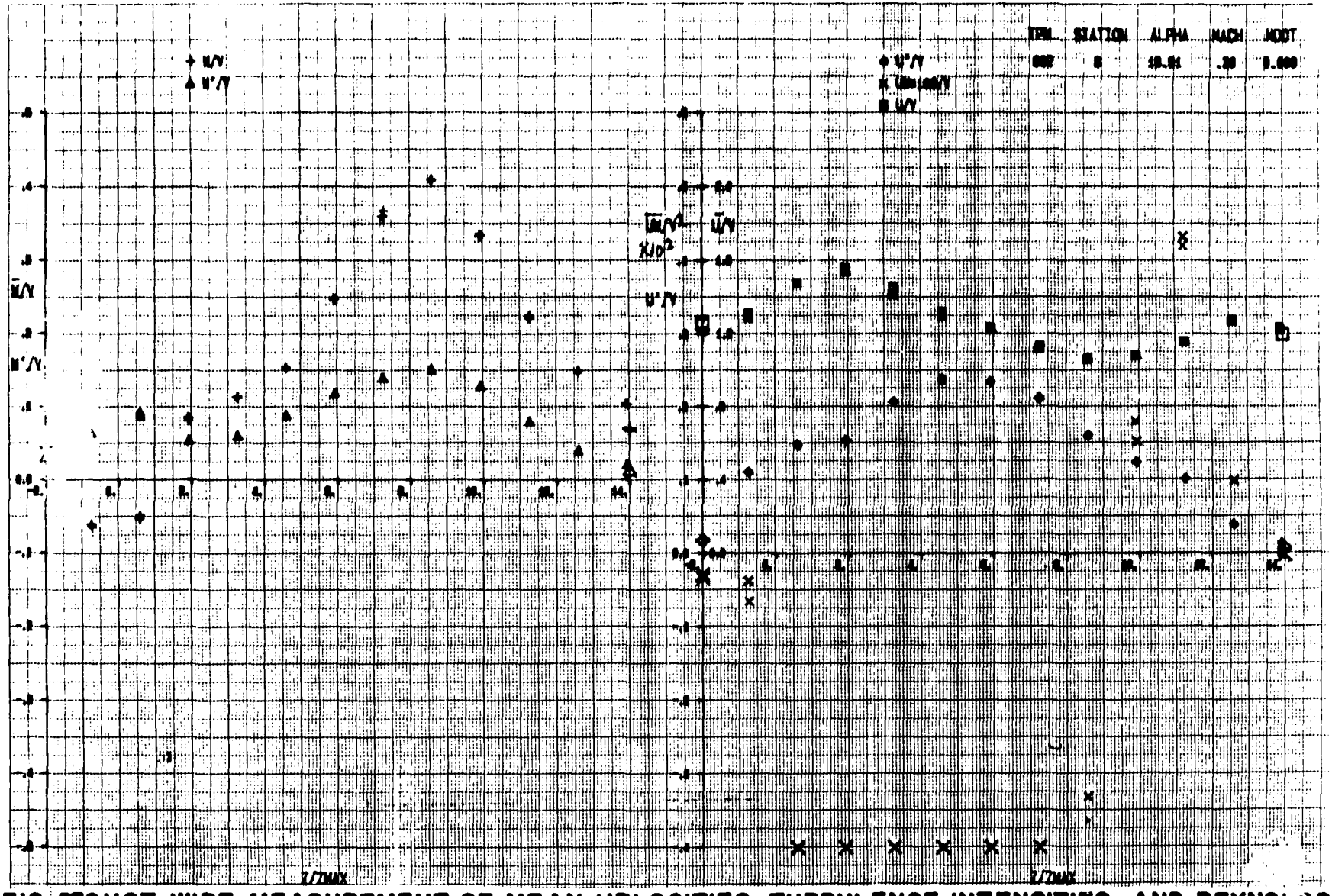

FIG. B36 HOT WIRE MEASUREMENT OF MEAN VELOCITIES, TURBULENCE INTENSITIES, AND REYNOLDS STRESSES WITHOUT BLOWING - COPLANAR CANARD - TGF - α = 20° STATION Q

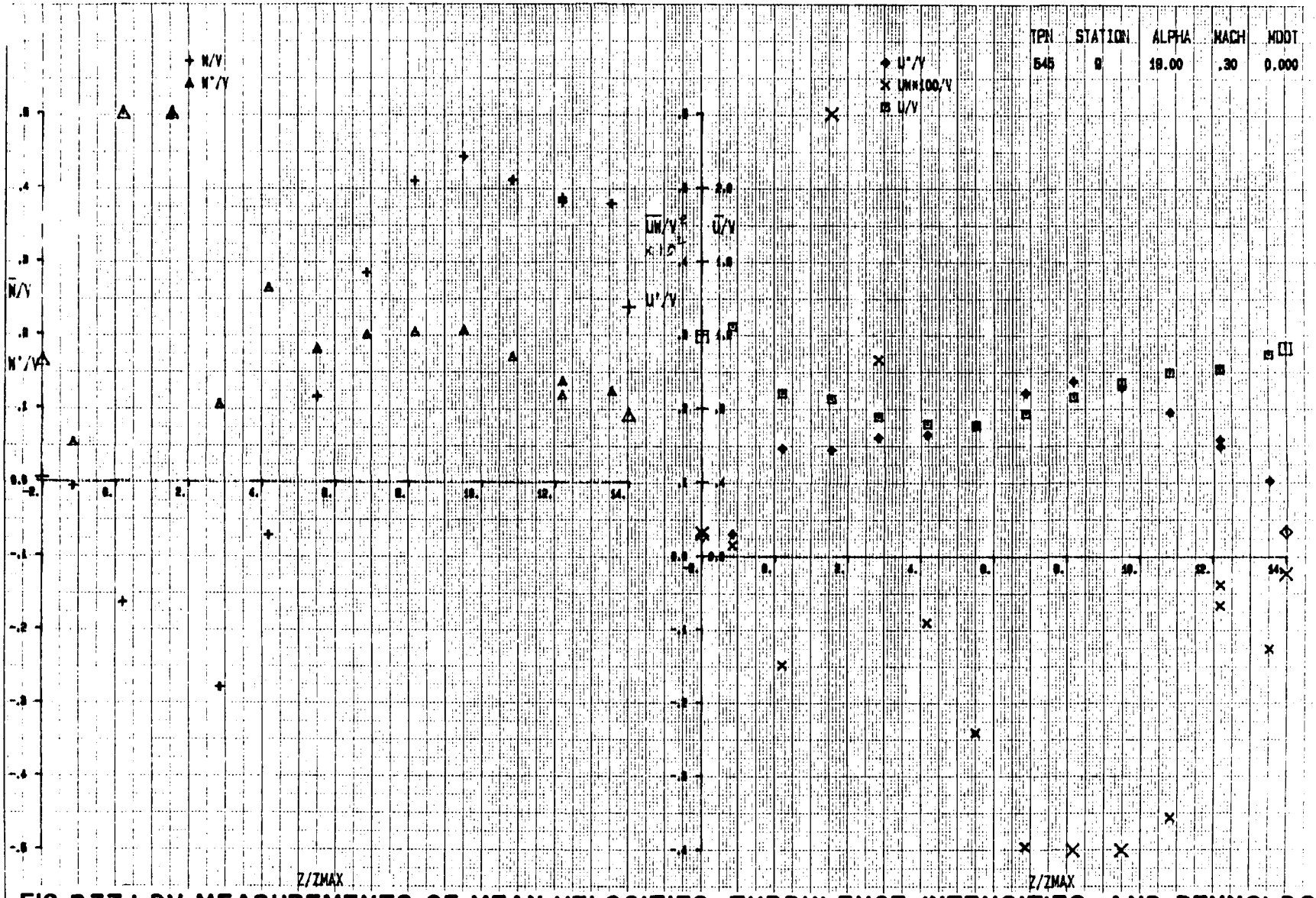

FIG. B37 LDV MEASUREMENTS OF MEAN VELOCITIES, TURBULENCE INTENSITIES, AND REYNOLDS STRESSES WITHOUT BLOWING - COPLANAR CANARD - TGF - $\alpha = 20^{\circ}$ STATION Q

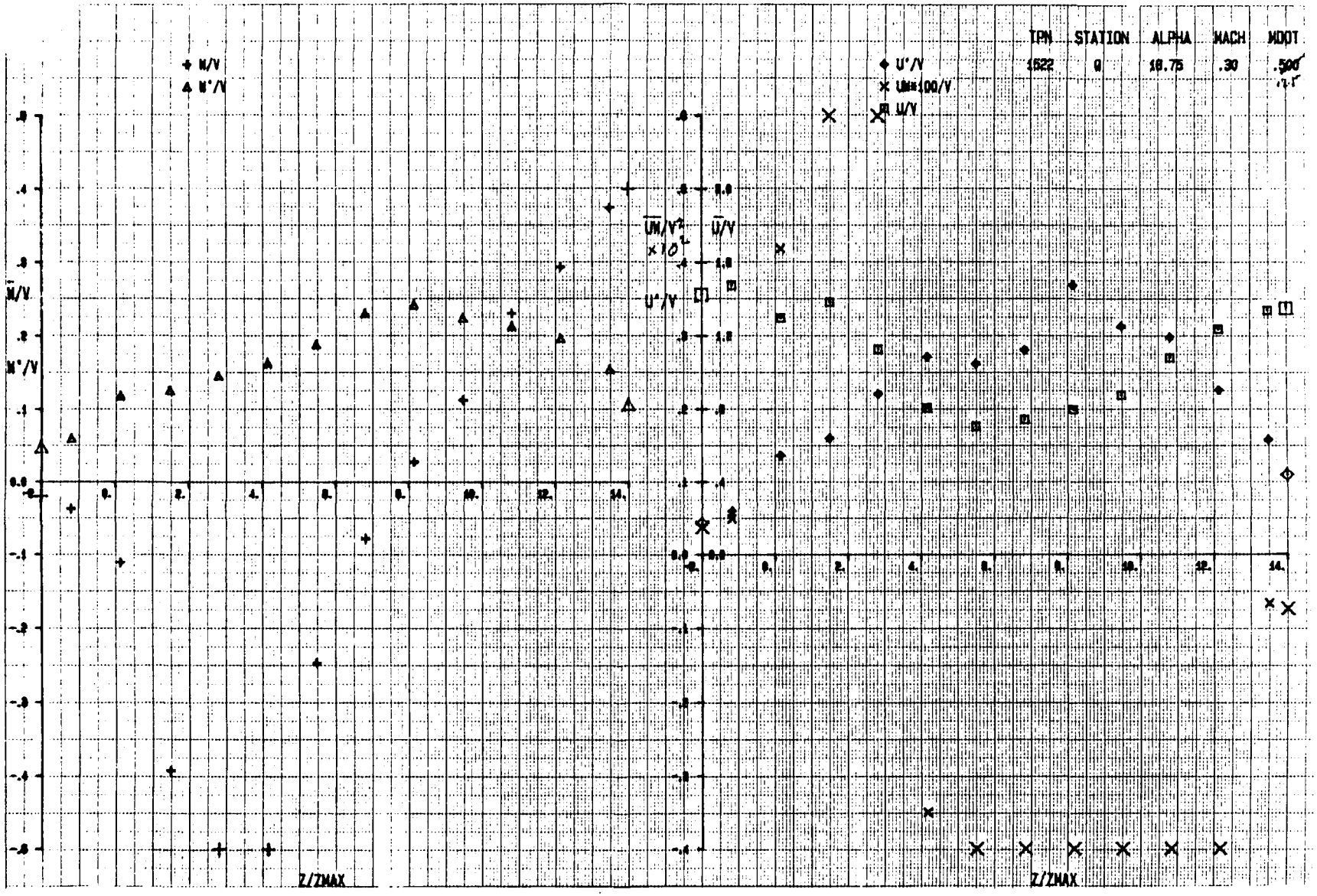

FIG. B 38 LDV MEASUREMENTS OF MEAN VELOCITIES, TURBULENCE INTENSITIES, AND REYNOLDS STRESSES WITH BLOWING - COPLANAR CANARD - TGF - $\alpha = 20^{\circ}$ - STATION Q

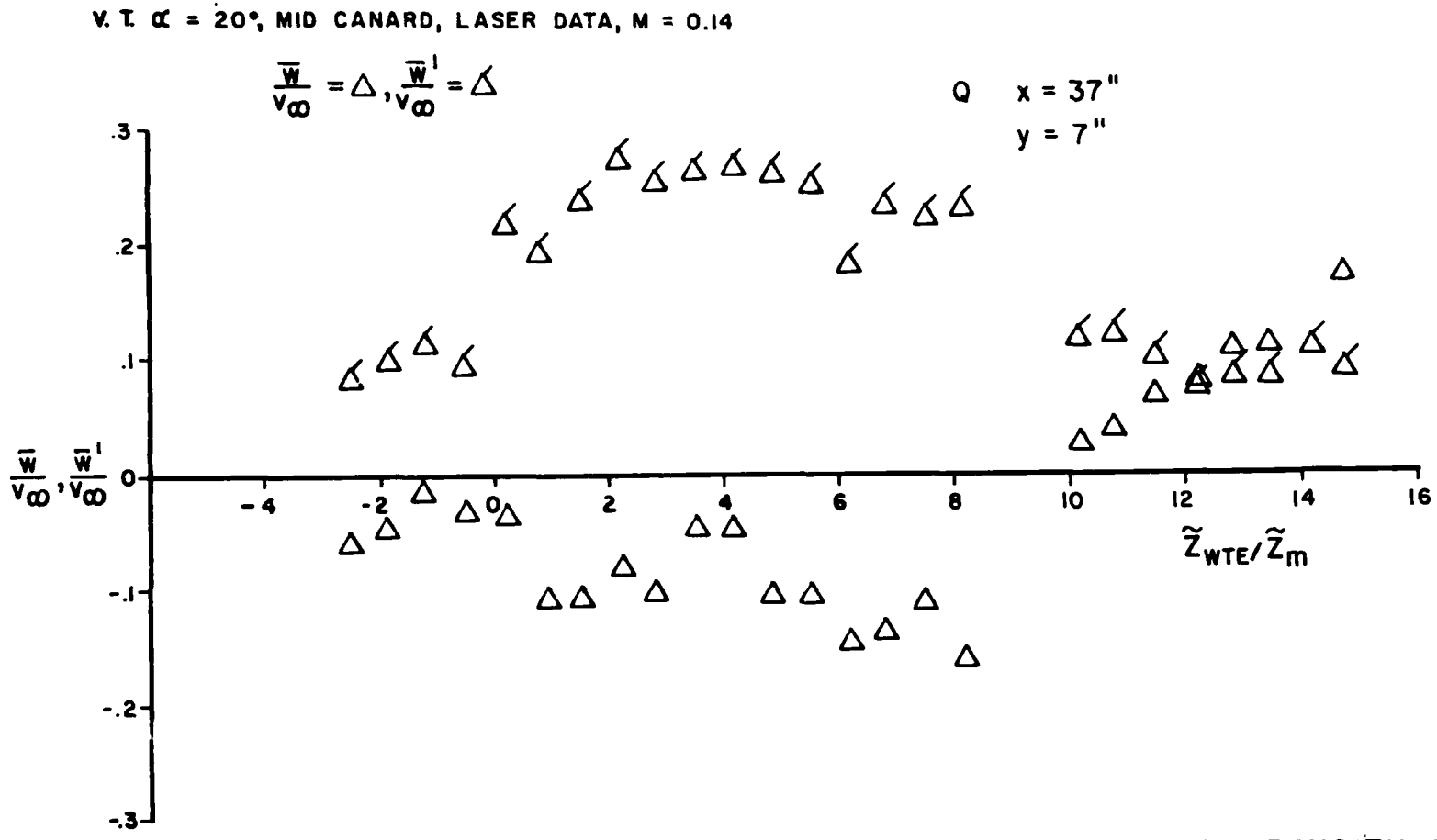

FIG. B39 LDV MEASUREMENTS OF VERTICAL MEAN VELOCITY AND TURBULENCE INTENSITY WITH THE COPLANAR CANARD WITHOUT BLOWING - V.W.T. - α = 20° - STATION Q

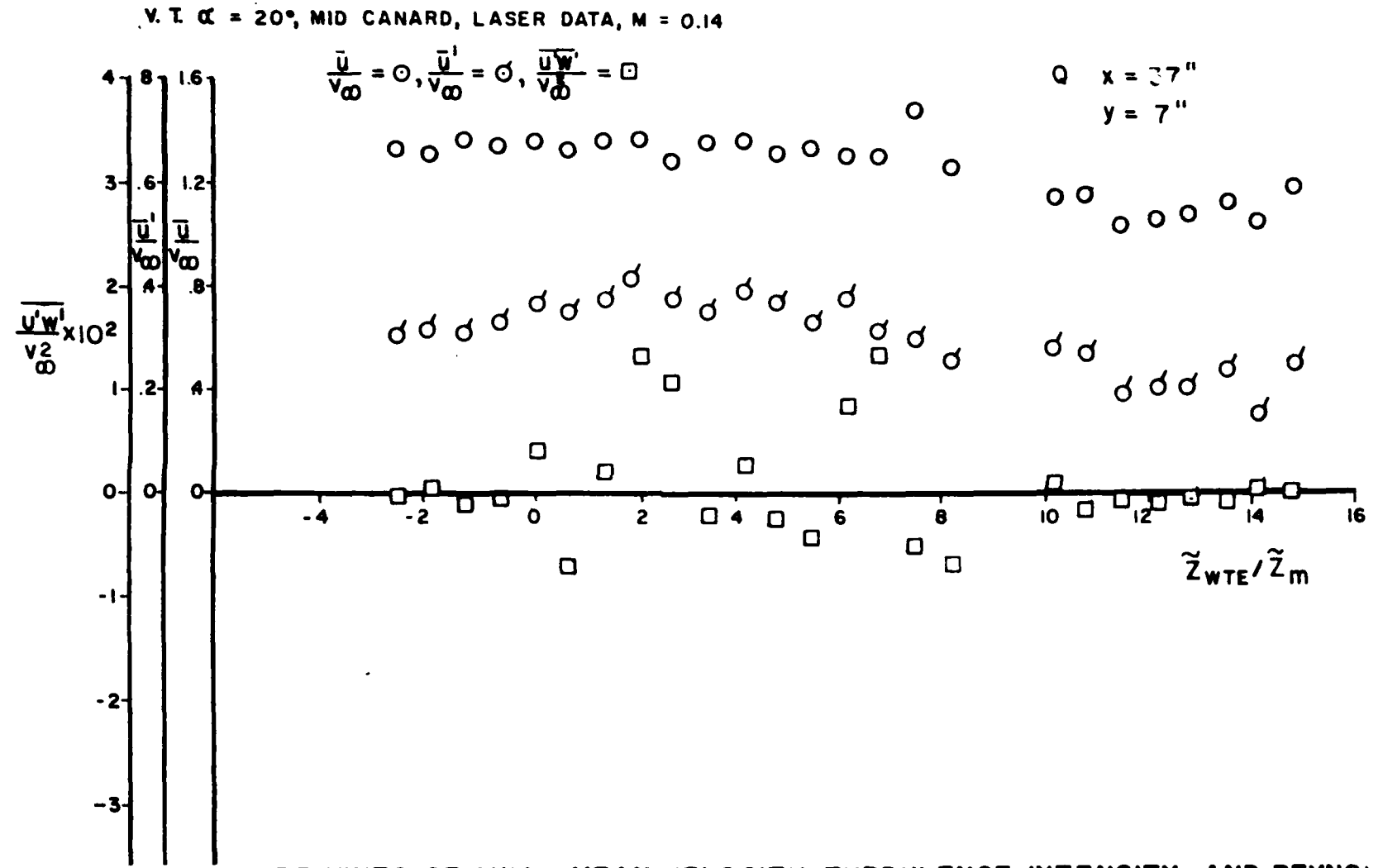

FIG. B40 LDV MEASUREMENTS OF AXIAL MEAN VELOCITY, TURBULENCE INTENSITY, AND REYNOLDS STRESSES WITH THE COPLANAR CANARD WITHOUT BLOWING - V. W. T. - α = 20° STATION Q

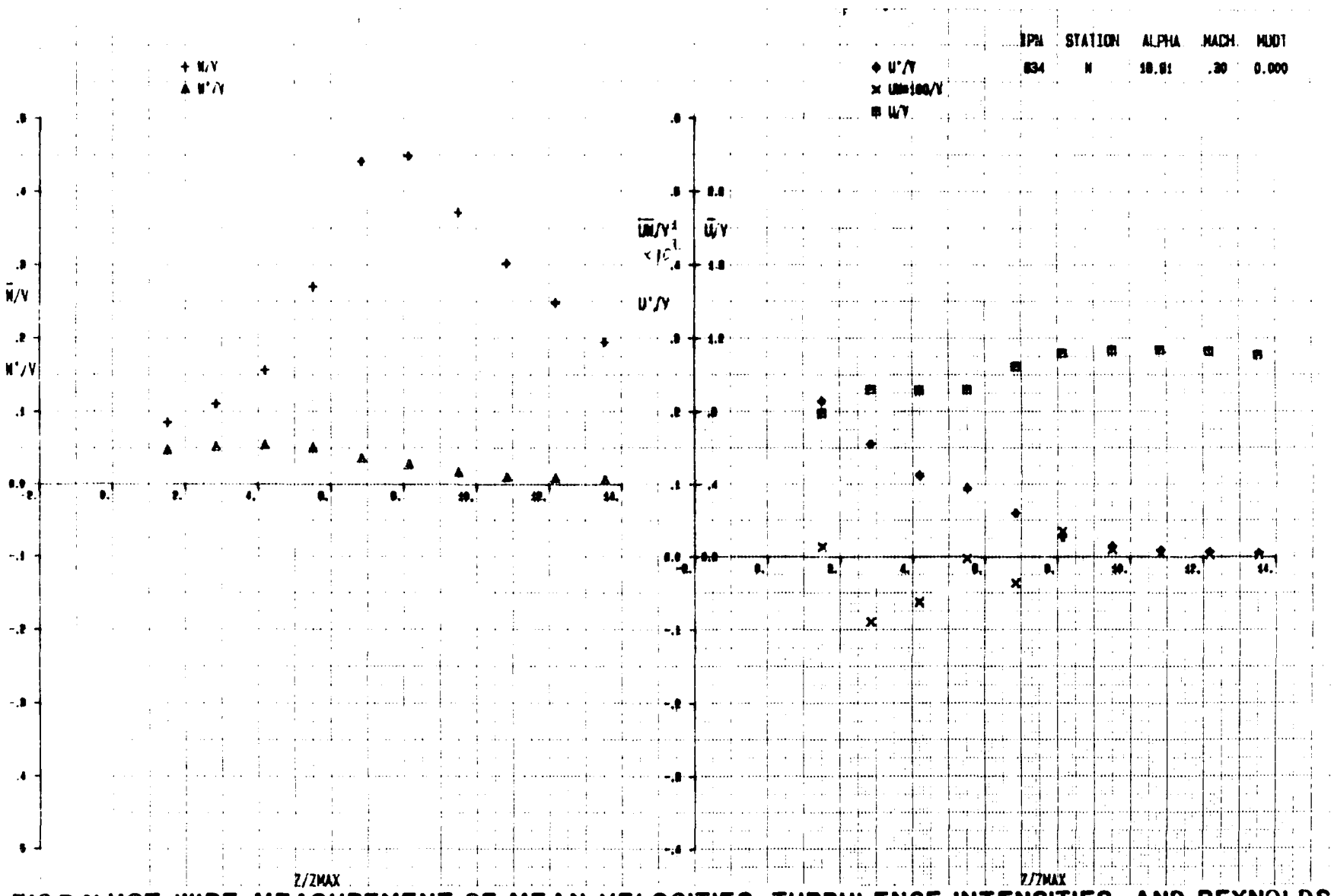

FIG.B41 HOT WIRE MEASUREMENT OF MEAN VELOCITIES, TURBULENCE INTENSITIES, AND REYNOLDS STRESSES WITHOUT BLOWING - COPLANAR CANARD - TGF - $\alpha = 20°$ STATION M

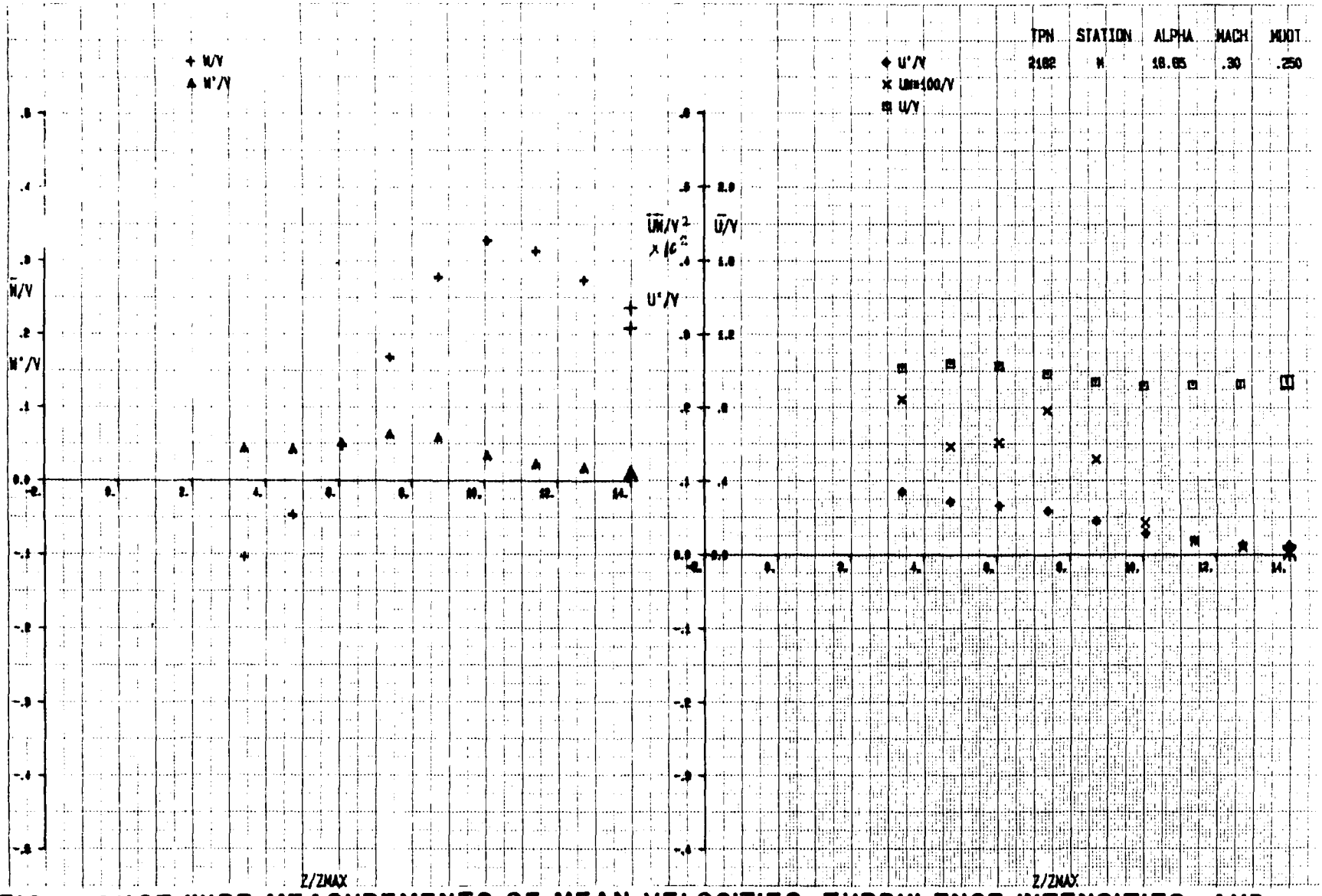

FIG. B42 HOT WIRE MEASUREMENTS OF MEAN VELOCITIES, TURBULENCE INTENSITIES, AND REYNOLDS STRESSES WITH BLOWING - COPLANAR CANARD - TGF - α=20°-STATION M

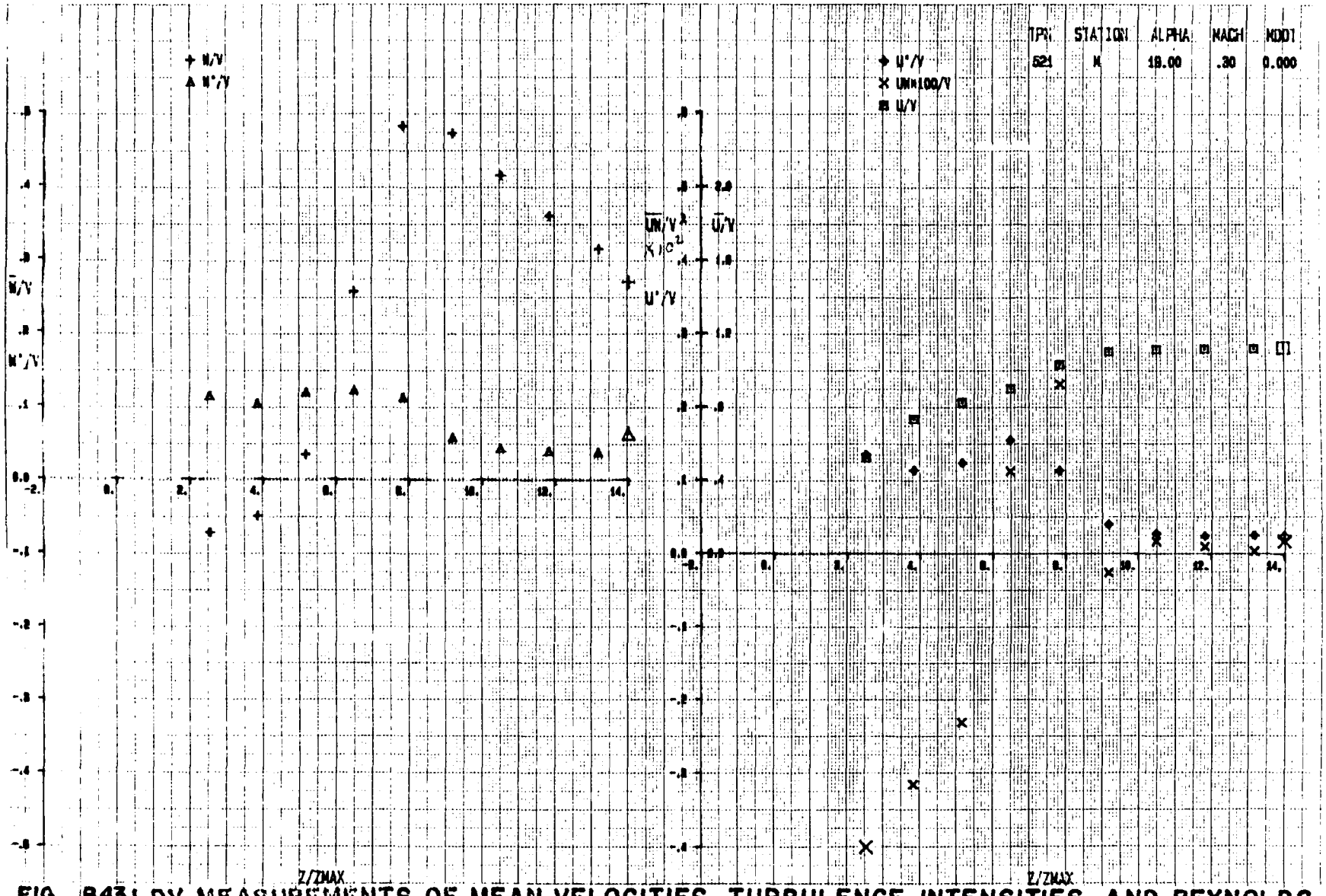

FIG. B43 LDV MEASUREMENTS OF MEAN VELOCITIES, TURBULENCE INTENSITIES, AND REYNOLDS STRESSES WITHOUT BLOWING - COPLANAR CANARD - TGF - α =20°-STATION M

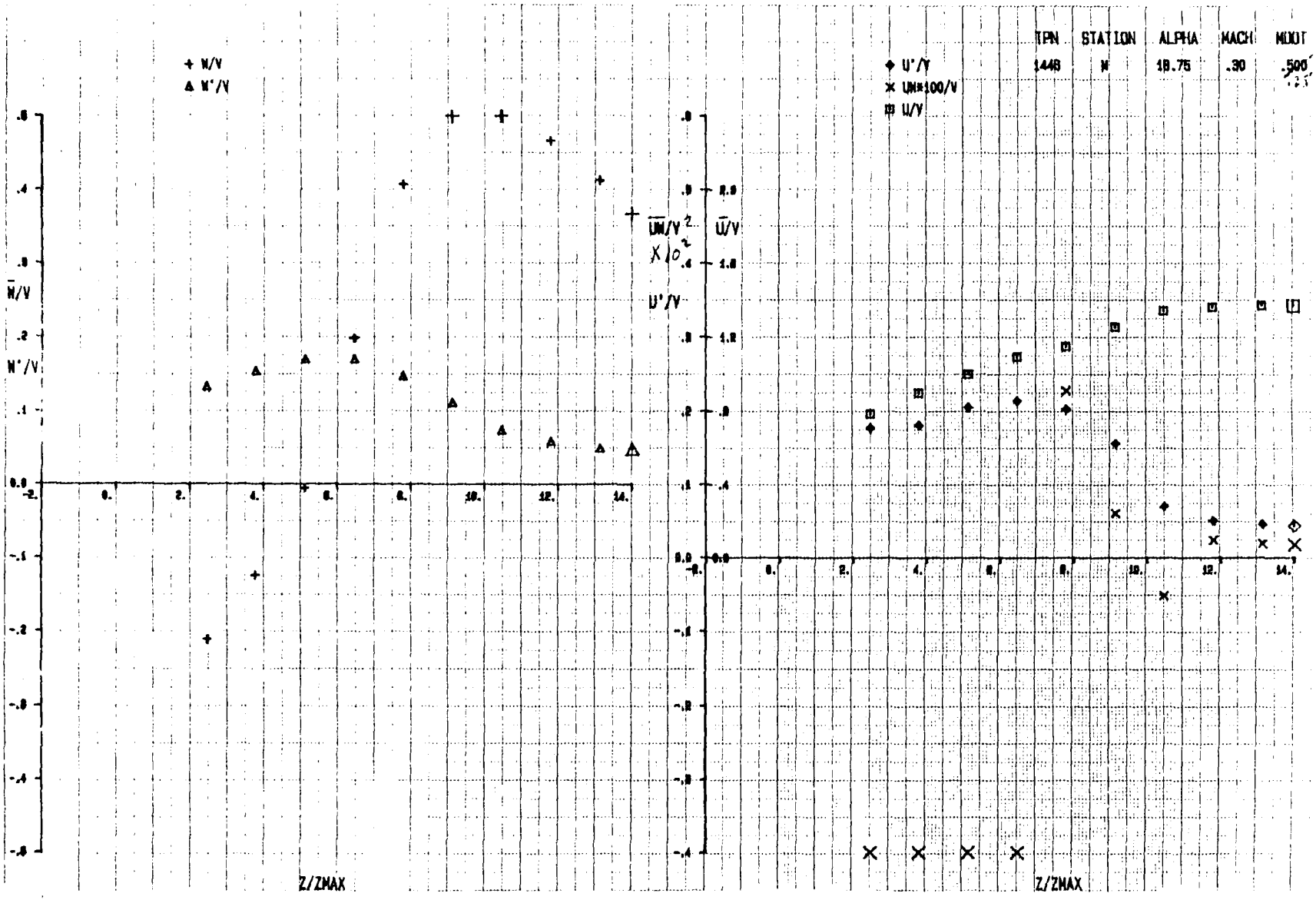

FIG. B44 LDV MEASUREMENTS OF MEAN VELOCITIES, TURBULENCE INTENSITIES, AND REYNOLDS STRESSES WITH BLOWING - COPLANAR CANARD - TGF - α = 20°-STATION M

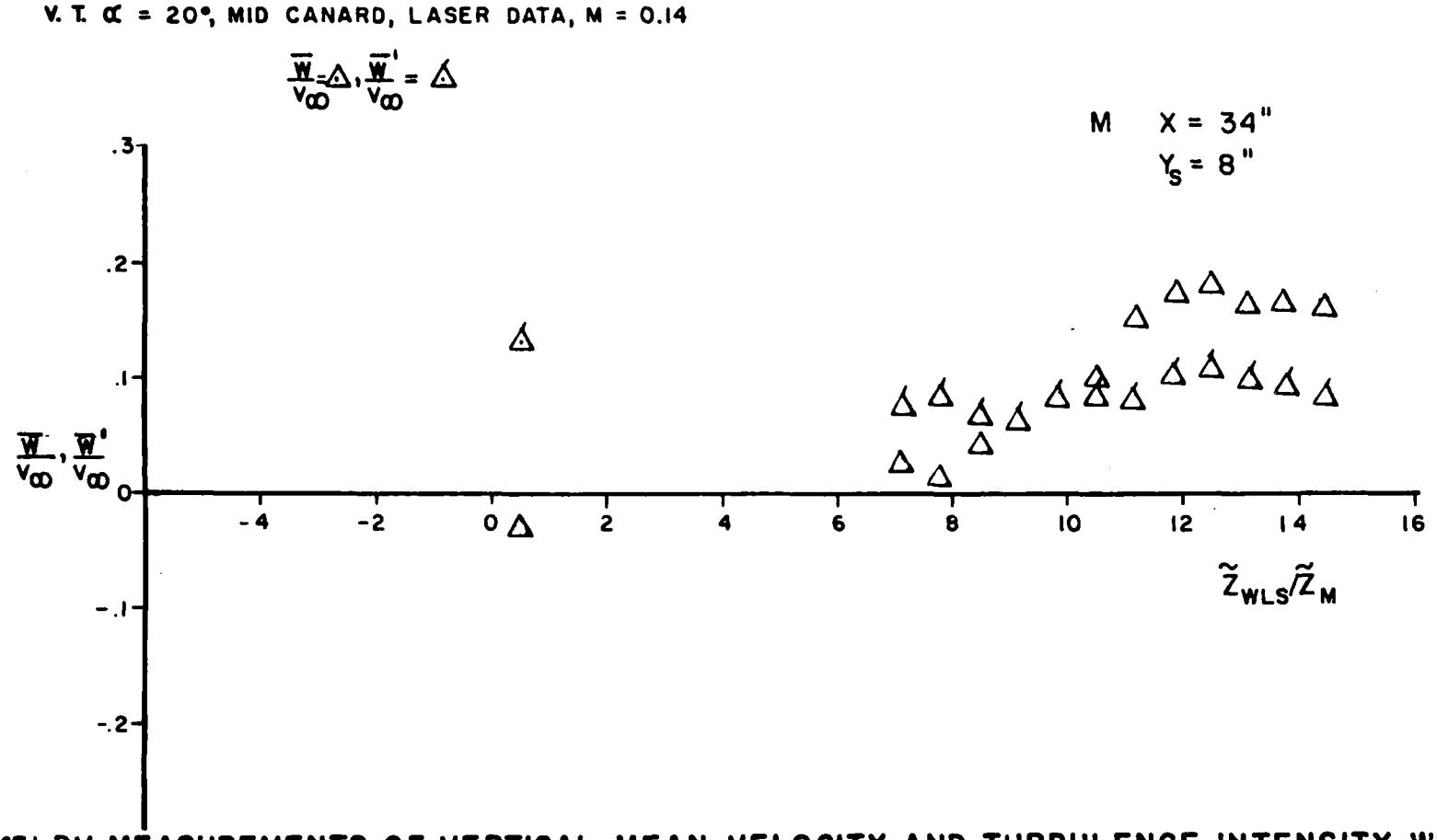

FIG. B45 LDV MEASUREMENTS OF VERTICAL MEAN VELOCITY AND TURBULENCE INTENSITY WITH THE COPLANAR CANARD WITHOUT BLOWING - V.W.T. - α = 20° STATION M

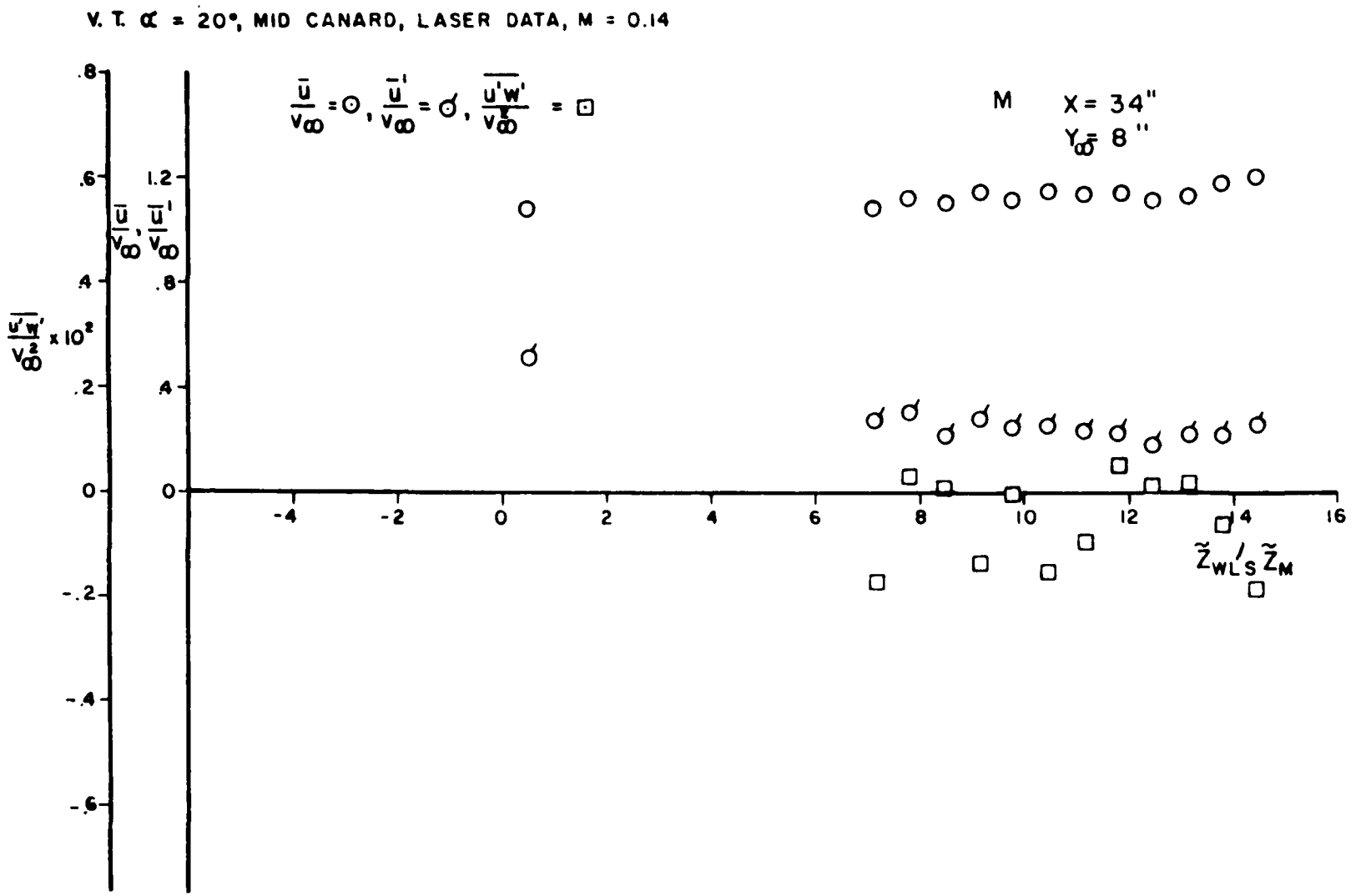

FIG. B46 LDV MEASUREMENTS OF AXIAL MEAN VELOCITY, TURBULENCE INTENSITY, AND REYNOLDS STRESSES WITH THE COPLANAR CANARD WITHOUT BLOWING - V. W. T. - α = 20° - STATION M

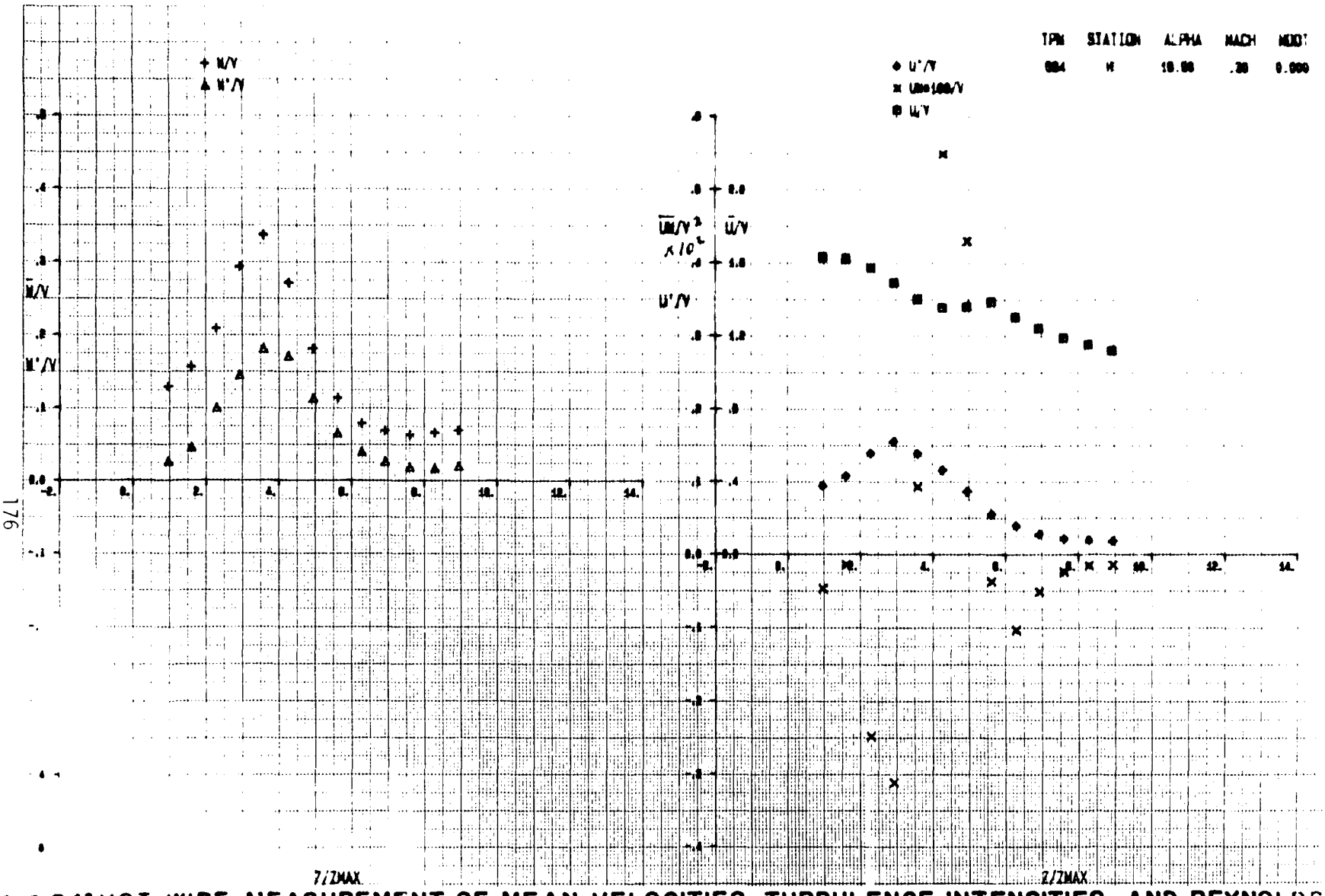

FIG 847 HOT WIRE MEASUREMENT OF MEAN VELOCITIES, TURBULENCE INTENSITIES, AND REYNOLDS STRESSES WITHOUT BLOWING - COPLANAR CANARD - TGF - α =20° STATION H

AD-A179 718 VORTEX INTERACTION ON A CANARD-WING CONFIGURATION(U) 3/3
AIR FORCE WRIGHT AERONAUTICAL LABS WRIGHT-PATTERSON AFB
OH W CALARESE OCT 86 AFWAL-TR-86-3100

UNCLASSIFIED F/G 1/1 NL

END
DATE
FILMED
F 87

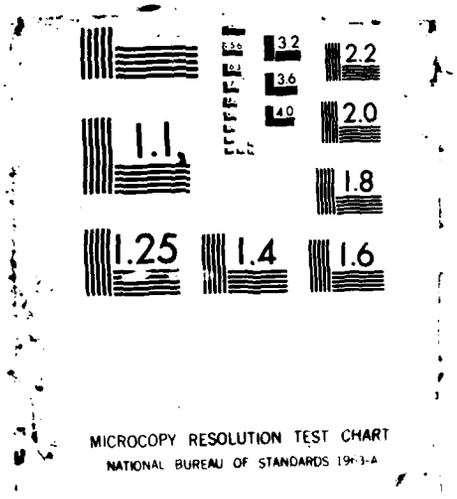
3.2
3.6
4.0
2.2
2.0
1.8
1.1
1.25
1.4
1.6
MICROCOPY RESOLUTION TEST CHART
NATIONAL BUREAU OF STANDARDS 1963-A

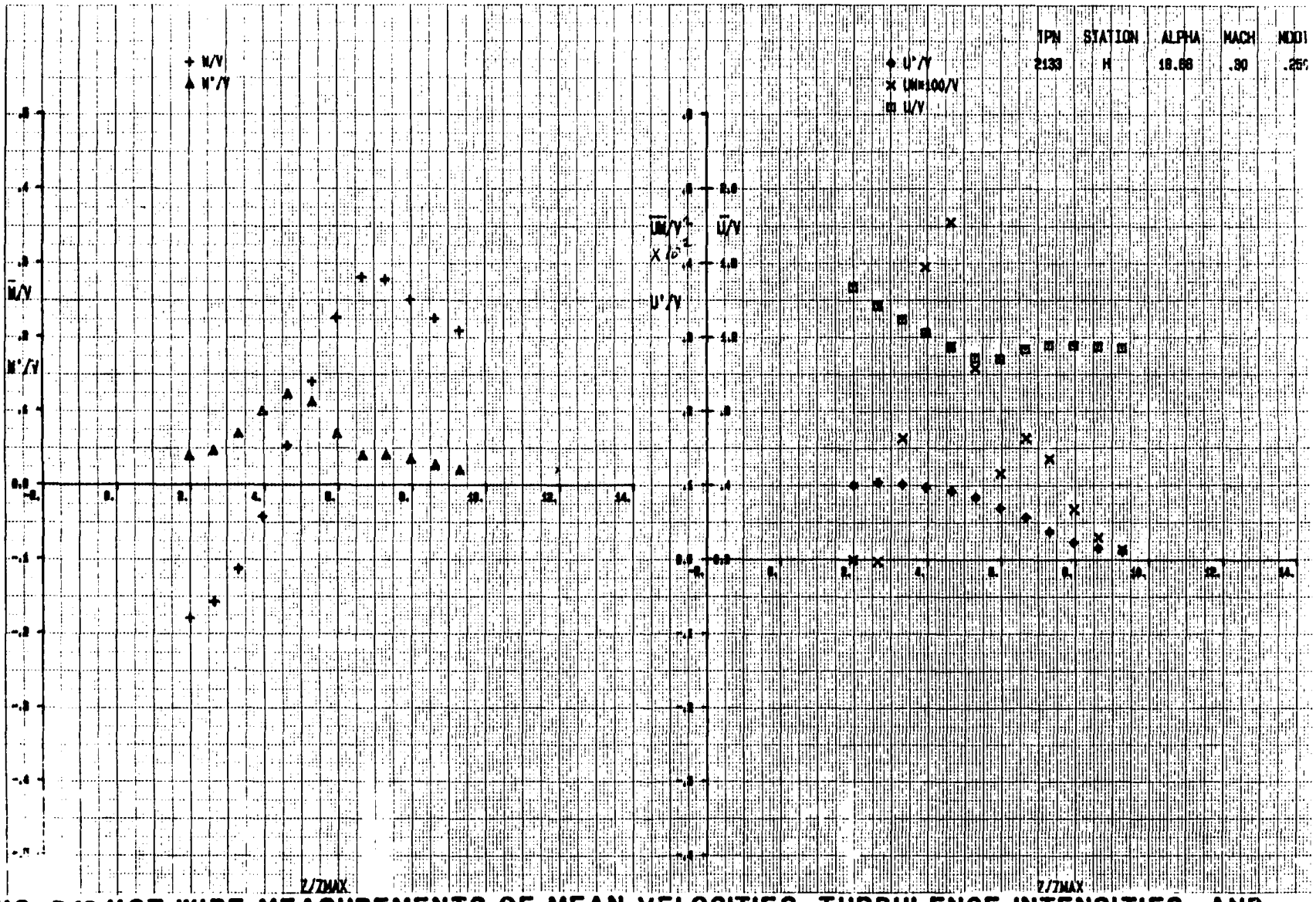

FIG. B48 HOT WIRE MEASUREMENTS OF MEAN VELOCITIES, TURBULENCE INTENSITIES, AND REYNOLDS STRESSES WITH BLOWING - COPLANAR CANARD - TGF - α=20°-STATION H

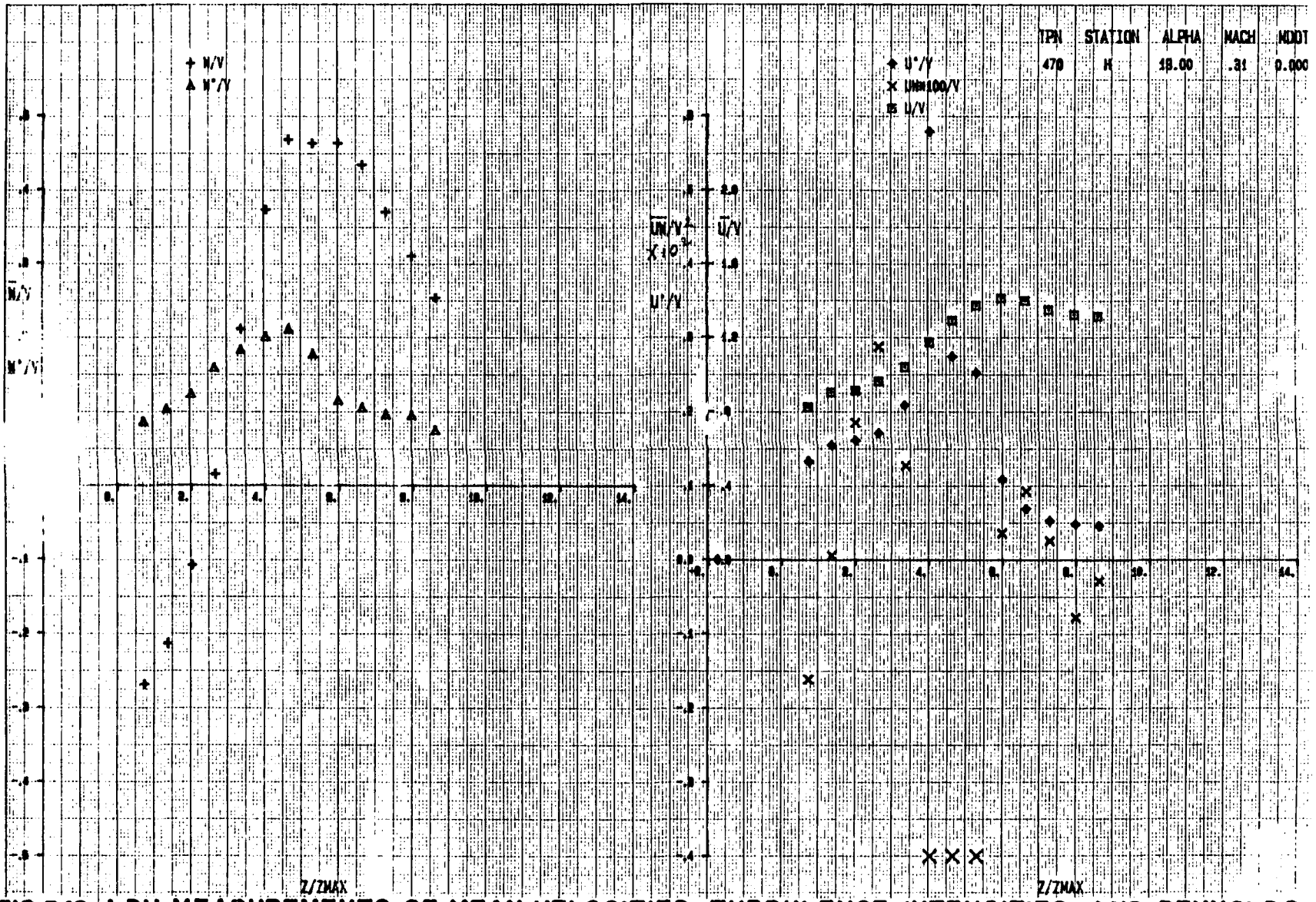

FIG.B49 LDV MEASUREMENTS OF MEAN VELOCITIES, TURBULENCE INTENSITIES, AND REYNOLDS STRESSES WITHOUT BLOWING - COPLANAR CANARD - TGF - α =20°-STATION H

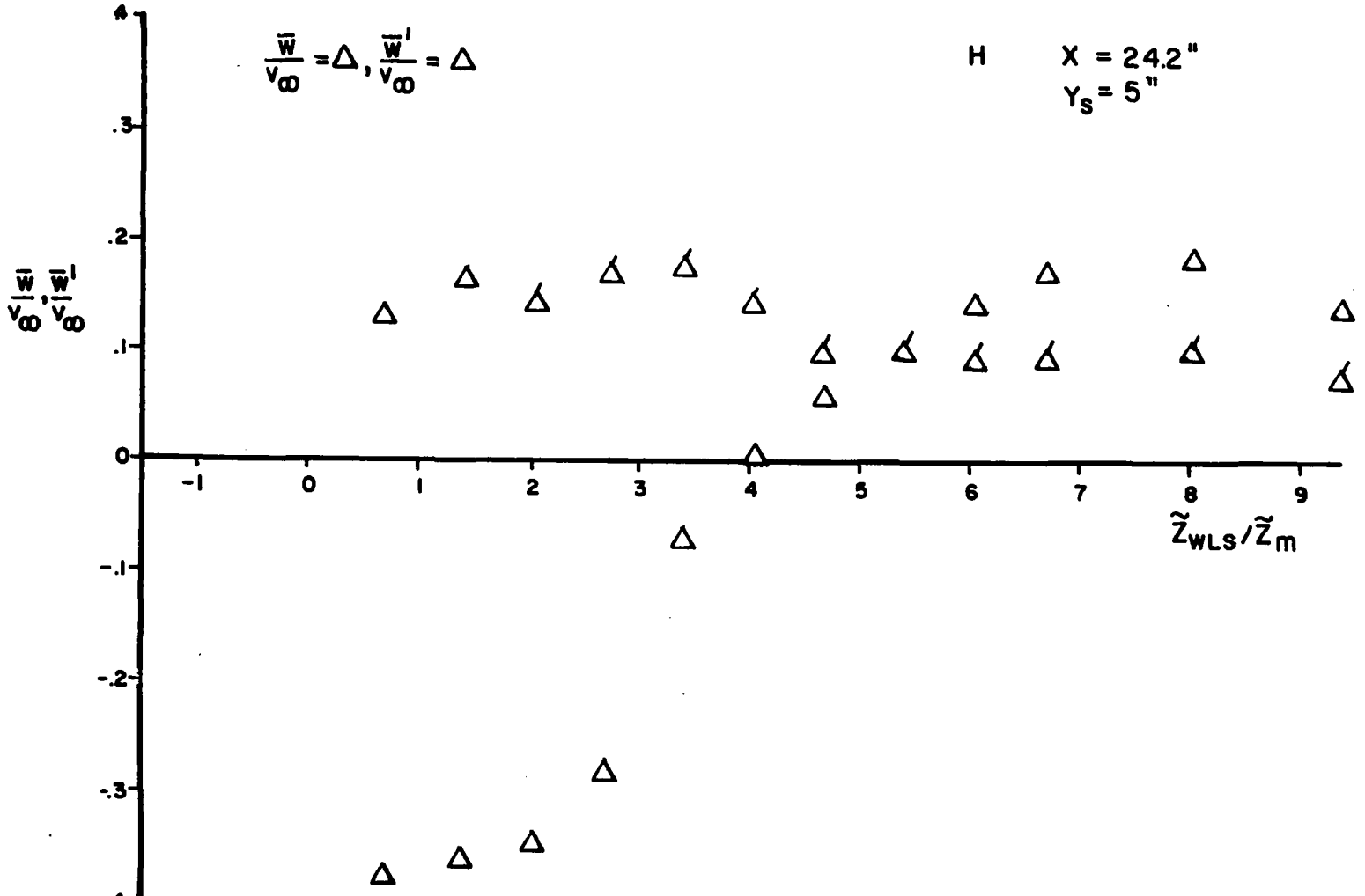

FIG.B5 LDV MEASUREMENTS OF VERTICAL MEAN VELOCITY AND TURBULENCE INTENSITY WITH THE COPLANAR CANARD WITHOUT BLOWING - V.W.T. - α = 20° STATION H

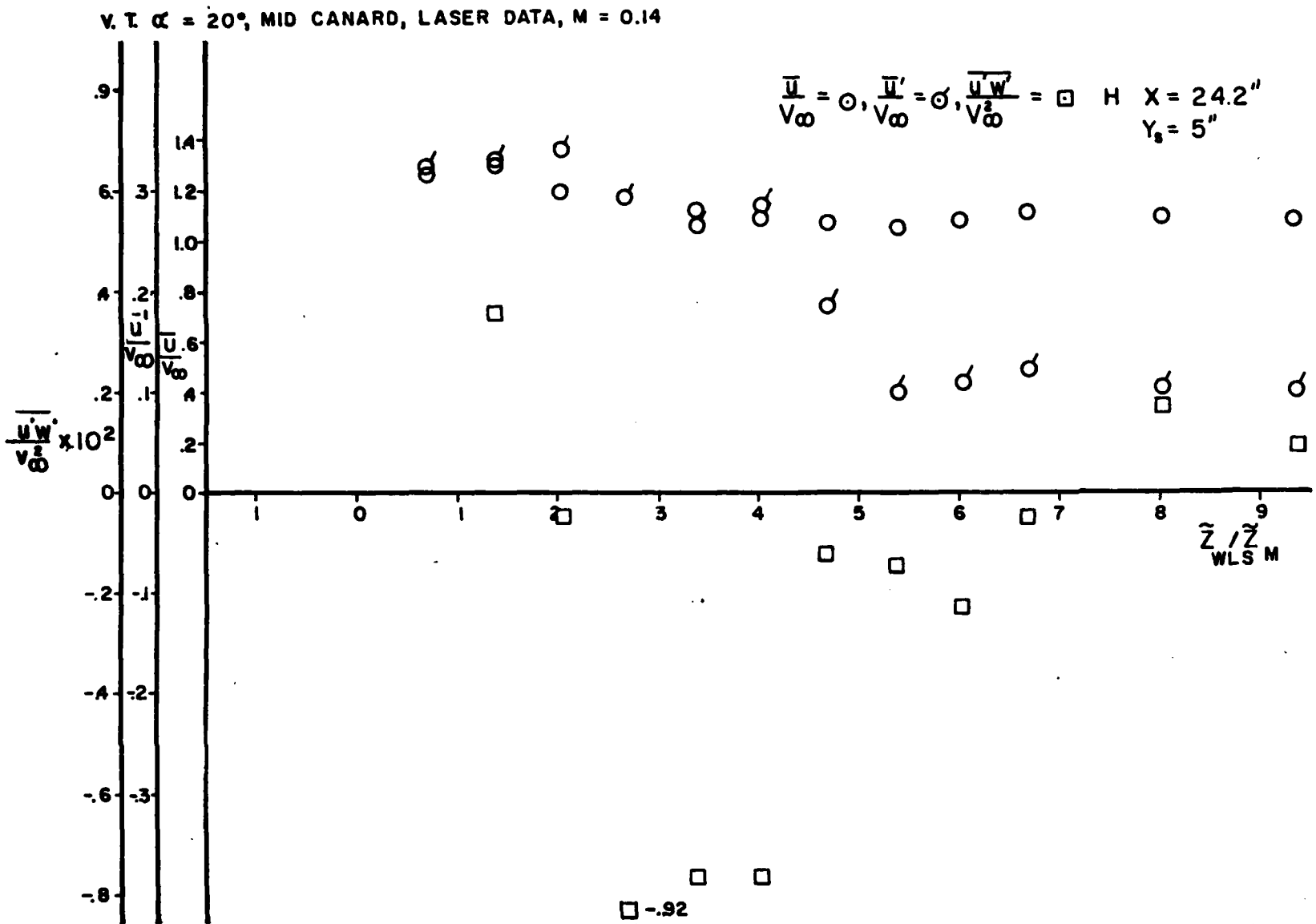

FIG. B52 LDV MEASUREMENTS OF AXIAL MEAN VELOCITY, TURBULENCE INTENSITY, AND REYNOLDS STRESSES WITH THE COPLANAR CANARD WITHOUT BLOWING - V. W. T. - α = 20° STATION H

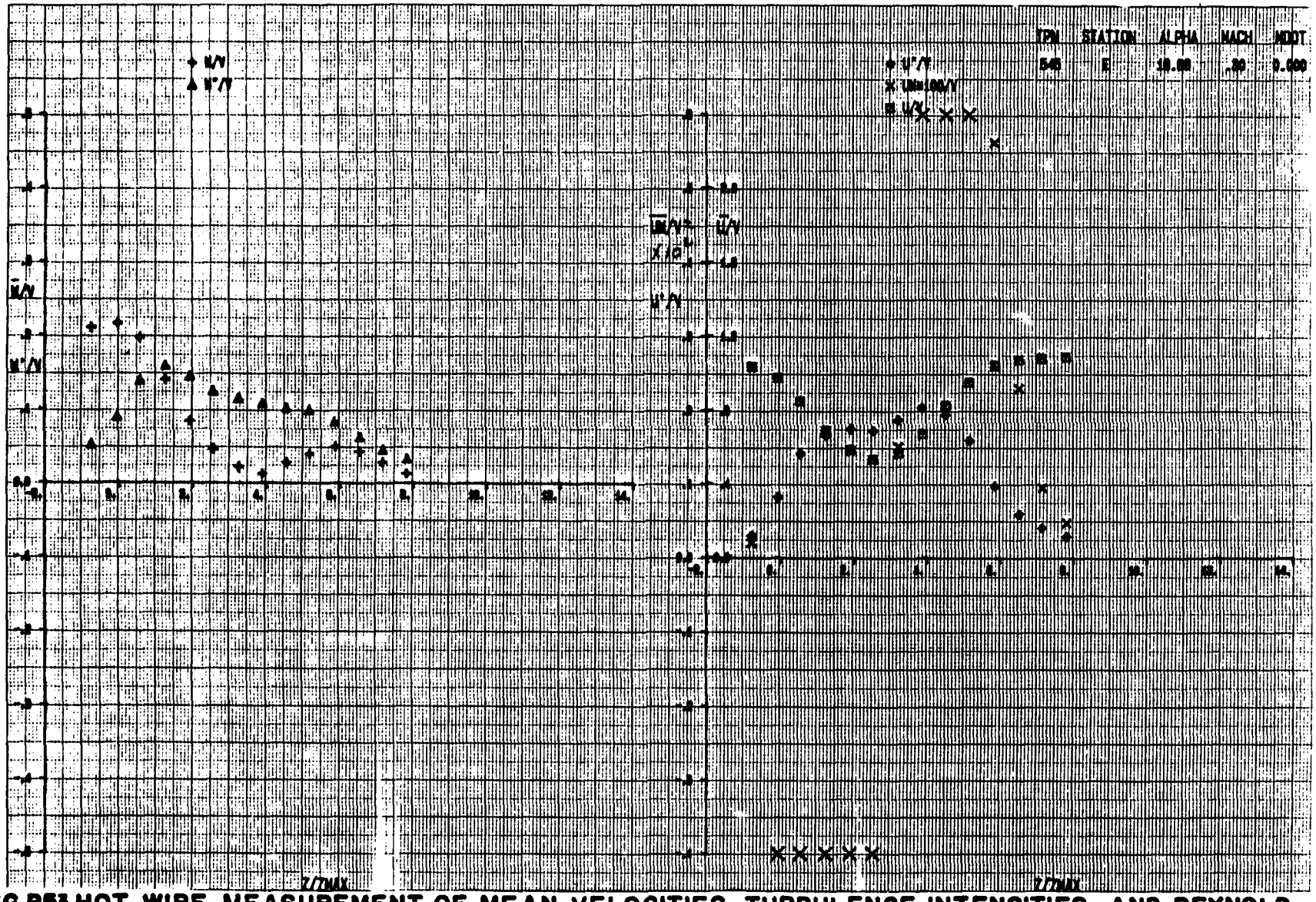

FIG. B53 HOT WIRE MEASUREMENT OF MEAN VELOCITIES, TURBULENCE INTENSITIES, AND REYNOLD STRESSES WITHOUT BLOWING - COPLANAR CANARD - TGF - $\alpha = 20°$ STATION E

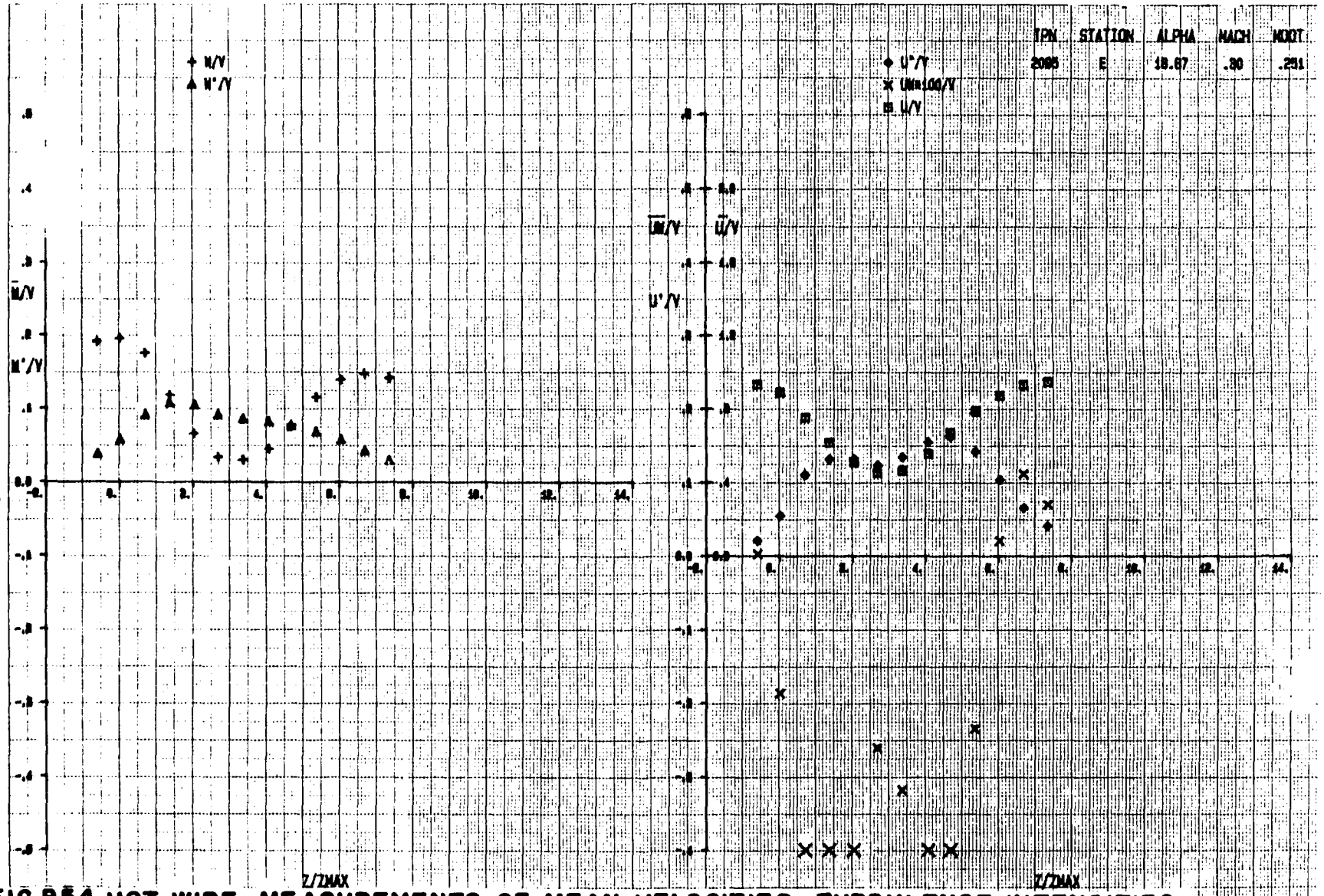

FIG.B54 HOT WIRE MEASUREMENTS OF MEAN VELOCITIES, TURBULENCE INTENSITIES, AND REYNOLDS STRESSES WITH BLOWING - COPLANAR CANARD - TGF - $\alpha = 20°$ - STATION E

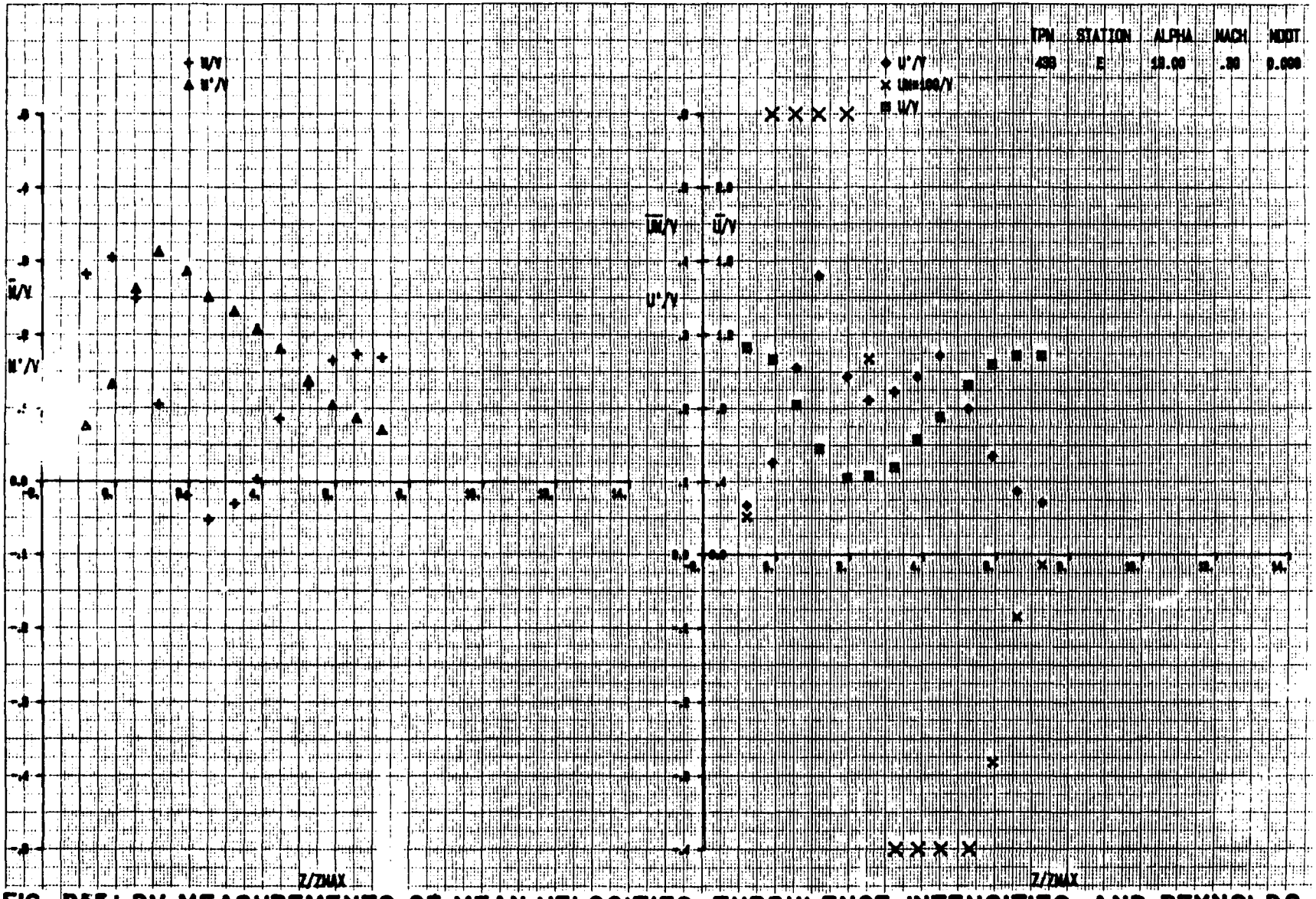

FIG. B55 LDV MEASUREMENTS OF MEAN VELOCITIES, TURBULENCE INTENSITIES, AND REYNOLDS STRESSES WITHOUT BLOWING - COPLANAR CANARD - TGF - α =20°-STATION E

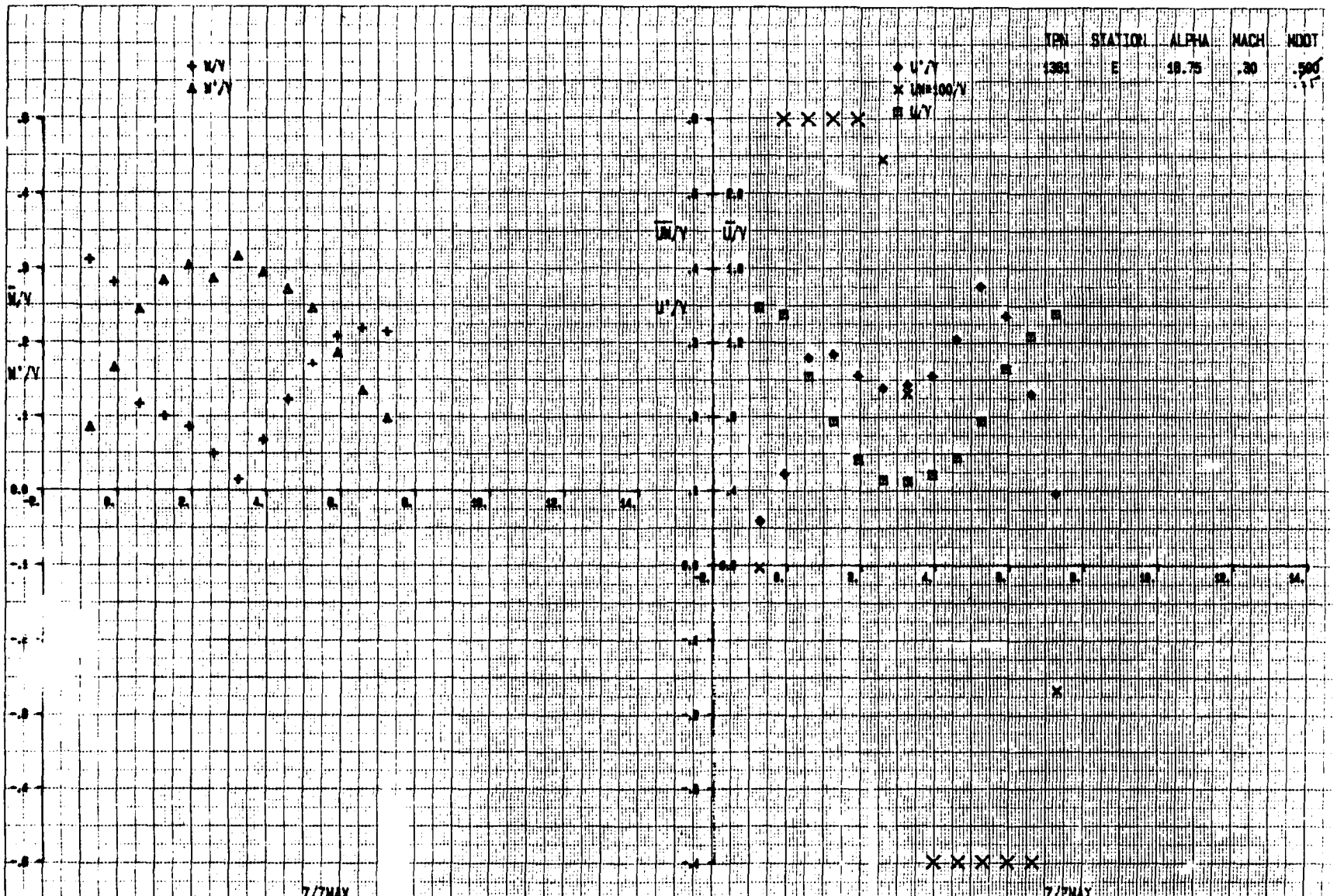

FIG. B56 LDV MEASUREMENTS OF MEAN VELOCITIES, TURBULENCE INTENSITIES, AND REYNOLDS STRESSES WITH BLOWING - COPLANAR CANARD - TGF - α = 20°-STATION E

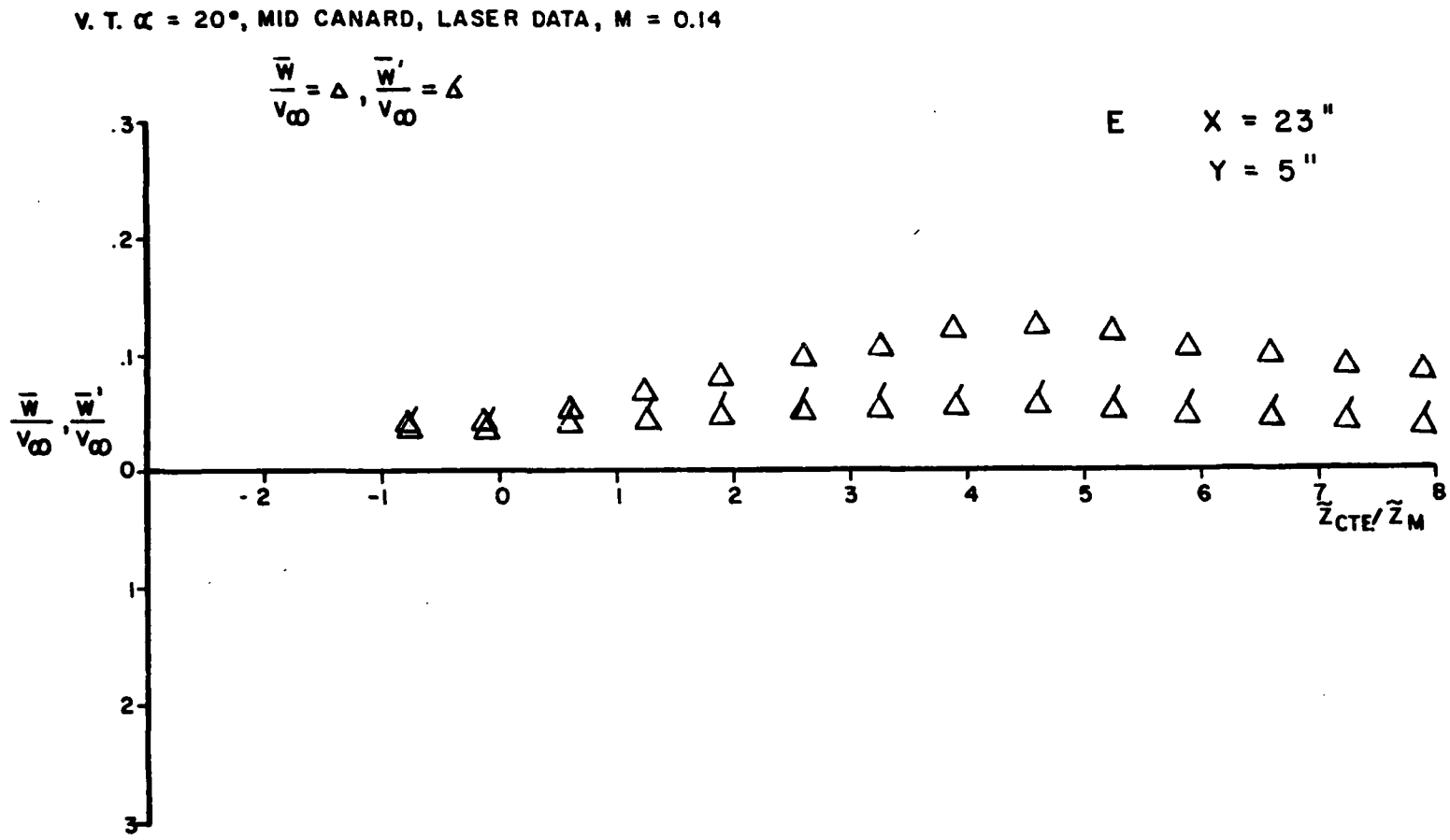

FIG. B57 LDV MEASUREMENTS OF VERTICAL MEAN VELOCITY AND TURBULENCE INTENSITY WITH THE COPLANAR CANARD WITHOUT BLOWING - V.W.T. - $\alpha = 20°$ - STATION E

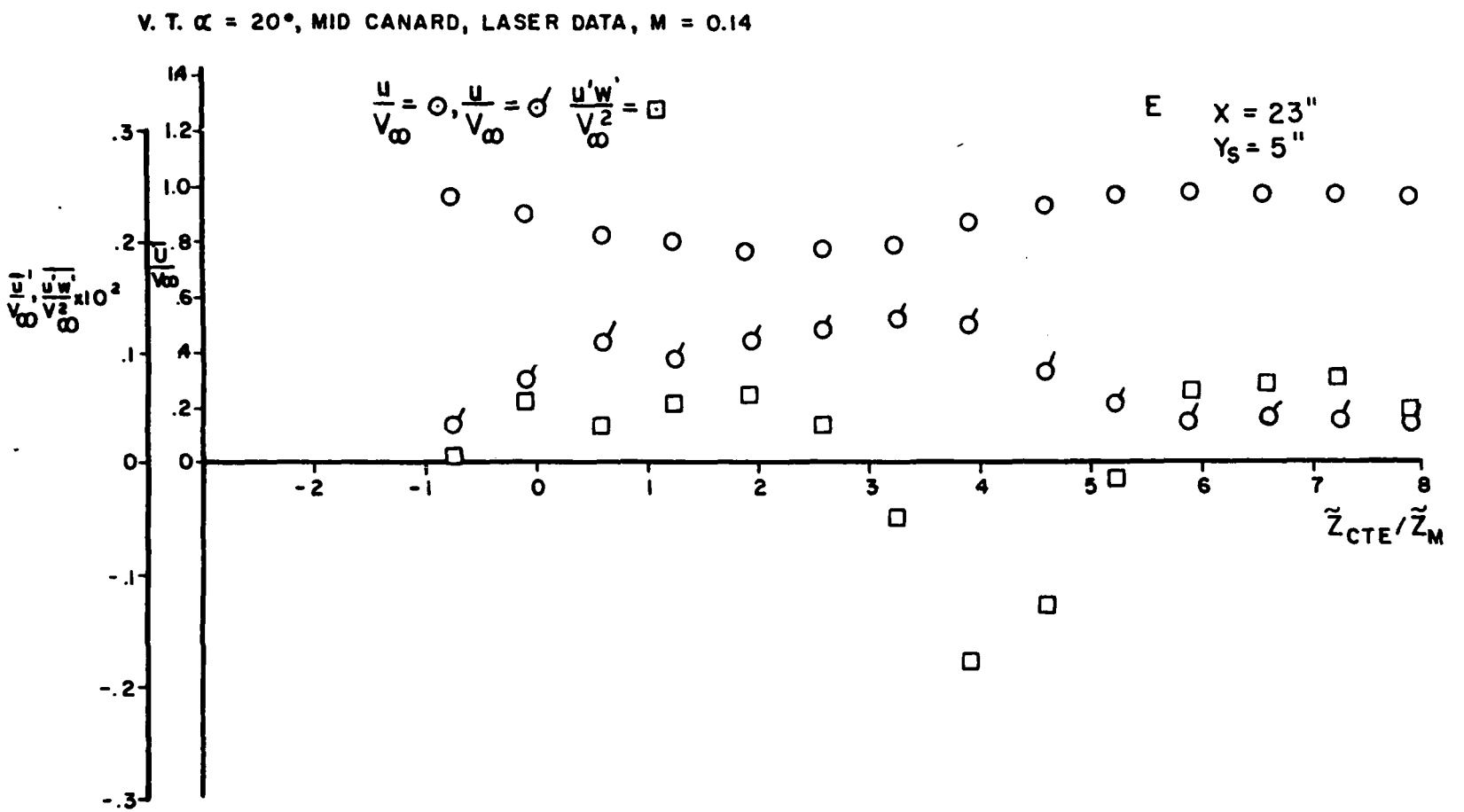

FIG.B58 LDV MEASUREMENTS OF AXIAL MEAN VELOCITY, TURBULENCE INTENSITY, AND REYNOLDS STRESSES WITH THE COPLANAR CANARD WITHOUT BLOWING - V. W. T. - α = 20° — STATION E

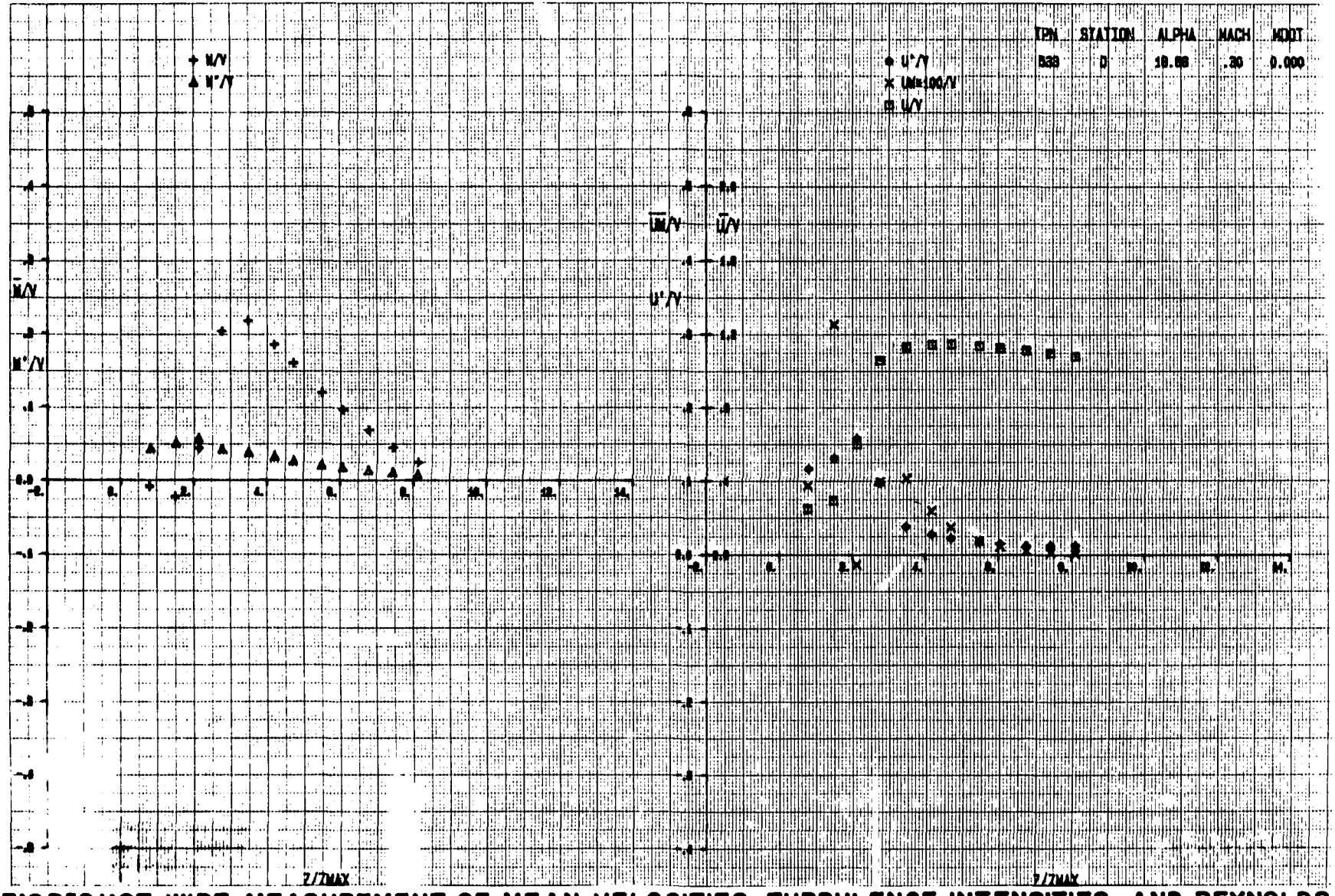

FIG.B59 HOT WIRE MEASUREMENT OF MEAN VELOCITIES, TURBULENCE INTENSITIES, AND REYNOLDS STRESSES WITHOUT BLOWING - COPLANAR CANARD - TGF - α =20° STATION D

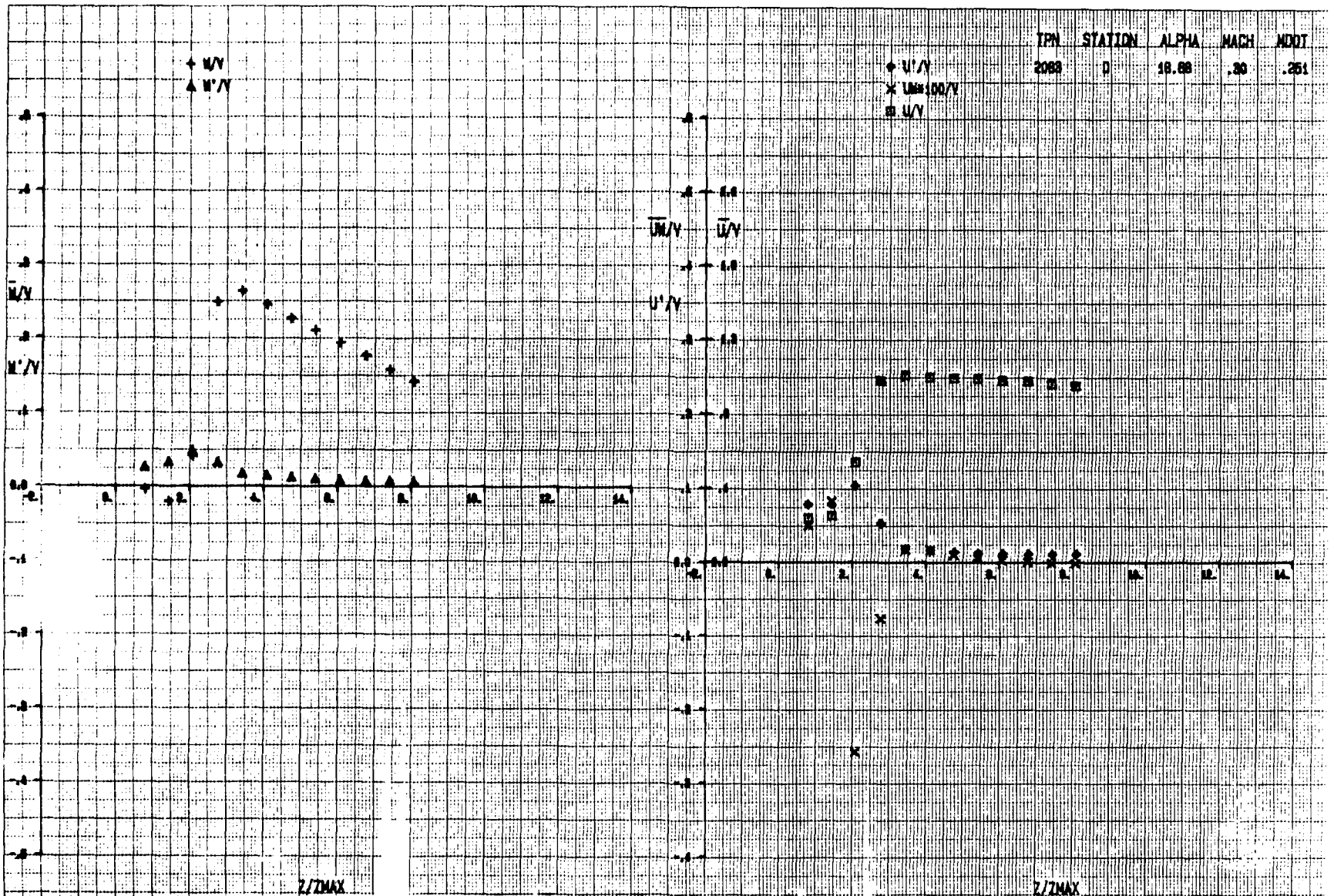

FIG. B60 HOT WIRE MEASUREMENTS OF MEAN VELOCITIES, TURBULENCE INTENSITIES, AND REYNOLDS STRESSES WITH BLOWING - COPLANAR CANARD - TGF - α=20°-STATION D

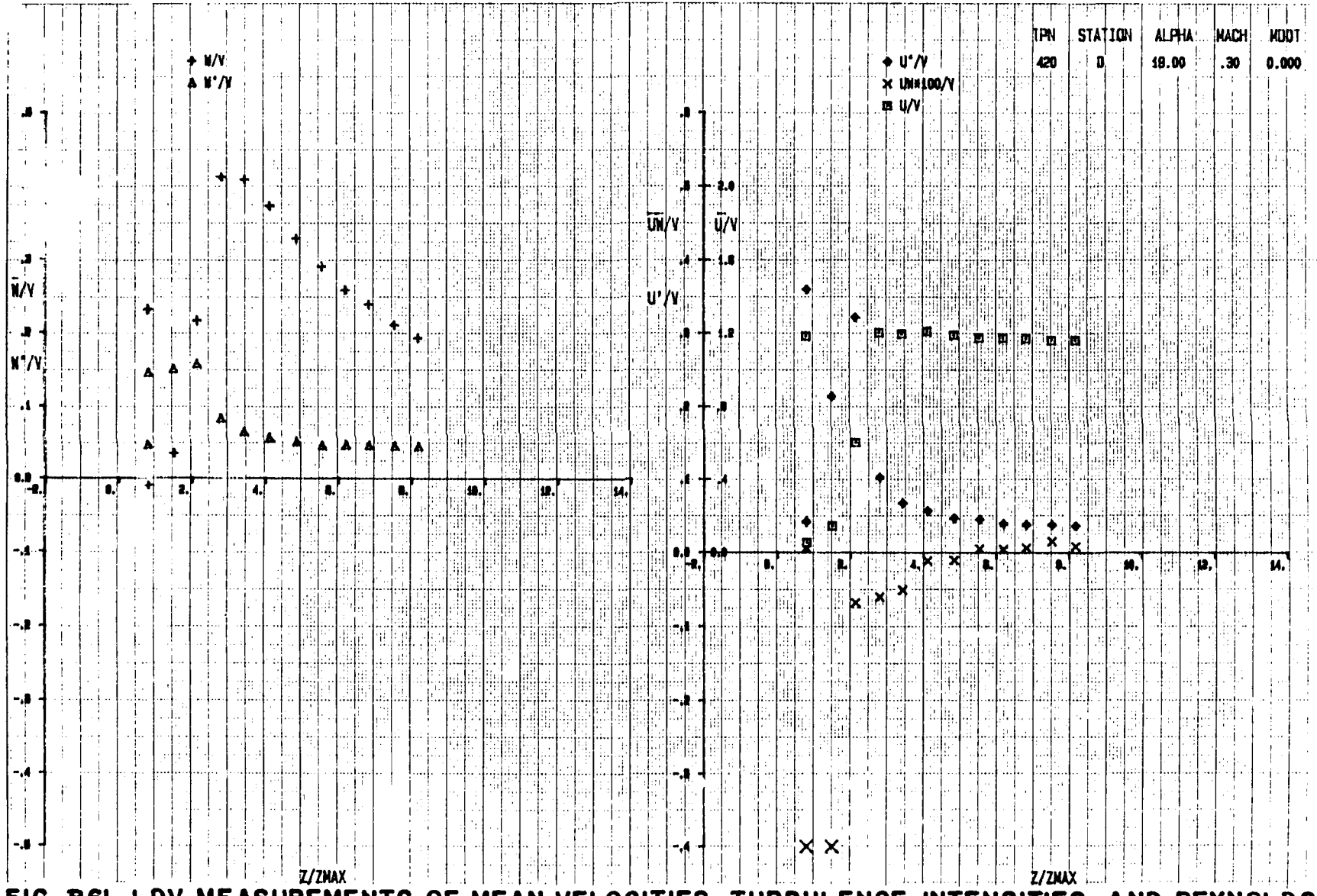

FIG. B61 LDV MEASUREMENTS OF MEAN VELOCITIES, TURBULENCE INTENSITIES, AND REYNOLDS STRESSES WITHOUT BLOWING - COPLANAR CANARD - TGF - α = 20° STATION D

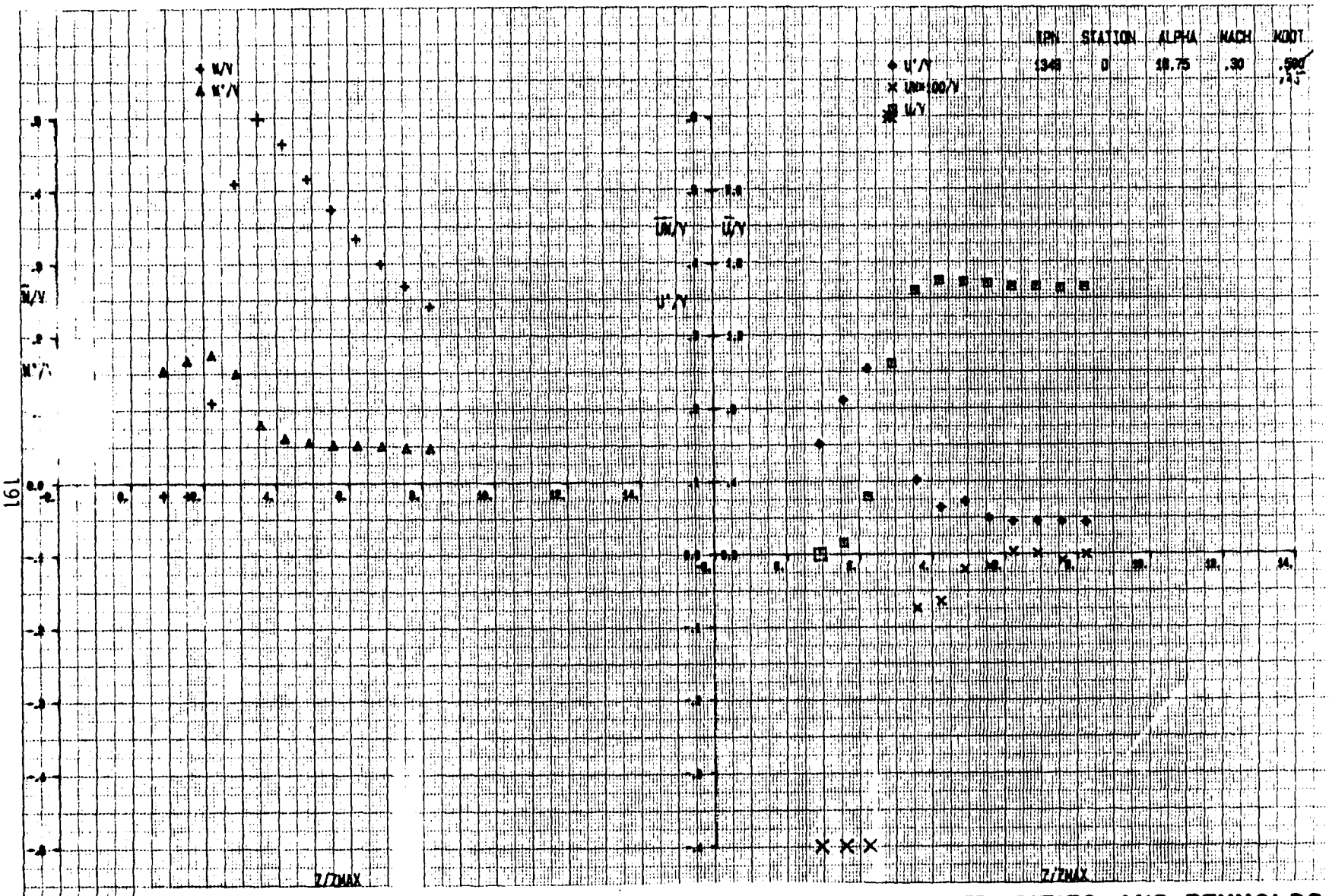

FIG. B62 LDV MEASUREMENTS OF MEAN VELOCITIES, TURBULENCE INTENSITIES, AND REYNOLDS STRESSES WITH BLOWING - COPLANAR CANARD - TGF - α = 20°-STATION D

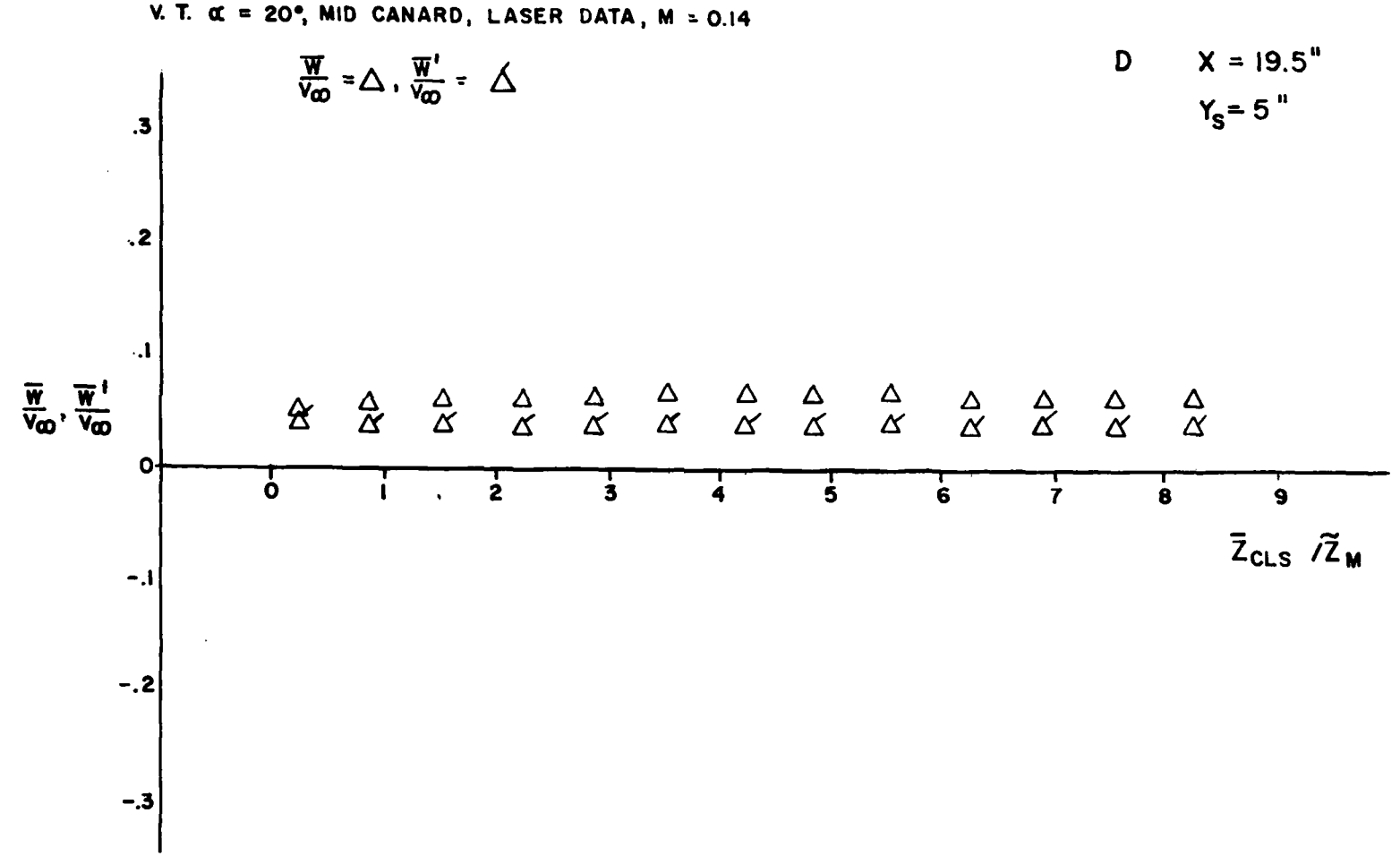

FIG. B63 LDV MEASUREMENTS OF VERTICAL MEAN VELOCITY AND TURBULENCE INTENSITY WITH THE COPLANAR CANARD – WITHOUT BLOWING - V.W.T. - α = 20° - STATION D

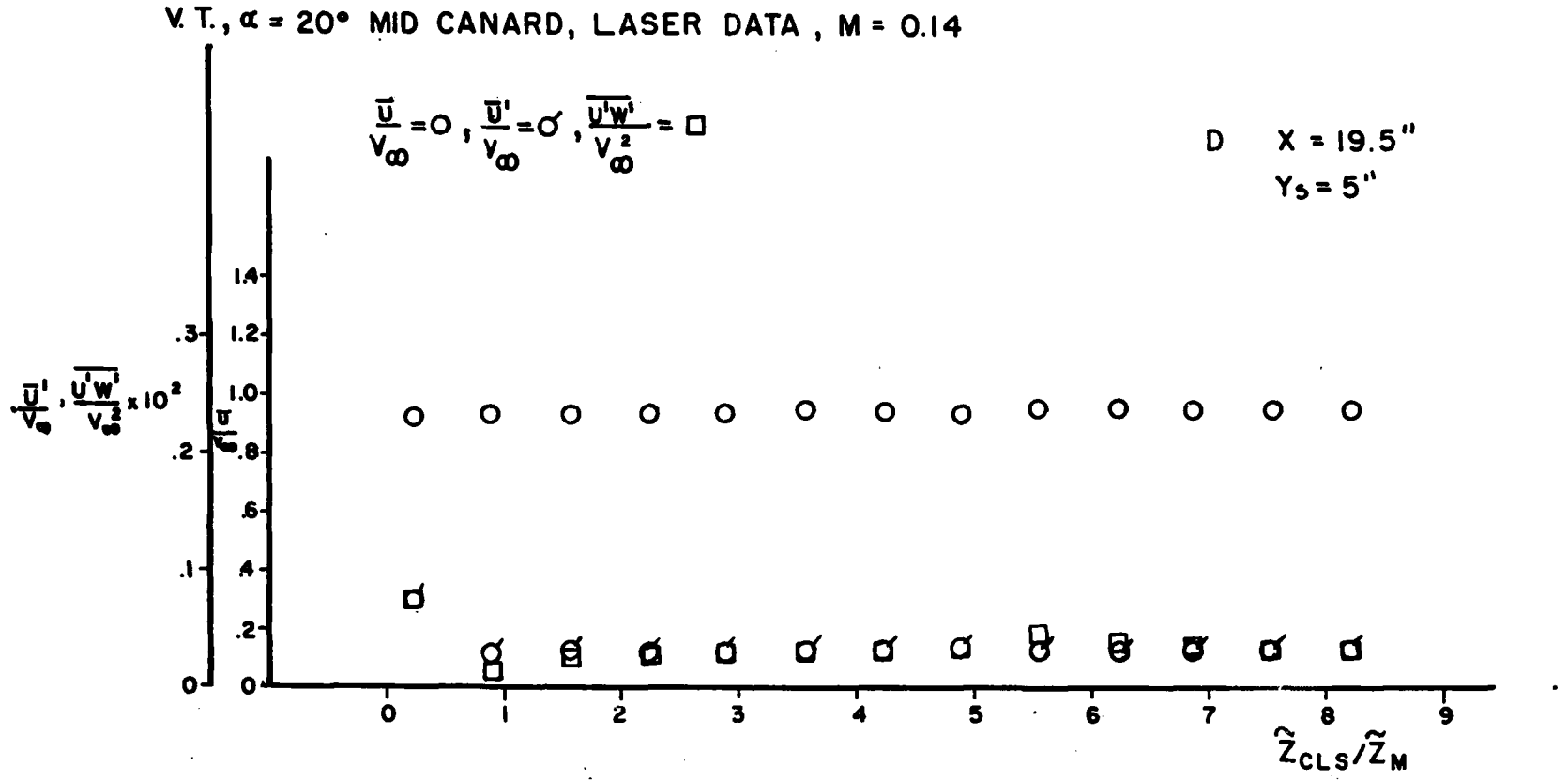

FIG. B64 LDV MEASUREMENTS OF MEAN VELOCITIES, TURBULENCE INTENSITIES, AND REYNOLDS STRESSES WITHOUT BLOWING - COPLANAR CANARD - V. W. T. - α = 20° - STATION D

FIG. B65 HOT WIRE MEASUREMENT OF MEAN VELOCITIES, TURBULENCE INTENSITIES, AND REYNOLDS STRESSES WITHOUT BLOWING - COPLANAR CANARD - TGF - $\alpha = 20°$ STATION B

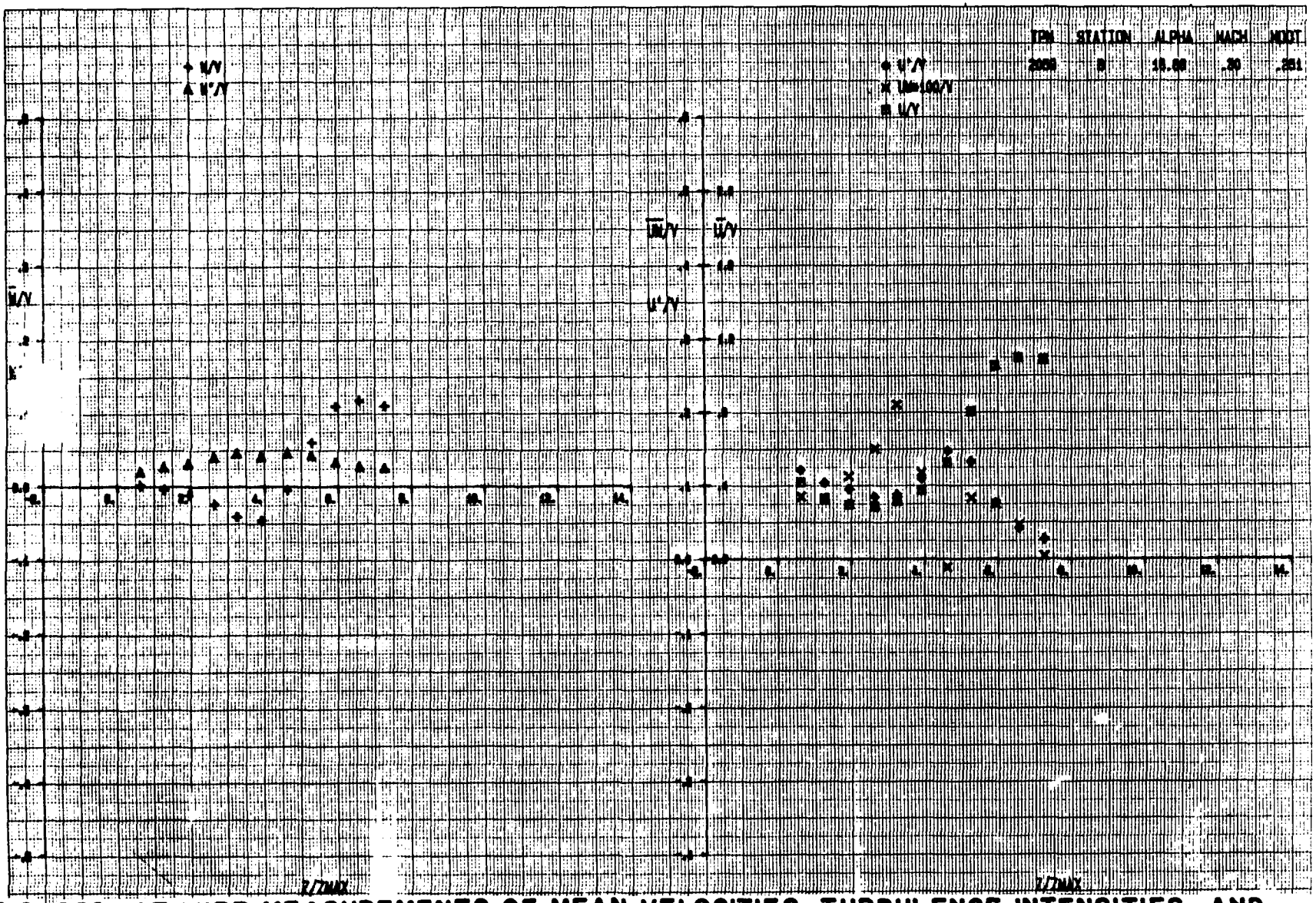

FIG. 866 HOT WIRE MEASUREMENTS OF MEAN VELOCITIES, TURBULENCE INTENSITIES, AND REYNOLDS STRESSES WITH BLOWING - COPLANAR CANARD - TGF - α=20°-STATION B

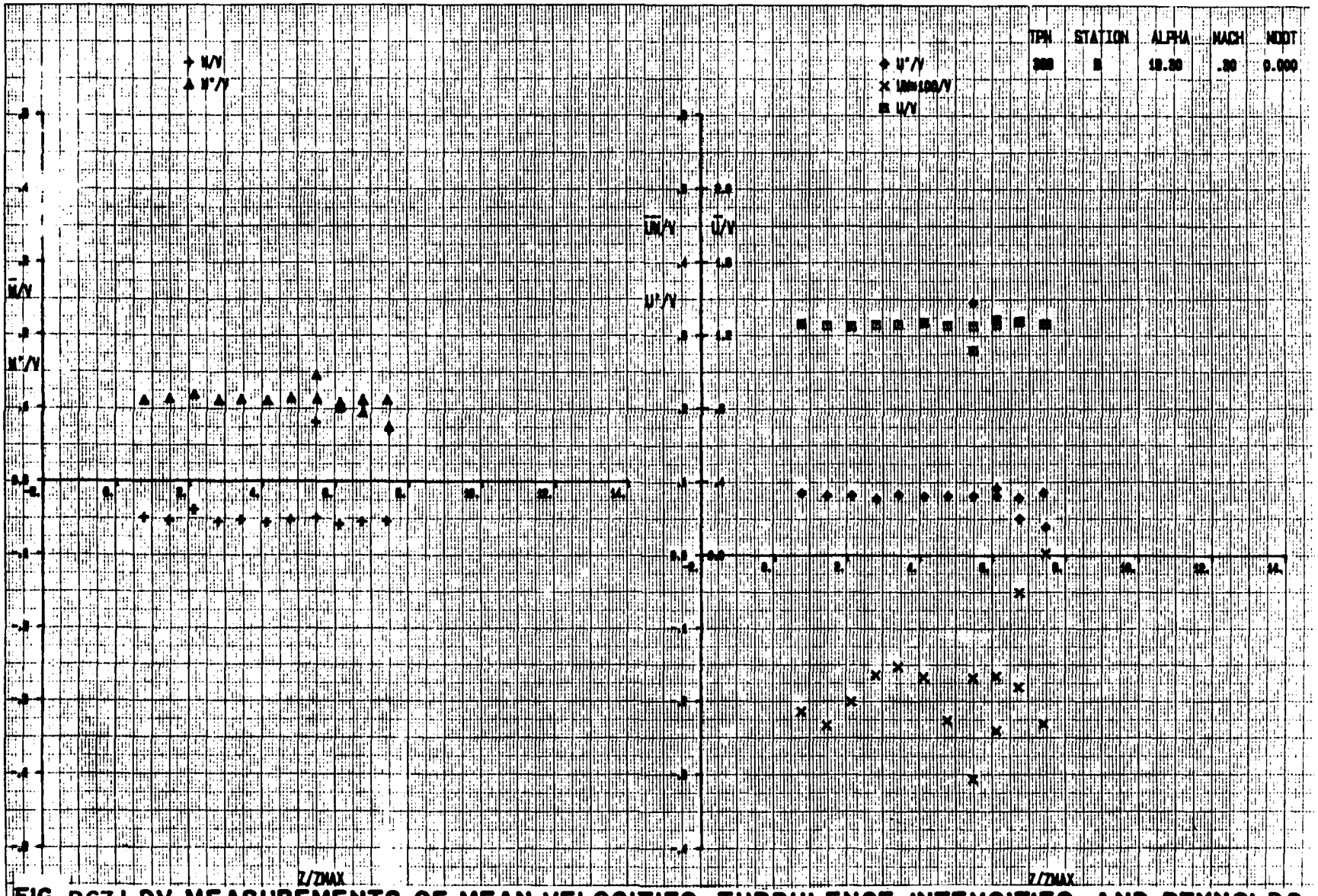

FIG. B67 LDV MEASUREMENTS OF MEAN VELOCITIES, TURBULENCE INTENSITIES, AND REYNOLDS STRESSES WITHOUT BLOWING - COPLANAR CANARD - TGF - α =20°-STATION B

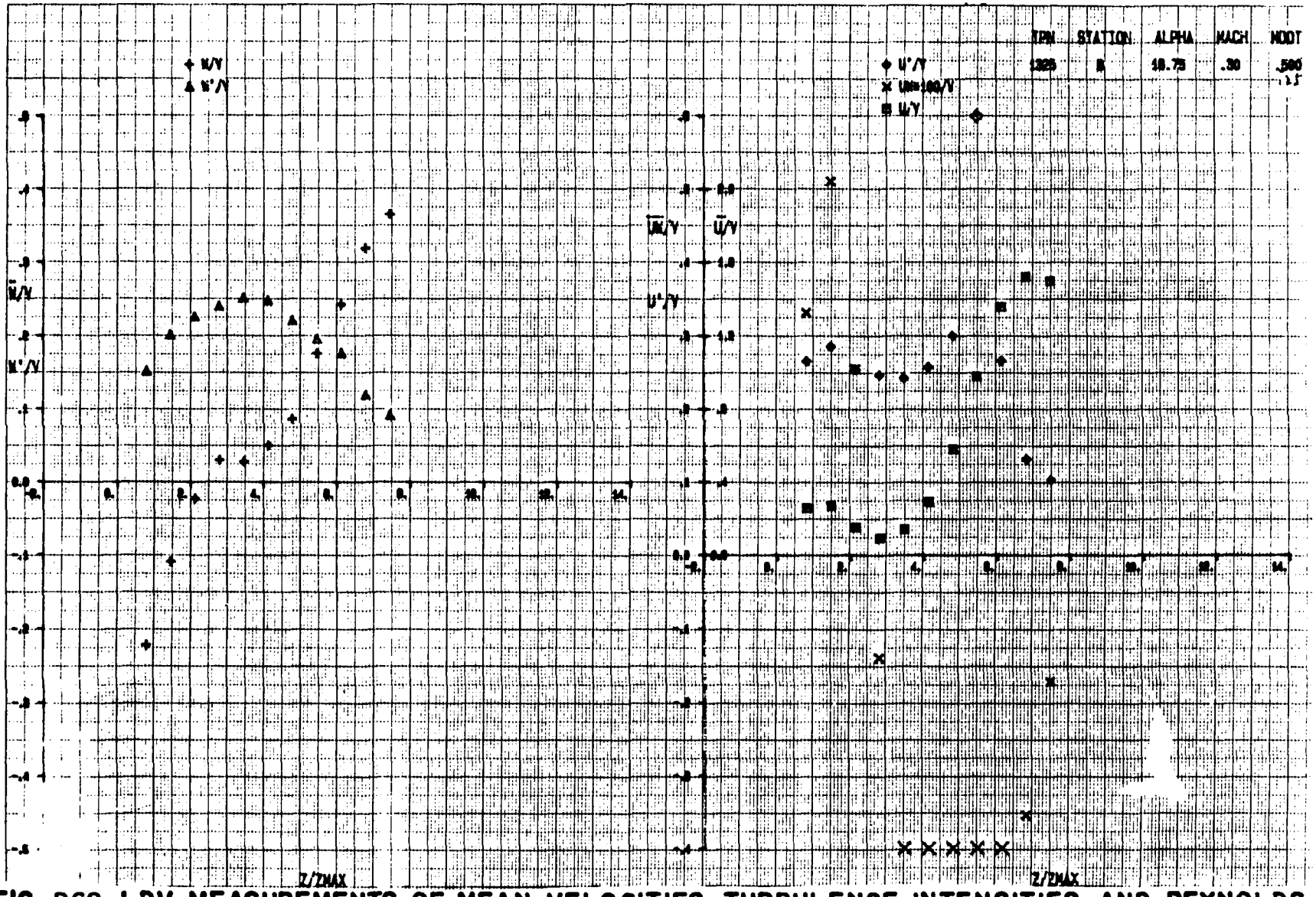

FIG. B68 LDV MEASUREMENTS OF MEAN VELOCITIES, TURBULENCE INTENSITIES, AND REYNOLDS STRESSES WITH BLOWING - COPLANAR CANARD - TGF - α = 20°-STATION B

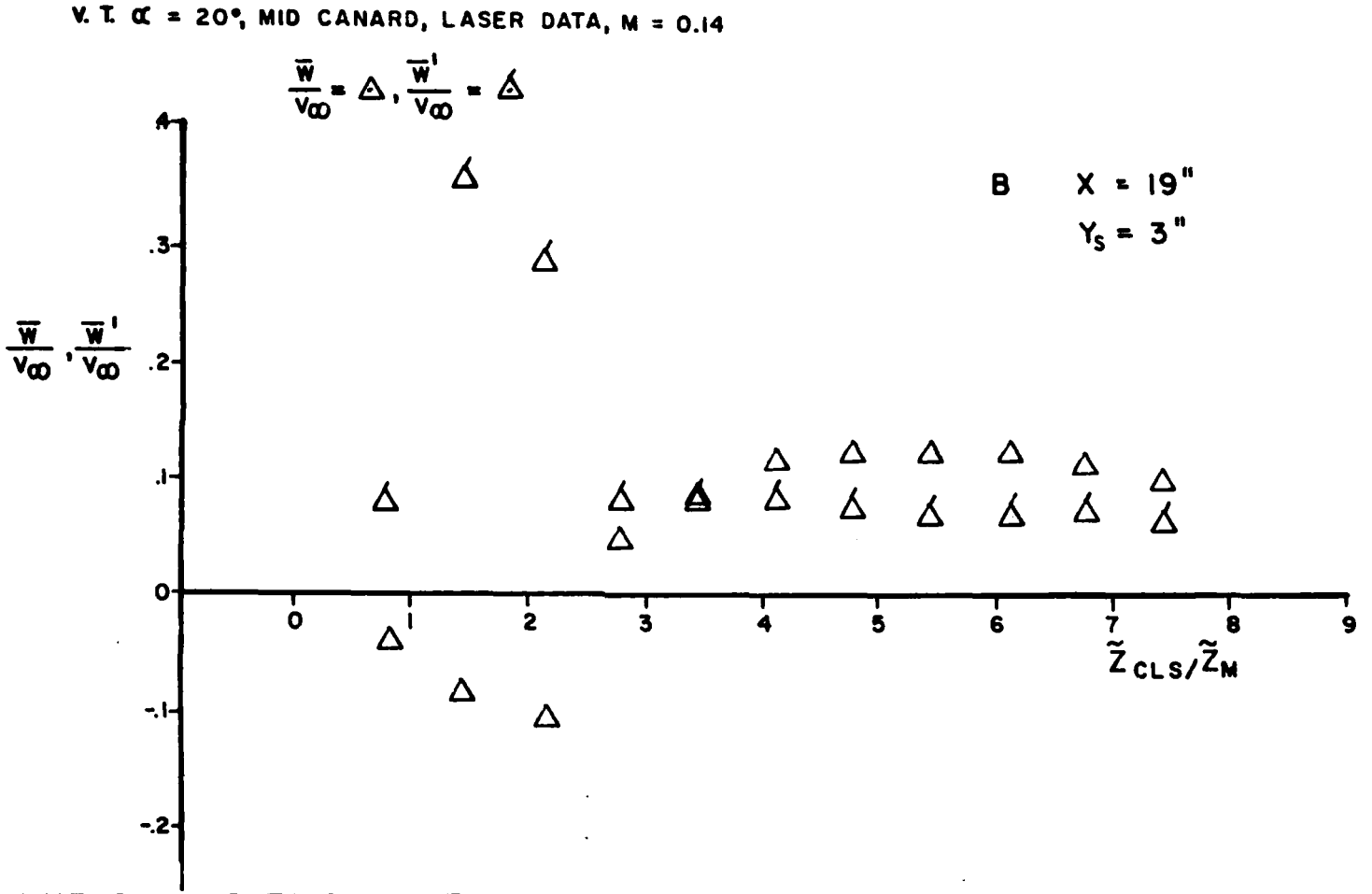

FIG. B69 LDV MEASUREMENTS OF VERTICAL MEAN VELOCITY AND TURBULENCE INTENSITY WITH THE COPLANAR CANARD WITHOUT BLOWING - V.W.T. - α = 20° STATION B

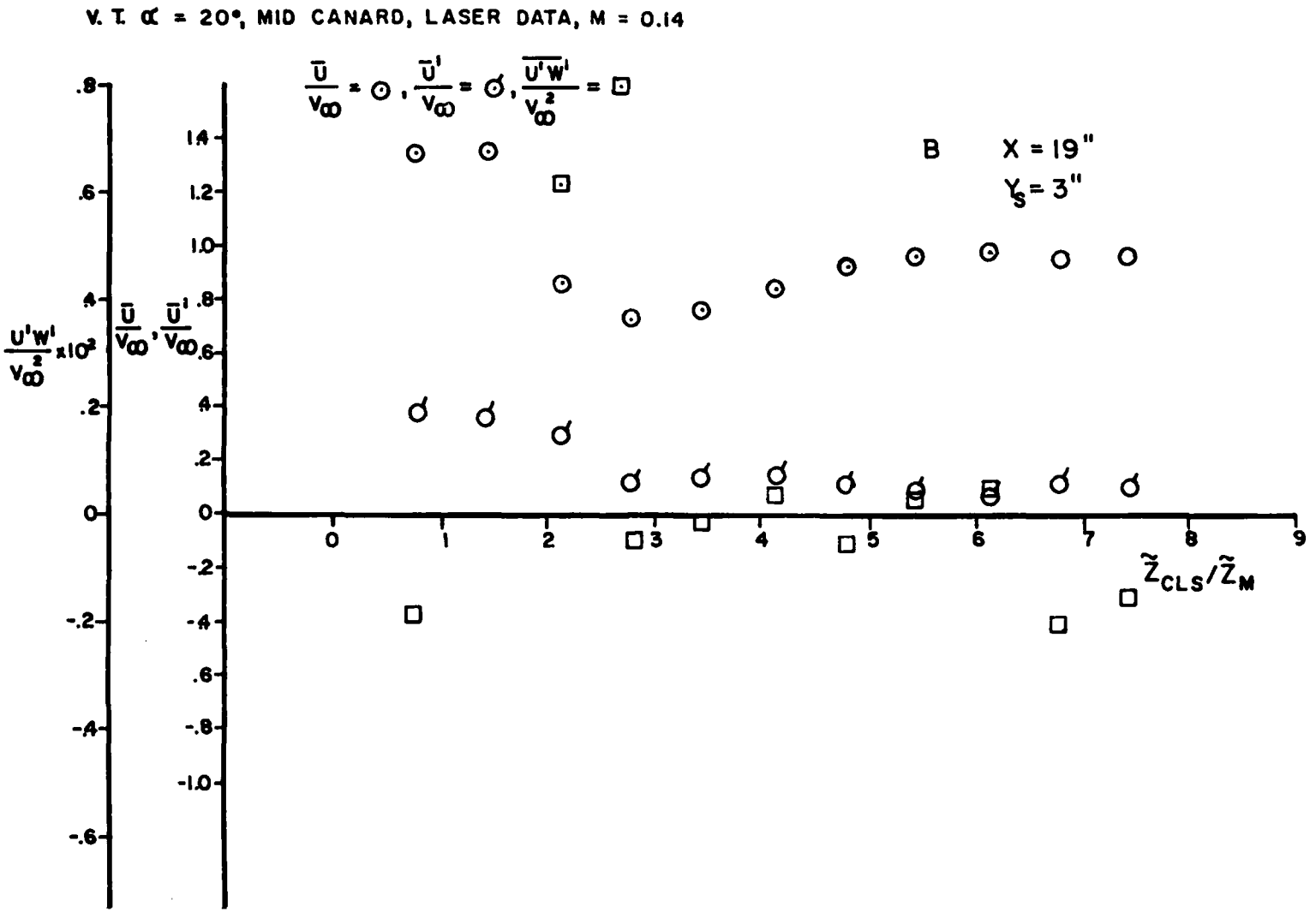

FIG. B 70 LDV MEASUREMENTS OF AXIAL MEAN VELOCITY, TURBULENCE INTENSITY, AND REYNOLDS STRESSES WITH THE COPLANAR CANARD WITHOUT BLOWING - V. W. T. - α = 20° - STATION B

APPENDIX C

The figures C1 to C22 compare data obtained in the VWT with the high canard to data with the mid canard for different configurations at different stations.

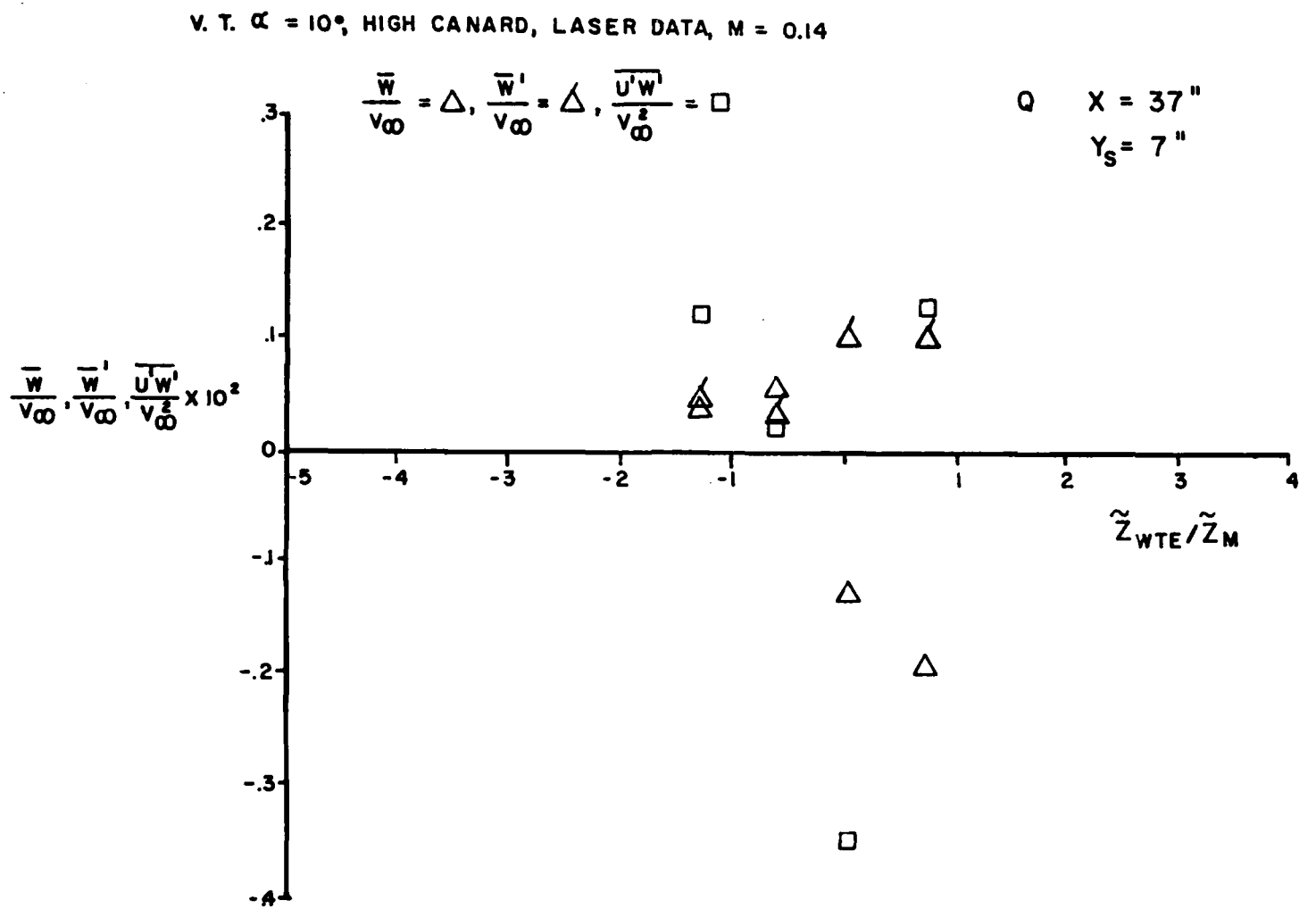

FIG. C1 LDV MEASUREMENTS OF VERTICAL MEAN VELOCITY, TURBULENCE INTENSITY, AND REYNOLDS STRESSES WITH THE HIGH CANARD WITHOUT BLOWING - V. W. T. - α = 10° STATION Q

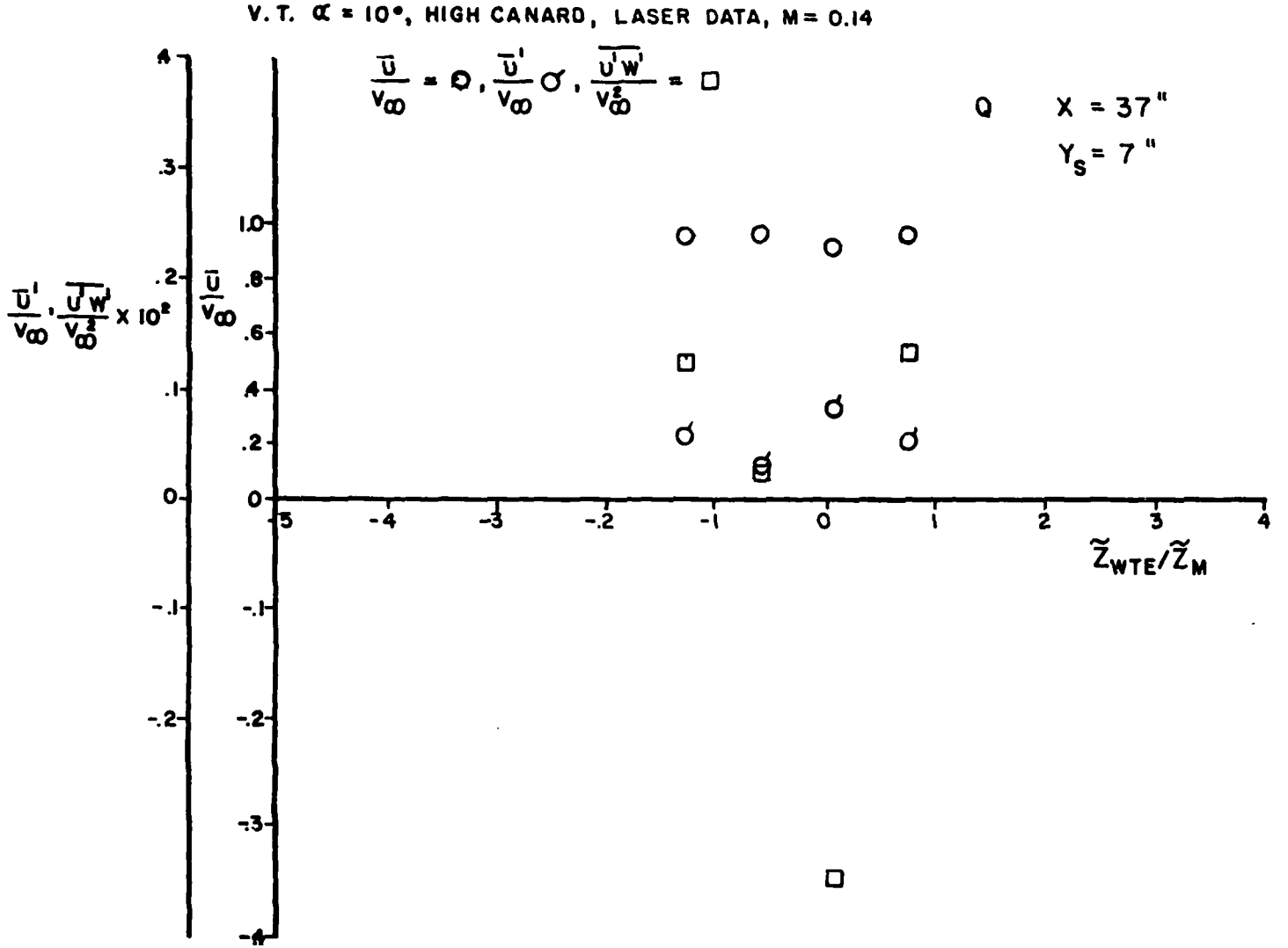

FIG. C2 LDV MEASUREMENTS OF AXIAL MEAN VELOCITY, TURBULENCE INTENSITY, AND REYNOLDS STRESSES WITH THE HIGH CANARD WITHOUT BLOWING - V. W. T. - α = 10° STATION Q

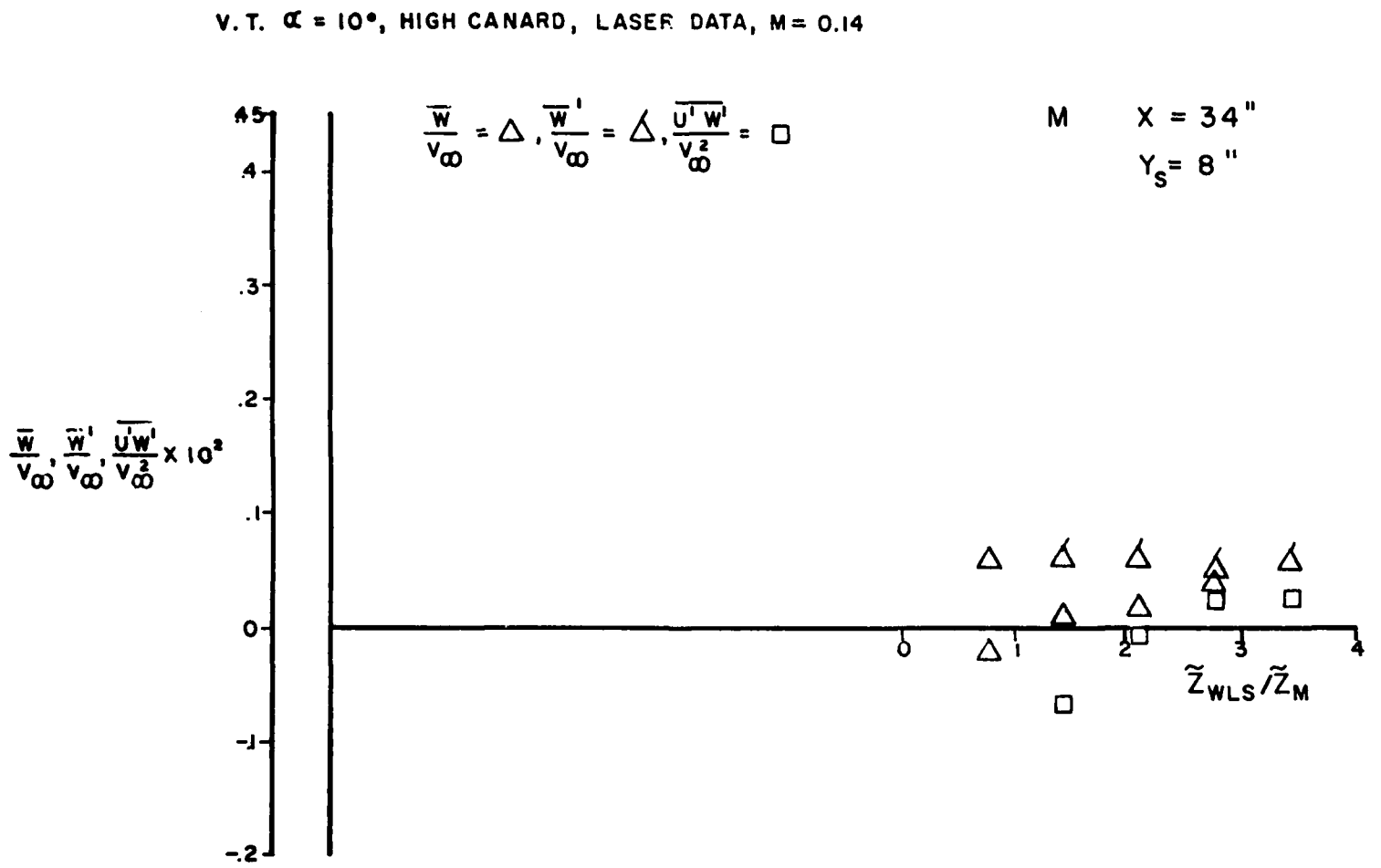

FIG. C3 LDV MEASUREMENTS OF VERTICAL MEAN VELOCITY, TURBULENCE INTENSITY, AND REYNOLDS STRESSES WITH THE HIGH CANARD WITHOUT BLOWING - V. W. T. - α = 10° STATION M

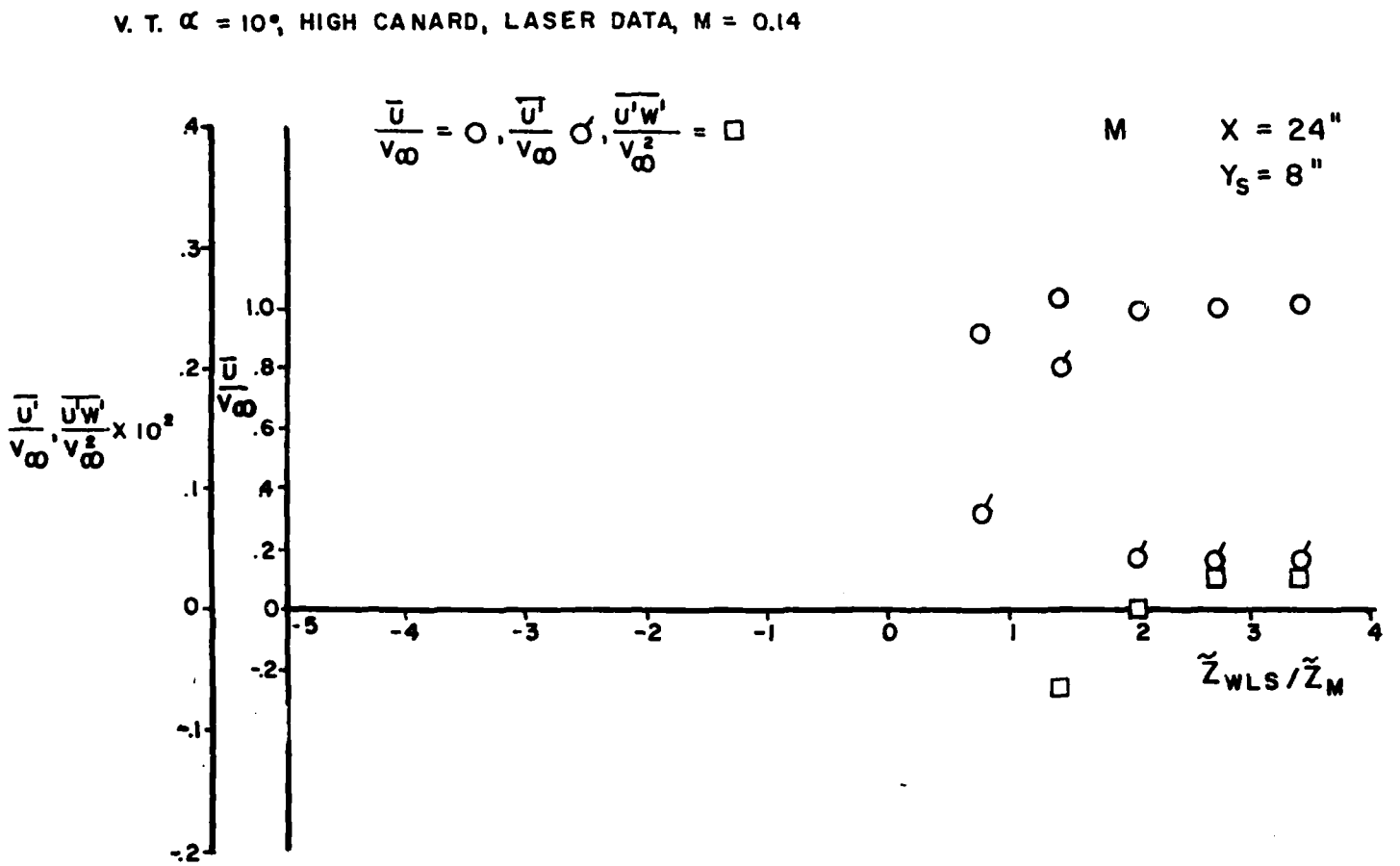

FIG. C4 LDV MEASUREMENTS OF AXIAL MEAN VELOCITY, TURBULENCE INTENSITY, AND REYNOLDS STRESSES WITH THE HIGH CANARD WITHOUT BLOWING - V. W. T. - α = 10° STATION M

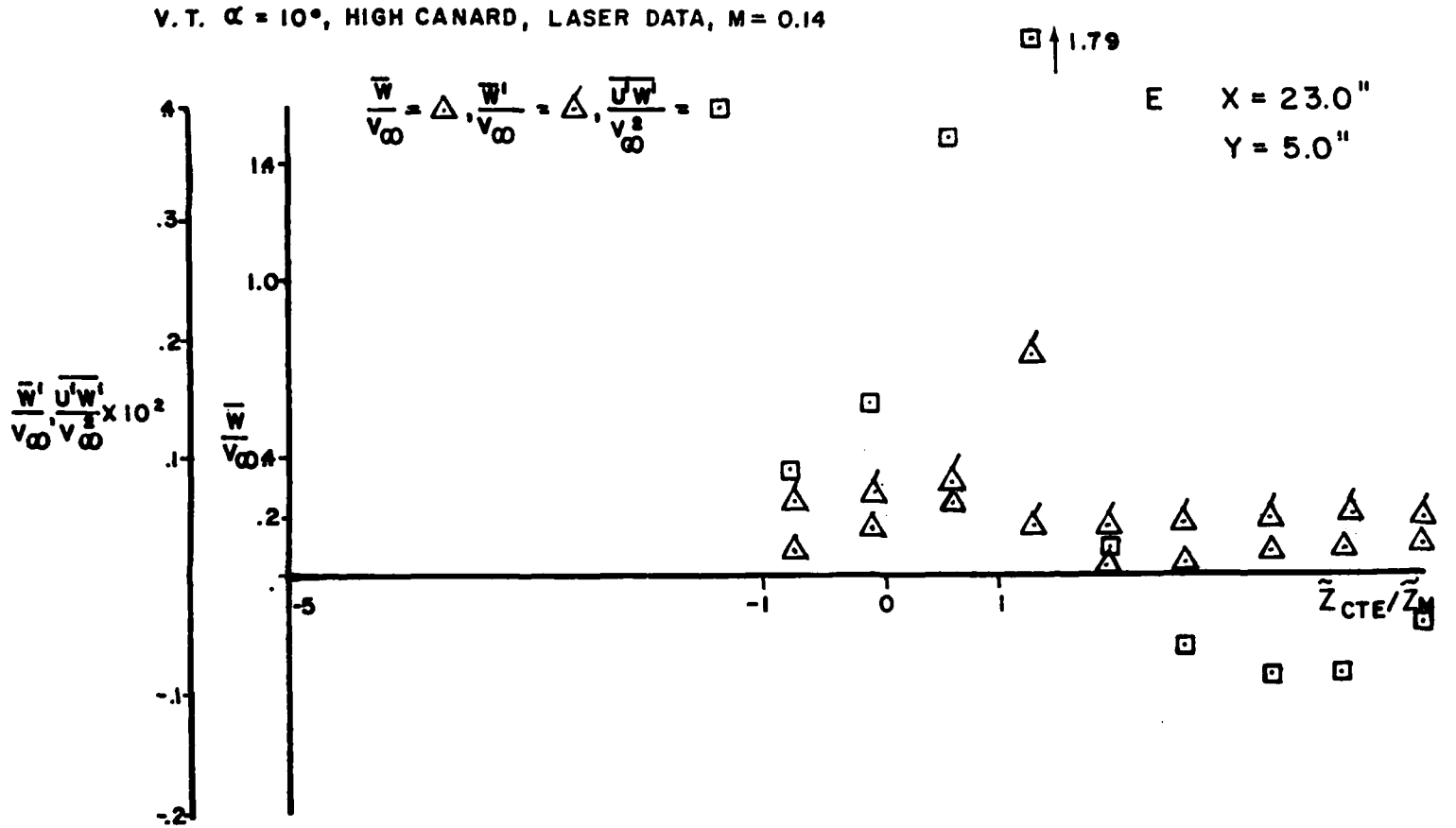

FIG. C5 LDV MEASUREMENTS OF VERTICAL MEAN VELOCITY, TURBULENCE INTENSITY, AND REYNOLDS STRESSES WITH THE HIGH CANARD WITHOUT BLOWING - V. W. T. - α = 10° STATION E

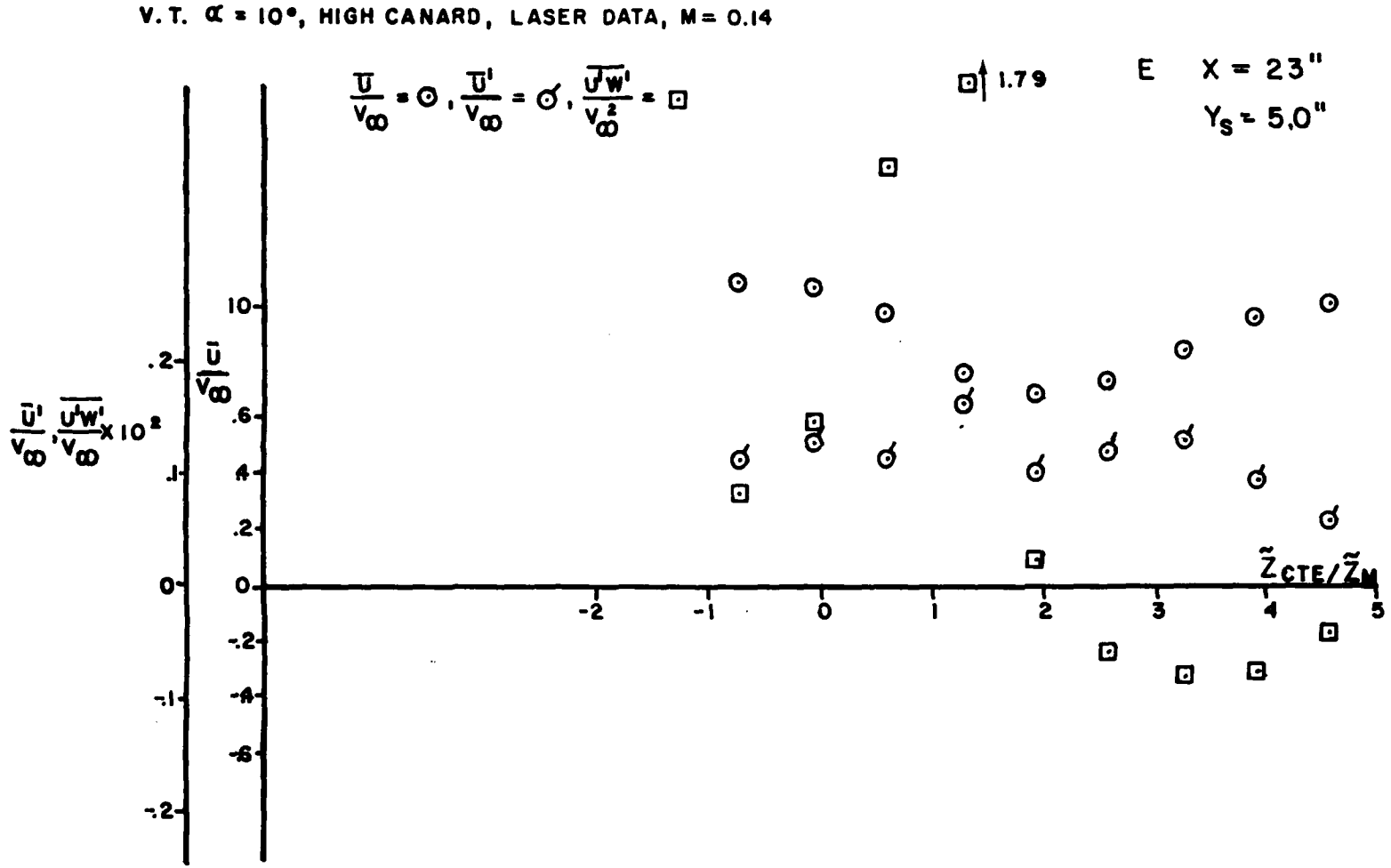

FIG. C6 LDV MEASUREMENTS OF AXIAL MEAN VELOCITY, TURBULENCE INTENSITY, AND REYNOLDS STRESSES WITH THE HIGH CANARD WITHOUT BLOWING - V. W. T. - α = 10° STATION E

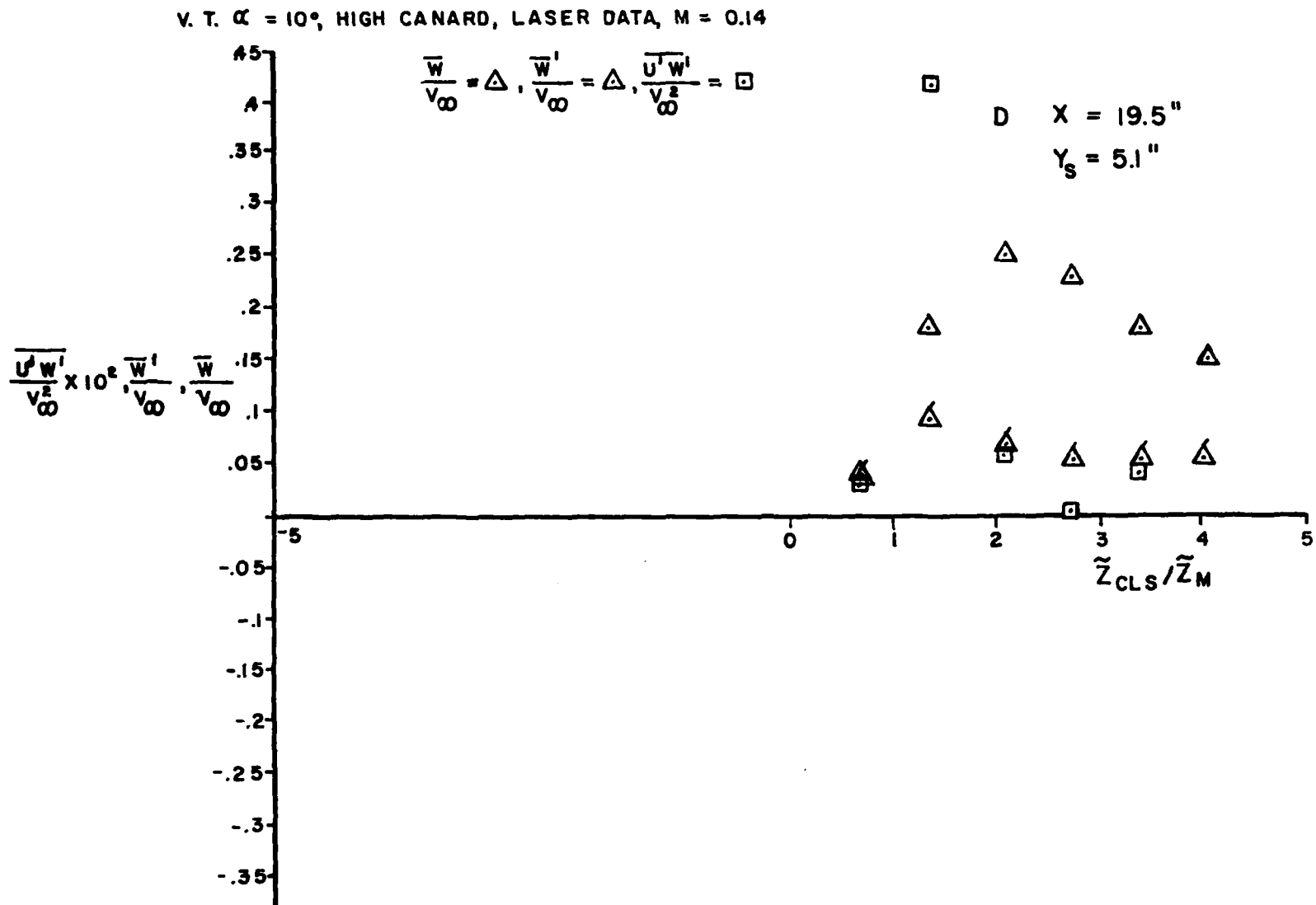

FIG. C7 LDV MEASUREMENTS OF VERTICAL MEAN VELOCITY, TURBULENCE INTENSITY, AND REYNOLDS STRESSES WITH THE HIGH CANARD WITHOUT BLOWING - V. W. T. - α = 10° STATION D

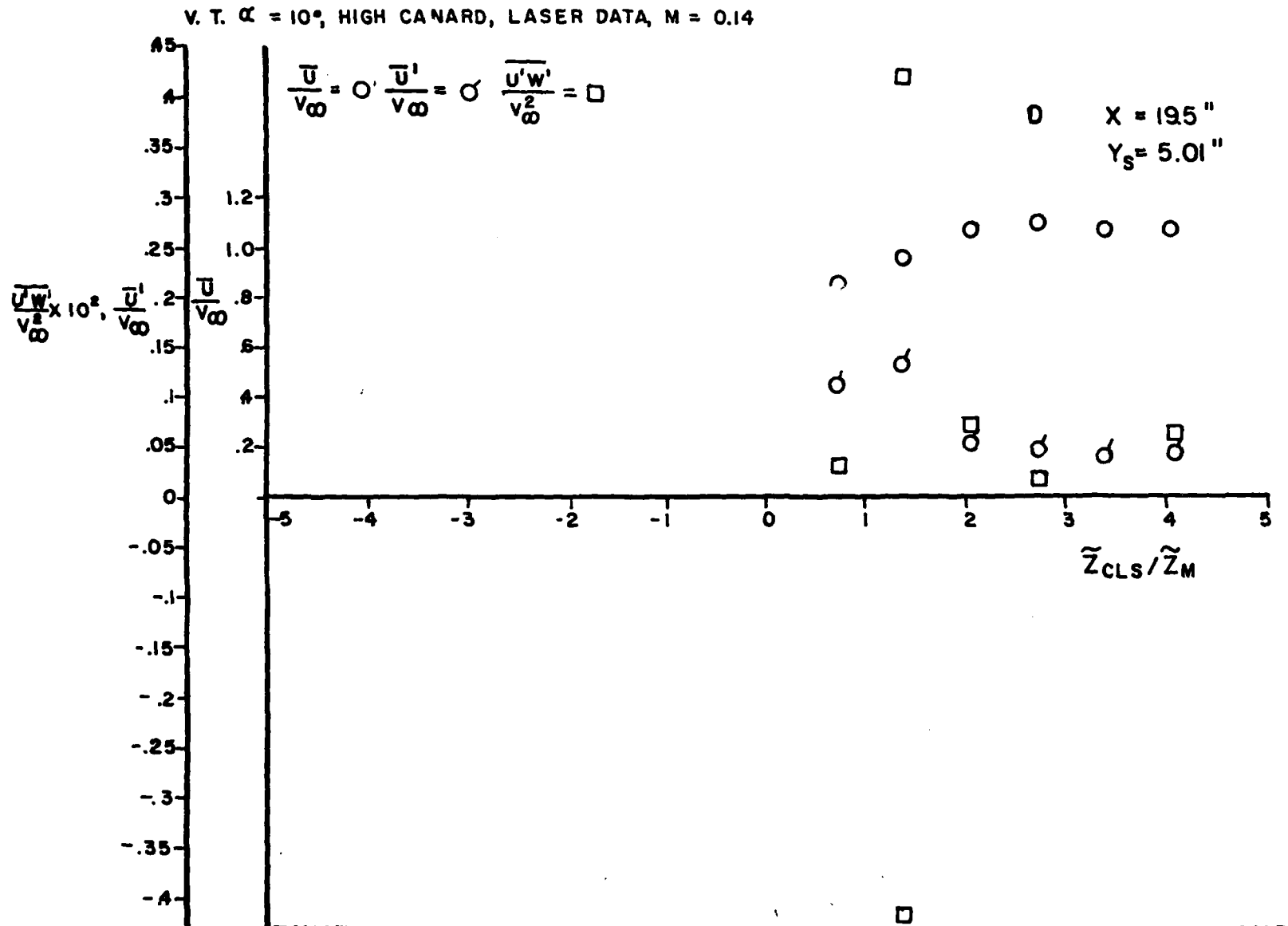

FIG. C8 LDV MEASUREMENTS OF AXIAL MEAN VELOCITY, TURBULENCE INTENSITY, AND REYNOLDS STRESSES WITH THE HIGH CANARD WITHOUT BLOWING - V. W. T. - α = 10° STATION D

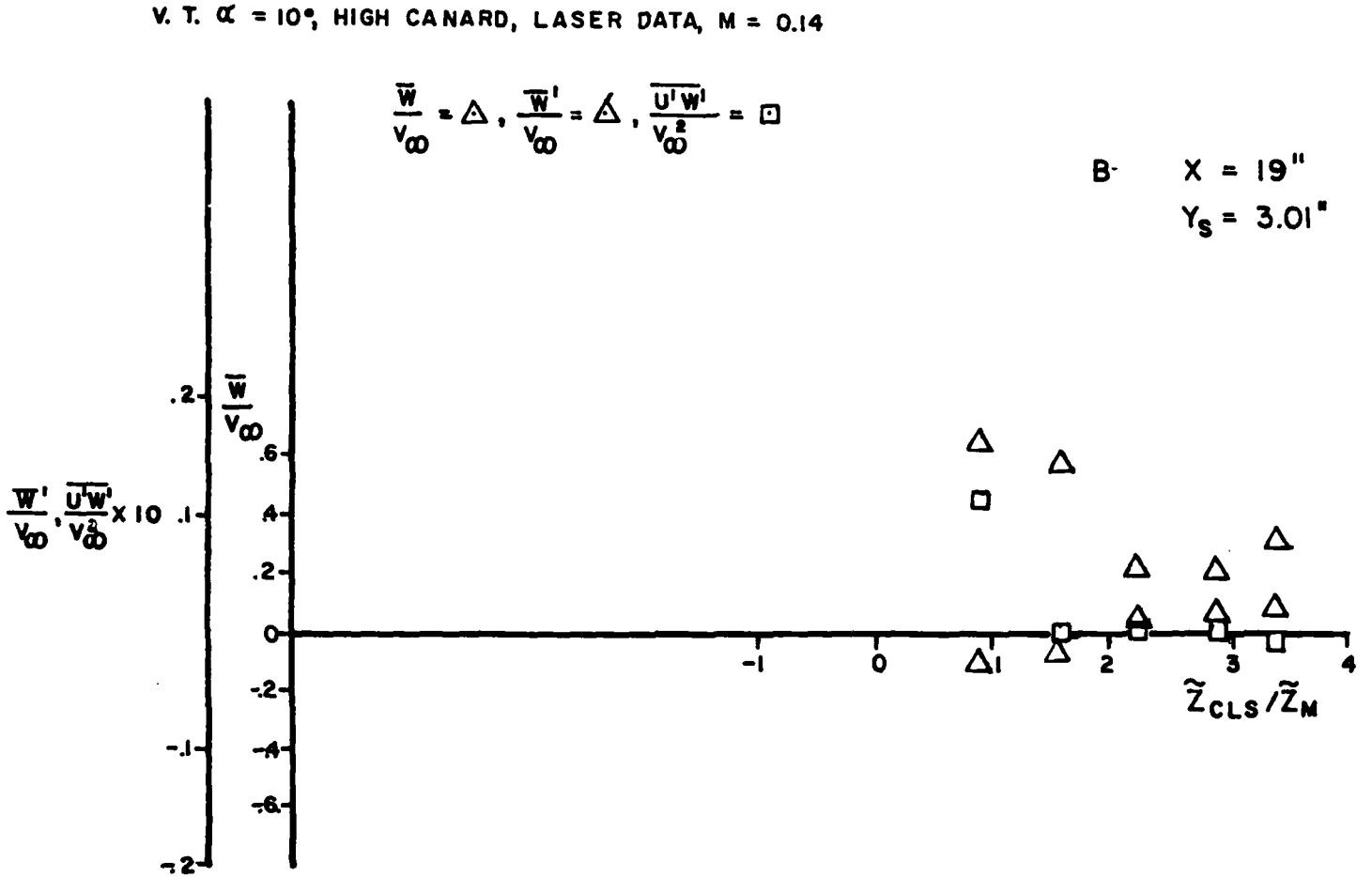

FIG. C9 LDV MEASUREMENTS OF VERTICAL MEAN VELOCITY, TURBULENCE INTENSITY, AND REYNOLDS STRESSES WITH THE HIGH CANARD WITHOUT BLOWING - V. W. T. - α = 10° STATION B

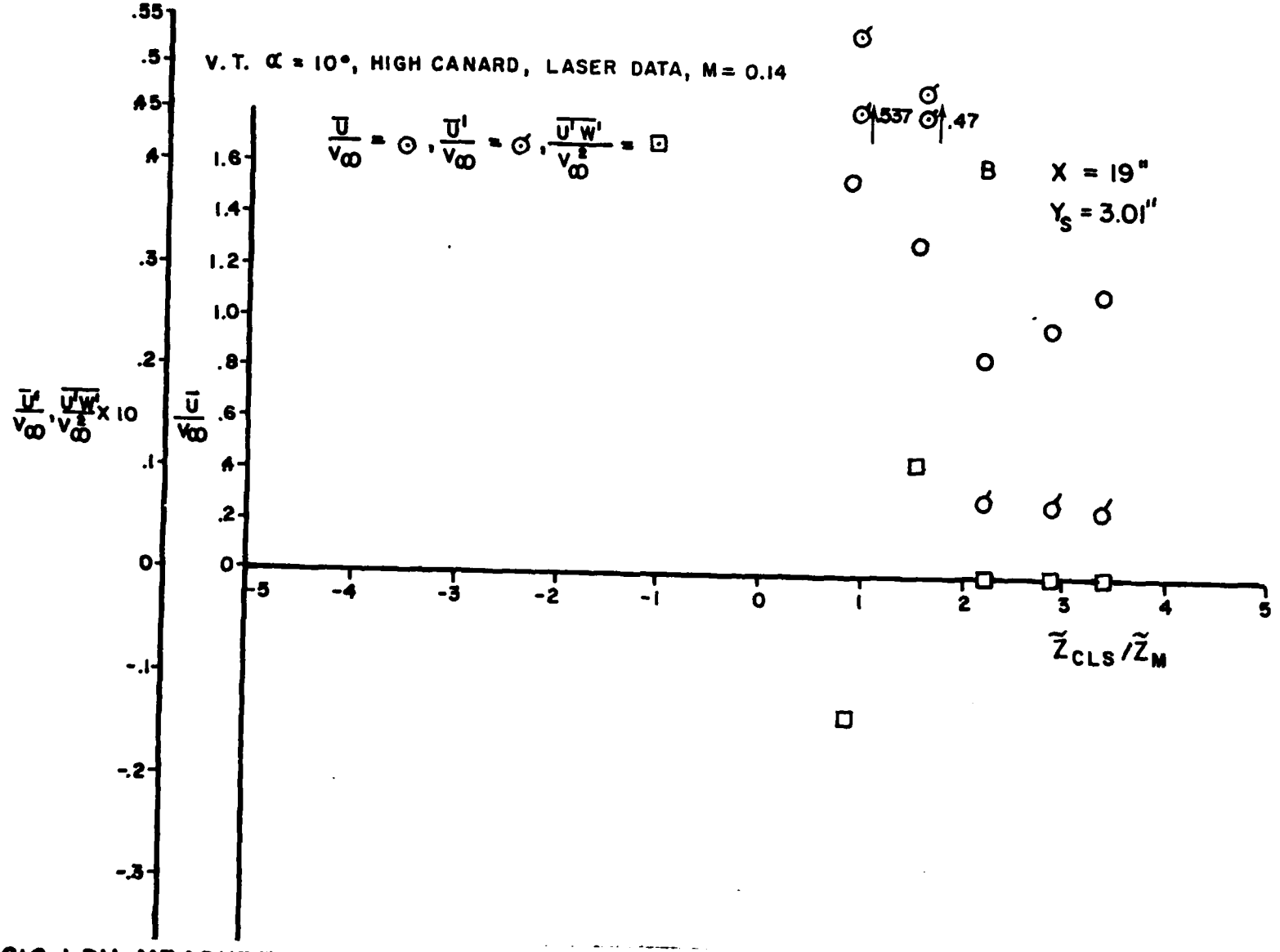

FIG. C10 LDV MEASUREMENTS OF AXIAL MEAN VELOCITY, TURBULENCE INTENSITY, AND REYNOLDS STRESSES WITH THE HIGH CANARD WITHOUT BLOWING - V. W. T. - α = 10° STATION B

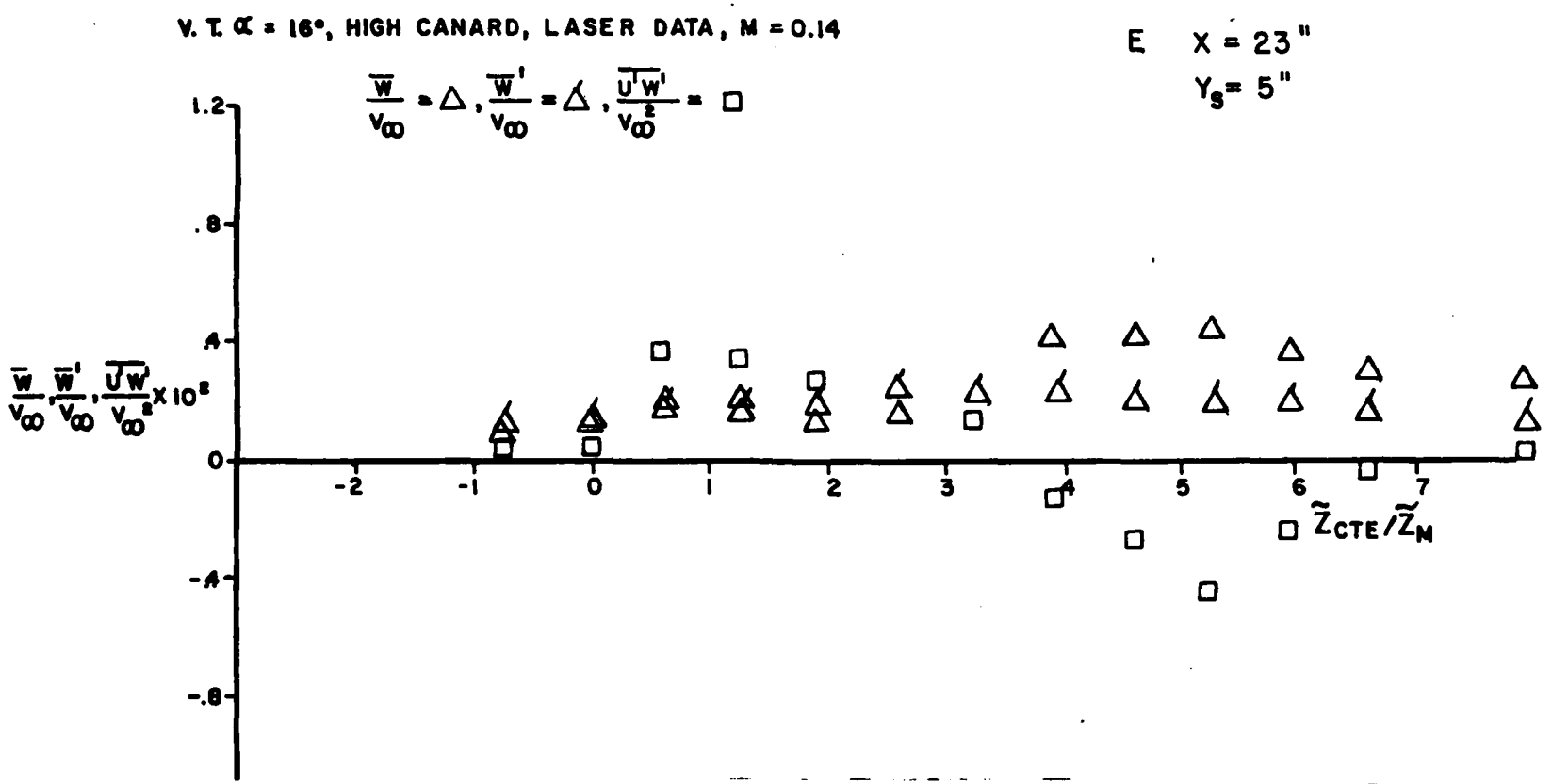

FIG. C11 LDV MEASUREMENTS OF VERTICAL MEAN VELOCITY, TURBULENCE INTENSITY, AND REYNOLDS STRESSES WITH THE HIGH CANARD WITHOUT BLOWING - V. W. T. - α = 16° STATION E

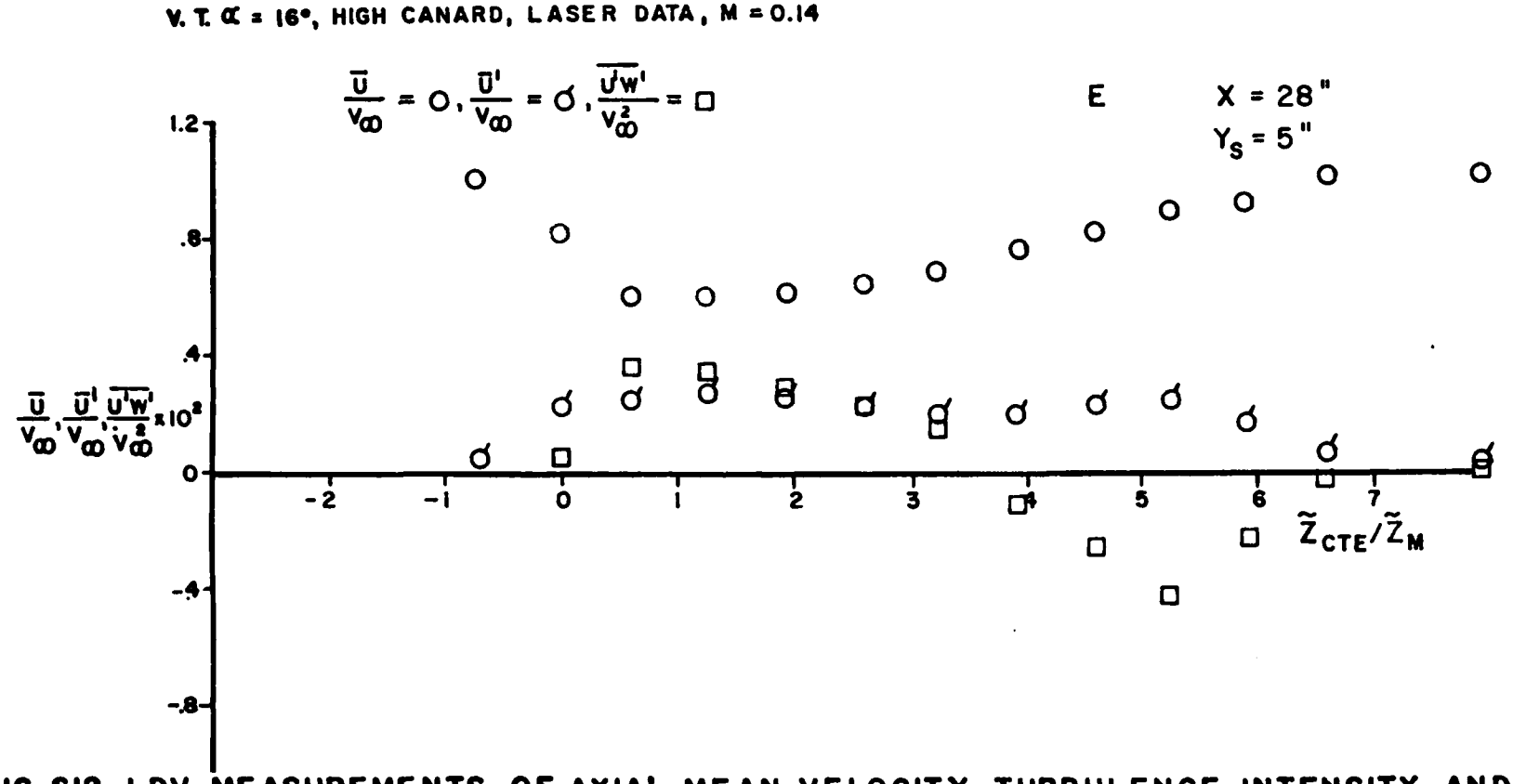

FIG. C12 LDV MEASUREMENTS OF AXIAL MEAN VELOCITY, TURBULENCE INTENSITY, AND REYNOLDS STRESSES WITH THE HIGH CANARD WITHOUT BLOWING - V. W. T. - α = 16° STATION E

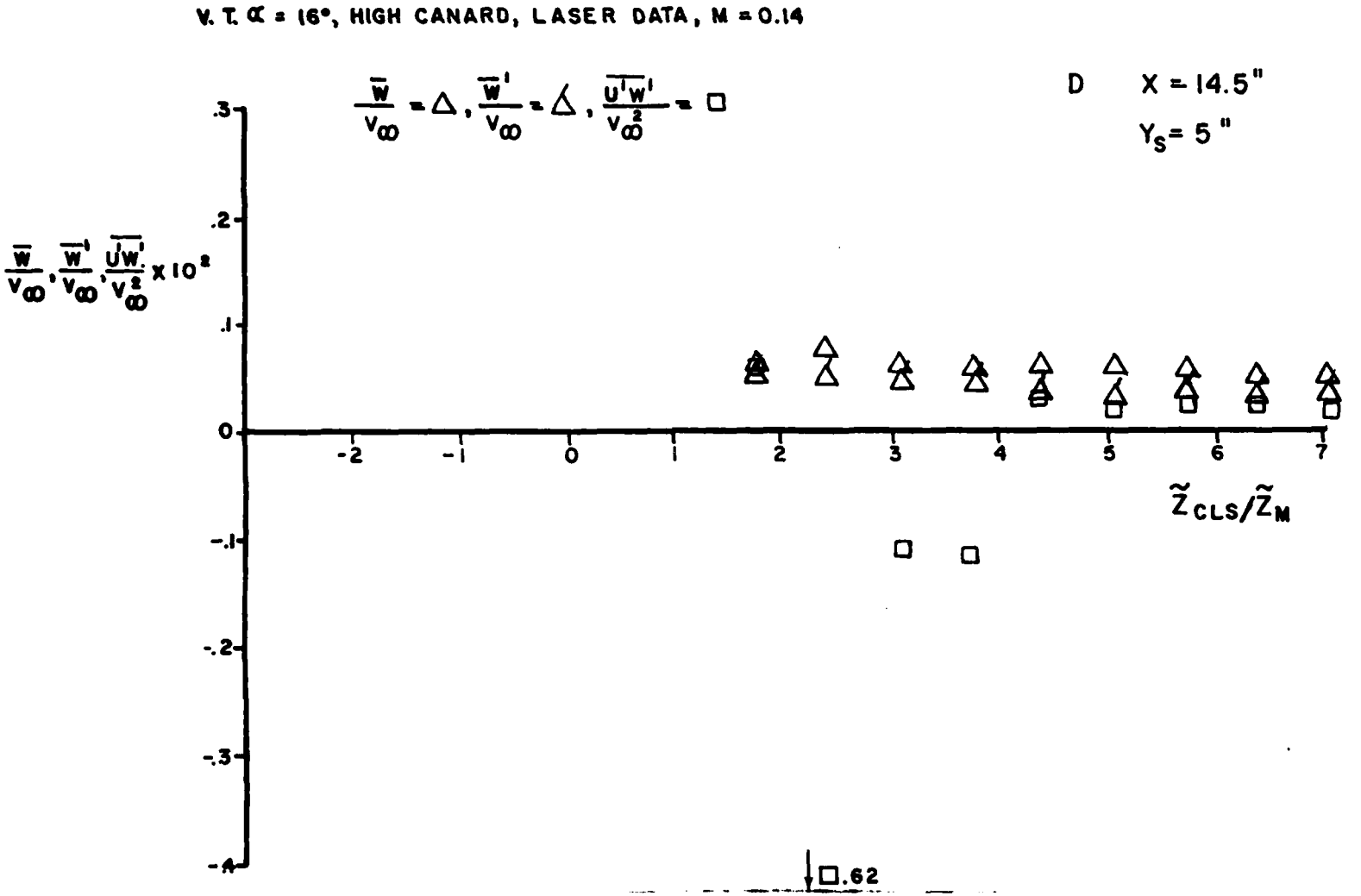

FIG. C13 LDV MEASUREMENTS OF VERTICAL MEAN VELOCITY, TURBULENCE INTENSITY, AND REYNOLDS STRESSES WITH THE HIGH CANARD WITHOUT BLOWING - V. W. T. - α = 16° STATION D

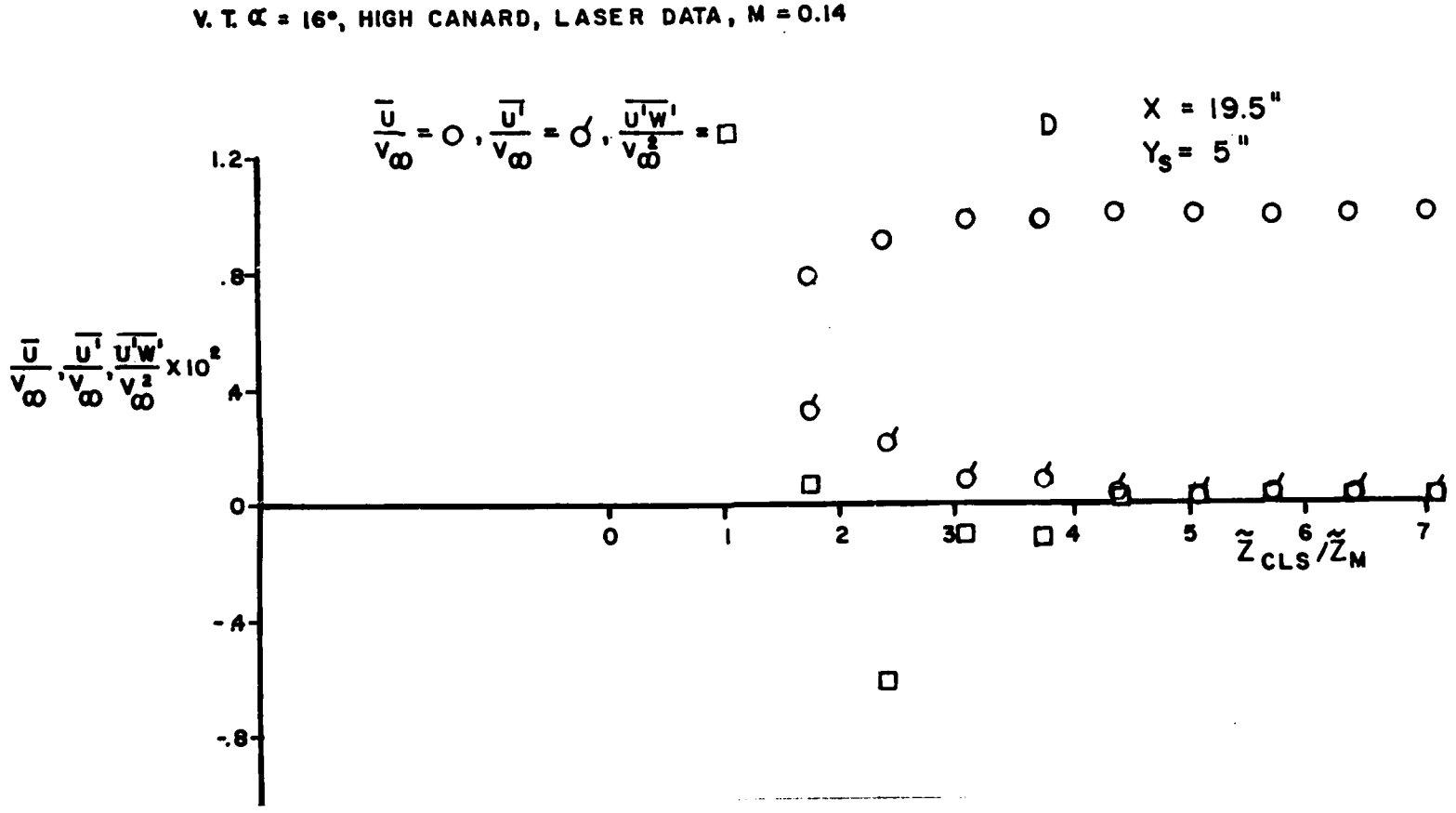

FIG. C14 LDV MEASUREMENTS OF AXIAL MEAN VELOCITY, TURBULENCE INTENSITY, AND REYNOLDS STRESSES WITH THE HIGH CANARD WITHOUT BLOWING - V. W. T. - $\alpha = 16°$ STATION D

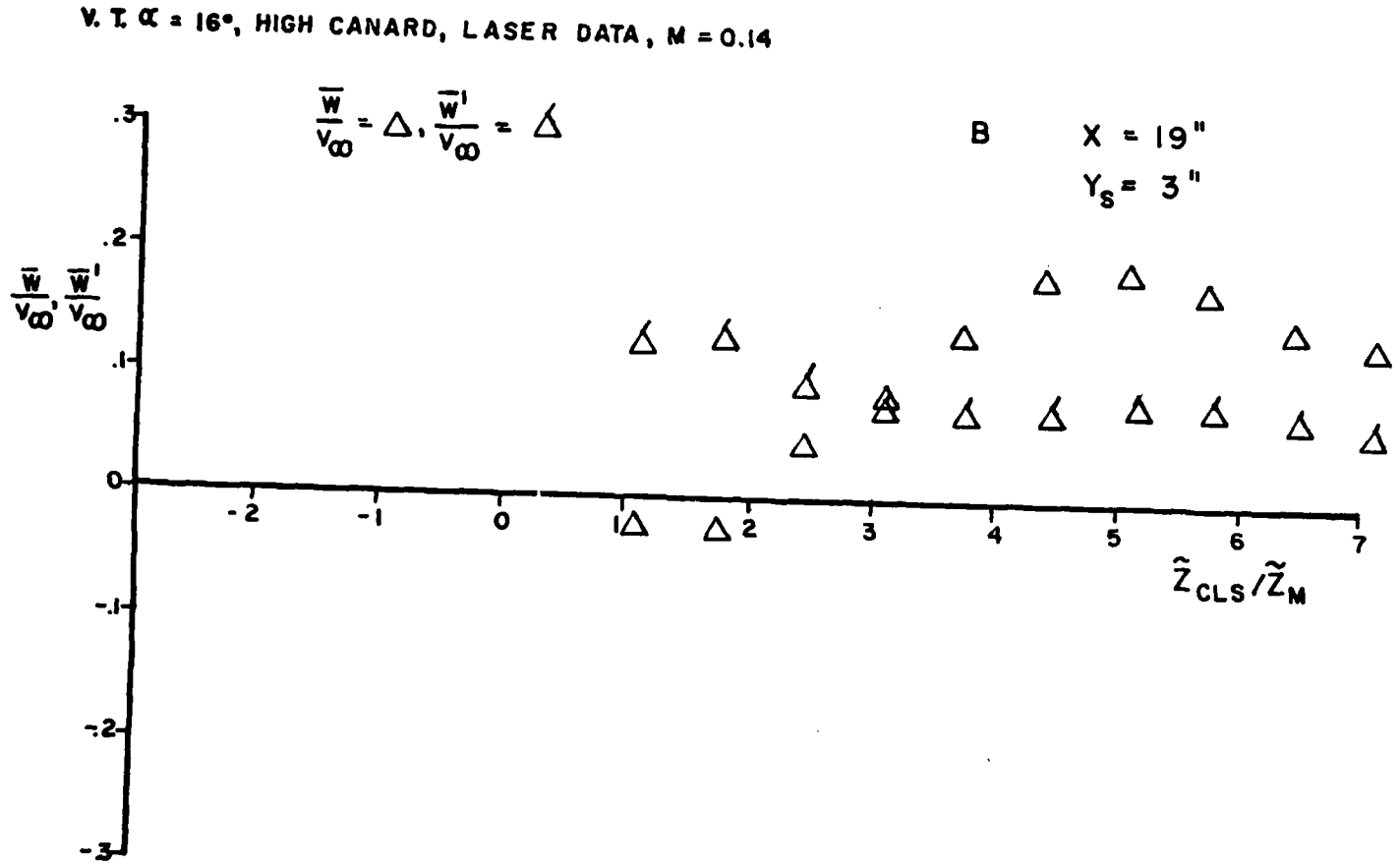

FIG. C15 LDV MEASUREMENTS OF VERTICAL MEAN VELOCITY AND TURBULENCE INTENSITY WITH THE HIGH CANARD WITHOUT BLOWING - V.W.T. - α = 16° STATION B

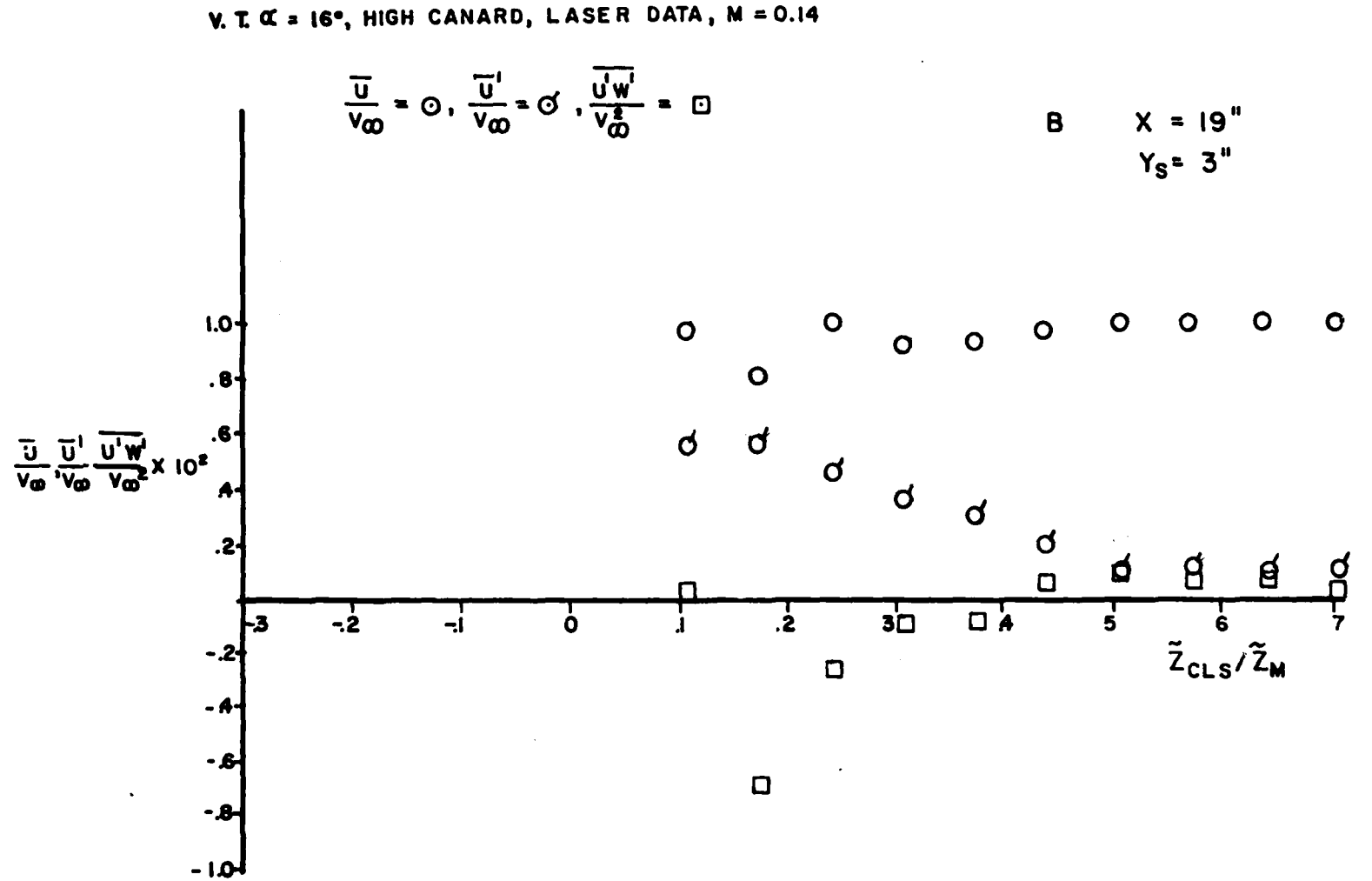

FIG. C16 LDV MEASUREMENTS OF AXIAL MEAN VELOCITY, TURBULENCE INTENSITY, AND REYNOLDS STRESSES WITH THE HIGH CANARD WITHOUT BLOWING - V. W. T. - $\alpha = 16°$ STATION B

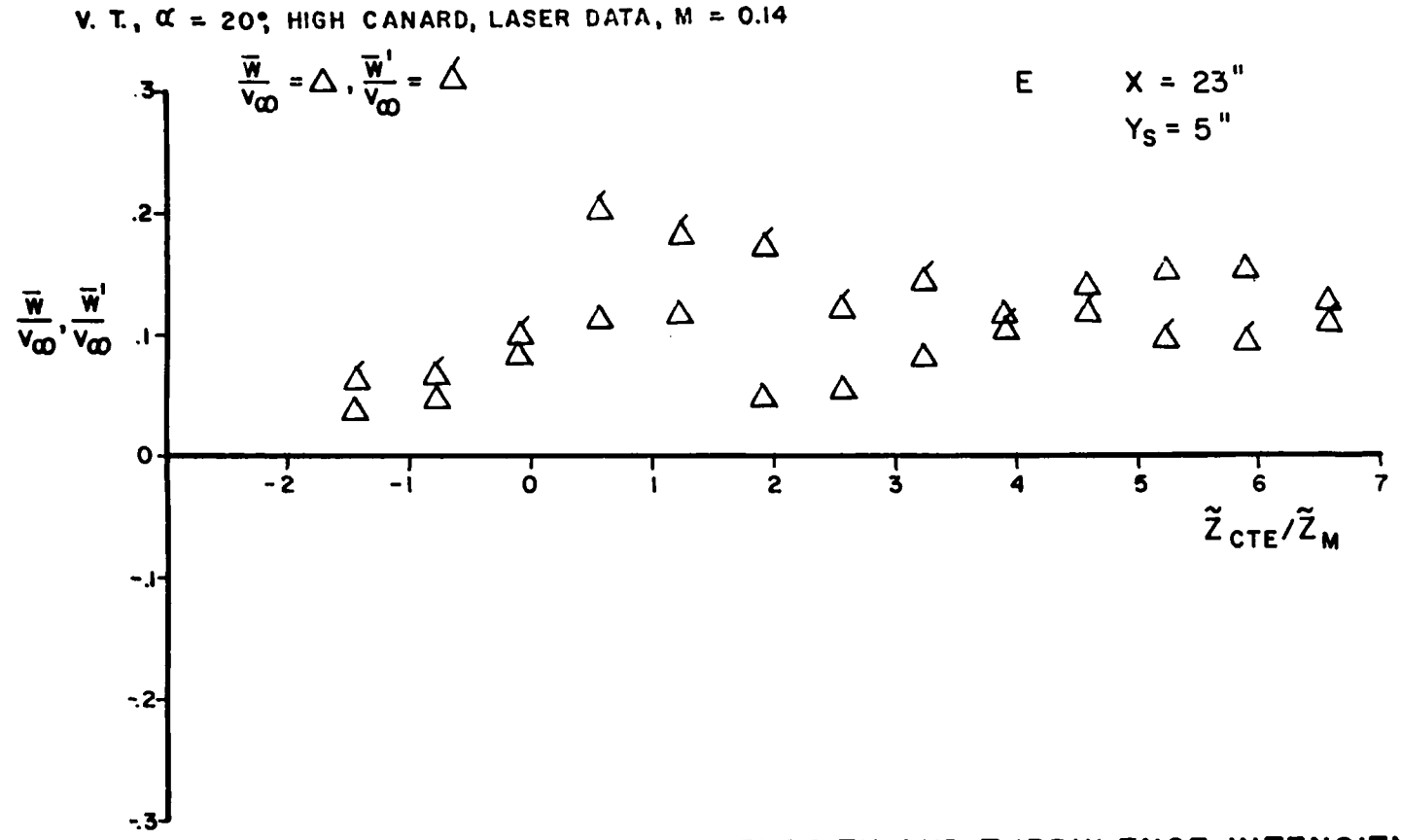

FIG. C17 LDV MEASUREMENTS OF VERTICAL MEAN VELOCITY AND TURBULENCE INTENSITY WITH THE HIGH CANARD WITHOUT BLOWING - V.W.T. - $\alpha = 20^\circ$ - STATION E

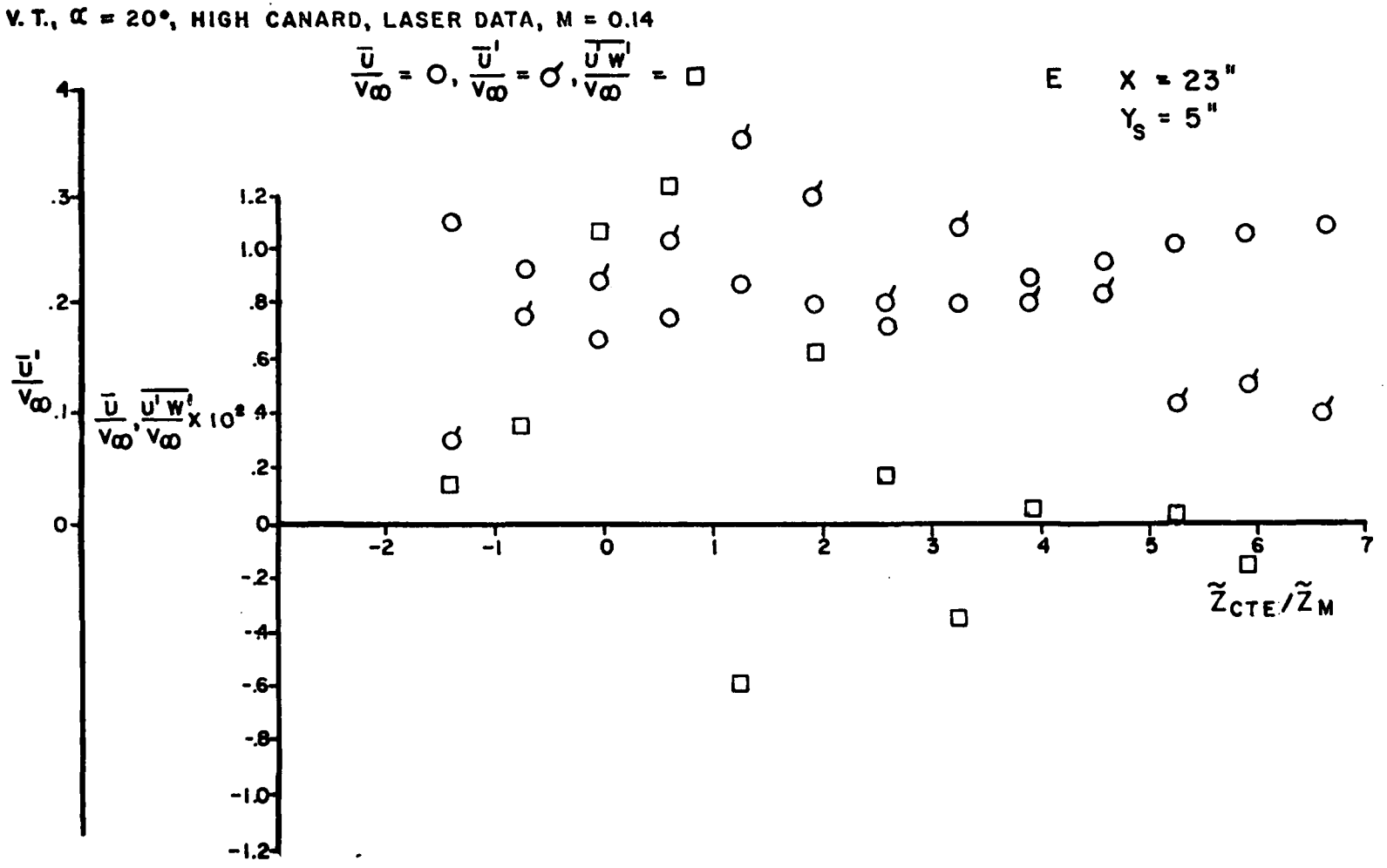

FIG. C18 LDV MEASUREMENTS OF AXIAL MEAN VELOCITY, TURBULENCE INTENSITY, AND REYNOLDS STRESSES WITH THE HIGH CANARD WITHOUT BLOWING - V. W. T. - α = 20° STATION E

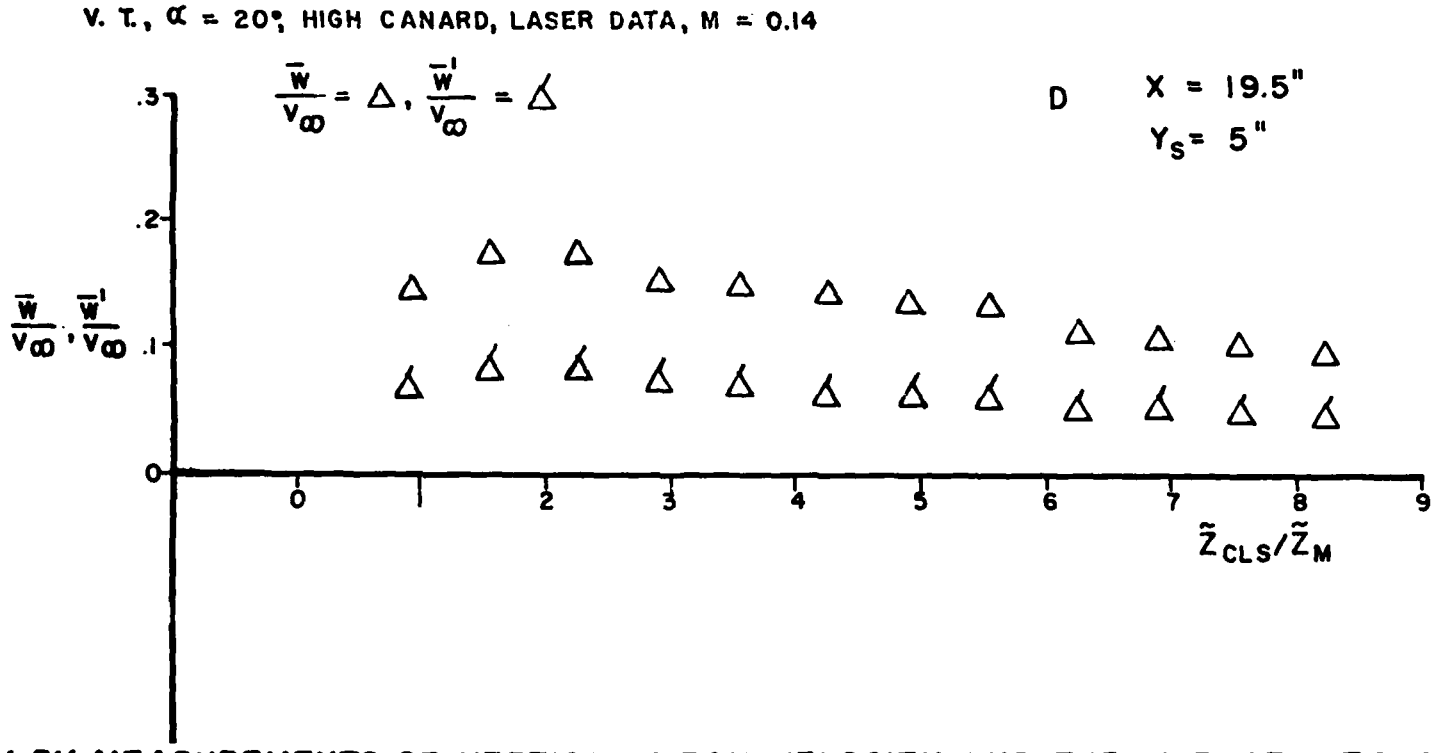

FIG. C19 LDV MEASUREMENTS OF VERTICAL MEAN VELOCITY AND TURBULENCE INTENSITY, WITH THE HIGH CANARD WITHOUT BLOWING - V. W. T. - α = 20° - STATION D

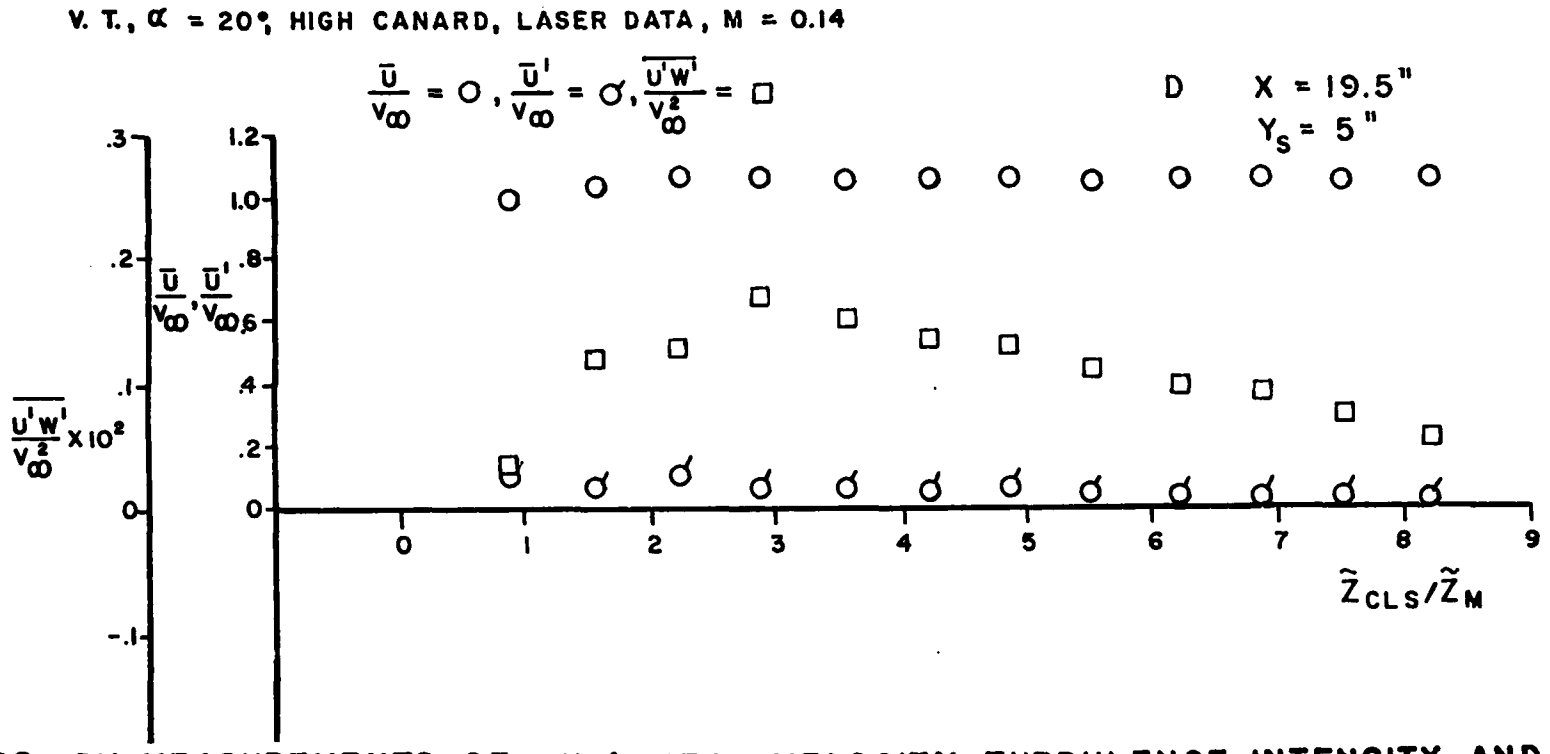

FIG. C20 LDV MEASUREMENTS OF AXIAL MEAN VELOCITY, TURBULENCE INTENSITY, AND REYNOLDS STRESSES WITH THE HIGH CANARD WITHOUT BLOWING - V. W. T. - α = 20° STATION D

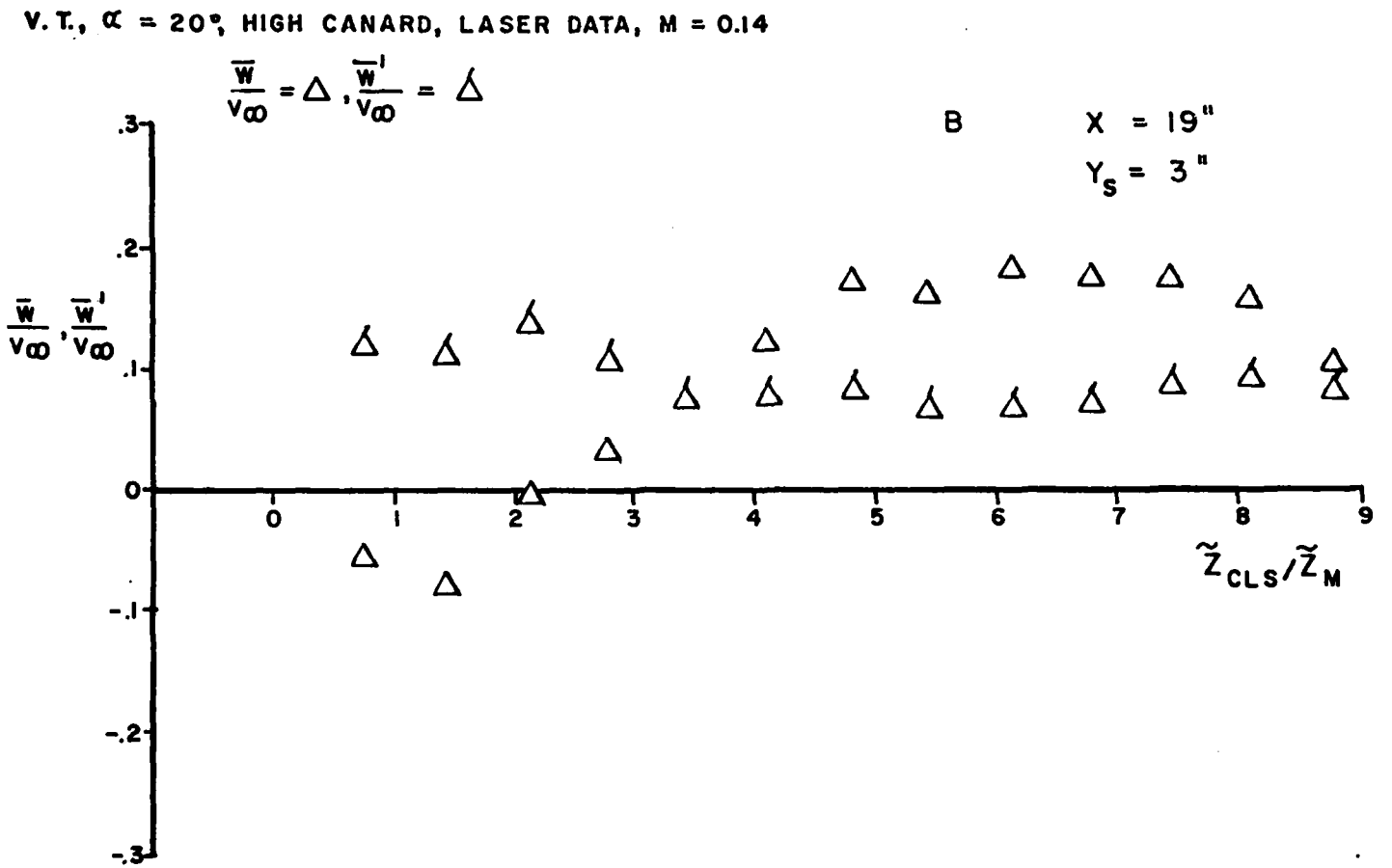

FIG. C21 LDV MEASUREMENTS OF VERTICAL MEAN VELOCITY AND TURBULENCE INTENSITY, WITH THE HIGH CANARD WITHOUT BLOWING - V. W. T. - α = 20° - STATION B

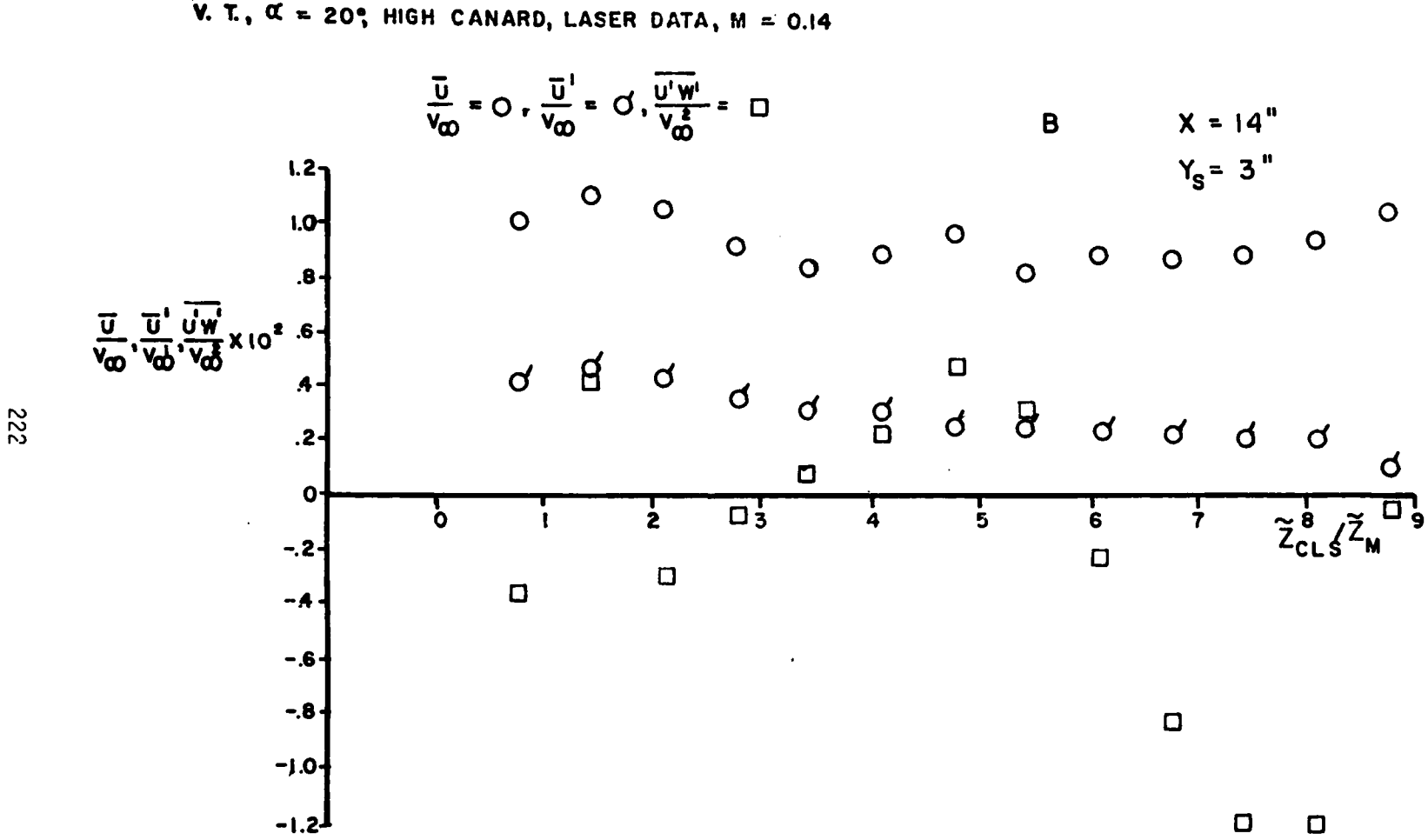

FIG. C22 LDV MEASUREMENTS OF AXIAL MEAN VELOCITY, TURBULENCE INTENSITY, AND REYNOLDS STRESSES WITH THE HIGH CANARD WITHOUT BLOWING - V. W. T. - α = 20° STATION B

APPENDIX D

The figures D1 to D27 compare data obtained in the TGF tunnel with the mid canard and without canard for different configurations at different stations.

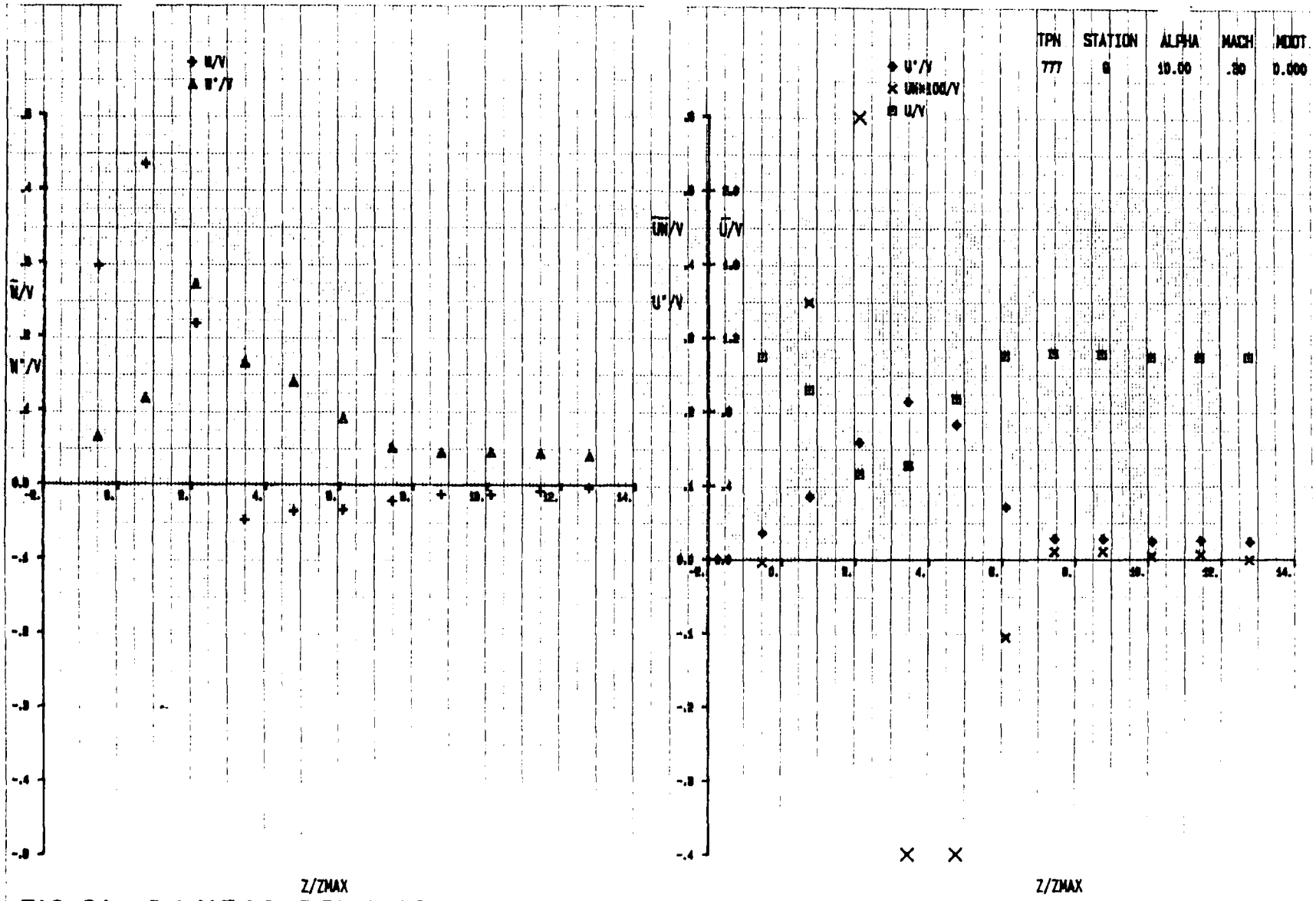

FIG. D1 LDV MEASUREMENTS OF MEAN VELOCITIES, TURBULENCE INTENSITIES, AND REYNOLDS STRESSES WITHOUT BLOWING - NO CANARD - TGF - $\alpha = 10°$ - STATION Q

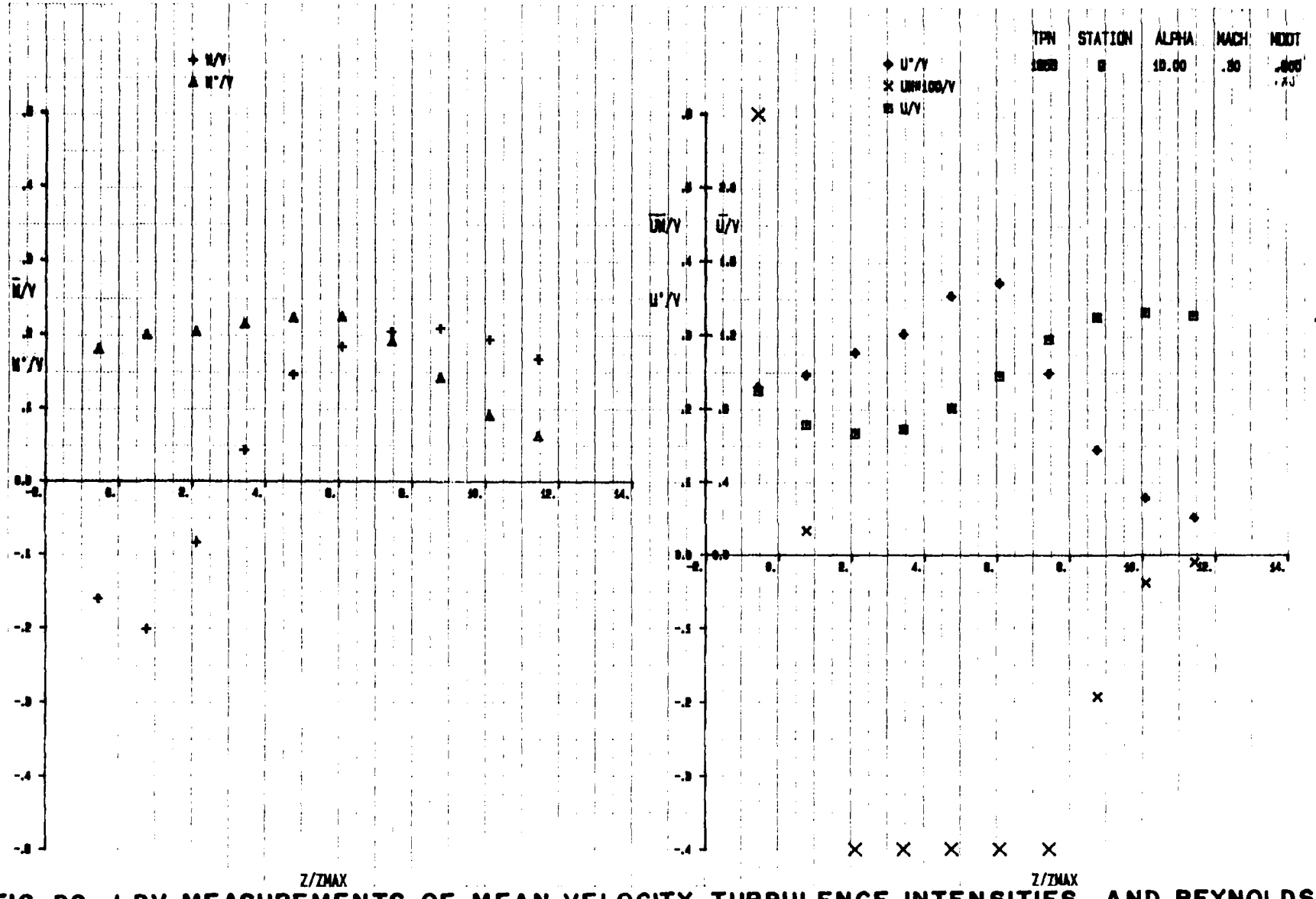

FIG. D2 LDV MEASUREMENTS OF MEAN VELOCITY, TURBULENCE INTENSITIES, AND REYNOLDS STRESSES WITH BLOWING - NO CANARD - TGF - $\alpha = 10°$ - STATION Q

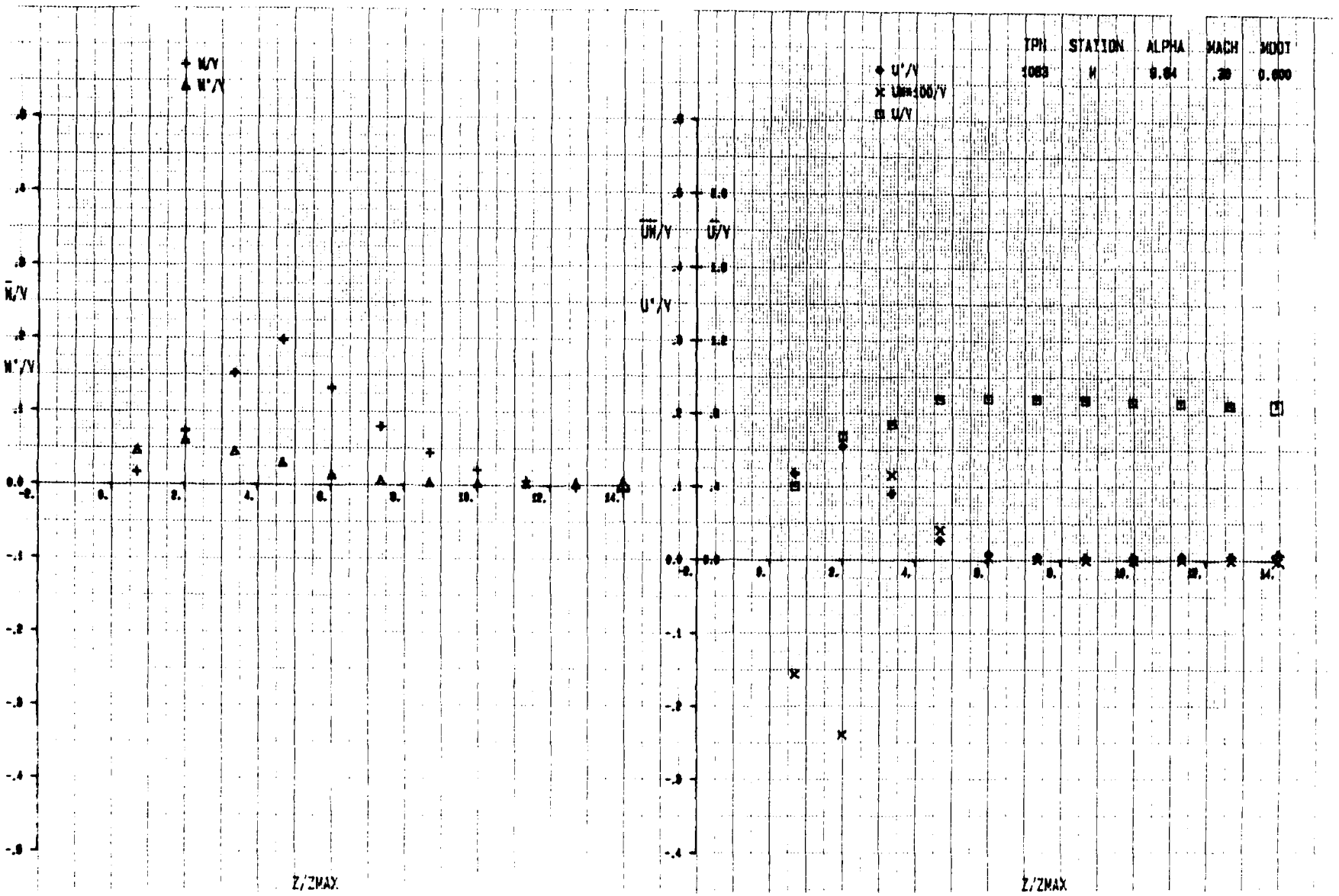

FIG. D3 HOT WIRE MEASUREMENT OF MEAN VELOCITIES, TURBULENCE INTENSITIES, AND REYNOLDS STRESSES WITHOUT BLOWING - NO CANARD - TGF - $\alpha = 10°$ STATION M

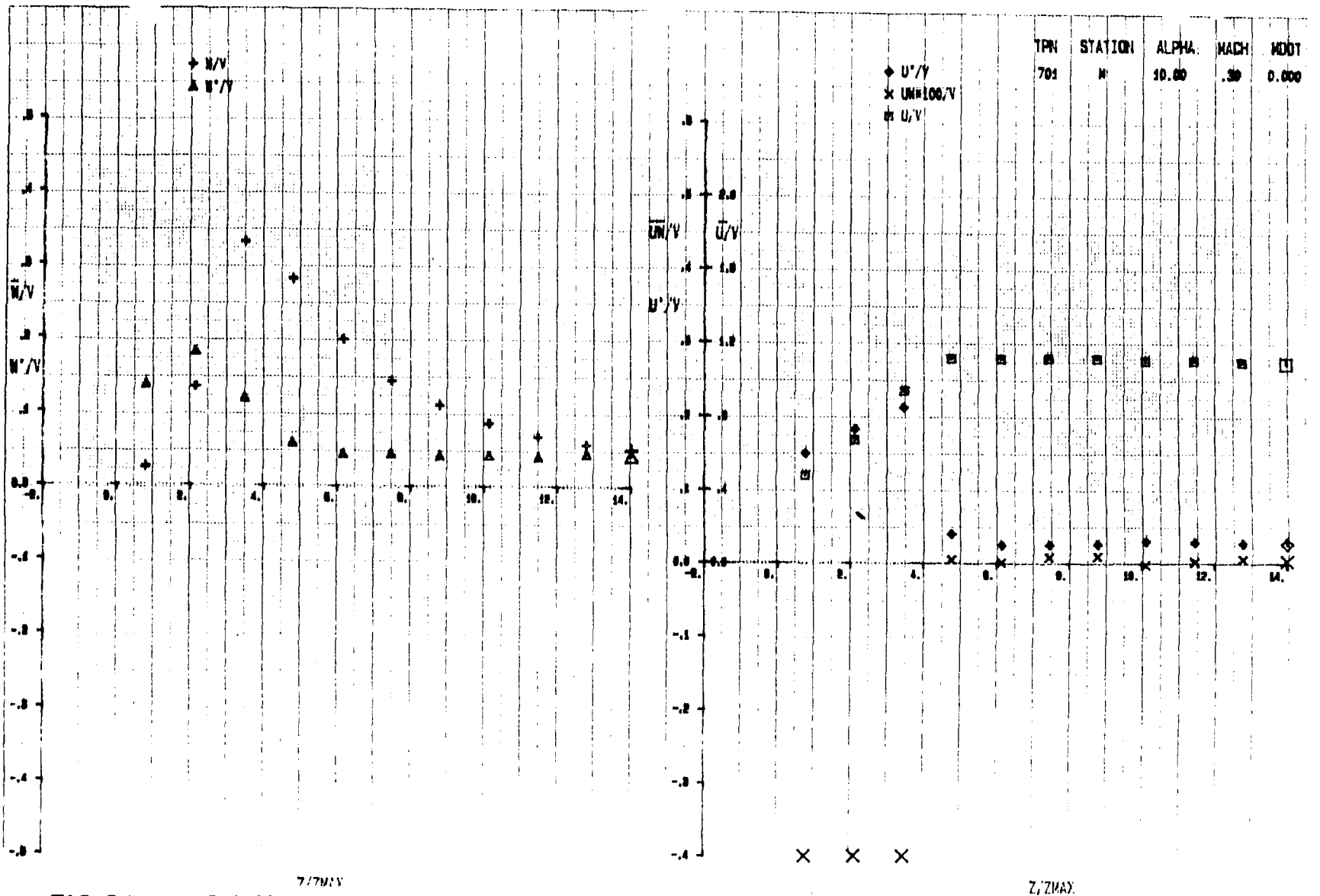

FIG. D4 LDV MEASUREMENTS OF MEAN VELOCITIES, TURBULENCE INTENSITIES, AND REYNOLDS STRESSES WITHOUT BLOWING - NO CANARD - TGF - $\alpha = 10°$ STATION M

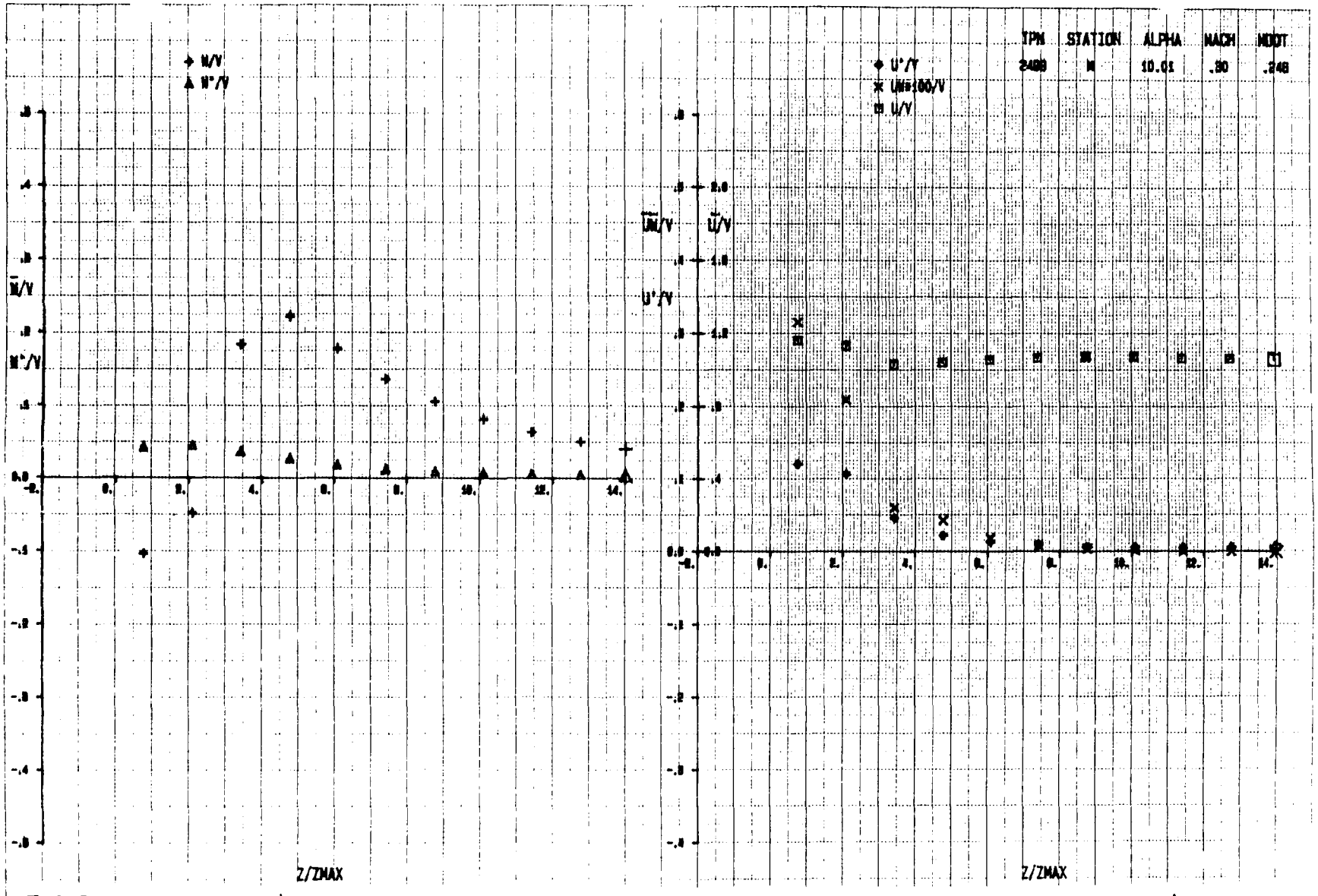

FIG.D5 HOT WIRE MEASUREMENT OF MEAN VELOCITIES, TURBULENCE INTENSITIES, AND REYNOLDS STRESSES WITH BLOWING - NO CANARD - TGF - $\alpha = 10°$ STATION M

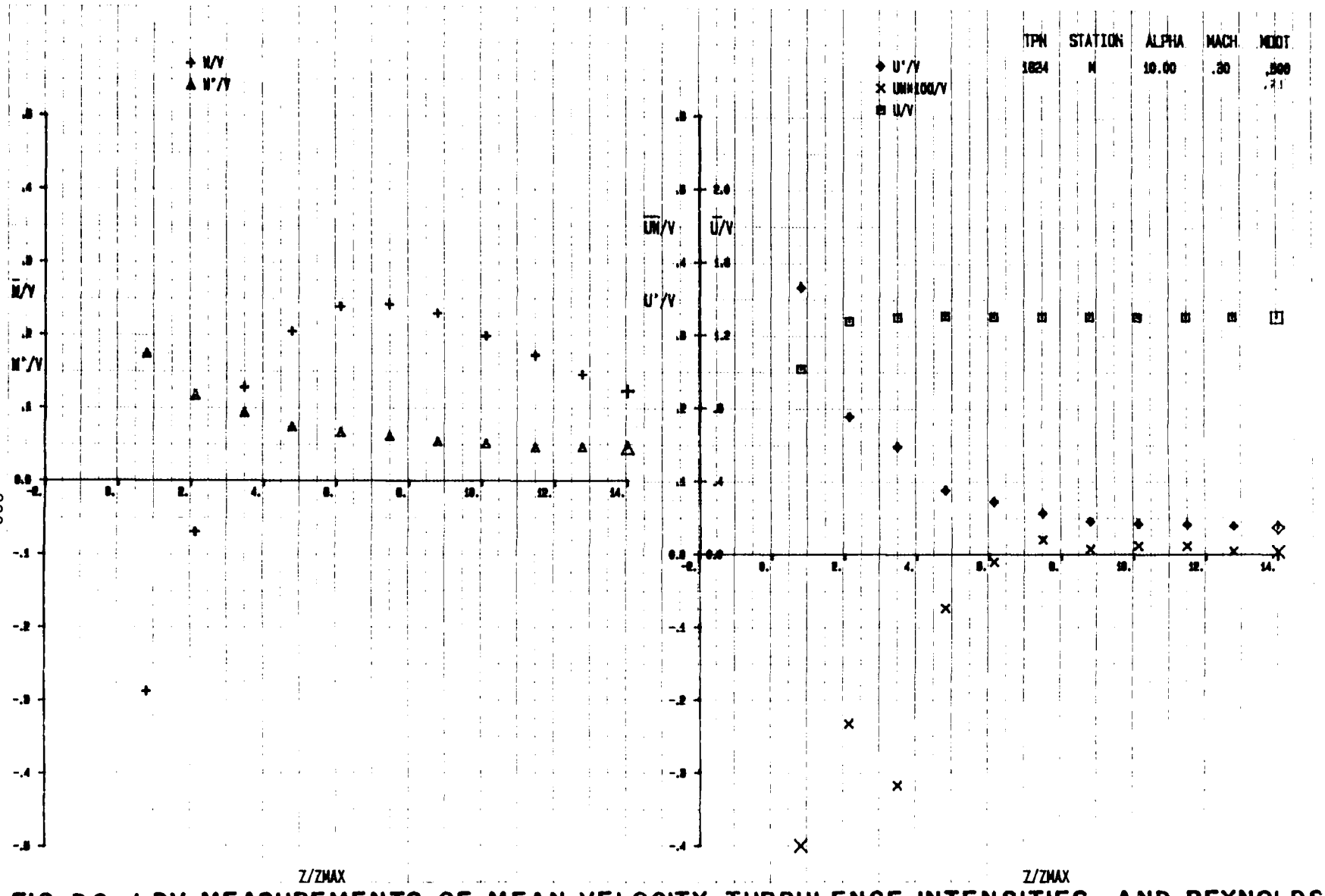

FIG. D6 LDV MEASUREMENTS OF MEAN VELOCITY, TURBULENCE INTENSITIES, AND REYNOLDS STRESSES WITH BLOWING - NO CANARD - TGF - α = 10° - STATION M

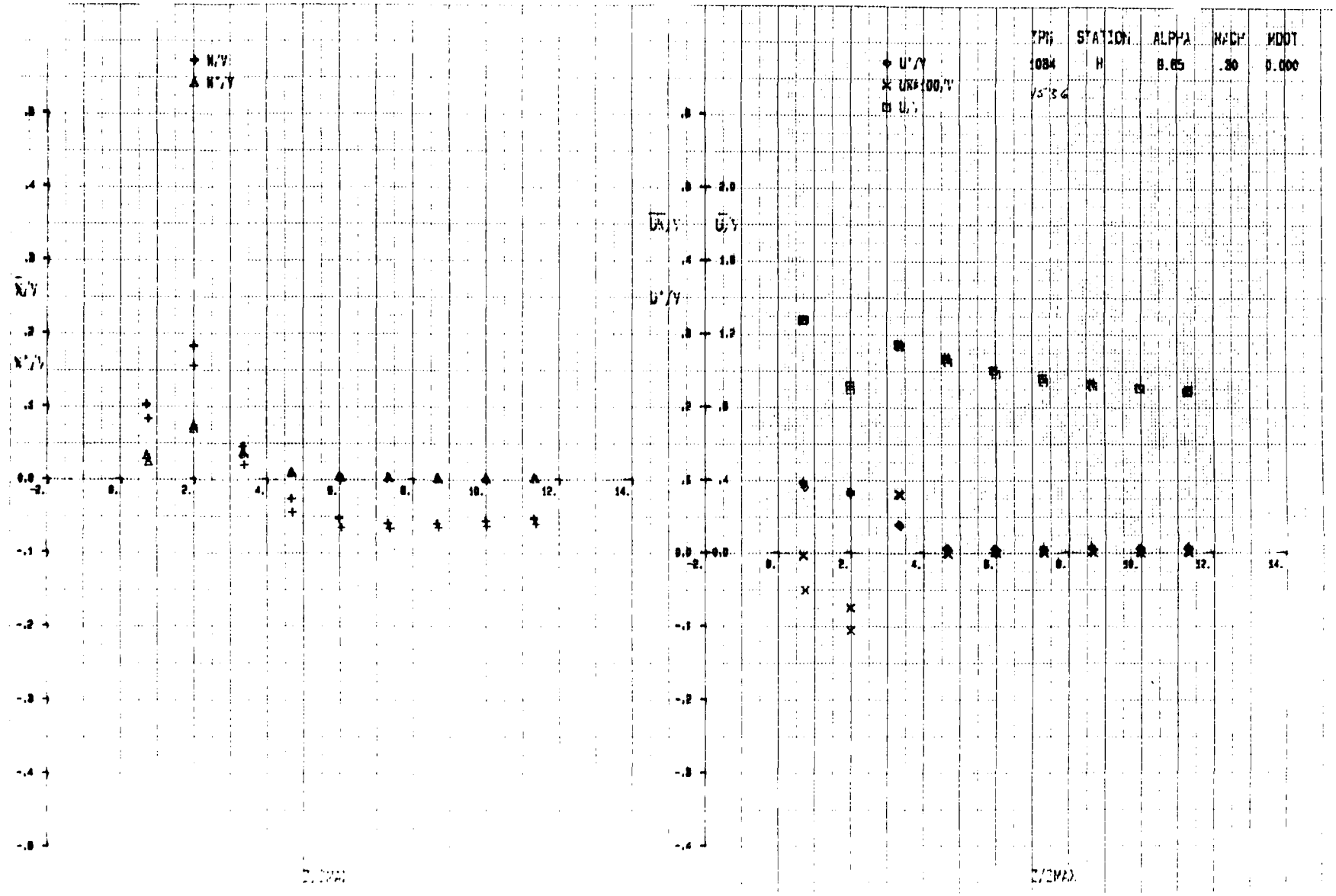

FIG D7 REPEATED HOT WIRE MEASUREMENTS OF MEAN VELOCITIES, TURBULENCE INTENSITIES AND REYNOLDS STRESSES WITHOUT BLOWING- NO CANARD -TGF - α = 10° STATION H

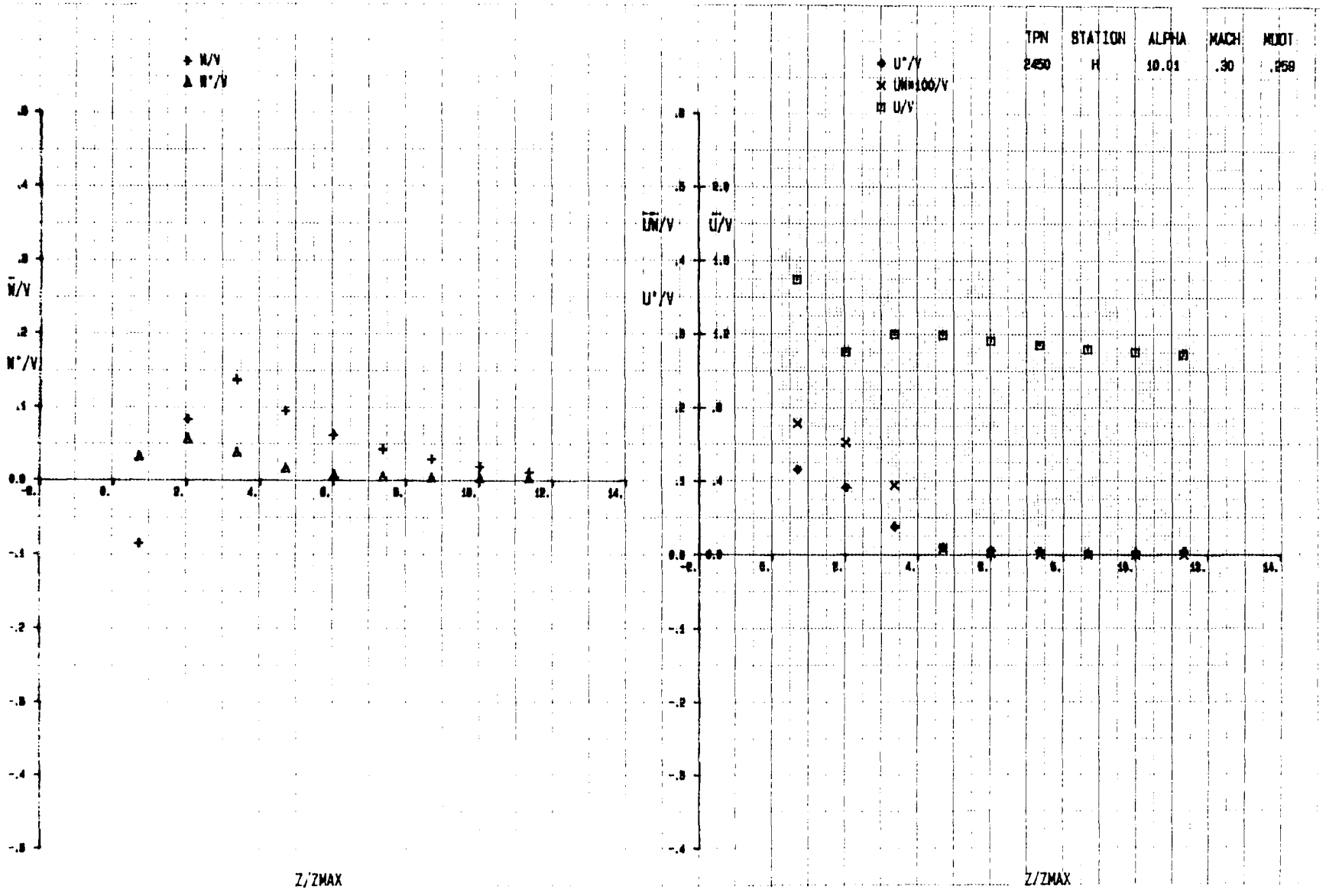

FIG. D8 HOT WIRE MEASUREMENT OF MEAN VELOCITIES, TURBULENCE INTENSITIES, AND REYNOLDS STRESSES WITH BLOWING - NO CANARD - TGF - $\alpha = 10°$ STATION H

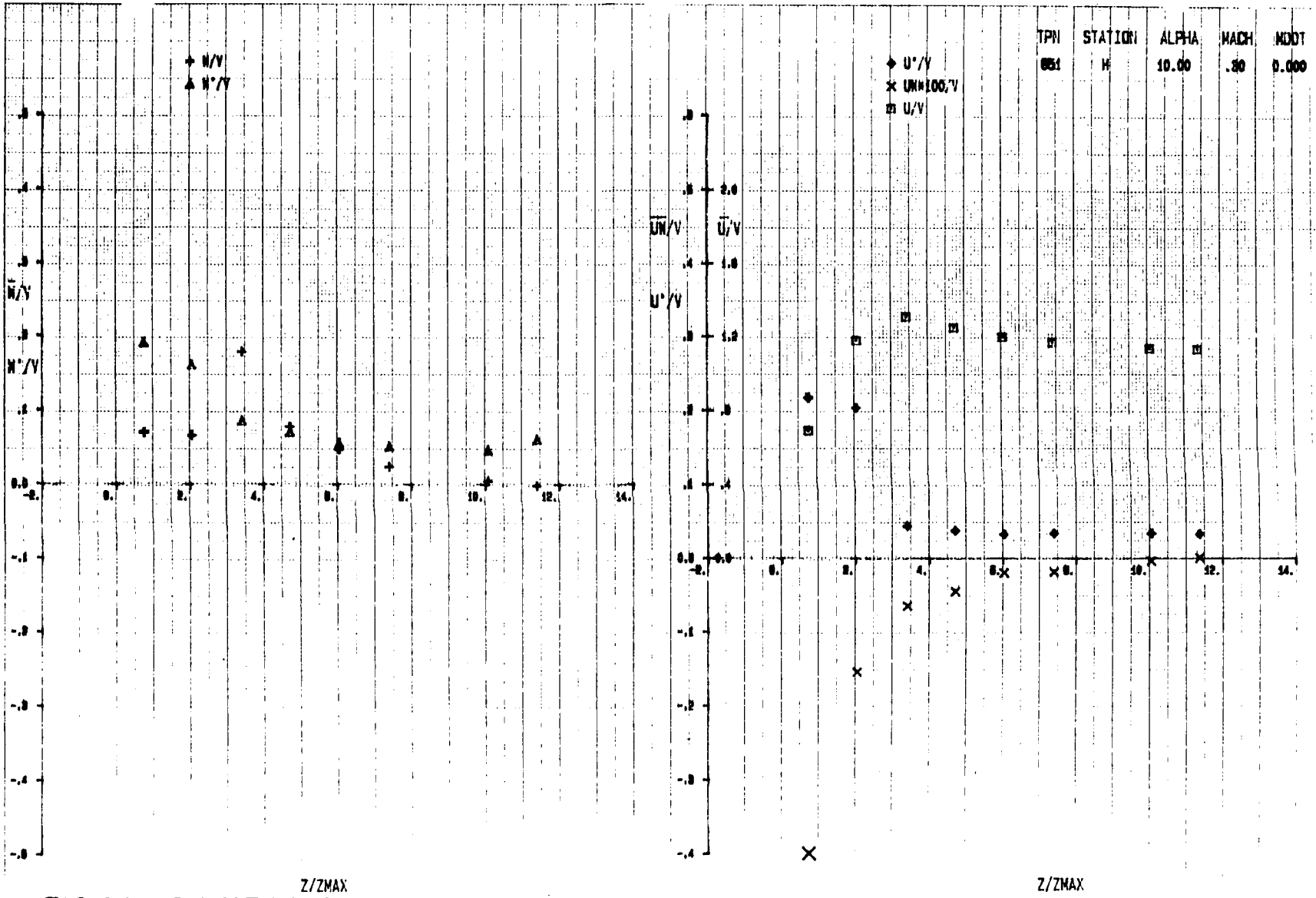

FIG. D9 LDV MEASUREMENTS OF MEAN VELOCITIES, TURBULENCE INTENSITIES, AND REYNOLDS STRESSES WITHOUT BLOWING - NO CANARD - TGF - $\alpha = 10°$ - STATION H

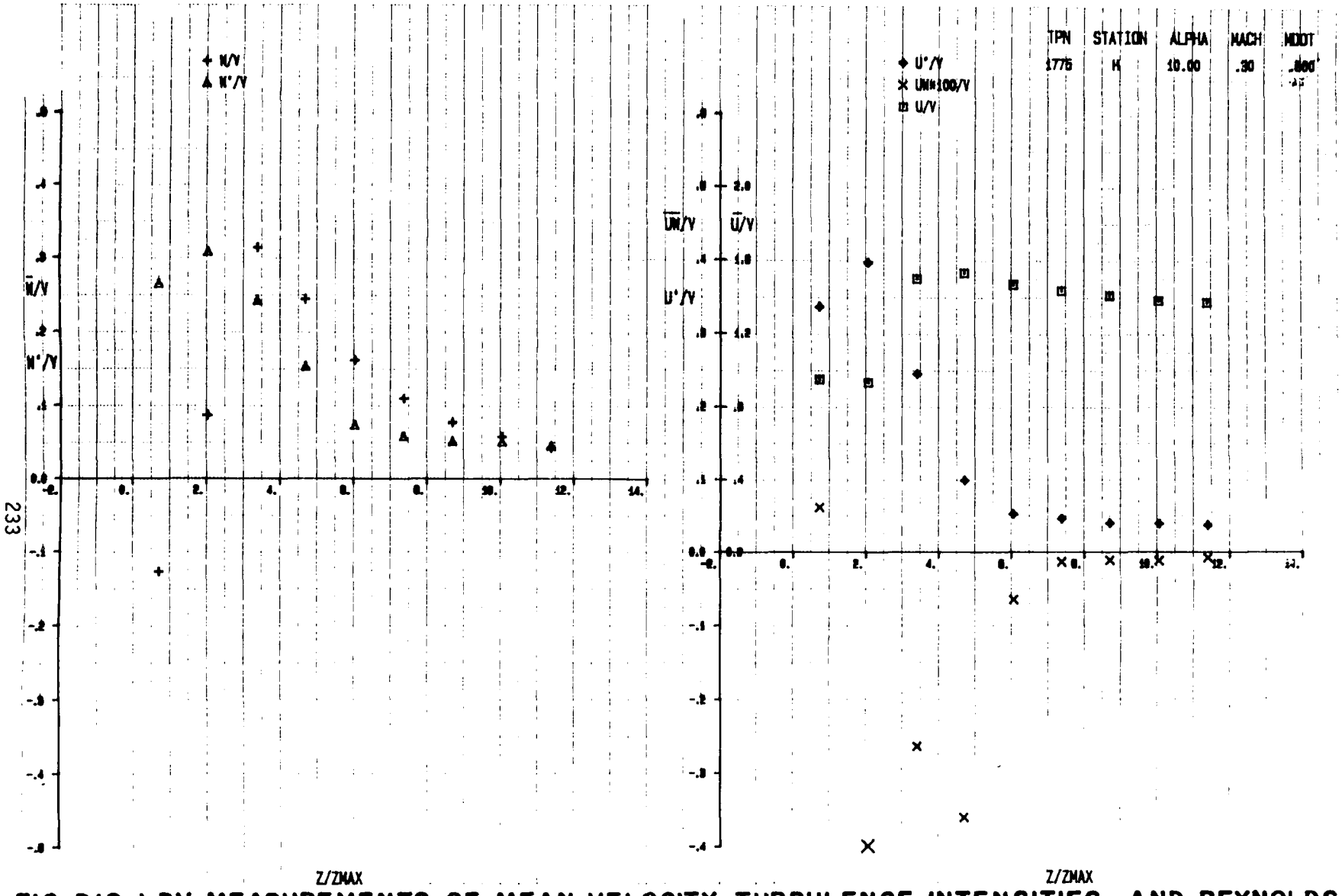

FIG. D10 LDV MEASUREMENTS OF MEAN VELOCITY, TURBULENCE INTENSITIES, AND REYNOLDS STRESSES WITH BLOWING - NO CANARD - TGF - $\alpha = 10°$ - STATION H

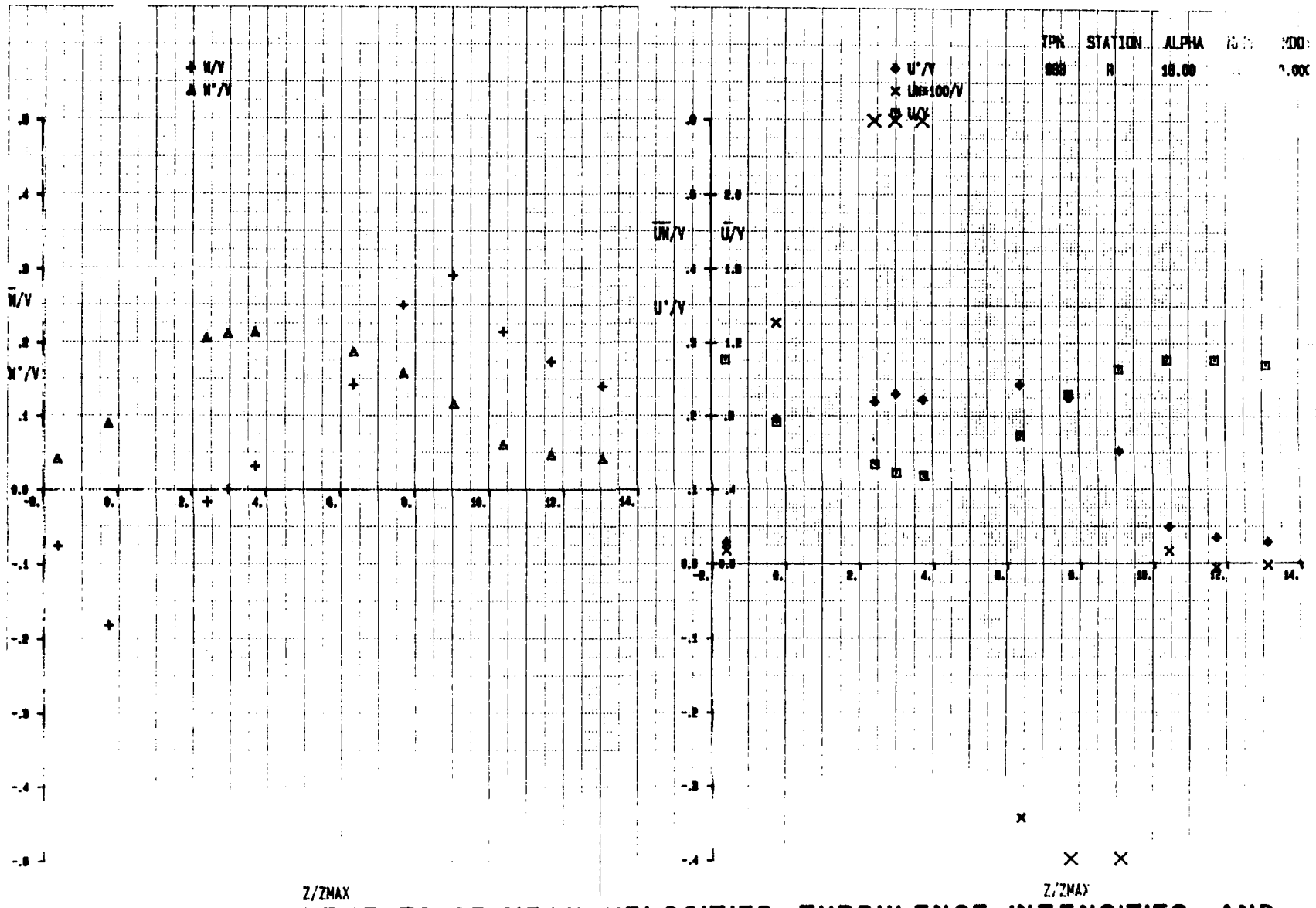

FIG. DII LDV MEASUREMENTS OF MEAN VELOCITIES, TURBULENCE INTENSITIES, AND REYNOLDS STRESSES WITHOUT BLOWING - NO CANARD - TGF - $\alpha = 16°$ - STATION R

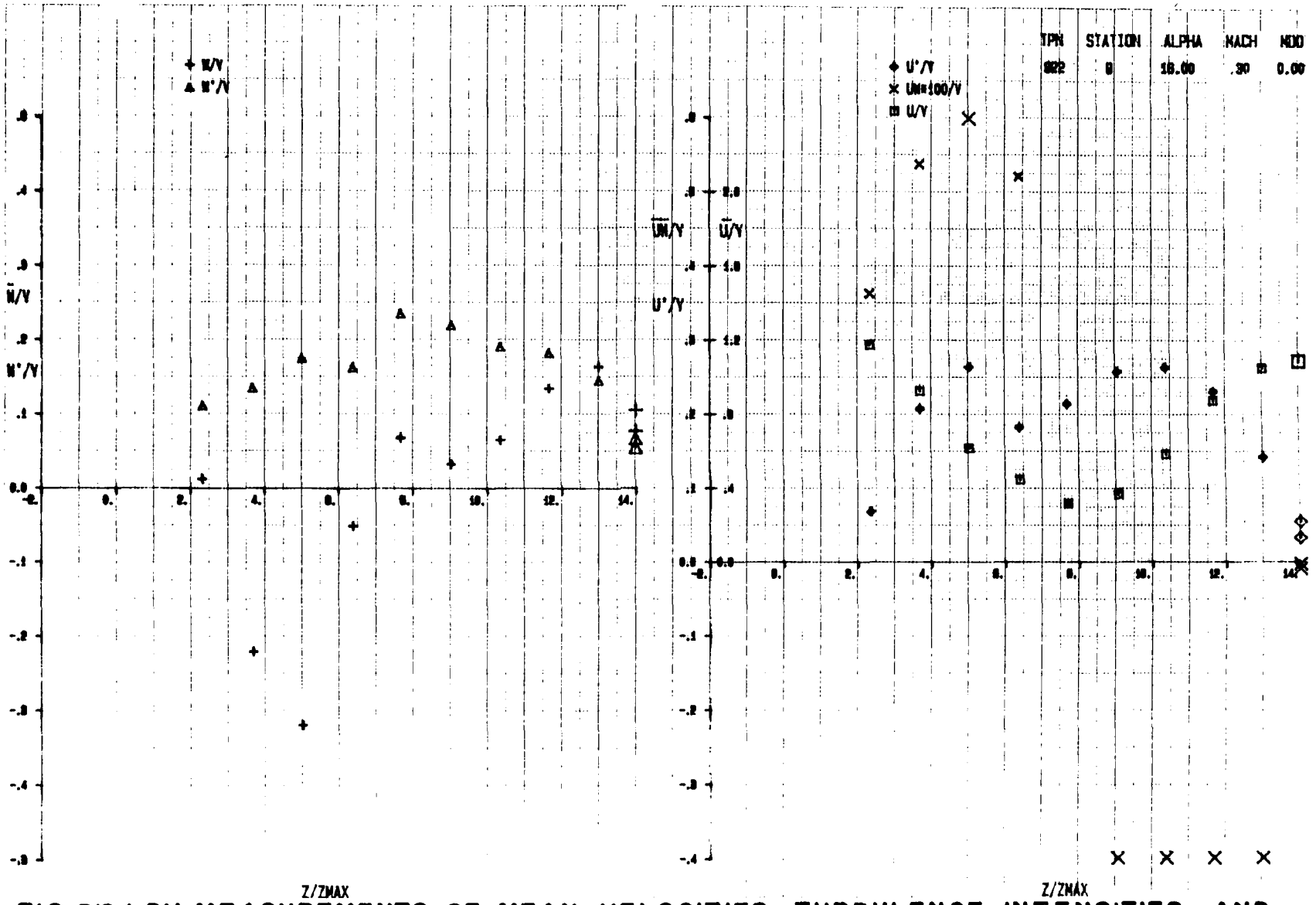

FIG. D12 LDV MEASUREMENTS OF MEAN VELOCITIES, TURBULENCE INTENSITIES, AND REYNOLDS STRESSES WITHOUT BLOWING - NO CANARD - TGF - $\alpha = 16°$ - STATION Q

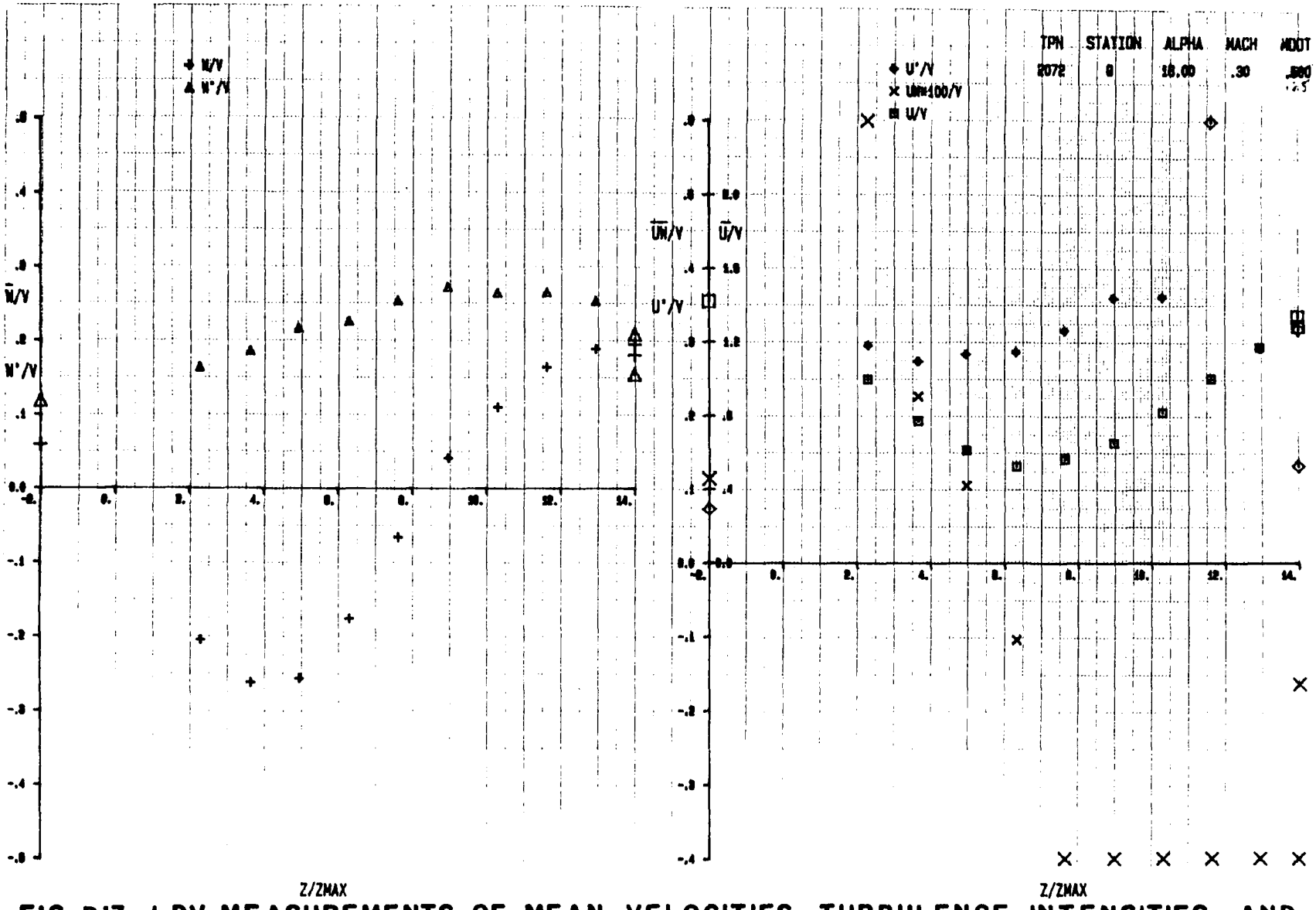

FIG. D13 LDV MEASUREMENTS OF MEAN VELOCITIES, TURBULENCE INTENSITIES, AND REYNOLDS STRESSES WITH BLOWING - NO CANARD - TGF - $\alpha = 16°$ - STATION Q

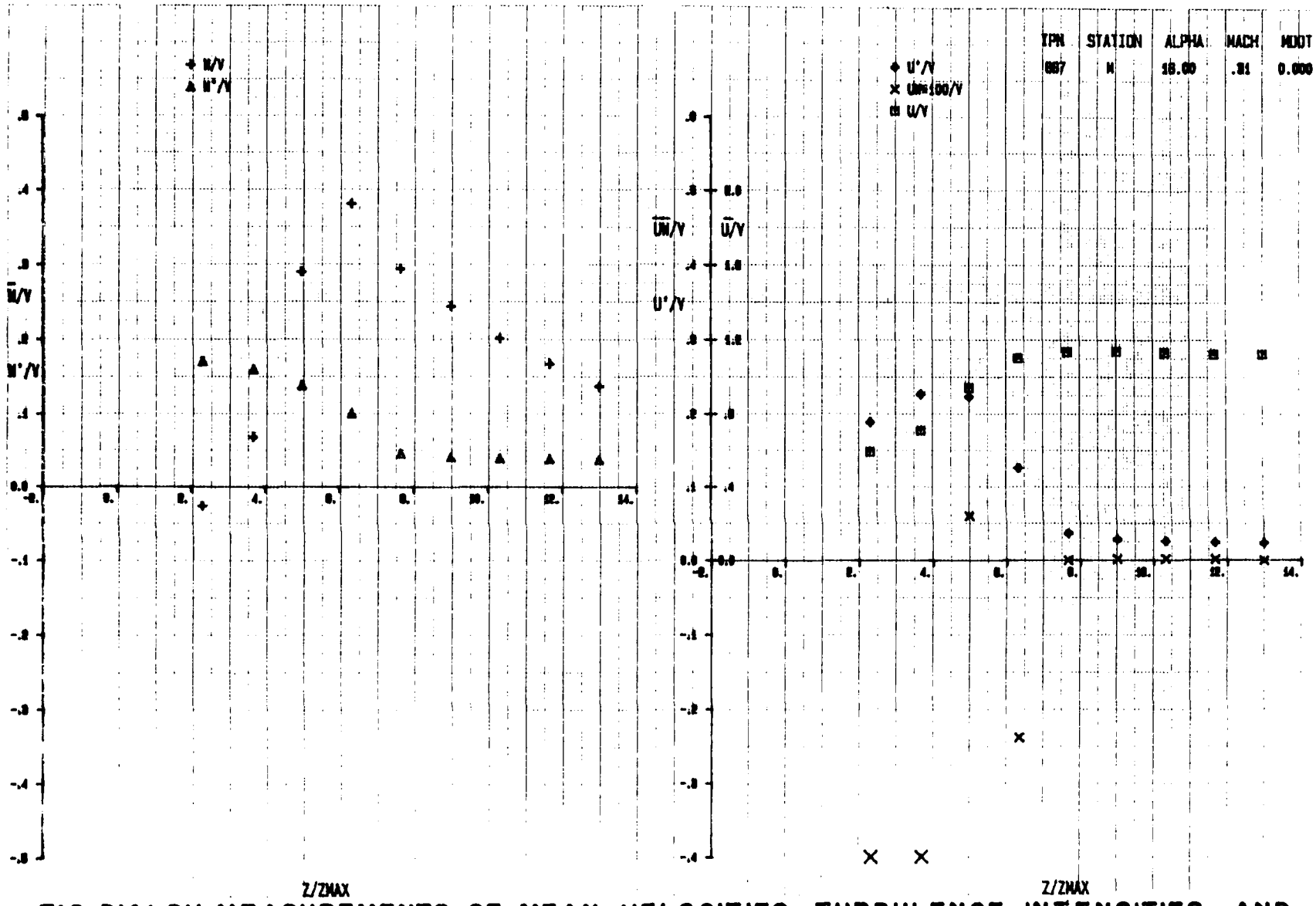

FIG. D14 LDV MEASUREMENTS OF MEAN VELOCITIES, TURBULENCE INTENSITIES, AND REYNOLDS STRESSES WITHOUT BLOWING - NO CANARD - TGF - $\alpha = 16°$ - STATION M

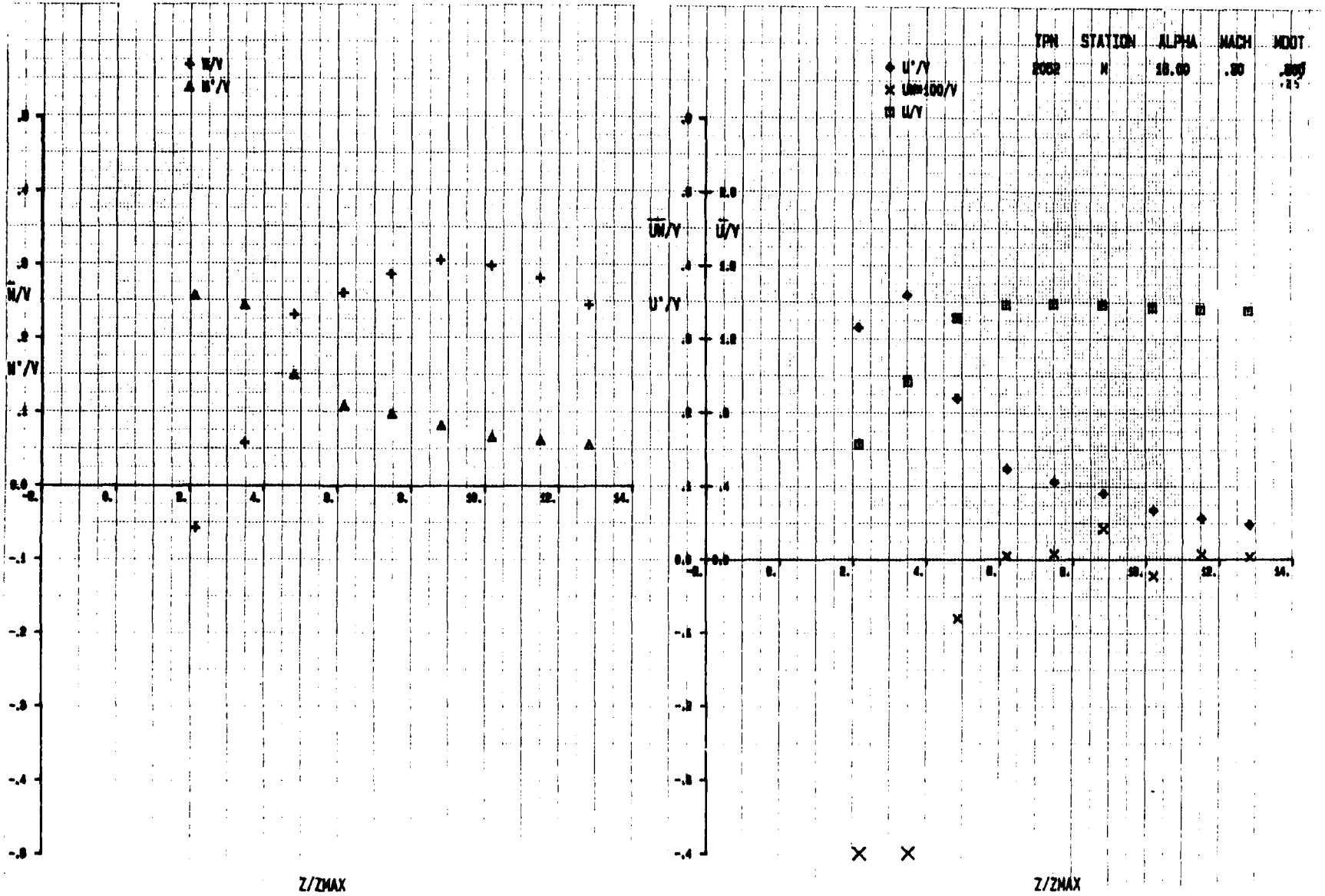

FIG. D15 LDV MEASUREMENTS OF MEAN VELOCITIES, TURBULENCE INTENSITIES, AND REYNOLDS STRESSES WITH BLOWING - NO CANARD - TGF - $\alpha = 16°$ - STATION M

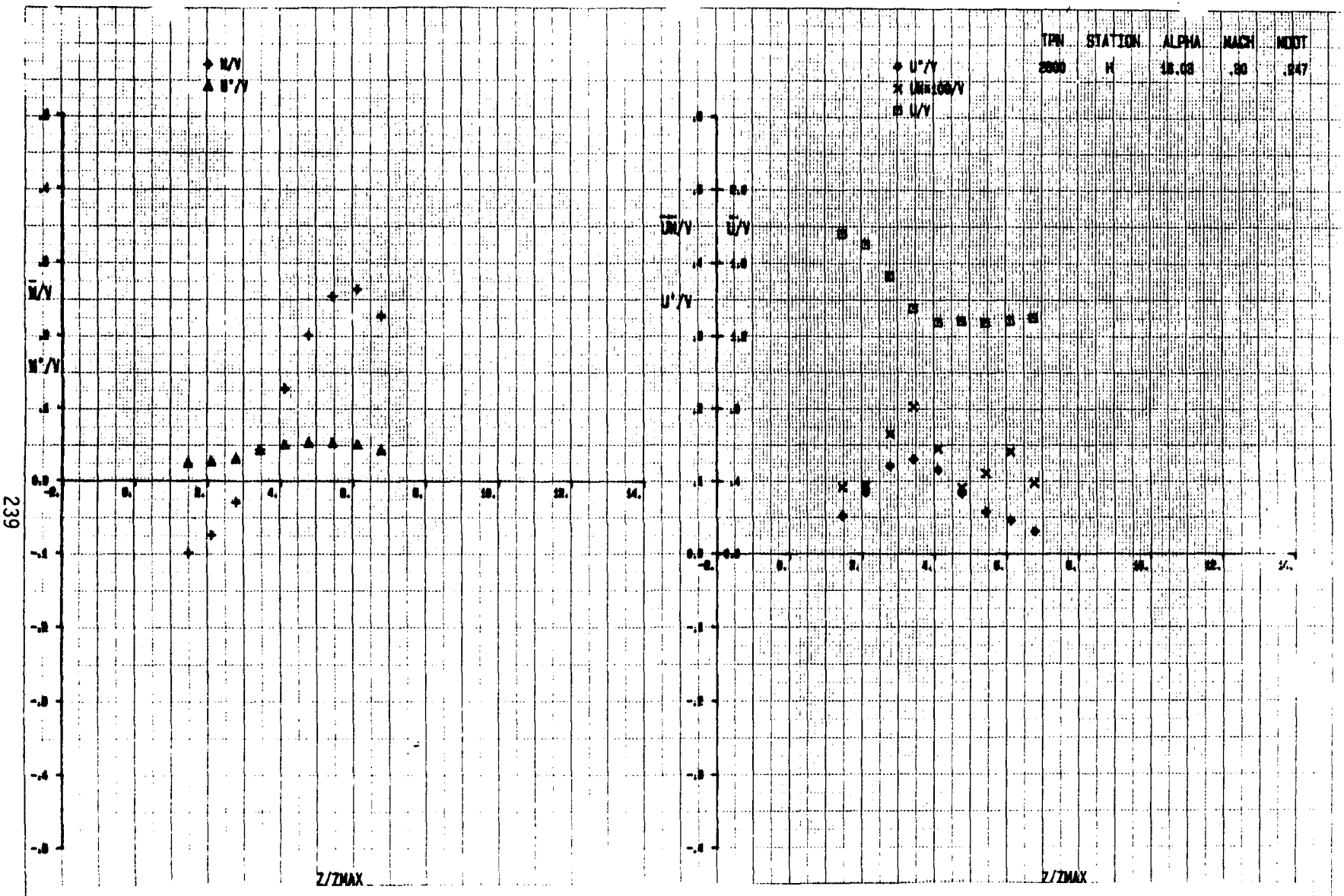

FIG. D16 HOT WIRE MEASUREMENT OF MEAN VELOCITIES, TURBULENCE INTENSITIES, AND REYNOLDS STRESSES WITH BLOWING - NO CANARD - TGF - $\alpha = 16°$ STATION H

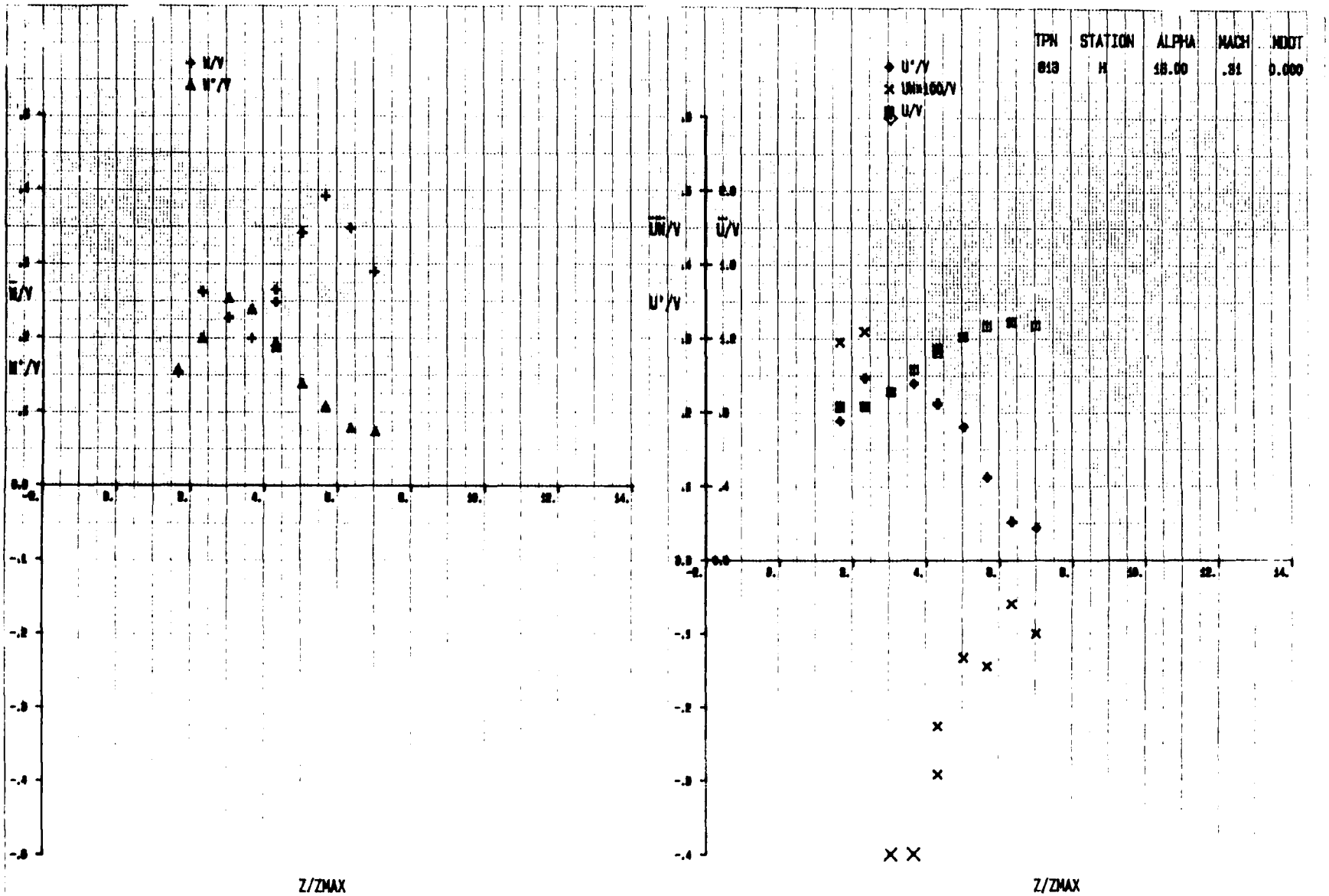

FIG. D17 LDV MEASUREMENTS OF MEAN VELOCITIES, TURBULENCE INTENSITIES, AND REYNOLDS STRESSES WITHOUT BLOWING - NO CANARD - TGF - $\alpha = 16°$ - STATION H

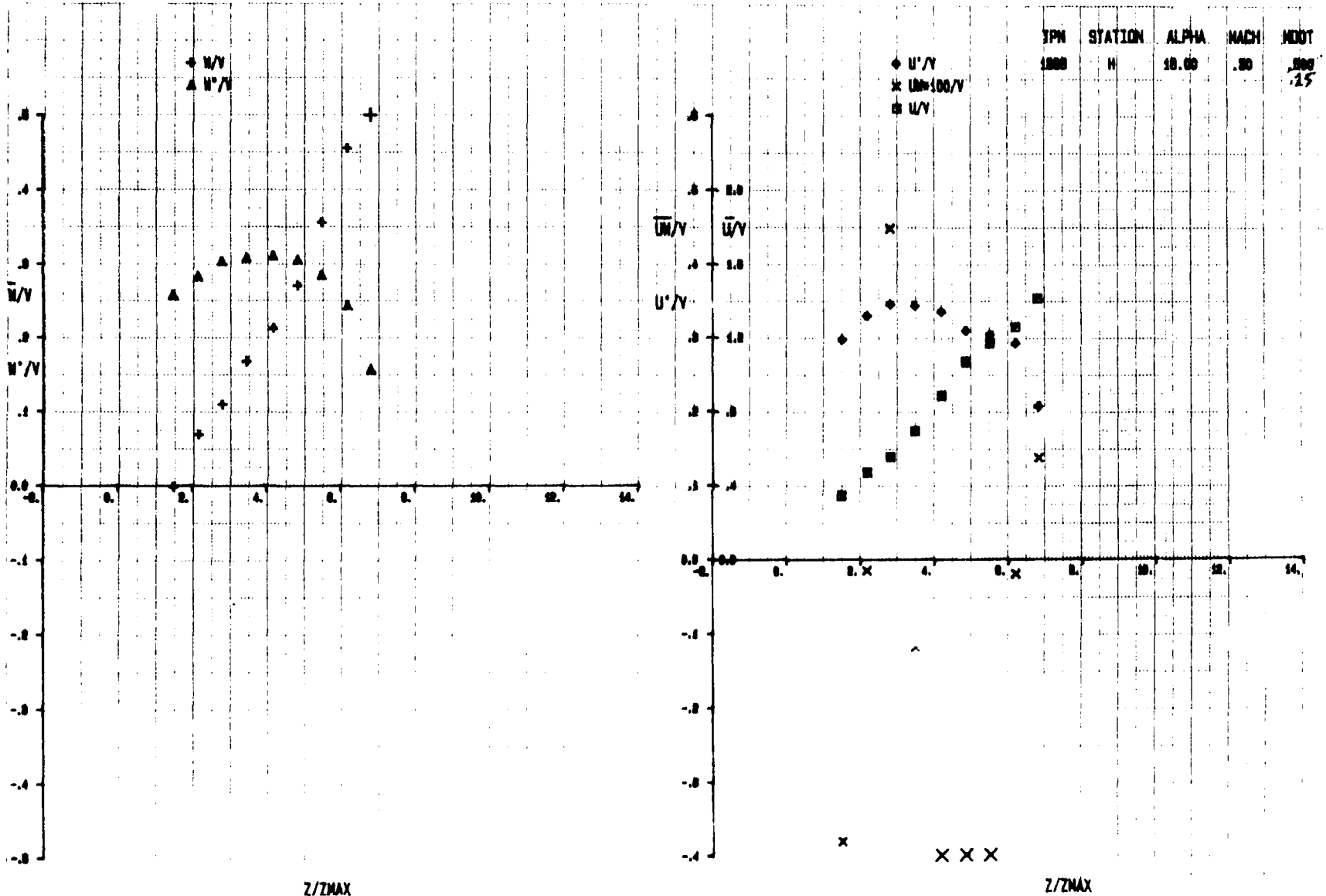

FIG. D 18 LDV MEASUREMENTS OF MEAN VELOCITIES, TURBULENCE INTENSITIES, AND REYNOLDS STRESSES WITH BLOWING - NO CANARD - TGF - $\alpha = 16°$ - STATION H

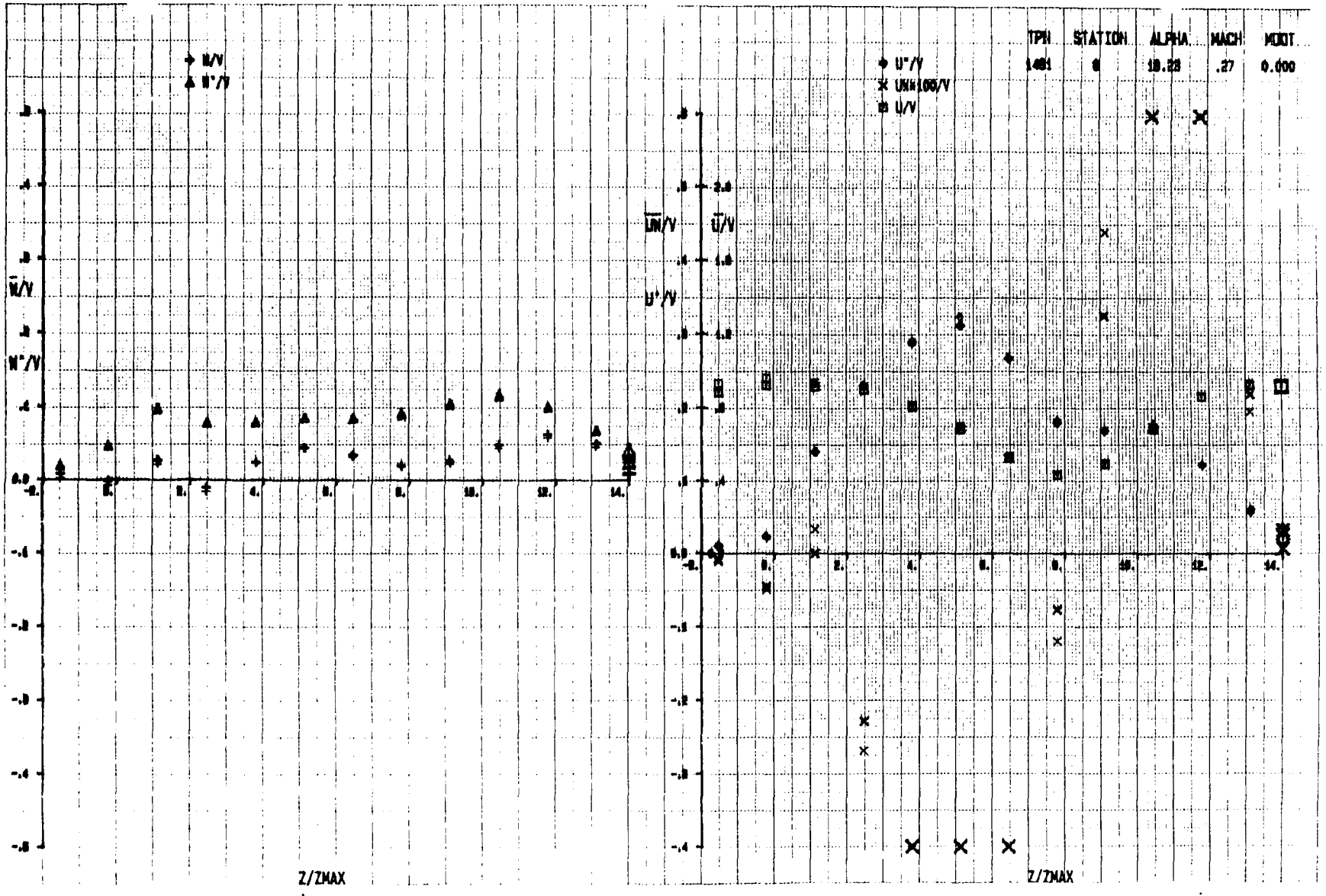

FIG. D19 HOT WIRE MEASUREMENT OF MEAN VELOCITIES, TURBULENCE INTENSITIES, AND REYNOLDS STRESSES WITHOUT BLOWING - NO CANARD - TGF - $\alpha = 20°$ STATION Q

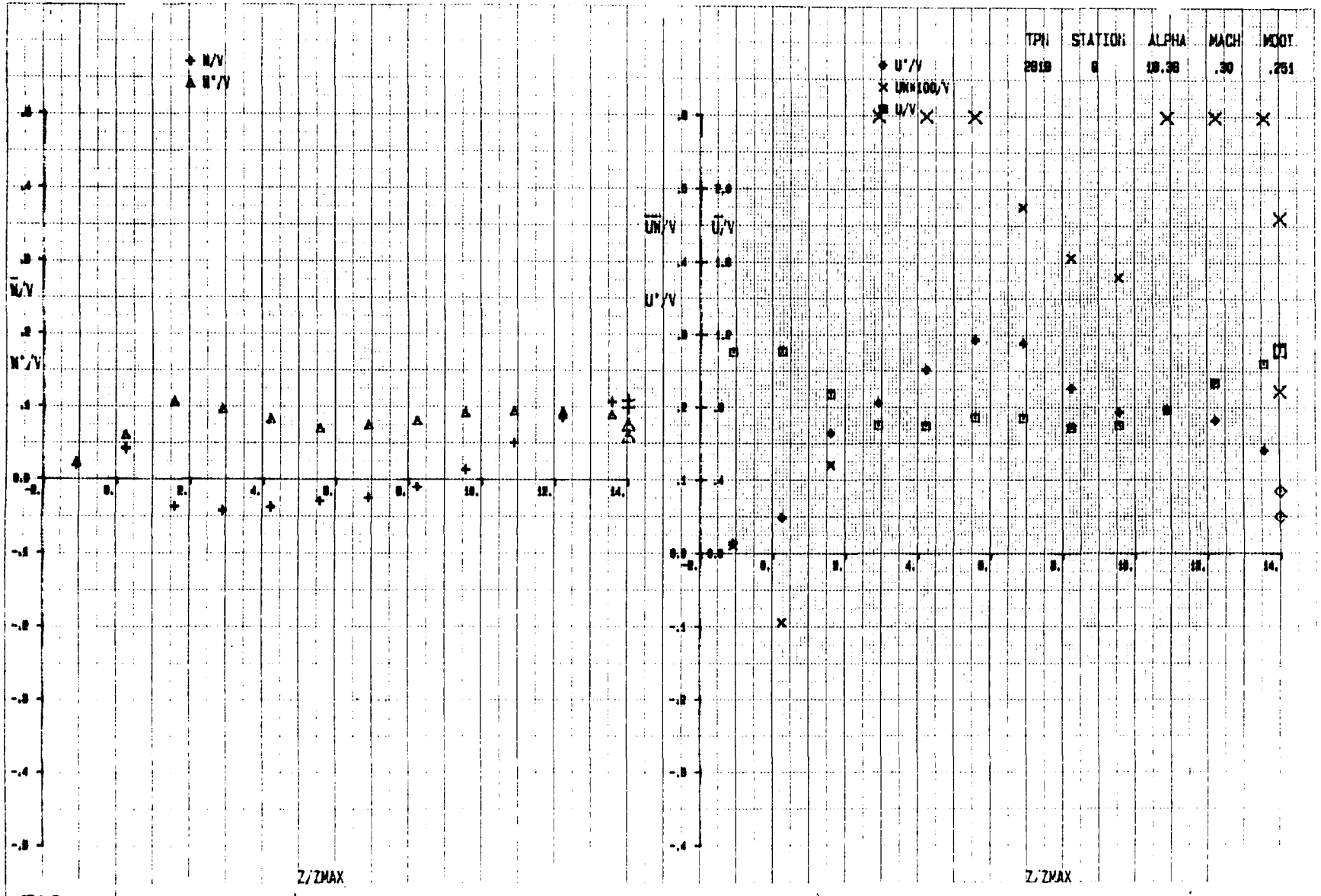

FIG.D20 HOT WIRE MEASUREMENT OF MEAN VELOCITIES, TURBULENCE INTENSITIES, AND REYNOLDS STRESSES WITH BLOWING - NO CANARD - TGF - α =20° STATION Q

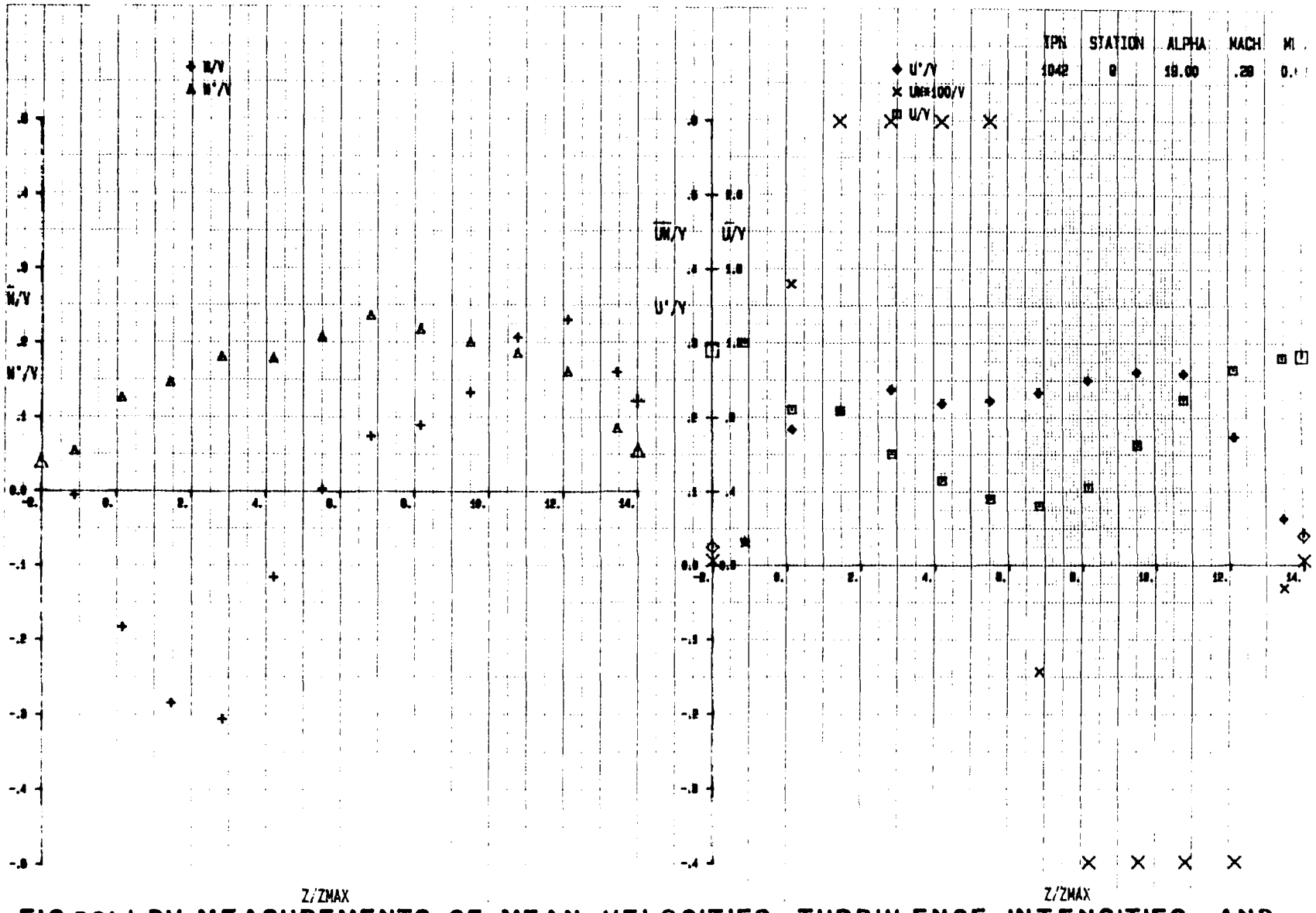

FIG.D21 LDV MEASUREMENTS OF MEAN VELOCITIES, TURBULENCE INTENSITIES, AND REYNOLDS STRESSES WITHOUT BLOWING - NO CANARD - TGF - $\alpha = 20^{\circ}$ - STATION Q

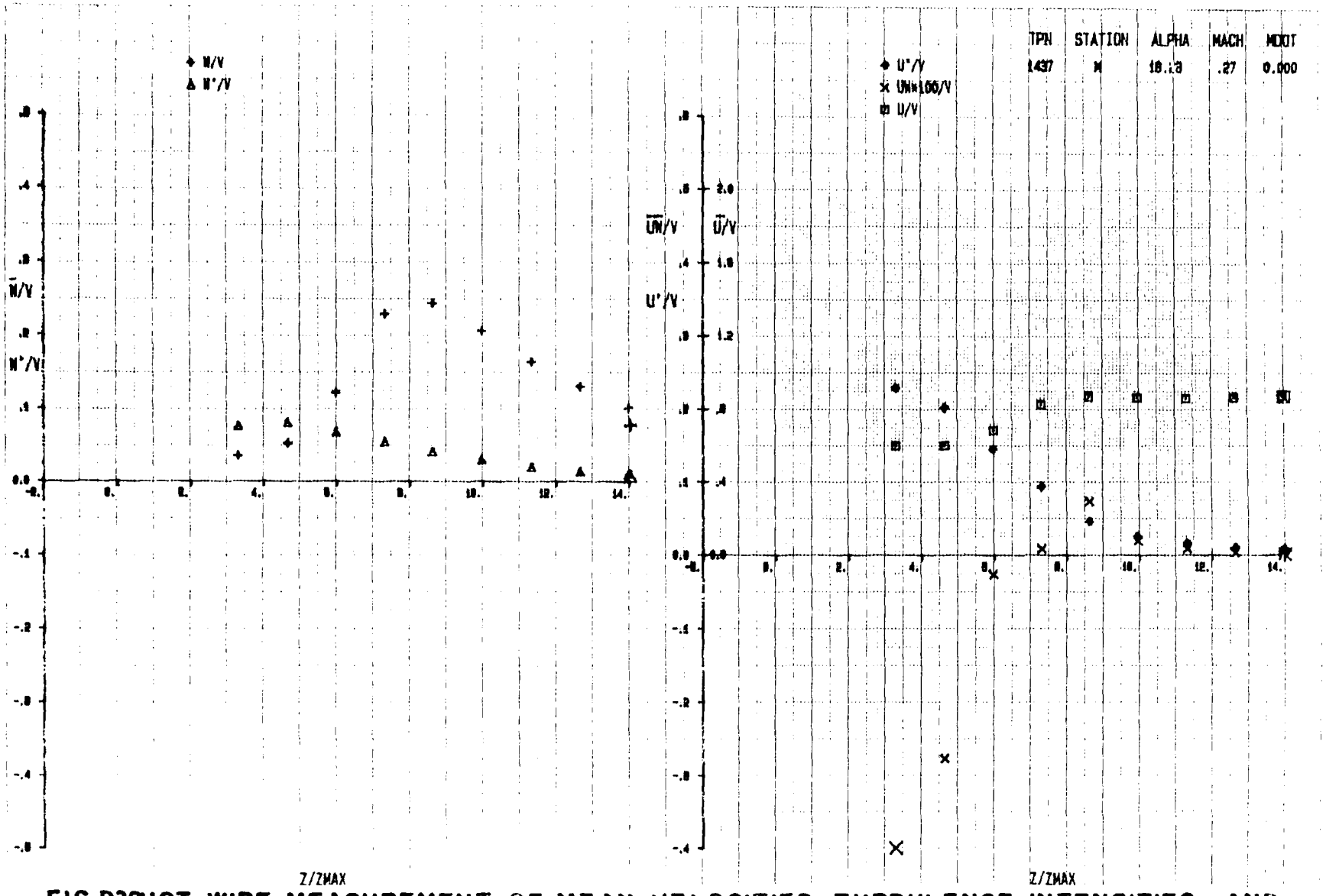

FIG. D22 HOT WIRE MEASUREMENT OF MEAN VELOCITIES, TURBULENCE INTENSITIES, AND REYNOLDS STRESSES WITHOUT BLOWING - NO CANARD - TGF - α = 20° STATION M

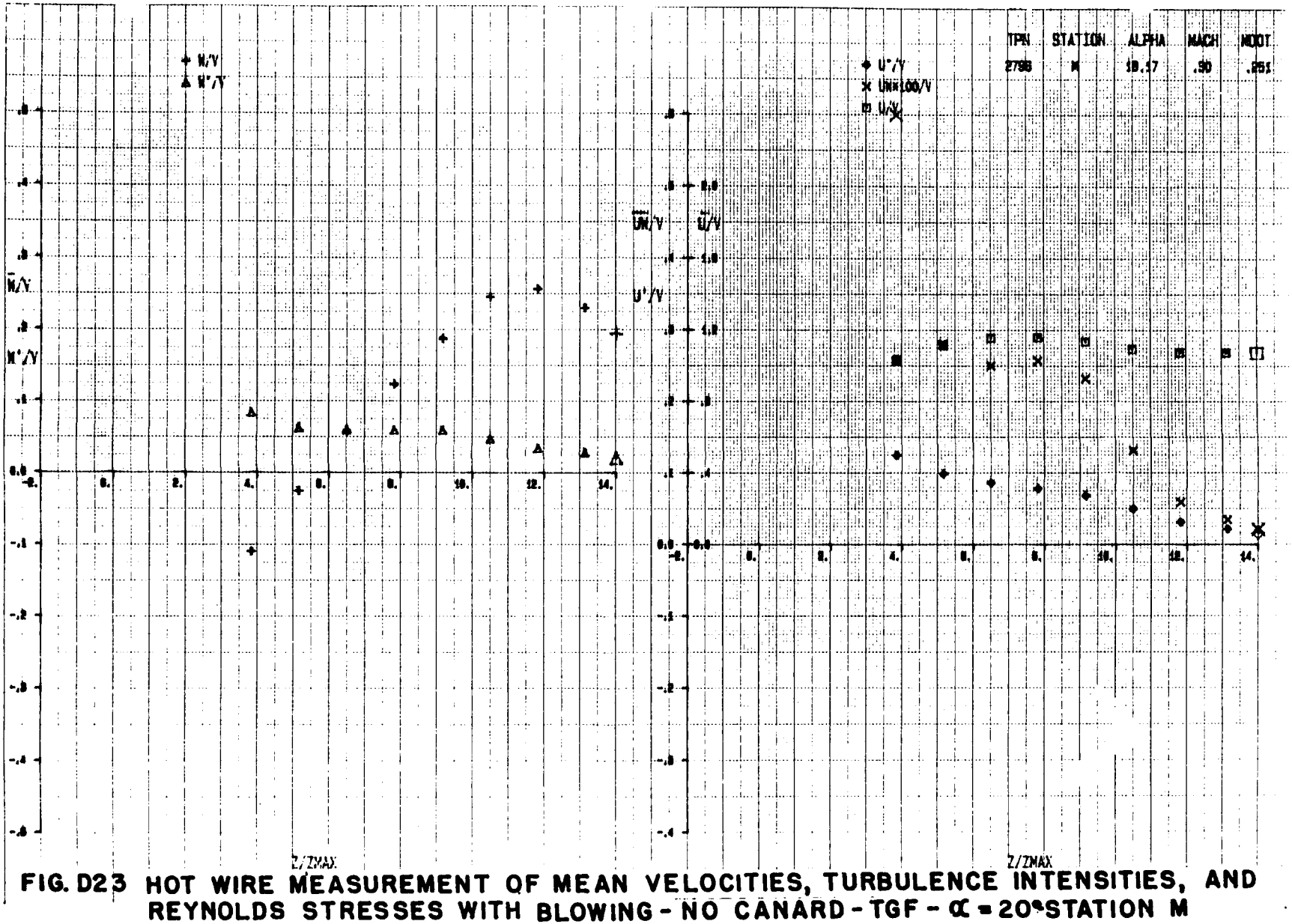

FIG. D23 HOT WIRE MEASUREMENT OF MEAN VELOCITIES, TURBULENCE INTENSITIES, AND REYNOLDS STRESSES WITH BLOWING - NO CANARD - TGF - $\alpha = 20°$ STATION M

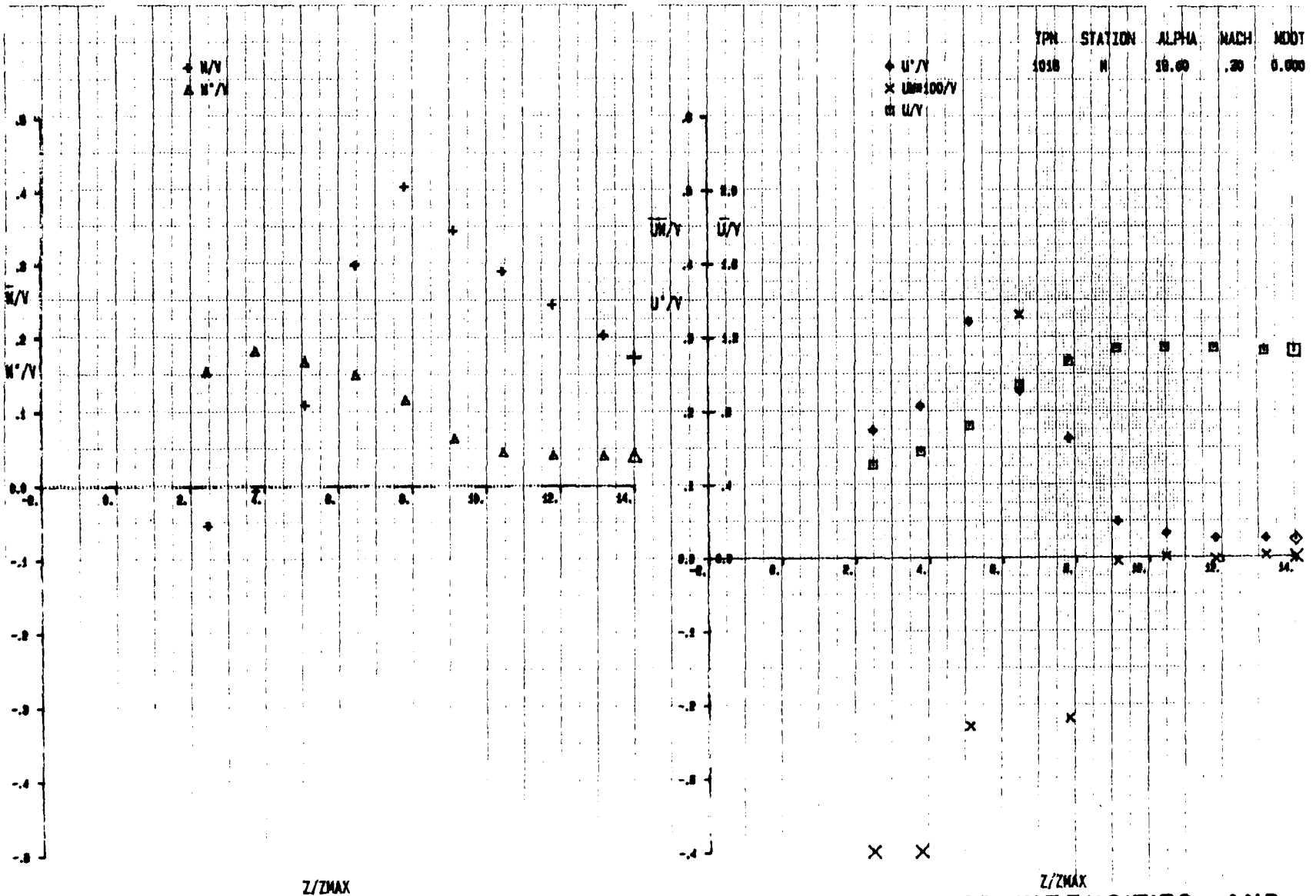

FIG.D24 LDV MEASUREMENTS OF MEAN VELOCITIES, TURBULENCE INTENSITIES, AND REYNOLDS STRESSES WITHOUT BLOWING - NO CANARD - TGF - α =20°- STATION M

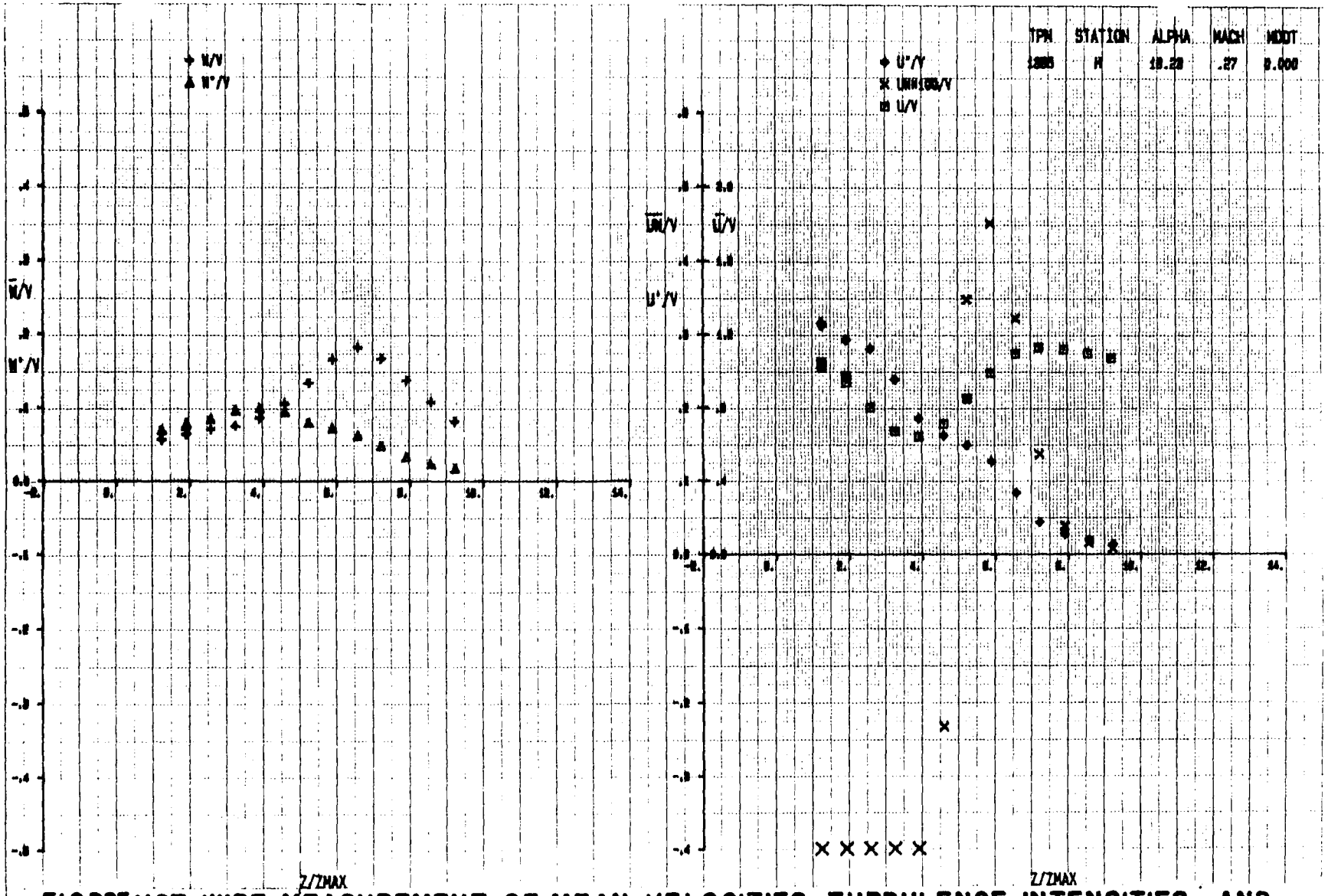

FIG.D25 HOT WIRE MEASUREMENT OF MEAN VELOCITIES, TURBULENCE INTENSITIES, AND REYNOLDS STRESSES WITHOUT BLOWING - NO CANARD - TGF - $\alpha = 20°$ STATION H

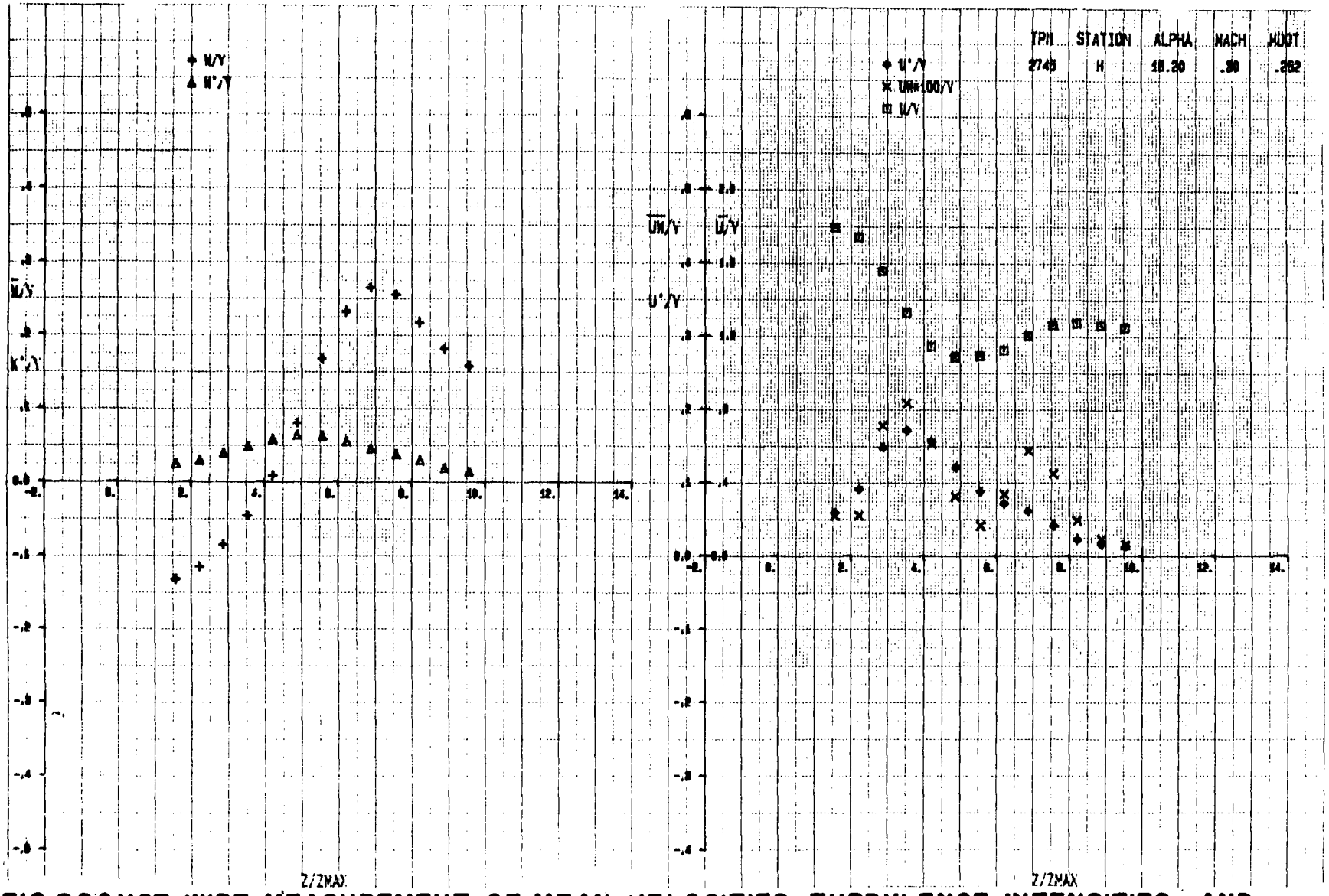

FIG. D26 HOT WIRE MEASUREMENT OF MEAN VELOCITIES, TURBULENCE INTENSITIES, AND REYNOLDS STRESSES WITH BLOWING - NO CANARD - TGF - $\alpha = 20°$ STATION H

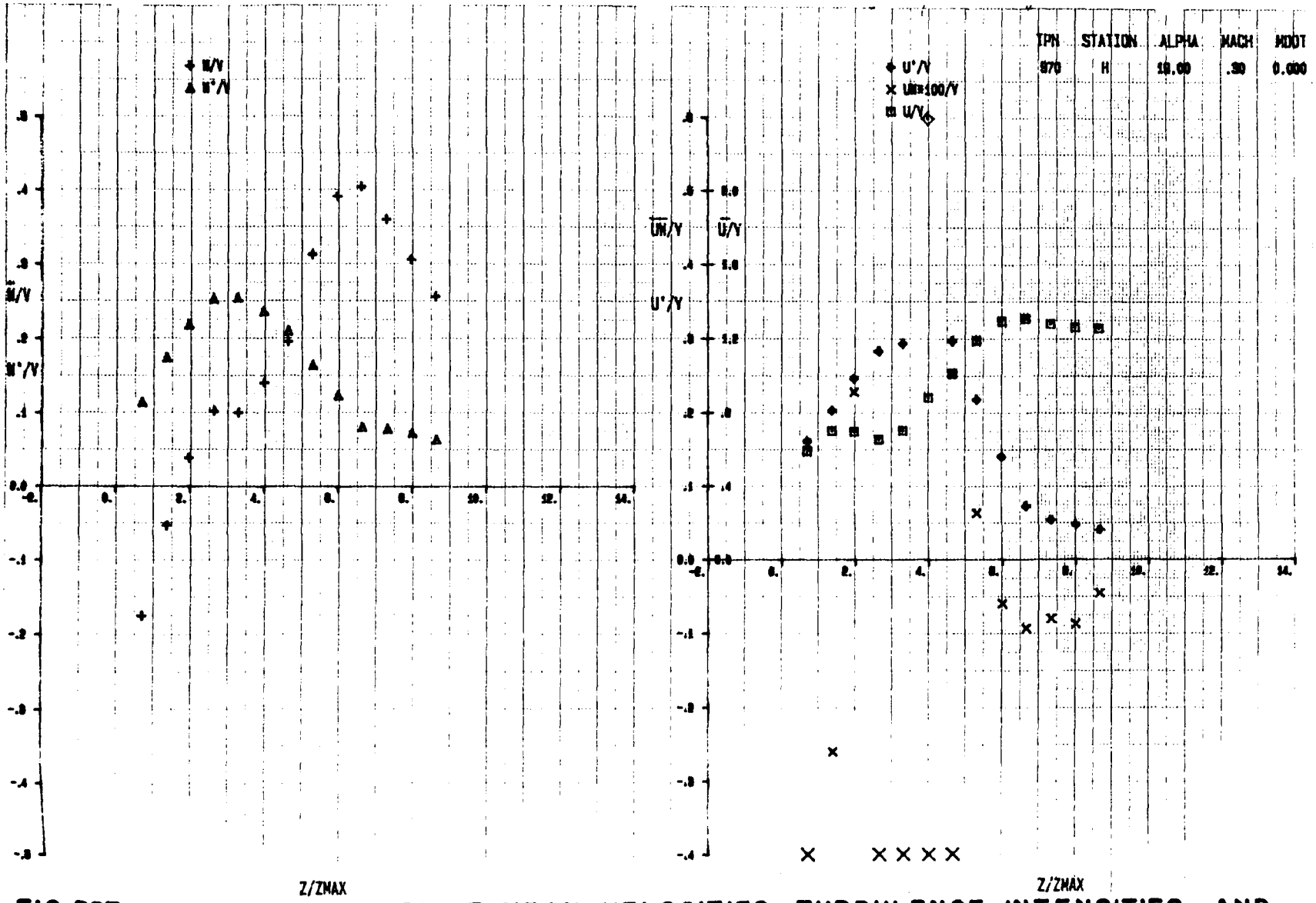

FIG. D27 LDV MEASUREMENTS OF MEAN VELOCITIES, TURBULENCE INTENSITIES, AND REYNOLDS STRESSES WITHOUT BLOWING - NO CANARD - TGF - $\alpha = 20°$ - STATION H

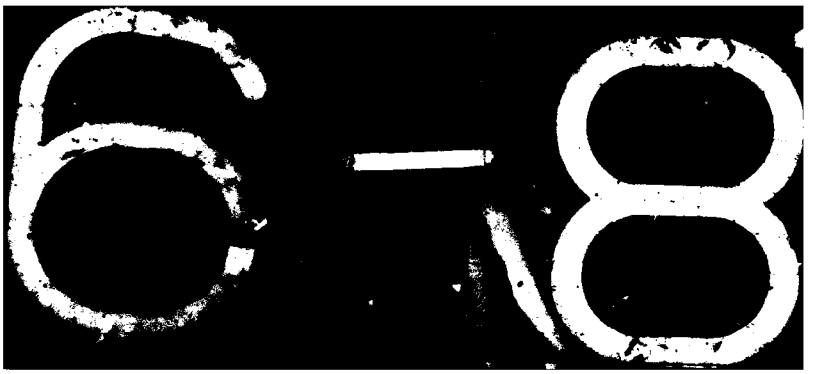
6-8